EMIW 2022

XXV ELECTROMAGNETIC INDUCTION WORKSHOP

11-17 September 2022

Grand Hotel Ontur ▪ Çeşme-Turkey

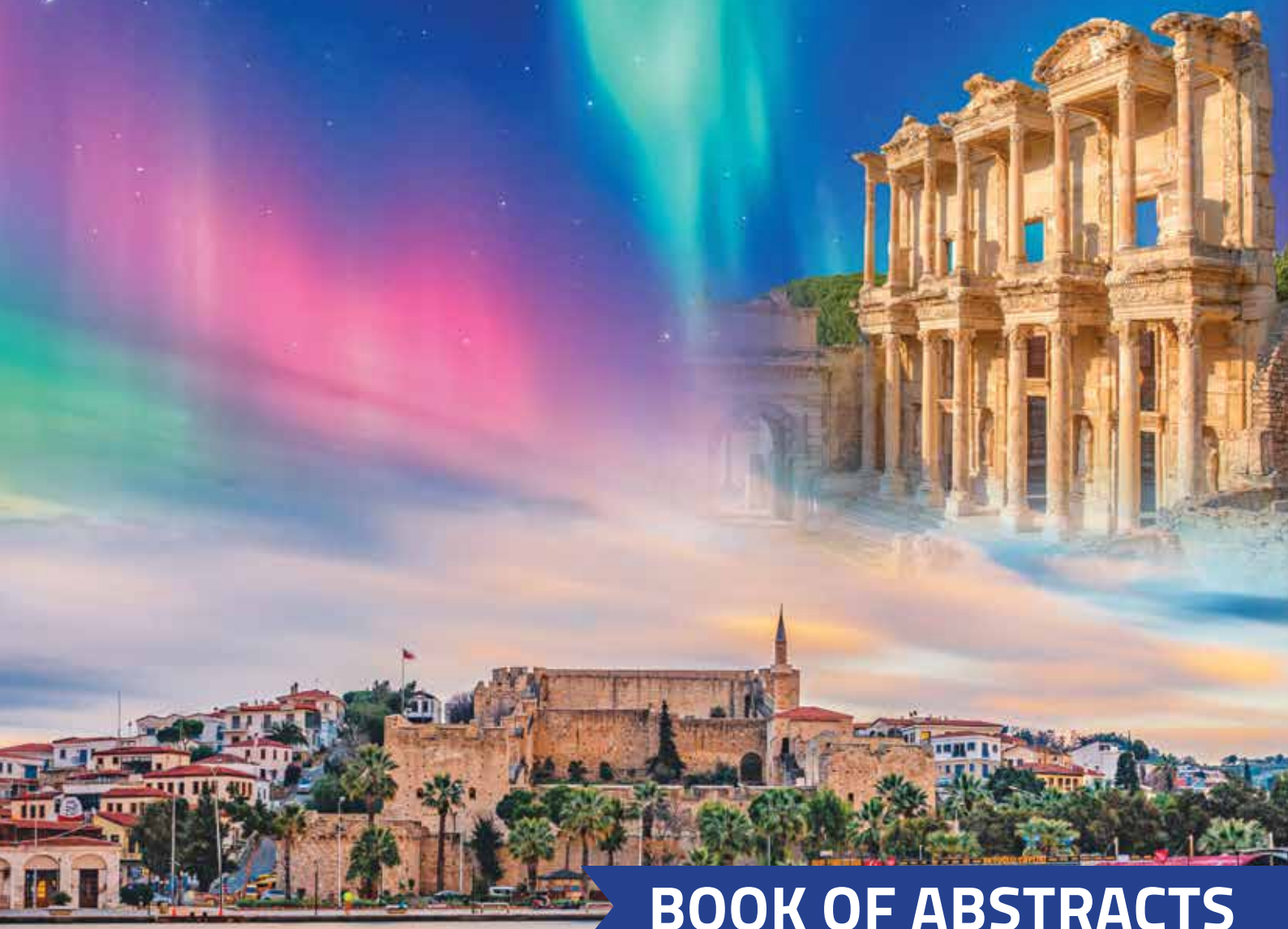

BOOK OF ABSTRACTS

emiw2022.emiw.org

EMIW 2022 XXV ELECTROMAGNETIC INDUCTION WORKSHOP

11-17 September 2022

Grand Hotel Ontur Çeşme-Turkey

25th EM Induction Workshop

11-17 September 2022

Çeşme-Turkey

emiw2022.emiw.org

BOOK OF ABSTRACTS

International Association of Geomagnetism and Aeronomy
Division VI Electromagnetic Induction in the Earth and Planetary Bodies

www.emiw.org

CONTENTS

Abstract, 25th EM Induction Workshop, Çeşme, Turkey, September 11-17, 2022

Near surface EM technologies – Archaeological and environmental applications

I. Akca[1]
[1] Ankara University, Department of Geophysical Engineering, Turkey, iakca@eng.ankara.edu.tr

SUMMARY

Electromagnetic methods (EM) are a special branch of geophysical studies applied for the solution of a variety of problems where the target depth ranges in centimeters to hundreds of kilometers. The majority of EM applications deals with deeper portions of the subsurface where the first few tens of meters generally disregarded. However, these depths also include valuable exploration targets from various point of views and EM also provide suitable tools for the investigation of such shallow targets. At this scale, the exploration targets are generally man-made or natural features/structures embedded into first few meters from the ground surface. The main EM tool used at near surface applications is the ground penetrating radar (GPR) a high frequency method providing high resolution images of subsurface. Therefore, this review is mainly focusing on the application of GPR method at investigations such as sinkhole detection, groundwater related surveys, agricultural investigations, ice and snow research and finally archaeological surveying. A recent trend in near surface application of EM studies is the determination of certain physical properties of soil and/or rocks directly from geophysical data. The review consists of three parts: (1) development in the instrumentation of shallow electromagnetic methods (mainly GPR), (2) latest data and image processing methodologies, (3) case histories and examples. The examples presented in the paper are mostly from archaeological surveys which have a significant weight in the literature as well.

Keywords: GPR, Data Processing, Archaeology, Environmental Geophysics

Unravelling electrical structure of the mantle with ionospheric, magnetospheric and oceanic electromagnetic sources

Alexander Grayver
[1]Institute of Geophysics, ETH Zürich, agrayver@ethz.ch

SUMMARY

This review presents the progress made in the last decade in the mantle studies with natural electromagnetic (EM) induction sources, which span periods from seconds to years and have diverse origins. These mechanisms produce field variations that can sense Earth's electrical structure at different scales in a depth range from the crust to the lower mantle. The last decade has seen substantial progress in different areas related to the methods, data collection and numerical modelling of EM phenomena. Specifically, new methods on handling complex ionospheric and magnetospheric sources were proposed, accompanied by more efficient forward and inverse modelling tools that allow us to combine several sources and constrain electrical conductivity on multiple scales simultaneously. Further, the launch of Swarm satellites in 2013 with extremely successful operation have marked a new era in the field of large-scale EM induction, presenting a set of new opportunities. These developments were backed by continuing new lab measurements of electrical conductivity for mantle minerals at temperatures and pressures that are closer to the actual conditions expected in the mantle. The latter enabled more accurate quantitative estimates of water content and temperature in the mantle. In parallel, crust and mantle conductivity models along with developed modelling techniques have become an integral part of geomagnetic field and geomagnetically induced current (GIC) modelling workflows.

Keywords: global induction, mantle conductivity, inversion, water content

Electromagnetic Measurements on Volcanic Islands

Duygu Kiyan
Dublin Institute for Advanced Studies, Ireland, duygu@cp.dias.ie

SUMMARY

Volcanic islands develop in the geodynamic context ranging from mid-ocean ridges (e.g., Azores Archipelago) to intraplate (such as the Hawaiian Islands, Cabo Verde) and to volcanic arcs (e.g., the Aeolian Islands, the Antilles). They are one of the most vulnerable environments on Earth not only because of their high exposure to the impact of multi-hazards (e.g., volcanic eruptions, landslides, tsunamis etc.) but also because of their isolation from the mainland. Many volcanic islands are densely inhabited, hence given the growing population and changing climate, the need to identify, monitor, and mitigate geohazards has been increasingly important to protect the public. Additionally, identifying and de-risking natural resources such as geothermal energy and freshwater are also essential to economies and societies. This review provides an overview of electromagnetic studies aimed at understanding and characterising the activity, dynamics and hazards of volcanoes on volcanic islands. These studies include passive and active electromagnetic data acquisition in the atmospheric, terrestrial, and marine (i.e., near-shore) realms. The review also addresses challenges related to survey planning, data acquisition, modelling, and interpretation. The particular challenges posed on volcanic islands include the following:

1. A potentially complicated internal structure of the volcanic edifice, which usually extends spatially below the ocean. Deep investigations thus will require marine measurements.
2. Depending on different tectonic and environmental settings, the subsurface can be extremely heterogeneous. The diversity of rocks present in and around the edifice is large, and often displays the work of multiple episodes of growth and collapse.
3. The presence of the ocean, where the near-shore bathymetry is often not well known, as well as the distribution of high-porosity sediments around the island, which are derived from the growth and collapse of the volcanic edifice.
4. Volcanic islands often have strong and steep topography, which poses not only considerable logistical problems, but also challenges for the model discretisation.
5. The ubiquitous presence of hydrothermal systems, which represent geochemically aggressive environments, and have the potential of interacting with the original rock, leading to considerable volumes of high-conductivity minerals and additional secondary heterogeneity.

Keywords: Electromagnetic induction, Electrical conductivity, Volcanoes, Volcanic islands

Abstract, 25^{th} EM Induction Workshop, Çeşme, Turkey, September 11-17, 2022

Electromagnetic Modeling Using Adaptive Grids - A Reflection on the Term Geometry

Klaus Spitzer
Institute of Geophysics and Geoinformatics, TU Bergakademie Freiberg, Germany
klaus.spitzer@geophysik.tu-freiberg.de

SUMMARY

The goal of electromagnetic (EM) modeling is to find mathematical and physical models that represent 'reality' as well as possible and allow us to predict and understand the behavior of EM fields in matter-filled space. Inevitably, these models are always an abstract and incomplete representation of reality. They therefore contain sources of error and are subject to a limited range of validity. Particularly, the geometry of our physical models in the Earth sciences is extremely challenging due to its multi-scale nature.

On a small scale, we may end up in microscopic, possibly self-similar structures where non-inductive polarization effects are not covered anymore by our chosen mathematical model due to a variety of pore-scale and inner-surface electrochemical processes. Electric conductivity can become complex-valued, frequency dependent and non-linear. Moreover, texture or heterogeneity below a certain spatial scale can appear as anisotropy, leading to a matrix representation of electromagnetic parameters in the equations to be discretized. Much of this is subject to current petrophysical research, which gives us new insights into the fundamental properties of these parameters.

On a large scale, and this is actually the main focus of my talk, there are sources of error associated with the representation of macroscopic geometry and its discretization. Whereas geometry modeling started with homogeneous and layered halfspaces with only a handful of parameters in the first half of the 20^{th} century, we were able to approximate 2D and 3D geometries in the 70s, 80s, and 90s using, in the end, millions of rectangular building blocks to construct geometric models in a brick-like and conformal fashion. This is simple and easy to handle but sometimes also inefficient, particularly when it comes to adopting to the geometric idiosyncrasies of our geo-reality. Staircase-like structures associated with rectangular Cartesian grids tend to introduce artifacts into the model response once the configuration of sources and receivers generates sensitivity towards the artificial geometric features. Therefore, more elegant ways of representing geometry evolved during the last 20 years incorporating unstructured and non-conforming grids or, recently, even meshless approaches.

I will focus on the numerical and computational side of modeling here and restrict myself to the classical scalar electromagnetic parameter set taking into account that computers will continue to expand our capabilities in the future. Since there are no closed solutions to Maxwell's equations with spatially arbitrarily varying coefficients, discrete solutions inevitably imply approximation errors whose magnitude is generally difficult to assess. A priori and a posteriori error estimators have provided us with some means to quantify the accuracy of the computed solution or, at least, allow us to tailor the properties of the used discretization to a desired level. Moreover, we realize that the description of the geometry itself, i.e., before we start discretizing it, represents a major problem. We need tools to disassemble the computational domain into 'water-tight' subdomains with arbitrary shapes. Large-scale structures, like underground voids, boreholes, bathymetry, or the topography of the Earth's surface can significantly influence the electromagnetic response within a specific frequency range or time interval. Ultimately, this means we have to deal with a multi-scale issue which requires an appropriate level of geometric detailedness and a flexible local refinement or coarsening to account for the true physical response once a reliable mathematical model has been chosen. It turns out that the sensitivity plays an important role to steer and direct the degree of resolution of meshes and geometry.

Due to brevity, the talk will not address the inverse problem and efforts to quantify uncertainty in a Bayesian sense. The talk much more tries to review some attempts to gain control over the error sources in the forward

process, particularly with respect to error estimators defined within the theory of finite elements. I will briefly review the different types of finite elements used in our approaches to model vector electromagnetic fields and scalar potentials, and discuss the types of meshes underlying the discretization schemes with respect to their ability to represent arbitrary geometry.

Keywords: Finite elements, unstructured grids, error estimators, geometry modeling, level of detailedness, adaptivity

Electromagnetic studies in the Eastern Mediterranean Region with Special Reference to Major Transform (Strike-Slip) Faults

S.B.Tank [1]

[1]Boğaziçi University, Kandilli Observatory and Earthquake Research Institute, bulent.tank@boun.edu.tr

SUMMARY

Even though extensively researched in the history of geosciences, human knowledge on the earthquake generation is still severely limited. This is primarily due to the complicated behavior of the medium, namely the seismogenic zone, where the earthquakes originate and variety of the numerous physical parameters used while acknowledging the earthquake phenomena. Leastways, our knowledge today reached to a certain level that allows us to affirm the fact that before, during and after earthquake processes are governed by the existence of sub-surface fluids (and/or geofluids) in and around the major fault zones. Depending mostly on fault's structural properties as well as its focal mechanism type, the geofluids present at the fault zone are held responsible for the occurrence of major and destructive earthquakes with their mechanical influence under various physicochemical conditions resulting in the weakening and lubricating effects. Thus, to comprehend the characteristics of the seismogenesis, imaging the geometry of fluid-sheltering fault structures, understanding the vivacity of the geofluids under varying stress conditions and determining the amounts of the geofluids have become indispensable apparatuses for the illumination of the earthquake related phenomena.

In this regard, together with some other fluid-sensitive geophysical and geological methods, the major fault zones worldwide are being examined with both time- and frequency-domain electromagnetic (EM) methods such as transient electromagnetics and magnetotellurics. Since 60s/70s when the earliest EM studies performed around the fault zones brought elementary results, there has been a tremendous amount of improvements in this field. However, the evolution of the equipment, the observation techniques and the modeling schemes brought further complexities. Particularly, the ongoing transition from the two-dimensional interpretation to the three-dimensional requires additional precautions and circumspections.

This narrative review attempts to shed some light on the pros and cons of utilizing some of these EM methods while investigating the structure and dynamic properties of the strike-slip fault zones in the Eastern Mediterranean region. The review begins with introducing the structural, rheological and electrical properties of the strike-slip faults in general. A historical perspective and global distribution of the EM studies on strike-slip faults will be given. Next, the tectonic, geodynamic and kinematic properties of the Eastern Mediterranean region will be presented. The remaining part of the review highlights several systematic studies performed at and around the major strike-slip faults of the Eastern Mediterranean Region, namely, the Dead Sea Transform Fault, the East Anatolian Fault and the North Anatolian Fault.

Keywords: Strike-slip Faults, Fluids, Eastern Mediterranean

Electromagnetic technology for prospecting unconventional hydrocarbon resources

Liangjun Yan[1,2,3]
[1]Key Laboratory of Exploration Technologies for Oil and Gas Resources (Yangtze University), Ministry of Education, China, 430100. yljemlab@163.com
[2]Cooperative innovation center of Unconventional oil and gas, Hubei, China
[3]Key Laboratory of Geophysical prospecting, CNPC

SUMMARY

Unconventional oil and gas (normally tight gas and oil, shale gas and oil, coal seam gas, natural gas hydrate, etc.), which generally have the characteristics of source-reservoir symbiosis, are widely distributed. Still, their high-quality reservoirs have large burial depths, small targets, complex electrical properties, and considerable inhomogeneity, making their a great challenge for electromagnetic (EM) exploration to detect them. In recent decade, A series of achievements have been made in the field of EM exploration of unconventional oil and gas worldwide, including the EM response mechanism of unconventional reservoir rocks, new methods and technologies in controlled-source EM exploration on land, identification and evaluation methods for oil and gas using EM parameters. These technologies have been successfully applied in unconventional oil and gas exploration and development with good effect and have been recognized by petroleum geology and development circles. Firstly, this paper introduced the complex resistivity characteristics of organic-rich shale, tight sandstone, and dolomite in southern China occurring in low porosity and permeability reservoirs, and discovered that organic-rich shale has the characteristics of low resistivity and high polarization. At next, an IP model for the shale reservoirs is established. Based on the mechanism of source-reservoir symbiosis in shale reservoirs, the identification mode for the sweet spot is proposed. It is then proved this paper that there exist a good petrophysics foundation for the EM exploration in the field of shale gas exploration and development. Secondly, there has been a research focus on how to use the multiple IP parameters, such as resistivity and polarizability, to estimate the characteristic parameters of the sweet spot of reservoir. The prediction method based on IP model for the parameters of reservoir is introduced. Thirdly, there is an outspring of the controlled-source EM exploration methods for unconventional oil and gas exploration, such as Wide Field Electromagnetic Method (WFEM), Wire-less Electromagnetic Method (WEM), Time-Frequency Electromagnetic Method (TFEM), Long Offset and Window Transient Electromagnetic Method (LowTEM) and Focused Source Electromagnetic Method (FSEM). These methods and technologies share a common feature of using a long wire source, with high-power, large current multi-waveform transmission, multi-component array acquisition and hybrid processing and inversion. Therefore, not only the signal-to-noise ratio, exploration depth, resolution and reliability, but also the efficiency, resolution, cost and adaptability have been significantly improved, making these methods able to deal with the geology problems in the exploration and development of unconventional oil and gas under complex conditions. Finally, several cases are given to indicate the apparent application effects of the new methods and technologies of controlled-source EM method in unconventional oil and gas exploration, sweet spot detection, fluid identification, fracturing monitoring, and at the same time, look into the broad application prospect of EM methods in the exploration and development of unconventional oil and gas. However, there are still plenty of unsuccessful cases. It is a long way to go in the effective application of EM methods in unconventional oil and gas exploration and development. Therefore, more achievements are expected to be made, especially on the EM response mechanism of unconventional oil and gas reservoirs, 3D high spatial and temporal density data collection technology under complex geological and topographical conditions, fast, stable and reliable high-precision inversion and imaging methods with constraints based on prior logging and seismic data, reservoir parameters prediction method based on refined IP model.
Due to the limitation of the author's ability and the paper's length, the new methods, technologies, and application cases referred to in this paper are mainly from China.

Keywords: Unconventional oil and gas, Resistivity, Chargeability, Sweet spot testing, Controlled source EM

INTRODUCTION

Due to the greenhouse effect and environmental concerns, human's yearn for clean energy has been inspired. However, the conventional oil and gas resources shortage has been a global headache in

the Post-Petroleum Era, therefore, the exploitation and development of unconventional oil and gas reserves are gaining more and more attentions worldwide among governments and energy companies. Unconventional oil and gas resources including tight gas and oil, shale gas and oil, heavy oil, coal seam gas, and natural gas hydrate, are significant parts of the global energy structure, which occupy about 80% of the total oil and gas reserves on the earth. The successful development of unconventional oil and gas resources, especially shale gas and tight sandstone gas in the United States (US) has enabled the country to become self-sufficient in natural gas for the first time in the last over 40 years. In 2009, the output of unconventional natural gas in the US first exceeded that of conventional natural gas. Since then, the US turned into an important shale gas exporter and the supply pattern of the global natural gas market has changed. China is the world's second-largest energy consumer, and its unconventional oil and gas reserves is equivalent to the US. To meet the social needs and to reduce the energy dependency, China has accelerated the research on unconventional oil and gas related geological theories, exploration technologies, development methods and technical equipment. So far, many advances have been made and huge achievements have been achieved. With the continuous rising of unconventional oil and gas output, the national energy structure is considerably improved.

1.1 Geological and geophysical characteristics of unconventional oil and gas reservoirs

- Geological characteristics

Unconventional oil and gas resources are different kinds of oil/gas reserves that cannot be explored and developed simply with regular technologies and methods. Generally, the reservoir forming conditions of unconventional oil and gas resources are less demanding than those of conventional oil and gas resources, thus, unconventional reservoirs are more common and their occurrence modes are more diverse, Unconventional reservoirs possess the following geological characteristics (Zou, 2015):
(a) source-reservoir symbiosis;
(b) large distribution area, deep burial depth, and blurred boundaries;
(c) tight, poor physical properties, low porosity, low permeability, extensive nanoscale cracks, and strong heterogeneity;
(d) lithological diversity (sandstone, limestone, shale, coal and migmatite, etc.), small effective reservoir;
(e) rich in organic matter, high maturity, poor phase segregation, no unified boundaries of oil, gas, and water.

- Geophysical characteristics

Reservoir rocks containing oil and gas usually possess the characteristics of high resistivity and high polarization (Zonge,1975; Lima and Sharma, 1992; Sigel et al., 2007; Davydycheva et al., 2006; Burtman, 2015; Hu 2022). He and Wang (2007) proposed the ‘Ring three storey’ model for oil and gas identification based on EM and IP parameters. They confirmed that oil-gas reservoirs were of high resistivity and high polarization, while the water-bearing reservoirs were generally of low resistivity and high polarization. Based on the spatial resistivity and polarization differences, oil, gas and water could be easily and effectively identified. With this model, numerous favorable geological results have been obtained by applying the EM method in oil and gas exploration (He, 2005; Davydycheva, 2006; He, 2010). However, the differences in geological characteristics make the electrical features of unconventional reservoirs noticeably different. Unconventional reservoirs are mainly shale, mud shale, tight sandstone, and mudstone, which present the features of low resistance, low permeability and low polarization. A great quantity of petrophysical experiments indicated that shale gas reservoirs in southern China generally demonstrated the characteristics of low density, low speed, high resistance, and low magnetism (Wang, 2015). By conducting substantive complex resistivity measurements, Yan et al. (2014) and Xiang et al. (2014) found that rich-organic shale in southern China had the characteristics of low resistivity and high polarization. Similar results were obtained by Burtman (2014) using TerraTek shale rock samples. Similarly, changes in electrical characteristics are also noticeable during thermal flooding and hydraulic fracturing process. For example, when SAGD technique is applied, steam chambers and possible steam channeling-paths may form, and phase-transformation zones would form surround the steam-injection wells. The resistivity variations within different phase-transformation zones can provide physical-property foundation to identify the steam-flooding front. (Yang et al. 2005; Hu, 2022). As for hydraulic fracturing in shale gas reservoir, low resistance and high polarization anomalous body would form when thousands of tons of fracturing fluid are injected into the reservoir (Chen, 2000). Therefore, EM method can be used to monitor the spatial distribution of fracturing fluid and shed light on fracturing optimization.

1.2 Exploration features of unconventional oil and gas

Unconventional reservoirs demonstrate different source, lithology and physical properties, as well as hydrocarbon conditions from conventional reservoirs, thus, the exploration methods, development and evaluation techniques can be totally different. To explore the unconventional oil

and gas reservoirs, there are three stages: firstly, screen out the core area based on the high-quality reservoir evaluation criteria; secondly, identify the 'Sweet Spots Area (Segment)' based on the reservoir integral/local tectonic characteristics, and fault and microfracture features; finally, drilling, production and 'Sweet Spots Area (Segment)' evaluation. Compared with conventional oil and gas, there are three changes in unconventional reservoirs exploration (Zou, 2015), one is from 'finding oil in trap' to 'finding oil in the strata', second is from 'oil/gas reservoir' to 'oil/gas layer', and third is from 'Sweet Spot' to 'Sweet Spot Area (Segment)'. The 'Sweet Spot Area (Segment)' of unconventional reservoirs refers to as the source-reservoir symbiosis development area, which is an unconventional hydrocarbon enrichment area with large distribution range, specific thickness, high-quality source rock, good physical properties, high oil/gas saturation, high formation energy (i.e., high gas-oil ratio, high formation pressure), high brittleness index, rich fracture and local structure developed. Evaluation and optimization of "Sweet Spots Area (Segment)" is the key of unconventional oil and gas exploration and development, which runs through the whole exploration and development process. The evaluation parameters slightly vary with different unconventional reservoirs. The main evaluation parameters include TOC, porosity, the development degree of microfractures, brittleness, range (burial depth and distribution area), etc. (Zou et al., 2015; Yang, 2019). To improve the economic recovery efficiency of unconventional reservoir, it is necessary to improve reservoir permeability or fluid viscosity by horizontal drilling, fracturing, and other techniques to guarantee the continuous or quasi continuous accumulation of oil/gas resources. According to the specific geological problems and electrical characteristics in the three stages of unconventional oil and gas exploration, EM exploration technology can give full play to the advantages to achieve the exploration, detection and evaluation of sweet spots.

1.3 Opportunities and challenges of EM exploration technologies

Due to the limitation of inherent method and theory, EM exploration is far less important than seismic exploration in oil and gas exploration, and only applied in the early stage of oil and gas exploration in basin survey. In unconventional reservoirs, the difference of seismic wave impedance between oil, gas and water is small, which makes seismic exploration difficult (Yuan, 2013). However, the difference of resistivity and dielectric constant between oil, gas and water is very large, and electromagnetic method has superior conditions for fluid identification and sweet spot detection (Yan, 2014). The high-power EM method can capture the high-resolution anomaly field distribution caused by resistivity and polarizability differences. When combined with seismic exploration methods, the distribution of 'Sweet Spots Area (Segment)', residual oil distribution, spatial distribution of steam or water injected can be elaborately described, and the reservoir permeability and oil/gas saturation can be accurately predicted. With the development of unconventional and ultra-deep oil and gas exploration, the cost of seismic exploration is increasing and the exploration is becoming more and more difficult. Electromagnetic exploration methods are facing great opportunities as well as severe challenges.

- Inherent limitations of EM methods

The essential difference between EM and seismic methods lies indifferent field properties. Seismic wave field belongs to the wave field, while electromagnetic field belongs to the diffusion field. Low-frequency EM methods are generally used for oil and gas exploration, which can be easily affected by volume effect, static offset, field source effect, overprint effect, shadow effect, etc. Fortunately, the development of high-precision 3D EM modeling technique has provided an effective tool to mitigate these adverse effects. For instance, the joint inversion of multiple field sources can effectively suppress the field source effect (He, 2019). Fictitious wave transformation for transient electromagnetic field improves the interpretation reliability and resolution (Chen, 1999; Li, 2005; Mittet, 2015, 2018; Stoffa et al. 2018). Full domain, full coverage, full waveform field, and uniform illumination three-dimensional EM data acquisition and processing, special wave field transformation and inversion imaging techniques are the keys to overcome the limitations of the EM exploration methods.

- EM response mechanism of reservoir rocks

EM response mechanism is closely related to the reservoir physical properties. The simplified resistivity model based EM methods is now facing great challenges to solve complicate geological problems, and the induced polarization (IP) mechanism of reservoir rocks should be valued (Kavian, 2012; Fiandaca, 2012). The time and frequency dispersion characteristics caused by the fluids and minerals in reservoir should be comprehensively considered and studied (Burtman, 2014, 2015). Meanwhile, the physical and structural characteristics of the conventional and unconventional oil and gas reservoirs should be distinguished, and an equivalent complex resistivity model comprehensively considering EM induction, IP and other effects should be established (Zhdanov, 2008). Moreover, the foundation of controllable source electromagnetic (CSEM) technology should be established based on the IP mechanism of reservoir rocks. Only by fully utilizing the sensitivity

of the IP parameters in complex resistivity model can the purpose of precise multi-parameter joint detection of oil and gas be realized. Therefore, it is essential to study the IP mechanism and anomaly extraction method of unconventional oil and gas reservoirs to improve the detection accuracy and the interpretation reliability. It is an inevitable trend in the development of EM exploration to seek IP multi-parameters based CSEM method.

- EM data acquisition

The effectiveness of exploration highly relies on the space-time density and the quality of EM data, and data acquisition technique is the prerequisite and the guarantee for the development of EM exploration methods. Acquisition technology requires a deep combination of methods, instruments, acquisition software, field geology and terrain conditions, geological targets and other factors, through feasibility analysis and simulation test, to develop an effective acquisition scheme. Firstly, In the acquisition method, it is necessary to achieve a substantial breakthrough in 3D acquisition, realize multi-field source coverage and uniform illumination, and synchronize acquisition with hundreds of thousands of instruments to record massive electromagnetic multi-component time series data, so as to meet the requirements of high spatial and temporal density data for high precision inversion. Secondly, high-quality acquisition software capable to conduct noise level analysis, feasibility analysis and data quality evaluation should be developed to improve the exploration efficiency. Finally, portable, intelligent, low-cost, low-power and low-noise EM multichannel receivers should also be manufactured to simplify the acquisition process.

- EM data processing

Data processing is significant part of the successful application of EM methods. Without a proper data processing technique, no matter how sensitive the instrument, how advanced the data collection techniques, and how high the quality of data, the results obtained will be worthless. Data processing mainly include data preprocessing, attribute parameter definition and extraction. Denoising and correcting is the first step in the data processing. Due to the cultural noise and the signal distortion caused by the method or the geological and topographical factors, targeted de-noising and correction methods are required. Many modern signal processing methods have been adapted to data de-noising, such as the robust estimation, median filtering, wavelet transform, recursive flood wave, and coherent analysis methods (Kass & Li 2011; Streich, 2011; Ji et al. 2016; Rasmussen et al. 2017; Wu, 2021). In contrast, the correction methods, such as the field source correction and static shift correction, are developed based on the characteristics of the methods. Because of the complexity of EM methods and noise, there is no universal correction and denoising techniques. Attribute parameter extraction is guaranteed to improve the reliability and effect of the inversion and interpretation. Conventional method is to define the apparent resistivity parameter. However, the complicated multidimensional source creates great difficulties in defining the apparent resistivity. Thus, using different field components or combinations of methods to define the attribute parameters by numerical calculations, such as the all-time apparent resistivity and all-time vertical conductivity, oil-water identification factor, differentially normalized quantities, has attracted research interest, and several good application results have been achieved (Yan, 1999; Davydycheva et al., 2006; He, 2015; Xue, 2020; He, 2021).

- EM inversion and interpretation methods

Theoretically, all geophysical inversions are underdetermined problems. It is difficult to infer the information about the abnormal underground targets accurately from a single type of geophysical data. Comprehensive inversion and interpretation by multiple geophysical datasets are becoming a significant research trend. Joint inversion using as many types of prior information as possible is an effective means of reducing the multiplicity of inversion, improving the data utilization, and modifying the inconsistency of the inversion model. Seismic information is relatively abundant in oil and gas exploration, and the method of joint inversion of EM and seismic data has attracted research attention and achieved better specific results (Peng and Liu, 2020, He, 2020). In unconventional oil and gas exploration, EM signals are sensitive to the sweet spot, and the electrical properties are consistent with the characteristic parameters, such as the porosity, brittleness, permeability, and TOC. With the constraints provided by the reservoir information obtained from the seismic data, the inversion resolution and interpretation reliability can be improved using EM data to predict the reservoir parameters. Furthermore, this method can reduce the risk of exploration and development.

There are two types of joint inversion: one type is based on petrophysical relationships and the other is based on structural similarity relationships (Peng and Liu, 2020). In oil and gas exploration and development, petrophysical and geological information can be acquired as the prior information. Integrating the prior information, such as petrophysical and geological data, into the inversion can reduce the non-uniqueness of the optimization problems and help obtain proper inversion results (Giraud et al., 2017; Astic and Oldenburg, 2019). Joint inversion based on the empirical relationships among the various geophysical parameters has undergone vigorous development (Jegen et al., 2009; Heincke et al., 2010; Lelievre et al., 2012), and the petrophysical empirical or statistical formula can be applied in industry. Via the intersection

analysis of the P-wave velocity and resistivity, Jegen et al. (2009) obtained the sectional empirical relationship between the P-wave velocity and resistivity. They confirmed that the empirical relationship can be locally effective under a specific geological background. Xu et al. (2016) and Peng et al. (2018) created marine EM and seismic data joint inversion frameworks based on the relationship between the reservoir and petrophysics and using the Archie formula and Gassmann formula, respectively. They both achieved global optimization one-dimensional joint inversion and extracted the reservoir porosity and saturation information. Hu et al. (2020) utilized the prior information obtained from the logging and seismic profile to perform constraint modeling, and they realized the artificial fish swarm joint inversion using the magnetotelluric (MT) and gravity data. Yang et al. (2021) proposed the petrophysical relationship between the velocity and resistivity based on the cross-variation function, and then, they adopted the guided fuzzy c-means clustering algorithm to carry out the multi-constraint inversion and completed the two-dimensional MT and seismic data joint inversion. However, there is still no standard petrophysical model that can link all of the physical parameters. Therefore, it is difficult to the directly integrate the petrophysical or other geological features into a standard geophysical inversion (Astic and Oldenburg, 2019).

Compared with the constrained inversion based on the empirical petrophysical relationship, the joint inversion built via structural coupling requires less prior information. Haber and Oldenburg (1997) first proposed the concept of structural coupling constraint inversion, and Gallando and Meju (2003 and 2004) subsequently proposed the cross-gradient inversion method. Multiple parameters joint inversion based on spatial structure similarity has gradually become the mainstream algorithm. Hu et al. (2009) applied the cross-gradient algorithm technique to joint inversion of two-dimensional seismic and EM data with multiplicative regularization and showed that the reservoir evaluation based on the joint inversion was better than that obtained through imaging interpretation of the individual seismic data. Zhdanov (2012) proposed a universal spatial structure constraint algorithm named Gramian spatial constraint method. It has many choices of operators for Gramian space; and when the operator is transformed into a gradient type, the cross-gradient method is obtained. Lelievre and Farquharson (2013) obtained a linear variation expression of the local model parameters and a solution for the change rate in all directions using the construction method, constructed Gramian spatial constraint operator using the obtained gradient of the model parameters, and finally achieved joint inversion of multiple datasets. Gao et al. (2017) proposed a cross-gradient joint inversion strategy using alternately updating model parameters, which reduced the complexity of algorithm. Yan et al. (2020) derived the three-dimensional (3D) discrete form of the cross-gradient operator and realized 3D joint inversion of gravity, magnetic, and MT data. Currently, the joint inversion of seismic and EM data is based on the petrophysical information constraints. Research on the structural coupling algorithm has primarily focused on joint inversion of gravity, magnetic, and EM data, and structural coupling joint inversion using seismic and EM data is the future goal in unconventional oil and gas EM exploration.

1.4 Level and ability of the EM exploration method

The EM method is an effective means of resource and energy exploration. The physical property foundation is the differences of the resistivity, dielectric constant, and polarization in rocks. The detection of underground geological targets can be realized by observing the spatial-temporal distribution of the EM fields. Although EM method has a good electrical basis in unconventional oil and gas exploration, the sweet spots of unconventional oil and gas reservoirs feature large burial depth, small target and strong heterogeneity, which require higher resolution, exploration depth and level of data processing and interpretation of electromagnetic exploration method. In the last 20 years of development, the methods of petroleum EM exploration have been comprehensively improved. In terms of the instruments, geophysical instrument companies such as Phoenix, Zong, KMS, Metronix, and Geonics have developed various types of high-power and strong current transmitting systems and multi-functional networked portable receivers. The wide frequency electromagnetic instrument developed by China's Jishan High-tech company, the high-power time-frequency electromagnetic system developed by BGP, CNPC, and the ultra-high power and ultra-low frequency transmitting and receiver developed by the Institute of Geophysics, Chinese Academy of Sciences, have also been put into oil and gas exploration. The Mag-power transmitter through a few kilometers to dozens of kilometers long ground wire to feed hundreds of amperes of current underground, can be convenient to emit a variety of waveform, for the time domain and frequency domain electromagnetic method to provide a powerful source of electromagnetic field. Low power consumption, broadband, low noise level, large dynamic range, portable, light weight, multi-function, distributed receivers can realize the data acquisition to thousands of channels array, which provided a hardware guarantee for 3D EM data acquisition and hydraulic fracturing monitoring under complex geology and terrain conditions. Lots of new control

source EM methods were emerging to improve the resolution, detection depth, and interpretation reliability, such as the Wide Frequency EM method (WFEM), Wire-less EM method (WEM), Time-frequency EM method (TFEM), Long offset, long window Transient EM method (LowTEM), and Focused Source EM method (FSEM). These methods have greatly improved the anti-noise ability, detection depth, resolution, reliability, work efficiency, cost, and adaptability. The use of new data processing, 3D inversion and interpretation techniques had significantly enhanced the ability of electromagnetic methods to serve unconventional oil and gas exploration. At the same time, the study of unconventional reservoir rocks physics of has been deepening, and the induced polarization mechanism of unconventional reservoirs has made new progress. The model that accurately describes the IP mechanism of unconventional reservoirs has been preliminarily established, and the parameter prediction method of unconventional reservoirs based on this model has also been basically formed (Tong, 2020; Burtman, 2015).

Lots of reviewers have summarized the EM methods and technologies in oil and gas exploration and development (He, 2010,2019; Strack, 2013,2014;Tietze 2014; Streich 2015; Di 2019, 2020; Xue 2016, 2020; Constable, 2010; Liu 2021). This paper focuses on the study of electrical characteristics of unconventional reservoir, the sweet spot detection and its characteristic parameters prediction methods based on the IP model, as well as the research progresses in regarding the new methods and technologies in EM exploration. In addition, several cases studies of shale gas the sweet spot detection and hydraulic fracturing monitoring with LowTEM were presented. The summary of the cases studies will benefit the wide application of new EM methods and technologies in unconventional oil and gas exploration and development.

2. Sweet spot detection and its character parameters prediction

The detection and evaluation technology of shale gas sweet spot is the key to shale gas exploration and development. Seismic exploration method undoubtedly plays an important role in sweet spot detection and development because of their high resolution and attribute identification capability. However, most of the shale gas exploration areas in southern China are rugged areas, and covered by limestone, seismic exploration is much more expensive and difficult to obtain high-quality data. In addition, the sweet spots are distributed in argillaceous source rocks with deep burial depth, high degree of evolution and rich organic matter. The seismic impedance characteristics are not obvious and there are no clear trap characteristics. The shale reservoir itself is a source rock with extremely low porosity and permeability, and strong heterogeneity. As a result, the seismic characteristics of the sweet spot are not obvious, which makes prediction difficult. Therefore, the development of high-precision seismic prediction methods for shale gas reservoirs faces great challenges, and the development of cost-effective non-seismic methods is an effective way to detect sweet spot in unconventional reservoirs.

As the most effective supplementary means of seismic exploration, the electromagnetic (EM) exploration method has the advantages of large exploration depth, high work efficiency, low cost and strong adaptability, and has been playing an important role in the early stage of basin oil and gas exploration. The EM exploration of oil and gas based on EM diffusion can only be effective when the resistivity of the oil and gas reservoir is high enough compared with the surrounding rocks. The importance of IP effect in rocks has been realized, and two IP parameters (resistivity and chargeability) have been tried to jointly detect oil and gas reservoirs (Davydycheva, 2006; He, 2010; Commer, 2011). Complex resistivity (CR) method, which is based on the IP theory, has been tried to identify conventional oil and gas in China for more than 30 years (Wu, 1996; Xu,2004; Su et al., 2005), and two kinds of IP anomaly models were put forward to interpret the CR date. One considered that the reservoir itself was a dynamic multiphase balance system, in which the double electric layer formed from bi-phase medium, and was the source in which the IP field came from (He, 2007). Another was called ‘the micro-seepage model’ which considered IP effect happened above the reservoir because the hydrocarbons migrated to the upper reducing zone, and resulted in the formation of the rich pyrite halo which was the source of strong IP effect (Veeken, 2009).

Shale gas is stored in the reservoir in free or adsorbed state, and has the typical characteristics of self-generation and self-storage and in-situ accumulation, which inevitably determines the difference in the IP anomaly model of data interpretation in shale gas exploration. Are the above two models suitable for shale gas exploration? What are the geoelectric characteristics of organic-rich shale? Does the shale gas reservoir have a strong IP effect? Can the resistivity and chargeability be integrated to identify the sweet spot? What is the sweet spot detecting pattern for EM exploration? Yan et al., (2014), Xiang (2014) collected hundreds of shale samples in southern China, performed compositional analysis, complex resistivity and Total Organic Carbon (TOC) measurements, and found a qualitative relationship between pyrite content and TOC. On this basis, combined with the IP theory study, the methods to predict the sweet spot’s characteristic parameters

and the detection pattern suitable for EM method were proposed.

2.1 Electrical characteristics of shale in southern China

Xiang et al. (2014) collected 243 geological outcrop samples in Yibin, Sichuan and Zunyi, Guizhou in southern China. The lithologies are mainly organic-rich shale, sandstone, dolomite and basalt (surrounding rock formations). Through the complex resistivity measurement and analysis, the IP parameters of the samples were obtained, and the physical properties of each formation were shown in Figure 1 and Table 1. Compared with the surrounding sandstone, dolomite and basalt, the average resistivity of the organic-rich shale is about 120 Ω·m, and the average polarizability is about 20% in Wufeng Group-Longmaxi Group; the average resistivity of the organic-rich shale is about 147 Ω·m, and the average polarizability is about 42% in the Qiongzhusi Group. These indicated that the organic-rich shale exhibited the characteristics of low resistivity and high chargeability, which was inconsistent with the low chargeability characteristics of conventional shale reservoirs.

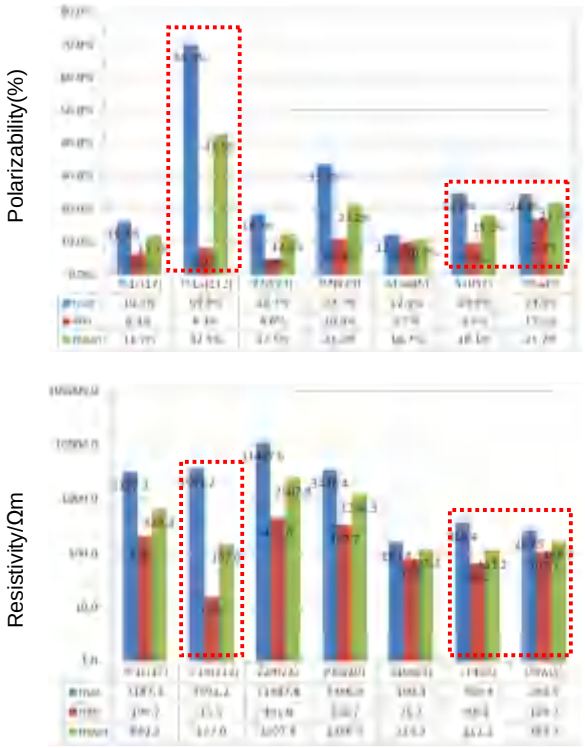

Figure 1. Polarizability and resistivity results of CR measurement for geological outcrop rocks at different groups (top: chargeability; bottom: resistivity)

2.2 Prediction of the sweet spot characteristic parameters

- TOC predicting

Organic-rich shale is abundant in Zhaotong, Yunnan, with shallow burial depth and large thickness. China National Petroleum Corporation (CNPC) has made breakthroughs in shale gas exploration in this area. The Well Z104 has successfully produced industrial gas, with a daily gas production of 20,000 cubic meters. The logging curves of Well Z104 (Figure 2) showed that the shale gas reservoir had obvious characteristics of low resistivity, low velocity and high gamma value. The mineral composition analysis of 34 cores from the groups of S_1l-O_3w and $Є_1$n in Well Z104 showed that the average content of quartz and feldspar was 30% to 60%, the average content of carbonate minerals is generally less than 30% (except mud shale), the average content of clay minerals is 10% to 35%, the content of pyrite is generally high, with a maximum value of 20% and an average content of 5% (Figure 3).

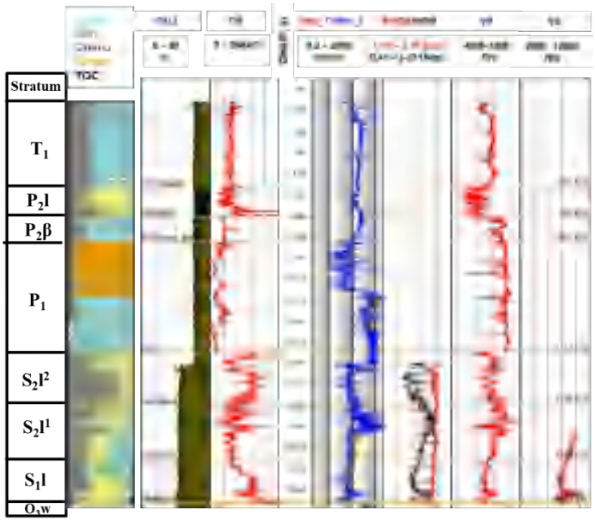

Figure 2. Z104 Geology Histogram and Logging Curves

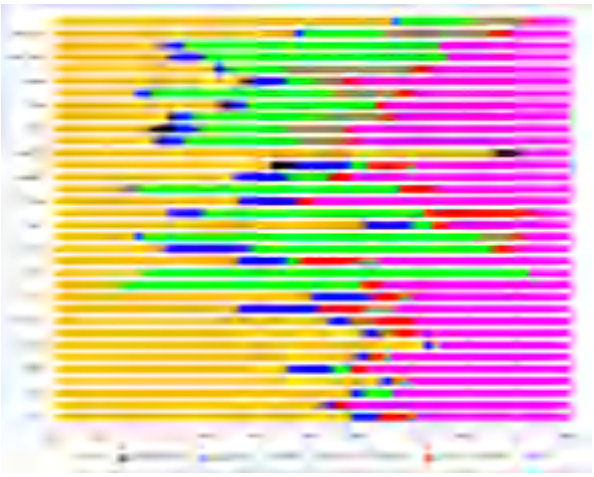

Figure 3. The mineral composition in the shales from S_1 l-O_3w and $Є_1$n (red: pyrite)

The complex resistivity measurement and TOC analysis were performed on 11 cores from Well Z104. Figure 4 indicated that the chargeability was

consistent with the variation of pyrite content, with a high positive correlation. Figure 5 presented a plot of TOC and pyrite content versus chargeability. The results showed that there was also a good correspondence between pyrite content and TOC. Apparently, pyrite is an indicator mineral for IP, and is it also an indicator mineral for TOC? If the relationship between TOC and chargeability could be established, it will have great significance for EM exploration.

Why is pyrite abundant in organic-rich shales? Is it necessarily related to TOC? A significant phenomenon is that pyrite is not only a characteristic mineral formed in organic-rich deposits, but also a marker of sedimentary environment and a characteristic mineral of strong IP effect. Veeken (2009) explained its formation process and controlling factors. The depositional environment of shale was a deep-water anoxic environment (reduction reaction environment), coupled with its self-generation and self-storage reservoir characteristics, the increase in TOC acted as a catalyst, providing a chemical reaction environment for the formation of secondary pyrite in the shale clay, the chemical process was as follows

$$CH_4 + Ca^{2+} + SO_4^{2-} \rightarrow CaCO_3 + H_2S\uparrow + H_2O$$

$$H_2S + Fe^{2+} + 2OH^- \rightarrow FeS_2 + H_2O$$

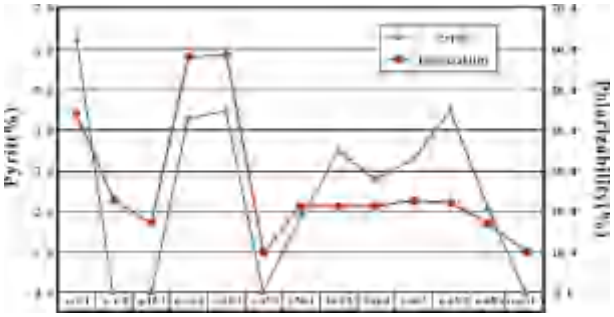

Figure 4. Relationship between pyrite and polarizability

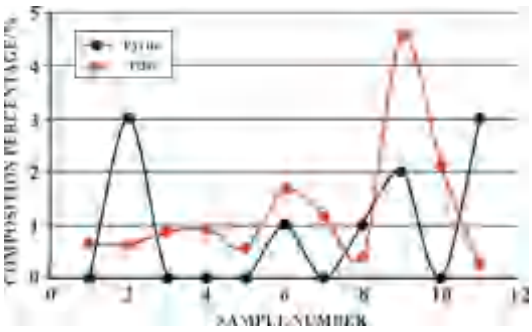

Figure 5. Relationship between TOC and pyrite

In addition, biodegradation and bacterial activity might give rise to organic origin of pyrite in the sedimentary pile. It was proved empirically that significant enrichment in pyrite was often related to hydrocarbon occurrences at deeper levels.

Based on the resistivity, polarizability and TOC of organic-rich shale, Xiang (2016) and Xu (2020) gave an empirical relationship model between polarizability and TOC, as shown in Figure 6.

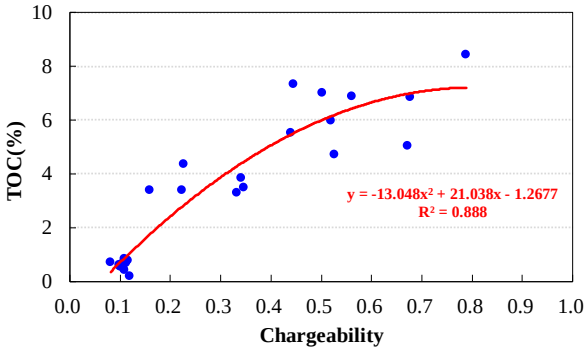

Figure 6. The Cross-plot of TOC and Polarizability

- Prediction of brittleness index

The mineral composition of shale reflected the depositional environment and depositional conditions of shale, and also determines the brittleness index of shale, which affects the fracturing and development of shale gas. It is of great significance to study the relationship between brittleness index and electrical parameters from the perspective of shale mineral composition. Quartz content is the main reason for the shale's brittleness, but the roles of other important brittle minerals cannot be ignored. There were many definitions of brittleness index. Xu et al. (2020) defined the brittleness index B as follows:

$$B = \frac{quartz + feldspar + Pyrite}{quartz + feldspar + Pyrite + carbonate + clay} \quad (1)$$

The above formula highlighted the relationship between pyrite content, brittleness index and electrical parameters (resistivity and polarizability). The brittleness of Well Z104 shale was statistically analyzed by formula (1), and the relationship between the brittleness index and the polarizability was established, as shown in Figure 7. It can be seen that the quadratic nonlinear relationship was obvious

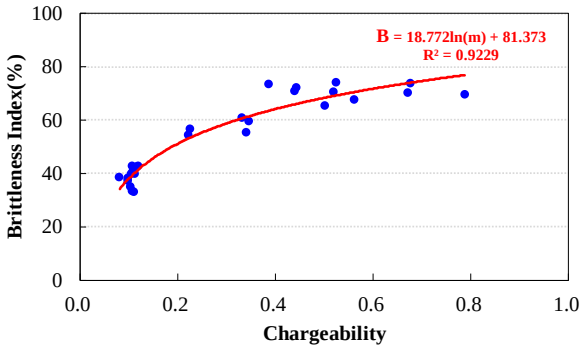

Figure 7. The cross-plot of brittleness index and polarizability

- Prediction of the permeability

Unconventional reservoirs usually have low porosity

and low permeability characteristics (porosity less than 10%, pore throat diameter less than 1 μm or permeability less than 1 mD). In order to achieve sustainable and effective oil and gas production, it is necessary to combine horizontal well drilling, formation fracturing and other technologies to increase reservoir permeability or reduce fluid viscosity (Zou et al., 2013).

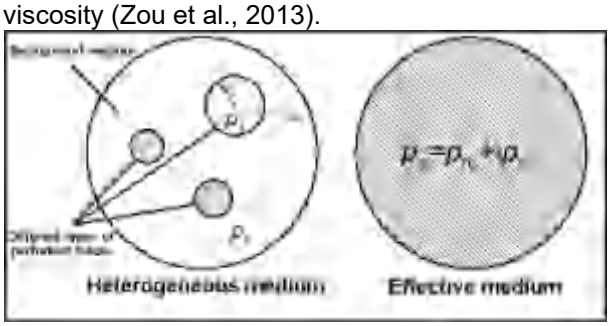

Figure 8. The schematic diagram of the effective-medium theory. A heterogeneous media contains many different types of perturbed media, each of which contains resistivity ρ_l , effective radius r_l , and surface-polarizability coefficient α_s^l . The resistivity of heterogeneous medium is equivalent to the CR of an effective medium through the effective-medium approach. (Tong et al., 2020)

Combining theoretical and experimental analysis of the electromagnetic characteristics of the 'sweet spot' region, establishing the theoretical relationship model between electromagnetic response and reservoir physical properties is the key to realize the EM detection and quantitative evaluation of sweet spot. Reservoir physical properties such as porosity, saturation, and permeability are sensitive parameters for reservoir IP characteristics (Slater, 2007). Archie (1942) gave the empirical relationship between pure sandstone conductivity and formation water conductivity, connected porosity and formation water saturation. However, the rock mineral composition and pore structure of unconventional reservoirs with low porosity and low permeability was complex, and the Archie's relationship was no longer applicable. The polarization effects (electric double layer polarization, Maxwell-Wagner dielectric polarization, etc.) existing at the interface of different minerals and pore fluids will cause the IP phenomenon of reservoir in the electromagnetic exploration frequency range. Pelton et al., (1978) first used the Cole-Cole model to characterize rock IP phenomena, and it was widely used in EM exploration. Zhdanov (2008) proposed the generalized effective-medium theory of induced polarization (GEMTIP) model based on strict mathematical and physical equations. GEMTIP is suitable for IP problems in anisotropic and multiphase media, and established a quantitative relationship between model parameters and rock physical properties, which is more conducive to reservoir prediction. Tong et al., (2020) extended the theoretical relationship between macroscopic IP parameters and microstructure in the GEMTIP, and established MGEMTIP model under the assumption of isotropic spherical perturbation (Figure 8).

MGEMTIP：

$$\rho_e = \frac{\rho_0}{M_0}\left\{1+\sum_{l=1}^{N}\eta_l\left[1-\frac{1}{i\omega\tau_l+1}\right]\right\}^{-1} \tag{2}$$

where $M_0 = 1-\sum_{l=1}^{N} 3f_l/2$, $\eta_l = 9\rho_0 f_l/\left[M_0(4\rho_l+2\rho_0)\right]$, $\tau_l = r_l/\left[2\alpha_s^l(2\rho_l+\rho_0)\right]$. ρ_0 is the DC resistivity of the background medium, $f_l, \rho_l, r_l, \alpha_s^l$ respectively correspond to the volume component of the l type perturbed medium, DC resistivity, equivalent spherical radius and surface polarization parameters N is the total amount of perturbed medium, the equivalent medium polarizability is $\eta_t = \sum_{l=1}^{N}\eta_l$. The relationship between η_t and the polarizability m of the Cole-Cole model is $m = \eta_t/(1+\eta_t)$. MGEMTIP is consistent with the polarization characteristics of discrete metallic minerals (Wong, 1979), and also explains the high polarization phenomenon in which the Mawell-Wagner polarization shifts to low frequencies under high oil saturation condition (Burtman and Zhdanov, 2015).

The electrical Kozeny-Carman (K-C) equation characterized the rock porosity and tortuosity through the formation factor F , and characterized the capillary radius r through the specific surface area S_{por} . The permeability relationship can be expressed as

$$k = \frac{Q}{F^b S_{por}^c} \tag{3}$$

Where Q, b, c are the fitting parameters (Slater, 2007).Since the seepage in unconventional reservoirs was dominated by the diffusion of non-Darcy flow, the validity of the electrical K-C equation was greatly reduced in low permeability rocks. Many studies proposed to use complex resistivity to estimate, thereby improving the prediction accuracy of permeability (Börner et al. 1996; de Lima and Niwas 2000; Slater and Lesmes 2002). Figure 9 showed the permeability prediction relationship based on normalized polarizability (Weller et al., 2015), but there was a large error in the prediction results of low permeability rocks. Figure 10 showed that S_{por} correlated with the imaginary conductivity σ''(which mainly controls the polarizability strength), but the quantitative relationship needed to be further determined in combination with clay minerals (Revil et al., 2013). Conductive minerals

such as clay and metals in unconventional reservoirs usually do not participate in the seepage process, but directly affect the rock IP phenomenon.

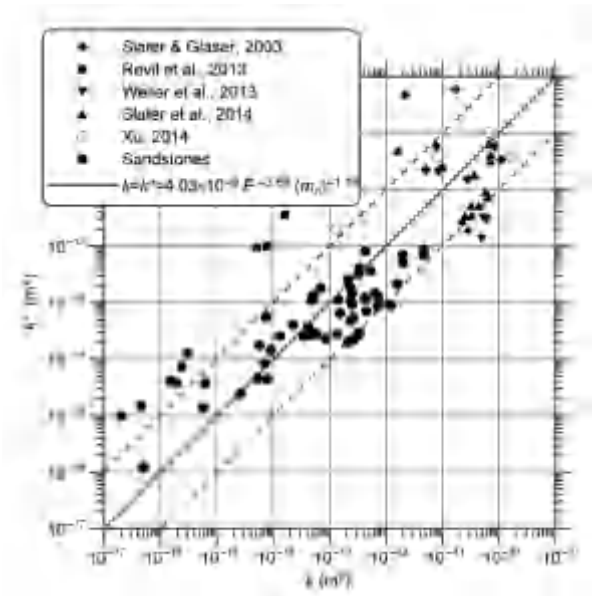

Figure 9. Permeability relationship between experimental measurement and electrical K-C model estimation based on normalized polarizability m_n ($m_n = m\sigma_0$)(Weller et al., 2015)

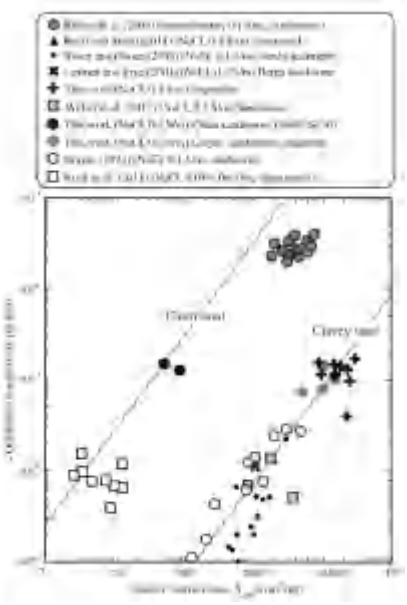

Figure 10. Experimental relationship between the imaginary conductivity and specific surface area between sandstone and clayey sandstone (Revil et al., 2013)

Whether conductive minerals actually produce conductance or polarization can be effectively analyzed by combining the mineral size, connectivity, and frequency band (Vinegar and Waxman, 1984; Xiang et al., 2014; Revil et al., 2015). Numerical simulations showed that there was a nonlinear effect between the permeability of

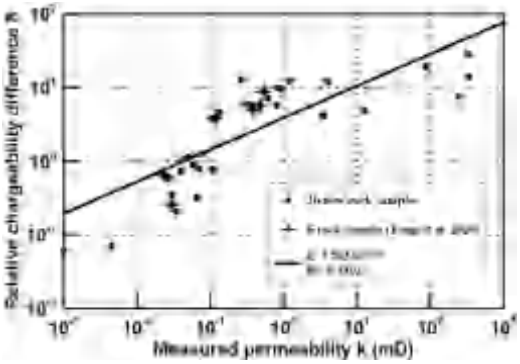

Figure 11. Relationship between relative polarizability difference and permeability of tight rock

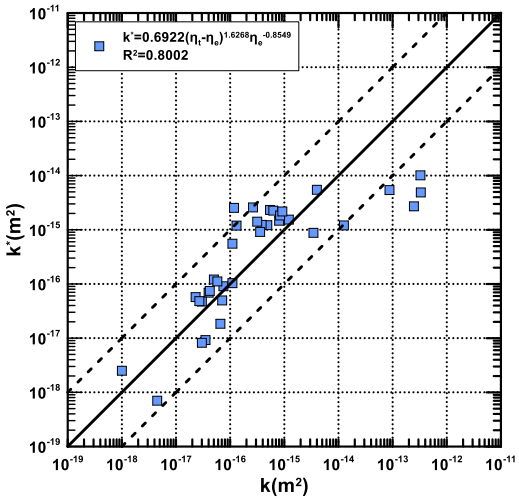

Figure 12. Permeability relationship between experimental measurement and MGEMTIP estimation based on polarizability difference

fractured tight reservoirs (limestone) and the conductivity of formation water (Kirkby et al., 2016). The electrical characteristics of these unconventional reservoirs seriously affect the permeability prediction based on the electrical K-C model. The existence of clay and minerals in unconventional reservoirs makes it difficult to distinguish the IP mechanism of unconventional reservoirs. Removing or suppressing polarization independent of pore fluid can effectively improve the prediction accuracy of permeability. There is a difference between the theoretical polarizability of the MGEMTIP (no seepage) and the measured polarizability of tight rocks (weak seepage). This difference has a good correlation with the rock permeability (Figure 11). The permeability prediction formula based on MGEMTIP was proposed

$$k^* = \frac{Q(\eta_t - \eta_e)^b}{\eta_e^c} = \frac{Q\Delta\eta^b}{\eta_e^c} \quad (4)$$

Where η_t and η_e correspond to the theoretical polarizability and measured polarizability of the rock, and Q, b, c are the rock characteristic indices. With

this model a good permeability prediction for low-porosity and low-permeability rocks containing low-resistivity minerals was achieved (Figure12).

2.3 Geo-electrical mode for sweet spot detection

Based on the complex resistivity test and analysis of unconventional reservoir rocks, there were three understandings: first, the excitation polarization of sweet spot was mainly generated by electron-conducting minerals such as pyrite, and its IP mechanism is the electron polarization mechanism. Second, the sweet spot region is characterized by high polarization and low resistivity. Third, the sweet spot area, its IP anomaly and resistivity anomaly overlap in space. Based on these three understandings, the geo-electrical mode of electromagnetic exploration for sweet spot was put forth(Yan, 2014；Figure 13). This mode provided a theoretical basis for the EM detection and comprehensive interpretation of sweet spot.

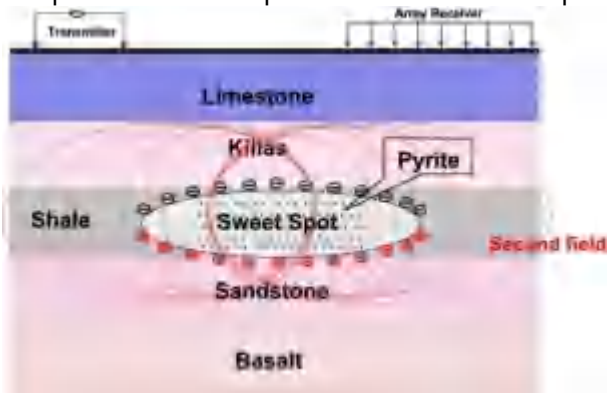

Figure 13. Sketch map of geo-electrical mode for sweet spot detection

3. The innovations in CSEM on land

In recent years, based on the development of methods and instruments, especially that of the CSAMT (Goldsten, 1975), CR (Zonge, 1975), LOTEM (Strack, 1989), and MTEM(Hobbs, 2006), a variety of new CSEM methods with a significant improvement in the adaptability, anti-interference ability, exploration depth, inversion effect, and resolution ability have been developed. These methods, including the TFEM, WEM, and FCEM, LowTEM are currently being applied in unconventional oil and gas exploration and development, and they possess the following innovations.

3.1 Definitions of EM property parameter

- Models and field components of the EM property parameter definitions

Because the horizontal electrical dipole has better attenuation characteristics in terms of offset and frequency than the magnetic dipole, the grounded line CSEM method has been generally applied in oil and gas and deep structure exploration. The horizontal electric field, the vertical magnetic field/the induced electromotive force (EMF) are the typical observed components. In terms of interpretation parameter definition, in addition to the uniformly conductive and non-polarized half-space model, the uniformly conductive and polarized half-space model and the earth-ionosphere model have also been developed, as shown in figure 14.

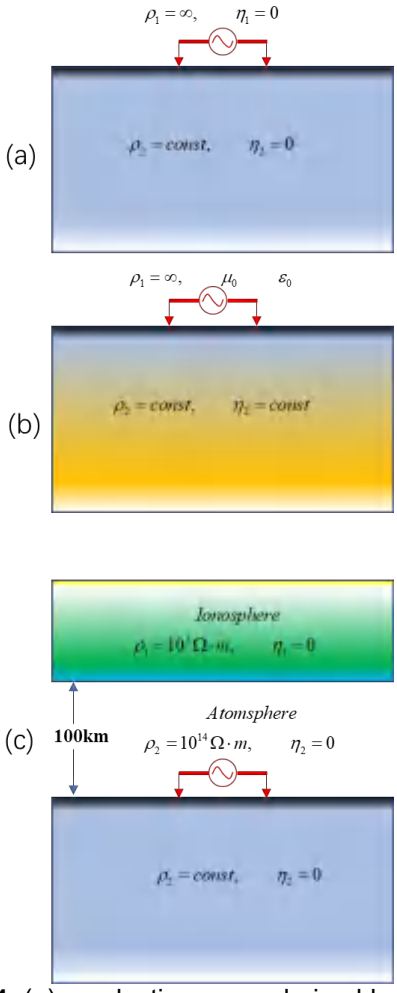

Figure 14. (a) conductive non-polarized half-space model; (b) conductive polarized half-space model and (c) the earth-ionosphere model

For the uniformly conductive and non-polarized half-space model, the time-domain electric and magnetic fields of the electric dipole were expressed as follows(Piao, 1990):

$$E_x=\frac{Idl\rho}{2\pi r^3}[\Phi(u)-\sqrt{\frac{2}{\pi}}ue^{-u^2/2}] \tag{5}$$

$$\frac{\partial H_z}{\partial t}=\frac{Idl\sin\theta}{\pi\mu_0 r^4}[\Phi(u)-\sqrt{\frac{2}{\pi}}u(1+\frac{u^2}{3})e^{-u^2/2}] \tag{6}$$

the frequency-domain electric and magnetic fields of the electric dipole were expressed as follows:

$$E_x=\frac{Idl\rho}{2\pi r^3}[3\cos^2\varphi-2+(1+ikr)e^{-kr}] \tag{7}$$

$$H_z = -\frac{3Idl\sin\theta}{2\pi k^2 r^4}[1-e^{ikr}(1+ikr-\frac{1}{3}k^2r^2)] \quad (8)$$

where $k=\sqrt{-i\omega\mu/\rho}$.

For the uniformly conductive and polarized half-space model, the time-domain electric field of the electric dipole can be written as follows (Davydycheva, 2006):

$$\begin{aligned} E_x(t) = \frac{Idl\rho}{2\pi r^3}\Bigg\{ & \left[\operatorname{erf}(u) - \frac{2u}{\sqrt{\pi}}e^{-u^2}\right] \\ & + \eta e^{n^2/u^2}\left[1-\operatorname{erf}(\frac{n}{u})\right] \\ & + \eta\left[\operatorname{erf}(u) - \frac{2nu}{\sqrt{\pi}}\right]e^{-u^2} \\ & + \eta e^{n^2/u^2}e^{2n}\left[1-\operatorname{erf}(\frac{n}{u}+u)\right] \\ & \times(1-2n+2n^2)\Bigg\} \end{aligned} \quad (9)$$

Where $u=\sqrt{\frac{\mu_0}{2\rho t}}r$, r is the offset, t is the observation time, ρ is the resistivity of the homogeneous half space, $n=0.5r\sqrt{\sigma\mu/\tau}$.

For the earth-ionosphere model, the expressions of the EM components of the ground source were as follows (Li, 2015):

$$\begin{aligned} E_x &= i\omega\mu\frac{Idl}{4\pi}\int_0^\infty F\cdot \mathrm{J}_0(\lambda r)\mathrm{d}\lambda \\ &+ \frac{i\omega\mu}{k_1^2}\frac{Idl}{4\pi}\cos^2\theta\int_0^\infty (FF-\frac{k_1^2}{\lambda^2}F)\cdot\lambda^2\cdot \mathrm{J}_0(\lambda r)\mathrm{d}\lambda \\ &+ \frac{i\omega\mu}{k_1^2}\frac{P_E}{4\pi}\frac{1}{r}(1-2\cos^2\theta)\int_0^\infty (FF-\frac{k_1^2}{\lambda^2}F)\cdot\lambda\cdot \mathrm{J}_1(\lambda r)\mathrm{d}\lambda \end{aligned} \quad (10)$$

$$\begin{aligned} H_y &= \frac{Idl}{4\pi}\int_0^\infty -\frac{u_1}{R_1(0)}F\cdot \mathrm{J}_0(\lambda r)\mathrm{d}\lambda \\ &+ \frac{Idl}{4\pi}\frac{1}{r}(1-2\cos^2\theta)\int_0^\infty\left[-\frac{R_1^*(0)}{u_1}FF+\frac{u_1}{R_1(0)}\frac{1}{\lambda^2}F\right]\cdot\lambda\cdot \mathrm{J}_1(\lambda r)\mathrm{d}\lambda \\ &+ \frac{P_E}{4\pi}\cos^2\theta\int_0^\infty(-\frac{R_1^*(0)}{u_1}FF+\frac{u_1}{R_1(0)}\frac{1}{\lambda^2}F)\cdot\lambda^2\cdot \mathrm{J}_0(\lambda r)\mathrm{d}\lambda \end{aligned} \quad (11)$$

where F and FF are related to the electric properties of the ionosphere layer (Li, 2015).

- EM attribute parameters

Owing to the complicated relationships between the components and the resistivity, polarizability in equations (5) - (11), the apparent resistivity and apparent polarizability can't be defined like the DC and MT method did, only by near field or far field approximation can the expression of near or far field apparent resistivity be given. This imposes restriction on the data collection area and creates great difficulties in the EM data processing and interpretation. In order to get effective attribute parameters the definition was mainly carried out from two aspects: the whole area numerical definition and the way of complex resistivity method and direct current method. Thus, new methods and techniques of electromagnetic exploration with different characteristics were produced.

Through further study on the numerical algorithms, it has become possible to define the apparent resistivity of the entire space using equations (5) – (11). Many scholars have proposed effective methods of defining parameters based on numerical algorithms. He (2010) defined the apparent resistivity of the whole region based on Equation (7) and proposed the WFEM, which organically unified the "near zone", "transient zone" and "far zone", improved the data distortion in the transient zone, and enabled electromagnetic sounding to be carried out in a vast region without being limited to the far zone. In addition, this definition was also introduced into the LOTEM, MTEM, and WEM, which has resulted in several breakthroughs regarding the data interpretation level and application effect (Yang,1986, Yan, 1999).

On the other hand, referring to the definition methods of apparent resistivity, apparent polarizability and charging rate in CR and DC to directly define the electromagnetic property parameters. According to the characteristics of the simultaneous data acquisition in TFEM, the EM attribute parameters, including the dual-frequency amplitude, dual-frequency phase, triple-frequency phase, and rate of change, were defined as follow:

$$\Delta A(\omega_i) = \frac{A(\omega_i)-A(\omega_{i3})}{A(\omega_i)} \quad (12)$$

$$\Delta\Phi_2(\omega_i) = \frac{\omega_{i3}\Phi(\omega_{i1})-\omega_i\Phi(\omega_{i3})}{\omega_{i3}-\omega_i} \quad (13)$$

$$\Delta\Phi_3(\omega_i) = \Phi(\omega_i) - \omega\frac{\mathrm{d}\Phi(\omega_i)}{\mathrm{d}\omega} + \frac{2}{3}\omega^2\frac{\mathrm{d}^2\Phi(\omega_i)}{\mathrm{d}\omega^2} \quad (14)$$

$$M_s = \frac{\frac{1}{t_m-t_{m-1}}\int_{t_{m-1}}^{t_m}\varepsilon(t)\mathrm{d}t}{\varepsilon_0} \quad (15)$$

Where ω_{i3} is the 3rd harmonic frequency of the fundamental frequency ω_i; A and Φ represent the amplitude and phase of the fundamental wave, respectively; ε_0 represents the initial potential, t_m and t_{m-1} represent the m^{th} and $(m-1)^{th}$ observation time, respectively; the difference between the t_m and t_{m-1} is the length of the m^{th} observation time window; $\varepsilon(t)$ is the potential decay curve of potential with time t.

The observation mode and the principle of the FSEM were shown in Figure 15. Using equation (5), Davydycheva (2006) defined four EM property parameters using voltages observed at the center of dual sources as follows:

$$\sum_{AB}\frac{\Delta_x U(t)}{\Delta_x U(t_0)},\ \sum_{AB}\frac{\Delta_x^2 U(t)}{\Delta_x U(t)},\ \sum_{AB}\frac{\Delta_t\Delta_x^2 U(t)}{\Delta_x U(t)},\ \sum_{AB}\frac{\Delta_t\Delta_x^2 U(t)}{\Delta_t\Delta_x U(t)} \quad (16)$$

Where

$$\Delta_x U(t) = U_{x2}(t)-U_{x1}(t)$$

$$\Delta_x U^2(t) = (U_{x1}(t)-2U_{x1}(t)+U_{x3}(t))$$

$$\Delta_t\Delta_x U(t) = \Delta_x U(t+\Delta t)-\Delta_x U(t)$$

$$\Delta_t\Delta_x{}^2 U(t) = \Delta_x{}^2 U(t+\Delta t)-\Delta_x{}^2 U(t)$$

It can be seen from Figure 15 that the FSEM has the characteristic of current vertical focusing, which improves the vertical resolution and the detection depth, and effectively suppresses the interference by the inhomogeneous sub-surface targets.

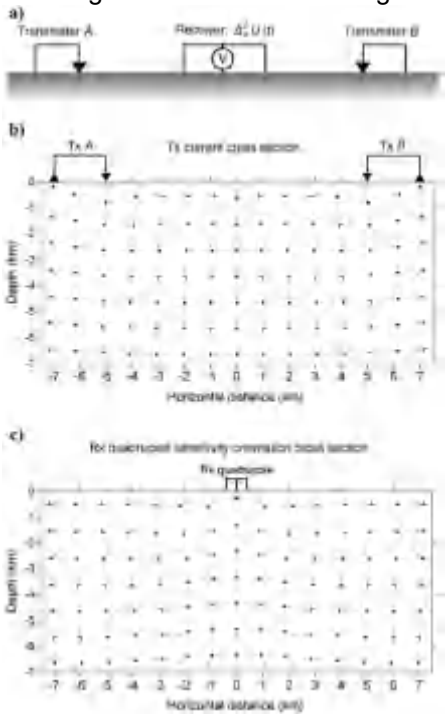

Figure 15. (a) The experimental setup with grounded electrodes (the earth is gray); (b)the dc current pattern for the transmitters, and (c) the receiver. Arrows indicate directions of current flow. The setup provides vertical current focusing. (Davydycheva, 2006)

3.2 Application of the Pseudo-random technique

The auto-correlation of pseudo-random time series (such as M-series) satisfies

$$R_{xx}(\tau) = K\delta(\tau). \quad (17)$$

The cross-correlation between signal and noise satisfies

$$R_{xn}(\tau) = 0 \quad (18)$$

Therefore, the cross-correlation between the earth response and the system input (transmitting signal) is

$$R_{xx}(\tau) = \int_0^{T_s} g(s)\cdot R_{xx}(\tau - s)ds = K\cdot g(\tau) \quad (19)$$

Equation (19) shows that due to the cross-correlation between the wider transmission band M-sequence and the observed EM field components, it is easy to remove the noise and obtain the earth impulse response with a high signal-to-noise ratio. Using the apparent resistivity expression defined by the impulse response of the homogeneous half-space, the apparent resistivity of can be easily calculated (Ou, 2019). In time-domain EM methods, such as the MTEM, WEM, and LowTEM, the pseudo-random technique of M-sequence current waveform was generally adopted, and thus, the data quality was significantly improved. Moreover, this ensured fast data processing and high-resolution inversion and imaging. Figure 16 and Figure 17 showed the impulse response for the homogeneous earth model obtained from the cross-correlation between the observation field and the pseudo-random MT sequence, which was consistent with the theoretical modeling results.

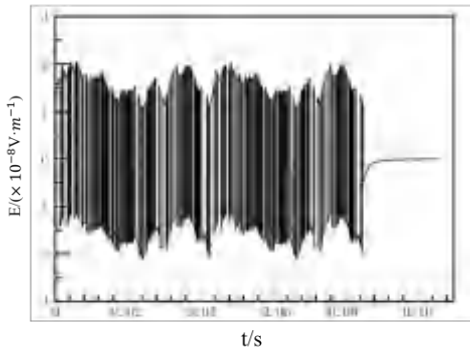

Figure 16. the electric fields inspired by the pseudo-random M-sequence.

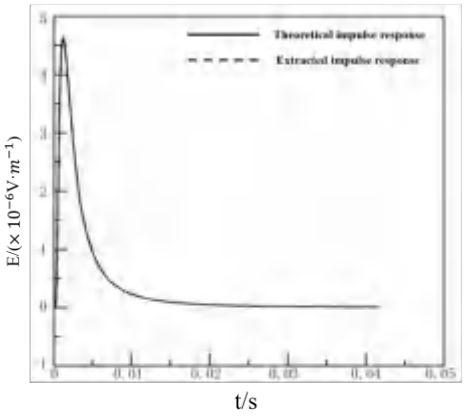

Figure 17. the obtained earth impulse response and the analytical solution.

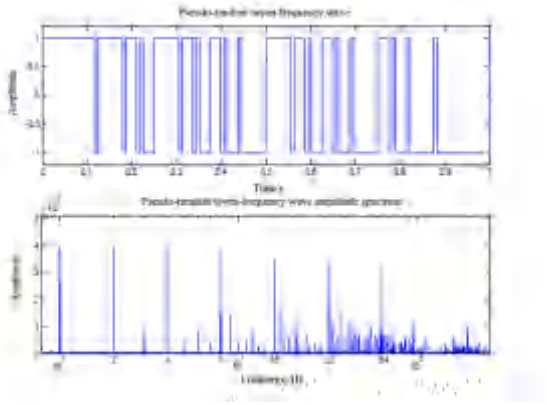

Figure 18. the pseudo-random seven-frequency waveform (A=1, T=1s), the time-domain waveform(top), and the spectrum (bottom, Jiang, 2010)

Another use of pseudo-random is the application of the 2^n sequence. Because the main frequencies of the 2^n sequence waveform are uniformly distributed along the logarithmic coordinate, the amplitudes and initial phases are essentially the same (Jiang, 2010). Using this waveform WFEM improved work efficiency and anti-interference ability, and ensured data quality. For example, the amplitudes and phases of seven frequencies can be obtained at one observation (Figure 18).

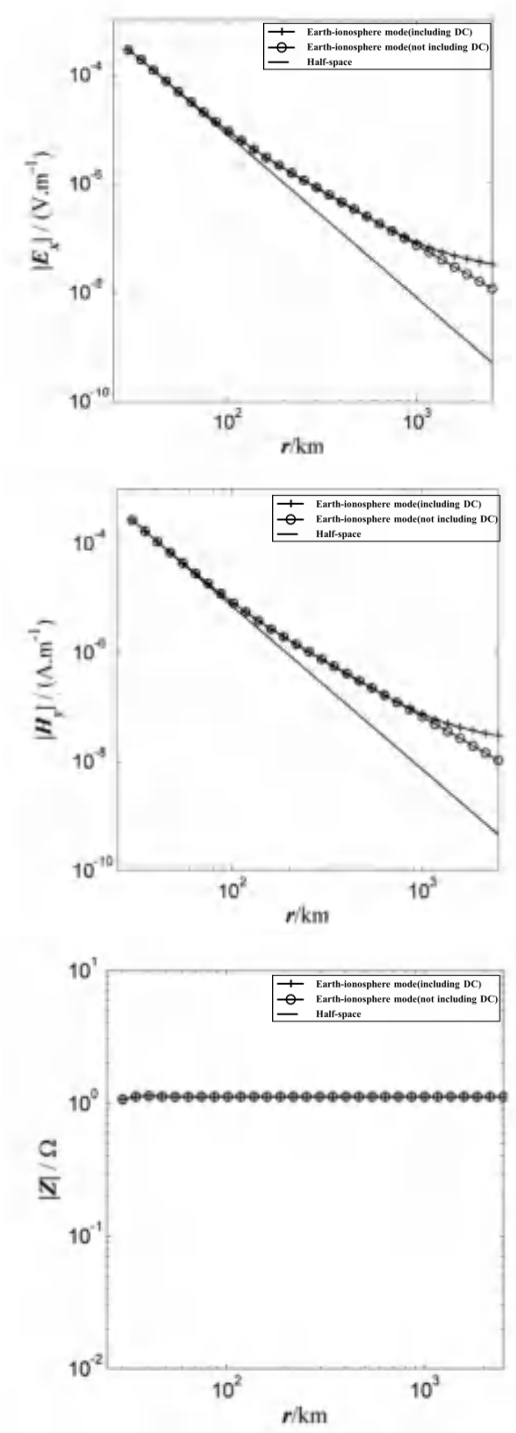

Figure 19. |Ex| (top), |Hy| (middle)and |Z| (bottom) field decay curves for axial array at 32 Hz (Li et al.,2015

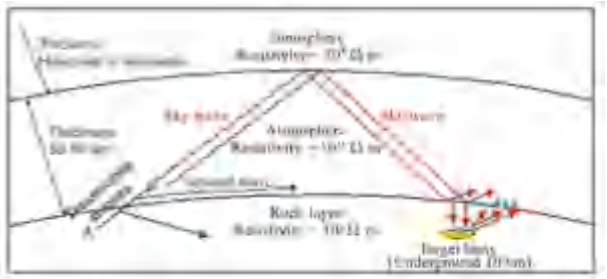

Figure 20. The EM waves propagation of WEM source (Di, 2020).

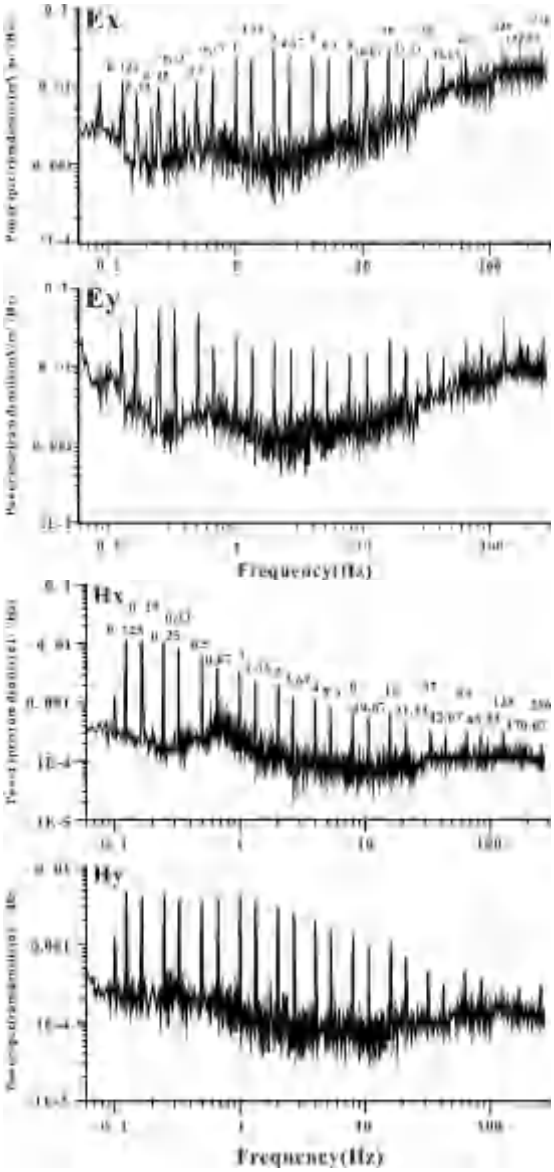

Figure 21. The comparison of power spectral density between WEM and MT fields.

3.3 Utilization of the sky-wave

From the modeling of field components for different lengths of wire source at different frequencies based on equations (6) and (7), Di et al. (2020) found that, when the source length is equal to the

height of the ionosphere, the influence of the sky-wave (wave guide) should be considered. Figure 18 showed that the electric field observed on the ground based on the earth model was significantly larger than that of the homogeneous half-space model when transmitter to receiver distance(r) was more than several hundreds kilometers. Based on this discovery, WEM was proposed by Di et al. (2008) Figure 20 is the principle map of WEM. Since the beginning of this century, China has carried out the research and construction of 'Extremely Low-frequency Ground Exploration Project', and established a fixed tensor source with a scale of over 100 kilometers in Central China, the transmitting power was up to 500kW, 21 frequencies were transmitted, and the frequency band ranged from 0.1Hz to 300Hz. Due to the existence of waveguide field, the WEM signal on the MT background can be observed effectively at far distance (Figure 21). Compared with MT data, the WEM data was considerable superior in quality (Figure 22), which has important theoretical and practical significance for EM exploration in mainland China.

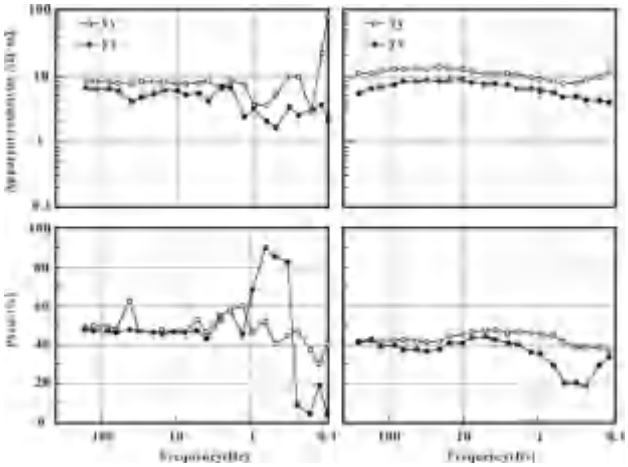

Figure 22. the comparison of apparent resistivity and phase curves between WEM(right) and MT (left)at site 31.

3.4 Reference observation and processing technology of CSEM

In addition to conventionally increasing the current, increasing the number of stacking and increasing the observation time to improve the data signal-to-noise ratio, the application of reference observation and processing technology of CSEM was also the key to ensure the quality of data. Yan (2012) proposed the near-reference magnetic field observation and processing technology for CSAMT. This technique improved the quality of the data by correcting the high-quality magnetic field component data from the near-reference observation and introducing it into the Cagniard apparent resistivity calculation of the CSAMT data of the observed profile. With the increasing

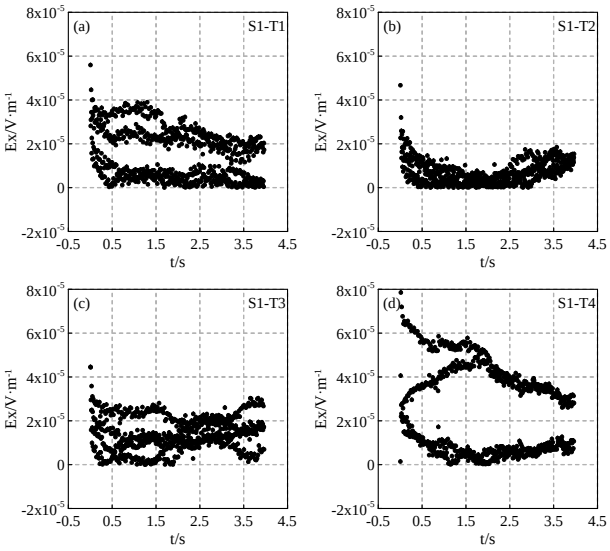

Figure 23. Raw data of 4 periods observed in the suburban area with strong culture noise.

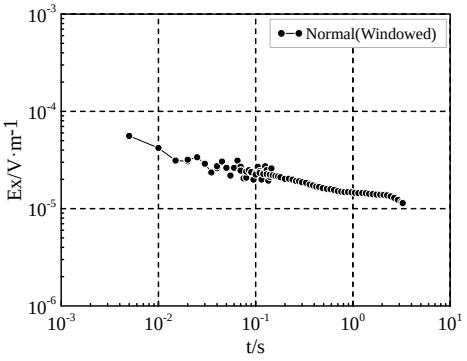

Figure 24. Ex Decay curve with stack and window filtering processing.

popularity of distributed design, array measurement and area data acquisition, the spatiotemporal characteristics of array data provided favorable conditions for reference processing technology. Zhou Cong and Tang Jingtian (2019) proposed a space-time array mixed-field source electromagnetic method (STAHSEM). It was based on multi-input and multi-output system analysis, established a spatiotemporal array equation system using multi-field sources and noise characteristics. By processing the array data synchronously observed by multiple stations, the high quality electromagnetic data of natural field source and controllable source can be obtained while suppressing the relevant noise effectively. In LowTEM data de-noise processing, a method of the local noise compensation (LNC) combined with the variational mode decomposition (VMD) was proposed, which can effectively suppress the noise in the time-domain EM data and improve the decay curve quality. Figure 23 was the LowTEM raw data of four periods observed in the strong cultural noise region. Figure 24 was the Ex decay curve obtained by conventional stacking and filtering. And Figure 25 was the decay curve processed by LNC & VMD.

After comparison, it can be seen that the quality of the head branch of the curve was obviously improved, and the tail branch was more reasonable.

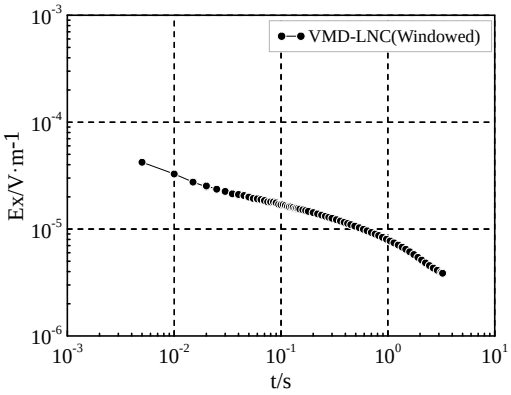

Figure 25. Ex Decay curve with the VMD and LNC joint processing.

Figure 26. TFEM parameter extraction and inversion route with seismic data constraint

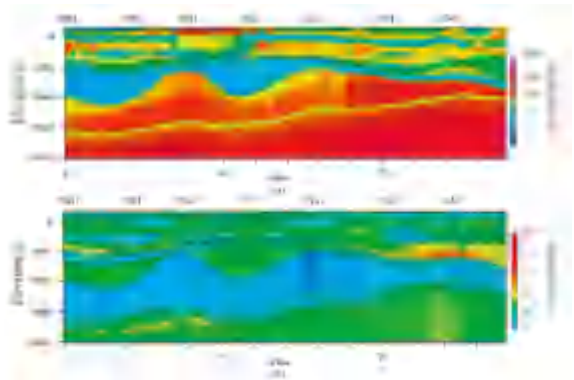

Figure 27. Inversion profile of resistivity and polarizability (top is for resistivity; bottom is for polarizability)

3.5 Joint and constraint data inversion

Various geophysical methods obtain the physical property information from different perspectives. Due to the existence of multiple interpretations in inversion, the different geophysical interpretation methods produce significant differences in the geological models, and even it cannot be reconciled. Joint inversion of multi-methods and multi-observation fields with the prior information constraints is the most effective way to improve the resolution and reliability (He, 2020, Liu, 2021). He (2020) established a joint objective function through TFEM multi-component data, and proposed a method to constrain parameters spaces of thickness, resistivity, and polarizability using prior seismic information and well loging. They combined the artificial fish and simulated annealing non-linear algorithms and the step-by-step constraint schemes together, which successfully overcame the non-uniqueness of inversion, ensured the exploration accuracy and effect. Figure 26 was the data-constrained inversion route. Figure 27 showed the resistivity and polarizability constrained inversion results of the application in the tight oil and gas exploration. In the inversion process, besides the priori interface information, it was also constrained based on logging and geological information (upper and lower boundaries). From the Figure 27, it can be seen that there existed a variation for resistivity and polarizability in the lateral direction in the same stratum, and the resolution of the thin layer in the vertical direction was significantly improved. Therefore, with more prior information, the inversion was more accurate for the unknown physical parameters.

4. Cases history

MT plays an important role in oil and gas exploration in the basin. At the beginning of this century, with the development of CSEM, this method has been expanded from exploration to development, from oil and gas structure exploration to trap exploration, and to oil and gas detection, and the status of EM method in oil and gas exploration has been rising. As oil and gas exploration moved to unconventional area, the geological and geophysical properties of exploration targets have changed greatly, new exploration fields, such as hydraulic fracturing monitoring of shale gas, tight gas and coalbed methane, and sweet spot detection of shale gas and tight gas, have put forward higher requirements for electromagnetic exploration methods and technologies. MT method did not meet the needs of oil and gas exploration in the strong electromagnetic noise environment. In recent years, with the further research on the geological and electrical characteristics of unconventional oil and gas reservoir, many new CSEM methods and techniques have emerged, and have been used in unconventional oil and gas exploration and development (Zhang, 2013; Zhang, 2017; Yan, 2018; Wang, 2019). In the following, this paper will present three cases on the sweet spot detecting, hydraulic fracturing monitoring and fluid property identification with TFEM, WFEM, and LowTEM methods.

4.1 WFEM application in shale oil and gas exploration

Jiangxi, China, is a province lacking conventional oil and gas resources, but there are several sets of mud shale and oil shale formations such as Cretaceous, Permian, Silurian, Cambrian, etc., which are widely distributed, thick and relatively stable. With the geological conditions for the formation of shale oil and gas reservoirs, shale oil and gas, tight oil and gas resources have great potential and good prospects for exploration and development. A basin to be explored in southern Jiangxi is mostly covered by red layers, developed underground volcanic rocks, and has many small local structures, and the geological and topographical conditions are complex, the shale target layer is generally buried at a depth of about 1500m. In this area sweet spot detection, seismic wave impedance difference was small, reflected energy was weak, seismic wave scattering was serious, and data quality is low. Conventional electromagnetic exploration data acquisition was difficult, and the detection depth and accuracy wee difficult to meet the requirements. To reveal the electrical characteristics and EM response principles for the source rocks in the basin, provide the theoretical basis for the geological evaluation, and determine the location of well drilling, A research group from Central South University carried out the WFEM exploration in this region. It deployed a survey line perpendicular to the structural trend of the basin. In this project, they expected to ascertain the basin structure, basement properties, stratigraphic distribution, and fault characteristics, determine the stratigraphic distribution of the lower Cretaceous Banshi formation for the main target layer, and circle the sweet spots. Table 2 showed the statistical results of stratigraphic lithology and resistivity stratification. From Table 2, we can see that from cover to basement, it can be divided into four electrical layers: the first layer includes sandstone, siltstone, and Mudstone of Guifeng group and Zhoutian formation, showed medium resistivity, and with a thickness of 700m; the second layer included conglomerate, glutenite and siltstone of Maodian, Lengshuiwu formations, showed sub-high resistivity, and with a thickness of about 600m; the third layer included shale, oil shale, and Mudstone of Banshi, showed obvious low resistivity, and with a thickness of about 700m, the fourth layer included limestone and quartz sandstone of Jilongzhang, Linshan formations, and showed high resistivity.

In order to analyze the feasibility of WFEM detection, two models of hydrocarbon-bearing shale (resistivity of 50Ω·m and non-hydrocarbon shale (resistivity of 200Ω·m) of the target layer (the third electric layer) were established according to Table 2 for forward calculation. The blue and red lines in Figure 28 were the apparent resistivity curves corresponding to the oil-gas shale and the oil-free shale, respectively. There was a significant difference afterward, and the maximum anomaly can reach 60%, which indicated that whether the Banshi formation contained carbonaceous shale can be identified according to the anomaly of the apparent resistivity curve of WFEM. Figure 29 was the pseudo profile of primary apparent resistivity curves formed by the electric field. According to the continuity and lateral variation in this figure, the structures can be qualitatively interpreted. There existed a sharp lateral variation of the curves between site 116 and site 129, which indicated that the structure of this section was complex, and the curve continuity of other sites performed well, which showed a relatively simple structure accordingly.

Table 2. Statistical results of lithology and resistivity for the Banshi formation and its upper and lower strata

Stratum	Main lithology	Resistivity (Ohm-m)	Electrical characteristics
K_2g	Fine sandstone, Sand mudstone, Conglomerate, Cobblestone	100~200	Intermediate resistivity
K_2z	Sandstone, Glutenite, Siltstone, Mudstone	50~300	
K_2m	Conglomerate, Glutenite, Siltstone	230~650	Secondary high resistivity
K_1l	Glutenite, Fine sandstone, Siltstone, Tuffaceous sandstone, Silty mudstone, Mudstone	300~500	
K_1b	Shale, Oil shale, Mud shale, Marl	36~125	Low resistivity
K_1b	Breccia lava, Siltstone, Conglomerate, Tuff	50~470	Intermediate resistivity
K_1j	Rhyolitic brecciated tuff	700~1800	High resistivity
J_1l	Sandstone	1014~2893	

Figure 30 was the profile of the 2D resistivity inversion and geological interpretation. It showed that the resistivity profile can be divided into three sections laterally: the first part was the southeast section (from site 101 to site 126) with the formation resistivity as a high-low-high distribution from top to bottom; the second part was the middle part (from site 126 to site 170) with the formation resistivity as a low-high-low distribution from top to bottom; the third part was the northwest section (from site 170 to site 195) with the formation resistivity as a high-

low-high distribution from top to bottom. In general, the survey line reflected a NE-dipping faulted basin. The strata at both ends of the survey line were uplifted as a whole, and the middle stratum was overall depression. In the depression, there was a wide and gentle anticline in the Cretaceous (from site 126 to site160).

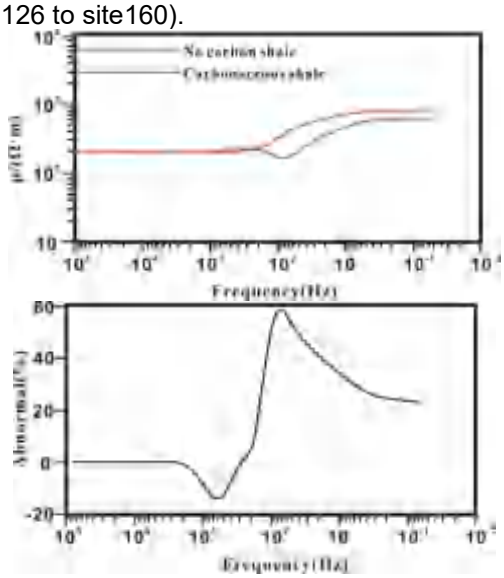

Figure 28. the apparent resistivity and abnormal amplitude curves corresponding to oil-gas and non-oil-gas shales

Figure 29. the primary apparent resistivity curves formed by the electric field for the survey line.

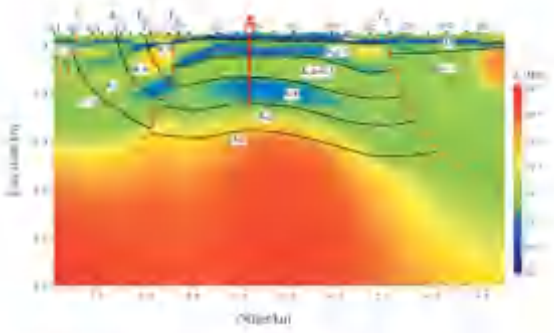

Figure 30. The profile of the 2D resistivity inversion and geological interpretation

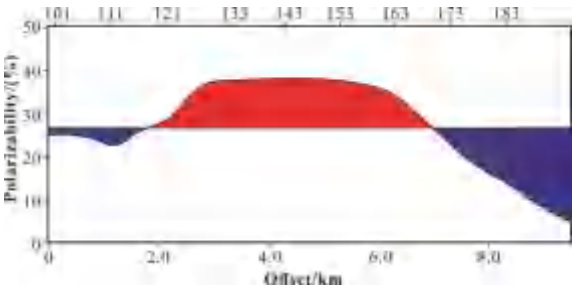

Figure 31. The profile of the polarizability curve

The uplift-in-concave feature in the middle of basin was obvious. The development of fault structure concentrated at the south and north ends of the profile was intense. F70 and F26 were the primary fault zones in the north and south faulted basins, respectively. These two fault zones were reverse faults, and some faults at the southern end of the profile controlled the shale layer. Oil shale, Mudstone, shale and other organic-rich source rocks in the Banshi formation were self-generated and self-stored, which was a favorable reservoir for shale oil and gas.

The fault structure at the middle part of the survey line (from site 126 to site 170) was relatively promising area for oil shale oil development with a deeper target layer depth and a good stratigraphic continuity. Figure 31 is the profile of polarizability curve. It showed that the section from site 116 to site 170 had a high polarized anomaly. Integrated information of resistivity and polarizability the sweet spot can be interpreted in the area between site126 to site 170, with a buried depth of 1000-1600m, an average thickness of 560m. Drilling well 1 is located between site 142 and site 143. Figure 32 is the depth histogram of drilling lithology formation. The buried depths of the bottom of Guifeng, Zhoutian, and Maodian formations were 116m, 466.53m, and 924.46m respectively. The depths of the three interfaces interpreted from the resistivity profile were 155m, 490m, and 920m, respectively. This showed that the inversion depths were very consistent with the drilling results. In addition, the drilling encountered a 2m thick fractured oil-bearing shale in the Banshi formation at a depth of 1500m. This indicated that the inversion depth was accurate, the interface of the electrical layer was clear, and the WFEM it was very sensitive to the conductive oil shale.

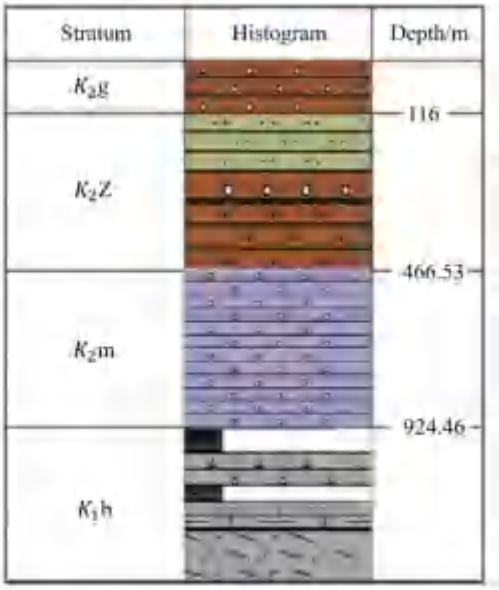

Figure 32. The histogram of the drilling stratum, lithology, and resistivity

4.2 TFEM Application in tight oil exploration

PM exploration area in the Middle East has been fully conducted by 3D seismic, with hundreds of oil Wells and abundant geological and geophysical data. However, the seismic method can not solved the distribution of source rocks under the tight reservoirs and deep gypsolytes. TFEM can easily penetrate the high resistivity layers and identify low-resistivity and high-polarization targets. BGP used TFEM to detect sweet spots in the upper and lower layer of the gypsolyte in the PM exploration area.

- The Geo-electrical Model

The main electrical marker layer in this area is a set of gypsolyte layer with a depth of 2000m and a maximum thickness of 1000m, which is partially missing. The seismic exploration have identified undulations in the top interface, the rock formation was characterized clearly by drilling data, and the resistivity was stable, about 2000Ω·m. There are three sets of reservoirs in the exploration area, the main reservoir is clastic reservoir of the upper Paleozoic Khlata Group, the other two are sandstone reservoir of the Safig formation on the top of the lower Paleozoic Ordovician and sandstone reservoir of the Haima group under the plaster rock.

Based on the geological and drilling information, the strata above 3500m depth can be divided into 16 layers, with the 8th layer being the targeted reservoir. The main oil area of this reservoir has been exploited. The resistivities of the water-bearing and oil-bearing reservoirs are 1.5 Ω·m and 200 Ω·m, and the average resistivity is 70 Ω •m. The Lithology and geo-electric model data were shown in Table 3 and Figure 32.

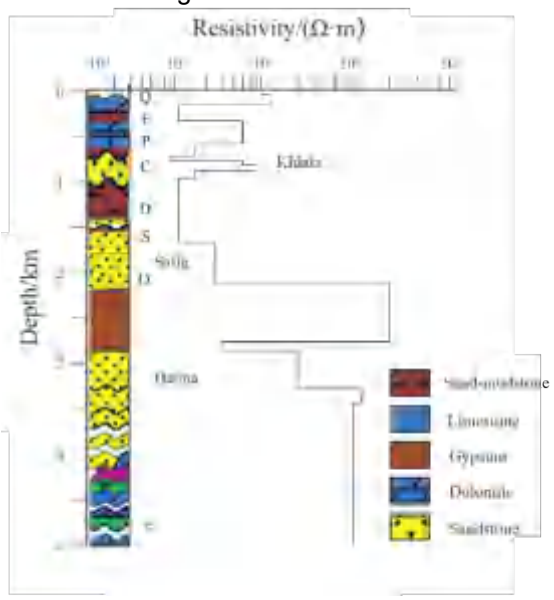

Figure 33. The layered geo-electric model

- Feasibility analysis of the methods

Based on the geo-electric model (Figure 33), and the ranges of the constraint model spaces were used in Table 3. The effectiveness of 1D model space constraint inversion method with artificial fish swarm no-linear algorithm can be tested. Table 4 showed the inverted resistivities. From Figure 33, and Tables 3 and 4, the inversion results were almost consistent with the model, which showed that the artificial fish swarm inversion was correct and feasible.

Layer number	Inversion results (Ω·m)	Theoretical model (Ω·m)
1	85.54	80
2	102.58	100
3	7.94	8
4	49.81	50
5	4.98	5
6	9.61	10
7	25.94	25
8	69.66	70
9	13.59	15
10	20.31	20
11	4.98	5
12	2211.80	2000
13	48.35	50
14	192.45	200
15	537.10	500
16	989.80	1000

Table 4. The inversion results of the electrical parameters

- Interface constrained resistivity inversion

Based on the interpretation results of 3D seismic data in PM exploration area and the well data nearby, a geometric model of formation interface of the survey line was constructed (the dot lines in Figure 35). The model interface was fixed when the TFEM data inversion was conducted, and then the resistivity model (Table 3) was applied in the constraint inversion, and the inversion results were shown in Figure 34. It showed that the resistivity coincided well with the formation interface, the gypsum resistivity coincided with the logging data, and it represented clear interfaces and strong horizontal continuity. In addition, the inversion results presented a clear Carboniferous oil-bearing reservoir (from site 1014 to site 1104). Compared with the drilling data, the interface depth was entirely consistent with the resistivity for each layer. The section from site 1054 to site 1074 was an oil field area that has been exploited for over ten years. Due to the water injection production, the resistivity was generally lower than that of the undeveloped area. The high resistivity anomaly between the site 1094 and site 1154 was quite apparent. Whether it was a favorable sweet spot can be comprehensively judged in combination with the anomaly of polarizability.

- Interface and resistivity joint constrained polarizability inversion

To improve the accuracy of polarizability inversion, an artificial fish swarm inversion with simultaneous constraints of interface geometry model and resistivity model was applied. Table 3 showed the polarizability model and the model space. The polarizability model space for different strata was determined based on the lithology analysis data, but the polarization of the reservoir was not constrained. Figure 34 showed the polarizability inversion profile. The section from site 1014 to site 1104 was the location of the known oil reservoir, it can be seen that the main Carboniferous reservoir had pronounced high polarization characteristics. Combined with the high resistivity characteristics for resistivity profile (Figure 35), the area from the site 1094 to site 1154 was circled as a sweet spot, and the high resistivity and low polarization anomaly near the site 1114 was not. The section of 1154-1184 was also characterized by high polarization and high resistivity, and it was also circled as a sweet spot, this interpretation was confirmed by the drilling results. Hence, joint interpretation of the sweet spot and its distribution area with resistivity and polarization increased the success rate of oil and gas exploration for TFEM.

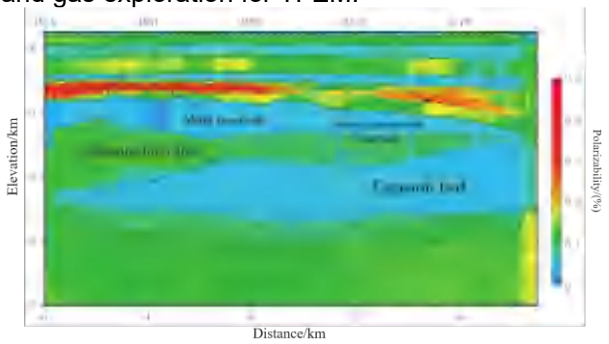

Figure 34. The interface and resistivity model constrained polarizability inversion profile

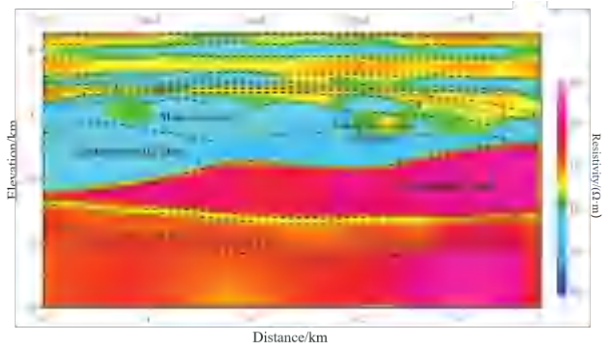

Figure 35. The interface constrained resistivity inversion profile.

4.3 Application in dynamic monitoring of hydraulic fracturing

Jiaoshiba shale gas field is the largest integrated gas reservoir in China. The effective application of hydraulic fracturing technology is conducive to stabilizing and increasing production in this area. Micro-seismic monitoring plays a vital role in improving the fracturing effect. However, affected by the complex terrain and surface geological conditions in southern China, the signal-to-noise ratio of micro-seismic monitoring was low, and the positioning accuracy was not high. In addition, limited by the micro-seismic method, the estimation of effective volume (ERV) is not accurate very much (Hoversten,， 2015). It is well known that when a large amount of fracturing fluid is injected into the reservoir rock, it will flow along the microfractures and continuously expand the fractures, this leads to the change of electrical properties. Due to the low resistivity characteristics of the fracturing fluid and the good connectivity caused by fracturing fluids, the stimulated reservoirs show good low resistivity and high polarizability characteristics, therefore, EM fracturing monitoring has a good physical property foundation. The application of EM methods can obtain sensitive parameters such as fluid trend, volume change and connectivity during the fracturing process, so as to achieve the purpose of monitoring in unconventional oil and gas reservoir fracturing.

In 2017, the EMLAB group of Yangtze University applied the LowTEM method to conduct continuous time-domain EM fracturing monitoring test in Jiaoshiba shale gas field. Through 224 Ex channels of data acquisition array, nearly 9 hours Ex component time series data had been acquired over three fracturing stages buried at a depth of 2800 meters. Through 4D LowTEM processing, the sensitive parameters of electrical changes caused by the fracturing of shale reservoirs were obtained, and the spatial distribution of the fracturing fluid was imaged. The results have guiding significance for fracturing production and well pattern adjustment.

- Electric characteristics of stratum

Table 5 showed the parameters the geo-electric model in test area based on JIAOYE #1 well logging. The model showed a good correspondence between resistivity and stratum, and the shale resistivity is obviously lower than that of the surrounding rocks.

- Electrical characteristics of fracturing fluid

Fracture liquids were sampled from three horizontal platforms (The base fluid is 2% potassium chloride). The measured complex resistivity results (Figure 36) showed that there were specific differences in the resistivity amplitude of fracturing fluids on different platforms, ranging from 0.8-6.4Ω·m. Still, they were all about an order of magnitude smaller than shales. The phase showed that they had different minimum values at frequency 50-500Hz, which indicated that they had strong polarization characteristics due to the presence of proppant.

- Normalized residual time-lapse imaging

All-time apparent resistivity was calculated from electric field components observed before and after

fracturing, then resistivity imaging was carried out based on the theory of chimney effect of current diffusion. To highlight the changing of resistivity caused by fracturing, a normalized residual processing method was developed in the log-log domain. The formula is

$$DF_\rho = 100 \times d\,|\log\rho_1 - \log\rho_2|\,/\,d\log\ \mathrm{h} \qquad (20)$$

Where DF_ρ is the value of normalized residual, ρ_1 is imaged resistivity before fracturing, ρ_2 is imaged resistivity after fracturing, and *h* is the depth.

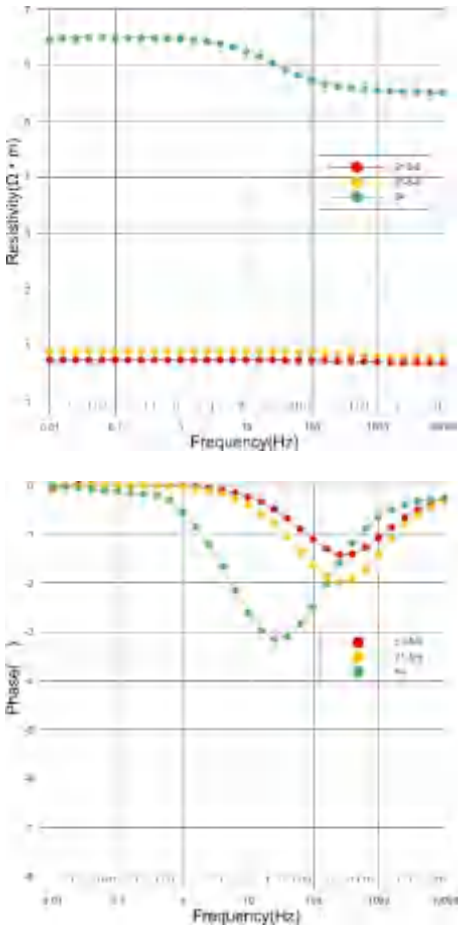

Figure 36. The complex resistivity of fracture liquid (Top: Amplitude; Bottom: Phase)

- Model testing

In geo-electric model(table 5), the resistivity of the reservoir stratum was assumed as 42Ω·m before fracturing, and 5Ω·m after fracturing. The normalized Ex and the normalized residual curves had shown in Figure 37. The top curve showed that the change was identified from decay time 5ms to 100ms when the reservoir stratum fracturing was conducted in the depth of 2330m. Normalized residual curve can depict the fracture change clearly in the range from 30ms to 40ms (bottom curve).

- LowTEM monitoring and analyzing

8 lines with length of 1400m each, 224 sites with 50m interval, were setup above the stage of 6, 7, 8 of the horizontal hydraulic fractured well. The length of the ground source was 4000m, in an east-west direction, the minimum offset was 5000m, the current was 65A, the current waveform was a bipolar square wave with a period of 8s and a duty cycle of 50%, the sampling rate was 400Hz. The schematic diagram of the field construction layout was shown in Figure 38.

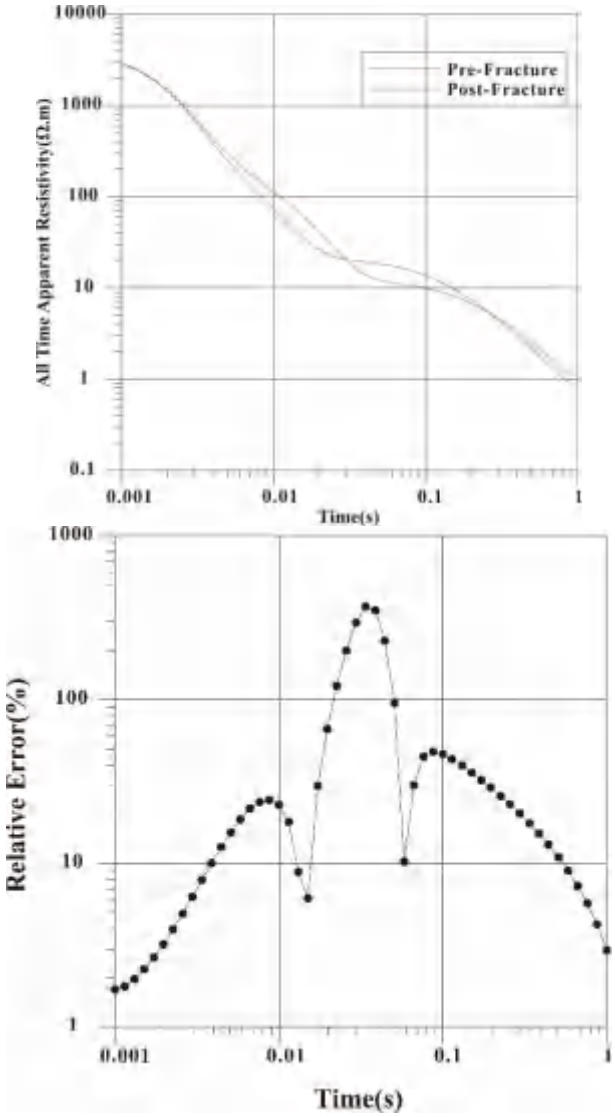

Figure 37. The EM field (top) and normalized residual (bottom) curves

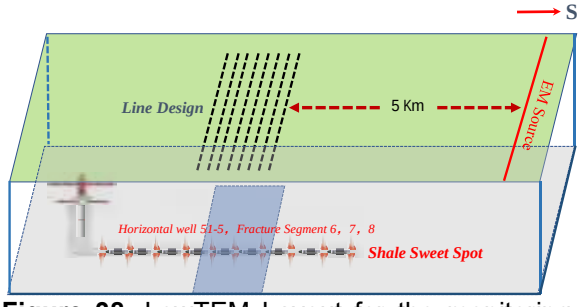

Figure 38. LowTEM Layout for the monitoring of shale fracture

The fracturing production information in the monitoring section is shown in Table. The continuous recording time of Ex while stage 6,7,8 were fractured was up to 9 hours, which ensured the whole process of the fracturing process of each stage. In order to guarantee the quality of decay curve, 30 minutes of electric field component time serious of segment 6, 7, 8 each was used to stack processing, and the normalized residual curves had been acquired on the sites of L01-14 and L01-16. In Figure 39, the weak changes of fracturing can be seen in the decay time range from 0.03s to 0.1s. The shape and time window were consistent with the forward results in Figure 37.

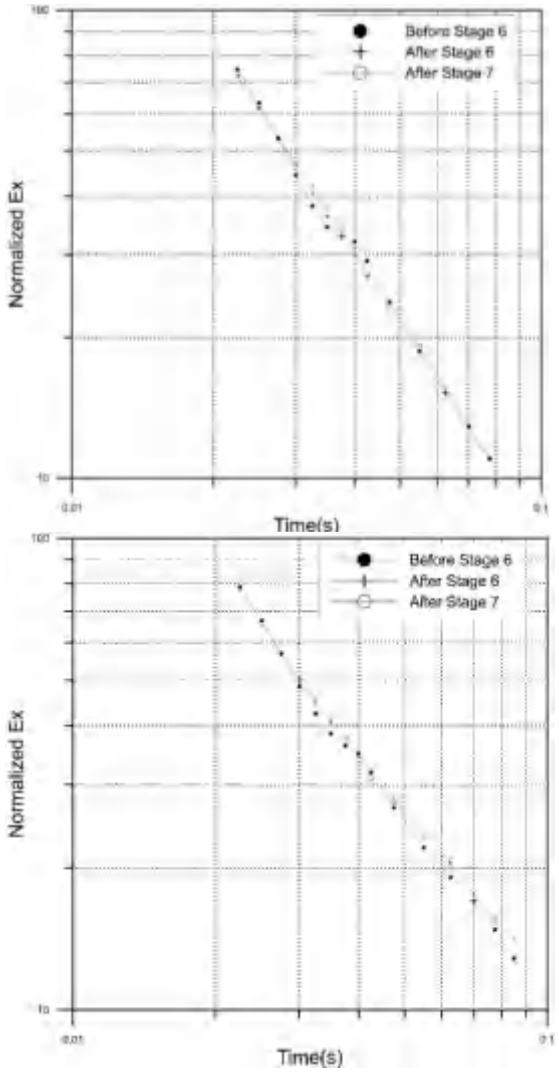

Figure 39. The curves of electric field component Ex observed at points 14 (top) and 16 (bottom) of L01 over the segment 6 and 7 in horizontal wells

The 3D fracturing anomalies showed in Figure 40 which were imaged based on the normalized residual curves, and at the same time the calibration was carried out with the help of seismic and well logging. The results showed that, after segment 6 fracturing the length of the fractured reservoir stratum in the direction of east to west was about 600 m, in which 400m was in the west of horizontal well, 200m was in the east of horizontal well. The width from north to south was about 200-300m. After segment 7 fracturing the length of the fractured reservoir stratum in the direction of east to west was about 700m, in which 400m was in the west of horizontal well, 300m was in the east of horizontal well. The width from north to south increased to 300-400m. Overall, the trend and spatial distribution of fracturing fluid were dumbbell-shaped, and the fracturing effect in the west area was better than that in the east area.

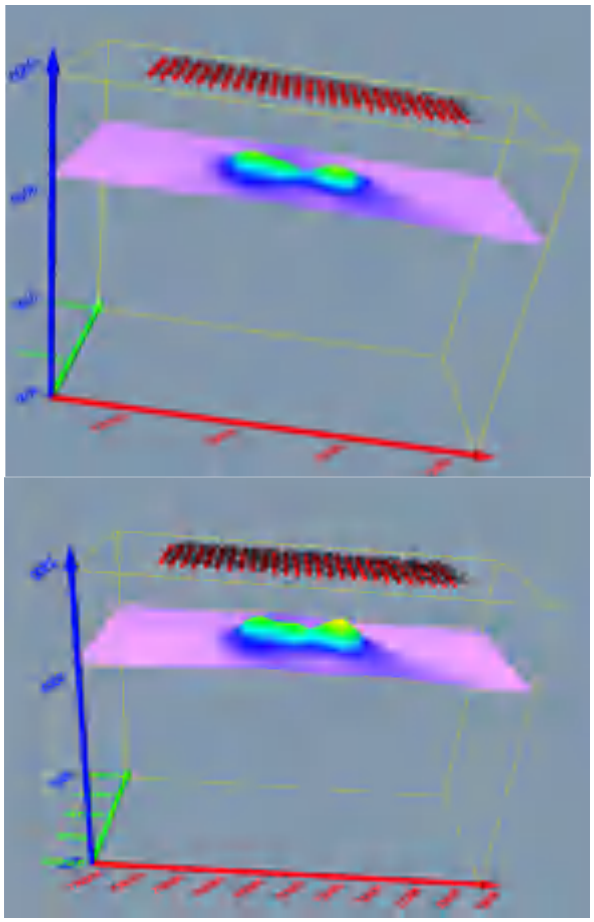

Figure 40. Anomaly in the space before and after fracture(top：after segment 6；bottom：after segment 7)

5 Conclusion and future

5.1 Conclusion

(a) The complex resistivity analysis of reservoir rocks showed that the organic-rich shale in southern China had the characteristics of low resistivity and high polarization. Tight oil and gas reservoirs were characterized by the high resistivity and high polarization. The hydraulic fracturing reservoir stimulation area had the characteristics of low resistance and high polarization. All these indicated that the CSEM detecting the sweet spots had a firm petrophysical basis.

(b) The high spatiotemporal density data collection, combining with updated methods, such as the high-power transmitters, pseudo-random waveforms, reference observation and processing, variational mode decomposition, have improved signal-to-noise ratio and guaranteed data quality, which can profit the accurate inversion.
(c) The new EM attribute parameter definitions greatly improved the sensitivity of CSEM to detect the target attribute and the fluid property, and also facilitated geological interpretation.
(d) With the prior information constraints, such as geology, seismicity, and well logging, the joint inversion of for multiple methods and multiple component data, can produce an accurate and reliable interpretation model.
(e) The sweet spot detection model and the parameter prediction method formed by the EM characteristics of shale reservoirs have laid a physical foundation for applying EM methods in geological evaluation. This techniques can be used for reference in the data interpretation of EM detection in other unconventional reservoirs.

5.2 Future

(a) Research on the inversion method based on IP model under seismic, logging and other prior information constraints should be carried out so that to improve the resolution and reliability of TDEM in unconventional oil and gas exploration.
(b) At present, the application of WEM method has played an essential role in engineering geology, mineral exploration, disaster prevention, and environmental governance. As the WEM source is improved further，it has become a dedicated fixed source that can transmit multi-segment frequency codes, which has improved exploration efficiency, reduced production costs, and ensured effective exploration depths up to 5km. the WEM method has become an essential means in the exploration and development of unconventional oil.
(c) The data collection methods should be continuously optimized. The EM forward model, analysis, and acquisition parameter evaluation before field work are the key to the success of EM survey. Softwires should be developed for EM data collection method and parameter optimization, further to provide robust means for data collection.
(d) The heterogeneity and electrical anisotropy of unconventional oil and gas reservoirs and hydraulic fracturing areas are pretty severe, which will lead to the misunderstandings in data processing and interpretation. It is an unavoidable problem to study the high-precision anisotropy forward modeling and inversion method.
(e) Based on the characteristics of EM exploration and micro-seismic monitoring, an acquisition array system that can simultaneously collect controlled-source EM methods and micro-seismic signals should be developed, effectively achieve the deep integration of EM and micro-seismic in all directions, and form a hydraulic fracturing controlled-source EM method and micros-seismic joint monitoring method.
(f) When we are faced with the difficulty of effectively suppressing the electromagnetic noise, the time-consuming and multi-resolution of 3D inversion, and the unsatisfactory application effect of sweet spot detection and evaluation, the arrival of artificial intelligence and big data show us a new hope. Through big data analysis, we are expected to find the real laws of the noise world, the model world and the underground electrical world hidden behind the big data of electromagnetic exploration. The analysis and prediction of big data through artificial intelligence and cloud computing will make the EM processing and interpretation more accurate, convenient and efficient, thus mining more hidden value of electromagnetic data.

Acknowledgements

This review was supported by Key Project (N0.: 42030805) of National Natural science foundation of China. In the process of references collection and writing this paper, I have received the assistance from Prof. Struck, Prof. Qingyun Di, Prof. Zhanxiang He, Dr. Zhigang Wang, Professor Jingtian Tang, Professor Zhengyong Ren, Professor Diquan Li, Dr. Kui Xiang, Dr. Lei Zhou, Dr. Xin Huang, Dr. Xiaoyue Cao, Dr. Tong Xiaolong and graduate students of EMLAB. All thanks here.

References

Archie GE (1942) The electrical resistivity log as an aid in determining some reservoir characteristics. Transactions of the AIME 146(01): 54–62

Astic T, Oldenburg DW (2019) A framework for petrophysically and geologically guided geophysical inversion using a dynamic Gaussian mixture model prior. Geophysical Journal International 219(3): 1989–2012. doi:10.1093/gji/ggz389

Börner FD, Schopper JR, Weller A (1996) Evaluation of transport and storage properties in the soil and groundwater zone from induced polarization measurements. Geophysical Prospecting 44: 583–601

Burtman V, Zhdanov MS, Fu H (2014) Spectral induced polarization effect in unconventional reservoir rocks. SEG Technical Program Expanded Abstracts 33: 907–911. doi:10.1190/segam2014-0419.1

Burtman V, Zhdanov MS (2015) Induced polarization effect in reservoir rocks and its modeling based on generalized effective-medium theory. Resource-Efficient

Technologies 1(1): 34–48. doi:10.1016/j.reffit.2015.06.008

Chen Benchi, Li Jinming, Zhou Fengtong (1999) Quasi wave equation migration of transient electromagnetic field. Oil Geophysical Prospecting 34(5): 546–554

Chen Feng, Xiu Jigang, An Jinzhen (2000) Research on dependence of resistivity changing anisotropy on microcracks extending in rock with experiment. Acta Seismiological Sinica 22(3): 310–318

Commer M, Newman GA, Williams KH (2011) 3D induced-polarization data inversion for complex resistivity. Geophysics 76(3): F157–F171. doi:10.1190/1.3560156

Constable S (2010) Ten years of marine CSEM for hydrocarbon exploration. Geophysics 75(5): 75A67–75A81. doi:10.1190/1.3483451

Davydycheva S, Rykhlinski N, Legeido P (2006) Electrical-prospecting method for hydrocarbon search using the induced-polarization effect. Geophysics 71(4): G179–G189. doi:10.1190/1.2217367

De Lima OAL, Niwas S (2000) Estimation of hydraulic parameters of shaly sandstone aquifers from geoelectrical measurements. Journal of Hydrology 235(1-2): 12–26

Di Qingyun, Wang Miaoyue, Wang Ruo et al (2008) Study of the long bipole and large power electromagnetic field. Chinese Journal of Geophysics (in Chinese) 51(6): 1917–1928

Di Qingyun, Xue Guoqiang, Yin Changchun et al (2020) New Methods of controlled-source electromagnetic detection in China. Scientia Sinica (Terrae) 50(09): 1219–1227

Di Qingyun, Zhu Rixiang, Xue Guoqiang et al (2019) New development of the Electromagnetic (EM) methods for deep exploration. Chinese Journal of Geophysics (in Chinese) 62(6): 2128–2138

Fiandaca G, Auken E, Christiansen AV et al (2012) Time-domain-induced polarization: Full-decay forward modeling and 1D laterally constrained inversion of Cole-Cole parameters. Geophysics 77(3): E213–E225. doi:10.1190/geo2011-0217.1

Gallardo LA, Meju MA (2003) Characterization of heterogeneous near-surface materials by joint 2D inversion of dc resistivity and seismic data. Geophysical Research Letters 30: 1658. doi:10.1029/2003GL017370

Gallardo LA, Meju MA (2004) Joint two-dimensional DC resistivity and seismic travel time version with cross-gradients constraints. Journal of Geophysical Research: Solid Earth 109: B03311. doi:10.1029/2003jb002716

Gao Ji, Zhang Haijiang, Fang Hongjian, Li Nan (2017) An efficient joint inversion strategy for 3D seismic travel time and DC resistivity data based on cross-gradient structure constraint. Chinese Journal of Geophysics (in Chinese) 60(9): 3628–3641. doi:10.6038/cjg20170927

Giraud J, Pakyuz-Charrier E, Jessell M et al (2017) Uncertainty reduction in joint inversion using geologically conditioned petrophysical constraints. Geophysics 82(6): 1–61. doi:10.1190/geo2016-0615.1

Goldstein MA et al (1975) Audio-frequency magnetotellurics with a grounded electric dipole source. Geophysics 40(1): 669–683

Haber E, Oldenburg DW (1997) Joint inversion: a structural approach. Inverse Problems 13(1): 63–77. doi:10.1088/0266-5611/13/1/006

Heincke B, Jegen M, Moorkamp M et al (2010) Adaptive coupling strategy for simultaneous joint inversions that use petrophysical information as constraints. SEG Technical Program Expanded Abstracts. doi:10.1190/1.3513426

He Jishan (2010) Wide field electromagnetic sounding methods. Journal of Central South University (Science and Technology) 41(3):1065–1072

He Zhanxiang (2019) Opportunities,challenges and development directions of electromagnetic exploration today. Computing Techniques for Geophysical and Geochemical Exploration 41(4): 433–447

He Zhanxiang, Dong Weibin, Zhao Guo et al (2021) Time-frequency electromagnetic (TFEM) technology: Data processing. Oil Geophysical Prospecting 56(6): 1391–1399

He Zhangxiang, Hu Wenbao, DongWeidong (2010) Petroleum electromagnetic prospecting advances and case studies in china. Surveys in Geophysics 31(2): 207–224 doi:10.1007/s10712-009-9093-z

He Zhanxiang, Hu Zuzhi, Gao Yan et al (2015) Field test of monitoring gas reservoir development using time-lapse continuous electromagnetic profile method. Geophysics 80 (2): 127–134. doi:10.1190/geo2014-0195.1

He Zhanxiang, Hu Zuzhi, Luo Weifeng, Wang Caifu (2010b) Mapping reservoirs based on resistivity and induced polarization derived from continuous 3D magnetotelluric profiling: Case study from Qaidam Basin, China. Geophysics 75(1): B25–B33. doi:10.1190/1.3279125

He Zhanxiang, Hu Zuzhi, Wang Zhigang (2020) Time-frequency electromagnetic(TFEM) technique: step-by-step constraint inversion based on artificial fish swarm algorithm. Oil Geophysical Prospecting 55(4): 898–905.

He Zhanxiang, Liu Xuejun, Qiu Weiting et al (2005) Mapping reservoir boundary by borehole-surface TFEM: Two case studies. The Leading Edge 24(9): 896–900. doi:10.1190/1.2056379

He Zhanxiang, Wang Xuben (2007) Geo-electrical anomalous pattern of reservoir and oil/gas detection by electromagnetic survey. Oil

Geophysical Prospecting 42(1): 102–106

Hobbs BA et al (2006) Multi-Transient Electromagnetics (MTEM) -controlled source equipment for subsurface resistivity investigation. 18th IAGA WG 1.2 Workshop on Electromagnetic Induction in the Earth. El Vendrell, Spain 17–23

Hoversten GM, Commer M, Haber E et al (2015) Hydro-frac monitoring using ground time-domain electromagnetics. Geophysical Prospecting 63(6): 1508–1526. doi:10.1111/1365-2478.12300

Hu Wenbao, Shen Jingshong, Yan Liangjun (2022) Reservoir Fluid Prediction Theory with CSEM and Application. Science Publish House, Beijing

Hu Wenyi, Abubakar A, Habashy TM (2009) Joint electromagnetic and seismic inversion using structural constraints. Geophysics 74(6): R99–R109

Hu Zuzhi, Shi Yanling, Liu Yunxiang et al (2020) Nonlinear constrained joint inversion of MT and gravity. Oil Geophysical Prospecting 55(01): 1110–1116

Jegen MD, Hobbs RW, Tarits P et al (2009) Joint inversion of marine magnetotelluric and gravity data incorporating seismic constraints: Preliminary results of sub-basalt imaging off the Faroe Shelf. Earth and Planetary Science Letters 282(1): 47–55. doi:10.1016/j.epsl.2009.02.018

Ji Yanju et al (2016) Noise reduction of time domain electromagnetic data: application of a combined wavelet denoising method. Radio Science 51(6): 680–689

Jiang qiyun (2010) Study on the key technology of wide field electromagnetic sounding instrument. PhD thesis, Central South University

Kavian M, Slob EC, Mulder WA (2012) A new empirical complex electrical resistivity model. Geophysics 77(3): E185–E191. doi:10.1190/geo2011-0315.1

Kass MA, Li Y (2011) Quantitative analysis and interpretation of transient electromagnetic data via principal component analysis. IEEE Transactions on Geoscience & Remote Sensing 50(5): 1910–1918

Kirkby A, Heinson G, Krieger L (2016) Relating permeability and electrical resistivity in fractures using random resistor network models. Journal of Geophysical Research: Solid Earth 121(3): 1546–1564

Lelievre PG, Farquharson CG, Hurich CA (2012) Joint inversion of seismic travel times and gravity data on unstructured grids with application to mineral exploration. Geophysics 77(1): K1–K15

Lelievre PG, Farquharson CG (2013) Gradient and smoothness regularization operators for geophysical inversion on unstructured meshes. Geophysical Journal International 195: 330–341. doi:10.1093/gji/ggt255

Li Diquan, Di Qingyun, Wang Miaoyue, David Nobes (2015) 'Earth–ionosphere' mode controlled source electromagnetic method. Geophysics 202: 1848–1858. doi: 10.1093/gji/ggv256

Lima OD, Sharma MM (1992) A generalized Maxwell-Wagner theory for membrane polarization in shaly sands. Geophysics 57(3): 431–440. doi:10.1190/1.1443257

Li Xiu, Xue Guoqiang, Song Jianping et al (2005) An optimize method for transient electromagnetic field-wave field conversion. Chinese Journal of Geophysics (in Chinese) 48(5): 1185–1190

Liu Jianxin, Guo Tianyu, Wang Bochen et al (2021) Review of marine electromagnetic methods for hydrocarbon exploration. Geophysical Prospecting for Petroleum 60(4): 527–538

Mittet, R (2015) Seismic wave propagation concepts applied to the Interpretation of marine controlled-source electromagnetic: Geophysics 80(2) E63–E81. doi:10.1190/geo2014-0215.1

Mittet, R (2018) Electromagnetic modeling of induced polarization with the fictitious wave domain method. SEG Technical Program Expanded Abstracts. doi:10.1190/segam2018-2994774.1

Ou Yangtao et al (2019) Identifying deep ore bodies using the Multi-Channel Transient Electromagnetic Method (MTEM): an example of a lead-zinc-silver mine in Inner Mongolia. Chinese J. Geophys (in Chinese) 62(5): 1981–1990

Pelton W, Ward S, Hallof P et al (1978) Mineral discrimination and removal of inductive coupling with multifrequency IP. Geophysics 43(3): 588–609

Peng Guomin, Liu Zhan (2020) An overview of joint electromagnetic-seismic inversion and its future development. Oil Geophysical Prospecting 55(2): 465–474

Peng Guomin, Xu Kaijun, Du Runlin, Liu Zhan (2018) Reservoir petrophysical parameter estimation with joint inversion of MCSEM and seismic AVA data. Oil Geophysical Prospecting 53(05): 1110–1116

Piao Huarong (1990) Principle of Electromagnetic Sounding. Geological Press, Beijing: Geological Publishing House

Rasmussen S, Nyboe NS, Mai S, Juul Larsen J (2017) Extraction and use of noise models from transient electromagnetic data. Geophysics 83(1): E37–E46.

Revil A, Abdel Aal GZ, Atekwana EA et al (2015) Induced polarization response of porous media with metallic particles—Part 2: Comparison with a broad database of experimental data. Geophysics 80(5): D539–D552. doi:10.1190/geo2014-0578.1

Revil A, Eppehimer J, Skold M et al (2013) Low-frequency complex conductivity of sandy and clayey materials. Journal of Colloid and Interface Science 398: 193–209. doi:10.1016/j.jcis.2013.01.015

Revil A, Woodruff WF, Torres-Verdin C et al (2013) Complex conductivity tensor of anisotropic hydrocarbon-bearing shales and mudrocks. Geophysics 78(6): D403–D418. doi:10.1190/geo2013-0100.1

Seigel HO, Nabighian M et al (2007) The early history of the induced polarization method. The Leading Edge 26(3): 312–321

Slater, L (2007) Near Surface Electrical Characterization of Hydraulic Conductivity: From Petrophysical Properties to Aquifer Geometries—A Review. Surveys in Geophysics, 28(2-3): 169–197. doi:10.1007/s10712-007-9022-y

Slater L, Lesmes DP (2002) Electrical-hydraulic relationships observed for unconsolidated sediments. Water Resources Research 38(10): 31–1–31–13. doi:10.1029/2001wr001075

Stoffa PL, Ziolkowski A (2018) Time evolution of the electric field – Part 1: using the rapid expansion method (REM) with pseudo-spectral evaluation of spatial derivatives. SEG Technical Program Expanded Abstracts. doi: 10.1190/segam2018-2995831.1

Strack, KM (2013) Future Directions of Electromagnetic Methods for Hydrocarbon Applications. Surveys in Geophysics 35(1):157–177. doi:10.1007/s10712-013-9237-z

Strack KM (2014) Future Directions of Electromagnetic Methods for Hydrocarbon Applications. Surveys in Geophysics 35:157–177

Strack KM et al (1989) Case histories of long-offset transient electromagnetic (LOTEM) in hydrocarbon prospective areas. First Break 7(12): 467–477

Streich R (2015) Controlled-Source Electromagnetic Approaches for Hydrocarbon Exploration and Monitoring on Land. Surveys in Geophysics 37(1): 47–80. doi:10.1007/s10712-015-9336-0

Streich R, Becken M, Matzander U, Ritter O (2011) Strategies for land-based controlled-source electromagnetic surveying in high-noise regions. The Leading Edge 30(10): 1174–1181. doi:10.1190/1.3657078

Su Zhuliu et al (2005) Appliacation of complex apparent resistivity (CR) method in prediction of oil/gas. Oil Geophysical Prospecting 40(4):467–471

Tietze K, Grayver A, Streich R et al (2014) Developments for Land-based Controlled-source Electromagnetic Surveying. Conference Proceedings, 76th EAGE Conference and Exhibition - Workshops. doi:10.3997/2214-4609.20140561

Tong, Xiaolong, Yan Liangjun, Xiang Kui (2020) Modifying the Generalized Effective-medium Theory of Induced Polarization Model in Compacted Rocks. Geophysics 85(4): 1–44

Veeken PC, Legeydo PJ, Davidenko YA et al (2009) Benefits of the induced polarization geoelectric method to hydrocarbon exploration. Geophysics 74(2): B47–B59. doi:10.1190/1.3076607

Vinegar HJ, Waxman MH (1984) Induced polarization of shaly sands. Geophysics 49(8): 1267–1287. doi:10.1190/1.1441755

Wang Mingfei, Chen Chao, Qu Dapeng et al (2015) The geophysical characteristics of shale gas reservoir from Wufeng member to Longmaxi member in Jiaoshiba block of Fulin shale gasfield. Geophysical Prospecting for Petroleum 54(5): 613–620

Wang Zhigang et al (2019) The use of time-frequency domain EM technique to monitor hydraulic fracturing. GEM 2019 Xi'an: International Workshop and Gravity, Electrical & Magnetic Methods and their Applications

Weller A, Slater L, Binley A et al (2015) Permeability prediction based on induced polarization: Insights from measurements on sandstone and unconsolidated samples spanning a wide permeability range. Geophysics 80(2): D161–D173. doi:10.1190/geo2014-0368.1

Wong J (1979) An electrochemical model of the induced-polarization phenomenon in disseminated sulfide ores. Geophysics 44(7): 1245–1265.doi:10.1190/1.1441005

Wu Changxiang et al (1996) The applleation of complex resistivity method in oil field exploration. Geophysical Prospecting for Petrole 35(4): 111–118

Wu Sihong, Huang Qinghua, Zhao Li (2021) De-noising of transient electromagnetic data based on the long short-term memory-autoencoder. Geophysical Journal International. doi:10.1093/gji/ggaa424

Xiang Kui, Hu Wenbao, Yan Liangjun et al (2014) Complex resistivity dispersion characteristics of shale samples in Sichuan and Guizhou area. Oil Geophysical Prospecting 49(5): 1013–1019

Xiang Kui, Yan Liangjun, Hu Hua, Hu Wenbao, Tang Xingong, Liu Xuejun (2016) Relationship analysis between brittle index and electrical properties of marine shale in South China. Geophysical Prospecting for Petroleum 55(6): 894–903

Xu Chuanjian et al (2004) Application effectiveness of complex resistivity (CR) method in oil and gas detection. Oil Geophysical Prospecting 39(S1): 31–35

Xu Fengjiao, Yan Liangjun, Xiang Kui et al (2020) Predicting the characteristic parameters of

shale sweet-spot with complex resistivity. Terrestrial, Atmospheric and Oceanic Sciences journal. doi: 10.3319/TAO.2020.03.22.01.

Xu Kaijun, Du Runlin, Liu Zhan (2016) Joint reservoir parameter inversion of 1D marine controlled source electromagnetic and seismic data. Oil Geophysical Prospecting 51(01): 197–203

Xue Guoqiang, Chen Weiying, Wu Xin (2020) Review on research of short-offset transient electromagnetic method. Journal of China University of Mining & Technology 49(2): 215–226

Xue Guoqiang, DI Qingyun, Wang Ruo et al (2020) Overview on data processing methods of multi-channel transient electromagnetic method. Progress in Geophysics (in Chinese) 35(1): 0211–0215

Xue Guoqiang, Wu Xin, Li Hai et al (2016) Progress of multi-transient electromagnetic method in abroad. Progress in Geophysics (in Chinese) 31(5): 2187–2191

Yan Liangjun, Hu Wenbao (1999) The estimation and fast inversion of All-time apparent resistivity for LOTEM. Oil Geophysical Prospecting 34(5): 532–538

Yan Liangjun (2014) Study on the induced polarization model in the exploration for shale gas in southern China. SEG Technical Program Expanded Abstracts. doi:10.1190/segam2014-0186.1

Yan LiangJun, Chen Xiaoxiong, Tang Hao et al (2018) Continuous TDEM for monitoring shale hydraulic fracturing. Applied Geophysics 15(1): 26–34. doi:10.1007/s11770-018-0661-1

Yan Liangjun et al (2012) Magnetic reference technique and correction method in 3D CSAMT. SEG Technical Program Expanded Abstracts. doi:10.1190/segam2012-0239.1

Yang Bo, Zhang Xiangguo, Liu Zhan, Xu Kaijun (2021) Technique and application of joint magnetotelluric and seismic modelling and constrained inversion based on clustering and multiviariate geostatistics. Oil Geophysical Prospecting 56(03): 670–677

Yang Chunmei, LI Hongqi, Zhang Fangle et al (2005) Resistivity drop mechanism during heavy oil thermal recovery. Petroleum Exploration and Development 32(2): 116–118

Yang Zhi, Zou Caineng, Fu Jinhua et al (2019) Characteristics and “Sweet Area (Section)” Evaluation of Continuous Tight & Shale Oil and Gas in Ordos Basin, North-central China. Journal of Earth Sciences and Environment 41(04): 459–474

Yang Sheng (1986) A single apparent resistivity expression for loop-offset transient electromagnetics. Geophysics 51(6): 1291–1297

Yan Zhengwen, Tan Handong, Peng Miao et al (2020) Three-dimensional joint inversion of gravity, magnetic and magnetotelluric data based on cross-gradient theory. Chinese Journal of Geophysics (in Chinese) 63(2): 736–752. doi:10.6038/cjg2020M0355

Yuan B, Diquan L, Bayless RC (2017) Wide field Electromagnetic Method for Shale Gas Exploration in Southern China: A case Study. Journal of Environmental & Engineering Geophysics 22(3): 279–289. doi:10.2113/jeeg22.3.279

Yuan Guiqin, Sun Yue, Gao Weidong et al (2013) Development Status of the Shale Gas Geophysical Prospecting Technology. Geology and Exploploration 49(5): 945–950

Zhang Chunhe, Liu Xuejun, He Lanfang et al (2013) A study of exploration organic rich shales using Time-Frequency Electromagnetic Method(TFEM). Chinese Journal of Geophysics (in Chinese) 56(9): 3173–3183. doi:10.6038/cjg20130930

Zhang Qiaoxun, Li Diquan, Tian Maojun (2017) Application of wide field electromagnetic method to the hydrocarbon exploration in a basin of South Jiangxi. Oil Geophysical Prospecting 52(5): 1085–1092.

Zhdanov M (2008) Generalized effective-medium theory of induced polarization. Geophysics 73(5): F197–F211

Zhdanov MS, Gribenko AV, Wilson GA, Funk C (2012) 3D joint inversion of geophysical data with Gramian constraints: A case study from the Carrapateena IOCG deposit, South Australia. The Leading Edge 12: 1382–1388

Zhou Cong, Tang Jingtian, Pang Cheng, Hu Shuanggui (2019) A theory and simulation study on the space-time array hybrid source electromagnetic method. Chinese Journal of Geophysics (in Chinese) 62(10): 3827–3842

Zhuo Xianjun et al (2007) Preliminary application of WEM in geophysical exploration. Progress in Geophysics 22(6): 1921–1924

Zonge KL, Wyna JC (1975) recent advance and application in complex resisivity measurement. Geophysics 40(5): 851–864. doi:10.1190/1.1440572

Zou Caineng, Zhang Guosheng, Yang Zhi et al (2013) Geological concepts, characteristics, resource potential and key techniques of unconventional hydrocarbon: On unconventional petroleum geology. Petroleum Exploration and Development 40(4): 385–399

Zou Caineng, Dong Dazhong, Wang Yuman et al (2015) Shale gas in China: Characteristics, challenges and prospects (I). Petroleum Exploration and Development 42(6): 689–701

Zou Caineng, Tao Shizhen, Bai Bin et al (2015) Differences and Relations between Unconventional and Conventional Oil and Gas. China Petroleum Exploration 20(1): 1–16

Zou Caineng, Zhai Guangming, Zhang Guangya et al (2015) Formation, distribution, potential and prediction of global conventional and unconventional hydrocarbon resources. Petroleum Exploration and Development 42(1): 13–25

Zou Caineng, Zhang Guosheng, Yang Zhi et al (2013) Geological concepts, characteristics, resource potential and key techniques of unconventional hydrocarbon: On unconventional petroleum geology. Petroleum Exploration and Development 40(4): 385–399

Zou Caineng, Zhu Rukai, Bai Bin et al (2015) Significance, Geologic Characteristics, Resource Potential and Future Challenges of Tight Oil and Shale Oil. Bulletin of Mineralogy, Petrology and Geochemistry 34(1): 3–17

Table 1. the laboratory measurement

Stratum	Lithology	Rock Number	Density (g/cm3)	Magnetisability (10^{-5}SI)	Permeability (mD)	Vp (m/s)	Vs (m/s)	Resistivity (Ohm-m)	Polarizability (%)
Longmaxi Group, Silurian	Shale	52	2.54	2.4	1.232	3580.00	2309.80	111.2	18.1
Wufeng Group, Ordovician	Shale	5	2.52	3.3	0.001	4898.94	2880.18	168.7	21.7
Qiongzhusi Group, Cambrian	Shale	112	2.43	5.4	0.933	4178.00	2623.62	147.0	42.5
Dengying Group, Sinian	Dolomite	23	2.81	1.9	3.606	4278.00	2877.97	2507.8	12.5

Table 3. the electric model and the model space for the PM area

Layer number	Thickness and model space (m)	Resistivity and model space ($\Omega \cdot m$)	Polarizability and model space
1	40(39.6,40.4)	80(50,100)	0.040(0.010,0.150)
2	110(109.9,110.1)	20(5,80)	0.120(0.010,0.200)
3	175(173.3,176.8)	10(1,30)	0.060(0.010,0.250)
4	250(2247.5,252.5)	50(10,70)	0.150(0.050,0.500)
5	140(138.6,141.4)	5(2,15)	0.050(0.010,0.350)
6	50(49.5,50.5)	10(5,15)	0.150(0.010,0.350)
7	50(49.5,50.5)	25(20,80)	0.250(0.010,0.450)
8	60(59.4,60.6)	70(1.5,200)	0.400(0.050,0.700)
9	90(89.1,90.9)	15(5,20)	0.100(0.010,0.400)
10	700(693.0,707.0)	20(2.5,100)	0.010(0.005,0.100)
11	450(445.5,454.5)	5(1.5,20)	0.075(0.010,0.150)
12	650(643.5,656.5)	2000(1950,2050)	0.005(0.000,0.001)
13	100(99.0,101.0)	50(10.80)	0.010(0.001,0.100)
14	400(396.0,404.0)	200(150,300)	0.100(0.010,0.200)
15	180(178.2,181.8)	500(100,2000)	0.120(0.010,0.200)
16	1000(990.0,1010.0)	1000(300,2000)	0.150(0.010,0.200)

Table 5. Geo-Resistivity model based on JIAOYE #1 Logging curve

Stratigraphy	Lithology	Burial depth(m)	Thickness(m)	Resistivity（Ω·m)
P_2ch-C2hl	Limestone	0--1430	1430	>2000
S_2h-S_1l	Mudstone	1430--2290	860	30-40
S_1l	Sandstone	2290--2330	40	244
S_1l -O_3w	Gas-bearing shale	2330--2410	80	42
O_3-O_1	Limestone	2410—		>1000

Table 6. Production information record of shale gas fracturing in test horizontal wells

Well section number	Fracturing date	Fracturing Start Time	Fracturing Termination Time	Fluid/Proppant Volume (m^3)
XX-6	February 29, 2016	18:07:23	20:35:03	1849.9/40.4
XX-7	March 1, 2016	08:41:33	11:37:00	1955.6/49.6
XX-8	March 1, 2016	17:07:50	19:53:00	1847.7/48.1

Archaeological prospecting using drone-towed electromagnetic and magnetic systems

Tobias Bjerg Vilhelmsen
tobjer@space.dtu.dk

SUMMARY

Drone-borne magnetic and electromagnetic sensor systems solutions have gradually expanded their use within geophysical prospecting. Magnetic and electromagnetic sensors in a drone setup allow much movability compared to a standard handhold walking survey and will also downscale the cost and risk typically associated with helicopter-borne surveys. Hence, a drone-based solution seems very attractive for magnetic and electromagnetic prospecting and could potentially replace some of the existing setups.

This abstract presents drone-towed magnetic and electromagnetic systems and datasets (Figures 1 and 2) from the same area in the southern part of Denmark (Thy), where both the magnetic and electromagnetic data show features from sub-surface structures in their raw data form. The area is known for its prehistorical flint mines, and using both magnetic and electromagnetic data will provide a better background for mapping these. To further enhance and verify any archaeological structures, we will apply levelling, micro levelling and grid the data to make interpretation possible.

The sensors and drone are off-the-shelf products, but the arrangement and construction of the survey are unique. We towed the sensors in a 6 meters wire configuration underneath the drone to avoid electromagnetic interference (Vilhelmsen and Døssing 2022) and flew with 0.7m line spacing approximately 1 meter above the surface. The vertical magnetic gradient shown in Figure 1 is measured in the same area as the quadrature response, and the legend is comparable. The quadrature response shown in Figure 2 is a stacked response from a transmission frequency of 40025Hz, 65675Hz, and 91275Hz measured with the multi-frequency broadband electromagnetic sensor GEM2-UAV from Geophex.

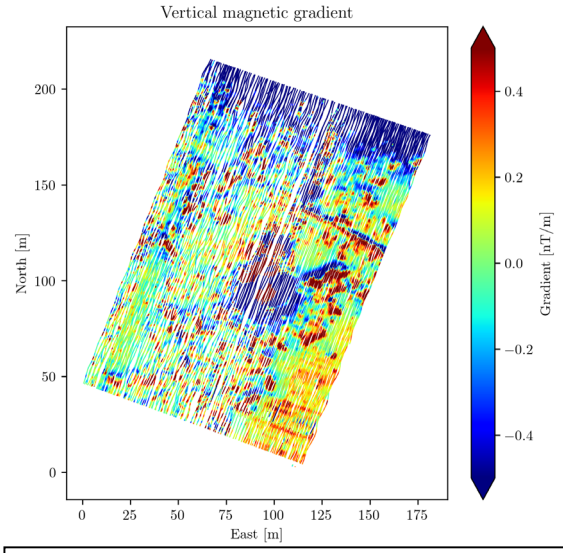

Figure 1: The raw vertical magnetic gradient from the drone-towed magnetic survey is plotted here in the limit +/- 1nT.

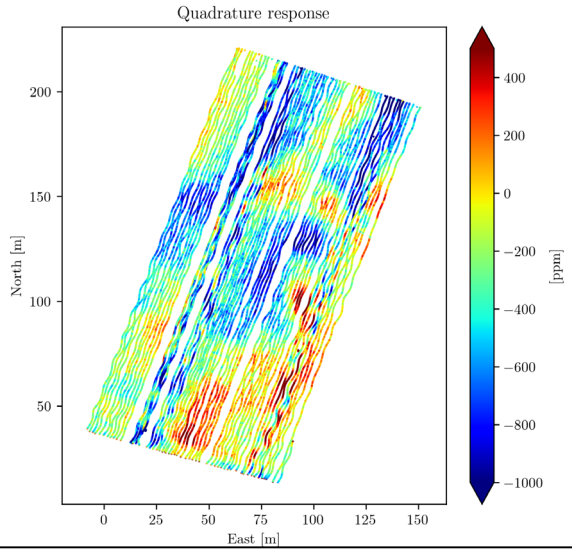

Figure 2: The stacked quadrature response from the drone-towed frequency-domain electromagnetic induction survey, with the transmission frequency of 40025Hz, 65675Hz, and 91275Hz.

Vilhelmsen, T. B. and Døssing, A.: Drone-towed CSEM system for near-surface geophysical prospecting: On instrument noise, temperature drift, transmission frequency and survey setup, EGUsphere [preprint], https://doi.org/10.5194/egusphere-2022-217, 2022.

Keywords: Drone-towed system, Archaeological prospecting, electromagnetic induction, and magnetic.

Abstract, 25th EM Induction Workshop, Çeşme, Turkey, September 11-17, 2022

Identifying the causes of the vertical component geomagnetic field anomaly at Eskdalemuir geomagnetic observatory, Scotland

G. Wang[1,2], J. Hübert[2] and K. A. Whaler[1]
[1]University of Edinburgh, UK, s2127818@ed.ac.uk
[2]British Geological Survey, Edinburgh, UK, guanren@bgs.ac.uk

SUMMARY

Magnetic field observations in the Scottish Southern Uplands reveal a dampened amplitude in the vertical component variations at Eskdalemuir when compared with the horizontal components for periods less than an hour. This relationship is not observed elsewhere. A high conductivity feature beneath Eskdalemuir has been the focal point of past literature to account for this local anomaly. However, the impact of solar activities on the external field variations at Eskdalemuir has yet to be investigated as a possible cause. This is an important factor to consider because it is assumed that large current systems are uniform at mid-latitude for geomagnetic depth sounding techniques to be applied. When this assumption is violated, the vertical magnetic field is most sensitive to the presence of non-uniform contributions. In this study we aim to characterise the space-weather driven external field contributions at different timescales to the measured vertical field component, using long time series of modern data recorded at the Eskdalemuir magnetic observatory.

Vertical magnetic transfer functions (tippers) are estimated using three-month datasets at one-minute and one-second cadences between 2003 and 2019 in order to examine their temporal variations due to the impact from source effects. Our results show that at Eskdalemuir, there are significant variations in the tipper estimates for periods above 1000 seconds between summer and winter months for the same year, especially in the Real T_x component. These findings have implications for data collected during other field campaigns with shorter recording times.

Keywords: magnetic induction, space weather, geomagnetic depth sounding, tipper

From Coast to Coast: Ongoing Magnetotelluric Data Processing for the National-Scale Survey, USMTArray-CONUS South

J. Crosbie[1], P. Bedrosian[2] and A. Kelbert[3]
[1]USGS Geology, Geophysics, and Geochemistry Science Center, Denver, CO - USA, kcrosbie@usgs.gov
[2]USGS Geology, Geophysics, and Geochemistry Science Center, Denver, CO - USA, pbedrosian@usgs.gov
[3]USGS Geologic Hazards Science Center, Golden, CO - USA, akelbert@usgs.gov

SUMMARY

The U.S. National Science Foundation's (NSF's) EarthScope program (2006-2018) produced many valuable geophysical datasets, including a large-scale, long-period magnetotelluric transportable array (USMTArray). Through EarthScope, approximately two-thirds of the conterminous U.S. was covered at a quasi-regular 70-km station spacing. NASA funded the project through 2019, and since June 2020, Oregon State University, cooperatively with the U.S. Geological Survey, has been completing the southern conterminous U.S., marching stations from California to Florida. Disseminating an ongoing, national-scale survey to the public is a novel undertaking in the magnetotelluric community, as it requires continuous processing of magnetotelluric array data, quality control for the raw time series, and maintaining an updated database of transfer functions. Transfer functions are used to estimate space weather power grid hazards; thus, timely processing is a national priority.

Here, we present the latest workflow for the ongoing real-time magnetotelluric data processing and archiving. We discuss processing and automation improvements to the workflow, including approaches to expand the range of long-period data into the "dead band." Weekly feedback is given to field crews about instrumentation issues as well as recommendations to continue data collection or to extract quality stations. We discuss the variety of field issues encountered, from cultural noise in California, to flooding issues in Florida. In addition, we focus on unidirectional noise in transfer functions in Florida and other gulf coast stations that may have oceanographic origins. The processing workflow for the USMTArray data has been expanded to work for wideband data, building upon the original USMTArray long-period workflow. We have applied the wideband processing workflow to a diversity of datasets and geologic settings including Yellowstone (Wyoming), Katmai (Alaska), and the Stillwater Complex (Montana). Finally, transfer functions are openly available and can be queried by survey (USMTArray) at the EM Transfer Function Product Query on IRIS SPUD (http://ds.iris.edu/spud/emtf).

Keywords: magnetotelluric, transfer functions, data processing, national-scale survey, archiving

ELMAR - the **EL**ectro**MA**gnetic **R**ecorder

Oliver Ritter[1], Stefan Rettig[1], Reinhard Schmitt[1], Martin Haxter[1], Carsten Müller-Brettschneider[1], Ute Weckmann[1]

[1]GFZ - German Research Center for Geosciences, oritter@gfz-potsdam.de

SUMMARY

For many years, the Geophysical Instrument Pool Potsdam (GIPP) of the German Research Centre for Geosciences (GFZ) has provided the international research community with geophysical and in particular Magnetotelluric (MT) instruments to conduct field experiments around the world. The instruments are provided free of charge, but with the obligation to archive and eventually publish the data. In total, recording equipment and sensors can be provided for about 50 broadband and 30 long-period MT stations. The most important workhorse in recent years has been the S.P.A.M. Mk IV data logger, which provides recordings in the frequency range from DC to about 10 kHz (max. 25 kHz sampling rate), with a typical power consumption of 6 – 8 W (no sensors connected).

Here we introduce ELMAR - the **El**ectro**ma**gnetic **R**ecorder - a new generation of data loggers designed and developed by the GIPP. The main advantages over existing systems are: a wider frequency range (max. 256 kHz sampling rate), lower power consumption (1.5 – 3 W), a wide range of supply voltages (8 – 36 V DC, Power over Ethernet, USB-C PD) and overall reduced dimensions and weight. User interaction is based on the *http* protocol, which means that ELMAR systems can be controlled from any web browser. A graphical user interface is provided to enter the required site information, check system status, monitor power consumption, voltages, and most importantly, the incoming data.

The analogue section provides software-controlled amplification (or attenuation) with variable gains. Gain control can be manual or automatic. All analogue inputs are differential with high impedance inputs (GΩ range). Optionally, a DC offset can be subtracted before the gain, e.g. to compensate for self-potentials of the electrical dipoles. Analogue-to-digital conversion is with 24-bit resolution.

The digital time series data can be filtered in a cascade decimation scheme, using a range of low-pass and high-pass filter settings. All data streams are continuous. Time series data, (calibrated) Fourier spectra, and MT transfer functions can be monitored (virtually) in real time. A comprehensive scheduler allows simultaneous acquisition of data streams with continuous data or pre-set (periodically recurring) intervals. An accurate time base is provided by a (dual) GNSS receiver and a voltage-controlled oscillator. The time series data is stored on SD cards.

The ELMAR recorder has a programmable test signal generator, which is used for self-testing the analogue electronics, but also for measuring contact resistances between the electrodes without polarizing them or for feeding a test signal into the induction coils.

Hybrid receiving dipole for broadband electric field measurement

N. Zorin[1,2*], D. Epishkin[1], D. Yakovlev[1] and A. Yakovlev[2]

[1]STC Nord-West, Moscow, Russia
[2]Moscow State University, Moscow, Russia
[*]corresponding author; nikita.zorin.geophys@gmail.com

SUMMARY

High-frequency electric field measurements with a regular receiving dipole with poor electrode contact are greatly influenced by capacitive leakage between the wires and the ground. At the same time, noncontact receiving lines are not generally suitable for low-frequency electric field measurements. We introduce a novel hybrid galvanic-capacitive receiving dipole, which could be used for broadband electric field measurement even with high contact resistance of grounded electrodes.

Keywords: poor electrode contact, capacitive leakage, ECR-effect.

INTRODUCTION

In electrical prospecting there are two ways to measure the electric field in the ground, that is, the contact, or “galvanic” method, and the noncontact or “capacitive” one. In the first case, the field sensor is a receiving line connected to a pair of grounded electrodes, while in the second case the receiving line includes special capacitive electrodes or just a pair of ungrounded wires. The galvanic method shows the best results when working at very low frequencies (up to ~100 Hz) and is widely used in resistivity methods, induced polarization (IP) and magnetotelluric (MT) sounding. The capacitive method shows best performance at very high frequencies (>1 kHz) and is successfully used in noncontact modifications of resistivity methods (Gruzdev et al. 2020; Kuras et al. 2006) and in radio-MT (RMT) exploration (Shlykov et al. 2020).

Unfortunately, the application of either of the indicated electric field sensors for carrying out measurements at both low and high frequencies is associated with serious difficulties. In particular, a conventional grounded array, as applied in the audio-MT (AMT) method, with a frequency ranging from ~1 Hz to ~10 kHz, requires very low grounding resistance values (<1 kΩ). Otherwise, the arising parasitic electrode contact resistance (ECR) effects may result in large distortions of the high-frequency parts of the sounding curves (Zonge and Hughes 1985). At the same time the non-contact technique is not applicable for frequencies well below ~1 kHz. This problem severely limits the applicability of such methods as AMT when working on frozen, sandy, or stony soils, rocks, etc.

Below we present a novel electric field sensor, which allows taking broadband measurements without any excessive requirements for the contact resistance of the grounded electrodes.

CLASSIC RECEIVING DIPOLE

The classic version of the receiving electric line and its simplified equivalent circuit are shown in Figure 1 (Vishnyakov and Vishnyakova 1974; Zonge and Hughes 1985). The following symbols are used in the figure: R_M (R_N) is the grounding resistance of the electrode M (N); C_M (C_N) is the capacitance between the cable M (N) and the ground; Z_0 is the complex input impedance of the receiver; D is the distance between the grounded electrodes; E is the electric field in the ground; and U_0 is the observed voltage at the receiver’s input. U_0 and E are related as follows:

$$U(\omega) = \left(\frac{0.5 + \frac{0.25}{1 + i\omega R_M C_M} + \frac{0.25}{1 + i\omega R_N C_N}}{1 + \frac{Z_{MN}(\omega)}{Z_0(\omega)}} \right) DE(\omega),$$

where ω stands for the angular frequency; i stands for the imaginary unit; $Z_{MN} = Z_M + Z_N$ is the complex contact impedance of the dipole MN; $Z_M = R_M/(1 + i\omega R_M C_M)$, $Z_N = R_N/(1 + i\omega R_N C_N)$.

Separating in this expression the coefficient K_{MN} due to wire-to-ground capacitive leakage from the coefficient K_0 due to voltage division at the receiver’s input, we get:

$$U_0(\omega) = K_0(\omega) K_{MN}(\omega) DE(\omega), \qquad (1a)$$

$$K_0(\omega) = \frac{Z_0(\omega)}{Z_0(\omega) + Z_{MN}(\omega)}, \qquad (1b)$$

$$K_{MN}(\omega) = 0.5 + \frac{0.25}{1 + i\omega R_M C_M} + \frac{0.25}{1 + i\omega R_N C_N}. \qquad (1c)$$

For a perfectly grounded dipole Equation 1 yields $K_{MN} \equiv K_0 \equiv 1$, and the observed voltage U_0 is related to the measured electrical field E with a simple expression:

$$U_0(\omega) = DE(\omega). \quad (2)$$

In a real grounded dipole, the voltage recorded by the receiver is always less than the expected value (2), and the degree of bias is governed by the values of complex coefficients K_{MN} and K_0.

HYBRID RECEIVING DIPOLE

The proposed hybrid "galvanic-capacitive" line and its simplified equivalent circuit are shown in Figure 2. It consists of an ordinary grounded dipole, supplemented with two more wires of the same length connected to each of the electrodes and stretched in different directions, as shown in Figure 2 (the far ends of the additional wire sections are insulated). Since the centers of the resulting M and N cables coincide with the grounding points of the corresponding electrodes, the effective length D of the hybrid dipole at very low frequencies ("galvanic mode") equals to that at very high frequencies ("capacitive mode"). As a result, the measured electric field in the ground is related to the observed voltage at the receiver's input as follows:

$$U_0(\omega) = K_0(\omega)DE(\omega), \quad (3a)$$

$$K_0(\omega) = \frac{Z_0(\omega)}{Z_0(\omega) + Z_{MN}(\omega)}. \quad (3b)$$

Comparison of Equations 1 and 3 shows that, irrespective of the contact resistivity of grounded electrodes, the electric field measurements with a hybrid receiving dipole are not vulnerable to the wire-to-ground capacitive leakage coefficient K_{MN}, and the only remaining source of possible distortion is the coefficient K_0 due to voltage division at the receiver's input. The influence of the latter could be minimized by using a receiver or pre-amplifier with sufficiently large input impedance Z_0 or by taking broadband *in situ* measurements of the complex contact impedance Z_{MN} at every observation site and correcting the acquired electric field data with the help of Equation 3.

CONCLUSIONS

Unlike conventional grounded or ungrounded electric field sensors, hybrid receiving dipoles are capable of performing equally well in galvanic, capacitive, and mixed operating modes. At very low frequencies this dipole behaves like a classic grounded line, at high frequencies – like a classic ungrounded line, and at intermediate frequencies there is a smooth transition from one mode of operation to another without changing the effective length of the receiving dipole. Thus, the hybrid setup successfully combines the advantages of grounded and ungrounded lines without showing their main drawbacks. The principal advantage of the hybrid dipole is its potential ability to record unbiased data in an unlimited frequency bandwidth, even under poor grounding conditions. At the same time, the way of its practical implementation proposed in our research is rather simple, requires minimal additional labor and, therefore, should not lead to a noticeable rise in the costs of field work.

REFERENCES

Gruzdev AI, Bobachev AA, Shevnin VA (2020) Determining the field of application of the noncontact resistivity technique, Moscow Univ Geol Bull 75 (6), pp. 644–651.

Kuras O, Beamish D, Meldrum PI, Ogilvy RD (2006) Fundamentals of the capacitive resistivity technique, Geophysics 71(3), pp. 135–152.

Shlykov A, Saraev A, Tezkan B (2020) Study of a permafrost area in the northern part of Siberia using controlled source radiomagnetotellurics, Pure Applied Geophys 177, pp. 5845–5859.

Vishnyakov AE, Vishnyakova KA (1974) Field excitation and measurement in electrical prospection. Nedra, Leningrad [in Russian].

Zonge KL, Hughes LJ (1985) Effect of electrode contact resistance on electric field measurements, Expanded Abstr. Technical Programme of 55th Ann. Intern. SEG Meeting, contrib. MIN 1.5. Tulsa. OK. pp. 231–234.

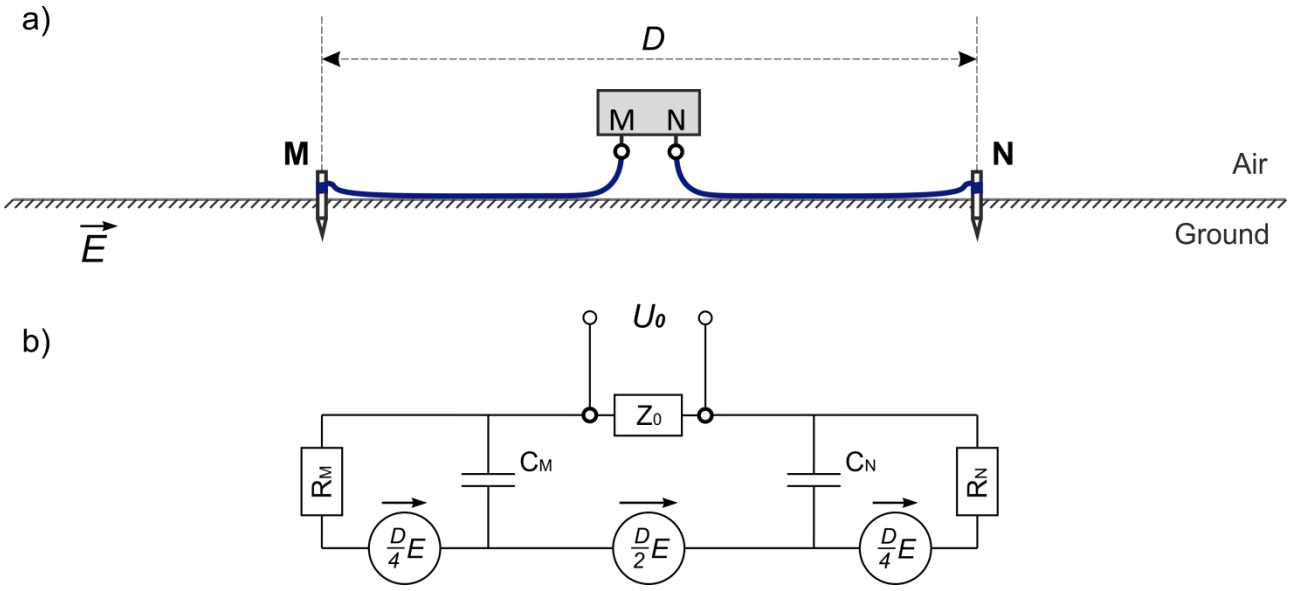

Figure 1. Classic receiving dipole (a) and its equivalent circuit (b).

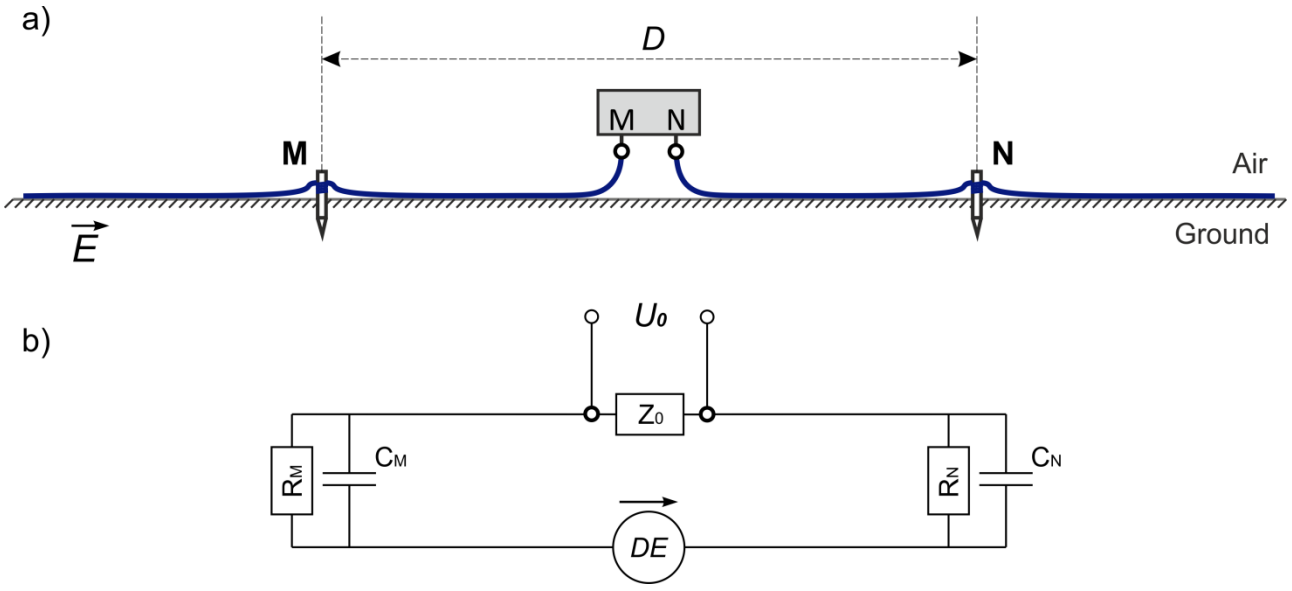

Figure 2. Hybrid receiving dipole (a) and its equivalent circuit (b).

Theory and practice of Controlled Source Audio-frequency Magneto-Tellurics: discussion on two case studies in France, at the Rochechouart impact structure and at the Strengbach catchment

P. Sailhac[1], Y. Quesnel[2], M. Lajaunie[3], S. Warden[4], C. Camerlynck[5], P. Lambert[6], J.-P. Malet[3]
[1]University of Paris-Saclay, France (UMR8148 GEOPS), pascal.sailhac@universite-paris-saclay.fr
[2]Aix-Marseille Université, France (UMR730 CEREGE), quesnel@cerege.fr
[3]University of Strasbourg, France (UMR 7063 ITES), m.lajaunie@hotmail.fr
[4]Hyperion, France, sheldon.warden@gmail.com
[5]Sorbone University, France (UMR 7619 METIS), christian.camerlynck@sorbonne-universite.fr
[6]Center for International Research and Restitution on Impacts and on Rochechouart, France (CIRIR), philippe.lambert@gmail.com

SUMMARY

Audio-frequency Magneto-Tellurics (AMT) is a passive noninvasive prospecting method; it is based on the electromagnetic induction in the ground from background electromagnetic plane waves caused by far distance sources of natural or anthropic origins; their frequency range is 20 Hz-20 kHz. Controlled Source Audio-frequency Magneto-Tellurics (CSAMT) method is an alternative to AMT which is considered to cope with practical field situations where background anthropic noise from near sources has high amplitudes compared to other incident electromagnetic waves; controlled source can be used to avoid high acquisition times or advanced robust processing that are necessary in AMT (Larnier et al. 2018). Controlled source is particularly interesting at frequencies in the so-called “AMT-dead band” of low natural activity near 1-3 kHz, corresponding to skin-depth of tens to hundreds of meters, depending on the underground resistivities.

In CSAMT theoretical principles, transmitter must be a set of large electric dipoles (hundreds of m) located far from the receiver area (tens of km); this geometry is necessary to eventually obtain good estimates of all impedance tensor components. However, actual field situations often impose different configurations with shorter dimensions, and one should deal with the measured electric and magnetic records by using the more general theoretical framework of Controlled Source Electro-Magnetic (CSEM) methods.

We consider two case studies of CSAMT surveys whose size of the electric transmitter antenna is relatively small (100-300 m). One study shows of a profile at the Rochechouart-Chassenon impact structure, France (Quesnel et al. 2021); CSAMT was used because of one High Voltage power line crosses the breccia area of interest. The other study shows the investigation of the Strengbach catchment, France (Lajaunie et al. 2022); CSAMT was used because one telecommunication antenna is on the summit, at one boundary of the catchment. Papers cited above essentially show CSAMT apparent resistivities and their inversion with shallow ERT resistivities; a very few information has been shown concerning the underlying CSAMT questions: Experimental set-up as well as simulation of radiation patterns, data processing, apparent resistivities and inversion will be discussed at EMIW22.

Keywords: Controlled-Source Audio Magneto-Tellurics, CSAMT, Power line noise, radiation pattern

References

Lajaunie M, Gance J, Sailhac P, Malet J-P, Warden S, Larnier H (2022) Hydrogeological structure of a granitic mountain catchment inferred from multi-method electrical resistivity datasets. Geophysical J. Int. (under review)

Larnier H, Sailhac P, Chambodut A (2018) Detection and characterization of lightning-based sources using continuous wavelet transform: application to audio-magnetotellurics. Geophysical J. Int. 212(1):103 - 118. doi:10.1093/gji/ggx418

Quesnel Y, Sailhac P, Lofi J, Lambert P, Rochette P, Uehara M, Camerlynck C, (2021) Multiscale geoelectrical properties of the Rochechouart impact structure, France, *Geochemistry, Geophysics, Geosystems* 22(9). doi:10.1029/2021GC010036

The maximum possible distances to the remote reference when working in medium and high latitudes

D. Epishkin[1*], A. Gubina[1], E. Shirokova[1], A. Yakovlev[1,2]
[1]Nord-West Ltd, Moscow, Russia
[2]Moscow State University, Moscow, Russia
[*]corresponding author: dmitri_epishkin@mail.ru

SUMMARY

This work compares the maximum possible distances to a magnetotelluric remote reference when operating in middle and high latitudes. Several illustrative examples show that the maximum distances at which the magnetotelluric fields correlate strongly depend on the latitude. In 2020-2021, we took magnetotelluric measurements in Yakutia region, on the regional profile 4-SB. Profile length is 900 km. Throughout all the work, registration was carried out at a fixed remote reference site. We analyzed the efficiency of using a remote reference for sites located at different distances from it (from 0 to 650 km). Also, we analyzed quality of horizontal magnetic tensors for sites located at different distances from each other. We used all measurements along the profile, which made it possible to study in detail the correlation of fields at different distances. The work carried out showed that at latitudes of about 60 degrees it makes sense to locate a remote reference at a distance of no more than a few hundred kilometers from the measurement sites. At large distances, the correlation between low-frequency field is lost, which must be taken into account when designing work in these latitudes. When carrying out work in middle latitudes, the distances at which fields correlate are increasing, and it is possible to locate remote reference at distances up to a thousand kilometers.

Keywords: remote reference, horizontal magnetic tensor, data processing

Abstract, 25^{th} EM Induction Workshop,Çeşmeı, Turkey, September 11-17, 2022

New long-period magnetotelluric measurements to improve ground electric field modelling in the UK during geomagnetic storms

E. Eaton[1], J. Huebert[1], C. Beggan[1], A. Montiel-Alvarez[2], A. Thomson[1], C. Hogg[3] and D. Kiyan[3]
[1]British Geological Survey, Edinburgh, UK, eleaton@bgs.ac.uk
[2]University of Edinburgh, a.montiel@ed.ac.uk
[3]Dublin Institute for Advanced Studies, Dublin, Ireland, duygu@cp.dias.ie

SUMMARY

To assess the hazard posed by space weather events to grounded technological infrastructure, such as Geomagnetically Induced Currents (GICs) in the UK and Irish power transmission networks, a key component is to accurately model how the ground electric field varies during geomagnetic storms. A model of electrical conductivity of the subsurface based on magnetotelluric data can be used for this purpose. For the UK-funded SWIMMR-SAGE (N4) project, we are currently planning to collect long-period MT data at more than 45 sites across England, Southern Scotland and Wales with $\sim$50 km grid spacing over two years between 2021 and 2023. Measurements of up to six weeks at each site are made using a rolling deployment of five LEMI-417 systems.

The measured magnetotelluric impedances provide a reliable method to compute the ground electric fields necessary for the elucidation of GIC estimates in the high voltage power grid model of Britain. Geoelectric fields can also be used to infer risk to pipelines and rail line infrastructure. Results from some of the 30 sites collected so far are presented, including magnetotelluric impedances, ground electric field data measured during large space weather events between May 2021 and June 2022, and improvements to the modelled geoelectric field at sites across the UK. Future work in the SWIMMR-SAGE project includes using the improved model of electrical conductivity of the subsurface and modelled geoelectric fields to provide nowcast and forecasts of the space weather impacts on ground-level infrastructure in Britain.

Keywords: Magnetotellurics, Space Weather

Hilbert transform of the frequency normalized impedance data: Application to the dispersion relations in magnetotellurics

Ahmet Tugrul Basokur
Lemnis Geosciences, basokur@ankara.edu.tr

SUMMARY

The real and imaginary parts of the Fourier transform of a causal signal can be obtained from each other by the Hilbert transform. The numerical computation can be carried out by the Fast Fourier Transform or the convolution of the data with an appropriate Hilbert kernel. However, magnetotelluric data are usually unequally sampled because the data points with less noise contribution are selected. A method and Python software are developed for the Hilbert transformation of unequally sampled data and applied to the real and imaginary part of the frequency normalized impedance to examine if the dispersion relations are satisfied for a given impedance tensor. The method involves the reconstruction of the measured data by a linear combination of an analytic interpolation function distributed along the horizontal axis. Then, the decomposition coefficients that provide a fit between the measured and the reconstructed data are solved by the linear least-squares method with singular value decomposition. Finally, the discrete Hilbert transformed data are constructed at any desired abscissa values by the sum of the analytic Hilbert transform of the interpolation function using the decomposition coefficients solved in the previous step. Examples from the magnetotelluric synthetic and field data, including out-of-quadrant phase cases, are given.

It is demonstrated that the dispersion relations of the frequency normalized impedance function are valid for all types of structures, including 1D, 2D and 3D cases. A set of theoretical data calculated for a 3D subsurface by ModEM software and corresponding dispersion curves computed with the suggested algorithm provided perfect fits. The dispersion relation for the FNI function is also valid for out-of-quadrant phase cases caused by 3D strong resistivity contrasts. However, electrical anisotropy and galvanic distortion could also be considered to explain the out-of-quadrant phase. Therefore, the validation of dispersion relations in such cases needs to be investigated.

Keywords: Magnetotellurics, Causal systems, Dispersion relations, Hilbert transform, Unequally sampled data.

Synchronization optimization providing for MT stations at grid survey

A. Prystai[1], V. Pronenko[1] and A. Bondarev[2]
[1]LLC "LEMI", Lviv, Ukraine, pron@isr.lviv.ua
[2]Lviv Polytechnic National University, Lviv, Ukraine, bondap@ukr.net

SUMMARY

Magnetotelluric (MT) survey is a leading electromagnetic method to probe the electrical conductivity structure of the Earth at depths ranging from few tens of meters to several hundreds of kilometers. As passive exploration technique, MT involves measuring fluctuations of the natural electric and magnetic fields in wide frequency range in two orthogonal directions at the Earth' surface. Recent application of multiple MT stations survey – remote reference or grid stations location – together with the modern computational technology allows significantly improve the quality of the results by eliminating noise and improving the signal-to-noise ratio and, as a consequence, to determine the parameters of Earth' geoelectric cross-section with a high degree of reliability.

It has to be stressed that the successful application of MT method greatly depends on the used instrumentation parameters. For grid survey, especially important is the precise synchronization of measurements simultaneously in every location. To organize the synchronous operation of all instruments, the systems for global positioning and time reference - GPS receivers - are widely used. However, despite GPS availability, the normally obtained synchronization precision is not enough because of the instability of the GPS synchronization signal, especially in the moments of the GPS signals loss.

To raise the synchronization accuracy, a new structure of the synchronization circuit has been developed. A linearized model of the circuit was constructed and its computer simulation was carried out. The stochastic model of a set of synchronization circuits is developed what allowed us to derive the equation of the evolution of cumulates of the random process of the clock. The computational experiments made it possible to identify the necessary parameters of the model and then the verification of the results was carried out using the structure of the broadband MT station LEMI-423. The experimental results confirmed a significant reduction of the obtained error from the instability of the GPS synchronization signal. As a result, we achieved sampling timing accuracy better than ± 60 ns, without phase jumps and distortion. To this, what is important for an autonomous field instrument, the obtained power consumption of the synchronization circuit was very low, what allowed us to reach the total power consumption of the LEMI-423 MT station below 1.7 W.

In conclusion, the short description of LEMI-423 MT station and its parameters are given.

Keywords: GPS synchronization, MT station, stochastic model.

Smart data selection – Using machine learning for RMT data processing

A. Platz[1], U. Weckmann[1,2]
[1]Helmholtz-Zentrum Potsdam, Deutsches GeoForschungsZentrum, Potsdam, Germany,
aplatz@gfz-potsdam.de
[2]University of Potsdam, Institute of Geoscienes, Potsdam, Germany

SUMMARY

The Radio-Magnetotelluric (RMT) method is a geophysical near-surface imaging technique with a broad range of possible applications. The GFZ Potsdam has recently acquired a newly developed horizontal magnetic dipole transmitter that allows the application of the RMT method even in regions with an insufficient coverage of radio transmitters serving as source signal. First measurements were conducted at three different locations in Chile in 2020. We have full control over the subsequent data processing by storing the raw time series. Processing the entire time series has a couple of drawbacks: The different emitted frequencies are transmitted in a sweep implying that only a smaller fraction of the time series contains the required signal for a particular target frequency and leading to an unfavourable signal-to-noise ratio. However, since it is technically impossible to have the same time base for the data logger and the transmitter with an accuracy of a few nanoseconds, an automated detection scheme is required to find time segments that contain the transmitter signal. Usually, several Gigabytes of raw time series are collected during field measurements, making manual editing and supervision of the time series virtually impossible. However, a careful selection of appropriate time segments is essential for the success of the data processing. Since the underlying physics are comparable to those of low-frequency MT, the same tools for statistical time series analysis and data processing can be used with partly significant modifications. The processing tools at GFZ include the modular processing suite EMERALD, which was originally designed for MT processing, but has recently been quickly adapted to process RMT data. One main difference is that in RMT the transmitter data is considered as signal, while in natural source MT this would be regarded as (near-field) electromagnetic noise that needs to be removed using automated robust statistical approaches. To address the challenge, machine learning algorithms have a high potential to solve both problems. Initial experience was gained with a recurrent neural network approach in order to identify suitable time segments (Patzer & Weckmann, EMTF 2021 – conference contribution and personal communication). However, many questions remained open, e.g. if other machine learning algorithms can result in better performances, which machine learning algorithms are in principle suitable for the characteristics and properties of RMT time series or which parameters should be used as input variables for the algorithms. A large number of machine learning algorithms exist, which can be divided into different groups according to their operating principle and their activity fields. We will test unsupervised methods, especially for clustering the data, as well as supervised methods as e.g. logistic regression, support vector machine or neural networks. We will present first results using the RMT data from Chile as training data set.

Keywords: Radio-Magnetotellurics (RMT), Machine learning, Neural networks

Shaky data and where to find them – MT on frozen lakes

C. Patzer[1], U. Autio[1] and J. Kamm[1]
[1]Geological Survey of Finland, GTK, cedric.patzer@gtk.fi

SUMMARY

Finland is commonly advertised as – a land of thousand lakes – in the media and public. However, in reality there are approximately 168 000 lakes covering up to 10% of the land area of the country. This large number of lakes can seriously obstruct planning and execution of any geophysical (in particular EM) fieldwork.

Within the BATCircle2.0 project (funded by Business Finland) GTK is currently collecting 3D MT data in north-eastern Finland north of the city of Kuusamo. In the centre of the study area lies the 240 km^2 lake Yli-Kitka which by applying traditional MT fieldwork procedures would cause a large gap in station coverage. As Finnish lakes reliably freeze over in winter, we used this opportunity to conduct a pilot study on the feasibility of measuring MT on the lake ice.

In beginning of February 2022, we installed 5 MT sites on the frozen lake Yli-Kitka with a site spacing of 2 km. For reference purposes we installed an additional site on land directly at the shoreline of the lake. While we obtained good data quality at the land site, we found very poor data quality between Periods of 100 s to 1 s at all lake sites. Closer inspection shows that this poor data quality is caused by a spurious signal on the magnetic channels. The measured signal is approximately 2 orders of magnitude larger than the natural MT signal simultaneously recorded at the land site, while the electric field channels seem to be unaffected by this effect.

This spurious signal is likely caused by movement of the lake ice due wind. This effectively prohibits standard single site processing of the measured time series to obtain MT transfer functions. Our findings are in accordance with McNeice and Jones (1998). One way to deal with such “shaky data” is to use magnetic fields from the land site to compute MT transfer functions. We are also discussing other options to remove or filter the spurious signal from the time series itself prior to any transfer function estimation.

Despite these challenges and difficult conditions in the field we found this pilot study to be successful. It shows that with some care it is possible to collect broadband MT data on frozen lakes. Allowing for easier survey planning with lake sites measured in winter and land sites during summer. In addition, being able to perform fieldwork during wintertime may also allow access of large frozen swamp areas which may not be accessible during summer months.

Keywords: MT, time series

McNeice, G. and A.G. Jones, 1998. Magnetotellurics in the frozen north: measurements on lake ice Contributed paper at: 14th EM Induction Workshop, Sinaia, Romania, August 16-23.

Results of FDEM-(CS)AMT test studies on the Alexandrovka area

E.Ermolin[1], N.Zorin[2], D.Epishkin[2] and D.Sapunov[1]
[1] "GM-Service" LTD, geophysmethod@gmail.com
[2]"Nord-West" LTD, mail@nw-geophysics.com

SUMMARY

The article presents the results of electrical surveying acquisition tests carried out in the winter of 2021 in the area of the educational and geophysical base of the Faculty of Geology of the Lomonosov Moscow State University "Alexandrovka" in the Kaluga region. The purpose of the experimental and methodological work was to obtain data in the "dead" frequency range of the audio magnetotelluric sounding (AMT) range. The paper describes the methodological features of the work performed by the method of frequency domain electromagnetic sounding (FDEM) and AMT with a controlled source (CSAMT). The obtained result is compared with a priori geological information, with geophysical studies of previous years. Some methodical features of test studies have been described in this paper.

Keywords: audio-magnetotelluric method, frequency-domain electromagnetics, skin-effect, resistivity

INTRODUCTION

The authors of this article performed test surveys of AMT and FDEM. The main purpose and objectives of these studies are as follows:

- combining the AMT technique with the method of frequency domain electromagnetic sounding (FDEM) and AMT with a controlled source (CSAMT) with the possibility of using the same set of equipment to record data from all methods;
- obtaining CSAMT data in areas complicated by cultural noise, as well as in the "dead" frequency range of AMT;
- obtaining data on the transverse resistance parameters of insulator layers based on the interpretation of the individual components frequency characteristics (curves) of frequency sounding.

Methods

Frequency domain electromagnetic sounding method providing information about changes in the resistance of the medium with depth by studying the frequency dependencies of the components of the electromagnetic field created by the artificial source.

In this paper, a horizontal electric dipole was used as a source. In a medium with resistivity ρ, the components of electric and magnetic fields in the far zone ($\omega\mu_0 r/\rho \gg 1$) of a source of HED type with dipole moment $P_{AB} = I_{AB} \cdot AB$, oriented along the x-axis, are expressed as follows (Modin et al. 2018):

$$E_x = \frac{P_{AB}(3\cos^2\varphi - 2)}{\pi r^3} \cdot \rho,$$

$$H_y = \frac{1}{\sqrt{-i\omega\mu_0}} \frac{P_{AB}(3\cos^2\varphi - 2)}{\pi r^3} \cdot \sqrt{\rho},$$

$$H_z = \frac{1}{-i\omega\mu_0} \frac{3P_{AB}\sin\varphi}{2\pi r^4} \cdot \rho, \quad (1)$$

$$Z_{xy} = \frac{E_x}{H_y} = \sqrt{-i\omega\mu_0\rho},$$

r – distance from source, φ – azimuth of the measurement point. Since the method works in the far zone, it is necessary to use a maximum spacing and a maximum current to perform measurements, which in turn leads to the need to use power generators and good grounding (<30 Ohm · m).

To achieve the objectives, the authors made an assessment of the parameters of the installation and practical measurements. Experimental and methodical works were performed on the territory of the scientific and educational geophysical base of the Lomonosov Moscow State University geological faculty "Alexandrovka" in Kaluga region.

AMT field measurements were performed with measurement of five components of the electromagnetic field. NORD stations (Nord-West LTD) were used as measuring devices, IMS 5 sensors (Vega LTD, Nord-West LTD) were used to register the magnetic field components, providing operation in the frequency interval from 1 Hz to 20 kHz. The electrical components of the field were recorded using nonpolarizing graphite electrodes NW-4 (LTD "Nord-West"). The works was performed using a cross-shaped system with a central electrode Figure 1. The length of each electrical line was 100 m (2 legs of 50 m). Azimuths of system of electrical lines and horizontal magnetic sensors: x – 73°, y – 163°. The x-axis is directed parallel to the HED. Induction sensors (two

horizontals, one vertical) were buried in the ground. The electrodes were grounded in pits 0.2–0.3 m deep in a mud mixture moistened with salt water.

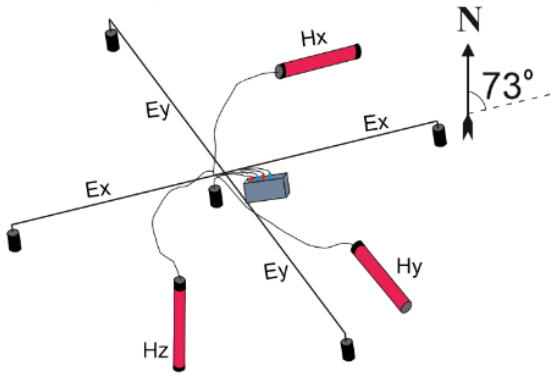

Figure 1. Measuring system for AMT, FDEM и CSAMT.

Evaluation of system parameters

Works by the FDEM are performed in a far zone condition corresponding to ($\omega\mu_0 r/\rho \gg 1$). In practice, in order to achieve the far-zone conditions, so that the distance from source exceeds the effective depth of the skin layer by several tens of times, using the very low frequency (Modin et al. 2018). The depth of the skin layer is calculated using the formula:

$$h_\delta \approx \frac{\sqrt{\rho T}}{2}\ (\text{km}) \qquad (2)$$

Let's estimate the distance satisfying the far zone condition for a structure with an average electrical resistivity of the order of 150 Ohm·m. This resistivity was determined by the results of acquisition tests performed by the authors in 2019 (Ermolin et al. 2020). The final stack according to the results of acquisition tests in 2019 is shown in Figure 2. The curve in Figure 1 is measured in the same area. A minimum at a frequency of 50 to 100 Hz corresponds to a conductor at an altitude of 0 to -100 meters in Figure 3. Thus, to study the "dead" frequency range, information is needed on the average electrical resistivity of rocks located above the altitude of 0 m. The average level of resistance in the depth range is an average of 150 Ohm · m.

In order to close the "dead" range of AMT, it is necessary to obtain high-quality data for the frequency of 800 Hz and above. The depht of the skin layer at 800 Hz can be estimated as:

$$h_\delta \approx \frac{\sqrt{\rho T}}{2} = \frac{\sqrt{\frac{150}{800}}}{2} \approx 0.2\ (\text{km}) \qquad (3)$$

As a result, a distance from the source of 6 km was used for work by the FDEM, providing the realization of the far zone condition ($\omega\mu_0 r/\rho \gg 1$).

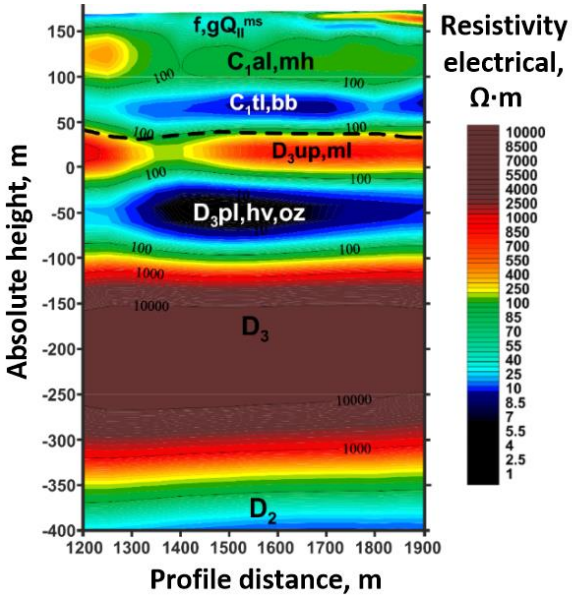

Figure 2. Electrical model from 2D inversion data AMT and ERT-IP (Ermolin et al. 2020).

The length of the transmitter line is 1150 m. The grounding resistance of the AB line is 30 Ohms, which made it possible to use a current of up to 7 A. The configuration is shown in Figure 3. The same figure shows the position of the profile along which the electrical model is built, shown in Figure 2. When performing the work of the FDEM, the most time-consuming is the organization of the HED (work shift of 4 operators), while the installation time of the measuring device is from 15 to 45 minutes (by two operators).

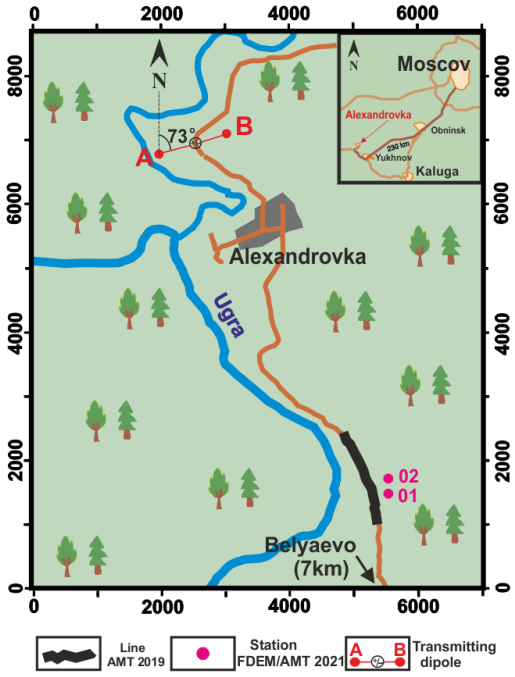

Figure 3. Scheme of acquisition tests perfomed

Due to the absence of time limits, all possible

frequencies of the transmitter GER-1000 from 1.22 Hz to 5000 Hz were used. The total time to use all frequencies (1.22, 2.44, 4.88, 9.77, 19.53, 39.06, 78.13, 156.25, 312.5, 625, 1250, 2500, 5000 Hz) was 15 minutes. A problem occurred while working with the transmitter. Due to the complex character of the transmitter line resistance at high frequencies, the output current had to be reduced to 3-4 A and the signal lost its rectangular shape, characteristic of a stabilized meander at low frequencies. An example of an unstabilized current is shown in Figure 4.

The lack of current stabilization is not a problem for the CSAMT method, as well as the classical FDEM, provided that the factual waveform in the transmitter line is registered witch a Hall sensor and taken into account during processing.

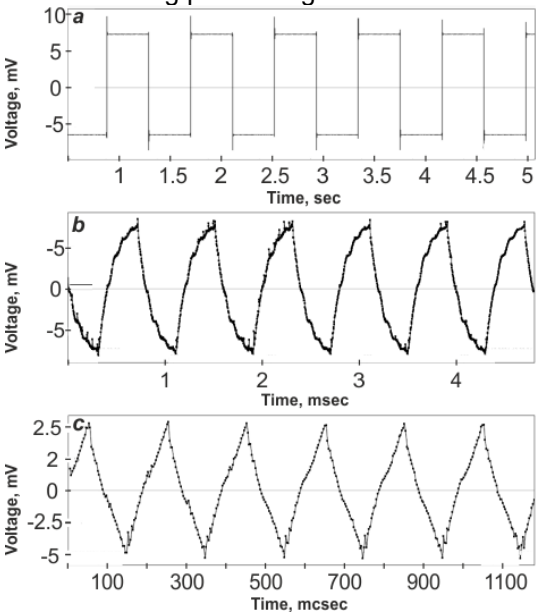

Figure 4. Example of transmitter line current record for frequencies: a) 1.22 Hz b) 1250 Hz c) 5000 Hz

Results

The result of processing of the FDEM field data are the curves of the electrical (Ex), magnetic components (Hy, Hz) and impedance (Zxy), shown in Figures 6-9.

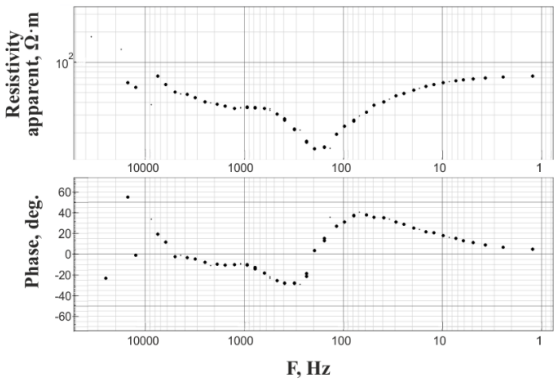

Figure 5. Component Ex, PK 01

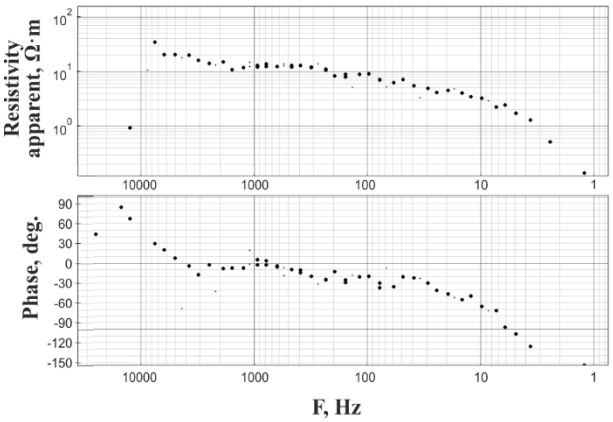

Figure 6. Component H_y, PK 01

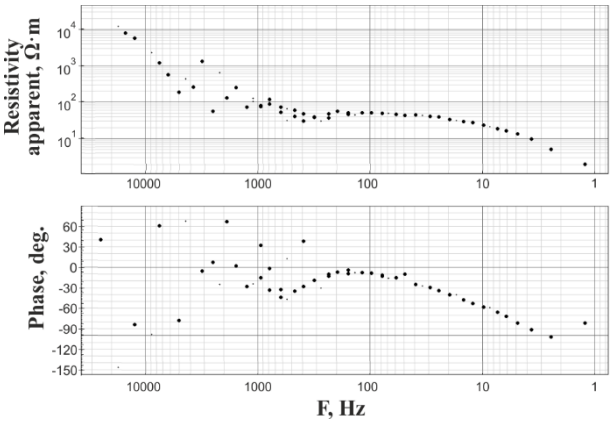

Figure 7. Component H_z, PK 01

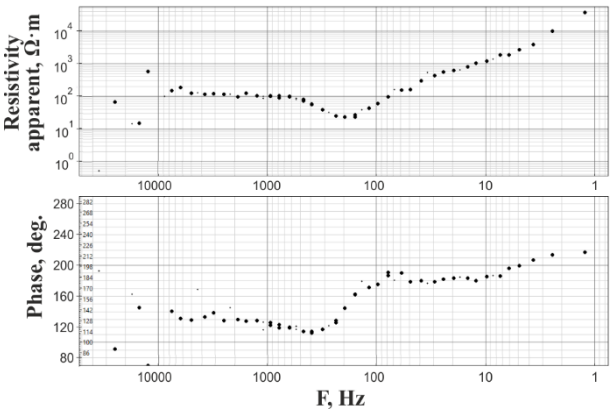

Figure 8. Component *Z*xy, PK 01

To interpretation the data of FDEM and CSAMT, selection was applied within the framework of 1D models, using the program CsmtSolver (author Dmitry Epishkin). An example of the selection performed for the CSAMT of the Zxy impedance component is shown in Figure 10.

Using a priori geological information the following geological interpretation of the model can be carried out at measurement point 01. The first three layers are interbedding of sands and loams. Next, a more conductive layer is clay with inclusion of coals of the Tula formation and Bobrikovian horizon of the Lower Carboniferous.

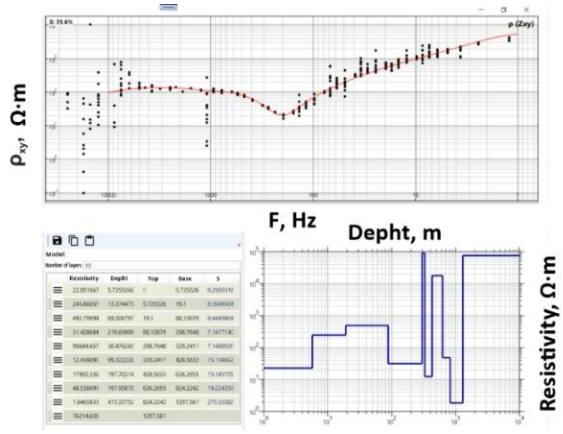

Figure 9. Selection of the geoelectric model by the Zxy impedance of frequency sounding in the CsmtSolver program window. PK 01.

Below is a high-resistivity layer represented by limestones, dolomites and marls of the Upper Devonian. This formation in the model is represented by the fifth, sixth and seventh layers. This range of resistances was selected to account for vertical anisotropy. The conductive layer is connected to the aquifer, the layers with high resistivity correlate with gypsified limestones, marls and dolomites. The eighth layer is terrigenous sediments, represented by clays, mudstones and sands of the Middle Devonian. The ninth layer is a conductive layer of Vendian sandstones with interbedded clays in which high-salt water is present. The tenth layer is a crystalline basement with high resistivity, composed of crystalline shists and gneisses of Lower Proterozoic and Archean age.

The result of AMT field data processing are splines. Figure 10 (left). At the next stage, a 1D inversion was performed using the AMT invariant curve Figure 10 (right). The results in Figure 10 (right) do not contradict the results of 2019 (Ermolin et al. 2020).

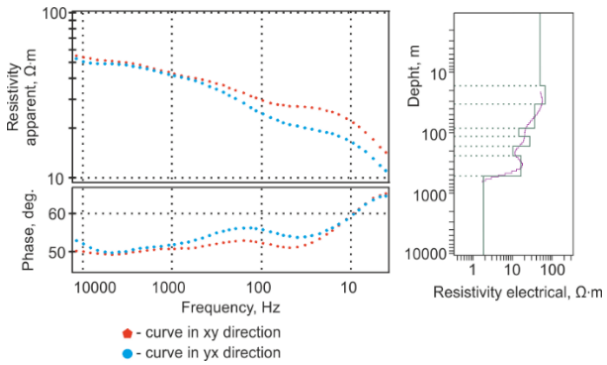

Figure 10. Example spline (left) and 1D inversion (left) smooth Occam inversion (model marked in pink) and eight-layer model (in green).

Conclusion

As a result of the acquisition tests, it was shown that the application of the FDEM allows obtaining data in the "dead" range of AMT for a component parallel to the direction of HED. In this experiment, the levels of the AMT and CSAMT curves did not coincide according to the measurement results.

In this test studies, it was not possible to perform an appropriate selection of the 1D resistivity model for the Ex component of the FDEM. But the results of the 1D interpretation of the AMT and CSAMT data are comparable. According to CSAMT data insulator layers (dolomites with interbedded gypsum) have a higher resistance value than according to the results of the interpretation of the AMT curve. Thus, the CSAMT results most correctly reflect the high resistances of gypsified dolomites, the resistivity of which exceeds tens of thousands of Ohm·m.

Importantly, it is necessary to register the transmitter line current when performing FDEM, because the signal at frequencies above 1000 Hz is not a correct meander.

References

Berdichevsky MN and Dmitriev VI. [2009] Models and methods of magnetotellurics. Book: Scientific World, 2009. 680 p.

Chave A.D., Jones A.G. [2012] The magnitotelluric method – theory and practice. Cambridge University. Press, 2012. 552 p.

Ermolin, E.Y., Ingerov, O., Yankilevich, A.A., Pokrovskaya, N.N. [2019] AMT soundings in the dead band within the chukotka region (Russian Far east). Journal of Mining Institutethis link is disabled, 2019, 236, p. 125–132

Ermolin, E., Kulikov, V., Melnikov, A., Asoskov, A. [2020] Features of experimental-methodical electrical exploration studies at the MSU training area (Aleksandrovka village). Engineering and Mining Geophysics 2020 - 16th Conference and Exhibition (Abstract)

Modin I.N., Yakovlev A.G., Pushkarev P.U.., Shevnin V.A. and others. [2018] geoelectric survey: a manual on electrical survey practice for students of geophysical specialties. Volume 1 - 2nd ed., revised. and ex. - Tver: "PolyPRESS", 2018 - p. 274

Rokityansky I.I. [1975] Investigation of electrical conductivity anomalies by geomagnetic-variation profiling. Kiev: "Scientific invention". 1975, p. 279

Vozoff K. [1972] Geophysics. 1972, 37, p. 98-141

Abstract, 25th EM Induction Workshop, Çeşme, Turkey, September 11-17, 2022

DISTRIBUTION OF SOURCE EFFECTS IN THE HIGH LATITUDE MAGNETOTELLURIC DATA

Sarasija Sanaka[1] Anne Neska[1]

[1]Institute of Geophysics Polish Academy of Sciences, Warsaw, Poland.,
ssanaka@igf.edu.pl

SUMMARY

The magnetotelluric (MT) and related passive electromagnetic induction methods work on the condition that the far-field assumption is fulfilled by the source signals. Whereas possible violations of this condition due to anthropogenic signals have been understood well, it becomes more and more evident that part of the natural electromagnetic signals is not homogeneous either, and unlike told in textbooks these near-field effects are not limited to polar and equatorial electrojet regions or the Sq variations with their harmonics. Such evidence comes mainly from long-term (monitoring) data, which results in transfer functions and induction arrows. The latter ones are most affected by source effects which expresses itself in the fact that they are not constant in time in a way that cannot be explained by changes in subsurface conductivity. To assess this problem, we have considered four years long time-series data of 15 stations from the IMAGE (International Monitor for Auroral Geomagnetic Effects) network. We have processed these data with Egbert's processing and also applied the Remote Reference Technique, which is necessary to eliminate cultural noise. Preliminary results clearly show temporal changes. In the induction arrows, the nonstationarity behaviour is prominently seen in the high but also in mid-latitude regions. The spatial and temporal pattern these source effects are exhibiting are partly familiar, in particular for seasonal changes in mid-latitude, and partly not understood well yet. We will further investigate them with the aim to identify their generation mechanism and to recommend ways to avoid MT results being influenced by them.

Keywords: Source effects, Seasonal changes

On the correctness of using plane-wave assumption and two-channel acquisition systems in MT exploration at high latitudes

D. Yakovlev[1], E. Pogrebnykh[2], D. Epishkin[1] and A. Yakovlev[2]
[1]STC Nord-West, stcnordwest@gmail.com, Moscow, Russia
[2]Lomonosov Moscow State University, Moscow Russia

SUMMARY

In 2019 about 5,000 MT sites were acquired during an MT survey in the Russian Arctic across the area of 120x80 km with a uniform site distribution over the network of 1x2 km. A single remote site was used for the remote reference processing. In the summertime we got a record at the reference site with duration for more than three months. These data allow us to better understand the applicability of the plane-wave assumption in such regions, since some experts suggest that application of classic Tikhonov-Cagniard source model in polar latitudes could lead to erroneous results due to the peculiarities of the local MT field source and proximity to it.

The whole record at the reference site was processed by 1-day fragments. Careful analysis of the frequency-time sections and graphs of variations of amplitude and phase of the impedance for 3 months, and graphs of their spectral density, we conclude that in the area of work located about 72° N the source-effect on the impedance tensor estimations is insignificant. Classic data processing based on plane-wave assumption yielded stable values of the impedance tensor and MT curves.

Maps of the horizontal magnetic tensor for several characteristic frequencies showed that within the study area the distance at which the magnetic field varies for less than 5% in amplitude and 3° in phase is about 2-3 km. Within this distance it is possible to consider the magnetic field recorded at an adjacent station as that recorded at the survey site, which could be employed for data processing acquired by two-channel MT acquisition systems.

Keywords: the plane-wave assumption, high latitudes, two-channel acquisition system

Measurement of noise characteristics of graphite electrodes in the field and comparison with other types of non-polarizing electrodes

D. Epishkin[1], N. Zorin[2]
[1]STC Nord-West, dmitri_epishkin@mail.ru
[2]STC Nord-West, nikita.zorin.geophys@gmail.com

SUMMARY

Graphite electrodes have been successfully used in MT measurements by a number of Russian companies for decades. This type of electrode has proven itself extremely well in practice. During the continuous use of graphite electrodes, an optimal design was developed, which made it possible to achieve a low level of noise and high reliability in various climatic conditions. However, up to the present time, this type of electrodes has hardly been mentioned even in large western review papers. This work aims to correct this omission. In the course of this work, a technique for measuring electrode noise was developed and an attempt was made to investigate the noise characteristics of graphite electrodes, as well as to compare them with other types of electrodes. It was found that the noise level of graphite electrodes is slightly lower than that of the widely used $Pb\text{-}PbCl_2$ and $Cu\text{-}CuSO_4$ electrodes. Also, this work demonstrates the importance of proper electrode maintenance for the best performance.

Keywords: magnetotelluric, non-polarizing electrode, parallel test

INTRODUCTION

Electrodes are the most critical component in the measurement of the telluric response, and indeed are often the weakest component of any MT system. If reasonable care is taken with all other aspects of the electric measurements, then it is the electrode noise that limits the quality of the electric field measurements (Petiau & Dupis 1980).

Most land MT surveys in the world are carried out with porous-pot $Pb\text{-}PbCl_2$ or $Cu\text{-}CuSO_4$ electrodes. In addition to these two types of non-polarizing electrodes, in the post-Soviet space, a number of geophysical companies actively employ graphite electrodes. Our numerous comparative tests and many years of practical experience show that graphite electrodes have an extremely low noise level and give good results over a wide frequency range under a wide range of temperature and humidity conditions.

This type of electrodes is not widely used outside Russia. Moreover, in a number of publications it is noted that graphite electrodes have a high noise level comparable to the level of the telluric field and, as a result, their use is not recommended for MT surveys (e.g., Petiau 2000; Ferguson at al. 2012). This contradicts our experience in the practical application of electrodes of various types.

The production technology of graphite electrodes was developed by Soviet geophysicists at the dawn of the MT method, and since then this type of electrode has not lost its relevance.

In a simplified form, graphite electrode is basically just a graphite rod placed in Zn-graphite powder (Figure 1). But, obviously, to make a high-quality electrode, it is important to comply with a number of conditions. Among other things, it is important to monitor the quality of all contacts. For example, the contact between the rod and cable must be well isolated from the environment; the shell of the electrode must be well permeable to moisture, etc.

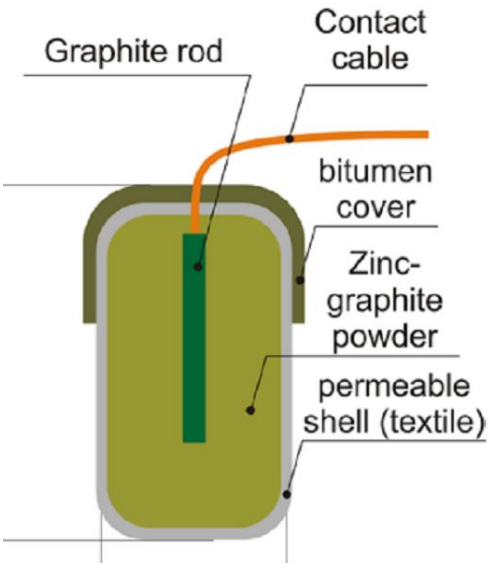

Figure 1. Graphite electrode.

If all conditions are met, then you can get a sensor with decent characteristics.

The main goal of this work is to study the noise characteristics of graphite electrodes and compare them with other types of non-polarizable electrodes. Another important point is to develop a suitable technique of measuring electrode noise in the field.

MEASUREMENTS AND PROCESSING

Comparative tests involved three types of widely used electrodes: graphite (manufactured by the Nord-West company), Cu-$CuSO_4$ and Pb-$PbCl_2$ (both manufactured by internationally recognized geophysical companies). We choose 8 electrodes of each type. All electrodes were brand-new and properly serviced before use.

To estimate the noise, a parallel test technique was applied. Electrodes of each type were grouped into pairs. Each pair formed an electrical line 1 meter long. All electric lines were located in parallel at a small distance from each other. Figure 2 shows two setups for measuring electrode noise (2 pairs of graphite electrodes installed on the left, and 2 pairs of Pb-$PbCl_2$ electrodes installed on the right).

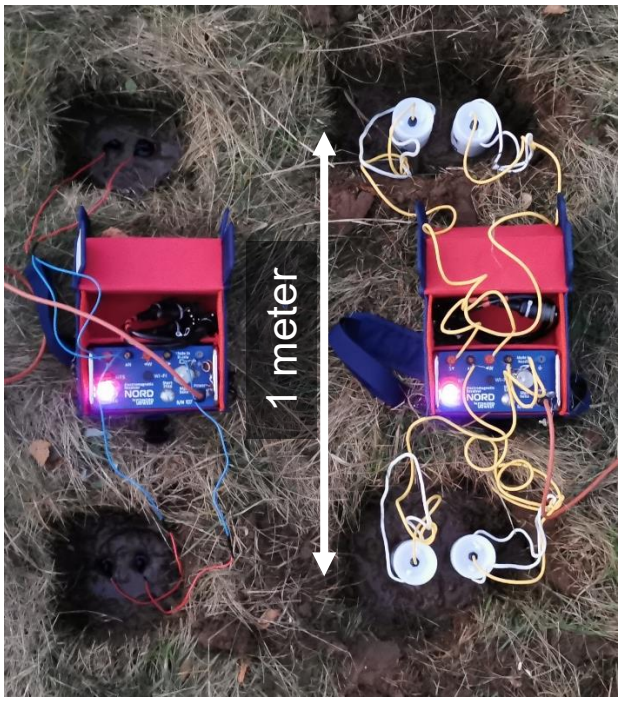

Figure 2. Simultaneous noise measurement for two types of electrodes. Left setup for graphite electrodes (4 electrodes), right setup for Pb-$PbCl_2$ electrodes (4 electrodes)

To study the stability of the characteristics of the electrodes, the signals were recorded periodically for 2 weeks.

Since the electric lines are very short, parallel and have the same length, the measured signals due to electric field in the ground are weak and roughly the same. Noise is the difference between the signals observed for different electrical lines and can be estimated using a simple formula:

$$Noise(t) = \frac{Ch_1(t) - Ch_2(t)}{2} \qquad (1)$$

For the noise function obtained this way, we have calculated the spectral density in a wide range of times (from 0.0001 to 1000 seconds). Examples of spectral density for different types of electrodes are given in Figure 3.

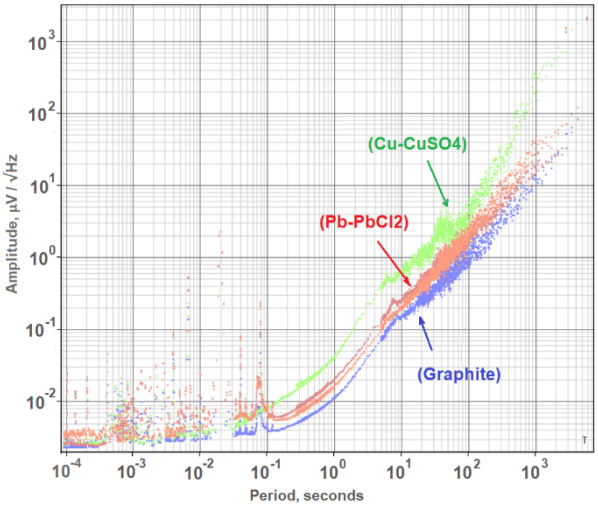

Figure 3. Noise spectral density of different types of electrodes after 24 hours of recording. Raw data (before applying the robust spline approximation).

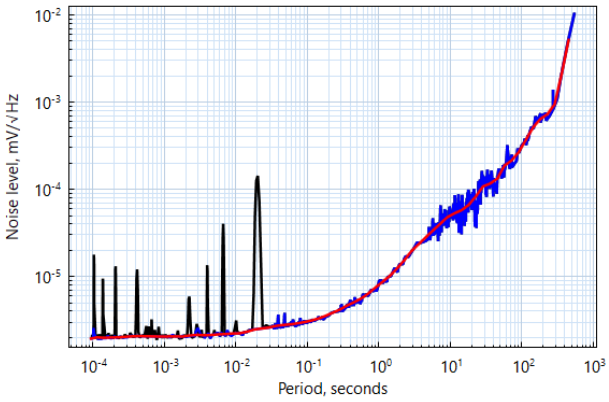

Figure 4. Robust spline approximation. Black line – raw spectra, blue line – spectra after industrial frequencies filtration, red line – smooth spline approximation

The place chosen for observations was located in the area of influence of industrial noise, therefore, distorted values were obtained at certain frequencies (50 Hz and harmonics). These peaks are not related to the self-noise of the electrodes; therefore, to obtain the final result, they were filtered. Then, spline approximation was carried out for the remaining values. This stage is shown in Figure 4.

RESULTS

As noted earlier, in order to obtain reliable noise estimates for each electrode type, it is necessary to ensure that each of the electrodes is in good condition and properly maintained. Figure 5 shows how the noise level of new (initially dry) graphite electrodes depends on the time elapsed after their first installation in moist soil. More than 12 hours should pass before the dry electrode starts to give the best results.

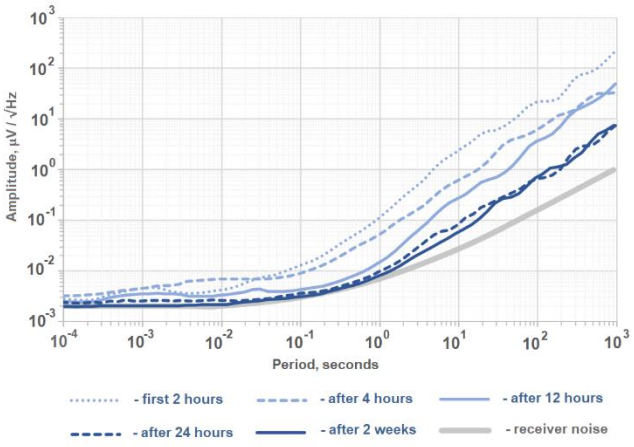

Figure 5. Change in noise level of a dry graphite electrode over time when placed in moist soil. Blue lines demonstrate noise levels for different times since installation. Gray line corresponds to receiver self-noise.

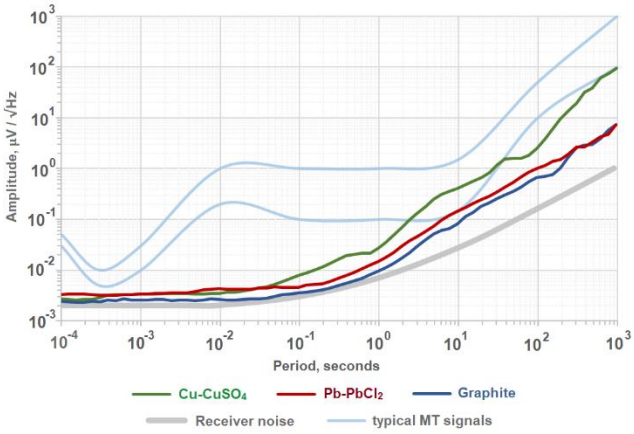

Figure 6. Comparison of the self-noise level of non-polarizable electrodes of various types

Figure 6 shows typical levels of noise of electrodes of different types. The highest noise level was consistently observed for Cu-$CuSO_4$ electrodes. Graphite and Pb-$PbCl_2$ electrodes both show noticeably better results quite similar to each other; but the noise level of graphite electrodes is slightly lower in the entire frequency range.

CONCLUSIONS

We believe that graphite electrodes deserve more attention of the international EM community than they used to have in last decades (e.g., see Lu and Macnae 1998). The presented work is the first step in our planned study of the characteristics of such electrodes. It is necessary to carry out long-term monitoring noise measurements and determine how the noise characteristics of the electrodes will depend on temperature, humidity and other factors.

However, according to the measurements already taken, it can be said with confidence that properly manufactured graphite electrodes demonstrate a noise level low enough to carry out magnetotelluric measurements in a wide frequency range. In all our observations, the noise level of graphite electrodes turned out to be consistently lower than that of the widely used Pb-$PbCl_2$ and Cu-$CuSO_4$ electrodes. Also, the graphite electrodes have a low production cost and are more environmentally friendly than most of metal-electrolyte electrodes, which makes them a very attractive option for MT exploration.

In addition, our measurements have demonstrated that the telluric field registration quality strongly depends on timely electrode maintenance. Before starting work, dry (new) electrodes should be kept in moist soil for about 1 day. This will provide the best measurement quality. This observation applies to any type of electrodes.

REFERENCES

Ferguson IJ (2012) Instrumentation and field procedures. In: Magnetotelluric method. Theory and Practice, ed. by Chave AD and Jones AG. Cambridge University Press, pp 421–479

Lu K, Macnae J (1998) The international campaign on intercomparison between electrodes for geoelectrical measurements. Explor. Geoph. 29: 484-488.

Petiau G & Dupis A (1980) Noise, temperature coefficient, and long time stability of electrodes for telluric observations. Geophys. Prosp., 28: 792–804

Petiau G (2000). Second generation of lead-lead chloride electrodes for geophysical applications. Pure Appl. Geophys., 157: 357-382

Aurora: An open source magnetotelluric data processing package in Python linking MTH5 to EMTF XML

Aurora: An open source magnetotelluric data processing package in Python linking MTH5 to EMTF XML

†K.N. Kappler[1], G. Egbert[2], A. Frassetto[3], L. Heagy[4], A. Kelbert[5], L. Keyson[3], D. Oldenburg[4], J.R. Peacock[5], and T. Ronan[3]

† Authors are listed alphabetically except the corresponding author.

[1]Independent, karl.kappler@berkeley.edu

[2]Oregon State University

[3] Incorporated Research Institutions for Seismology (IRIS)

[4]University of British Columbia

[5]United States Geological Survey

SUMMARY

Aurora is a software package that calculates robust estimates of electromagnetic transfer functions (EMTF) from magnetotelluric time series data. It is being developed for two primary purposes: first, to streamline the generation of high-quality, exchangeable EMTFs for archiving at the IRIS data center and second, to provide an open-source software package to the EM community that has been benchmarked against the legacy Egbert's EMTF codes. Aurora is a Python representation of Egbert's latest EMTF Matlab code that is designed to interface with the self-descriptive MTH5 data structure for magnetotelluric time series. We use Numpy, Pandas, Scipy, and Xarray as package dependencies. Comprehensive tracking of data provenance is provided within the pipeline via Xarray. Data products are outfitted with MTH5 metadata which can be converted to FDSN StationXML for surveys and EMTF XML for transfer function archiving. The Aurora software package, which includes worked example datasets, will be released via both PyPI and Conda-Forge in the autumn of 2022. We present an overview of these codes and outline a path forward over the following 1-2 years. The longer term vision includes capability for time and frequency domain data cleaning, data visualization, and data QC as well as novel array deployment geometries and controlled source data processing. We invite members of the community to join us in using these codes and collaborating on their future development.

Keywords: Magnetotellurics, Processing, Open Source, Python, Transfer Function

Open-source Python software for the visualization of magnetotelluric data and three-dimensional resistivity models

Ahmet Tuğrul Başokur
Lemnis Geosciences, basokur@ankara.edu.tr

SUMMARY

I present an open-source Python software (MTdmv) for MT data and three-dimensional (3D) model visualization that is available for academic use. The code can be directly run from a Python console without installation. The matplot.lib is the main library to create plots and picture files. The Google Earth 'kml' files can be produced from the edi files, or the coordinates and information in the edi files can be changed from a text file. The data visualization consists of plotting the frequency normalized impedance, apparent resistivity definitions, and Schmucker and Bostick transformations. The mentioned MT quantities can also be plotted as pseudo-section and maps for the measured and model response data. The real and imaginary parts of the frequency normalized impedance can be estimated from one another using the Hilbert transform to validate the dispersion relation.

The model visualization part could read ModEM and other data formats and shrink, modify and resave in different file formats. The extraction of a resistivity section in any direction can be achieved by defining the coordinates of two points or a point and angle pair. A resistivity section can be created along a crooked line, such as a seismic line through the coordinates given in a text file. The resistivity variation with depth can be plotted for a given coordinate. The model maps can be superimposed on Google Earth images. The software could automatically create all possible maps and sections for a given attribute.

All colourmaps contained in matplot.lib library can be activated. The picture files can be saved in pdf, jpg and all other formats supported by matplotlib and in any desired resolution. Furthermore, the image files can be obtained in any language after adding someone's native language to the language text file.

Keywords: Magnetotelluric, Python, Data visualization, Model visualization, Three-dimensional visualization.

The effect of radar trace number on tomographic images of cylindrical objects obtained using GPR

O. Apaydın[1], T. İşseven[2], Y. Çıtır[3], S. Paker[4] and I. Erer[5]
[1]Istanbul Technical University, Department of Geophysical Engineering, apaydinor@itu.edu.tr
[2]Istanbul Technical University, Department of Geophysical Engineering, isseven@itu.edu.tr
[3]ARAR Oil and Gas Exploration Production Marketing Inc., ycitir@arar.com.tr
[4]Istanbul Technical University, Department of Electronics and Communication Engineering,spaker@itu.edu.tr
[5]Istanbul Technical University, Department of Electronics and Communication Engineering, ierer@itu.edu.tr

SUMMARY

Ground penetrating radar (GPR) method is a non-destructive method that has been used in geological, archaeological, military and engineering researches for many years. GPR can be used to investigate structures at different depths, from several centimetres to a few hundred meters. In recent studies, it has also been used to image the internal structures of objects with shallow depths, such as tree trunks and historical building columns. With GPR, discontinuities, cavities and cracks in these structures can be detected. While investigating the internal structures of cylindrical objects, measurements are taken around the objects with GPR at certain angle intervals along a circular line. And by using the radar traces taken from these different angles in the backprojection method, tomographic images showing the interior of cylindrical objects are created. Vector network analyzer (VNA) and Vivaldi antenna pair are used to take radar measurements. The measurement system is fixed at one point and the object to be investigated is placed on a table that can be rotated with certain angle intervals around its own axis. Thus, measurements are taken at desired angle ranges. In this study, the effect of radar traces collected with different measurement intervals on tomographic images is compared and examined.

Keywords: GPR, backprojection, cylindrical objects

Full correction of the electric field data biased by the ECR-effects

N. Zorin[1,2*], D. Epishkin[1], D. Yakovlev[1] and A. Yakovlev[2]

[1]STC Nord-West, Moscow, Russia
[2]Moscow State University, Moscow, Russia
[*]corresponding author; nikita.zorin.geophys@gmail.com

SUMMARY

Electrical exploration on frozen or stony soil is associated with high difficulties in achieving good quality of electrode grounding. In such conditions, the results of high-frequency electric field measurements are often biased due to the electrode contact resistance (ECR) effects, i.e., the capacitive leakage between wires and ground and voltage division at the receiver's input. In this paper we discuss a new method of full analytical correction of the ECR-distorted data.

Keywords: poor electrode contact, capacitive leakage.

INTRODUCTION

High contact resistance of grounded receiving dipoles can significantly distort alternating electrical field measurements in the ground (Vishnyakov and Vishnyakova 1974; Zonge and Hughes 1985). These distortions are mostly due to various kinds of capacitive effects in the receiving circuit, which increase with operating frequency. Thus, in the DC resistivity, induced polarization and magnetotelluric (MT) methods, electrode contact resistance up to 10-20 kOhm is usually considered to be acceptable, while in the audio-MT (AMT) and controlled-source EM induction (CSEM, CSAMT) methods it is generally recommended to achieve values less than 1 kOhm.

In many cases (for example, when working on ice, frozen, sandy and rocky soil), making a dipole with less than 10-20 kOhm grounding resistance is very labor-intensive, not to mention the almost infeasible values of 1 kOhm or less. Unfortunately, electrical explorations with the above methods are often carried out exactly in such unfavorable conditions, especially typical for the Polar Regions. Thus, better understanding of the electric field distortions caused by poorly grounded electrodes, as well as elaborating new ways to solve this problem, is a relevant task for EM scientists.

Below we present a novel approach of full analytical correction of the ECR-distorted electrical field data.

RECEIVING DIPOLE MODEL

To quantify the distortions associated with high grounding resistance, or, as called by Zonge and Hughes (1985), ECR (electrode contact resistance) effects, let us review the equivalent circuit of a grounded receiving dipole (Figure 1).

The following symbols are used in the figure: $R_M\,(R_N)$ is the grounding resistance of the electrode M (N); $C_M\,(C_N)$ is the capacitance between the cable M (N) and the ground; Z_0 is the complex input impedance of the receiver; D is the distance between the electrodes; E is the electric field in the ground; and U_0 is the observed voltage at the receiver's input. U_0 and E are related as follows:

$$U(\omega) = \left(\frac{0.5 + \frac{0.25}{1 + i\omega R_M C_M} + \frac{0.25}{1 + i\omega R_N C_N}}{1 + \frac{Z_{MN}(\omega)}{Z_0(\omega)}} \right) DE(\omega),$$

where ω stands for the angular frequency; i stands for the imaginary unit; $Z_{MN} = Z_M + Z_N$ is the complex contact impedance of the dipole MN; $Z_M = R_M/(1 + i\omega R_M C_M)$, $Z_N = R_N/(1 + i\omega R_N C_N)$.

Separating in this expression the coefficient K_{MN} due to wire-to-ground capacitive leakage from the coefficient K_0 due to voltage division at the receiver's input, we get:

$$U_0(\omega) = K_0(\omega) K_{MN}(\omega) DE(\omega), \qquad (1a)$$

$$K_0(\omega) = \frac{Z_0(\omega)}{Z_0(\omega) + Z_{MN}(\omega)}, \qquad (1b)$$

$$K_{MN}(\omega) = 0.5 + \frac{0.25}{1 + i\omega R_M C_M} + \frac{0.25}{1 + i\omega R_N C_N}. \qquad (1c)$$

For a perfectly grounded dipole Equation 1 yields $K_{MN} \equiv K_0 \equiv 1$, and the observed voltage U is related to the measured electrical field E with a simple expression:

$$U_0(\omega) = DE(\omega). \quad (2)$$

In a real grounded dipole, the voltage recorded by the receiver is always less than the expected value (2), and the degree of bias is governed by the values of complex coefficients K_{MN} and K_0.

CORRECTION OF BIASED DATA

A known way to deal with ECR distortions due to voltage division at the receiver's input is their partial correction based on the estimates of $R_{MN} = R_M + R_N$ values obtained *in situ* at each survey site. It is especially important for receivers with high input capacitance (and hence low input impedance values at high frequencies). For this, many modern MT/AMT stations are capable to autonomously measure the R_{MN} value, which is saved in the device memory and then taken into account at the stage of data processing by normalizing the results by $Z_0/(Z_0 + R_{MN}) \approx K_0$.

A natural development of the method of partial data correction described above is their full correction according to Equation 1 with *in situ* estimates of all necessary parameters – R_M, R_N, C_M and C_N. Such estimates can be obtained using a simple portable LCR-meter or a specially designed impedance meter using the "auxiliary grounding" technique (Bursian, 1972). For this purpose, it is required to ground an auxiliary electrode A at a sufficient distance from electrodes M and N and measure the impedance values Z_{MN}, Z_{AM} and Z_{AN} of the three obtained dipoles at two (at least) frequencies: ω_1 and $\omega_2 \gg \omega_1$. Then, using the following formulas, we estimate the impedance values of the half-dipoles M and N:

$$Z_M(\omega_i) = \frac{Z_{MN}(\omega_i) + Z_{AM}(\omega_i) - Z_{AN}(\omega_i)}{2}, \quad (2a)$$

$$Z_N(\omega_i) = \frac{Z_{MN}(\omega_i) - Z_{AM}(\omega_i) + Z_{AN}(\omega_i)}{2}. \quad (2b)$$

Then we solve with regard to the unknowns R_M, R_N, C_M and C_N the obtained determined (with $i = 1,2$) or over-determined (with $i = 1,2,\ldots$) equation systems:

$$Z_M(\omega_i) = \frac{R_M}{1 + i\omega_i R_M C_M}, \quad (3a)$$

$$Z_N(\omega_i) = \frac{R_N}{1 + i\omega_i R_N C_N}. \quad (3b)$$

Finally, for all operating frequencies, using Equation 1 and known complex input impedance of the receiver we calculate the distortion coefficients K_0 and K_{MN}, and then divide by them the obtained values of the electrical field after processing.

CONCLUSIONS

There are two principal ways of solving the problem of biased data in EM prospecting: 1) – to eliminate/minimize the distortion value in the field, and 2) – to correct the distorted data later at the processing/interpretation phase. In this paper we consider the second approach, which involves the *in situ* estimation of one or more parameters of the receiving dipole with further partial or full correction of the biased data during processing.

The proposed approach of full data correction may help to greatly expand the range of maximum permissible values of electrode contact resistivities for many EM methods with little additional effort. Note that in the capacity of an auxiliary electrode A one may use the central electrode of the receiver (if any) or, in MT/AMT methods – any electrode of the orthogonal receiving dipole.

REFERENCES

Bursian VR (1972) Theory of electromagnetic fields used in electrical exploration, 2nd ed., rev. and add. Nedra, Leningrad [in Russian].

Vishnyakov AE, Vishnyakova KA (1974) Field excitation and measurement in electrical prospection. Nedra, Leningrad [in Russian].

Zonge KL, Hughes LJ (1985) Effect of electrode contact resistance on electric field measurements, Expanded Abstr. Technical Programme of 55th Ann. Intern. SEG Meeting, contrib. MIN 1.5. Tulsa. OK. pp. 231–234.

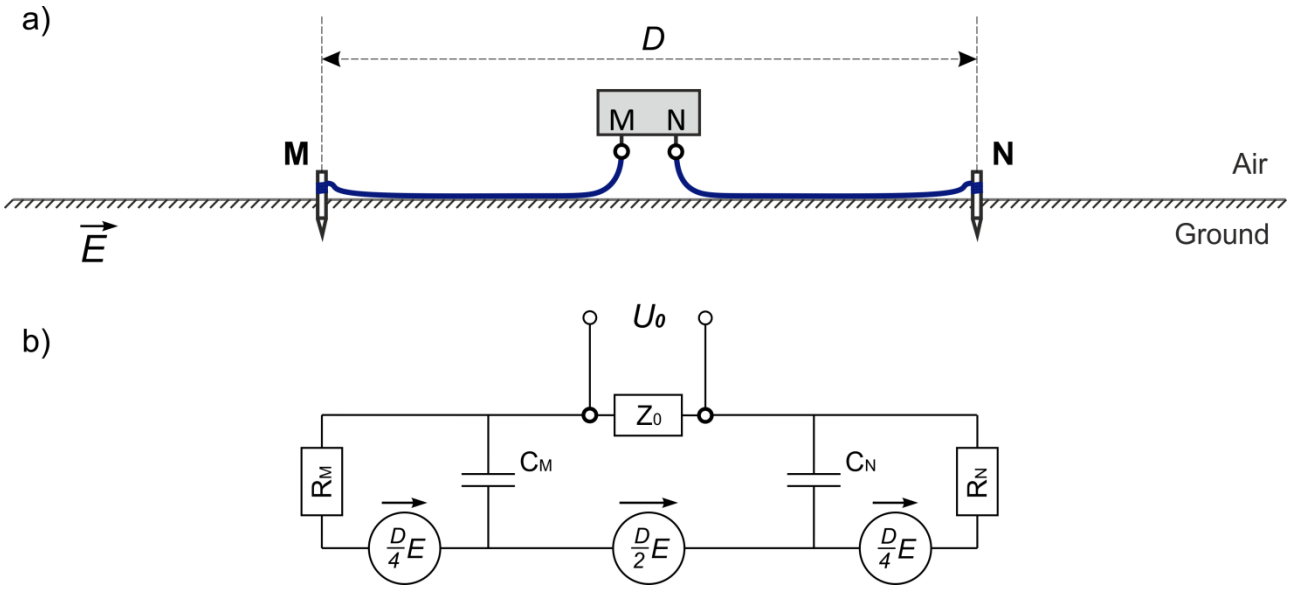

Figure 1. Classic receiving dipole (a) and its equivalent circuit (b).

Cloud connected low power, low noise systems for LMT & MT

V. Pronenko[1], K. Strack[2], and A. Prystai[1]
[1]LLC "LEMI", Lviv, Ukraine, pron@isr.lviv.ua
[2]KMS Technologies, Houston, USA, kurtstrack@me.com

SUMMARY

Over the past years, we developed and field tested two easy to operate low power, low-noise magnetotelluric systems, LEMI-423 (wideband) and LEMI-424 (long period). Recently, both systems were adapted to be connected via a noise-free web access box for continuous data streaming allowing near real-time remote reference application.

The key feature of both systems is the low noise amplifiers and the sensors. The LEMI-424 is used already in many countries for low-frequency magnetotelluric work and past field experience has shown their high field reliability. The system is also used for magnetic studies of the magnetosphere. The sensor has a noise level of 10 pT/sqrt(Hz) at 1 Hz. Other sensors can also be connected. The entire system weighs less than 3 Kg (plus environment-friendly non-polarized electrodes). Its total power consumption is less than 1 W.

The sister system is the LEMI-423 which addresses the standard magnetotelluric band from 0.0001 Hz to 1000 Hz. It can go up to 4 kHz sampling rate while still keeping the power consumption including sensors under 1 W. The LEMI-423 uses the well-established LEMI-120 coils, used not only for magnetotellurics but also for many space research projects. The system weights under 3 Kg (excluding cables) and the sensors each under 6 kg.

The construction peculiarities and application examples are presented in the report.

Keywords: web access box, LMT & MT system, low-noise, low-power station.

EM-ACROSS System: Installation at the Kusatsu-Shirane Volcano, Japan

Serita, S.[1], Ogawa, Y.[1,2], Ishizu, K.[2,3], Tseng, K.H.[1], Kunitomo, T.[4],
Minami, T.[5], Ichihara, H[4], Caldwell, T.G.[6], Heise, W.[6], Bertrand E.A.[6]
[1]Department of Earth and Planetary Sciences, Tokyo Institute of Technology, Japan
[2]Volcanic Fluid Research Center, Tokyo Institute of Technology, Japan
[3] Graduate School of Science, University of Hyogo, Japan
[4] Earthquake and Volcano Research Center, Nagoya University, Japan
[5] Department of Planetology, Kobe University, Japan
[6] GNS Science, New Zealand

We have been working on establishing an electromagnetic routine monitoring system called EM-ACROSS. ACROSS stands for Actively Controlled Routinely Operated Signal System. The source signal is composed of a set of sine waves with multiple line frequencies and is precisely controlled by the synchronization with a 10MHz GPS signal. This allows stacking receiver signals for a long time, even with a relatively small power transmitter.
EM-ACROSS system was installed at Kusatsu-Shirane volcano, located 200km NW of Tokyo. The Kusatsu-Shirane volcano is an andesitic-to-dacitic volcano known for its phreatic activity in historical times. The internal structure of the most active crater, Yugama, was modeled to the depth of 2km by magnetotelluric soundings with 91 sites, and a three-dimensional resistivity structure was obtained (Tseng et al., 2020). We now aim to image the temporal variation of the resistivity structure in four dimensions.
The transmitter system is composed of a GPS-controlled function generator that can output arbitrary signals at two channels. For each channel, the signal time series consists of a set of 8 frequencies. The two sets have slightly different frequencies, so two sets of independent signal time series can be recorded in the receiver without interference. The amplitudes of the transmitter signals have a larger amplitude toward lower frequencies to counteract the natural signals. The phases of the sine components are randomized to avoid generating a peaking. We installed two current dipoles in NS and EW directions. The signals from the two channels of the function generator were 80 times amplified by the two power amplifiers.
The receiver sites measure electric and magnetic signals using MT receivers. As we have two current dipoles, we can obtain tensor responses simultaneously. In addition, as the transmitter signal consists of a set of specific line frequencies, we can also measure magnetotelluric signals without disturbances.

Keywords: controlled source, frequency domain, stacking, ACROSS

Abstract, 25^{th} EM Induction Workshop,Çeşmeı, Turkey, September 11-17, 2022

Towards a AFMAG-capable airborne EM Sensor Platform - Identification of Noise Sources

A. Thiede, M. Becken
Institute of Geophysics, University of Münster, Germany; athiede@uni-muenster.de

SUMMARY

Airborne electromagnetic (EM) measurements using natural signal provide a dense data coverage of large areas in short time and with small effort. The audio-magnetotelluric signal is much weaker than the signal of a nearby artificial transmitter. Hence, airborne systems require an extremely low noise level for purely passive measurements.
The strongest noise source of airborne EM data is motion noise due to sensor movements in the Earth's magnetic field. As part of the DESMEX II project, we aim to optimize the DESMEX induction coil airborne system to meet passive EM requirements and improve semi-airborne EM data quality aspiring to penetration depths of > 1000 m. We use an Inertial Navigation System (INS) to measure sensor movements and predict the signal input caused by motion. The INS samples with 400 Hz, thus allows for low frequency corrections.
However, the "cleaned" data recorded with undamped sensors are still afflicted with remaining motion noise and the resulting signal-to-noise ratio is insufficient for natural signal analysis. To reduce the noise level, we built a damped sensor platform using vibration-insulating foam material. Damping characteristics were tested on the ground and under flight conditions.
The vibration-insulated sensor platform reduces motion noise on all components with a factor of more than 10 at high frequencies (> 50 Hz). Passive airborne EM using the DESMEX induction coil system seems to be feasible in a limited frequency range. Accessing lower frequencies is essential for greater penetration depth hence further improvement is necessary. We identified internal EM and further motion noise sources affecting airborne EM data quality. Ongoing work focuses on the removal of noise sources and the design of an optimized sensor platform.

Keywords: Audio-frequency Magnetics; semi-airborne Electromagnetics; Airborne Sensor Platform; Motion Noise

Abstract, 25th EM Induction Workshop, Çeşme, Turkey, September 11-17, 2022

3D inversion of an integrated TEM survey

Longying Xiao[1], Gianluca Fiandaca[2], Pradip K. Maurya[3], Anders Vest Christiansen[4]
[1] Geological Survey of Finland (GTK), longying.xiao@gtk.fi
[2] University of Milano, gianluca.fiandaca@unimi.it
[3] Aarhus University, pradip.maurya@geo.au.dk
[4] Aarhus University, anders.vest@geo.au.dk

SUMMARY

Recent instrument advancements in the field of the transient electromagnetic (TEM) method enable applications adapted to different environments. To invert integrated datasets from ground-based and waterborne TEM surveys under one model domain, the complexity increases for two factors: i) significant multi-dimensionality effects from settings with strong conductivity contrasts such as a coastline. ii) sensitivity footprints vary depending on the systems. We address these challenges by utilizing a previously developed 3D octree-based inversion scheme, where the decoupling between forward and inversion mesh allows local meshes for individual soundings, and a commonly shared model for the inversion domain. We demonstrate the framework environments through synthetic and field case studies. These experiments show that: i) for such surveys, the 3D inversion outperforms the 1D inversion in terms of a lower data misfit and more accurate predicted model; ii) a careful forward mesh refinement is required to effectively explain the data collected at the settings with thin and highly conductive top layers.

Keywords: Time-domain electromagnetic, 3D, Inversion, Borehole

INTRODUCTION

The transient electromagnetic method is an efficient and non-invasive geophysical tool for characterizing the resistivity distribution of the subsurface. Nowadays, many TEM systems are developed for improved maneuverability and acquisition, allowing for measurements in a variety of environments – e.g. airborne, ground-based, or waterborne surveys. An integrated survey, which consists of a mix of several TEM systems, can be a helpful solution in some circumstances, since different systems may offer superior resolution by concentrating at different sensitivity depths or surveying different types of land/sea. Following TEM measurements, a 1D inversion is routinely applied, assuming the subsurface is quasi-1D. However, it is difficult to resolve the subsurface structures with little ambiguity if major 2D or 3D effects are present (Rabinovich, 1995; Bauer-Gottwein et al., 2010), such as salinity-related anomalies, even if there is a strong agreement between predicted and measured data. Furthermore, the inevitable mix of system configurations result in varied sensitivity footprints horizontally and vertically, necessitating individually tailored meshing for 3D modeling.

The outlined challenges are especially prominent in coastal surveys. First, both ground-based and waterborne (or airborne) TEM systems are used to image the resistivity distribution below land and seawater. Second, the strong conductivity contrast between seawater and/or lithologies affected by high salinity and freshwater lithologies results in significant 2D and 3D effects in the data. As a result, a standard 1D inversion framework is unable to appropriately resolve subsurface structures correctly, which could be crucial for effectively conceptualizing seawater intrusion problems. To address the issues, we use a developed 3D multi-mesh inversion scheme (Xiao et al., 2022): i) 3D octree-based forward modeling is employed to describe the multi-dimensional environment and simulate the electromagnetic field diffusion. ii) a decoupling between the forward and the inversion mesh is utilized to provide the flexibility of modeling each sounding separately to minimize computational costs while accounting for differences in configuration and sensitivity. The mesh decoupling further allows for a continuation of the model-domain across the land-sea interface during inversion, in comparison to an approach that uses independent model domains for the land-based and waterborne sub-surveys. We investigate the problem on a synthetic example and demonstrate our solution on a field dataset collected from a coastal area, where borehole data is available to verify the result.

METHODS

TEM Modeling and inversion

Assuming that the media is isotropic, non-magnetizable and that electrical properties are independent of time, the time-domain forward

problem is formulated as a diffusion equation in terms of the electrical field $\mathbf{e}(\mathbf{x},t)$:

$$\nabla \times \nabla \times \mathbf{e}(\mathbf{x},t) + \mu\sigma(\mathbf{x})\frac{\partial \mathbf{e}(\mathbf{x},t)}{\partial t} = -\frac{\partial \mathbf{j_s}(t)}{\partial t} \qquad (1)$$

where the electric field $\mathbf{e}(\mathbf{x},t)$, is a function of space, $\mathbf{x}(\mathbf{x} \in \Omega)$, and time, $t \in (0,T)$; μ is the magnetic permeability of free space, σ denotes the electric conductivity, and $\mathbf{j}_s$ denotes the current source. The modeling and inversion used a previously developed octree-based scheme (Xiao et al., 2022). In particular, the multi-mesh approach (Zhang et al., 2021) is employed in the scheme, which is beneficial in this dual-system ground-based and waterborne TEM inversion. In the inversion, one regular mesh is used for the full-scale model update. The forward modeling and Jacobian calculation, however, are performed on sounding-based, with a local mesh description for the different systems.

Modeling mesh design

TEM techniques are highly sensitive to conductors. When doing a survey in saline water, the eddy currents diffuse horizontally in the water for a long time rather than moving downwards, resulting in a shallow vertical resolution. For such cases where conductive structures are present in the top subsurface, additional mesh refinement is required to attain acceptable numerical accuracy. First, the mesh elements in the seawater layer must be refined to depict rapid field variations near the TEM system. At the same time, the refinement must cover vast horizontal footprints to account for the lateral extension of the eddy currents with time.

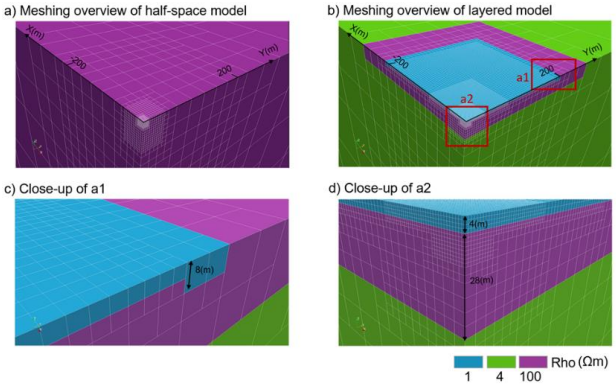

Figure 1. Illustration of the octree mesh refinement for a three-layered (1/4/100 Ωm) model. a) shows a normal half-space meshing while b) shows a refined mesh for a highly conductive and thin top layer. c) shows a close-up of the mesh in b) at the end of the fine mesh (a1), laterally, and d) shows a similar close-up just below the transmitter (a2).

RESULTS

Synthetic example

To replicate a coastal environment (Figure 2-b) similar to the field case scenario, we created a three-layer 3D synthetic model. The measurement for the synthetic example (Figure 2-c) uses tTEM (Auken et al., 2019) and FloaTEM (Maurya et al., 2021) systems to cover an area of 140mx70m with a 10 m sounding distance. We selected a profile perpendicular to the driving direction consisting of 6 tTEM soundings and 7 FloaTEM soundings. We compared the relative difference between the 1D response from AarhusInv (Auken et al., 2015) and the 3D response from the forward solution (Xiao et al., 2022).

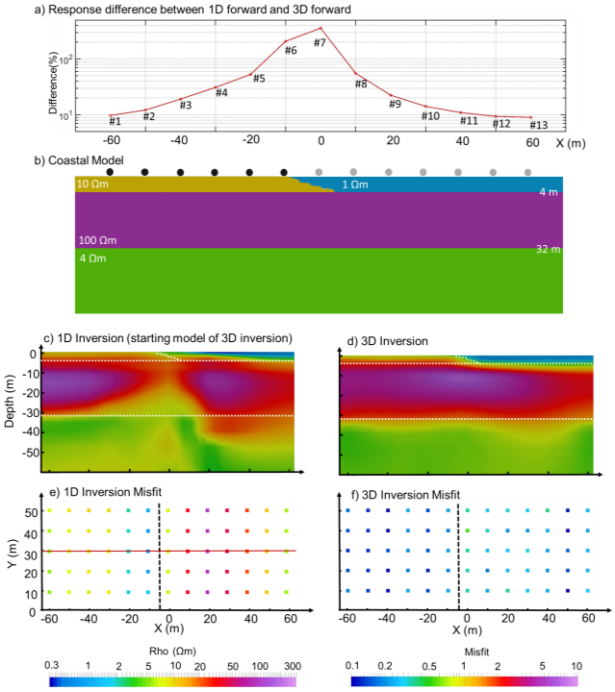

Figure 2. The 1D/3D forward and inversion result on a coastal model: a) Forward response difference; b) Coastal model illustration, where the tTEM and FloaTEM soundings are symbolized by black and grey dots, respectively; c) 1D inversion section (starting model of 3D inversion); d) 3D inversion section; e) 1D inversion misfit map; f) 3D inversion misfit map. The dotted white lines outline the structures of the true model. The dotted black lines symbolize the coastline. The solid red line indicates the section location of inversion results in subfigure (c) and (d).

The modeling test has revealed a significant difference between a 1D and a 3D response, in the instance of strong 2D effects from a coastline (Figure 2-a). As a result, it has illustrated the importance of using multi-dimensional simulation instead of 1D modeling in such an area. To compare the inversion performance of different dimensions, we performed both 3D (Xiao et al., 2022) and 1D inversions (Christensen et al. ,2017) using the same model space, i.e. a voxel mesh with the same

spatial discretization. Although we started the inversion with correct parameters, the seawater layer in 1D inversion result is too shallow compared to the true model; also, a conductive pant leg is reaching into the high-resistivity layer. The 3D inversion starting model (i.e.,1D inversion result), on the other hand, did not include a layer to represent the proper water table, but it recovered the true model substantially. This includes a more reasonable resistivity model without the pant leg.

Field case

Himmark Beach is a contaminated area in southern Denmark due to the deposition of chemical waste. The local government aims to characterize the pollution pathways to the sea using the TEM method and make a removal strategy for the environmental problem. We use a small subset from the TEM campaign to illustrate our solution to the inversion problem, due to the large computational complexity and the access to existing borehole information. The presented dataset (Figure 3) consists of 18 tTEM soundings and 41 FloaTEM soundings. In general, the distance between acquisition lines is around 20 m and the distance between soundings is 5 m.

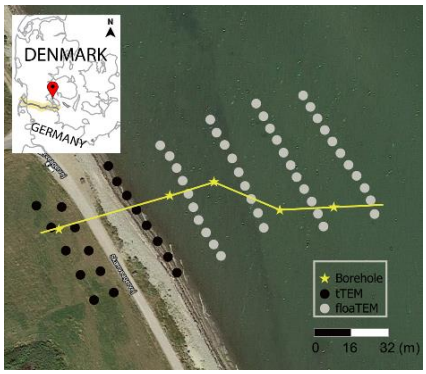

Figure 3. Survey map. The solid yellow line represents a profile along the existing boreholes.

In 1D inversion result (Figure 4-a), what appears to be a 2D pant leg effect, similar to the one seen in the synthetic example inversion. For the 3D result (Figure 4-d), the top resistive till layer (~20 Ωm) is only aligned with the borehole reported sand-clay interface. We further calculate the formation factor of the 1D/3D inversion models within the depth range of the saline-water-saturated sand layer observed in the boreholes. Following Archie's law (Archie, 1942), we find that the 1D result yields a formation factor of 20, whereas the 3D inversion predicts a value of ~4-5. Based on published lab measurements of saline sand formation properties (Frings et al., 2011; Kadhim et al., 2013), we learn that the 3D result gives a more reasonable estimation of the resistivity in the sand layer.

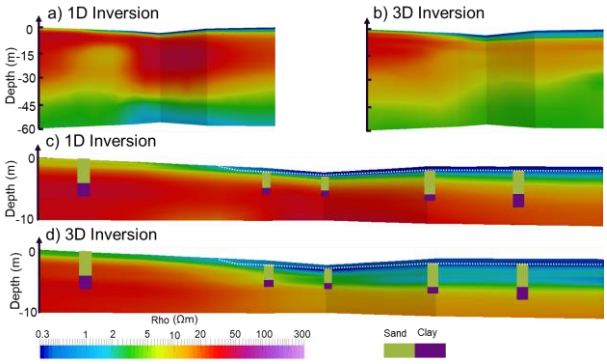

Figure 4. The result from inversions. The white dashed line represents the bathymetry based on measurements at the borehole locations.

CONCLUSIONS

In this study, we investigated the 3D effects present in integrated TEM surveys at coastal sites by applying a previously developed 3D inversion scheme, both with synthetic and field examples. In the synthetic coastal model, we analyzed both forward responses and inversion results using a 1D and a 3D forward code. The forward response difference increases significantly when the soundings are closer to the coastline, which was up to 400% on a sounding basis. As for the inversion, the 1D result did not recover the water depth properly. Furthermore, a clear pant leg effect appeared in the onshore survey area. The 3D inversion, however, reproduced the model fairly accurately with no particular artifacts and a low data misfit. In the inversions of the field data, many results from the synthetic study reappear. Existing borehole data verified that the 3D inversion provided accurate characterization of a particular interface between sand and clay, which was the primary target of the investigation.

ACKNOWLEDGEMENTS

The authors would like to thank the region of Southern Denmark for allowing the data for publication. We would like to thank Jesper Pedersen for providing the background of the field data collection and Dr. Nikolaj Foged for extracting borehole information from the Jupiter database. We thank Dr. Paul McLachlan for the language polishing.

REFERENCES

Archie, G. E., 1942, The electrical resistivity log as an aid in determining some reservoir characteristics: Trans. AIME, 146, 54-62.

Auken, E., N. Foged, J. J. Larsen, K. V. T. Lassen, P. K. Maurya, S. M. Dath, and T. T. Eiskjær,

2019, tTEM—a towed transient electromagnetic system for detailed 3d imaging of the top 70 m of the subsurface: Geophysics, 84, no. 1, E13-E22.

Auken, E., A. V. Christiansen, G. Fiandaca, C. Schamper, A. A. Behroozmand, A. Binley, E. Nielsen, F. Effersø, N. B. Christensen, K. I. Sørensen, N. Foged, and G. Vignoli, 2015, An overview of a highly versatile forward and stable inverse algorithm for airborne, ground-based and borehole electromagnetic and electric data: Exploration Geophysics, 2015, no. 46, 223-235.

Bauer-Gottwein, P., B. N. Gondwe, L. Christiansen, D. Herckenrath, L. Kgotlhang, and S. Zimmermann, 2010, Hydrogeophysical exploration of three-dimensional salinity anomalies with the time-domain electromagnetic method (tdem): Journal of Hydrology, 380, no. 3-4, 318-329.

Christensen, N. K., T. P. A. Ferre, G. Fiandaca, and S. Christensen, 2017, Voxel inversion of airborne electromagnetic data for improved groundwater model construction and prediction accuracy: Hydrology and Earth System Sciences, 21, no. 2, 1321-1337.

Frings, R. M., H. Schüttrumpf, and S. Vollmer, 2011, Verification of porosity predictors for fluvial sand-gravel deposits: Water Resources Research, 47, no. 7.

Kadhim, F. S., A. Samsuri, and A. Kamal, 2013, A review in correlation between cementation factor and carbonate rock properties: Life Sci. J, 10, no. 4, 2451-2458.

Maurya, P. K., F. E. Christensen, M. A. Kass, J. B. Pedersen, R. R. Frederiksen, N. Foged, A. V. Christiansen, and E. Auken, 2021, Technical note: Efficient imaging of hydrological units below lakes and fjords with a floating, transient electromagnetic system (FloaTEM): Hydrol. Earth Syst. Sci. Discuss., 2021, 1-21.

Rabinovich, M., 1995, Errors of 1-d interpretation of 3-d tdem data in the application of mapping saltwater/freshwater contact: Journal of Applied Geophysics, 34, no. 1, 23-34.

Xiao, L., G. Fiandaca, B. Zhang, E. Auken, and A.V. Christiansen, 2022, Fast 2.5D and 3D Inversion of transient electromagnetic surveys using the octree-based finite element method: Geophysics, 0: 1-53.

Zhang, B., K. W. Engebretsen, G. Fiandaca, H. Cai, and E. Auken, 2021, 3d inversion of time-domain electromagnetic data using finite elements and a triple mesh formulation: Geophysics, 86, no. 3, E257-E267.

Abstract, 25^{th} EM Induction Workshop,Çeşmeı, Turkey, September 11-17, 2022

Joint Probabilistic Inversion of 3D Magnetotelluric and Seismic Data in Southeast Australia

M.C. Manassero[1], J.C. Afonso[2] , S. Özaydin [1], A. Kirkby[3], I. Fomin[1] A.G. Jones[4, 5], and K. Czarnota[6]
[1]Macquarie University, Australia (constanza.manassero@hdr.mq.edu.au, sinan.ozaydin@hdr.mq.edu.au)
[2]University of Twente, Netherlands (j.c.afonso@utwente.nl)
[3]
[4]Complete MT Solutions Inc., Canada
[5]University of Western Australia, Australia
[6]Geoscience Australia, Canberra, Australia

SUMMARY

Multi-observable inversions are gaining popularity for imaging the structure of the lithosphere (Afonso et al., 2016). Of particular interest is the joint inversion of magnetotelluric (MT) with seismic data as their complementary sensitivity to the thermal structure, hydrogen content and small volumes of fluid or melt offer a powerful means to detect fluid pathways in the lithosphere including the locus of partial melting, ore deposits and hydrated lithologies. This unique potential has given impetus to the acquisition of collocated MT and seismic data over large regions (e.g., AusLAMP/AusArray in Australia).

Probabilistic inversions provide complete information about the unknown parameters and their uncertainties conditioned on the data and modelling assumptions. Joint probabilistic inversions of MT and seismic data have been successfully implemented in the context of 1D MT data only. For the cases of 2D and 3D MT data, however, the large computational cost of the MT forward problem has been the main impediment for pursuing probabilistic inversions. To overcome this limitation, we have presented a novel strategy (Manassero et al., 2020, 2021) that reduces the computational cost of the 3D MT forward solver and allows us to perform full joint probabilistic inversions of MT and other datasets for the 3D imaging of deep thermochemical anomalies and fluid pathways.

As part of the Exploring for the Future program, we present preliminary results of the first joint probabilistic inversion of 3D MT in southeast Australia using the AusLAMP data and a seismic velocity model derived from teleseismic tomography (Rawlinson et al.,2016). We also make interpretations of our conductivity models using the code MATE (Özaydin and Selway, 2020). These results demonstrate the capabilities of our conceptual and numerical framework for 3D joint probabilistic inversions of MT with other geophysical data sets and open up exciting opportunities for elucidating the Earth's interior in other regions.

Keywords: 3D Magnetotellurics, Probabilistic Inversion, Joint Inversion, Numerical modelling, Lithospheric structure

Abstract, 25^{th} EM Induction Workshop,Çeşmeı, Turkey, September 11-17, 2022

Petrophysical-based constrained and joint inversions of magnetotelluric (MT) and gravity data-sets on unstructured tetrahedral meshes

M. Kangazian[1], C. Farquharson[1]
[1]Memorial University of Newfoundland, St. John's, NL, Canada, Department of Earth Sciences.
mkangazianka@mun.ca, cgfarquh@mun.ca

SUMMARY

Geophysical inverse problems can identify significant subsurface features by the means of measured physical quantities such as gravity, magnetic, electric, and electromagnetic (EM) fields. The minimum-structure algorithm, or Occam's style, is one of the most common inversion methods that has been extensively employed for the inversion of geophysical data due to its robustness and reliability. This method can be adapted and extended in many ways. Perhaps the two most important of which are constrained and joint inversion methods, and on which this study focusses. The geophysical Earth models constructed from multiple, complementary geophysical survey types or constrained independent inversions are more likely to represent the true subsurface than a model constructed from an independent unconstrained inversion.

Joint inversion methods can be divided into two main types, structural-based and petrophysical-based joint inversion methods, depending on the type of coupling measure used between physical property models. This study develops a joint MT and gravity inversion methodology based on a petrophysical-based approach. Petrophysical-based joint inversions result in a less challenging, although not easy, optimization problem compared with the structural-based approaches. The fuzzy *c*-means clustering technique (FCM) is the petrophysical-based joint inversion method that this studying uses as a coupling measure. Also, independent constrained MT and gravity inversions using the FCM method are compared with the joint inversion results.

The capability of the joint and constrained MT and gravity inversions are investigated using synthetic and real-data examples. The conductivity and density models constructed by the clustering method represent a reasonable definition of the anomaly's boundaries and a reasonable range of the recovered physical property values of the true model compared to the models constructed by the independent MT and gravity inversions.

Keywords: Constrained inversion, Gravity method, Joint inversion, Magnetotelluric method

True 3D Land CSAMT Modeling

W. Soyer[1] and R.L. Mackie[1]

[1]CGG Multiphysics
Wolfgang.Soyer@cgg.com
Randall.Mackie@cgg.com

SUMMARY

Controlled source audio magnetotellurics “CSAMT” is a grounded electromagnetic imaging technique used primarily in the mining industry and is a closely related predecessor to the marine controlled source electromagnetic method “CSEM” more familiar to the oil and gas community. Both methods involve injecting alternating electric current into the Earth through long transmitter dipoles, and making measurements of the Earth’s response at an array of EM receivers. Historically, CSAMT data have been interpreted using readily available MT modeling algorithms, but this means using only the data considered far enough away from the dipole source to be interpretable using the MT-inherent assumption of a uniform, or “far-field”, source. In this work, we show the advantages of carrying out complete earth, three-dimensional modeling of all grounded dipole EM fields, including those near the source, and avoiding the commonly employed, ad-hoc methods that throw away otherwise valuable “transition-zone” data that are unusable in MT-only modeling workflows. The CSEM inversion modeling is applied to a synthetic and a real data example, and inversion of complex field amplitudes is compared with impedance inversions.

Keywords: 3D inversion, true layout, CSEM, CSAMT, MT

INTRODUCTION

Controlled source, grounded electrode EM surveys have a long and successful history in mineral exploration geophysics, where the most commonly deployed configuration is CSAMT, using single, fixed, kilometer-long transmitter dipoles in broadside configuration (e.g., Zonge and Hughes 1991). More recently, however, hybrid survey configurations are gaining in popularity, including surveys using multiple transmitter and receiver dipole locations and orientations (e.g., Grayver et al. 2014, Darnet et al. 2018).

Despite continuous advancements in computing power and algorithms, the analysis and modeling of CSAMT data is still generally restricted to “far-field” data, where the standard magnetotelluric (MT) uniform source field assumption is valid, and readily available MT modeling tools are employed (e.g., Sasaki et al, 1992, Wannamaker, 1997). In general, far-field conditions are met at higher frequencies and longer source-receiver offsets. This restriction not only limits the depth of exploration, but also removes the potentially beneficial sensitivity characteristics of EM fields in the transition zone between near-field and far-field behavior, where vertical current components are sensitive to thin resistive layers otherwise invisible to MT. While three-dimensional inversion modeling of land CSAMT is being developed (e.g., Lin et al 2018, Wang et al 2018) it is not yet the industry standard that 3D inversion modeling is for land and marine MT, and marine CSEM.

3D CSEM IMPLEMENTATION

Here we discuss extensions of electromagnetic modeling algorithms (Mackie et al, 2020) for generic, land CSEM array data, including CSAMT configurations. The objective is to provide accurate and efficient modeling of the typically km-long grounded transmitter dipoles, with rugged topography and realistic geology at both receiver and transmitter array locations. We model EM fields using a staggered grid, finite difference technique which is a subset of the more general Finite Integration Technique. In our modeling code, long grounded dipoles are draped over topography. We can model and invert far-field, transition zone, and near-field data in a single workflow, as complete controlled source EM data.

Code verification was carried out using a sequence of 1D models of increasing complexity and comparing 3D results to those obtained with analytical 1D CSEM codes (not shown here). This confirmed that with reasonable gridding we can obtain accuracies to better than 2%, in line with typical finite difference numerical solutions.

SYNTHETIC EXAMPLE

We designed a test 3D model using real topography with about 800m relief (Figure 1). The 3D model has a background resistivity of 100 Ωm and hosts two pairs of 3200×2800×500 m anomalies of 10 Ωm and 5000 Ωm, respectively, draped below 1000m depth (Figure 1). Two perpendicular transmitter orientations were modeled. Receivers were spaced every 400 m, and offsets to the transmitter ranged from 3 km to 12 km. We modeled CSEM forward responses at 28 frequencies from 0.2 Hz to 500 Hz, using all components.

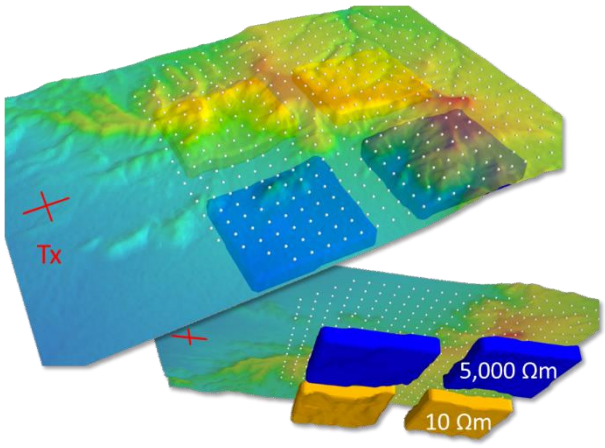

Figure 1. Setup of CSAMT simulated array over topography. The transmitter location (red cross) is to the west at 3 km from closest receivers. The four anomalous 500m thick bodies inserted at 1km below the surface are shown in orange and blue.

Figure 2 shows results from a number of 3D inversions of complex field amplitudes, all of which started from the background resistivity and used low structural regularization. Prior to the inversions we added 1.5% random Gaussian noise to the electric and magnetic fields of the CSEM data. Both the electric broadside data (top row) and the combined electric (scalar) broadside and inline data inversion (middle row) reveal the resistivity structure reasonably well, however the inversion involving the inline component resolves the resistor closer to the transmitter better due to the stronger vertical current flow in this configuration (Figure 3). Magnetic field inversions yield only a very smooth representation of the resistivity structure (Figure 2, bottom).

A question being discussed is whether field amplitude inversions have an advantage over impedance inversions (Routh and Oldenburg 2000). Here we have carried out an impedance inversion for the synthetic broadside setup, and these resulted in higher structural detail than the inversion of the corresponding electric field amplitudes, resulting in better impedance data fits (Figures 4 and 5).

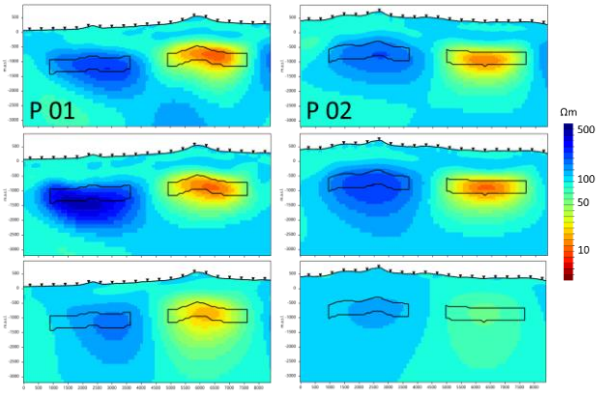

Figure 2. 3D CSEM field inversion results. Data input: top) broadside electric fields; middle) broadside & inline electric fields; bottom) broadside & inline magnetic fields.

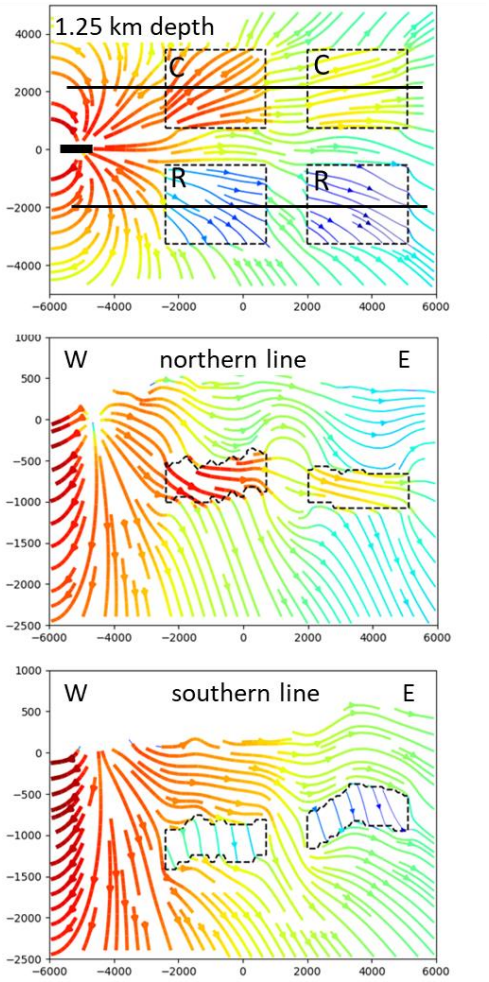

Figure 3. 3D current density for the transmitter in the inline configuration, at 0.2 Hz. Top: depth slice at 1.25km below surface; middle and bottom: cross sections, vertical exaggeration is 2.5. Warm colors and thicker lines mark higher current density.

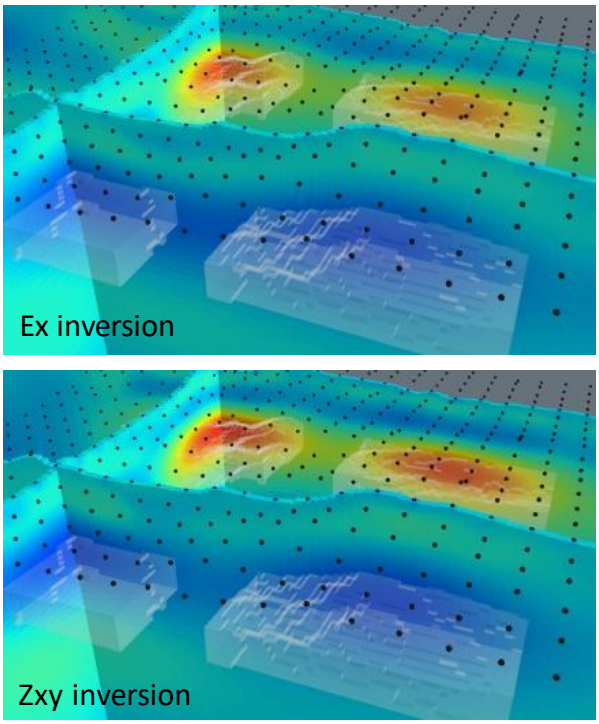

Figure 4. 3D CSEM electric field amplitude inversion (top) compared to the sharper 3D CSEM impedance inversion (bottom). Broadside data were used in both cases.

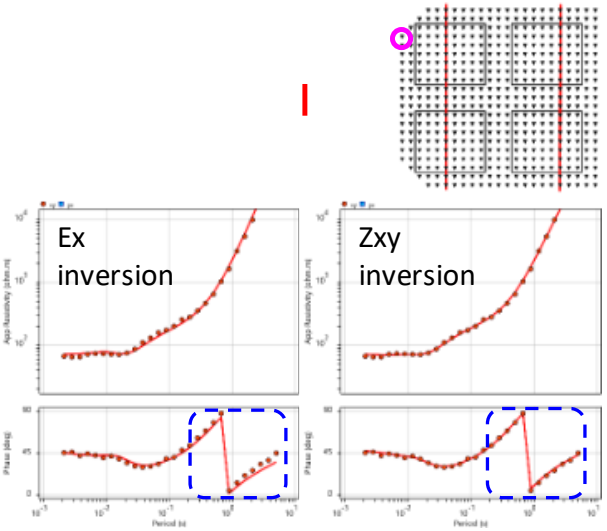

Figure 5. Impedance data fit at high angle from transmitter axis for electric field amplitude (Ex, left) and impedance (Zxy, right) 3D CSEM inversion. The impedance inversion achieves a better fit, as might be expected, as magnetic fields are not inverted in the Ex only inversion.

REAL DATA EXAMPLE - SILVERBELL

We applied our new inversion algorithm to a 1993 CSAMT legacy data set from the Silverbell mine in Arizona. Line and site spacing is 240m and 60m, respectively, and other geometric parameters are shown in Figure 6.

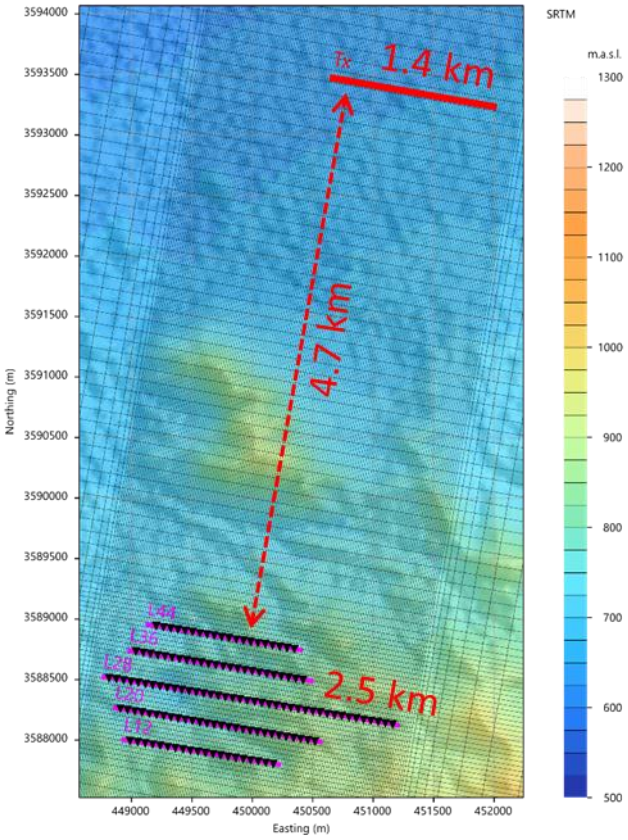

Figure 6. Scalar, broadside CSAMT survey at Silverbell. Transmitter-receiver distance is >4.7 km.

A 3D mesh was created with 20x60x10 m spacing in the topographic core, and a wider 100m crossline spacing between the transmitter and the receivers (1.5 million cells total). Input data for 3D CSEM inversions were scalar impedances at all 9 frequencies between 32 Hz and 8192 Hz. A homogeneous 150 Ωm was used as starting model.

The 3D CSEM inversion gives a good data fit across the full frequency range (Figure 7). Results are shown along line L28 in Figure 8 (bottom) in comparison with 1D and 2D MT inversions (TM-mode data). The 3D inversion provides a smooth image, without strong imprint from statics.

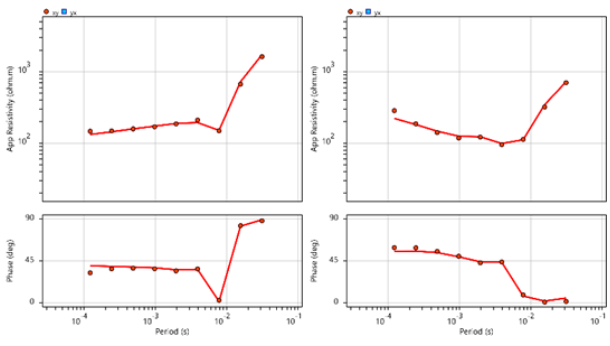

Figure 7. Data fit examples from 3D CSEM inversion impedance inversion at Silverbell.

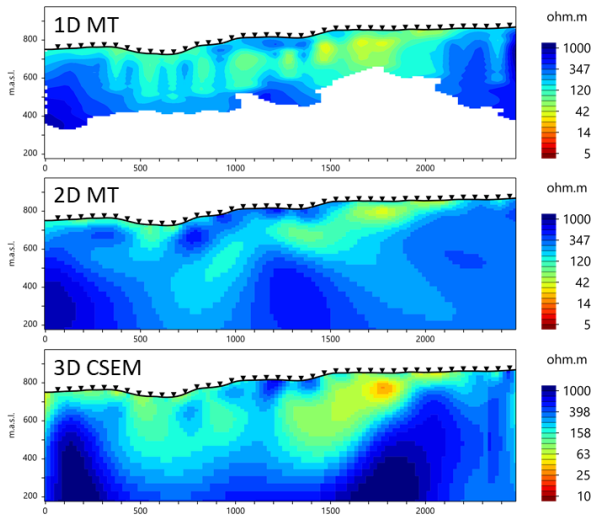

Figure 8. Comparison between 1D & 2D MT, and 3D CSEM impedance inversion, along line L28. Input data to MT TM-mode inversions excluded the lowest three frequencies. 1D inversions are affected by statics.

The 3D CSEM results also match well with earlier published 2D results (comparison not shown here). Note the Silverbell mine has evolved dramatically since the acquisition of this data set.

Conclusions

We have extended our land, marine and airborne 3D EM inversion modeling algorithms to include generic land controlled-source EM modeling. While we can now model any arbitrary set up of transmitter and receiver dipole orientations and locations, here we have concentrated on the typical CSAMT field deployment with one or two long grounded transmitter and an array of receivers at a certain offset. True controlled source inversion of the CSEM data results in good recovery of resistivity anomalies for the synthetic setup, especially when inverting impedances or inverting electric field data from two polarizations. An additional benefit is the ability to model all data from near-field through the transition zone and into the far-field, eliminating ad hoc methods to remove near-field and transition zone data.

Acknowledgements

We would like to thank Scott Urquhart and Scott McInnes from Zonge Intl. for providing the Silverbell data. We highly appreciate the sharing of industry insight by these and additionally Simon Mann (Zonge Australia), Roger Sharpe (Quantec) and Yann Avram (Phoenix).

References

Darnet M, Wawrzyniak P, Coppo N, Nielsson S, Schill E, Fridleifsson GO (2018) Monitoring geothermal reservoir developments with the Controlled-Source Electro-Magnetic method – A calibration study on the Reykjanes geothermal field: Journal of Volcanology and Geothermal Research: 391, doi:10.1016/j.jvolgeores.2018.08.015.

Grayver AV, Streich R, Ritter O (2014) 3D inversion and resolution analysis of land-based CSEM data from the Ketzin CO2 storage formation: Geophysics 79(2): E101–E114, doi:10.1190/Geo2013-0184.1.

Lin C, Zhong S, Auken E, Cai H, Tan H, Peng M, Kong W (2018) The effects of 3D topography on controlled-source audio-frequency magnetotelluric responses. Geophysics 83(2): WB97–108.

Mackie RL, Meju MA, Miorelli F, Miller RV, Scholl C, Shahir AS (2020), Seismic image-guided 3D inversion of marine controlled-source electromagnetic and magnetotelluric data. Interpretation 8: SS1-SS13.

Routh PS, Oldenburg, DW (2000) Advantages of field component inversion of CSAMT data, SEG Tech Program Expand Abstr doi:10.1190/1.1815997.

Sasaki Y, Yoshihiro Y, Matsuo K (1992) Resistivity imaging of controlled-source audiofrequency magnetotelluric data. Geophysics 57: 952-955.

Wang T, Wang K, Tan H (2017) Forward modeling and inversion of tensor CSAMT in 3D anisotropic media. Applied Geophysics 14: 590–605, doi:10.1007/s11770-017-0644-7.

Wannamaker P (1997) Tensor CSAMT survey over the Sulphur Springs thermal area, Valles Caldera, New Mexico, Part I: Implications for structure of the western caldera / Part II: Implications for CSAMT methodology: Geophysics 62: 451-465 / 466-476.

Zonge KL, Hughes LJ (1991) Controlled source audio-frequency magnetotellurics, in M. N. Nabighian, ed., Electromagnetic Methods in Applied Geophysics 2b: 713-809, Soc. Expl. Geophys, Tulsa

Abstract, 25^{th} EM Induction Workshop,Çeşmeı, Turkey, September 11-17, 2022

Using deep learning for model error estimation in 3D probabilistic inversion of controlled-source electromagnetic data

Matías W. Elías[1], Marina Rosas-Carbajal[2] and Fabio I. Zyserman[1]
[1]CONICET - Facultad de Ciencias Astronómicas y Geofísicas, Universidad Nacional de La Plata, Provincia de Buenos Aires, Argentina, melias@fcaglp.unlp.edu.ar, zyserman@fcaglp.unlp.edu.ar
[2]Université de Paris, Institut de physique du globe de Paris, CNRS, F-75005 Paris, France, rosas@ipgp.fr

SUMMARY

We propose a 3D Markov Chain Monte Carlo (MCMC) inversion of controlled-source electromagnetic (CSEM) data to image oil reservoirs. Simulation of the CSEM response with complex 3D geological structures becomes challenging when a large number of forward computations are required, which is the case when performing a probabilistic inversion. We use a parallel structure and an efficient nonconforming finite element algorithm to calculate the electromagnetic response by discretizing the diffusive frequency-domain Maxwell's equations. We compute the differences between solutions calculated with the same forward solver but with two different discretization sizes, and we use deep learning techniques to determine a low-dimensional probabilistic representation of this model discrepancies. We use this representation as prior information in the probabilistic inversion, which is then set to characterize not only the subsurface model parameters, but also the model errors caused by the use of the computationally-cheap coarse discretization.
Based on an array of receivers, we construct multichannel images of the field discrepancy between models for different frequencies and field components. We train a spacial generative adversarial network (SGAN) with those images, demonstrating that the network is able to capture the distribution function of the model error. The trained generator is added to the MCMC inversion algorithm. Then, at each step of the MCMC computation the forward response is corrected with a model error realization of the network.
We propose a synthetic marine CSEM experiment to test the MCMC recovery of model parameters and model error. We evaluate the feasibility of the method and emphasize the advantages of estimating modeling error and the use of a computationally-cheap forward model. This approach provides a complete probability distribution of the model parameters retrieved by the inverse problem. Assessing model uncertainty contributes to a more comprehensive interpretation of the geophysical measurements.

Keywords: Probability distributions, Neural networks, Controlled source electromagnetics

Abstract, 25^{th} EM Induction Workshop, Çeşmeı, Turkey, September 11-17, 2022

Surface geometry inversion of marine CSEM data

Xushan Lu[1,3*], Chris Galley[2], Peter Lelièvre[1], and Colin Farquharson[3]
[1]Department of Mathematics and Computer Science, Mount Allison University
[2]Department of Earth and Environmental Sciences, University of Ottawa
[3]Department of Earth Sciences, Memorial University of Newfoundland
xlu@mta.ca

SUMMARY

Traditional minimum-structure style inversion recovers models that are generally smooth due to the incorporation of the model roughness terms in the objective function being minimized. For certain models with a localized anomaly that have a distinct physical property contrast with the surrounding host rocks, such as seafloor massive sulphide (SMS) ore deposits, it is difficult to extract the boundary information of the ore body from the recovered models of minimum-structure inversion. We present a surface geometry inversion (SGI) method which directly inverts for the geometrical information of the ore body's boundary wireframe surface. The objective function of our SGI algorithm only has one data misfit term per geophysical data type. Regularization can be applied but is not required. For this example, we use only a single data misfit term. The minimization of the objective function is an over-determined problem, and we solve it using a global optimization algorithm, namely, the genetic algorithm. We present a synthetic study where we apply our SGI to the inversion of a marine controlled-source electromagnetic (CSEM) dataset. The synthetic model considers realistic bathymetry and the ore body has a complex shape based on a realistic SMS ore body. The surface of the ore body is constructed by connecting a small number of control nodes into triangular facets. We then use a subdivision algorithm to further subdivide the connected facets, which produces a model that has a more serpentine boundary surface although it is still characterized by the original set of control nodes. Constraints can be easily incorporated into the model by fixing certain nodes during the inversion when drilling data are available. In this study, we use our SGI algorithm to invert for the three-dimensional coordinates of these control nodes given a priori physical properties. However, it is possible to invert for physical properties of the ore body simultaneously, although it would increase the nonuniqueness of the inversion significantly. The physical property of the background model is always fixed during the inversion.

We discretize the entire model with unstructured tetrahedral meshes and then calculate the forward response using a finite-element solver. Our SGI algorithm iteratively searches for the best model that can fit the data. We parallelized our SGI using a hybrid MPI+OpenMP technique to speed up the inversion as there could be up to several hundreds of models required to be calculated in each iteration. Our synthetic inversion examples show that the developed SGI could recover models whose shapes are close to those of the true model.

Keywords: Marine CSEM, Seafloor massive sulphide, surface geometry inversion

Applying a multi-transmitter hybrid Conjugate Gradient-Occam algorithm to the inversion of 3D mCSEM data

W. Lima[1], G. Egbert[2] , N. Meqbel[1], A. Benevides[1], S. Fontes[1], E. LaTerra[1] and P. Werdt[1]
[1]Observatório Nacional Brazil, williamslima@on.br
[2]Oregon State University Corvallis USA, egbert@coas.oregonstate.edu

SUMMARY

We present the results of applying a hybrid conjugate gradient-Occam inversion algorithm to 3D marine CSEM data. The Occam scheme is a very effective way of dealing with the particular problem of choosing a value for the regularization parameter in an inverse problem. However, in the traditional implementation, the full Jacobian matrix is required—something which is not feasible for realistic 3D problems. Thus, iterative search algorithms which do not require the full Jacobian, such as NLCG, LBFGS, or iterative solution of the Gauss-Newton (GN) normal equations, are most commonly used for solving 3D EM inverse problems. Hybrid algorithms offer another option. In the basic hybrid scheme, the dataspace GN normal equations are solved iteratively (without computing the full Jacobian), but results of the forward and adjoint calculations required for each iterative step are saved. These are then used to construct a low dimensional approximation to the full Jacobian, and hence the GN equations. By solving the low-dimension approximate GN equations multiple times with different regularization parameters, an approximate Occam scheme can be efficiently realized. In addition to allowing use of GN methods such as Occam, generation of an approximate Jacobian through this hybrid approach will allow more complete and efficient exploration of trade-offs between fitting different data types (e.g., MT as well as CSEM), and provides an approximation to the linearized resolution operator.

For most EM inverse problems there are in fact multiple transmitters, characterized by source frequency and/or location. Gradient based optimization schemes (such as NLCG, as used in ModEM) require solving adjoint problems for every transmitter. Each of these is essentially the gradient (in the model space) of the data misfit penalty, restricted to data from that transmitter. The standard schemes merge these into a single gradient vector. With the multi-transmitter hybrid scheme we save all of this information about penalty functional gradients, and then uses this to form an improved approximation to the full Jacobian. We can anticipate that saving all of this information will be especially useful for mCSEM, and joint mCSEM/MT inversions – primarily because the transmitters (different dipole locations for mCSEM; plane wave sources for MT) are all quite different, so the corresponding gradient components will be more nearly independent. We are currently testing this idea using a mixture of Matlab and Fortran—the inversion algorithms being tested are coded in Matlab, and forward and sensitivity calculations are implemented through calls to ModEM. Communication between the two codes is through disk I/O. Although there is some loss of efficiency with such an approach, development and testing new algorithmic concepts is much faster in Matlab (especially since we already have a substantial Matlab code base). In our presentation we will present details on the new algorithms, and compare performance against other algorithms (e.g., NLCG) in terms of memory, number of iterations required for convergence, and total computing time.

Keywords: mCSEM inversion, Occam, hybrid, Conjugate Gradient

Abstract, 25^{th} EM Induction Workshop,Çeşmeı, Turkey, September 11-17, 2022

Real-time simulation of the electromagnetic field spatiotemporal evolution due to geomagnetic disturbances

M. Kruglyakov[1], A. Kuvshinov[2] and E. Marshalko[3]
[1]University of Otago, New Zealand, mikhail.kruglyakov@otago.ac.nz
[2]ETH Zurich, Switzerland, kuvshinov@erdw.ethz.ch
[3]Finnish Meteorological Institute, Finland, elena.marshalko@fmi.fi

SUMMARY

We present a methodology for real-time simulation of the electromagnetic (EM) field spatiotemporal dynamics in a given 3-D conductivity model of the Earth and continuously augmented inducing source data. The formalism relies on the factorization of the source by spatial modes and time series of respective expansion coefficients, works both on a global and regional scale (i.e. in spherical and Cartesian geometries) and allows researchers to compute high-resolution EM field in a fraction of seconds.

To validate the formalism, we invoke a 3-D conductivity model of Fennoscandia and consider a realistic source built using the Spherical Elementary Current Systems (SECS) method as applied to magnetic field data from the IMAGE network of observations. The factorization of the SECS-recovered source is then performed using the principal component analysis. Taking the 7–8 September 2017 geomagnetic storm as a space weather event, we show that real-time high-resolution 3-D modelling of EM field is feasible, requiring less than 0.025 seconds to compute the field at a given time instant on a 512×512 lateral grid.

We also discuss an application of the presented technique to global-scale simulations of magnetic and electric fields.

Keywords: Numerical methods, EM induction, 3-D modelling, Now-casting

HIP-FEM: A Hierarchical, Induced Polarization Finite Element Method for analysis of thin, dispersive, geoelectric features

C.J. Weiss[1,2] , G.D. Beskardes[1], and A. Darrh[1,3]

[1] Geophysics Department, Sandia National Laboratories, Albuquerque NM, USA, cjweiss@sandia.gov
[2] Earth and Planetary Science Department, University of New Mexico, Albuquerque NM, USA
[3] Geophysics Department, Colorado School of Mines, Golden CO, USA

Summary

One of the persistent challenges in computational geophysical electromagnetics is balancing the tension between the high computational cost of maximizing geologic realism and the necessity of rapid throughput of simulation results, whether for inversion, “real-time” decision making, experiment design, or construction of machine learning training sets. To this end, considerable effort has been spent over the decades on various effective medium methodologies, exotic reformulations of Maxwell’s equations in terms of non-local (fractional) operators, and a growing expanse reduced order model approaches. Here we expand on the latter by focusing on the hierarchical finite element approach (Weiss, 2017; Beskardes et al., 2021) and its extension to the physics of induced polarization through review of the relevant mathematics and analysis of model studies inspired by relevant and challenging mineral exploration scenarios. The occurrence of alteration halos around massive mineral bodies or mineral alteration along the complex fluid migration pathways in a leach pile or fault zone represent instances where the conductive feature of interest is intrinsically “thin” when compared to the surrounding geologic structures. Such conductive features – often with frequency-dependent electrical properties – discretize naturally in the hierarchical finite element framework which decomposes the electrical model into bulk contributions from volumetric elements, supplemented by infinitesimally thin contributions associated with the elements’ facets and edges where needed. This avoids the costly volumetric discretization of the latter and lies at the heart of the method’s overwhelming efficiency. The application and extension of the method we describe here represents a novel contribution toward further tilting the balance of geologic realism in the analyst’s favor while addressing the future of mineral exploration in developing tools to meet the demands of an emergent and global, green energy economy.

Keywords: mining geophysics, induced polarization, fractures, finite element modeling

Acknowledgements

Sandia National Laboratories is a multimission laboratory managed and operated by National Technology and Engineering Solutions of Sandia, LLC., a wholly owned subsidiary of Honeywell International, Inc., for the U.S. Department of Energy’s National Nuclear Security Administration under contract DE-NA-0003525. Finite-element meshes used for this analysis were generated by Cubit, available at http://cubit.sandia.gov. Funding support was provided by the Sandia National Laboratories LDRD program.

References

Beskardes, G.D., Weiss, C.J., Um, E., Wilt, M. and MacLennan, K., 2021. The effects of well damage and completion designs on geoelectrical responses in mature wellbore environments. *Geophysics*, **86**, no. 6, pp. E355–E366.

Weiss, C.J., 2017. Finite-element analysis for model parameters distributed on a hierarchy of geometric simplices. *Geophysics*, **82**, no. 4, pp. E155–E167.

Abstract, 25th EM Induction Workshop, Çeşme, Turkey, September 11-17, 2022

3-D radio-frequency CSEM at the Weidenpesch waste site in Cologne

M. Smirnova[1], B. Tezkan[1], A. Shlykov[2], S. Fadavi[1], A. Saraev[2], P. Yogeshwar[1]
[1]University of Cologne, maria.smirnova@uni-koeln.de
[2]Saint-Petersburg State University

Summary

A classical radio-magnetotelluric (RMT) method is routinely applied to various environmental, engineering, and exploration problems. The technique uses the radio-transmitters broadcasting electromagnetic fields at frequencies above 10 kHz. A significant disadvantage of RMT is a lack of robust radio transmitters in remote areas and a limited depth of investigation. To overcome these problems, the controlled sources can be used as an active source – the CSRMT method. Such modification allows measurements in remote areas and the extended frequency range (from 1 kHz to 1 MHz). However, with controlled sources, maintaining the plain-wave assumption at all frequencies and throughout the survey area is often problematic. In this contribution, we present an implementation of the CSRMT method with sources installed in the survey area (near-to-far-field zones). This is, in fact, a CSEM method working in the radio-frequency band. However, we consider impedance tensor and tipper vector transfer functions, which require measurement and modelling of two source polarisations. Here, we present the results of the radio CSEM measurements collected at the Weidenpesch waste site in Cologne. In the obtained 3-D model, the waste site is well resolved. The model agrees with the boreholes' interpretation and the area's known geology.

Keywords: CSRMT, CSEM, 3-D inversion, Weidenpesch waste site

Introduction

The concept of using controlled sources (CS) to improve the data quality and depth of investigation of AMT and RMT methods has earlier shown its potential (Hughes&Carlson 1987; Bastani 2001). There, sources were installed in the far-field to fulfil the plane-wave assumption. One of the disadvantages of such far-field CSAMT/CSRMT (Saraev et al 2017) is that there are still some source effects in the data (Li&Pedersen 1991), or if the source is too far, the signal-to-noise ratio decreases substantially. Here, we present the CSRMT method, with sources installed in the survey area (measurements in near-to-far-field zones), which is, in fact, a CSEM method working in the radio-frequency band. In this case, the source geometry must be considered during modelling. We have implemented the modelling and inversion for the 3-D case using our finite-difference code in Matlab (Egbert et al., 2017, Cherevatova et al., 2018). We consider two perpendicular sources (horizontal electric dipole (HED) lines) to estimate the impedance tensor and tipper vector transfer functions. Such an approach avoids measurements of the current strength time series, which is difficult at high frequencies.

Several CSRMT field surveys have been conducted to verify the method. Here, we present the results of the CSRMT survey over the Weidenpesch waste site in Cologne, Germany. This area was selected because the conductive waste site is buried in a contrasting, more resistive host rock. The geology of the sub-surface, composition and history of the waste site is well known. The waste site is about 400 m by 90 m in lateral size and about 10 m thick. It comprises various building debris, household wastes, dust, grinding, and stone materials and is surrounded by relatively resistive gravel and sand. The site is closed and covered with a thin layer of fine silty sand (0.5-2.5 m thick). In addition to CSRMT measurements, ERT, magnetic and TEM data were acquired and will be used later for comparison.

Methods

The 3-D radio-frequency CSEM modelling and inversion was implemented within the MR3DMod framework – an object-oriented code in Matlab. The code was initially created as a prototype of MT ModEM software (Egbert&Kelbert 2012, Egbert et al. 2017), later extended for other methods, e.g., CSEM, TEM, DC, gravity and magnetics. Thus, as in ModEM, the modelling is performed using finite-difference approximation on a staggered grid. For CSEM, we followed the scattered-field approach (Newman&Alumbaugh 1995), where the total field (we solve for $\mathbf{E}$ field) is split into the background and anomalous (scattered) parts: $\mathbf{E} = \mathbf{E}_b + \mathbf{E}_a$. The background EM field is calculated using 1-D quasi-

analytical code of Key (2009). The anomalous field is calculated by solving a system of partial equations:

$$\nabla \times \nabla \times \mathbf{E}_a + i\omega\mu_0\sigma\mathbf{E}_a = -i\omega\mu_0(\sigma - \sigma_b)\mathbf{E}_a, \quad (1)$$

where the right-hand side is an external source term, μ_0 is the magnetic permeability of free space, ω is the angular frequency, and σ_b is the background conductivity (1-D half-space). In this study, we neglect the displacement currents as the sub-surface's resistivity is below 1000 Ωm, and there is no evidence of the strong polarisation effects in the field example discussed later. Once the solution for the anomalous electric field is obtained, the anomalous magnetic field is computed as

$$\mathbf{H}_a = \frac{1}{i\omega\mu_0}\nabla \times \mathbf{E}_a. \quad (2)$$

The total magnetic field is then calculated as a superposition of the background field and anomalous field: $\mathbf{H} = \mathbf{H}_b + \mathbf{H}_a$. Equations 1 and 2 are calculated twice, once for each source polarisation. Then, EM fields are interpolated from grid edges/faces to the site locations, and impedance tensor or tipper vector transfer functions are estimated. The subsequent procedure for calculating the Jacobian is the same as in Egbert&Kelbert 2012 with a non-zero source (CSEM and adjoint cases). For inversion, we used the data space-Occam method (Siripunvarapon et al. 2004).

Results

The Weidenpesch survey was conducted in two phases. The first phase was CSRMT/RMT far-field measurements. The second phase, discussed in this contribution, was the transition zone CSRMT (Figure 1). Two perpendicular HED sources (Tx1 – 215 m, Tx2 – 465 m) were installed in the survey area. Source current was variable between 1 A and 7.5 A. Measurements were performed along a set of profiles (red circles in Figure 1) crossing the waste site (dashed grey line in Figure 1). The distance between profiles is about 30 m and between sites about 10 m. At each site, six recordings were done, three for each source at base frequencies of 0.5, 5, and 50 kHz, to cover the complete frequency range from 1 kHz to 1 MHz. The data were processed using the KMSProMT software (Smirnov 2003), which was adopted for CSEM processing by adding the discrete frequency selection (Smirnova et al. 2019).

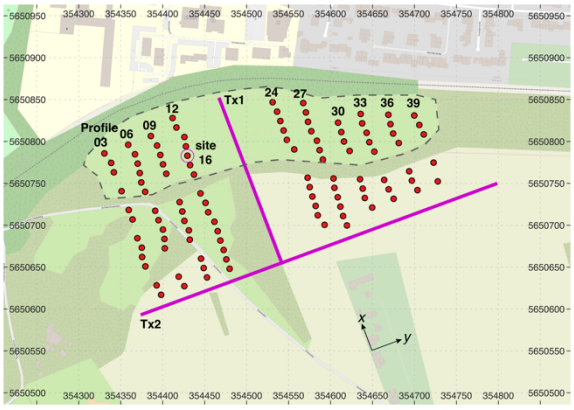

Figure 1. Survey plan for CSRMT measurements in the transition zone at Weidenpesch, Cologne. Red circles mark the location of the receivers; magenta lines are source locations. The waste site is outlined with a dashed grey line. Local coordinate system *xy* is shown on the map.

Figure 2 shows a pseudo-section of the *yx* component of the apparent resistivity and impedance phase for profile 12 (Figure 1). The apparent resistivity ranges from around 1 Ωm to 1000 Ωm. There is a clear boundary between the conductive waste site in the NW of the profile and the resistive background in the SE. The data are consistent from site to site and with a period, indicating good data quality.

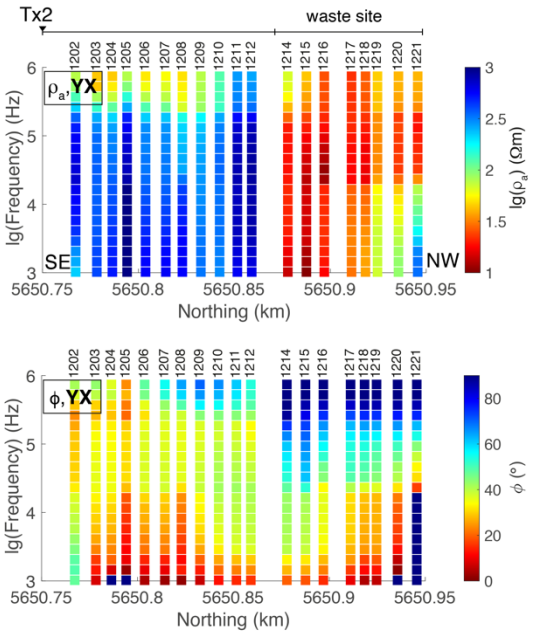

Figure 2. Pseudo-section of the *yx* apparent resistivity (top) and impedance phase (bottom) at profile 12 (see location in Figure 1).

In Figure 3, an example of a typical sounding curve at the waste site is shown (site 16 along profile 12 in Figure 1).

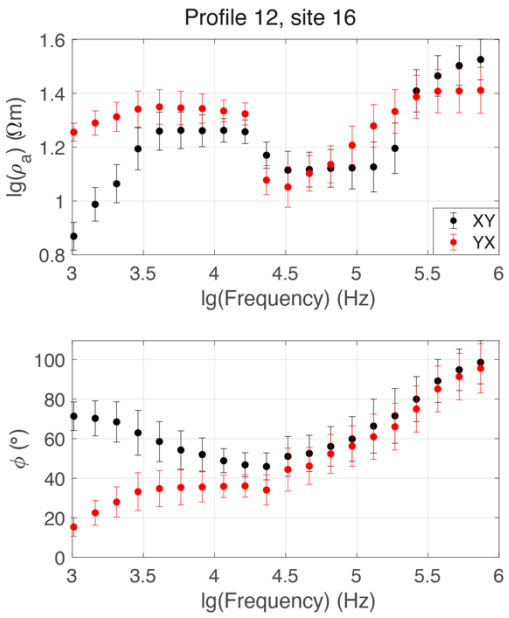

Figure 3. Apparent resistivity and impedance phase of the off-diagonal components of the impedance tensor at the selected site (see location in Figure 1).

In Figure 3, the *xy* slices from the 3-D model are shown at different depths (1 m, 2.1 m, 3.3 m, and 9.5 m). The model was obtained after inverting the impedance tensor at 114 sites in the frequency range from 1 kHz to 524 kHz. Error levels were set at 5% $\sqrt{|Z_{xy}Z_{yx}|}$ for all impedance components. The coordinate system was rotated by $20°$ to reduce the mesh size. The modelling domain was then discretised into 96x96x50 cells with a minimum 11 m cell size in the *x*-direction, 6 m in the *y*-direction and 1 m in the *z*-direction. A half-space of 50 Ωm was used as the initial model. The inversion converged to an RMS of 2.5.

Discussion

The highly conductive (1-10 Ωm) waste site is well resolved in the 3-D model (see slice at a depth of 3.3 m in Figure 4). The top of the anomaly is at a depth of around 2 m, and its thickness is about 7 m. The waste is covered by a resistive layer of fine silty sand (up to 1000 Ωm and about 1 m thick). The waste is underlain by a more resistive layer of gravel and sand (around 100 Ωm). This layering structure agrees with borehole interpretations, suggesting the top 2 m layer of fluviatile clays, underlain by a 20 m thick Pleistocene gravel and sand layer.

Conclusions

We presented a radio-frequency CSEM method (CSRMT in the transition zone) in this contribution. We developed and tested an algorithm for CSRMT 3-D modelling and inversion for the case when data are acquired in the vicinity of the source. Such an approach allows us to extend the measurement frequency range, depth of investigation and improve the signal-to-noise ratio. Additionally, it simplifies the survey planning and logistics, as sources can be installed directly in the survey area. We presented a real-field case study for the Weidenpesch waste site in Cologne. The 3-D model clearly outlines the waste site's location and shape and agrees with borehole data and geology.

Acknowledgements

The project was funded by the German Research Foundation (DFG) under grant number TE 170/21-1 and by the Russian Science Foundation, project number 21-47-04401.

References

Bastani M (2001) EnviroMT: A new controlled source/radio magnetotelluric system. PhD thesis, Uppsala University, Uppsala

Cherevatova M, Egbert GD, Smirnov MY (2018) A multi-resolution approach to electromagnetic modelling. Geophysical Journal International 214: 656—671

Egbert GD, Kelbert A (2012) Computational recipes for electromagnetic inverse problems. Geophysical Journal International 189: 251—267

Egbert GD, Smirnov MY, Cherevatova M (2017) Development of Flexible Object-Oriented MATLAB Codes for 3D EM Modeling. 6th International Symposium on Three-Dimensional Electromagnetics, Expand Abstr.

Hughes L, Carlson N (1987) Structure mapping at Trap Spring Oil eld, Nevada, using controlled-source magnetotellurics. First Break 5(11)

Key K (2009) 1D inversion of multicomponent, multifrequency marine CSEM data: Methodology and synthetic studies for resolving thin resistive layers. Geophysics 74: F9—F20

Li X, Pedersen LB (1991) Controlled source tensor magnetotellurics. Geophysics 56: 1456–1461

Newman GA, Alumbaugh DL (1995) Frequency-domain modelling of airborne electromagnetic responses using staggered finite differences. Geophysical Prospecting 43: 1021—1042

Saraev A, Simakov A, Shlykov A, Tezkan B (2017) Controlled source radiomagnetotellurics: A tool for near surface investigations in remote regions. Journal of Applied Geophysics 146: 228—237

Siripunvaraporn W, Uyeshima M, Egbert G (2004) Three-dimensional inversion for network-magnetotelluric data. Earth, Planets and Space 56: 893—902

Smirnov MY (2003) Magnetotelluric data processing with a robust statistical procedure having a high breakdown point. Geophysical Journal International 152: 1—7

Smirnova M, Becken M, Nittinger C, Yogeshwar P, Moerbe W, Rochlitz R, Steuer A, Costabel S, Smirnov MY, DESMEX Working Group (2019) Three-dimensional inversion of semi-airborne data from the flight experiment over an ancient mining area near Schleiz, Germany. Geophysics 84: E281—E292

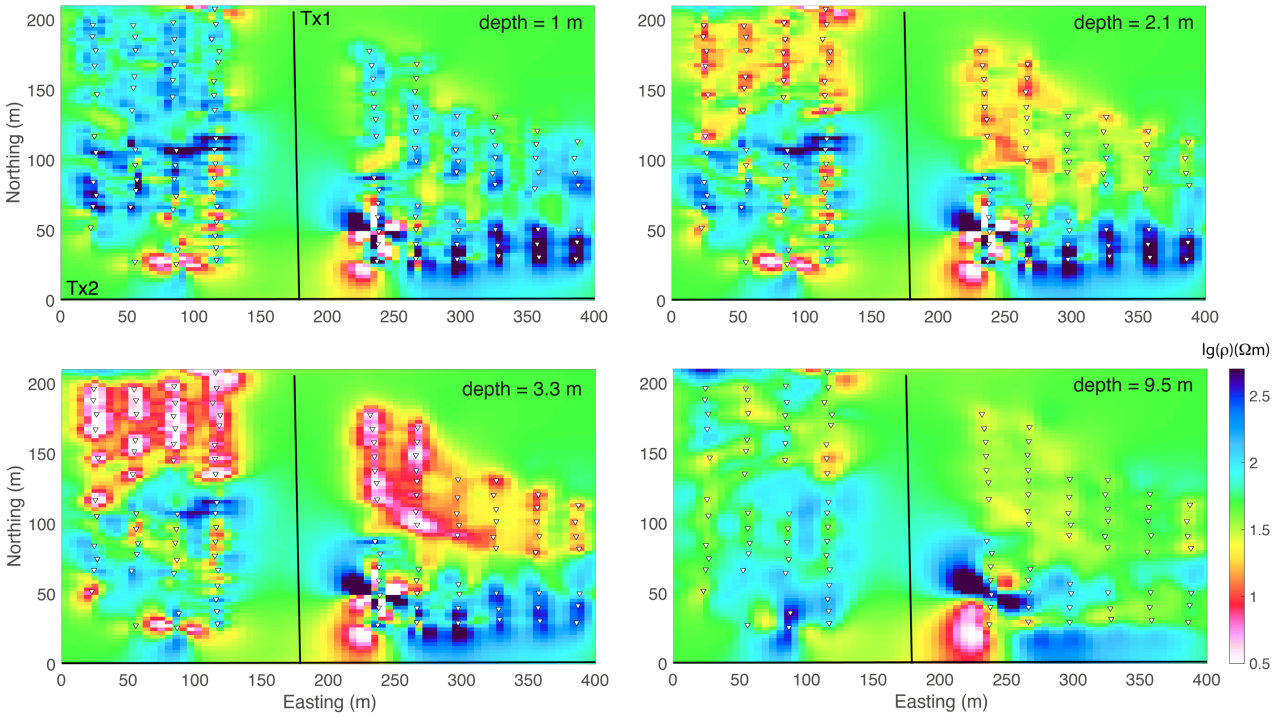

Figure 4. 3-D Weidenpesch waste site model. Horizontal *xy* slices at different depths. Black lines indicate the location of the source, and white triangles – represent sites.

Hybrid GPU solution to regularized divergence-free curl-curl equations for electromagnetic inversion problems

Hao Dong[1,2]*, Kai Sun[3], Gary Egbert[4], Anna Kelbert[5] and Naser Meqbel[6]

[1]China University of Geosciences, Beijing,
[2]State Key Laboratory of Geological Process and Mineral Resources, Beijing
[3]Nvidia Corporation, Beijing
[4]Oregon State University, Corvallis
[5]United States Geological Survey, Denver
[6]3D Consulting-GEO GmbH, Berlin
*donghao@cugb.edu.cn

SUMMARY

The Curl-Curl equation is the key to the time-harmonic electromagnetic (EM) problems in geophysics. The efficiency of its solution is decisive to the performance of EM simulations, which account for over 90% of the computation cost in inversions like Magnetotellurics or controlled source EM problems. However, most published EM computation codes are still CPU-based and cannot utilize the recent computation techniques with GPUs. Based on the previously proposed divergence-free algorithm developed on CPUs, this study demonstrates the current limits of the CPU-based inversion procedure. To exploit the high throughput computational ability of GPUs, the study proposes a hybrid CPU-GPU framework to solve the forward and adjoint problems of the EM inversions. The large sparse linear systems arise from the staggered-grid finite difference approximation of curl-curl problems are solved with a new mixed-precision Krylov subspace solver. The algorithm is implemented with the ModEM modular inversion package and with both synthetic and real-world magnetotelluric examples. The results show a promising 15-30x speed-up for the solution stage of the curl-curl equations over single-CPU calculations. On real-world inversion test cases, the overall performance of a GPU-attached computation node with the new hybrid framework is comparable to that of four CPU-only nodes with conventional ModEM implementation. This would make the large-scale frequency domain EM inversions possible on smaller modern GPU platforms with reduced carbon footprint.

Keywords: divergence-free, curl-curl equation, GPU, magnetotellurics, inversion

Speeding up the inversion of the 3D MT problem

D. Varılsüha[1]
[1]Istanbul Technical University, deniz.varilsuha@itu.edu.tr

SUMMARY

In this study, I have investigated different algorithms that can greatly reduce the inversion time of a 3D Magnetotelluric problem. These algorithms include the right choice of the partial differential equations to solve an EM problem, a hybrid finite-difference and finite-elements numerical technique, employment of multiple GPUs for the calculations, the mesh decoupling technique, and other good implementation practices. When all of them are applied in conjunction, the inversion time for a medium-sized 3D problem can be completed in around an hour.

Keywords: 3D, Magnetotellurics, GPU computing, Hybrid Numerical Technique.

Introduction

Any 3D interpretation or inversion of geophysical data is computationally challenging. Researchers who develop such software have to deal with long compute times that can vary from hours to days to obtain reasonable 3D models. In reality, an inversion tool should be rerun several times with different parameters to be sure of the final results. This may even lead to greater compute time and also it limits the possibility of one experimenting with the existing code. In this study, the 3D MT inversion problem is investigated and different algorithms are applied to the forward and inverse parts of the problem to speed up the inversion.

Methods

For the MT problem, either second-order E field or H fields obtained from Maxwell equations are solved in quasi-static approximation for the forward problem. The resulting linear system can be solved either by direct methods such as LU decomposition or iterative methods such as conjugate gradients (CG). The latter approach is better and more efficient for larger systems. However, the iterative solution's convergence might be affected by round-off errors and it may need an additional routine called divergence correction of E fields for low frequencies as the linear system gets more and more ill-conditioned when the frequency value gets closer to zero. For that reason, there are many different partial differential equations (PDE) to solve for various reasons to obtain the same fields. Varılsüha and Candansayar (2018) investigated these PDEs that can be solved iteratively in the least amount of time and the following is found to be the fastest when compared to others.

$$\nabla x \nabla x \mathbf{A} + \mu_0 \sigma (\mathrm{i}\omega \mathbf{A} + \nabla \psi) = 0 \quad (1)$$

$$\mu_0 \nabla . \sigma \mathbf{A} + \frac{\mu_0}{\mathrm{i}\omega} \nabla . \sigma \nabla \psi = 0. \quad (2)$$

E-fields are calculated via

$$\mathbf{E} = -\mathrm{i}\omega \mathbf{A} - \nabla \psi \quad (3)$$

The iterative solution of the coupled system of (1) and (2) reduce the number of iterations required by half on average when compared to the classical E-field formulation.

The most common numerical techniques to solve a given problem are finite-differences (FD) and finite-elements (FE) approaches. When a model has a flat surface, it is a common approach to use simple blocks and employ the FD technique due to its simplicity. The FE technique is necessary when distorted hexahedral elements or tetrahedral elements are present. Implementation-wise, it can be a good approach to start with a structured and non-distorted mesh. Later topographic features such as hills and valleys can be added by distorting the mesh. This will result in a partially distorted mesh and the suggested technique by Varılsüha (2019) can be used to take advantage of both FE and FD techniques by employing both of them in a single mesh.

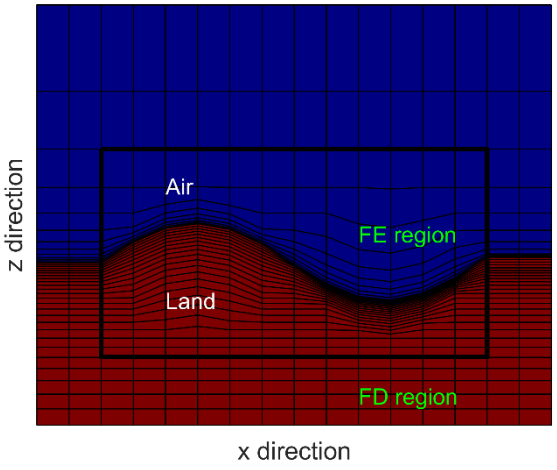

Figure 1. A depiction of the hybrid numerical technique is given for a 2D mesh. While the distorted FE region is solved with finite elements, the undistorted blocks are solved with finite-difference methods

The main advantage of this hybrid technique is its

computational cost. The linear systems resulting from the pure FD technique can be solved with half of the time required by the FE technique. It also requires one-third of the memory required by the FE method. The meshes formed and used in this study have only 5 to 20 percent of their cells distorted and thus require the FE method. So, this ultimately means that the hybrid method is almost as efficient as the FD approach while being able to represent the topographic features for the model used in this study. It is also worthy to state it reduces the required memory space which could be very important when GPUs are used to solve the equations and considering their limited amount of memory space.

It is the most straightforward approach to use a single mesh for all data, frequencies, and receivers. It is also a common approach to use multiple smaller meshes for different receivers to reduce computational overburden, especially for airborne EM and time domain EM studies. It can be possible to employ this technique for the frequency domain MT problem. Varılsüha (2020) showed that different meshes can be created for different frequency groups since higher and lower frequencies have different penetration depths. In this study, the same technique is employed and smaller meshes are later mapped to the parameter mesh with a mapping matrix. Figure 2 depicts a picture of a parameter mesh and two local meshes for a high-frequency group and a low-frequency group. By using different smaller meshes for different frequencies, as opposed to using a single large mesh, it was possible to at least halve the total number of cells for the forward modeling meshes used in this study. This ultimately means halving the time for the forward modeling and thus inversion time.

High performance and parallel computing can also reduce computational time. It is common to use multi-core CPUs or multiple CPUs in a workstation to divide up the work using libraries such as MPI or OpenMP. In the last decade, GPU computing has become popular and the platform itself has shown to have the potential to speed up numerical computations. It is also possible to plug in multiple GPUs to a single computer to speed-up calculations even more. This could be also an important feature because one doesn't need to deal with large and complicated shared or distributed memory clusters since it is easy to plug in more GPUs to a single computer and it is easy to configure the new hardware. For these reasons, in this work, I have used 8 GPUs (Nvidia RTX 3090) along with a 10-core CPU (Intel 10900K) to do the numerical crunching using Matlab. The experimentation showed that using 8-GPUs in parallel speed-up the computations by 8-fold when compared with parallel computing using the multi-core CPU.

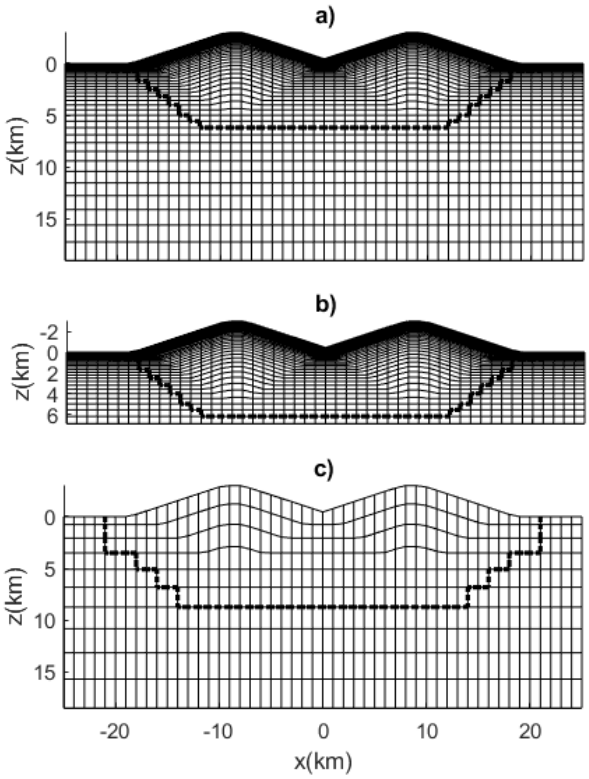

Figure 2. a) The parameter mesh and the forward modeling mesh without the mesh decoupling technique. b) mesh for the highest frequency group and c) mesh for the lowest frequency group when the mesh decoupling technique is employed. The dashed line shows the barrier between FE and FD regions for the hybrid numerical technique.

A regular consumer-grade CPU could have a core count between 1 and 64. On the other hand, a consumer-grade GPU might have a core count of 10000. In addition to that, GPUs have their dedicated memory and the memory bandwidth on the GPU can exceed the bandwidth between CPU and RAM by 10 to 20 times. This is an important detail because the linear algebra for sparse matrices is often memory-bounded as opposed to being compute-intensive. This means higher memory bandwidth of a system can greatly reduce the computation times. For that reason, multiple GPUs are employed to solve the linear system iteratively using a Conjugate gradient (CG) method in this study to achieve significant speed-ups. However, to make the algorithm converge to a solution in a fast manner, the CG system must be preconditioned using a preconditioner matrix. Usually, the preconditioner matrix is decomposed into two triangular matrices using the incomplete lower-upper algorithm (ILU(0)) and it is applied to a given vector in every step of the iterative solver by forward and backward sweeping. This operation can be challenging for GPUs because sometimes it can be difficult to find parallelism for a given preconditioner matrix. My experimentation also

confirmed that 80 to 90 percent of GPU time is spent doing the triangular matrix solutions. I also noticed that solving larger linear systems makes the GPU more efficient, however, this ultimately means larger models and longer inversion times. To make the computations more efficient, I came up with an implementation detail that resulted in a 15-20 percent decrease in forward modeling time. For the 3D MT problem, a linear system such as $Ax = b$ is solved for two polarizations. Instead of solving it twice for different RHS vectors, I've found that solving the following is more efficient,

$$\begin{bmatrix} \mathbf{A} & 0 \\ 0 & \mathbf{A} \end{bmatrix} \begin{bmatrix} \mathrm{x}_1 \\ \mathrm{x}_2 \end{bmatrix} = \begin{bmatrix} \mathrm{b}_1 \\ \mathrm{b}_2 \end{bmatrix} \quad (4)$$

where x_1 and x_2 are the solution for two polarizations. This technique is implemented in the inversion algorithm fully.

To test all the techniques presented in this work all at once, a previously published dataset that would require a medium-sized model is chosen. This dataset is also inverted by other people so it was possible to compare the inversion results to test the accuracy of this algorithm. The dataset named two mountain model's data is first created and used by Usui (2015) and I obtained it by contacting the author. It has 40 receiver points and 16 frequencies. Every receiver has 4 components of the impedance tensor and 2 components of Magnetic Transfer Function (MTF) for all frequencies. The data also has additional noise and real-valued distortion components to make it harder to invert. In this study, I inverted the data to obtain the original model and the distortion tensors as parameters. In Figure 3 the true model that the data is obtained from is given.

The inversion is carried out by minimizing the following objective functional by the L-BFGS algorithm.

$$\phi(\mathbf{m_\sigma}, \mathbf{m_C}) = \phi_\mathrm{d}(\mathbf{m_\sigma}, \mathbf{m_C}) + \lambda\phi_\mathrm{m}(\mathbf{m_\sigma}) + \kappa\phi_\mathrm{C}(\mathbf{m_C}) \quad (5)$$

where ϕ_d , ϕ_m and ϕ_C are data misfit, model roughness, and distortion intensity. λ and κ are trade-off parameters that would be adjusted as the inversion is carried out. $\mathbf{m_\sigma}$ and $\mathbf{m_C}$ are model parameters for the conductivity and the distortion tensor that are being obtained in inversion.

In Figure 4, it can be seen the inversion results are side by side with the true model. In this inversion, the impedance tensor (**Z**) and the MTF vector (**W**) are used as data. In addition to those, the distortion tensor for both **Z** and **W** is estimated as a parameter to obtain better models. Distorted tensors could be expressed as

$$\mathbf{Z}_\mathrm{D} = \mathbf{C}_\mathrm{h}\mathbf{Z} \quad (6)$$

$$\mathbf{W}_\mathrm{D} = (\mathbf{W} + \mathbf{C}_\mathrm{z}\mathbf{Z}) \quad (7)$$

$\mathbf{Z}_\mathrm{D}$ and $\mathbf{W}_\mathrm{D}$ are the distorted forms of data. $\mathbf{C}_\mathrm{h}$ and $\mathbf{C}_\mathrm{z}$ are the horizontal and vertical distortion tensor and vectors respectively. In this study, they are estimated as a parameter to obtain much correct inversion.

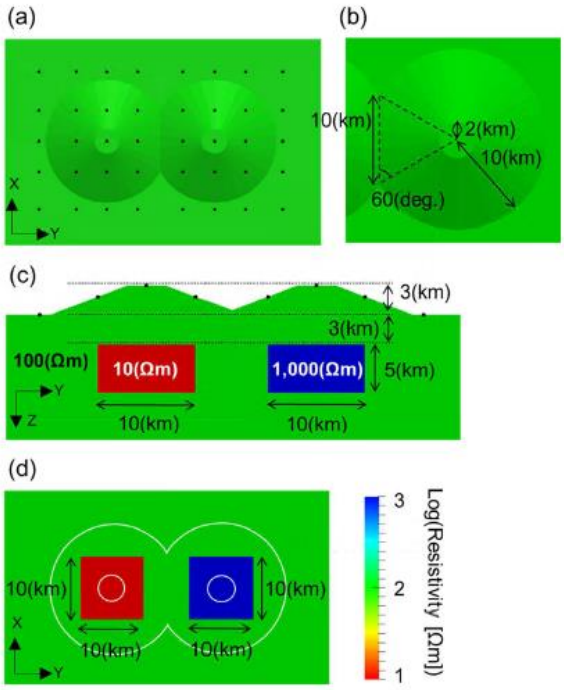

Figure 3. The figure is taken from the work by Usui, 2015. a) and b) shows the surface topography in detail. c) and d) show the exact spot and sizes of conductive and resistive anomalies. In this study, x and y directions are reversed and named y and x directions respectively.

Results

It took 45 inversion steps to obtain the results given in Figure 4. The location of both conductive and resistive anomalies are found correctly however the resistivity value of the resistive structure is estimated at 300 Ωm which is far away from its true value. However, considering the nature of the MT method and its insensitivity to resistive structures, these findings can be considered normal. The same inversion is also carried out by using only the impedance data (while estimating the distortion tensor also) and a very similar model is obtained from it. However, it took 52 steps to complete the inversion and this ultimately means that the joint inversion solves the problem in a lesser amount of time. It should be noted that the joint inversion of different data types can potentially reduce the computation times significantly.

The model given in Figure 4 had 116K parameters and 50 31 and 75 cells in x, y, and z directions respectively. Using all techniques described in this study helped to reduce the total inversion time to an hour. Even though the inversion code requires special hardware such as GPUs to run, the algorithms described here can be coded for any architecture and run on any hardware. These

results also prove that the same techniques could be applied to other EM problems or other elliptic problems to achieve similar results.

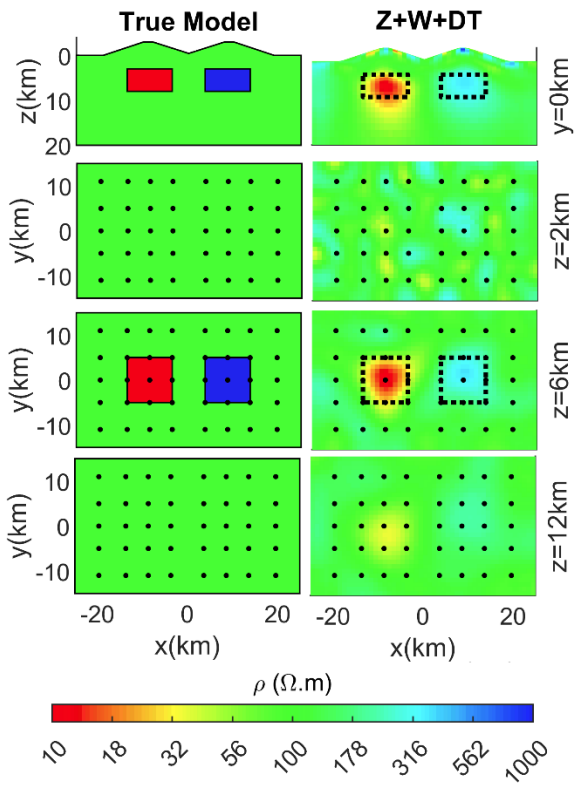

Figure 4. The true model and the model obtained by the joint inversion of impedance tensor and MTF vector. The dashed lines indicate the position of true anomalies. The inversion is performed by jointly inverting the impedance (**Z**) and MTF (**W**) data while estimating the distortion tensor (**DT**)

Discussion

When dealing with anisotropic forward modeling for an EM problem, the Lebedev grids can be employed especially when an FD grid is in mind with E fields defined on the edges. This not only helps with the numerical discretization of the anisotropic PDE but also helps to reduce the size of the mesh. The Lebedev grid technique requires 3 more meshes shifted to the original mesh so the total computational time seems to get quadrupled however at the same time it significantly increases the accuracy of the forward solution. This can also mean that a coarser mesh can be adapted and the same accuracy of a single mesh could be achieved. The important detail about the Lebedev grids is that they will generate 4 independent meshes for the isotropic case instead of one. When coupled with the idea given in Equation 4, it will make the forward solution on a GPU even more efficient. I have experimented with this idea and a model with no topography, and I've seen a further increase in efficiency. However, due to the topography of the model used in this study, it is not considered here.

Conclusions

There is no single answer when it comes to speeding up a geophysical inverse problem. In this study, I show that various techniques must be implemented together to achieve significant results. Simple parallelization techniques or better/faster hardware alone may not be enough. A correct choice of the PDE, hybrid numerical techniques, the mesh decoupling approaches also play a great role to achieve exceptional timings because every technique shown in this study has the potential to reduce the computational time significantly however when all of them are employed together the final speed-up is the multiplication of the speed-ups of all of them. This study concludes that these techniques can reduce the total inversion time by almost 2 orders of magnitude.

References

Usui Y (2015) 3-D inversion of magnetotelluric data using unstructured tetrahedral elements: applicability to data affected by topography, Geophysical Journal International 202, 828-849.

Varılsüha D (2019) Fast Three Dimensional Inversion of Magnetotelluric data based on Finite Difference and Finite Element Hybrid Forward Modeling, Ph.D. thesis, Ankara University, Ankara.

Varılsüha D (2020) 3D inversion of magnetotelluric data by using a hybrid forward-modeling approach and mesh decoupling, Geophysics 85, E191-E205.

Varılsüha D, Candansayar ME (2018) 3D magnetotelluric modeling by using finite-difference method: Comparison study of different forward modeling approaches, Geophysics 83, WB51-WB60.

Abstract, 25^{th} EM Induction Workshop,Çeşmeı, Turkey, September 11-17, 2022

Open-source 3D inversion of semi-airborne electromagnetic data

R. Rochlitz[1], T. Günther[1] and M. Becken[2]
[1]Leibniz Institute for Applied Geophysics, Hanover, Germany, raphael.rochlitz@leibniz-liag.de
[2]Department of physics, University of Münster, Germany, michael.becken@uni-muenster.de

SUMMARY

We present a new 3D inverse modeling scheme for semi-airborne controlled-source electromagnetic data building upon the open-source modeling software custEM and the open-source inversion framework pyGIMLi. The underlying geometries include arbitrarily shaped transmitters on the surface with topography and airborne receivers in the air or on the ground. The topography prohibits the exploitation of secondary-field formulations with semi-analytic primary-field solutions, such as commonly used in marine or airborne environments. We are able to account for realistic survey geometries with an irregular tetrahedral discretization of the modeling domain. We use a finite-element electric-field approach with a total-field formulation and first- or (preferably) second-order polynomial basis functions as implemented in custEM. Solving the resulting linear systems of equations with a direct solver enables us calculating explicit sensitivities with comparatively cheap back-substitutions for hundreds of airborne or ground receiver stations in multiple flight areas with several transmitters. The pyGIMLi framework provides a fast-converging Gauss-Newton minimization scheme for the inversion process. We apply our developed tools on a synthetic model and a semi-airborne data set of combined flight areas with 4 transmitters. The data with 12 frequencies in the range of 7 to 1000 Hz cover a total area of approximately 50 km2 and provide a penetration depth of up to 1000 meters. Our final 3D resistivity model matches well the available geological information. Reference inversion results from the analysis of 2D ERT and EM data on a central profile are overall consistent with the 3D inversion results but provide also insights about the limitations of 2D methods in a 3D geological environment. The developed procedure is not only applicable for semi-airborne data sets, but also capable of handling other controlled-source electromagnetic survey geometries. The presented results and tools are freely available as the underlying software.

Keywords: numerical solutions, electromagnetic theory, inversion, finite element method, controlled-source electromagnetics

Abstract, 25^{th} EM Induction Workshop, Çeşmeı, Turkey, September 11-17, 2022

Application of the total and scattered field decomposition and perfectly-matched layers to improve the accuracy in electromagnetic modelling

L. M. Buntin[1], T. Kalscheuer[2], G. Kreiss[3] and Z. Ren[4]
[1]Dept. of Earth Sciences, Uppsala University, Uppsala, Sweden, laura.buntin@geo.uu.se
[2]Dept. of Earth Sciences, Uppsala University, Uppsala, Sweden, thomas.kalscheuer@geo.uu.se
[3]Dept. of Information Technology, Uppsala University, Uppsala, Sweden, gunilla.kreiss@it.uu.se
[4]School of Geo-science and Info-Physics, Central South University, Changsha, China, renzhengyong@csu.edu.cn

SUMMARY

Inhomogeneous Dirichlet boundary conditions are routinely applied in 2D magnetotelluric forward modelling. However, the finite size of the modelling domain results in false reflections of the anomalous field at the boundaries, because the prescribed boundary fields are normal fields. Hence, the anomalous field is not accounted for, and the solution accuracy may be significantly reduced. To eliminate such false reflections, we introduce the *total and scattered field decomposition* (TSFD) to geophysical modelling. This makes it possible to apply fully absorbing boundary conditions to the scattered (often anomalous) field, and we apply perfectly-matched layers. In the TSFD, the modelling domain is split into two regions: in the total-field region, encompassing receiver sites and geological targets, the unknowns are total-field values, and in the scattered-field region, consisting of boundary regions, the unknowns are scattered-field values. At the TSFD interface, that separates these regions, the incident plane-wave field is impressed as a source. At the outer boundaries of the scattered field region, perfectly-matched layers attenuate the outward propagating scattered field to zero. We develop TSFD setups for two types of models. The *horizontal TSFD* divides the domain along a horizontal TSFD interface in air, with perfectly-matched layers at the top and Dirichlet boundary conditions at the other boundaries. It is designed for models with different layerings at the left and right boundaries. In such cases the total field at the top boundary cannot be correctly computed, which always leads to reflections using standard Dirichlet boundary conditions. The horizontal TSFD solution is shown to be significantly more accurate. The *surrounding TSFD* is designed for horizontally layered background models. Here, the scattered field region comprises all boundaries, which can be placed closer to the area of interest without diminishing solution accuracy by using perfectly-matched layers. This results in significantly diminished computational problem size.

Keywords: total and scattered field decomposition, perfectly-matched layers, finite-element modelling, computational accuracy

Abstract, 25th EM Induction Workshop,Çeşmeı, Turkey, September 11-17, 2022

An efficient 3D EM modeling scheme based on a radiation boundary approach

Rahul Dehiya[1] and Arun Singh[2]
[1]Indian Institute of Science Education and Research, Pune, rahul.dehiya@iiserpune.ac.in
[2]Indian Institute of Technology (Indian School of Mines), Dhanbad, aruns@iitism.ac.in

ABSTRACT

We present the development of an efficient 3D forward modeling algorithm of electromagnetic data based on a radiation boundary scheme. The proposed scheme computes the response at the desired resolution in two steps. The first step involves coarse-grid finite-difference modeling and the computation of a radiation boundary field vector at the boundaries of a relatively fine mesh. In the second step, modeling is performed for the fine mesh with boundary conditions modified using the computed radiation boundary vector. An initial solution derived from coarse-grid modeling is also used for fine-grid modeling. The fine-mesh discretization includes partial or no air medium and does not contain the stretched grid. The boundary of the finer mesh can have an arbitrary shape that depends on the sensors' positions. The ability to have an arbitrarily shaped boundary of the computational domain optimizes the computation in forward modeling and reduces the degree of freedom when the algorithm is used in an inversion. The proposed algorithm derives computational efficiency from a stretch-free discretization, air-free computational domain, and a better initial guess for an iterative solver. The proposed scheme is based on the finite-difference method; however, the concept of radiation boundary conditions can be employed along with other numerical techniques as well. The robustness and versatility of the algorithm are illustrated for both controlled-source electromagnetic and magnetotelluric data. Numerical experiments demonstrate that the developed algorithm is one order faster than the finite-difference modeling algorithm in most of the cases presented. The scheme is particularly suitable for data analysis of large models resulting due to the fine discretization or the large survey area such as USArray and AusLAMP.

Abstract, 25^{th} EM Induction Workshop,Çeşmeı, Turkey, September 11-17, 2022

Electromagnetic imaging using high-order FE and goal-oriented meshing

O. Castillo-Reyes[1], P. Rulff[2] and E. S. Um[3]
[1]Barcelona Supercomputing Center (BSC), octavio.castillo@bsc.es
[2]Department of Earth Sciences, Uppsala University, paula.rulff@geo.uu.se
[3]Lawrence Berkeley National Laboratory, Earth and Environmental Sciences, evanum@gmail.com

SUMMARY

Electromagnetic (EM) modeling routines development has increased in the last decade. Given the recent advances in numerical methods and increased computing power, there are several options to solve the forward EM problem today. However, regardless of the computational meshes used, most of these modeling tools do not support high-order polynomial discretization methods and adaptive meshing.

In this work, we present numerical experiments about goal-oriented adaptive mesh refinement and the high-order edge finite element method (HEFEM) for the solution of challenging 3D controlled-source electromagnetic (CSEM) surveys. Each test case presents a particular modeling challenge (e.g., topography, presence of metallic boreholes), suitable for studying the numerical schemes capacities in realistic setups. We use two 3D EM modeling routines to compute synthetic EM responses: elfe3D and PETGEM. We investigate the performance of the goal-oriented meshes and HEFEM discretizations in terms of accuracy and computational cost (e.g., run-time, memory consumption).

Our assessment provides relevant information for an in-depth understanding of the pros and cons of employing HEFEM and goal-oriented meshes. The numerical experiments show that high-order polynomial basis functions in conjunction with goal-oriented meshes can obtain synthetic EM responses in agreement with the reference. This conclusion is valid for all the test cases under consideration. However, the code performance depends on the input model: frequency, resistivity, scale variations, mesh quality, source discretization, and computational architecture. Therefore, an aware meshing scheme that considers the polynomial basis order is required to obtain competitive performance ratios. We believe that our numerical experiments will prove useful for the EM community.

Keywords: Geo-electromagnetics, numerical solutions, goal-oriented refinement meshing, high-order finite element, parallel computing

Abstract, 25^{th} EM Induction Workshop,Çeşmeı, Turkey, September 11-17, 2022

2D Electrical Resistivity Modelling on highly distorted, non-smooth, rough grids

Deepak Suryavanshi[1], Rahul Dehiya[1]
[1]IISER Pune, deepak.suryavanshi@students.iiserpune.ac.in
[2]IISER Pune, rahul.dehiya@iiserpune.ac.in

SUMMARY

DC Resistivity method is a geophysical technique that has been widely used in subsurface investigations such as groundwater mapping, critical zone studies, and mineral exploration. In this study, we present a 2D modeling of the DC Resistivity data, keeping in mind that the constructive approach should be based on the very fundamentals of the governing physics and should be able to extend its realms for the complicated cases as well. We have developed a C++ code that aims at solving the 2D DC resistivity problem.

The novelty of our development lies in the construction of the proposed finite difference scheme (FDs) that is based on the Mimetic finite difference methods (MFDM). MFDMs are a class of numerical methods that attempts to mimic the fundamental properties of the governing physics like the conservation laws, symmetry properties, and discontinuity of the coefficients. It further enables the development of modeling algorithms based on non-orthogonal grids required to account for irregular topography. It is difficult for the FDs to accommodate non-orthogonal grids and, hence, varying topography. The finite elements (FEs) methods are generally used for modeling variable topography models. However, FDs have advantages over FEs in inverse modeling where dual discretization is not required in FDs, as is the case with FEs. The MFDM meets both of these objectives, making them a suitable scheme for DC modeling. Hence, we implemented MFDM to develop an algorithm that solved the DC resistivity problem.

A dyke model is utilized to verify the accuracy of the developed algorithm by comparing the numerically-simulated responses to the analytical solution. The benchmarking exercise is done on varying conductivity contrasts for the dyke models to establish the algorithm's accuracy. Further, the developed algorithm is tested for different 2D models by comparing its responses with a 3D modeling algorithm. The proposed algorithm is capable of handling anisotropy. Hence, the developed algorithm is suitable for analyzing DC data of anisotropy and variable topography subsurface. We have carried out a series of experiments to establish the robustness of our code when the grids become very irregular, non-smooth, and the orthogonality is violated. This is achieved by distorting the orthogonal girds using pseudo-random numbers, which follow a uniform distribution. The angles for all the grid nodes are calculated, and the ones having an angle outside 20 to 160-degree intervals are classified as highly distorted. The numerical tests are conducted on highly distorted cells ranging from 1% to 10% of the total cells. The error analysis suggests that the algorithm performs very well for non-orthogonal, non-smooth, highly distorted rough grids and the observed errors were appreciably low.

Keywords: 2D DC Resistivity Modelling, MFDM, Non-orthogonal rough grids.

Abstract, 25th EM Induction Workshop, Kuşadası, Turkey, September 11-17, 2022

Regularization of VLF inversion using rank order smoothing

Gökhan Karcıoğlu[1], Anisya B.Tekkeli[1], Ümit Avşar[2], Mehmet Ali Üge[1,3], Mehmet Safa Arslan[1]

[1] Istanbul University-Cerrahpasa, Engineering Faculty, Department of Geophysical Engineering. Istanbul 34500, Turkey, gkarci@istanbul.edu.tr

[2] Istanbul Technical University, Mining Faculty, Geophysical Engineering Department, Ayazağa, Turkey, avsaru@itu.edu.tr

[3] Japan Agency for Marine-Earth Science and Technology (JAMSTEC), Showa-machi 3173-25, Kanazawa-ku, Yokohama 236-0001, Japan

SUMMARY

Least-squares inversions are generally applied to recover resistivity distribution models from electromagnetic induction data. Since the defined inversion problems are underdetermined and ill-posed, various operators are implemented to regularize the process. Smoothing operators, which are simple finite difference matrices penalizing the resistivity differences between neighboring cells, are implemented in the most applications and aims to result with smooth structure boundaries. These smooth models often have over-smoothing structure boundaries which are rather difficult to interpret. Considering this, we have defined a smoothing operator based on rank order filtering. These non-linear filters are known with their ability to eliminate low-frequency changes while keeping boundary information. In image processing, rank order filters are implemented by determining ranks of pixels within a given filter window and assigning the value of the pixel corresponding to the desired rank, defined by the user, to the central pixel. Filtering is completed by repeating the process for all pixels. Correspondingly, we have penalized the difference of each cell from its neighboring cell corresponding to the defined rank value. Contributions from other cells are also calculated and damped with a Gaussian curve according to their difference from the defined rank. In our implementations we have used median (50%) as the desired rank value since higher or lower values were biasing the inversion to minimize resistors or conductors. In the trials with synthetic data, inversion with the rank order smoothing is observed to be able to recover boundaries successfully while minimizing misfit. For the field implementation, we used the VLF-R measurements collected over the rupture area of the North Anatolian Fault Zone. The data are modeled using both rank order smoothing and traditional smoothing operator for comparison. The recovered models show that the rank order smoothing resulted with models with more evident boundaries, revealing the known faults better.

Keywords: VLF-R, North Anatolian Fault Zone, 2D Inversion

Abstract, 25th EM Induction Workshop,Çeşmeı, Turkey, September 11-17, 2022

Frequency dependent complex resistivity inversion in 3D from Controlled-Source Electromagnetic data

J. Porté[3], F. Bretaudeau[1] and J-F. Girard[2]
[1]BRGM (French Geological Survey), f.bretaudeau@brgm.fr
[2]Strasbourg University, ITES-CNRS, UMR7063, France
[3]Formerly 1 2, now at SINTEF Industry, julien.porte@sintef.no

SUMMARY

In some rocks and soils, induced polarization (IP) phenomena are occurring when an electric perturbation is applied. These mechanisms are described by a *frequency dependent complex resistivity (CR)*. The study of relaxation model parameters describing these phenomena allows to access indirectly to several properties of interest of the underground, as properties linked to the pore space geometry, fluid content or presence and discrimination of disseminated metallic particles. Complex resistivity is usually studied using electrical method with a direct current hypothesis, in time or frequency domain. Electromagnetic induction coupling with the ground or cable layout are then neglected or considered as a source of noise, as they increase with frequency and larger offset. Thus, strong limitations appear to recover a complex resistivity image of buried target.
It leads several authors to rely on empirical EM induction retrieval techniques (Routh and Oldenburg, 2001) to manage IP data contaminated by EM effects. Lately, other authors worked to implement the problem of CR to Controlled-Source Electromagnetic method (CSEM), a resistivity imaging technique using multi-frequency electromagnetic signals fully taking into account EM induction. It uses thus the geometrical and the frequency sounding information of the ground for a larger investigation depth. Ghorbani et al (2009) developed, CR1Dinv, a 1D inversion code taking into account EM induction and IP effects for SIP data. Some codes at larger dimension exists but usually take into account only a constant complex resistivity as the work of (MacLennan et al, 2014) in 2.5D. Nevertheless, there still are a strong need of a method able to manage both effects in this domain. In this work, we implemented frequency dependent complex resistivity inversion in POLYEM3D, a 3D finite-difference modelling and inversion code for controlled-source electromagnetic data (CSEM) (Bretaudeau et al, 2021) in order to fully recover IP information contained in EM data. Through a three layers synthetic example, we present the inversion method developed to constrain the multi-parameters problem using an 1D inversion module fully implemented to the 3D code for methodological developments. Secondly, a 3D synthetic example is showed to illustrate a transposition of the developed inversion method to the 3D code.

Keywords: CSEM, complex resistivity, 3D inversion

METHOD

Frequency dependent CR implementation to the inversion problem leads to the multiplication of the number of parameters and so, to the number of equivalent solution. In order to constrain efficiently the multi-parameters problem, we decomposed the inversion through a multi-stages strategy. Indeed, the problem is decomposed in a two stages procedure, based on the electrical field sensitivity to CR. In a first stage, the resistivity norm $|\rho^*|$ is solved inverting the amplitude of the electrical field response which present a low sensitivity to the CR phase ϕ_{cpx} (1). From the retrieved model in the first stage, we invert in a second stage the electric field phase residual to obtain the CR phase ϕ_{cpx} image.

Furthermore, to manage the increasing number of parameters several empirical relaxation models are commonly used to describe CR spectrum, as the most used one, the Cole-Cole (CC) resistivity model (Cole and Cole, 1941)(Pelton et al, 1978). In this study, we chose to keep a general formulation of

the frequency dependent CR by using a $2^n d$ order polynomial parameterization. CR norm $|\rho^*|(\omega)$ and phase ϕ_{cpx} are the n parameters according to following equations :

$$|\rho^*(\omega)| \propto \mathcal{P}_2\omega^2 + \mathcal{P}_1\omega^1 + \mathcal{P}_0 \quad (1)$$

$$\Phi_{cpx}(\omega) \propto \mathcal{Q}_2\omega^2 + \mathcal{Q}_1\omega^1 + \mathcal{Q}_0 \quad (2)$$

The inversion problem is then reduced to 6 parameters per cell independently to the number of frequency used. In the multi-stages procedure describes above, only 3 parameters per cell are solved simultaneously. Method was developed using a 1D inversion module based on the semi-analytic solution forward code used to solve the primary electrical field of the 3D code and a gradient solved by perturbation. The optimisation is based on a Gauss-Newton estimation of the model update and a linesearch based on a bracketing strategy (Métivier and Brossier, 2016). In following example, we minimize the L2 norm of the logarithm of the data augmented by a Tikhonov regularisation with a maximum smoothness constrain (Grayver et al, 2013).

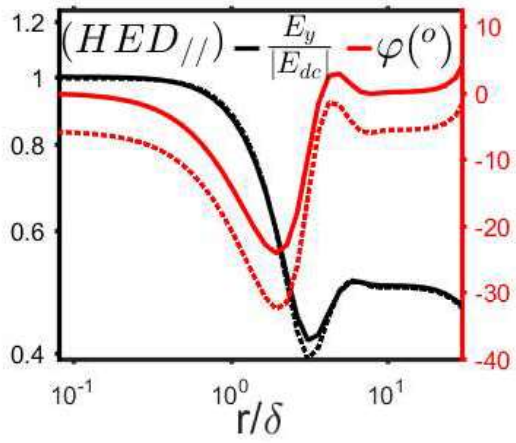

Figure 1: Normalized amplitude and phase of the electric response relative to the offset/skin depth δ ratio over a constant resistivity half-space with (dotted) and without (solid) -100 mrad of CR phase

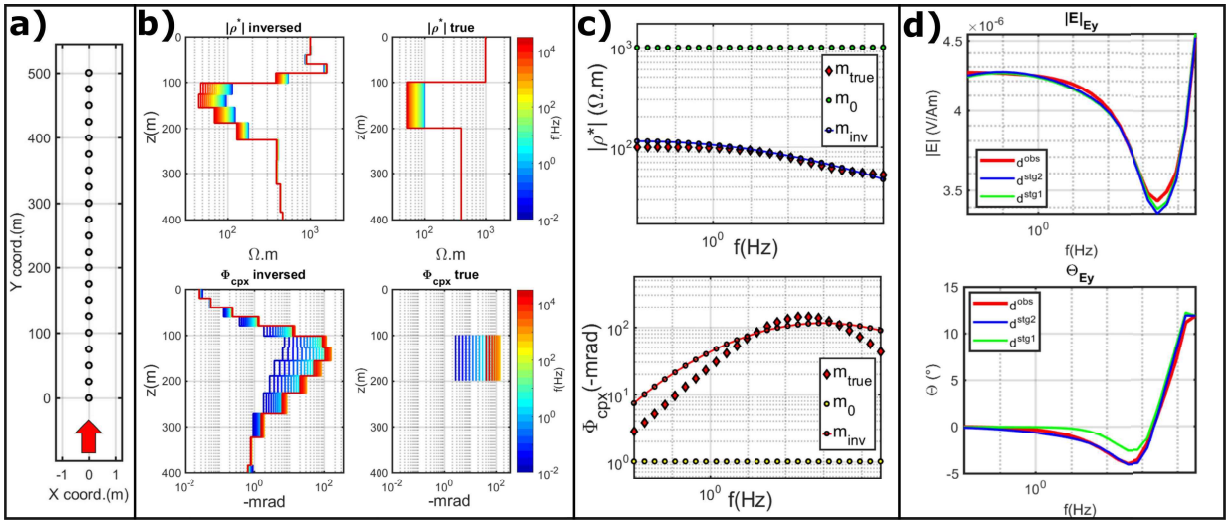

Figure 2: 1D inversion results (Gauss-Newton optimization and L2 norm) for a three layers synthetic model including a conductive polarizable layer accordingly to a Cole-Cole model ($\rho_0 = 100\Omega.m$ $m = 0.5$ $\tau = 0.001s$ $c = 0.5$). Final data $rms < 1\%$. a) Acquisition geometry using a horizontal electric dipole (HED) (red arrow); b) Inverted and true CR model sounding at each frequency (color lines); c) CR spectrum in the cell layer at z=150m for the starting model m_0, the true model m_{true} and the resulting model m_{inv}; d) Data fit (Electrical amplitude (top); Electrical phase (bottom)) at the station $y = 250m$: observed data in red, inverted data at end of stage 1 in green and the final data fit at end of stage 2 in blue

COMPLEX RESISTIVITY INVERSION RESULTS

Figure 2 presents the results from an 1D synthetic three layers model using our inversion strategy in 2 stages and a 2^{nd} order polynomial parametrization of CR. The second layer is a 100 meters conductive and polarizable layer according to a CC relaxation

model (ρ_0= 10 $.m$; m= 0.5; τ= 0.001 s; c = 0.5). We used inline electric field of an 500 meters acquisition profile with a 25 meters spacing, from an inline horizontal electric dipole (HED). 25 frequencies spaced logarithmically from 0.01 Hz to 30 kHz were used and starting model as a constant homogeneous half-space of $500\Omega.m$ and a CR phase of $-1mrad$.

Figure 2 b) shows CR soundings results at each frequency compared to the true CR model. The CR norm image is the result of the first stage whereas the CR phase image the result from the second stage of our inversion procedure. The layer geometry is well defined for $|\rho^*|$ and ϕ_{cpx} and the shape of the CR spectrum is correctly retrieved in the layer as shown in c). The data fit after each stage can be seen in d) for one of the reception sites. We can notice the residual remaining after stage 1 on the electrical phase being fitted in stage 2, without alterring significantly the fit on the amplitude.

Following the 1D development phase and previous results, the method was transposed to the 3D case in the main code POLYEM3D. l-BFGS optimization is used here. Gradient was computed using the adjoint-state method (Plessix and Mulder, 2008) for the CR case and appropriate change of variables were implemented in order to properly precondition the inverse problem and compensate the sensitivity heterogeneity. Figure 4 presents the results obtained for a simple 3D CR synthetic model inversion with a conductive and polarizable cube according to a CC model within a constant half-space with negligible CR phase ($100\Omega.m$ and $-1mrad$).

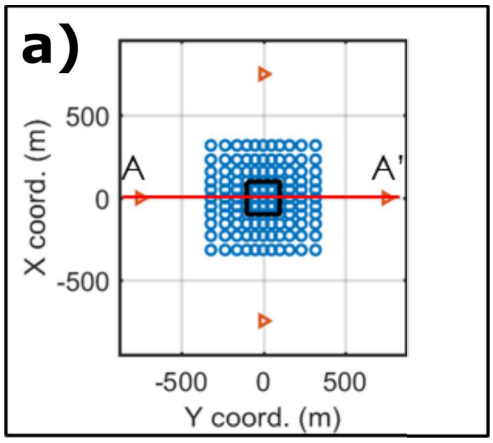

Figure 3: Surface acquisition geometry using 4 HED transmitters oriented to the center of a reception grid measuring the electrical field response (blue circles);

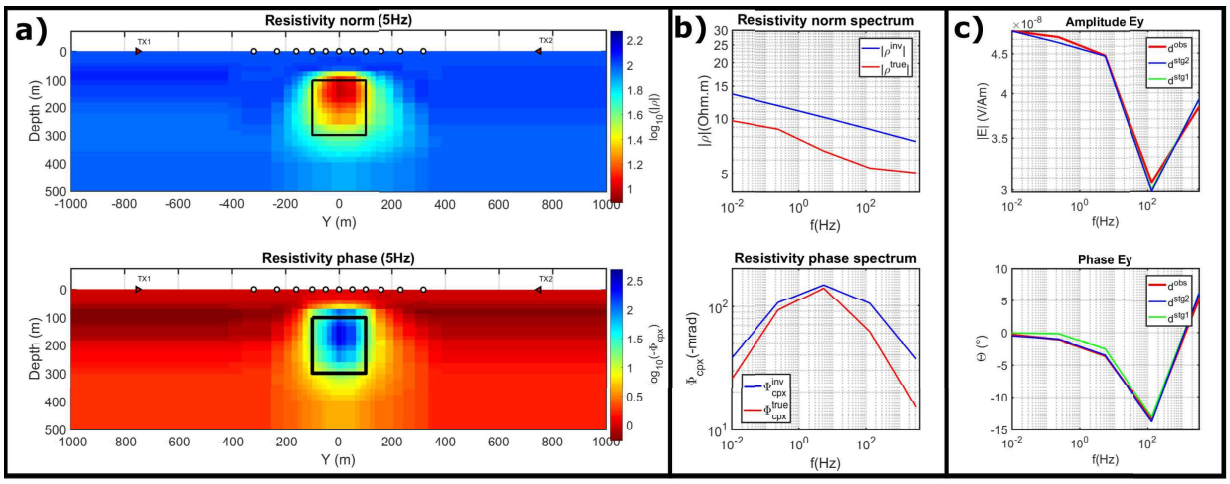

Figure 4: Results of the 3D inversion (l-BFGS optimization and L2 norm) of a polarizable cube (black square) accordingly to a Cole-Cole model ($\rho_0 = 10\Omega.m$ $m = 0.5$ $\tau = 0.1s$ $c = 0.5$) in a homogeneous background ($100\Omega.m$ and $-1mrad$). Final data $rms < 1\%$. b) Norm and phase image of the CR at 5 Hz extracted for the profile AA' in figure 3 . c) CR spectrum at the top-center of the cube ; d) Data fit at the reception site directly above the center of the cube

CONCLUSIONS

We show through 1D synthetic data inversions and preliminary 3D results that we are able to estimate a complex resistivity and its frequency variation from CSEM data by considering all the IP/EM coupling, when IP signals are sufficiently large compared to

EM induction. Our inversion strategy allows then to access to IP parameters of the medium in an extended frequency domain as well as for greater depth of investigation. A 3D CSEM survey was undertaken in December 2020 on the former mining site of La Porte-Aux-Moines (CÃ´tes-d'Armor, France) presenting strong IP responses, to validate our inversion method for a 3D in-situ dataset.

ACKNOWLEDGEMENTS

The research leading to these results has received fundings from the french ANR in the framework of projects EXCITING. Large scale modeling and inversion was performed using the CINES (Centre Informatique National de lâEnseignement SupÃ©rieur) supercomputer OCCIGEN.

REFERENCES

Bretaudeau F, Dubois F, Bissavetsy Kassa S, Coppo N, Wawrzyniak P, Darnet M (2021) Time-lapse resistivity imaging: Csem-data 3-d double-difference inversion and application to the reykjanes geothermal field. Geophysical Journal International 226(3):1764–1782

Cole KS, Cole RH (1941) Dispersion and Absorption in Dielectrics I. Alternating Current Characteristics. The Journal of Chemical Physics 9(4):341–351, DOI 10.1063/1.1750906, URL https://aip.scitation.org/doi/abs/10.1063/1.1750906, publisher: American Institute of Physics

Ghorbani A, Cosenza P, Revil A, Zamora M, Schmutz M, Florsch N, Jougnot D (2009) Non-invasive monitoring of water content and textural changes in clay-rocks using spectral induced polarization: A laboratory investigation. Applied Clay Science 43(3-4):493–502

Grayver AV, Streich R, Ritter O (2013) Three-dimensional parallel distributed inversion of CSEM data using a direct forward solver. Geophysical Journal International 193(3):1432–1446

MacLennan K, Karaoulis M, Revil A (2014) Complex conductivity tomography using low-frequency crosswell electromagnetic data. Geophysics 79(1):E23–E38

Métivier L, Brossier R (2016) The seiscope optimization toolbox: A large-scale nonlinear optimization library based on reverse communication-the seiscope optimization toolbox. Geophysics 81(2):F1–F15

Pelton WH, Ward SH, Hallof PG, Sill WR, Nelson PH (1978) Mineral discrimination and removal of inductive coupling with multifrequency IP. Geophysics 43(3):588–609

Plessix RE, Mulder W (2008) Resistivity imaging with controlled-source electromagnetic data: depth and data weighting. Inverse problems 24(3):034012

Routh PS, Oldenburg DW (2001) Electromagnetic coupling in frequency-domain induced polarization data: A method for removal. Geophysical Journal International 145(1):59–76

Abstract, 25^{th} EM Induction Workshop,Çeşmeı, Turkey, September 11-17, 2022

Gradient and roughness regularization operators for geophysical inversion on unstructured meshes using ℓ_2 and ℓ_1 norms

M. Kangazian[1], C. Farquharson[1]
[1]Memorial University of Newfoundland, St. John's, NL, Canada, Department of Earth Sciences.
mkangazianka@mun.ca, cgfarquh@mun.ca

SUMMARY

Minimum-structure, or "Occam's", style of inversion requires proper regularization strategies to gain sensible geophysical models. Designing the spatial matrix operators required for the regularization term for unstructured meshes is not as straightforward as for structured meshes because of the complex geometric and spatial properties of unstructured meshes. Perhaps the simplest method of calculating the spatial gradient operators for unstructured tetrahedral meshes is the one that calculates the physical property differences across all internal mesh faces. However, this type of regularization is not able to incorporate structural orientation information such as strike, dip, and tilt angles into an inversion, which can be particularly important information for survey methods with limited depth resolution such as gravity and magnetics, as well as for electrical and electromagnetic methods such as magnetotellurics. Hence, other methods have been proposed for calculating the gradient operators for unstructured tetrahedral meshes that allow one to incorporate the structural orientation information of geological features into the inversion framework and obtain more sensible geophysical models.

The majority of these methods consider a cell along with the nearest neighbours of that particular cell as a package to prevent a patchwork pattern being created, and commonly an ℓ_2 norm is used for the measure of the regularization term. These methods work well and allow the orientation information of a geological structure to be incorporated into the inversion to give desirable methods. However, the models constructed using these regularization methods are not as sharp as hoped for when the regularization function uses ℓ_1-norm measures instead of an ℓ_2 norm due to the package issue.

In this study, the effect of the package issue is investigated for the scenarios in which an ℓ_1-norm measure is employed in the regularization term. Also, the method that calculates the gradient operators across the interior faces of the mesh is extended so that geological orientation information of a body can be incorporated into an inversion. It shall be shown that the models constructed by this method have sharper boundaries compared to the models constructed using methods that consider each cell as a package with its neighbours.

Keywords: Inversion, Regularization, Unstructured tetrahedral meshes

1D and 3D Inversion and Modelling of Airborne Transient Electromagnetic and Magnetic Data From Over a Potential Volcanogenic Massive Sulphide Deposit, Cripple Creek, Newfoundland

Alican Demirbas[1], Colin G. Farquharson[2]
[1]General Directorate of Mineral Research and Exploration, Ankara, Turkey, alican.demirbas@mta.gov.tr
[2]Memorial University of Newfoundland, Department of Earth Sciences, St John's, Canada, cgfarquh@mun.ca

SUMMARY

Electromagnetic (EM) methods, including transient electromagnetics (TEM), and magnetic methods are commonly used in mineral exploration. In this study, airborne TEM, ground-based frequency-domain EM and magnetic data are used to investigate possible mineralization zones suggested by the airborne TEM data on the Cripple Creek Property, in the Gander area, Newfoundland, Canada. This study's main goal is to invert the airborne TEM data in 1D to recover the conductive structures that are possible mineralization zones. Airborne magnetic and ground-based frequency-domain EM data are also considered. The ground-based frequency-domain EM data, which are available for just a limited area, and the TEM responses are compared and their respective responses shown to be mostly consistent. A 3D inversion of the magnetic data not only helps better define the physical properties of the targets identified from the EM data-sets but also helps define the background regional geology. The geometry of a mineralized zone suggested by the TEM inversion is then refined by further forward modelling (using the software "Maxwell"). The resulting models are compared and discussed in terms of reliability of the inversion. The results show that the 3D models of the conductivity generated from the stitched together 1D TEM inversion results recover the near-surface structures quite well but become inaccurate at depth. It is shown that the models resulting from the 3D magnetic inversion are partially consistent with the TEM results. This is possible because of the physical property of the structure of interest, which means that the area of interest does not show the same magnetic properties everywhere. Both magnetic and conductive features are only coincident on one of the flight lines. However, when the magnetic inversion result is considered separately, it helps to reveal the magnetic properties reasonably well around the structure of interest.

Keywords: Airborne Transient EM, Magnetic, Inversion

2D U-Net convolutional networks for 1D inversion of magnetotelluric data

Mehdi Rahmani Jevinani[1], Banafsheh Habibian Dehkordi[2], Mohammad Hossein Rohban[3] and Ian J. Ferguson[4]

[1]Institute of Geophysics, University of Tehran, Tehran, Iran, mehdirahmanijevinani@yahoo.com

[2]Institute of Geophysics, University of Tehran, Tehran, Iran, bhabibian@ut.ac.ir

[3]Department of Computer Engineering, Sharif University of Technology, Tehran, Iran, rohban@sharif.edu

[4]Dept. of Geological Sciences, University of Manitoba, Winnipeg, Manitoba, Canada, Ij.Ferguson@umanitoba.ca

SUMMARY

Deep convolutional networks as one of the main developments in deep learning approaches have been applied increasingly in geophysical inverse problems in recent years. The capabilities of 2D U-Net convolutional network for 1D inversion of magnetotelluric data are examined in this study. We apply an innovative method to generate the large number of sample data that are generally required by deep learning-based approaches. Layers with fixed and variable thicknesses and (apparent resistivity) data with and without phases are considered. From the total of 1 million data samples, 95% of them are used as training and validation sets and 5% as test data. Input data are scaled for training and rescaled to form output data or predictions.

The original 2D U-Net is used for segmentation problems. To 1D inverse modeling of magnetotelluric data, a 2D U-Net with 36 layers is designed including two main modifications: First, at the beginning and end of the compression and decompression path, filter 32 is replaced by filter 64. Second, instead of tow, four convolutional layers are used for each filter. The kernel size is 3×2 and batch normalization and ReLU activation functions are considered. Dropout ratios of 0.5, 0.3 and 0.1 are also added to prevent overfitting. Finally, the Adam algorithm with learning rate of 0.0001 and Huber loss are used as optimization algorithm and loss function, respectively.

In the random design of one-dimensional models, there is a possibility of creating layers that due to the values of their electrical conductance cannot be easily identified in magnetotellurics. Therefore, subsurface resistivity values as outputs of the deep learning model are also recovered with similar limitations in resolution.

Keywords: Magnetotellurics, Inverse Modelling, Convolutional Neural Networks

Abstract, 25th EM Induction Workshop,Çeşme, Turkey, September 11-17, 2022

3D Minimum-structure Inversion for CSEM Problems Using Potentials and Unstructured Tetrahedral Grids

Kadir B. Kara[1,2], Colin G. Farquharson[1]
[1]Memorial University of Newfoundland, Department of Earth Sciences, St. John's, Newfoundland A1B 3X5, Canada.
[2]Kocaeli University, Faculty of Engineering, Department of Geophysical Engineering, Kocaeli 41380, Turkey.
E-mail(s): kbkara@mun.ca; cgfarquh@mun.ca.

SUMMARY

Electromagnetic (EM) methods, including profiling and sounding techniques, are used to determine the changes in the electrical conductivity of the earth with both depth and laterally. Frequency-domain EM measurements are conducted at a number of frequencies at fixed source and receiver locations, with the strength of the measured EM fields depending on the earth's conductivity.

Many methods have been used for the numerical modelling of controlled-source electromagnetic methods (CSEM) as a result of developments in computer science. In this study, the finite-element (FE) method in which differential equations are weighted, or a functional minimized whose minimum occurs at the solution to the differential equations is used. CSEM modelling can be done by using either direct E-field methods or potential methods. A potential formulation, specifically the decomposition of the electric field into vector and scalar potentials for the Helmholtz and the conservation of charge equations, namely an $\mathbf{A}$-ϕ decomposition, is used. Vector and scalar basis functions are used for the potentials. The equations are discretized using the weighted residual method, which results in a sparse linear system. The resulting linear system is solved by a sparse direct solver with LU factorization. Modelling domains are subdivided into unstructured tetrahedral grids which are suitable for real geological features such as contacts between rock units and for topography.

Inversion methods can be mainly separated into local (gradient-based) and global methods. Global methods have the ability to reach the global minimum and use less memory. These methods, however, have to call the forward-modelling operator too many times, and hence, gradient-based methods have become more attractive for higher-dimensional inversions. A minimum-structure inversion procedure based on the Gauss-Newton (GN) method which is one of the gradient-based methods is used for the inversion. The procedure aims to find the simplest and most robust model that reproduces the observed data by dividing the problem region into many fine cells. Therefore, the inversion procedure is a highly under-determined inverse problem that achieves the goal by iteratively minimizing an objective function that includes data misfit and model structure terms. Iterative preconditioned conjugate gradient (CG) and nonpreconditioned generalized minimal residual (GMRES) methods are used to solve the linear systems of equations for the model updates. These solvers do not request explicit calculations of the matrices; therefore, this significantly reduces memory demand.

The aim of this study is to develop a powerful and flexible interpretation tool for CSEM problems. The new algorithm was tested with three synthetic examples. One of the three examples was a realistic model that includes an amorphous body and topography. The EM fields (e.g., E_x and H_z) were used as data, and Gaussian random noise was added before inversions. The inversions of models were completed with a common-or-garden laptop and in reasonable time e.g., 85 hr. Both iterative solvers could reduce the residual norms down to the desired level. The recovered models were almost the same for both iterative solvers, and the buried bodies of the three examples were fully recovered.

Keywords: Inversion, Potentials, CSEM, Unstructured Grids

ModEM software: An update on the improvements, availability, and performance metrics

Kelbert, A.[1,2], Egbert, G.[2], Dong, H.[3], Meqbel, N.[4], Zhongyin, L.[5]

[1] *Geomagnetism Program, US Geological Survey, Golden, CO, USA*
[2] *Oregon State University, Corvallis, OR, USA*
[3] *China University of Geosciences, Beijing, China*
[4] *3D Consulting-Geo GmbH, Berlin, Germany*
[5] *Institute of Geology, China Earthquake Administration, Beijing, China*

SUMMARY

ModEM 3D is a parallelized Fortran magnetotelluric (MT) modeling and inversion code [Egbert and Kelbert, 2012; Kelbert et al., 2014] that is freely available for academic use, and has been widely used for 3D MT modeling and inversion by the global MT community. Since the code was initially released, multiple extensions and improvements have been implemented. An upcoming release of an updated version of ModEM allows for flexible air layers and boundary conditions, flexible data orientations, and improved memory usage. It also includes an efficient sparse-matrix solver, a variety of inversion algorithms, and provides (with some limitations) for MT modeling in spherical coordinates. This updated version of ModEM 3D will be better suited for the modeling of electromagnetic induction in the Earth in the context of modern large-scale MT and space weather applications. We will report on the timelines and procedures for availability of these improvements and the related performance metrics, and on the budding efforts to share and distribute auxiliary toolboxes that provide assistance to scientists in setting up ModEM software and in the analysis of results.

Keywords: Magnetotelluric Inversion, Numerical Modeling, ModEM Community of Practice

Abstract, 25th EM Induction Workshop, Çeşme, Turkey, September 11-17, 2022

A MATLAB FE Library for the Simulation and Inversion of EM Problems

Jan Blechta[1], Ralph-Uwe Börner[2], Oliver Ernst[1], Mathias Scheunert[2] and Klaus Spitzer[2]
[1] Faculty of Mathematics, TU Chemnitz, Germany, jan.blechta@math.tu-chemnitz.de, oliver.ernst@math.tu-chemnitz.de
[2] Institute of Geophysics and Geoinformatics, TU Bergakademie Freiberg, Germany, rub@geophysik.tu-freiberg.de, mathias.scheunert@geophysik.tu-freiberg.de, klaus.spitzer@geophysik.tu-freiberg.de

SUMMARY

The electromagnetics working group of the Freiberg Institute of Geophysics and Geoinformatics looks back on a long history of research in the field of simulation and inversion of electromagnetic problems. Together with the Faculties of Mathematics of the Universities of Chemnitz and Freiberg, a wide variety of individual software solutions have been developed over the years. A collaborative software project over the last three to four years has enabled the pooling, unification, and re-implementation of all the acquired knowledge into a single Matlab finite element software library, which is currently being tested and is on its way to becoming an open source application for the EM community. In our poster, we present the key features of this library which allow for the implementation of the forward and inverse problem of any type of time- or frequency dependent geophysical electromagnetic application in 2D and 3D. For this purpose, case studies for magnetotellurics (MT) and geoelectrics (DC) as well as examples for controlled source electromagnetics (CSEM) and induced polarization (IP) are shown. We would like to invite all interested parties to discuss with us possible applications as well as technical or theoretical aspects of electromagnetics and its numerical implementation.

Keywords: Finite elements, unstructured grids, simulation, inversion, Matlab, library

Abstract, 25^{th} EM Induction Workshop,Çeşmeı, Turkey, September 11-17, 2022

3D modeling of CSEM data in the radio frequency band with different sources

S. Schöttle[1*], M. Smirnova[1], B. Tezkan[1], P. Yogeshwar[1] and M. Smirnov[2]
[1]University of Cologne
[2]Luleå University of Technology
* stefan.schoettle@uni-koeln.de

ABSTRACT

Radio-magnetotellurics (RMT) is a passive electromagnetic (EM) technique in geophysics often used for shallow environmental and geotechnical applications. The method uses remote radio antennas broadcasting in a range of around 10-1000 kHz as transmitters. Due to the natural limitations of RMT in its depth of investigation and its dependency on remote radio transmitters, the technique has been extended to use control source in wide frequency range in the past decade. Here, we term it as CS/RMT measurements, as they combine the plane wave RMT range and the source intermediate zone (CSEM). Therefore, the approach can be thought, especially in terms of 3D inversion, as a combined CSEM and RMT method. The CS/RMT measurement frequency range extends from 1-1000 kHz.

Considering the source intermediate zone has several advantages over the previous approach of considering only the far-field: (i) easier logistics, as we do not need to place the source far enough to maintain far-field conditions; (ii) better signal-to-noise ratio; (iii) combined resolution of CSEM and RMT, among others. Such implementation requires modelling of the EM field considering the source. Here, we study the resolution capabilities of different source types in the radio-frequency band over the 3D sub-surface. For this we develop our modelling software – an object-oriented code in Python – MR3DMod.py.

To calculate the background 1D solution for different source types, general 1D field formulations were implemented, following the computational recipes of the well established 3Dinv. Moreover, we combine the fast Hankel transform (different filters) with direct quadrature via optimised Python routines to derive the field components.

We will show the advantages and disadvantages of the various sources at high frequencies for the selected synthetic models and give recommendations for the CS/RMT survey planning.

Keywords: forward modelling, CSEM, RMT, CS/RMT

CRT3DMT: A three-dimensional magnetotelluric inversion package with adaptively refined unstructured inversion grid and an application to lithospheric conductivity structure beneath North China

Huang Chen, Zhengyong Ren and Jingtian Tang
School of Geosciences and Info-Physics, Central South University, 410083, Changsha, China,
csuchenhuang@csu.edu.cn

SUMMARY

Currently, three-dimensional magnetotelluric inversion often uses a fixed inversion grid. Too sparse inversion grid cannot accurately describe the distribution of the complex subsurface conductivities, and may also lead to inversion results failing to converge. While, too inversion grids will increase not only the computational cost, but also the non-uniqueness of the inversion. Aiming to solve the above problems brought by using fixed inversion grid, we have developed a three-dimensional magnetotelluric adaptive inversion algorithm and package with adaptively refined unstructured inversion grid. Firstly, based on the unstructured finite element method, the highly accurate forward responses of the three-dimensional geo-electric model with arbitrary complex topography and conductivity distributions can be obtained. Then, the nested forward and inversion tetrahedral grids are utilized to satisfy their different requirements on grid density. The Thikhonov regularization objective function with smooth constraint is established and minimized by using limited memory BFGS algorithm with inexact line search procedure, where the gradient of the objective function is solved by using the adjoint principle. Most importantly, an inversion grid refinement strategy commonly driven by the data fit gradient and the model parameter gradient is proposed, which is used to guide the automatic refinement of inversion grid in the optimization process. Successively, several synthetic models are used to validate and test the performance of the developed adaptive inversion algorithm and package. The results show that the developed algorithm and package can significantly improve the accuracy and convergence rate of three-dimensional magnetotelluric inversion with less inversion knowns. Finally, a geologically significant three-dimensional lithospheric conductivity structure beneath North China is obtained by using the developed package.

Keywords: Magnetotellurics; Finite element method; Unstructured grids; Adaptive inversion; L-BFGS

UHOMT: A novel 3D finite element Magnetotelluric forward modeling code with unstructured meshes.

Ruiz-Aguilar, D., Gallardo-Romero, E.U.

We introduce to the EM community a 3D magnetotelluric forward modeling program which computes the distribution of the electric field on an unstructured mesh. We employ high order edge elements and implement the Edge Finite Element method to accurately simulate magnetotelluric data in the form of impedance tensor. The program is open-source and optimized for both high-performance computing (HPC) architectures and non-HPC architectures. At first, the implemented methodology and code work-flow are shown. Then, we evaluate the accuracy of our algorithm with various synthetic test models and compare our results with other Finite Element (FE) and Finite Difference (FD) algorithms. The experiments show that the implemented high order elements are effective in providing highly accurate solutions for multiple frequencies with few elements independently of the model's geometry. Hence, leading to reduced computing times. Finally, we compare results using FD and FE codes considering real topographic variations.

3D Inversion of Controlled-Source Electromagnetic Data using Non-linear Conjugate Gradients

P. Rulff[1], T. Kalscheuer[2]
[1]Uppsala University, Department of Earth Sciences, Uppsala, Sweden, paula.rulff@geo.uu.se
[2]Uppsala University, Department of Earth Sciences, Uppsala, Sweden, thomas.kalscheuer@geo.uu.se

SUMMARY

We present first results of our 3D inversion software developed to image the resistivity distribution of the subsurface with frequency-domain controlled-source electromagnetic data.

Our 3D finite-element forward solver was implemented into an inversion framework using non-linear conjugate gradients. The software can handle CSEM setups with multiple source locations. Impedance tensor elements generated by a set of two coincident perpendicularly oriented horizontal electric or horizontal magnetic dipole sources serve as input data for the inversion. Using tensor measurements instead of scalar or vector measurements or single field components brings two advantages: First, complex 3D structures can be better resolved. Second, the source current strength, which is not always recorded alongside the field data, does not have to be known for the inversion as the amplitude and phase of the source current cancel out in the tensor formulation.

In our contribution, we investigate the influence of different regularisation schemes and structural weights on the inversion of synthetic datasets. The regularisation on unstructured meshes is a non-trivial part in the inverse computation, especially the regions around the sources must be handled with caution. To prevent large model updates near sources and receivers, we designed a depth weighting function. A similar depth weighting has been successfully applied to 3D magnetic and gravity inverse problems in order to distribute the model update more evenly in the domain.

Keywords: Three-dimensional inversion, controlled-source, frequency-domain, regularisation, conjugate-gradients

Abstract, 25^{th} EM Induction Workshop,Çeşmeı, Turkey, September 11-17, 2022

2D and 3D Forward modeling of electromagnetic fields in the time domain using Discontinuous Galerkin Method and Spectral Element Method.

Beatriz Valdés-Moreno[1], Marco A. Pérez-Flores[2], and Jonás D. De Basabe[3]
[1] Department of Applied Geophysics, CICESE, valdesb@cicese.edu.mx
[2] Department of Applied Geophysics, CICESE, mperez@cicese.mx
[3] Department of Seismology, CICESE, jonas@cicese.mx

SUMMARY

Electromagnetic methods in the time domain have been widely used in geophysics exploration, and their application in complex media increases the necessity to get better forward and inverse modeling. With the increase of computational power, we can create more extensive and complex earth models and use more sophisticated numerical algorithms.

The boundary conditions of the electromagnetic problem dictate that the tangential electric field must be continuous, and the normal electric field is discontinuous. Thus, the finite element method based on nodal elements is unsuitable for this problem. An alternative is to use the Discontinuous Galerkin method, where the discontinuity of the normal electric field is preserved, and the jump in the tangential electric field is penalized for continuity.

This ongoing research project explores the spectral element method and the interior-penalty discontinuous Galerkin method (IP-DGM) to model transient electromagnetic fields in two and three dimensions in anisotropic media. IP-DGM allows us to have better control over the boundary conditions of the electromagnetic fields; furthermore, it is a highly parallelizable method and allows adaptation to geometries and complex boundary conditions. Finally, we tested explicit schemes such as finite differences, the Lax-Wendroff method, and the Backward Euler implicit method for time stepping.

Keywords: Discontinuous Galerkin Method, Time-domain, Electromagnetic fields.

Abstract, 25^{th} EM Induction Workshop, Çeşme, Turkey, September 11-17, 2022

Time-dependent adaptive mesh refinement for 3D forward modelling of transient electromagnetic fields in volcanic environments including topography

C. Schneider[1], K. Spitzer[1] and M. Hort[2]
[1]TU Bergakademie Freiberg, Germany, carolin.schneider@geophysik.tu-freiberg.de,
klaus.spitzer@geophysik.tu-freiberg.de
[2]Universität Hamburg, matthias.hort@uni-hamburg.de

SUMMARY

Numerical forward modelling of transient electromagnetic (TEM) fields in topographically demanding terrain is a rather challenging task but inevitable to identify reasonable measurement configurations and to correctly interpret acquired field data when investigating mountainous regions. Since the propagating electromagnetic fields change with time and space, an adaptively refined grid would ideally be time-dependent, too. Generating large unstructured tetrahedral grids tailored manually to each specific time-step is, however, very time consuming. Moreover, the system matrix also changes with time causing additional numerical work in the solution process. We tackle both problems by using a very efficient Krylov-subspace method which projects the system matrix onto a low-dimensional space and, therefore, enables us to evaluate the solution for any given time. Additionally, we propose an adaptive approach including hanging edges within our modelling domain. With this, an initial mesh is refined according to the requirements of the propagating electromagnetic field. The development is driven by the application of TEM at volcanic sites. There is an enormous volcanological interest in magmatic pathways and hydrothermal systems within volcanic structures aiming to understand processes occurring prior to a volcanic eruption. Therefore, we apply our TEM simulation routine to a model of Stromboli volcano, Italy, created from a digital elevation model (DEM).

Keywords: modelling, transient electromagnetics, Krylov subspace, adaptive mesh refinement

INTRODUCTION

Numerical modelling using finite elements (FE) is a common tool in geoelectromagnetics. Its accuracy is strongly affected by the underlying mesh as has been vividly demonstrated by the work of Schwarzbach (2009). Several approaches exist to generate an appropriate mesh: Usually, an experienced user sets up an *a-priori* refined mesh with high resolution in the vicinity of the receiver and transmitter locations. On the other hand, *a-posteriori* error estimators are used to quantify the discretization error associated with a specific mesh, which has been proposed by, e.g., Ren et al (2013). In frequency-domain modelling the fineness of the mesh is also related to the frequency. Consequently, the mesh has to be a function of time in time-domain modelling. We therefore suggest to create a series of meshes adapted to the individual time step. This is usually prohibitively expensive but becomes feasible with the Krylov subspace technique we are using here. In order to tailor the mesh to specific times in the TEM forward problem, we use an extension of the hanging node approach on Nédélec elements. The refinement routine guided by an error indicator can be applied to a DEM derived topographic model. Here, we apply our technique to a model of Stromboli volcano, Italy.

MATHEMATICAL BACKGROUND

TEM utilizes the turn-off of a DC current in a usually square loop on the Earth's surface to induce eddy currents in the underground decaying in intensity and expanding in space. They can be modeled by solving the field equation for the electric field $\mathbf{E}$ derived from Maxwell's equations. The TEM mea-

surand, a normalized temporal variation of the magnetic flux density at the Earth's surface, is then extracted using Ampère's law $\partial_t \mathbf{B} = \nabla \times \mathbf{E}$.

Electric field equation

We state the time domain formulation of transient electromagnetic induction in terms of the electric field $\mathbf{E}$ as an initial-boundary value problem (e.g. Afanasjew et al, 2013; Börner et al, 2008, 2015)

$$\nabla \times (\mu^{-1} \nabla \times \mathbf{E}) + \sigma \partial_t \mathbf{E} = \mathbf{0} \quad \text{on } \Omega \times \mathbb{R}_+, \tag{1a}$$

$$\mathbf{E}|_{t=0} = \sigma^{-1} \mathbf{j} \quad \text{on } \Omega, \tag{1b}$$

$$\mathbf{n} \times \mathbf{E} = \mathbf{0} \quad \text{on } \partial\Omega \times \mathbb{R}_+, \tag{1c}$$

where $\mu = \mu_0$ represents the magnetic permeability of free space, $\sigma = \sigma(\mathbf{x})$ the spatially varying electrical conductivity, and $\mathbf{j}$ the source current density associated with a current shut-off at time t_0.
The spatial discretization on an unstructured tetrahedral grid using curl-conforming Nédélec elements yields an ODE initial value problem reading

$$\partial_t \mathbf{u}(t) + A\mathbf{u}(t) = \mathbf{0}, \quad t \in \mathbb{R}_+, \tag{2a}$$

$$\mathbf{u}(0) = \mathbf{b}, \tag{2b}$$

where $\mathbf{u}$ is the coefficient vector of the FE approximation of $\mathbf{E}$ with respect to the Nédélec basis at times $t > 0$ and $\mathbf{b}$ denotes the vector of initial values. The matrix *A* includes both the spatial approximation of the curl-curl operator and the spatially varying conductivity $\sigma(\mathbf{x})$.
Now, we find a solution to Equation 2 using a matrix exponential function

$$\mathbf{u}(t) = e^{-tA}\mathbf{b}, \tag{3}$$

which can be evaluated by developing a rational Arnoldi approximation at any given time $t > 0$ (Afanasjew et al, 2008; Börner et al, 2015).

Hanging edge approach

Adaptive mesh refinement using hanging nodes for octree finite volume discretizations has already been described by, e.g., Haber et al (2007). However, records are scarce for extending the approach to FE simulations based on Nédélec elements.
In Figure 1, a uniformly refined tetrahedron is depicted, where the original vertices enumerated 1-4 are indicated in black, while the vertices constructed within the refinement process are denoted by red numbers. When refining adjacent tetrahedra, new degrees of freedom are generated. However, if at least one adjacent tetrahedron is not refined, this causes hanging nodes and, consequently, hanging edges. Therefore, hanging edges only appear in the outskirts of a refined area, adjoint to the original (i.e. unrefined) mesh.

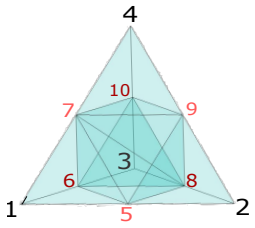

Figure 1: Uniformly refined tetrahedron, black digits enumerate the original vertices of the unrefined tetrahedron, red digits indicate vertices emerging from the refinement process.

Uniform refinement results in bisecting every single edge. Consequently, a set of geometrical constraints can be derived from the original, large edges ("parents") on the newly created, small edges ("children"), where edge $\vec{e}_{ij}$ denotes the edge linking vertices i and j (cf. Figure 1). The constraints derived from edge $\vec{e}_{12}$ read

$$\vec{e}_{15} = {}^1\!/_2\ \vec{e}_{12} \quad \text{and} \quad \vec{e}_{25} = {}^{-1}\!/_2\ \vec{e}_{12}. \tag{4}$$

Furthermore, the new edges emerging on the front facet of the depicted tetrahedron can be constrained using

$$\vec{e}_{57} = {}^1\!/_2\ \vec{e}_{24},\ \vec{e}_{59} = {}^1\!/_2\ \vec{e}_{14} \text{ and } \vec{e}_{79} = {}^1\!/_2\ \vec{e}_{12}. \tag{5}$$

In such a manner, each new edge can be constrained, except for an edge created inside the tetrahedron, such as edge $\vec{e}_{78}$ in Figure 1. Since the latter edge is embedded in the surrounding tetrahedra, it is a complete edge in the mathematical sense.
The stated constraints are mapped to the FE degrees of freedom on each refined tetrahedron and incorporated into the system matrix using the work of Abel and Shephard (1979).
Note, that the constrained degrees of freedom are a linearly interpolated and, consequently, do not yield additional information. The advantage of the hanging edge approach is the ability to refine a mesh straightforwardly without the need to treat hanging nodes at the level of grid generation.

RESULTS

In order to demonstrate the use of adaptive mesh refinement including hanging edges, we consider two applications common in 3D modelling: firstly, automatic refinement around the transmitter location and secondly, time-dependent tracking of the electric field in the subsurface.

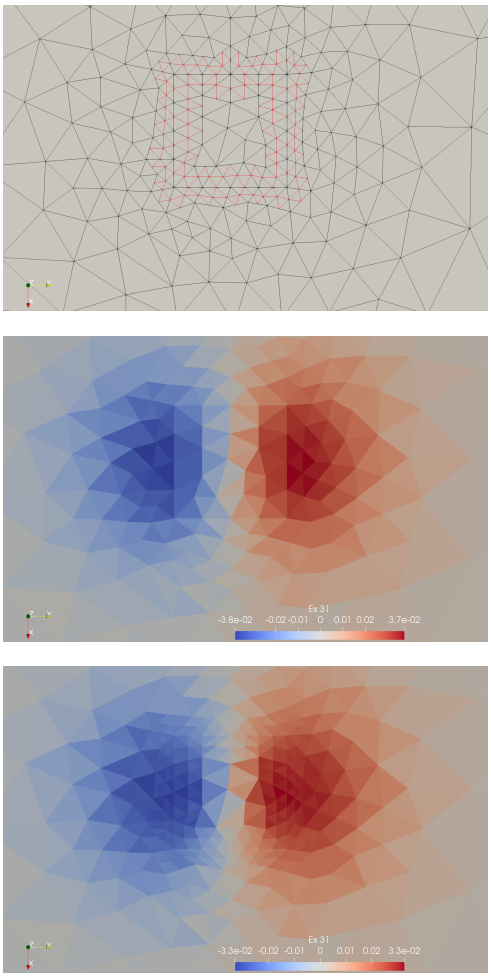

Figure 2: Unrefined (black) and refined (red) grid at the transmitter location (top) and E_x at time $t_1 = 10^{-6}\,\mathrm{s}$ in the unrefined (central) and refined mesh (bottom).

Homogeneous Halfspace

When modelling in the time domain, the fineness of the initial value condition severely affects the solution. Therefore, we automatically refine the region around the transmitter location within a homogeneous halfspace model with electrical conductivities $\sigma_{air} = 10^{-9}\,S/\mathrm{m}$ and $\sigma_{Earth} = 10^{-3}\,S/\mathrm{m}$ based on the solution E_x at time $t = 10^{-6}\,\mathrm{s}$ shown in Figure 2. In the uppermost panel, one can clearly observe hanging nodes where the refined mesh (red colour) borders the original mesh (black colour). As can be seen in the central and lowermost subplot, respectively, the solution on the fine mesh (lowermost figure) exhibits a smoother E_x distribution in contrast to the rather coarse solution on the original mesh (central figure). Due to the higher resolution in the initial step, the accuracy of the solution at later times is also raised.

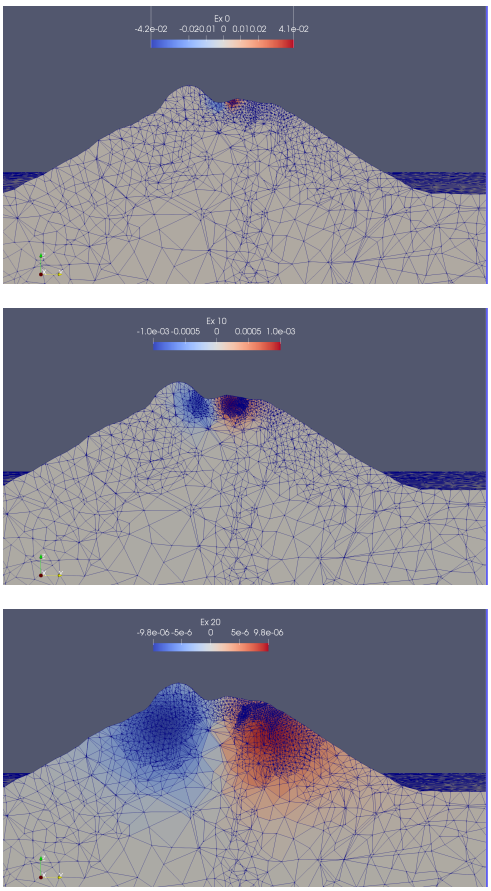

Figure 3: Tracking E_x in the underground using adaptive mesh refinement at times : $t_1 = 10^{-6}\,\mathrm{s}$, $t_2 = 10^{-5}\,\mathrm{s}$, $t_3 = 10^{-4}\,\mathrm{s}$ (from top to bottom).

Application to a DEM

As a second application for automatic adaptive refinement, we consider a homogeneous model of Stromboli volcano, Italy, derived from a DEM. Due to the steep topography, the electrical conductivities are set to $\sigma_{air} = 10^{-6}\,S/\mathrm{m}$ and $\sigma_{Earth} = 10^{-3}\,S/\mathrm{m}$

in order to maintain numerical stability at the Earth-air interface. An experienced user would generate a mesh with appropriate fineness in the vicinity of the receiver location, the transmitter location and at the Earth-air interface mapping the topography to a certain level of detailedness. However, additional refinement in the underground is necessary in the vicinity of conductivity anomalies and for accurately resolving the temporal behaviour of the electric field. In Figure 3, the tracking of E_x using the subset $\mathcal{T}_{ref}$ with

$$\mathcal{T}_{ref} = \{\, T \subset \Omega | E_x > 1/2 \max(E_x) \vee E_x < 1/2 \min(E_x) \,\}$$

is visualized at times $t_1 = 10^{-6}\,\mathrm{s}$, $t_2 = 10^{-5}\,\mathrm{s}$ and $t_3 = 10^{-4}\,\mathrm{s}$. Note that, due to the nature of unstructured meshes, the interface of the clipped model may contain a variety of slices through tetrahedra which need not necessarily be triangular. The time-dependency of the underlying mesh is clearly visible, the fine regions follow the extrema of E_x. Apparently, the region, in which E_x is greater or less than half of its maximum/minimum value, respectively, widens with increasing time. This is in accordance with the diffussive nature of electromagnetic fields.

CONCLUSIONS

3D simulations of electromagnetic fields are highly useful to image electromagnetic fields in the underground. However, the accuracy of the results depends on the underlying mesh. In order to enhance the distribution of degrees of freedom we propose a strategy of time-dependent adaptive mesh refinement using hanging edges based on the extrema of the electric field. Future investigations will focus on the quantitative description of the refinement process.

ACKNOWLEDGMENTS

The SRTMGL1 V003 data product was retrieved in July 2017 from the online Data Pool, courtesy of the NASA Land Processes Distributed Active Archive Center (LP DAAC), USGS/Earth Resources Observation and Science (EROS) Center, Sioux Falls, South Dakota,
https://lpdaac.usgs.gov/data access/data pool.

REFERENCES

Abel JF, Shephard MS (1979) An algorithm for multipoint constraints in finite element analysis. International Journal for Numerical Methods in Engineering 14(3):464–467, DOI 10.1002/nme.1620140312

Afanasjew M, Eiermann M, Ernst OG, Güttel S (2008) Implementation of a restarted Krylov subspace method for the evaluation of matrix functions . Linear Algebra and its Applications 429:2293–2314

Afanasjew M, Börner RU, Eiermann M, Ernst OG, Spitzer K (2013) Efficient Three-Dimensional Time Domain TEM Simulation Using Finite Elements, a Nonlocal Boundary Condition, Multigrid, and Rational Krylov Subspace Methods. 5th International Symposium on Three-Dimensional Electromagnetics, May 7 - 9, 2013, Sapporo, Japan p 4p

Börner RU, Ernst OG, Spitzer K (2008) Fast 3-d simulation of transient electromagnetic fields by model reduction in the frequency domain using krylov subspace projection. Geophysical Journal International 173(3):766–780, DOI 10.1111/j.1365-246X.2008.03750.x

Börner RU, Ernst O, Güttel S (2015) Three-Dimensional Transient Electromagnetic Modeling Using Rational Krylov Methods. Geophys J Int 202(3)

Haber E, Heldmann S, Ascher U (2007) Adaptive finite volume method for distributed non-smooth parameter identification. Inverse Problems 23(4):1659–1676, DOI 10.1088/0266-5611/23/4/017

Ren Z, Kalscheuer T, Greenhalgh S, Maurer H (2013) A goal-oriented adaptive finite-element approach for plane wave 3-d electromagnetic modelling. Geophysical Journal International 194(2):700–718, DOI 10.1093/gji/ggt154

Schwarzbach C (2009) Stability of finite element solutions to Maxwell's equations in frequency domain. PhD thesis, TU Bergakademie Freiberg

A parallel adaptive finite-element method for 3-D large-scale controlled-source electromagnetic forward modelling with hierarchical tetrahedral grids

Zhengguang Liu[12], Zhengyong Ren[1], Hongbo Yao[1], Jingtian Tang[1], Xushan Lu[2], Colin Farquharson[2]
[1] School of Geosciences and Info-Physics, Central South University
[2] Department of Earth Sciences, Memorial University of Newfoundland
Email: liuzhengguang@csu.edu.cn

SUMMARY

Three-dimensional forward modeling software that can quickly solve large-scale problems, provide precise electromagnetic responses for complicated geo-electrical models, and can be easily incorporated into inversion algorithms are required to effectively and efficiently model and interpret controlled-source electromagnetic (CSEM) data acquired in areas with the kinds of arbitrary topography and complex geological environments that are typical of real-life situations. We have developed a parallel, adaptive, finite-element approach for frequency-domain 3-D CSEM forward modeling. Our algorithm is capable of using hierarchical tetrahedral grids with an adaptive mesh refinement (AMR) technique, which yields more accurate electromagnetic responses for large-scale complex models. Our algorithm solves the total electric field vector equation. The geo-electrical model is discretized by unstructured tetrahedral grids which can deal with complex underground geological models with arbitrary surface topography. Unlike previous adaptive finite-element software working on unstructured tetrahedral grids, we implemented a novel mesh refinement technique named the longest edge bisection method to generate hierarchically refined grids. New cells obtained from the refinement method are all part of the original cells in the coarser grid. Therefore, a one-to-one mapping relationship between the newly refined cells and the original cells could be efficiently and precisely obtained such that the conductivity model represented by the refined mesh stays the same as that represented by the original mesh. This means there will be no inconsistency in the conductivity model in the inversion while transitioning from early-stage coarser meshes to late-stage refined meshes to obtain better recovered models. In addition, we employ a parallel domain-decomposition technique to accelerate the computational speed of our forward modeling algorithm. The flexible generalized minimum residual (FGMRES) iterative solver with an auxiliary-space Maxwell preconditioner is used to solve the final large-scale linear system of equations. We validate the performance of the proposed scheme using one synthetic model and one realistic model. We demonstrate that accurate electromagnetic fields can be obtained by comparison with the analytic solutions and that the code is highly scalable for large-scale problems with millions or even hundreds of millions of unknowns. For the realistic model with complex geometry, our solutions match well with the results calculated by the existing 3D CSEM forward modelling code. Both synthetic and realistic examples demonstrate that our newly developed code is an effective, efficient forward modeling engine for interpreting CSEM field data acquired in areas of complex geology and topography.

Keywords: Numerical simulation; Large-scale; Goal-oriented adaptive mesh refinement; Longest edge bisection method; Parallel iterative solver

3D EM modeling and inversion with a mixed finite-element and finite-difference approach to handle high topography and bathymetry variations

S. Védrine[1], R. Rochlitz[2] and F. Bretaudeau[1]
[1]BRGM, 3 Av. Claude Guillemin, Orléans 45060, France, s.vedrine@brgm.fr
[2]Leibniz Institute for Applied Geophysics, Hanover, Germany, raphael.rochlitz@leibniz-liag.de
[1]BRGM, 3 Av. Claude Guillemin, Orléans 45060, France, f.bretaudeau@brgm.fr

SUMMARY

3D CSEM modeling is usually performed by finite-difference (FD) discretization, but new players have entered the scientific community with finite-element (FE) modeling codes. FDs are suitable for simple cases, but are unsuitable for complex geometries, while FEs are very effective in the presence of high topography and/or bathymetry variations. The open-source 3D FE modeling code custEM has demonstrated its efficiency and reliability and is freely available to the scientific community. The recent work done by its development team has made it possible to integrate the inversion part with the Guauss Newton minimization algorithm, but there is not yet enough user feedback and tools available on this new module to be operational for the general public. On the other hand, POLYEM3D is a 3D FD modeling and inversion code that has a wide range of inversion algorithms and reparametrization and regularization tools but faces numerical errors in presence of high topography or bathymetry variations such as in coastal areas or volcanic environments due to the sea/land interface and large variations in near-shore bathymetry and topography. We tested a mixed FE and FD approach that aims to reduce the modeling errors inherent in the FD scheme in such complex problems. A secondary field formulation is available in POLYEM3D and instead of classically using a semi-analytical 1D code to compute the primary field, we use 3D fields computed in a simple isotropic homogeneous model with custEM incorporating topographic and bathymetric variations. The accuracy of the mixed approach was evaluated by modeling with a simple synthetic model incorporating topographic and bathymetric variations, and comparing the responses of the FE and mixed FE/FD codes. In addition, an inversion on a complex CSEM case demonstrated the good behavior of the mixed approach in inversion thanks to the panel of reparametrization and regularization tools offered by POLYEM3D.

Keywords: 3D CSEM modeling, topography, bathymetry, Volcanic islands, Separated field, Finite-element, Finite-difference

Abstract, 25th EM Induction Workshop, Çeşme, Turkey, September 11-17, 2022

Multi-scale conductivity model of the contiguous US from inversion of the MT USArray

Federico Munch[1], Alexander Grayver[2]
[1]Berkeley Seismological Laboratory, University of California, Berkeley, United States, fmunch@seismo.berkeley.edu
[2]Institute of Geophysics, ETH Zürich, agrayver@ethz.ch

SUMMARY

The MT component of the USArray consists of a high quality data set of magnetotelluric measurements that addresses both of these problems. Covering ~70% of the contiguous United States on a quasi-regular 70 km spaced grid, this unique publicly available data led to the development of several regional 3-D electrical conductivity models. However, an inversion of the entire data set demands novel multi-scale imaging approaches that can handle and take advantage of a large range of spatial scales contained in the data. We here present a 3-D electrical conductivity model of the contiguous United States derived from the inversion of the 1100 highest quality USArray magnetotelluric stations. The use of state-of-the-art modeling techniques based on high-order finite-element methods allows us to take into account complex coastline and reconstruct Earth's conductivity across many scales. The retrieved electrical conductivity variations are consistent with well-known continental structures such as the active tectonic processes within the western United States (e.g., Yellowstone hotspot, Basin and Range extension, and subduction of the Juan de Fuca slab) as well as the presence of deep roots (~250 km) beneath cratons. Furthermore, we interpret the conductivity variations in terms of upper mantle water content by coupling electrical conductivity with constrains on mantle thermochemical structure derived from the analysis of seismic data. Our results suggest the existence of a relatively upper mantle beneath the United States, with slight lateral variations. In particular, we find an increase in upper mantle water content from west to east, with largest values underneath the Midcontinent Rift System and the Appalachians.

Keywords: global induction, mantle conductivity, inversion, water content

Joint inversion of magnetotelluric data and receiver functions using Pareto-based swarm intelligence algorithm

E. Büyük[1] and E. Zor[2]
[1]Department of Geophysical Engineering, Faculty of Engineering and Natural Science, Gümüşhane University, Gümüşhane, Turkey,
[2]TÜBİTAK Marmara Research Center, Kocaeli, Turkey, ekrem.zor@tubitak.gov.tr

SUMMARY

The increasing popularity in joint inversion could be attributed to the successful determination of structures that are difficult to detect by restricting the models using priori information in conventional modelling. In recent years, joint inversion of magneto-telluric data and receiver functions also provides valuable information on structures extending from the upper crust to the lower crust such as detached and folded metamorphic complex structures, weakly layered crust, etc. Another well-known disadvantages of the derivative-based conventional modeling algorithms used to determine these structures is that the solution has a dependency to an initial model and the possibility of trapping in a local minimum.

The seismic velocity and electrical conductivity parameters solved with the inversion of receiver function and magnetotelluric data are not well correlated physically, and jointly inverting them in the scientific literature is generally used in two ways: 1) to obtain a solution with the empirical relationships extracted from the laboratory experiments, the so-called petrophysical approach, 2) the cross-gradient approach, which aims to obtain a solution using structural constraints. Since the relationship between seismic velocities and conductivity is largely unknown in the petrophysical approach, a weak coupling between them increases the resolution but can also lead to misleading and incorrect results. These physical parameters can have different responses to the inputs such as porosity, permeability, temperature. As a commonly accepted approach, the cross-gradient method looks for the solution having structural similarities between the two models. However, the two different datasets does not always respond to the structural similarities equally, thus obtaining more convincing solution may involve the consideration of different structural couplings with a regularization term added to the objective function as a multiplier or a weighted sum.

In this study, Particle Swarm Optimization integrated with the Pareto optimality approach (Pareto-PSO) applied to the receiver function and magnetotelluric data to jointly invert them. PSO is a metaheuristic global optimization algorithm inspired by the social behavior of flocks of birds or fish, and is an excellent alternative to traditional geophysical modeling techniques that suffer from initial model dependence, linearization problems, and trapping at a local minimum. Pareto-PSO also provides the opportunity to model in a joint system without reducing the resolution of individual datasets that have different physical sensitivities. Similar to the cross-gradient approach in modeling receiver functions and magnetotelluric data that provide one-dimensional model responses, this study examines the gradient approach in the vertical direction only. By using the advantage of the Pareto approach, apart from the classical weighted sum approach in the objective function, the structural differences have been added to the objective function space as a third axis alongside the misfit of the receiver function and magnetotelluric data to search for the solution without the need for weighting and combining in the objective function.

We tested a series of synthetic models containing noise-free and noisy data of the magnetotelluric and receiver functions by using Pareto-PSO. Since the seismic velocity and electrical conductivity parameters may indicate different responses to the same physical phenomena, the variation of the parameters was applied in the same direction but with different percentages. Our modeling approach is successfully solved the structures by using the Pareto front, which presents the joint and individual solutions for the two datasets, also allows to analyze the non-uniqueness of the solution from the Pareto-front solutions.

Abstract, 25^{th} EM Induction Workshop,Çeşmeı, Turkey, September 11-17, 2022

Development of an efficient 3D inversion algorithm for large-scale MT data

Arun Singh[1] and Rahul Dehiya[2]
[1]Indian Institute of Technology (Indian School of Mines), Dhanbad, aruns@iitism.ac.in
[2]Indian Institute of Science Education and Research, Pune, rahul.dehiya@iiserpune.ac.in

ABSTRACT

We developed an efficient 3D magnetotelluric inversion algorithm employing a forward modeling scheme based on the radiation boundary method. The radiation boundary vector is estimated using coarse-mesh modeling for the user-defined inversion domain. Therefore, the proposed algorithm allows an arbitrarily shaped boundary of the inversion domain. Consequently, it minimizes the degree of freedom in an inversion process by reducing the number of cells for which the conductivity ought to be estimated. The developed algorithm is helpful for large inversion domains that arise due to the vast survey area or high-resolution imaging. The algorithm is created by augmenting these features into the AP3DMT algorithm. The versatility and efficiency of the inversion scheme are illustrated for synthetic and real field data. We considered the Rubik model for the synthetic experiment where data is simulated on two profiles intersecting at a right angle. The proposed algorithm estimates the resistivity of conductive blocks better than the inversion scheme based on the conventional modeling approach. At the same time, the computation time in this experiment reduces by more than six times. We also invert the SAMTEX MT data using the developed algorithm to illustrate the robustness of the proposed algorithm. The inverted model is in overall agreement with well-known structures (e.g., Kaapvaal and Zimbabwe cratons, Ghanzi-Chobe Belt).

3-D Modeling of Airborne and Land-based Controlled-Source Electromagnetic Data: Comparison on CPU and GPU Platform

İsmail Demirci[1]

[1]Ankara University, Faculty of Engineering, Geophysical Engineering Department, Geophysical Modelling Group, Ankara, TURKEY. E-mail: idemirci@eng.ankara.edu.tr

SUMMARY

In last decades, thanks to the developed semi-airborne/airborne geophysical measurement methods and data acquisition systems, it is aimed to make the data acquisition possible and increase the data acquisition speed in areas where working condition is difficult. Airborne geophysical studies have generally focused on Magnetic methods, transient Electromagnetic methods and Very Low Frequency Electromagnetic methods. However, due to the weakness of the methods in terms of depth information, the use of airborne-based controlled-source electromagnetic methods has gained importance in recent years. The realization of geophysical studies in forested and mountainous areas depends not only on the development of measurement acquisition systems, but also on the development of software to be used in the evaluation processes of the measurements taken. In this study, 3D forward solution algorithm is developed to use for inversion stage of natural and controlled source electromagnetic data collected on ground and airborne studies. In addition, direct and iterative solution methods are used in the software developed during the study, and their performance is tested in CPU-GPU platforms and the results are discussed.

Keywords: Airborne Electromagnetic, Modeling, Three-Dimensional, Graphical Processing Unit

INTRODUCTION

In recent years, studies have done on aerial measurement methods for many geophysical methods (Radiometric, Magnetic and Electromagnetic methods, etc.). Thanks to the developed airborne-based geophysical measurement methods and measurement taking systems, it is possible to work in topographic conditions where it is not possible or difficult to take measurements from the land, covered with dense vegetation and where it is not possible to carry the equipment for measurement taking. However, due to the weakness of methods such as Radiometric and Magnetic methods in terms of depth information, the use of electromagnetic methods measured from the air vehicle has gained importance. Airborne EM methods are used in many subjects such as environmental problems (Doll et al., 2001), infrastructure surveys (Pfaffhuber et al. 2010), groundwater and pollution (Gunnink et al., 2012), geological mapping (Steuer et al., 2009) and mineral surveys (Wolfgram and Golden, 2001).

In parallel with the developments in the measurement methods and applications of airborne EM methods, the development of 3-D modeling and inversion algorithms used in the evaluation of data has accelerated. 3-D forward solution algorithms are the most important part of inversion algorithms used to obtain reliable 3-D underground models. Therefore, the development of stable and fast 3-D forward solution algorithms is vital for obtaining more reliable underground models.

In recent years, there are many studies on 3-D forward solution in frequency domain EM methods. Finite Differences (Newman and Alumbaugh, 1995, 2002; Streich, 2009), Finite Elements (Badea et al., 2001; Mitsuhata and Uchida, 2004; da Silva et al., 2012), Finite Volume (Mackie et al., 1994; Haber and Ascher, 2001; Constable and Weiss, 2006) and Integral Equation (Wannamaker, 1991; Avdeev et al., 2002) methods are generally used for forward solution methods. Finite element method is the most flexible method in terms of defining model geometry (Avdeev, 2005, Erdoğan et al. 2008, Demirci et al., 2012). Although integral equation methods are very useful for simple models, there are difficulties in computation for complex models (Mackie et al. 1993). For this reason, the Finite Difference method and the closely related Finite Volume method are preferred because of their ease of calculation and application and solution stability. In addition, there are a limited number of studies on modeling 3-D airborne-based EM methods (Newman and Alumbaugh, 1995; Avdeev, 2005; Cox et al., 2010; Liu and Yin, 2014), and the finite difference method was generally preferred in the studies. During this study, airborne and land-based CSEM 3-D forward modeling algorithm was developed by using Finite Difference method.

METHOD

In EM methods, to calculate model responses, we solve the vector Helmholtz equation for the secondary electric field $\mathbf{E}^S$

$$\nabla \times \nabla \times \mathbf{E}^s + \mathrm{i}\omega\mu_0\sigma^* \mathbf{E}^s = -\mathrm{i}\omega\mu_0 \mathbf{J} \qquad (1)$$

where $\mathbf{J} = (\sigma^{*} - \sigma^{P*})\mathbf{E}^{P}$ define source term, ω denotes angular frequency, the complex conductivity $\sigma^{*} = \sigma + j\omega\varepsilon$ includes conductivity σ and permittivity ε, μ_0 denotes free-space magnetic permeability and σ^{P*} is the conductivity of a layered background model. If the source term on the right hand side of the equation is used, the methods are defined as controlled source, otherwise natural source methods. The primary electric field $\mathbf{E}^{P}$ is computed for conductivity σ^{P*} using quasi-analytic expressions for 1D media (Streich & Becken 2011). The Helmholtz equation given above cannot be solved analytically for complex models. For this reason, one of the numerical solution methods should be used in the solution of the equation. Finite Difference method (Newman and Alumbaugh, 1995; Alumbaugh et al., 1996; Champagne II et al., 2001; Weiss and Newman, 2002, Streich, 2009) is one of the most preferred methods due to its ease of application and speed of solution. In this study, Finite Difference method is preferred in the solution of the Helmholtz equation.

The Finite Difference expression of Eq.1 is obtained using Yee(1966)'s staggered grid approach, scaled symmetrically, and Dirichlet boundary conditions (usually Dirichlet boundary conditions have been used in previous studies so that the resulting equation is symmetrical, see Newman and Alumbaugh, 1995; Streich, 2009) is used, a system of linear equations is obtained in the form given below.

$$\mathbf{K}\mathbf{E}^{S} = \mathbf{S} \qquad (2)$$

where **K** defines a hermitian and sparse matrix with at most 13 nonzero elements in each row, and **S** defines the source term. **E** field values are obtained by solving the system of equations, and **H** fields can be derived from electric fields by using auxiliary equations. In order to solve the system of equations, it is necessary to invert the matrix **K** (direct methods) or to solve the system of equations with Krylov space solvers (iterative methods).

Recently, direct solvers have used for relatively small modeling meshes. Since the inverse of the matrix is taken with direct solvers, there is no need to solve the equation again for each source and polarization, and the solution speed increases. Depending on the developments in computer technology, the use of direct solution methods has increased in the last decades and the use of Multifrontal methods in the CPU environment has become widespread (Streich, 2009; da Silva et al., 2012; Kordy et al., 2015; Puzyrev et al., 2016; Mütschard et al., 2017 ; Liu et al., 2018). Although the RAM usage of direct solvers are reduced with Multifrontal methods, it is not preferred for large model meshes. During the study, Multifrontal methods are used to compare solution speeds for small model meshes.

The number of rows or columns of the K matrix in the equation system to be solved can be expressed in hundreds of thousands or even millions, depending on the number of elements in the designed 3-D model mesh. For this reason, stationary and fast solvers used in the solution of the system of equations directly affect the speed of the method. Krylov space solvers are often preferred because RAM usage is much lower than direct solvers. In the 3-D EM method, the main Krylov space solvers used in the forward solution are CG (Zhdanov et al., 2000; Haber, 2004; Zhdanov et al., 2011), BICG (Sasaki et al., 2010; Farquharson ve Miensopust, 2011; Sasaki, 2012), BICGSTAB (Xiao et al., 2018; Singh et al., 2017; Plessix ve Mulder, 2008), QMR (Kelbert et al., 2014; Tang et al.,2015; Wang ve Tan, 2017) and GMRES (Cox et al., 2010; Grayver, 2015; Grayver and Kolev, 2015). Hursan and Zhdanov (2002) compared the methods and said that BICGSTAB, QMR and GMRES methods are the most effective solvers in their study. These three methods are often preferred in the solution of the equation.

These solvers are used in the developed algorithm and CPU performances are tested in the solution of frequency domain CSEM 3-D modeling algorithm. Using the results obtained, it is preferred to use BICGSTAB in GPU. The results of the algorithm and comparison of the solvers are discussed and their results presented in the following section.

MODEL STUDY

The initial results of the developed algorithm has been tested for the resistivity model given in Table-1 with using 1-D semi-analytical straight solution algorithm (Streich and Becken, 2011) and the previously developed 3D CSEM forward modeling algorithm (CUSTEM- Rochlitz et al., 2019). The E and H field amplitudes of the developed algorithm were compared with the CUSTEM and semi-analytical solution algorithm for the 1Hz frequency on each measurement point, which were obtained as a result of the resistivity model given in table-1 (Figure 1). The source used in the study is located at y=-3km and parallel to the x-axis. The dipole length of the source is used as 1 Km. The result of developed algorithm coincides with the results obtained with both the analytical solution and the CUSTEM algorithm. The performances of the solvers are tested on the CPU and it is seen that the BICGSTAB solver was the fastest and most stable solver (Figure 2). However, it is seen that direct solvers reach the solution in the most effective solution time when more than one source is used. In Figure 2, the results are given according to the

use of a single source. In iterative solvers, it is necessary to recalculate for each source, while in direct solvers, there is no significant increase in computation time when more than one source is used. Therefore, as a result of the study, it is concluded that using direct solvers would be efficient in case of using multiple sources for small model meshes. When the CPU and GPU performances of the BICGSTAB algorithm, which is the chosen iterative solver, are examined, it is observed that the acceleration in the solver is 2,5 times higher, especially at low frequencies, and the algorithm developed on the GPU platform is more efficient (Figure 3).

Table 1. 1-D resistivity model used in the test study

	***z* (m)**	**Resistivity (Ωm)**
B 1	0 to 300	100
B 2	300 to 700	10000
B 3	700 to infinity	1000

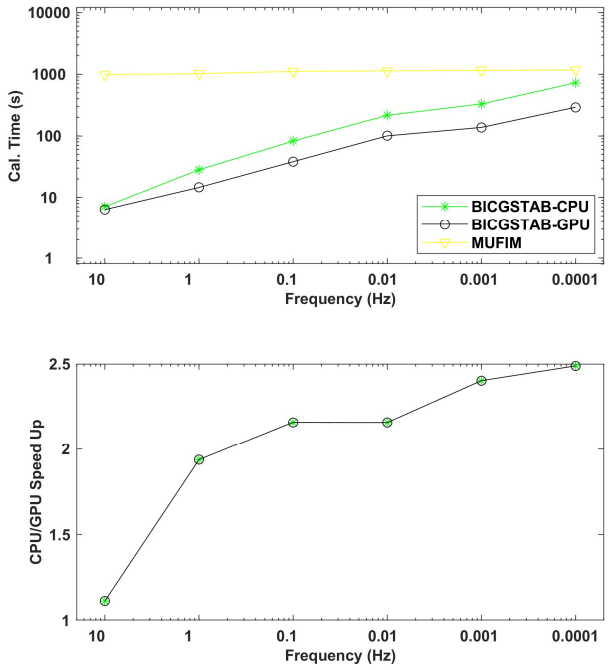

Figure 3. CPU and GPU performances and relative acceleration graphs of the selected iterative solver (BICGSTAB)

CONCLUSIONS

The findings obtained on the CPU revealed that the BICGSTAB algorithm is an efficient algorithm for 3D CSEM forward modeling. Therefore, it was also coded in the GPU environment. In this way, it has been observed that the algorithms coded on the GPU reach a solution 2.5 times faster, especially at low frequencies. In the case of multiple sources, multifrontal methods is converging to the solution faster for high frequencies and for small model networks. It is thought that the selection of the solvers in the developed algorithm chosed as hybrid in the light of the information obtained, which will increase the solution speed. For this purpose, in order to optimize the solution speed, the use of BICGSTAB at high frequencies and the multifrontal method at low frequencies is recommended in cases where the number of sources is more than one.

ACKNOWLEDGEMENTS

This work was supported within the scope of TÜBİTAK BİDEB with grant no 1059B191800610.

REFERENCES

Avdeev DB, Kuvshinov AV, Pankratov OV, Newman GA (2002) Three-dimensional induction logging problems, Part I: An integral equation solution and model comparisons. Geophysics, 67(2), 413-426.

Badea EA, Everett ME, Newman GA, Biro O (2001) Finite-element analysis of controlled-source electromagnetic induction using Coulomb-gauged potentials. Geophysics, 66(3), 786-799.

Constable S, Weiss CJ (2006) Mapping thin resistors and hydrocarbons with marine EM methods, Part II—Modeling and analysis in 3D. Geophysics, 71(6), G321-G332.

da Silva NV, Morgan JV, MacGregor L, Warner M (2012) A finite element multifrontal method for 3D CSEM modeling in the frequency domain. Geophysics, 77(2), E101-E115.

Demirci I, Erdoğan E, Candansayar ME (2012) Two-dimensional inversion of direct current resistivity data incorporating topography by using finite difference techniques with triangle cells: Investigation of Kera fault zone in western Crete. Geophysics, 77(1), E67-E75.

Doll WE, Nyquist JE, Beard LP, Gamey TJ (2000) Airborne geophysical surveying for hazardous waste site characterization on the Oak Ridge Reservation, Tennessee. Geophysics, 65(5), 1372-1387.

Erdoğan E, Demirci I, Candansayar ME (2008) Incorporating topography into 2D resistivity modeling using finite-element and finite-difference approaches. Geophysics, 73(3), F135-F142.

Gunnink JL, Bosch JHA, Siemon B, Roth B, Auken E (2012) Combining ground-based and airborne EM through Artificial Neural Networks for modelling glacial till under saline groundwater conditions. Hydrology and Earth System Sciences, 16(8), 3061.

Haber E, Ascher UM (2001) Fast finite volume simulation of 3D electromagnetic problems with highly discontinuous coefficients. SIAM Journal on Scientific Computing, 22(6), 1943-1961.

Mackie RL, Smith JT, Madden TR (1994) Three-dimensional electromagnetic modeling using finite difference equations: The magnetotelluric example. Radio Science, 29(4), 923-935.

Mitsuhata Y, Uchida T (2004) 3D magnetotelluric modeling using the T-Ω finite-element method. Geophysics, 69(1), 108-119.

Newman GA, Alumbaugh DL (1995) Frequency-domain modelling of airborne electromagnetic responses using staggered finite differences. Geophysical Prospecting, 43(8), 1021-1042.

Newman GA, Alumbaugh DL (2002) Three-dimensional induction logging problems, Part 2: A finite-difference solution. Geophysics, 67(2), 484-491.

Pfaffhuber AA, Grimstad E, Domaas U, Auken E, Foged N, Halkjaer M (2010) Airborne EM mapping of rockslides and tunneling hazards. The Leading Edge, 29(8), 956-959.

Rochlitz R, Skibbe N, Günther T (2019) custEM: Customizable finite-element simulation of complex controlled-source electromagnetic data. Geophysics, 84(2), F17-F33.

Steuer A, Siemon B, Auken E (2009) A comparison of helicopter-borne electromagnetics in frequency-and time-domain at the Cuxhaven valley in Northern Germany. Journal of Applied Geophysics, 67(3), 194-205

Streich R (2009) 3D finite-difference frequency-domain modeling of controlled-source electromagnetic data: Direct solution and optimization for high accuracy. Geophysics, 74(5), F95-F105.

Streich R, Becken M (2011) Electromagnetic fields generated by finite-length wire sources: comparison with point dipole solutions. Geophysical Prospecting, 59(2), 361-374.

Wannamaker PE (1991) Advances in three-dimensional magnetotelluric modeling using integral equations. Geophysics, 56(11), 1716-1728.

Wolfgram P, Golden H (2001) Airborne EM applied to sulphide nickel-examples and analysis. Exploration Geophysics, 32(3/4), 136-140.

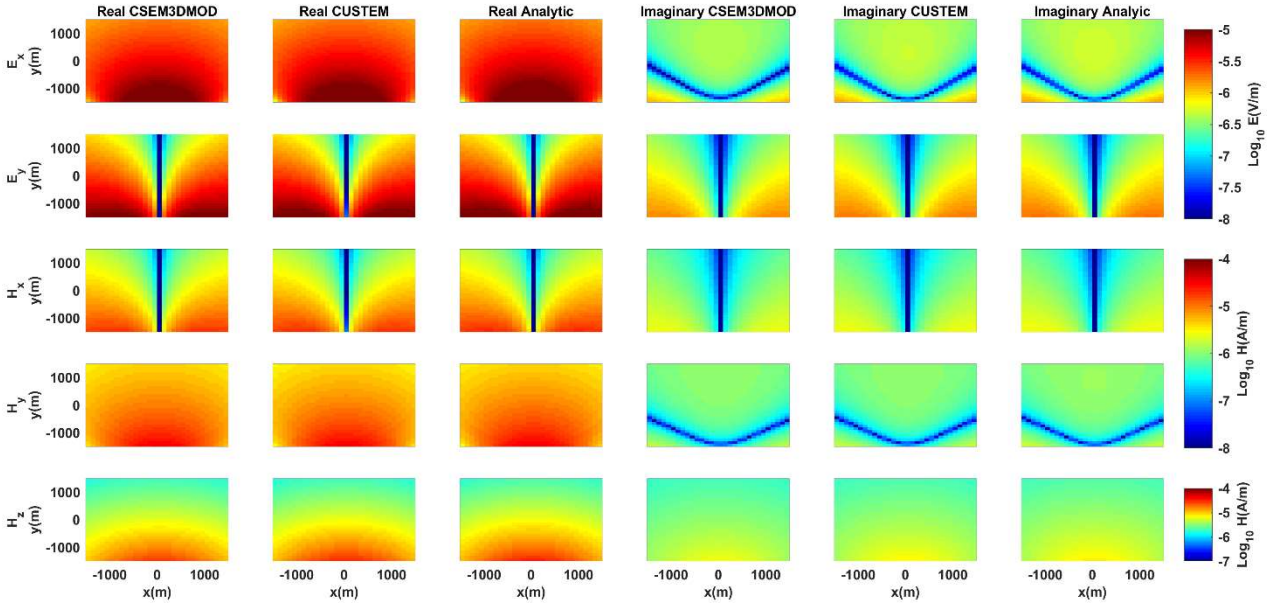

Figure 1. Comparison of our algorithm electric and magnetic field results (Ex, Ey, Hx, Hy, Hz) with CUSTEM and Semi-analytic solution for 1 Hz

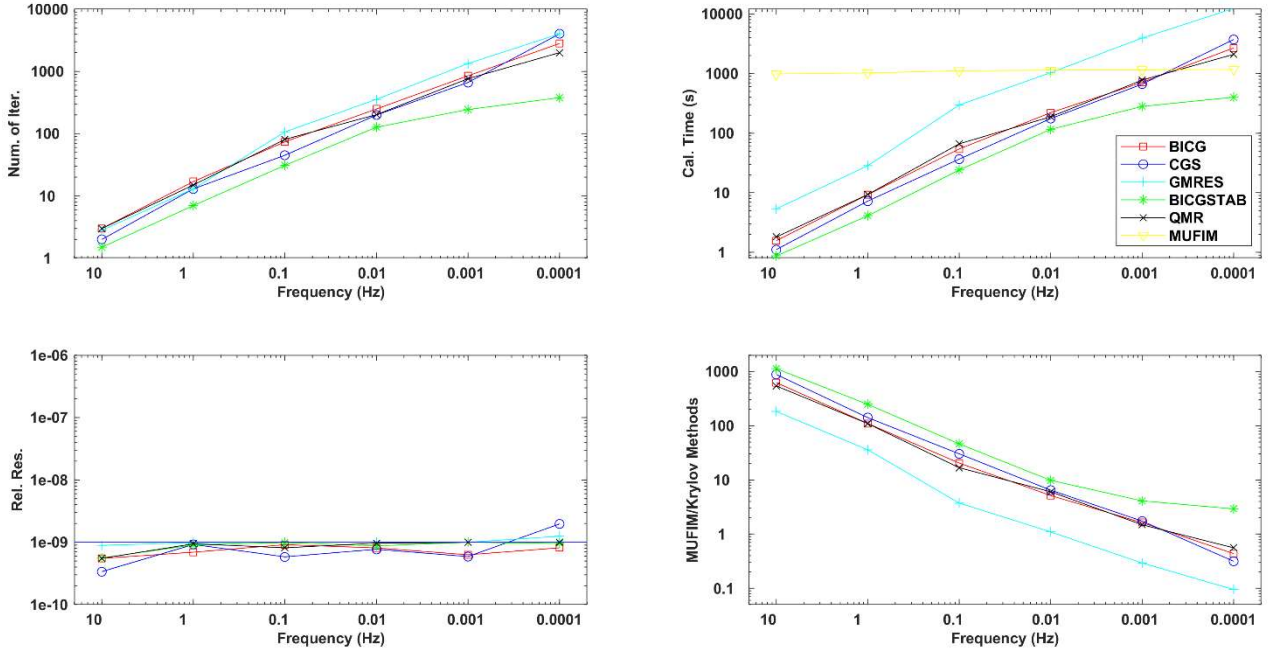

Figure 2. Comparison of iterative solvers in terms of iteration number, computation time, relative error and speed-up relative to direct solvers

POLYEM3D : A flexible 3D CSEM and MT modeling and inversion code

F. Bretaudeau [1,*], F. Dubois [1], J. Porté [1,2,3], S. Védrine [1,4]

[1]BRGM (French Geological Survey) f.bretaudeau@brgm.fr
[2] Strasbourg University, ITES-CNRS, UMR7063, France
[3] Formerly 1 & 2, now at SINTEF Industry, Norway
[4] University of Western Britany - EO-OCEAN, UMR6538, France

SUMMARY

We developed the massively parallel 3D finite-volume modeling and inversion software POLYEM3D, dedicated to the modeling and inversion of various type of EM data. POLYEM3D relies on a separated primary/secondary fields approach and can therefore handle both MT, and CSEM with very flexible acquisition configurations for sources and receivers: far or near field, marine, land, coastal, dipoles, long wires, loops and interactions with boreholes and metallic pipes. Coupling with other modeling codes such as FE to improve topography/bathymetry modeling or interactions with complex structures such as casings are possible.
The algorithm includes various solvers (MUMPS, WSMP) and can support both gradient-based (l-BFGS) and Gauss-Newton optimization to adapt to the data and computation constraints.
Many tools are available to tune the inversion of real world data, such as flexible parameterization with arbitrary 1D/2D/3D splines of several orders, automatic and user-defined inversion preconditioners, data reformulations and weighting, various L2 and robust norms, joint MT and CSEM, fast check 1D modeling/inversion, as well as including prior and constrains from borehole or AEM.

POLYEM3D was designed to be operational and efficient with real EM data, but also as an open research tool. In particular, it made it possible to explore new possibilities for EM such as 3D CSEM complex resistivity inversion (Porté et al. 2021), CSEM/MT inversion in a coastal context (Védrine et al. 2022, Védrine et al. EMIW22), joint inversion of several EM methods (Védrine et al. EMIW22), CSEM time-lapse differential inversion (Bretaudeau et al. 2021), CSEM deep imaging for geothermal energy in urbanized areas and sedimentary environments (Bretaudeau et al. 2022, Darnet et al. 2022), or CO2 storage and monitoring, or other shallow land CSEM configurations.

Keywords: 3D modeling, 3D inversion, MT, Controlled Source EM, direct solver, flexible, land, marine, coastal, joint inversion, IP inversion, topography, bathymetry, geothermal exploration

Magnetotelluric system NORD

D. Epishkin[1*], A. Yakovlev[1,2], D. Yakovlev[1], N. Zorin[1,2],
[1]Nord-West Ltd, Moscow, Russia
[2]Moscow State University, Moscow, Russia
[*]corresponding author: dmitri_epishkin@mail.ru

SUMMARY

This work presents the testing results of a new magnetotelluric system NORD. The key features of the system are: wireless operation with options of real-time data processing and quality assessment, measuring complex impedance of electric lines, low self-noise, low power consumption, light weight, compactness, reliability, robust data processing algorithms. The receiver has a built-in calibration system as well as telemetry that allows to monitor the status of the device and identify common problems. At the moment, the NORD allows to obtain high-quality MT data in the range from 50 000 seconds up to 20 000 Hz. We carried out a large number of field tests and comparisons with equipment from leading manufacturers, which showed excellent performance of the system. Also in recent years, a few large-scale production works have been carried out using this system.

Keywords: instrumentation, self-noise, testing, data processing

INTRODUCTION

The use of high-quality modern equipment is one of the important components of the successful implementation of magnetotelluric (MT) work. A number of review papers and textbooks discuss land MT instrumentation (Kaufman and Keller 1981; Simpson and Bahr 2005; Ferguson et al. 2012). Other reviews are focused on magnetic (Poliakov et al. 2017) and electric (e.g. Perrier et al. 1997; Lu et al. 1998) field sensors.

At present, a number of requirements are imposed on magnetotelluric systems. The system should have low level of self-noise, wide frequency range, the receiver input impedance should be sufficiently high to minimize the distortions of electric signal associated with poor grounding conditions. The equipment should be reliable, robust and able to operate in various climatic conditions; it also should be as simple as possible to use. We focused on these requirements when developing the station.

The NORD magnetotelluric system consists of 3 main parts: 1) 5-channel receiver 2) magnetic and electric field sensors 3) software for communication with the station and for data processing. This work describes the distinctive features of the NORD system and presents the results of testing.

MAIN FEATURES OF THE SYSTEM

The NORD system has a number of features that distinguish it from other magnetotelluric systems.

An innovative feature of the NORD receiver is that it has the ability to measure the overall complex impedance of the grounded dipoles, which include the capacitive effects in the wires. This allows taking less biased electric field measurements in the regions with poor grounding conditions.

The station has the ability to process data in real-time without stopping the record. It is also possible to view telemetry, time series, spectra and coherences in real-time, which allows you to quickly estimate the quality of the data.

All interaction with the station is carried out via Wi-Fi, which increases the reliability of the device in the field. Operation of the system is carried out by any Android / iOS / Windows / Linux – based device with a Wi-Fi module and an Internet browser.

The small dimensions and weight of the receiver make it possible to adapt it for marine measurements (Epishkin et al, 2018).

For advanced processing (Epishkin 2016) of raw time series acquired by NORD system one should use EPI-KIT — a modern and universal software solution for processing of MT and CSEM data. This software can process data received by equipment from a number of manufacturers, which allows you to combine different types of equipment in one project.

Receiver

The first component of the NORD system is a modern digital receiving unit (Figure 1), specially designed to register the EM field signals in wide

frequency range. The receiver has 2 electric and 3 magnetic channels, each one equipped with a separate 32-bit ADC with a base sampling rate of 2400 Hz and 24-bit ADC with a base sampling rate of 312.5 kHz for radio-magnetotellurics (RMT) or audio-magnetotellurics (AMT). It is possible to save the time series simultaneously at 5 sampling rates: 15 Hz, 150 Hz, 2400 Hz, 78.125 kHz, 312.5 kHz. The sampling rate schedule is easily configurable, and allows to control the final size of raw data files. High accuracy of the acquired MT or CSEM data is ensured by low internal noise level (~ 3.5 nV/√Hz for AMT frequency range) and modern ADCs of NORD receiver, combined with using robust data processing algorithm implemented in the EPI-KIT software. The main characteristics of the receiver are given in Table 1.

Figure 1. Receiver NORD

Parameter	Value
Number of channels	2 electric + 3 magnetic
Frequency range	DC – 35 kHz
ADC per channel	32 bit + 24 bit
Sampling frequencies	312.5 kHz, 78.125 kHz, 2.4 kHz, 150 Hz, 15 Hz
Input resistance	10 MΩ
Input capacitance	< 0.5 nF
Max. input voltage	E channels: ± 600 mV H channels: ± 2500 mV
Self-noise level	~ 3.5 nV/√Hz
Data interface	Wi-Fi 802.11n
Time synchronization	± 30 ns (RMS)
Integral solid-state drive	32 GB Industrial Grade (optionally up to 256 GB)
Power consumption	6 – 8.5 W
Power supply voltage	12 V
Weight	1.8 kg
Dimensions	20x10x13 cm
Temperature range	-40 … +85 °C

Table 1. Technical characteristics of the NORD receiver

Electric field sensors

Electric field measurement in the NORD system is performed with NW-4 sensors, which is a special type of compact, environmentally sound and relatively inexpensive non-polarizable graphite electrodes with low self-noise level.

Magnetic field sensors

NORD system set includes induction coils of the IMS series – low-noise magnetic field sensors with smooth and stable frequency characteristics. There are three types of sensors: IMS-5 – high-frequency sensors for AMT (0.1 Hz – 20 kHz), IMS-10 – classic MT band sensors (0.00002 Hz – 1000 Hz), IMS-15 – broadband sensors which allows obtaining a single AMT+MT (BBMT) curve without changing different types of sensors (0.00002 Hz – 10 kHz). The main characteristics of the IMS sensors are shown in Table 2. The amplitude-frequency characteristics of the sensors are given in Figure 3.

Parameter	IMS-5	IMS-10	IMS-15
Methods	AMT, CSEM	MT, CSEM	AMT+MT, CSEM
Operation frequency range, Hz	0.1 – 20000	0.00002 - 1000	0.00002 - 10000
Power consumption, W	0.96	1.2	1.7
Dimensions: length, cm	55	105	105
Dimensions: diameter, cm	6	7.6	6
Weight, kg	3	7	5.5

Table 2. Technical characteristics of the induction magnetic sensors (IMS series) used in the NORD system

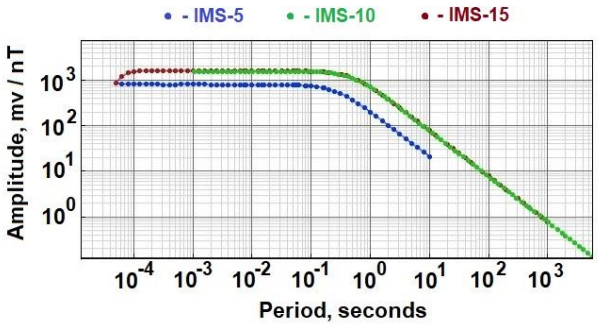

Figure 3. Magnetic sensors IMS-5, IMS-10, IMS-15 amplitude-frequency characteristics

TESTING RESULTS

Receiver self-noise

The measured internal noise level of the receiver is shown in Figure 2 in orange.

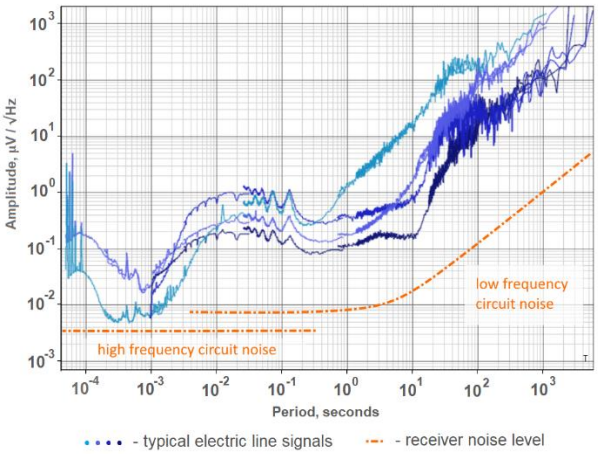

Figure 2. Self-noise of NORD receiver compared to typical electric line signals. There are different noise floors for high- and low-frequency receiving circuits.

Magnetic sensors self-noise testing

For all types of inductive magnetic sensors, we carried out numerous parallel tests, on the basis of which the self-noise of each sensor was calculated. Also, for some sensors self-noise measurements were carried out in a shielded camera. The noise levels obtained by both methods agree with each other. Tests have shown that the sensors have a stable and predictable noise level. Figure 4 shows results of self-noise measurements for different types of IMS sensors.

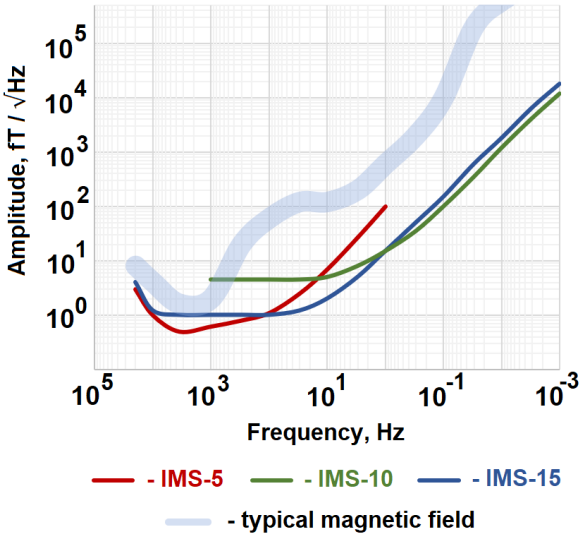

Figure 4. Self-noise of IMS sensors compared to a typical magnetic field

Synchronization testing

One of the important requirements for MT units is accurate time synchronization. To check the NORD receivers' synchronization accuracy we developed a special test. The same sinusoidal signal with a frequency f of several hundred Hz was applied simultaneously to several receivers, and for each moment of time the phase difference in degrees (Δφ) between the registered signals at the given frequency was calculated. Next, according to Equation 1, the time shift (Δt) was calculated:

$$\Delta t = \frac{\Delta\varphi}{360}\,\frac{1}{f} \qquad (1)$$

Figure 5 shows an example of a two-hour observation of timing accuracy between two NORD receivers. During the entire observation period, the synchronization accuracy between instruments was better than 60 ns, which is sufficient for synchronous processing of time series at frequencies up to 100 kHz.

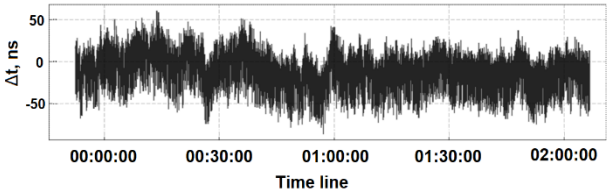

Figure 5. Time shifts (Δt) between signals from two NORD stations synchronized by GPS

Field testing

NORD system is being actively tested for several years, and dozens of pilot instruments have been already used in commercial MT and CSEM projects in Ural Mountains, Taymyr Peninsula, Siberia and Kazakhstan. To date, thousands of measurements have been carried out using the NORD system in various climatic conditions.

As a demonstration of the system's capabilities, Figures 6 and 7 show 2 measurement results.

The first result was obtained in Kamchatka (eastern part of Russia). The measurements were carried out in the MT mode. For 3 days of measurements, it was possible to obtain high-quality curves in the range from 0.001 seconds to 30 000 seconds.

The second result was obtained in the central part of the East European Plain. In this example, the recording was carried out in the BBMT mode. With 12 hours of data, high-quality results were obtained in the range from 0.0001 seconds to 1000 seconds.

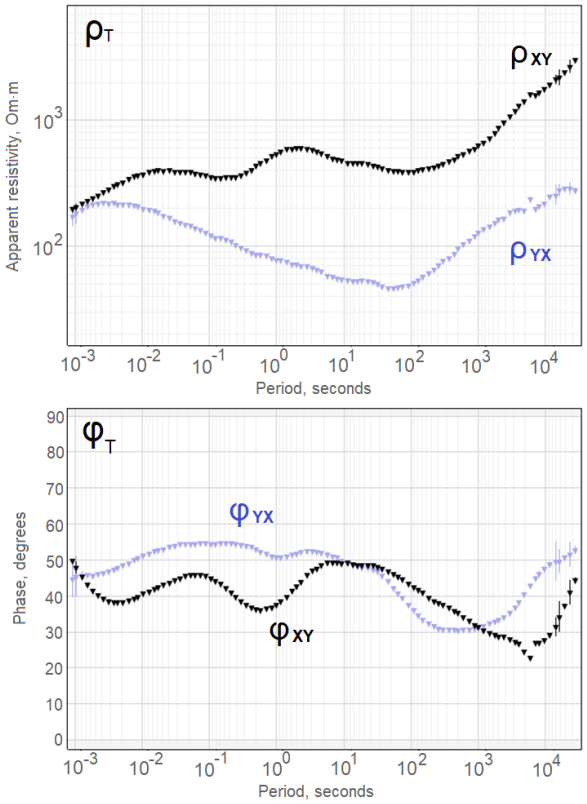

Figure 6. Processing result of 3-day record at Kamchatka region (East of Russia) with the IMS-10 magnetic coils in the MT frequency range

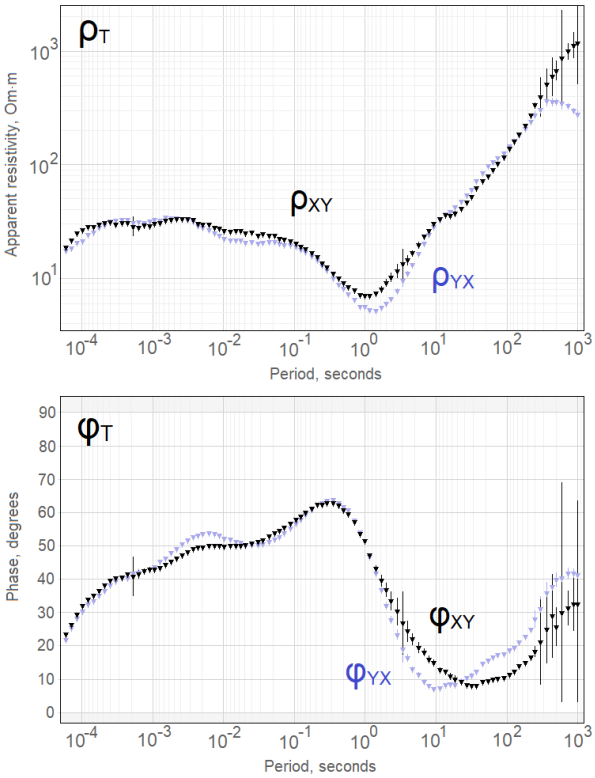

Figure 7. Processing result of 12-hours record at the East European Plain (Russia) with the IMS-15 magnetic coils in the BBMT frequency range

Conclusions

The conducted tests have shown that the receiver and field sensors work at a high level and meet the most modern requirements for accuracy and reliability. The new solutions applied in the Nord complex (measurement and accounting of the complex resistance of electrical lines, processing and quality control in real time, control through any device with a browser) improve the quality of the received MT and CSEM data and increase work productivity.

References

Epishkin DV (2016) Improving magnetotelluric data-processing methods. Moscow Univ. Geol. Bul. 71(5):347–354.

Epishkin D, Palshin N, Yakovlev A, Yakovlev D (2018) Technology of marine magnetotelluric sounding in transition zone. In: Paper presented at the 24th EM Induction Workshop, Helsingor, Denmark, 13-20 August 2018. https://doi.org/10.13140/rg.2.2.33684.60808

Ferguson IJ, Chave AD, Jones AG, Mackie R, Rodi W (2012) Instrumentation and field procedures. In: Magnetotelluric method. Cambridge University Press, pp 421–479

Kaufman AA, Keller G (1981) The magnetotelluric Sounding Method. Elsevier, Amsterdam

Lu K, Macnae J (1998) The international campaign on intercomparison between electrodes for geoelectrical measurements. Explor. Geoph. 29: 484-488.

Perrier FE et al. (1997) A 1-year systematic study of electrodes for long period measurements of the electric field in geophysical environments. J. Geomagn. Geoelectr. 49: 1677-1696

Poliakov SV, Reznikov BI, Shchennikov AV, Kopytenko EA & Samsonov BV (2017) The range of induction-coil magnetic field sensors for geophysical explorations. Seismic Instruments 53: 1-18

Simpson F & Bahr K (2005) Practical Magnetotellurics. Cambridge University Press, Cambridge

Abstract, 25th EM Induction Workshop, Çeşme, Turkey, September 11-17, 2022

Well integrity monitoring with electric fields by using hierarchical geo-electric models

G.D. Beskardes[1] and C.J. Weiss[1]

[1] Geophysics Department, Sandia National Laboratories, Albuquerque NM, USA, gdbeska@sandia.gov

Summary

Failure of wellbore integrity is one of the key concerns in operating oil and gas fields as well as abandoned mature fields that are typically considered for long-term CO_2 storage, and may cause dramatic negative environmental impacts. Here, we present a numerical study on the well integrity monitoring by using electric (E) field measurements. The survey setting includes a steel-cased well whose condition is unknown (i.e., intact or damaged) and a surface profile along where the E field is measured once the casing is energized at the well head (i.e., the top-casing method; Wilt, 2016; MacLennan et al., 2018). The changes in the surface E field can be used to detect and constrain the location of well damage.

Here, we obtain the E field responses of the steel-cased wells from the simulated electrical potentials in the DC limit by utilizing the hierarchical finite element method (*Hi*-FEM; Weiss, 2017). The method allows us to represent the electrical conductivity not only on volume elements but also on lower dimensional elements such as facets (2D) and edges (1D) in the unstructured finite element mesh. Since the well casing is represented by a subset of connected edges within the 3D tetrahedral finite element mesh, the surface E field data can be simulated without the need of extensive mesh refinement and high computational cost. Our results support the findings of the previous studies that well breakage results in an anomalous increase in the amplitude of the surface E field inversely proportional to the length of the path from the wellhead. Moreover, our analysis of surface E field data obtained from an energized, damaged well also shows that regardless of the amount, type, and location of well damage, surface E field measurements can identify the presence of damage and provide a reasonable estimate for the compromised portion of the well. In this study, we present various model scenarios to investigate the feasibility of an automated well integrity monitoring with the surface EM data.

Keywords: DC resistivity, electric fields, well integrity monitoring, finite element modeling

Acknowledgements

Sandia National Laboratories is a multimission laboratory managed and operated by National Technology and Engineering Solutions of Sandia, LLC., a wholly owned subsidiary of Honeywell International, Inc., for the U.S. Department of Energy's National Nuclear Security Administration under contract DE-NA-0003525. Finite-element meshes used for this analysis were generated by Cubit, available at http://cubit.sandia.gov. Funding support was provided by the Sandia National Laboratories LDRD program.

References

Beskardes, G.D., Weiss, C.J., Um, E., Wilt, M. and MacLennan, K., 2021. The effects of well damage and completion designs on geoelectrical responses in mature wellbore environments. *Geophysics*, **86**, no. 6, pp. E355–E366.

MacLennan, K., G. Nieuwenhuis, M. Wilt, E. Um, and J. M. Pendleton, 2018, Evaluating well casing integrity with non-invasive electromagnetic methods: Presented at the Annual Technical Conference and Exhibition, SPE.

Weiss, C.J., 2017. Finite-element analysis for model parameters distributed on a hierarchy of geometric simplices. *Geophysics*, **82**, no. 4, pp. E155–E167.

Wilt, M., 2016, Wellbore integrity mapping using well-casing electrodes and surface based electrical fields: Final Report for SBIR phase 1 Grant DE-SC0015166.

Magnetotelluric imaging of the Mitidja Basin structure, North of Algeria

Naïla. Kerbadj[1,2], Abderrezak. Bouzid[1] and Ahmed Seddik. Kasdi[1,2]
[1] Centre de Recherche Astronomie, Astrophysique et géophysique CRAAG, 16340, BP 63 route de l'Observatoire Bouzaréah, Algiers, Algeria.
[2]Université des sciences et de la technologie Houari Boumediene, BP 32 El Alia Bab-Ezzouar, 16111, Algiers, Algeria.

SUMMARY

The Mitidja basin is located in central northern Algeria, thus it is an active seismic zone. Studies have shown destructive earthquakes along the southern and northern sides of the area. It is associated with Quaternary compressive deformation revealed by thrust focal mechanisms (Maouche et al. 2011; Meghraoui 1991). Due to a lack of deep geophysical data, evidences about the lithospheric structures related to the formation of the Mitidja basin are limited. Magnetotelluric data from 10 stations on an 11 km N-S profile were acquired and inverted to derive an electrical resistivity model. Phase tensor analysis indicates a 2D resistivity structure with presence of 3D local features. The 2D inversion model illustrates electrically conductive basin with depth of ~ 3.5 km. The lack of seismic profiles and deep wells throughout the basin makes it impossible to know its depth, exact development time, geometry and dip of surrounding faults. Only modeling of recent gravity data highlights the direction of deep and steep north-dipping NE-SW tectonic contact at the northern basin boundary (Hamai 2011). The subject of this work is to image the underlying geoelectric structures beneath Mitidja basin.

Keywords: Mitidja Basin, Tipasa, Magnetotellutic, inversion, Algeria.

INTRODUCTION

The north of Algeria is one of the most active seismic area in northern Africa. The Mitidja basin is located within the central northern Algeria. This basin is marked by E-W to NE-SW trending fold structures and related reverse and thrust faults, accommodating 2 to 3 mm/yr shortening across the Tell Atlas (Guemache 2010; Maouche et al. 2011; Meghraoui 1991).

In order to obtain a geoelectrical model of the Mitidja basin, a magnetotelluric survey was performed. Basically it consisted of an 11 km N-S profil in Sidi-Rached, near Tipasa town in the western part of Mitidja basin. MT method uses natural origin electric and magnetic fields (Electrical thunderstorms and ionosphere-magnetosphere interactions). It is the most effective method to characterize the electrical resistivity of the subsoil (Aymé et al. 1954). A frequency dependent impedance tensor (Z) is obtained from the time variations of the horizontal electric and magnetic fields measured at the surface.

This paper presents a 2D inversion results obtained from minimizing the misfit of calculated model responses and observed data. This work is made to image the underlying geoelectric structures beneath Mitidja basin which is the focus of interest of the scientists working on seismic hazards and risk.

Geological setting

The Mitidja basin is situated in the central Tell Atlas in the north of Algeria. It is interpreted as a syncline bounded by compressive structures. It is characterized by E-W to NE-SW trending fold structures, over 150 km, being more or less parallel to the coastline (Maouche et al. 2011; Meghraoui 1991).

The most important active structure of Algiers area form the southern and northern edges of the Mitidja Quaternary basin, are the Blida thrust and fold system and the Sahel anticline respectively. The main part of the Mitidja basin is filled by sediments and volcanic rocks. NW-SE to NNW-SSE compressions formed the actual frame of the Mitidja region, between lower Pliocene and Quaternary (Derder et al. 2018; Guemache 2010; Maouche et al. 2011; Meghraoui 1991).

To the north of the basin, a 70 km long Sahel asymmetrical anticline shows a blind reverse fault (Guemache 2010; Maouche et al. 2011; Meghraoui 1991) which is probably at the origin of several earthquakes in the North of Algeria. The Mitidja basin is an active structure; many seismological studies have shown the existence of destructive earthquakes along both the southern and northern sides of the basin (Heddar et al. 2013; Maouche et al. 2018).

Data acquisition and processing

The Mitidja broadband MT sites were collected between 2008 and 2022, where the data was acquired on an 11 km profile of 10 stations, with sites spacing between 0.6 and 3 km.
Sites MTJ02, MTJ03, MTJ06 and MTJ07 are located over the Sahel fold. MTJ09 was located above the limit between the Sahel fold and the Mitidja basin. The rest of sites were installed on top of the Quaternary deposits of the Mitidja basin. The sites are distributed along N-S profile, that is, orthogonal to the geological structures direction. At each sounding the electrical (E_x , E_y) and magnetic components (H_x , H_y H_z) are recorded using MTU-5A of Phonix Geophysics. The AMT recordings were performed during approximately 1 hour, whereas the MT ones were carried out over a time range of 3 to 24 hours.
The observed time series were processed using SSMT2000 software, yielding impedance tensors Z and Tipper T_Z within the period rang 10^{-4} – 10^{3}s.

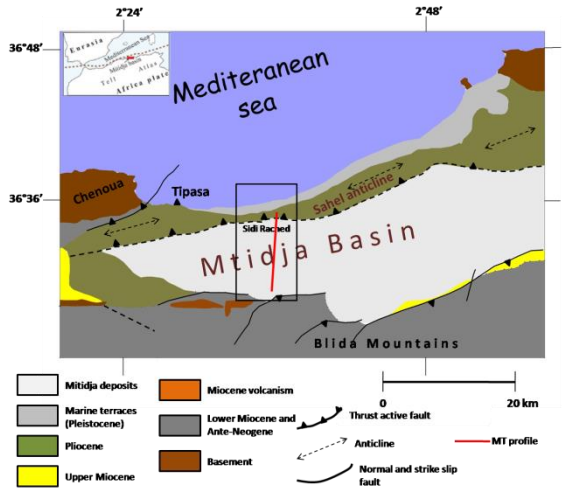

Figure 1. Simplified geological map of Mitidja basin modified from (Maouche et al. 2018). The red line indicates the position of MT profile.

Figure 2. MT sites distribution plotted in red circle along a N-S profile (Google earth image)

Dimensionality and strike analysis

The MT data were edited to remove estimations that were clearly contaminated by noise. A dimensionality analysis using phase tensor was carried out. This approach provides also estimates of regional strike starting from the analysis of the magnetotelluric impedance tensor (Caldwell et al. 2004).
To measure the structural dimensionality (Caldwell et al. 2004), a skew angle β was calculated from phase tensor. When $|\beta| < 3$, a 2D structure is interpreted while for $|\beta| > 3$ a 3D structure should be considered. The phase tensor can be displayed by an ellipse. The shape of the ellipse represents a dimensionality of the resistivity responses: Circular for 1D and elliptical for 2D or 3D.
Figure 3 shows that for most of the periods β values are below the threshold ($|\beta| < 3$). Some large β values appear at the longest period ($|\beta| > 3$). Accordingly, the subsurface structure may be regarded as 2D, in general.
In this study, induction vectors were useless due to the high level noises contaminated the measured vertical magnetic field.
Figure 4 shows the rose diagram values for all periods at each station. The results suggest a strike angle of N80°E which coincides well with the regional geology. The rotated xy and yx curves were assigned to the TE and TM mode, respectively.

Two dimensional resistivity modeling

The MT data was inverted using the finite element inversion algorithm MARE2DEM (Key 2016) to derive a 2D smoothest resistivity model that fits the data. In order to find the best inversion strategy, several tests were carried out.
Both transverse electric (TE) and transverse magnetic (TM) modes were inverted jointly using 50 Ωm homogenous half space as a starting model. An error floor of 10% was applied to the apparent resistivity and 2.87° in the phases. Figure 5 shows the model obtained finally. This model achieved an RMS misfit of 2.03. In order to check the consistency of the result, sensitivity tests were carried out. The latter have shown that there are no inversion artifacts.

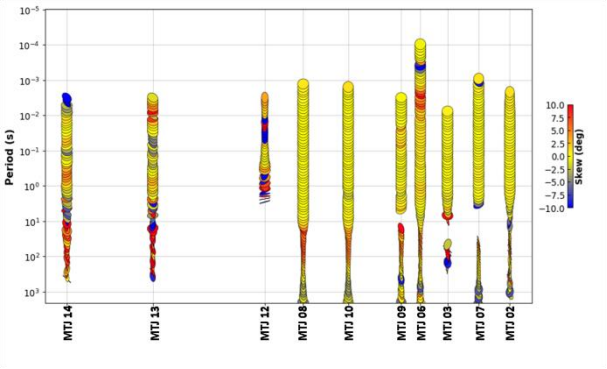

Figure 3. Skew angle β plot along the profile

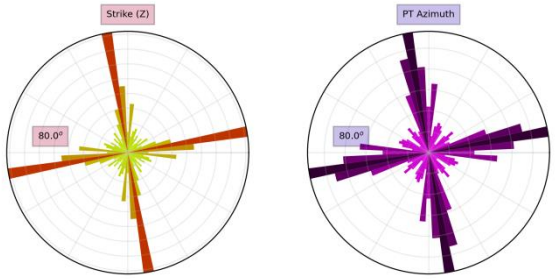

Figure 4. Rose diagram of strike angles obtained by the phase tensor method for all sites and all periods.

Results and discussion

The subsurface of the Mitidja basin appears mainly as conductive intersected by various conductors' bodies (Kerbadj et al. 2022).

From N to S, the model (figure 5) shows in the upper part a conductive zone UC1 (0.1 ~ 1Ωm) a resistive zone UR1 (150 Ωm), a second conductor zone UC2 (10 Ωm), a second very resistive zone (1000 Ωm) and an alternation of conductors and resistors UC-R (10 – 150 Ωm). A very conductive zones C1 and C2 (0.3 – 1 Ωm) are identified in depth that extends to 3 km. This high conductivity might be related to fluid content within the marine Pliocene formation.

A number of resistive anomalies shown in the obtained model (figure 5) could be related to active deformation causing juxtaposition of older geological formation with the younger basin sediments.

The model illustrate well the Sahel anticline Neogene structure, this anticline shows thrust and flexural faulting affecting the vertical bedding of Quaternary units of the Mitidja basin. Between the upper Miocene and the Quaternary, NW-SE to NNW-SSE compressions forms the syncline of the Mitidja basin.

Minimum depth extent of the shown model can be determined as approximately deeper than 3.5 km due to the highly intense effect of the conductive structures which prevent the deep structures from being resolved properly.

Conclusions

Magnetotelluric profile was carried out in the central part of northern Algeria, into the east of Mitidja basin in order to reveal its structure at depth.

The phase tensor dimensionality analysis suggested that the data are generally consistent with 2D assumptions. The finite elements code MARE2DEM was used to resolve the 2D inverse problem. Sensitivity tests were carried out to confirm that resistivity structures are robust. The obtained model reveals structures that correlate with geological information and complementing them despite the noisy data.

Acknowledgements

The equipment for the field work was supplied by the research center of Astronomy, Astrophysics and Geophysics (CRAAG) and Houari Boumediene university (USTHB Algeria). This project has required intensive field work which would have not been possible without the effort from researchers and students from the research center of Astronomy, Astrophysics and Geophysics (CRAAG, Algeria) and Houari Boumediene university (USTHB Algeria) which we gratefully acknowledge.

References

Aymé A, Aymé J-M, Magne J (1954) Etude des terrains Néogènes de la cluse du Mazafran Sahel d'Alger). Bulletin n°1, Fascicle 11,129-150

Caldwell T.G, Bibby H.M, Brown C (2004) The magnetotelluric phase tensor. Geophys. J. Int., 158, 457-469

Derder M.EM, Djellit H, Henry B, Maouche S, Amenna M, Bestandji R, Ymel H, Gharbi S, Abtout A, Dorbath C (2018) Strong Neotectonic block-rotation, related to the Africa-Eurasia convergence in northern Algeria: Paleomagnetic evidence from the Mitidja basin. Tectonics 10.1029/2018TC005394

Guemache M-A, Djellit H, Ymmel H, Gharbi S, Dorbath C (2010) La faille post-Astienne de Bouinan-Soumâa (région de Blida, bordure sud du bassin de la Mitidja, Algérie) : Expression néotectonique et implication dans l'évaluation de l'aléa sismique. Bulletin du service géologique national Vol.21, n°1, PP. 75-94,11 fig.

Hamai L, (2011) Etude gravimétrique de la Mitidja occidentale

Heddar A, Authemayou C, Djellit H, Yelles A-K, Déverchère J, Gharbi S, Boudiaf A, Van Vliet Lanoe B (2013) Preliminary results of a paleoseismological analysis along the Sahel fault (Algeria): New evidence for historical seismic events. Quaternary International, 302, 210-223

Kerbadj N, Abderrezak B, Boukhlouf W, Bougchiche S, Deramchi A, Guemache M-A, Djellit H, Abtout A (2022) Underlying geological structure of the northern edge of the Mitidja basin and the Sahel fold near Tipasa town (Algiers, Algeria) using magnetotellurics: First result. CAJG 2019 pp 489–491

Kerry K (2016) MARE2DEM: A 2-D inversion code for controlled-source electromagnetic and magnetotelluric data. Geophys. J. Int 207, 571–588

Maouche S, Harbi A (2018) The active faults of the Mitidja basin (North Central Algeria): what does the seismic history of the region tell us? A review. Euro-Mediterranean Journal for Environmental Integration, 3:21

Maouche S, Meghraoui M, Morhange C, Belabbes S, Bouhadad Y, Hddoum H (2011) Active coastal thrusting and folding, and uplift rate of the Sahel Anticline and Zemmouri earthquake area (Tell Atlas, Algeria). 2nd edn. Publisher, Location (1999). Tectonophysics, 509, 69-80

Meghraoui M (1991) Blind reverse faulting system associated with the Mont Chenoua-Tipaza earthquake of 29 october 1989 (north-central Algeria). Terra Nova, 3, 84-93

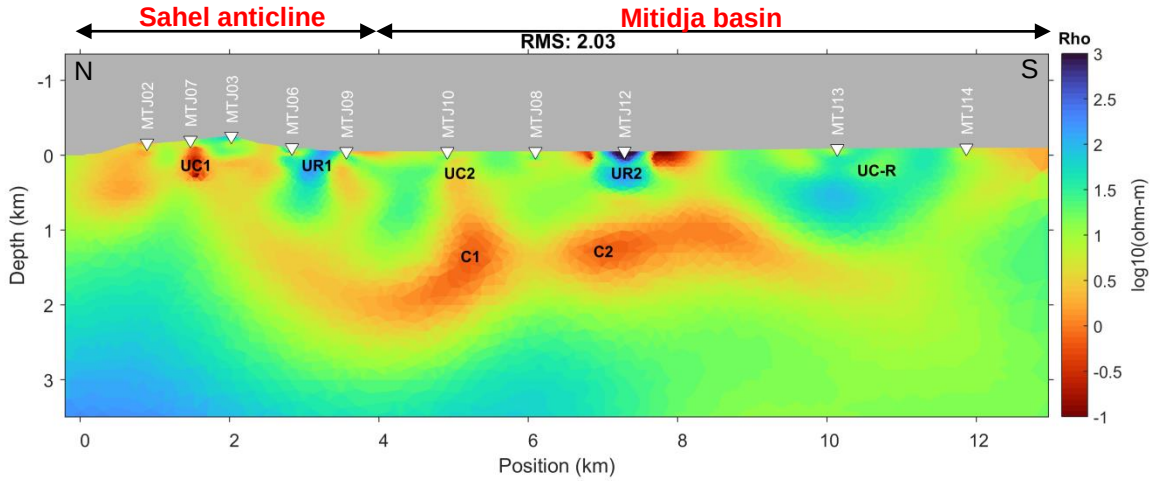

Figure 5. 2D Inversion results model obtained with RMS of 2.03

Sensitivity of phase tensors to absolute resistivities in a 3-D world

L. Dambly[1a], F. Samrock[1], A. V. Grayver[2] and M.O. Saar[1]

[1]ETH Zürich, Institute of Geophysics, Geothermal Energy and Geofluids Group, [a]luise.dambly@erdw.ethz.ch
[2]ETH Zürich, Institute of Geophysics, Earth and Planetary Magnetism

SUMMARY

Galvanic distortions represent one of the greatest challenges when dealing with magnetotelluric datasets. Several methods exist that try to mitigate the effect of distortions on inversion. One solution to avoid this major issue was provided with the introduction of the phase tensor, a transfer function that is free of galvanic distortion. However, the nature of the phase tensor makes it predominantly sensitive to relative changes of resistivity and its ability to constrain absolute resistivities is still under debate. So far, case studies have shown that phase tensor inversion works effectively if (i) the subsurface resistivity distribution has significant 3-D heterogeneities, (ii) MT site spacing is sufficiently dense, and (iii) data-constrained starting models are employed. There is presently a lack of systematic investigations to what extent phase tensors constrain absolute resistivity values in 3-D subsurface models.

To shed light on this discussion we systematically analyse to what degree variations of absolute resistivities influence the fit of phase tensor data. We use a dataset with measurements from 127 MT stations in an area of about 340 km^2 covering a volcanic geothermal field in the Main Ethiopian Rift. To ensure the eligibility of the dataset for 3-D phase tensor inversion we introduce a quantitative criterion for “sufficiently” dense station spacing. Using a homogenous starting model derived from the average apparent resistivity we retrieve a model with a good data fit, that acts as a reference model.

In a first test the fit of the reference model is compared to models obtained from inversion using arbitrary (i.e. not data-constrained) starting models consisting of homogenous halfspace models of 20, 50, 100 and 1000 Ωm. This results in poorer data fit and less geologically plausible models, thereby demonstrating the importance of using starting models that are constrained by data. In a second test we use the reference model and vary the resistivity values using algorithms from image processing such as contrast adjustment and linear stretching. Detailed analysis of the modelled responses and residuals reveals significant changes in the misfit relative to the reference model.

We conclude that in a realistic 3-D settings with sufficiently dense MT site spacing phase tensor inversion can be considered as a reliable method to recover true subsurface resistivities. If performed properly, phase tensor inversion is an elegant and straight-forward method to obtain models not affected by galvanic distortion.

Keywords: Magnetotellurics, Phase tensor, 3-D inversion, Galvanic distortion

Conductivity structure beneath Australia constrained by 3-D inversion of tippers in spherical geometry

F. Cicchetti[1], A. Grayver[1], R. Rigaud[1], A. Kuvshinov[1] and A. Yoshikawa[2]

[1]Institut für Geophysik - ETH Zürich, agrayver@erdw.ethz.ch
[2] Department of Earth and Planetary Sciences - Kyushu University, yoshikawa.akimasa.254@m.kyushu-u.ac.jp

SUMMARY

We present a new 3-D conductivity model of the Australian continent for part of the crust and upper mantle. The model was derived by inverting vertical magnetic field transfer functions (tippers), estimated from a combined data set at periods between 300s and 10000s. Specifically, we used data from the Australian Wide Array of Geomagnetic Stations (AWAGS) project and complemented them with geomagnetic observatory data from the MAGnetic Data Acquisition System (MAGDAS) and the British Geological Survey (BGS) data sets.

The challenging task of inverting tippers at a continental scale was addressed by performing inversion in a spherical frame and using a multi-scale approach with adaptively refined meshes to accurately account for the ocean effect and decrease of resolution with depth. This was made possible by a new formalism that allows modelling tippers on a sphere within the inversion code GoFEM. Furthermore, a spherical geometry set-up eliminates potential distortions caused by cartographic projections and paves the way to a natural integration of tippers with other longer-period electromagnetic (EM) responses from global sources.

Despite the limitations posed by the data set and survey layout, obtained conductivity model successfully images conductivity variations that correspond to major geologic features and boundaries, thereby providing new insights into the electrical structure beneath Australian continents and potentially serving as an initial guess for more detailed studies.

We consider this work as the first step in a broader study aiming at jointly inverting tippers and longer-period EM responses to obtain a 3-D conductivity model beneath Australia down to lower mantle depths.

Keywords: EM Induction – Magnetotellurics – Tippers – Electrical Conductivity – Australia

Constraining the 1-D electrical conductivity of the crust and mantle beneath continents by the joint inversion of multi-source electromagnetic transfer functions

R. Rigaud[1], A. Kuvshinov[1], A. Grayver[1], F. Perrier[2] and M. Kruglyakov[3]

[1] ETH Zürich, rafael.rigaud@erdw.ethz.ch
kuvshinov@erdw.ethz.ch
agrayver@erdw.ethz.ch
[2] Institute de Physique du Globe de Paris, perrier@ipgp.fr
[3] University of Otago, mikhail.kruglyakov@otago.ac.nz

SUMMARY

In this study, we present an approach that enables probing the Earth's conductivity structure from the crust to the lower mantle beneath geomagnetic observatories equipped with electric field measurements. This approach is based on a joint inversion of multi-source electromagnetic (EM) responses, namely, magnetotelluric impedances and longer-period global-to-local (G2L) transfer functions (TFs) originating from signals due to ionospheric and magnetospheric sources. Using the G2L TFs paradigm instead of the conventionally used C-responses allows us to account for the spatial complexity of the external sources. We validate the approach by inverting the responses estimated from the magnetic and electric data collected at the Chambon-le-Foret (CLF) geomagnetic observatory in France. We discuss the incurred challenges when working with CLF data, which arise due to the contamination of daily variations of ionospheric origin with the signals induced by the oceanic tides. We mitigate this problem through a high-resolution 3-D modelling of tidal signals and their subtraction from the data.

Keywords: EM Induction – Magnetotellurics – Geomagnetic Depth Sounding – Electrical Conductivity – Chambon-le-Foret

Dual L-shape model: a possible cause of anomalous magnetotelluric phase in central India

Khasi Raju & Prasanta K Patro

Magnetotelluric division
CSIR-National Geophysical Research Institute, Hyderabad, India

Summary

The anomalous magnetotelluric phase is a distinct characteristic of magnetotelluric (MT) data, which can be represented as a distortion in the MT data or anisotropy in the subsurface formations. In the present study, we notice an anomalous phase at several stations along the Narmada river course normal to the Tan Shear Zone (TSZ) in central India. We made efforts to derive a possible cause of the anomalous phase using synthetic studies and the obtained results are correlated with measured impedance tensor data as well as local geological conditions. In central India, multiple reactivations of the TSZ lead to the formation of a damage zone parallel to it and conjugate Riedel shear zone (parallel to the Narmada River course) normal to the TSZ. Based on the geographical position of the damage zone and conjugate Riedel shear zone in the study area we presented a dual L-shape model. From the response of the model, we noticed that near-surface 3-D heterogeneity across the TSZ critically distorted the transverse component of MT data (YX component of measured data) due to the strong current channeling. When the current flows across the conjugate Riedel shear zone i.e. along the Narmada river course, charges are accumulated at the boundaries of surficial 3-D structures. The charges associated with the current channeling leads to the reverse of the telluric current direction that is reflected in the form of anomalous phase in the transverse component of impedance tensor in measured data.

Keywords: Anomalous phase, dual L-shape model, CITZ, Tan shear zone, distortion, current channeling

Three-Dimensional Inversion of Magnetotelluric Data from the Tarawera Dome Complex, New Zealand

Authors: P. Semper, E. A. Bertrand, G. Caldwell, W. Heise, M. Scheunert, K. Spitzer

We have merged our long-term numerical software developments at TU Bergakademie Freiberg and TU Chemnitz into a finite element toolbox that now provides blueprints for the implementation of forward operators and inversion routines for arbitrary geophysical EM problems.

Here we present an application of this toolbox to the magnetotelluric method by inverting both synthetic and real MT field data sets to study the behaviour of the implemented numerical solutions and prove the applicability to large field data sets. The MT data were acquired by GNS Science at 68 sites over an area of 25 x 30 km^2 at the Tarawera Dome Complex, New Zealand, from 2006 to 2017. For the 3D inversion, we have used 16 periods between 0.013 s and 341.297 s and placed particular emphasis on an appropriate representation of the rugged topography. In a first attempt, we adapted the level of detailedness of the topography using an inverse distance weighting scheme, which for the time being sufficiently resolves the features of the topography that are important for this particular survey setup. We explicitly show that parts of the data are strongly affected by the topography at sites that are less than 2 km away from steep slopes and that these topographic features have to be resolved with sufficient accuracy. The free software programs gmsh and MUMPS are used to discretize the model domain and solve the forward problem.

For the synthetic case, we have used the targeted field dataset as a guide. A simplified model of the Tarawera Dome Complex has thus been created to generate a synthetic data set. The model is based on the knowledge of the regional geology and an analysis of the raw data. It consists of four main layers and two conductive plume-like structures. In addition, the lakes in the study area and the Pacific Ocean have been included using rough geometric approximations of their true shape. We can clearly see that the lakes cause static shifts at nearby sites and that the ocean affects the longest periods at all sites.

For the inversion of the synthetic data, we have restricted ourselves to the impedances which leads to the resolution of the stratigraphy in terms of layer thicknesses and resistivities. However, the plume-like structures were not resolved, which is probably due to their low significance within the synthetic data.

The 3D inversion of the impedances of the real data set yields very similar results to the ones obtained in previous studies by Heise, et. al. (2016) and Bertrand et. al. (in review). Two conductive plume-like structures, which seem to rise from a larger conductive zone at depth, are well resolved. These have been previously interpreted to be either high temperature fluids or partial melt rising from a partial melt body at depth.

Both studies give us positive feedback regarding the practical inversion of extensive MT field datasets with our toolbox.

Plane wave correction and 3D inversion of tensor CSRMT data

A. Shlykov[1], A. Saraev[2], N. Bobrov[3] and B. Tezkan[4]
[1] St. Petersburg State University, a.shlykov@spbu.ru
[2] St. Petersburg State University, a.saraev@spbu.ru
[3] St. Petersburg State University, n.bobrov@spbu.ru
[4] Cologne University, tezkan@geo.uni-koeln.de

SUMMARY

The plane wave correction of tensor CSRMT data measured in the transition zone of controlled source for the subsequent 3D inversion is proposed. Using 1D controlled source inversion of transition zone CSRMT data the plane wave curves were derived for main components of the impedance tensor. Efficiency of proposed correction was confirmed by the comparison with AMT curves. Corresponding CSRMT plane wave responses: apparent resistivity and phase curves were combined with AMT data and inverted using the ModEM three-dimensional code including topography. The obtained model was validated by the a priori geological information.

Keywords: Plane wave correction, Transition zone, Controlled-source radiomagnetotellurics, Audiomagnetotellurics, 3D inversion

INTRODUCTION

3D inversion of radiomagnetotelluric (RMT) data and controlled source radiomagnetotelluric (CSRMT) data in the far-field zone is based on the solution of the plane wave forward problem and is usually performed using magnetotelluric codes (Newman et al, 2003, Bastani et al, 2012). Modern computers and developed inversion codes like ModEM (Kelbert et al, 2014) permit to fulfill the inversion quite fast. Controlled source 3D inversion considering data in the transition zone of a source is the much more time-consuming task. There are still no publications about 3D transition zone inversion of the CSRMT data. Usually CSRMT measurements are performed both in the far-field and transition zones. Here we propose a relatively simple and fast procedure for the transformation of the mixed transition and far-field zone curves into fully plane wave equivalent curves without losing the phase and applicable for tensor CSRMT datasets (main components of impedance tensor). Validation of the proposed procedure was performed using the joint inversion of transformed CSRMT and audiomagnetotellurics (AMT) data and the comparison with a priori geological information.

Dataset

Field measurements were performed on the geophysics test site near St. Petersburg, Russia. For CSRMT measurements we used the RMT-F 5-channel recorder and two GTS-1 transmitters (Saraev et al, 2017) with perpendicular grounded wires of 620-630 m length. Measurements by the CSRMT were fulfilled in the broadside area of perpendicular wires at offsets from 13 to 640 m along 9 profiles with 50 m step and 20 m separation between stations along a profile. At the realization of soundings three main frequencies were used: 0.5, 5 and 50 kHz with 9 odd subharmonics for each main frequency to cover the range 0.5-950 kHz with 27 points on the sounding curve. Tensor CSRMT measurements were performed using traditional consecutive switching on transmitters: one measurement when the first transmitter is switched on and second one when the second transmitter is switched on.

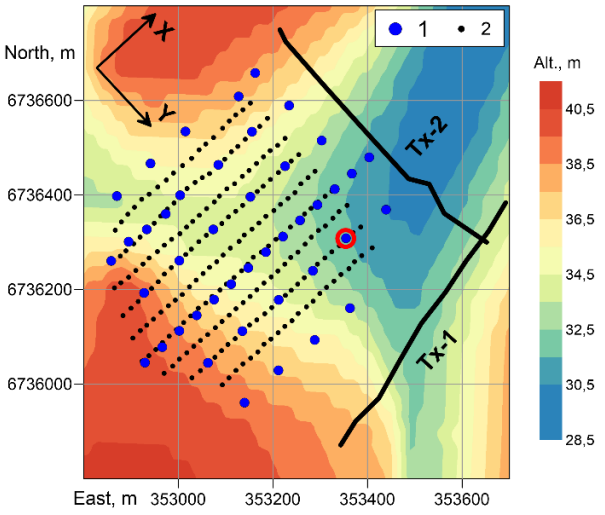

Figure 1. The layout of the sources and measuring stations in the topography map. 1 – AMT stations, 2 – CSRMT stations. Local coordinate system is shown in the map. Red circle shows the selected station for the analysis of transition zone effect.

Tensor AMT measurements were carried out using the 4-channel ACF-4M recorder (Saraev et al, 2014)

in the frequency range 3-400 Hz. AMT stations were located on the regular mesh 100x100 m within the studied area. The layout of the measurement stations in the topography map is presented in Figure 1.

The range of topography changing is about 10 m in this area. Inversion was done accounting the topography. Local X-axis is directed along the profiles and local Y-axis – is across profiles.

An example of the CSRMT and AMT sounding curves is presented in Figure 2. A station was selected near the sources (red circle in Figure 1) to illustrate the impact of the transition zone effect on CSRMT data. We can see the significant gap between AMT and CSRMT curves because of transition zone effect.

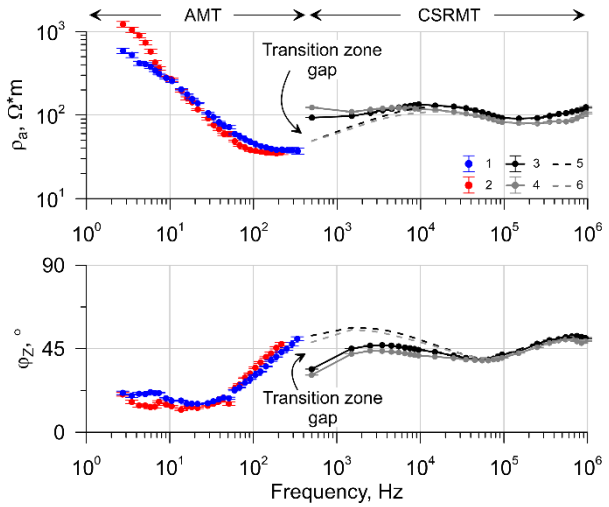

Figure 2. An example of sounding curves. 1 – XY AMT curve, 2 – YX AMT curve, 3 – XY CSRMT curve, 4 – YX CSRMT curve, 5 – synthetic plane wave curve after 1D inversion of XY CSRMT data, 6 – the same for YX CSRMT data. Position of the station is marked by a red circle in Figure 1.

Plane wave correction procedure

The correction procedure for transforming of the transition zone CSRMT data into the fully plane wave equivalent curves is described below.

Following to the principle of equivalence, we can say that any 1D model can be considered as an equivalent to the 3D model or the real distribution of the resistivity in the subsurface media if the electromagnetic (EM) response from this 1D model is close enough to the 3D response or measured data. It is valid for the plane wave and controlled source response (both, in transition and far-field zones). Almost any transition zone CSRMT data can be fitted with some acceptable tolerance using 1D controlled source inversion. For the obtained 1D model a plane wave response can be computed. We can assume that the computed 1D plane wave response is equivalent to the plane wave response from the real resistivity distribution on the measurement station.

In this context the task of 1D inversion of the transition zone CSRMT data is the fitting of measured data as close as possible but not the finding of a geologically reasonable model. The layered Marquardt inversion can be a good candidate for this procedure. For tensor data such correction has an obvious limitation. It is no way to correct diagonal XX and YY components but the main XY and YX components only. But the advantages of this approach are the independent fitting of each curve (XY and YX) and the joint correction of apparent resistivity and phase contrary to existing transition zone correction procedures like (Bartel, Jacobson, 1987).

Figure 2 contains an example of results of the application of proposed procedure. Dotted lines on the CSRMT curves are the corrected ones. It is clearly visible that both apparent resistivity ρ_a and impedance phase φ_z AMT curves are naturally continued by the corrected plane wave CSRMT curves and we have smooth common curves over six decades of the frequency. For tensor CSRMT data in the transition zone when the diagonal components of the impedance tensor are small enough this procedure can be a reasonable alternative to controlled source 3D inversion.

Results of 3D plane wave inversion

For the 3D inversion we used the ModEM code (Kelbert et al, 2014). The full AMT impedance tensor data at 43 stations and the main components of the transformed CSRMT impedance tensor data at 222 stations were used at the inversion. The finite difference rectangular model had 65x58x62 cells with the inner horizontal part 700x540 m with size of cells 20x20 m. The first (top) 12 m part of the model was divided into 8 equal layers with 1.5 m thickness to discretize the topography. Each other layer of the model had the thickness 1.2 times bigger than a previous layer down to 68 km. Total size of the model was 53x53x68 km.

Inversion was performed using the nonlinear conjugate gradients (NLCG) algorithm (Rodi, Mackie, 2001). We used 2% error-floor for the main components of the impedance tensor and 15% error-floor for the diagonal components of the AMT data. Start resistivity of the model under the “air” cells was 40 Ωm. All AMT data and a priory geological information show that the basement of the section is presented by the resistive crystalline rocks. Using the smooth Occam inversion, the

position of such sharp (by resistivity) border will be blurred and cannot be mapped confidently. In areas where the distance between AMT and CSRMT stations was less than 5 m we applied the 1D Marquardt joint inversion with 5 layers in the model using TM curves. For this inversion the original (not corrected) CSRMT data were used. As results of the 1D inversion the depths to the roof of the resistive basement were obtained in the range 220-310 m with slightly dipping toward the east with near to homogeneous the overlaying layer with resistivity around 30-60 Ωm and thickness around 140-180 m. According to a priory geological information this layer corresponds to the Riphaean sandstones and siltstones. Most of inhomogeneous are located in the top part of the section represented by Quaternary sediments. We estimated the topography of the top border of crystalline rocks and inserted this information to the start 3D model with the resistivity of basement 10000 Ωm.

For the 3D inversion the start RMS was 15.3% and final one after 60 iterations – 2 %. An example of fitting of the measured curves is presented in Figure 3. An example of section across the 3D model is shown in Figure 4 with overlapped a priori borehole information. The top part of section is the resistive Quaternary sands and loams. Its thickness matches the borehole data quite well. Lower we can see the more conductive layer with local resistive areas in the top, which corresponds to the Riphaean sandstones with gravel and pebbles. Lower part of model above the basement is the homogenies layer with resistivity of 30-40 Ωm which corresponds to Riphaean sandstones, siltstones and metasandstones. The resistive basement remained without any significant changes from the start model. This confirmed that our 1D estimation of the basement topography was correct. The top border of the basement according to geological information from one borehole in the vicinity of this area. It is presumed and shown by the dashed line in Figure 4. Our survey clarified the relief of this border. General view on the 3D model is presented in Figure 5.

Conclusions

The procedure for the plane wave correction of tensor CSRMT data in transition zone is proposed. Procedure is based on the 1D controlled source inversion of measured CSRMT data and the calculation of plane wave response for the derived model. The inversion is performed independently for XY and YX curves. As a result, we obtained the plane wave response, which is an equivalent to the AMT-RMT response which we can expect to obtain on the measuring station. Comparison with AMT data show that proposed procedure gets CSRMT response which naturally continue AMT curves. Using the 3D plane wave inversion of AMT and corrected CSRMT data we obtained the model which is in good agreement with a priori geology information.

Acknowledgements

The presented results were obtained with the support of the Russian Science Foundation, project No 21-47-04401, the Center GEOMODEL of St. Petersburg State University and the German Science Foundation, (project TE 170/21-1).

References

Bartel LC, Jacobson RD (1987) Results of a controlled-source audiofrequency magnetotelluric survey at the Puhimau thermal area, Kilauea Volcano, Hawaii. Geophysics 52(5):665.

Bastani M, Hubert J. Kalsheuer T, Pedersed LB, Godio A, Bernard J (2012) 2D joint inversion of RMT and ERT data versus individual 3D inversion of full tensor RMT data: an example from Trecate site in Italy. Geophysics 77(4):WB233.

Kelbert A, Meqbel N, Egbert GD, Tandon K (2014) ModEM: a modular system for inversion of electromagnetic geophysical data. Computers & Geosciences 66:40.

Newman GA, Recher S, Tezkan B, Neubauer FM (2003) 3D inversion of a scalar radio magnetotelluric field data set. Geophysics 68(3):791.

Rodi WL, Mackie R (2001) Nonlinear conjugate gradients algorithm for 2-D magnetotelluric inversion. Geophysics 66(1):174.

Saraev A, Simakov A, Shlykov A, Tezkan B (2017) Controlled source radiomagnetotellurics: a tool for near surface investigation in remote regions. Journal of Applied Geophysics 146.

Saraev A, Antashchuk K, Pertel M, Eremin I, Golovenko V, Larionov K (2011) The software-hardware system of audiomagnetotelluric sounding ACF-4M. The V Russian Workshop on the electromagnetic soundings of the Earth (EMS-2011), St. Petersburg.

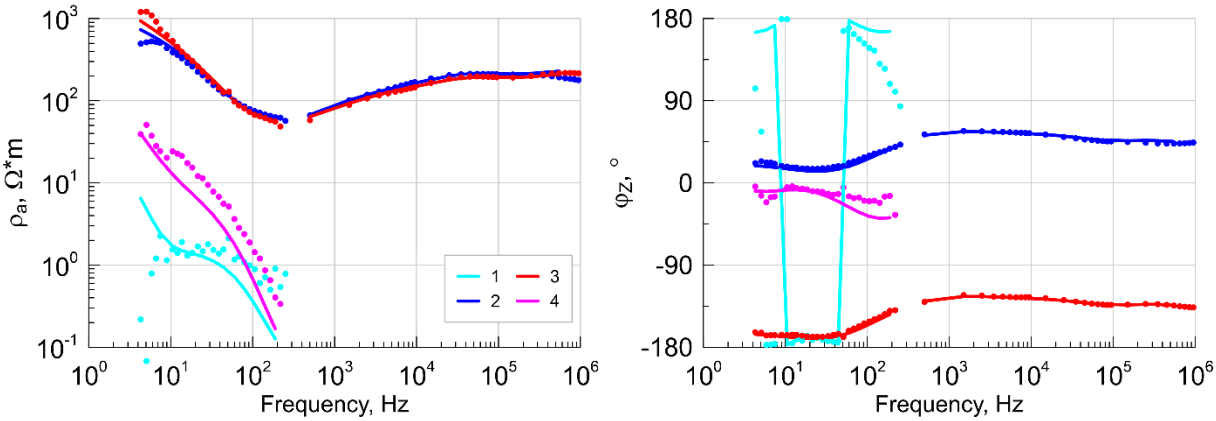

Figure 3. Comparison of synthetic and measured data for one station close to the sources. 1-4 – components of impedance tensor (1 - XX, 2 – XY, 3 – YX, 4 – YY), dots – measured data, lines – synthetic data.

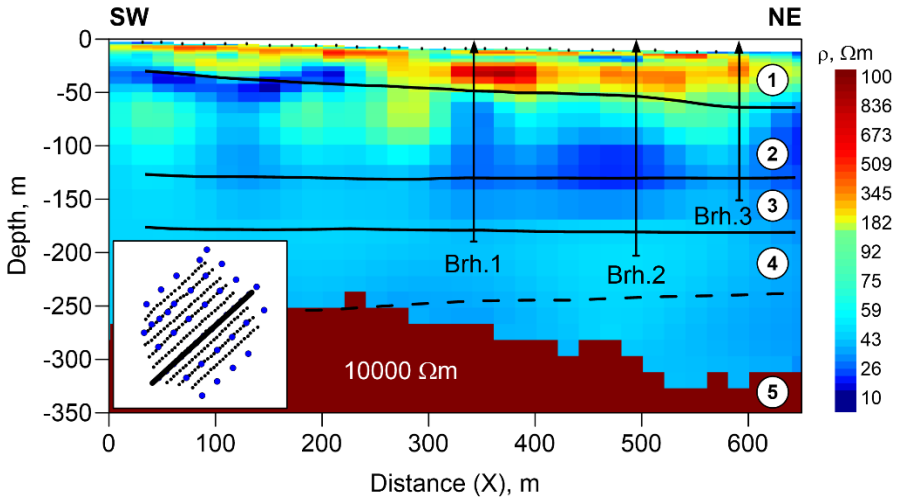

Figure 4. A section across the 3D model along the X-axis with overlapped borehole data. 1 – Quaternary sands and loams, 2 – Riphaean sandstones with gravel and pebbles, 3 – Riphaean sandstones and siltstones, 4 – Riphaean metasandstones, 5 – Precambrian crystalline basement (gneisses). The top border of the gneisses is not confident with borehole data but clarified by the resistivity section.

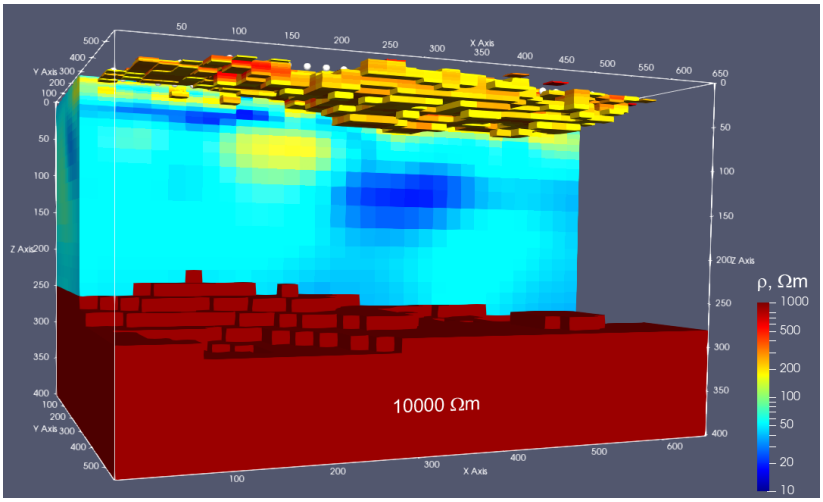

Figure 5. General view of the 3D model. Top resistive bodies correspond to the Quaternary sands. ~~and~~ Bottom resistive layer is the crystalline basement.

Abstract, 25^{th} EM Induction Workshop, Çeşme, Turkey, September 11-17, 2022

Convolutional Neural Networks Applied to 2D and 3D DC Resistivity Inversion

S. Weit[1], R.-U. Börner[1], M. Brändel[2], P. Gödickmeier[1], R. Gootjes[2], S. Kost[2], O. Rheinbach[2], M. Scheunert[1] and K. Spitzer[1]
[1]Institute of Geophysics and Geoinformatics, TU Bergakademie Freiberg
[2]Institute of Numerical Mathematics and Optimization, TU Bergakademie Freiberg

SUMMARY

A neural network approach has been developed to invert 2D and 3D apparent resistivity data. The network utilizes convolutions as well as pooling and unpooling operations to transform pseudosections into an underground resistivity model. To train the network, synthetic data were produced using an in-house finite element routine. The subsurface models to produce the data consist of homogenous halfspaces with 0 to 5 conductive spherical anomalies per simulated measurement. The anomalies, if present, have a constant total cross-sectional area. The network was trained on 15300 simulated measurements in 2D and 7500 in 3D. Results show a fairly accurate match of anomaly resistivity and location between ground truth and prediction for larger anomalies, while smaller anomalies often blend together in the prediction. The Background resistivity is often overestimated by the network. Due to the way training was performed, the applicability of the network is currently limited to a small number of scenarios. Despite its limitations, the speed of the prediction and the lack of required a-priori information are advantageous. Possible applications of neural networks in DC resistivity inversion lie in the generation of suitable starting models for other, more traditional inversion techniques.

Keywords: Machine Learning, Convolutional Neural Network, DC, Inversion

INTRODUCTION

Geophysical Inversion is often very time consuming and requires previous knowledge on the geological environment of the survey area. Both of these factors could be avoided or alleviated by utilizing neural networks for geophysical inversion. Distinguishing the effects of anomalies from the effects produced by a geologic background is very similar to an image segmentation approach. This approach is very established and has been shown to work in a variety of fields. Image segmentation is traditionally accomplished using convolutional neural networks. Here, we present an approach of utilizing convolutional neural networks for the task of regression applied to DC data. Network architecture, forward modelling and preliminary results will be discussed.

ARCHITECTURE

Architecture for segmentation often follows an encoder/decoder scheme (see Figure 1). During the encoding, convolutional layers and pooling layers are used to filter out the most important information. This information is then distributed and transformed during the decoder step with the use of unpooling layers and more convolutions. The traditional SegNet architecture (Badrinarayanan et al, 2017) uses a varying number of pooling and unpooling layers, with a final activation function (usually softmax) for pixel classification. Here, this architecture is slightly modified to perform regression by replacing the final activation function with a fully connected layer (see Figure 1). This way, not the categories of each cell (anomaly/background) but the value of each cell (resistivity) are predicted. This 2D network also mirrors the approach to an architecture used by Vu and Jardani (2021). To reduce the amount of overtraining and therefore make the network generalize more, dropout layers were introduced into every convolutional block. These set random entries of the input tensor to 0. In the 3D case, the unpooling layer is replaced by a combination of upsampling the output from the previous step as well as concatenating it with the output of the respective layer during the encoder.

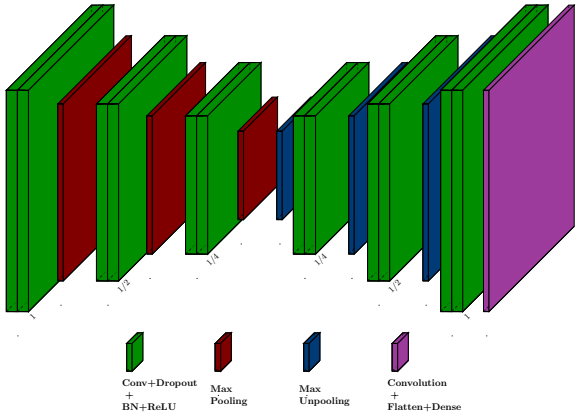

Figure 1: Architecture used for training 2D inversion

This approach effectively turns the network into a U-Net (Ronneberger et al, 2015) for the 3D case. This decision was made due to the lack of an established unpooling approach in 3D that utilizes the positional information of the pooling step. All training and evaluation were performed using the Keras API for Tensorflow (Abadi et al, 2016).

Data Simulation and Preparation

To attain the amount of data needed for training a neural network, synthetic DC data were generated. The synthetic forward modeling was performed using Matlab with an in-house finite element routine (Scheunert et al, 2022). We simulated DC measurements along 17 Profiles with 17 Electrodes each in a dipole-dipole configuration. Each simulated 3D measurement (17 dipole-dipole profiles with 17 electrodes each) will be called a "sample" in the following. The distance between profiles and electrodes was $3\ m$. This setup was deliberately chosen to compare results with Vu and Jardani (2021).

Dataset	n_{train}	n_{eval}
Dataset 1 (base)	7500	1563
Dataset 2 (no anomalies)	800	200
Dataset 3 (varying ρ for BG)	7000	1000

Table 1: Amount of training and evaluation data for each dataset.

For training, 3 sets of data were used: A basic one with spherical anomalies in an otherwise homogenous background of constant resistivity, one dataset with fully homogenous background and one with spherical anomalies in a homogenous background of varying resistivity. The amount of data in each set are shown in Table 1. The 0-5 spherical anomalies were randomly placed, with their centres below the central profile.

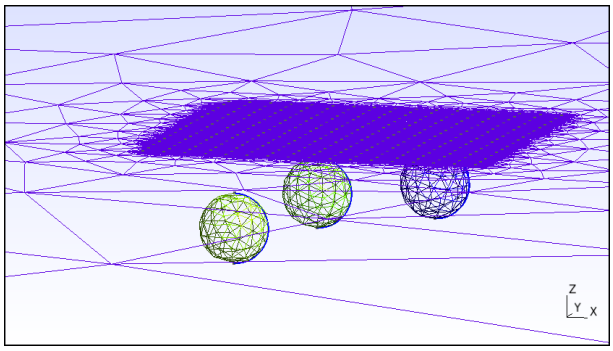

Figure 2: Mesh example for 3 spheres. Mesh is only shown on boundary surfaces.

The sum of the cross sectional area of all spheres was constant among all samples (excluding the homogenous halfspace set). Background resistivity was set to $4,000\ \Omega m$ for the base data set and varied from $4,000 - 40,000\ \Omega m$ for the third data set. Anomaly resistivity varied from $10\ \Omega m$ to $2,000\ \Omega m$. An example with 3 spheres is shown in Figure 2.

The 17 pseudo sections were mapped onto a 32x32x16 grid with grid cells of the size 1.5m in every spatial direction (see Figure 3 for one profile). Background resistivity was assumed for every cell not corresponding to a value from the pseudo section (again note Figure 3).

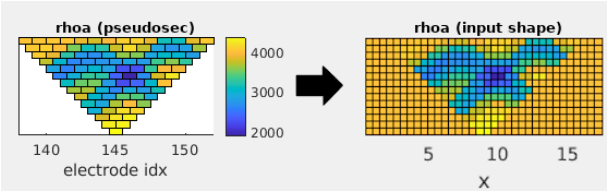

Figure 3: Mapping of a pseudo section to a 32x16 grid.

Inputs ρ_a and ρ were then finally transformed before being supplied to the network:

$$\rho_{a,in} = 10(log_{10}(\rho_a) - 3.5) \quad (1)$$

$$\rho_{in} = log_{10}(\rho) \quad (2)$$

Noisy data were created by the addition of normally distributed random numbers ($\mu = 0$ and $\sigma = 75$) onto every grid point value belonging to the pseudosection.

RESULTS

Figure 4 shows the 2D network prediction for data from all 3 datasets by a network that was trained using samples from all 3 datasets. The samples themselves have not been part of the training but were separated before. Structures close to the surface can be resolved fairly accurately for both cases with anomalies. Deeper structures often blend together or are not resolved at all.

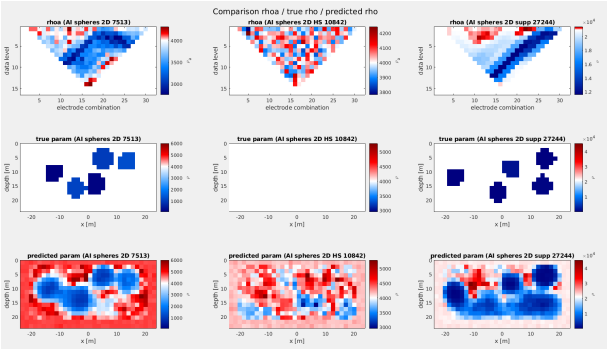

Figure 4: Results for image regression in 2D with all 3 datasets. Top represents the input grid, middle the ground truth, bottom the prediction.

This can be expected due to deeper structures being masked by shallower structures in the data. The background resistivity is generally wrong across evaluations and often shows small-scale variations not present in the ground truth. This is particularly visible in the evaluation of the pseudosection for the homogenous halfspace. There, a wide range of resistivities is predicted, with a great amount of local, small-scale variation, despite none of it being present in the ground truth. This effect can result from a variety of factors, such as small network complexity, dataset structure, noise level, amount of data, etc.

Figure 5 shows network prediction in 3D for the first dataset. A lot of the same effects as in the 2D case can be observed (missing resolvability of deeper anomalies, strong local variation in background resistivity) for this case as well. The general resolvability for smaller structures is worse than in the 2D case.

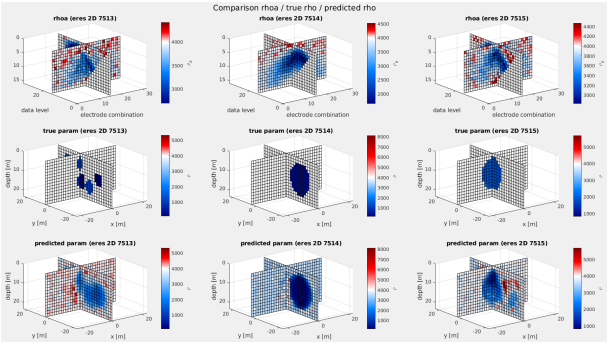

Figure 5: Results for image regression in 3D with the base dataset.

This could be attributed to the fact that a smaller percentage of underground cells belongs to an anomaly compared to the 2D case. Larger Scale anomalies (such as the right and center cases in Figure 5), are resolved well with regards to their position and resistivity.

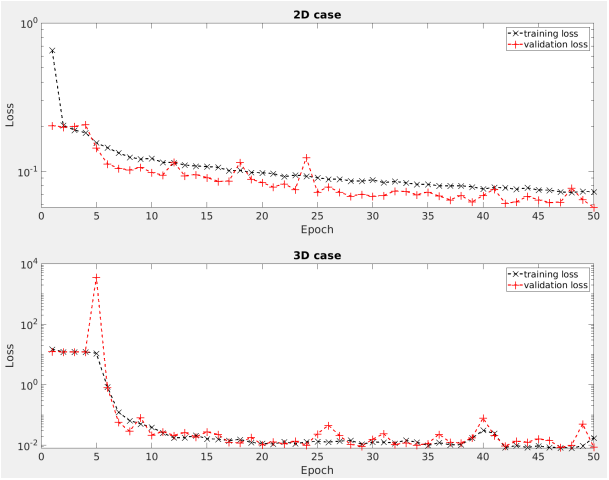

Figure 6: Loss for the training of 2D (above) and 3D networks (below).

Figure 6 shows the loss during training and validation. The curves showcase a small plateau during the start of training, followed by a large drop in loss during a few iterations . After around 10 iterations, improvement of the loss is small for the rest of the training process in 3D. No overtraining (divergence of training and validation loss) can be noticed in either case.

A limitation of the approach is illustrated in Figure 7. There, data from a subsurface model with a more resistive anomaly leads to a prediction that does not match the ground truth.

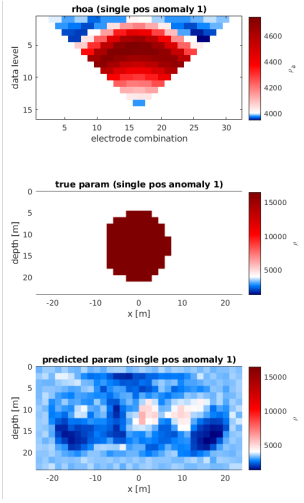

Figure 7: An example of an untrained scenario being evaluated poorly.

As there are no samples covering this case present in the dataset, the network is not able to evaluate cases like these correctly. This illustrates the high dependency on the training data for this type of network.

Conclusions

The presented approach shows promising results for resolving large to medium sized spherical anomalies. Huge limitations lie in the evaluation of scenarios that have not been used for training, such as positive resistivity anomalies. Some of these limitations could potentially be overcome by training with more data and data covering more scenarios. A strong dependency on training data will always be present for this type of network and therefore, alternative approaches should be considered to attain stronger generalization.

References

Abadi M, Barham P, Chen J, Chen Z, Davis A, Dean J, Devin M, Ghemawat S, Irving G, Isard M, et al (2016) Tensorflow: A system for large-scale machine learning. In: 12th {USENIX} symposium on operating systems design and implementation ({OSDI} 16), pp 265–283

Badrinarayanan V, Kendall A, Cipolla R (2017) Segnet: A deep convolutional encoder-decoder architecture for image segmentation. IEEE transactions on pattern analysis and machine intelligence 39(12):2481–2495

Ronneberger O, Fischer P, Brox T (2015) U-net: Convolutional networks for biomedical image segmentation. In: International Conference on Medical image computing and computer-assisted intervention, Springer, pp 234–241

Scheunert M, Blechta J, Börner RU, Ernst O, Spitzer K (2022) A matlab fe library for the simulation and inversion of em problems. In: 29. Schmucker-Weidelt-Kolloquium für Elektromagnetische Tiefenforschung, Deutsche Geophysikalische Gesellschaft e. V., pp 132–132

Vu M, Jardani A (2021) Convolutional neural networks with segnet architecture applied to three-dimensional tomography of subsurface electrical resistivity: Cnn-3d-ert. Geophysical Journal International 225(2):1319–1331

Multivariate statistical analysis of geophysical data and models by neural network approaches

R. Vadoodi[1], T.M. Rasmussen[1], M. Abdolmaleki[2]
[1]Luleå University of Technology, Sweden, roshanak.vadoodi@ltu.se
[2]University of Toronto, Canada

SUMMARY

Combination of geophysical data including magnetotelluric and potential field data provide useful information for mapping and interpreting geological units. Application of neural network approaches has proven to have potential to analyze and classify complex multivariate and high-dimensional data. Results from application of quantitative classification based on the unsupervised Self Organizing Map (SOM) neural network (Kohonen, 1982) to regional-scale potential field data combined with newly acquired broadband magnetotelluric data (Vadoodi et al., 2021) were presented by Vadoodi and Rasmussen (2022). The data covered a 200 km by 250 km area located in the Paleoproterozoic Norrbotten ore province (northern Sweden). The quantitative analysis integrated the petrophysical parameters associated with three data types (obtained from 3D individual inversions of gravimetric and magnetic fields and magnetotelluric data). The input parameters to the SOM algorithm were defined such that the information on depth variation of each petrophysical property enters the classification jointly with actual values. The input data contained 3D resistivity, magnetic susceptibility, and density model parameter values for six selected depth levels covering the entire crust. The SOM analysis provided an easy way to map and characterize three petrophysical models jointly to find the locations in the crust that are similar with respect to all three petrophysical parameters as well as similar depth-wise distribution. The domain classification is discussed with respect to the geological boundaries and composition of the crust. In general, consistency was observed regarding the visual comparison between the SOM domains and the mapped geological units. However, some discrepancies were noted in specific areas where more work is needed to analyze the reasons for the discrepancies.

Deep learning algorithms have been profoundly used in the earth science during the last few years for a variety of scientific problems such as image processing and classification. It uses multiple layers to progressively extract higher-level features from the input data. In the current study, we present results from the application of an unsupervised deep learning algorithm (stacked auto-encoder) for the above-mentioned data including resistivity, magnetic susceptibility and density values obtained from 3D inversion models for the same depth sections presented by Vadoodi and Rasmussen (2022). The domain classification is further discussed and compared with the results from the SOM analysis.

Keywords: Magnetotelluric, Potential field, 3D inversion, Neural network, Deep learning

Application of the skew parameters in 1-D and 2-D inversion of MT data

D. Yakovlev[1], K. Koryagin[1], D. Epishkin[1], N. Zorin[1,2] and A. Yakovlev[2]
[1]STC Nord-West, stcnordwest@gmail.com, Moscow, Russia
[2]Lomonosov Moscow State University, Moscow Russia

SUMMARY

1-D and 2-D magnetotelluric (MT) inversion is often used in practice. However, some MT data used in such inversions may show 3-D behavior in a certain frequency range, and the question is how these effects should be accounted for. The idea we present here is to increase the confidence intervals for the data within the frequency range, where they correspond to a higher-dimensional media, proportionally to the values of the observed skew (inhomogeneity) parameters.

For example, the following criteria may be used to prepare MT curves for 1-D inversion. For amplitude data the values N, $Skew_S$ and $Skew_B$ are used. These parameters are dimensionless and range from 0 to 1, indicating deviation of the medium from 1-D (N) and 2-D ($Skew_S$, $Skew_B$) models. Then the modified confidence intervals $\Delta lg|Z|$ for the amplitude curves may be calculated as: $\Delta lg|Z| = \Delta lg|Z|_{original} + N + Skew_S + Skew_B$. For phase data, the phase tensor parameters $\Delta\varphi$ and β are used. These parameters are measured in degrees and also indicate deviation of the medium from 1-D ($\Delta\varphi$) and 2-D (β) models. Accordingly, the modified confidence intervals for the phase curves $\Delta arg(Z)$ may be defined as: $\Delta arg(Z) = \Delta arg(Z)_{original} + \Delta\varphi + \beta$. The MT curves prepared in this way during inversion will make it possible to fit data more accurate in those frequency ranges where the dimension of the medium corresponds to the dimension of the inversion used.

This technology is implemented in the Inversio program, which is designed for analysis and 1-D/2-D inversion of large amount of MT data. At the analysis stage the interpreter, looking at the frequency sections of the skew parameters, decides which of the parameters to use to penalize the curves. The simplicity of the technology makes it very convenient in large-scale MT projects with a variable geological structure of the environment.

Keywords: Skew parameters, 1-D inversion, 2-D inversion

Impedance of capacitive electrodes and wires on the ground surface

N. Zorin[1,2*], D. Epishkin[1], D. Yakovlev[1] and A. Bobachev[2]

[1]STC Nord-West, Moscow, Russia
[2]Moscow State University, Moscow, Russia
[*]corresponding author; nikita.zorin.geophys@gmail.com

SUMMARY

In this paper we derive corrected for the edge effects formula for the capacitance of a thin disk over a conducting plane, and offer a number of generalized expressions for assessing the transfer impedance of a capacitive electrode over the ground with finite conductivity. It is shown that the transfer impedance of an insulated wire on the ground surface in a wide frequency range is described by the Cole-Cole formula with an exponent parameter slightly less than 1.

Keywords: contact impedance, disc capacitance.

3D imaging of electrical conductivity structures in the Eastern Cheb Basin across the Hartoušov and Bublák mofettes

B. Aleid[1&2], U. Weckmann[1&2], A. Platz[1], J. Pek[3], S. Kováčiková[3] & R. Klanica[3]
[1] Helmholtz Centre Potsdam - GFZ German Research Centre for Geosciences, aleid @gfz-potsdam.de
[2] Institute of Earth and Environmental Science, University of Potsdam, Germany
[3] Institute of Geophysics of the Czech Academy of Sciences, Prague, Czech Republic

SUMMARY

The mofette fields of Bublák and Hartoušov are among the most prominent CO_2 degassing centers in Europe, which are locacted in the Cheb Basin, a shallow Neogene intracontinental basin in the western part of Czech Republic. The massive degassing of CO_2 in the Cheb Basin, especially in the mofette fields, originates from great depths. These mantle/lower-crustal derived fluids might use fault zones for their ascent. In addition, Quaternary volcanoes were discovered in the area; their magmatic ascent paths and the interaction of the other deep magmatic processes as well as the observations at the earth's surface such as mofettes are not yet fully understood. With our research, we would like to contribute to a comprehensive and holistic interpretation of the tectonic regime, and image the ascent paths of fluids. In this context, the magnetotelluric (MT) method was applied which is sensitive to electrically conductive phases such as brines and fluids, partial melts or metallic compounds. We expect that the pathways for fluids from the mantle towards the mofettes have a much higher electrical conductivity than the surrounding crystalline rocks. As part of an ICDP drilling programme, two overlapping experiments along a regional profiles were conducted and one local grid of MT stations were measured in the Cheb basin close to mofette fields. The local dense grid of 97 MT stations, the scope of this work, has an average sites spacing of 500 m. We measured five component broad-band MT data in a frequency range of 0.0001–1000 s with an average recording time of three days. Unfortunately, there are many man-made electromagnetic noise sources such as power plants, DC electrified railways, and the heavily populated study area with its infrastructure. These disturbances had to be removed from the recorded data within the course of data processing prior to any modelling and inversion. It was finally possible to improve the data quality to 1s by advanced processing approaches. The presented high resolution 3D image of the electrical conductivity of the area surrounding the mofettes matches with available drill logs from the Czech Geological Survey and the previous geophysical studies. A shallow high resistivity layer is related to Quaternary deposits NE of the mofette fields. The high conductive layer around and beneath the mofettes might be related to the ascent paths of fluids. A prominent contrast between the sedimentary and the phyllitic-granitic basement can be observed. Large-scale regional models hint at deep reaching pathways fostering the ascend of mantle derived fluids into the regions of mofettes and swarm earthquakes. However, The most prominent large-scale conductivity features of the other two regional models are several channels from the lower crust to the surface, possibly representing pathways for fluids into the earthquake swarm region, mofette fields, and known spas. However, such a conductive channel is absent in our local model beneath the surface expression of the mofettes. To assess whether the experimental layout, the reduced data quality or inversion issues are responsible for the lack of such an ascending pathway, or if fluid migration in this area is rather horizontal than vertical, we applied synthetic inversion test. Results from synthetic modelling studies and available geoscientific constraints hint that such a channel might exist directly beneath the mofette field. Still, it seems to be challenging to resolve due to the given data quality, station distribution, and the subsurface conductivity structure within a conductive sediment basin.

Keywords: Magnetotellurics; West Bohemia; Earthquake swarm; Fluids; 3D inversion

Abstract, 25^{th} EM Induction Workshop,Çeşmeı, Turkey, September 11-17, 2022

Time-lapse resistivity imaging : CSEM-data 3D double-difference inversion and application to the Reykjanes geothermal field

Frédéric Dubois[1], François Bretaudeau[1]
[1]BRGM, 3 Av. Claude Guillemin, Orléans 45060, France

SUMMARY

Time-lapse resistivity tomography bring valuable information on the physical changes occurring inside a geological reservoir. In this study, resistivity monitoring from CSEM data is investigated through synthetic and real data. We present three different schemes currently used to perform time-lapse inversions and compare these three methods: parallel, sequential and double difference. We demonstrate on synthetic tests that double difference scheme is the best way to perform time-lapse inversion when the survey parameters are fixed between the different time-lapse acquisitions. We show that double difference inversion allows to remove the imprint of correlated noise distortions, static shifts, and most of the non-linearity of the inversion process including numerical noise and acquisition footprint. It also appears that this approach is robust against the baseline resistivity model quality, and even a rough starting resistivity model built from borehole logs or basic geological knowledge can be sufficient to map the time-lapse changes at their right positions. We perform these comparisons with real land time-lapse CSEM data acquired one year apart over the Reykjanes geothermal field.

Keywords: Controlled-Source Electromagnetics, time-lapse, inversion, geothermal monitoring, resistivity

INTRODUCTION

Geological reservoirs are exploited for various economic reasons: oil and gas production, power and heat generation from geothermal energy, C02 storage or water supply management. Monitoring of time-lapse resistivity changes in the reservoir properties using geophysical techniques can provide valuable information about the reservoir evolution, and is becoming more and more common, facilitated by permanent or semi-permanent acquisition systems. It consists in carrying out at different time a geophysical acquisition over a same region, and produce a structural image showing the temporal changes between the two acquisitions.

More specifically, electrical resistivity provides valuable information in many applications trough its sensitivity to permeability, fluids, clay content or temperature, and can be obtained using a large range of diffusive geophysical methods such as DC electrical resistivity tomography, time-domain electromagnetics, magnetotellurics or frequency domain controlled source electromagnetics (CSEM). Therfore monitoring electrical resisitivity may be very usefull.

For monitoring process, the first acquisition or reference dataset is generally called baseline and the following acquisitions are considered as monitors. In time lapse electric imaging studies, inversion of the baseline and monitor data sets are generally performed separately, or in cascade using baseline model as a starting guess for the monitor inversion. Then the difference between the two inverted models is presented as the time-lapse variation in resistivity of the reservoir. We call those schemes parallel and sequential time-lapse inversion. The high non-linearity and non-uniqueness of the resistivity imaging problems make the inversion results still strongly dependent of the path taken by the inversion. This effect may be exacerbated in presence of high level of noise, which can result in very different inverted models, even without significant model changes.

To overcome problems of parallel inversions, different time-lapse inversion schemes have been pro-

posed, mostly based on the used of constrains between the time-lapse models to force the stability and keep consistency between the time lapse models. For common-acquisition setup between surveys (same geometry, same acquisition parameters), an alternative inversion technique is available to obtain more stable results by reducing the effect of noise and non-linearity of the inversion process. This scheme called double difference or differential inversion is based on the combination of baseline and monitor data. It is commonly applied in medical imaging, is used in seismic travel-time inversion and have been applied successfully to seismic Full Waveform Inversion by Asnaashari et al (2014). But its evaluation on time-lapse resistivity problems have not been reported yet.

METHODS

CSEM inversions are intrinsically non-linear, and iterative optimization methods have to be employed. For each iteration k, we try to minimized the data residual vector which is typically defined as the difference between observed data and data calculated in the current model m_k:

$$\delta d_k = d_{obs} - d_{cal}(m_k) \quad (1)$$

with the computed data d_{cal} related to the resistivity model m_k by the forward operator G.

We define two different data sets corresponding to a baseline acquisition (d_{obs1}) and a monitor acquisition (d_{obs2}). First, a baseline reconstruction needs to be done by minimizing the difference between d_{obs1} and d_{cal} generated in a m_0 starting model. However, at the end of this first inversion, discrepancies remain between observed and predicted data coming from our inability to properly build the true resistivity model.

We can split the different contribution of each data set as follows

$$d_{obs1} = d_{m_0} + \delta d_{m_0} + d_{static} + d_{noise_1} \quad (2)$$

$$d_{obs2} = d_{m_0} + \delta d_{m_0} + d_{static} + d_{noise_2} + d_{pert}. \quad (3)$$

with d_{m_0} the data predicted by the forward modelling, δd_{m_0} un-modelled effects in the forward modelling, d_{noise} and d_{static} the uncorrelated and correlated noise between the two acquisitions , and finally d_{pert} the time-lapse signal related to geological variations.

In case of *parallel* scheme, baseline and monitor inversions are completely decoupled. We compute the time-lapse image by taking the difference between the final inverted models. Baseline and monitor data set do not need to have the same geometry (number of data, number of receivers/sources). This seemingly advantage is a potential pitfall for inversion tuning. However, we may compare models with potentially different inverting mesh, regularization parameters and thus very different local resolution. This will induce signals in the time-lapse model mainly related to the resolution difference between baseline and monitor inversion. Besides, the inverse problem is highly non-linear which implies complex noise propagation between data and model estimates. In *double difference inversion*, extra care should be taken on the perfectly match between baseline and monitor data set geometry. First, the baseline is reconstructed exactly as in parallel inversion. However, in the second step instead of inverting the monitor data we invert the data difference (Asnaashari et al, 2014). We thus define data difference as $\Delta d = (d_{obs_2} - d_{obs_1})$. Then, we rewrite the data residual vector at an iteration k as:

$$\begin{aligned} \delta {d_2}^{dble} &= (d_{obs_2} - d_{obs_1} + d_{cal}(m_1)) - d_{cal}(m_1) \\ &= d_{pert} + (d_{noise_2} - d_{noise_1}). \end{aligned} \quad (4)$$

A very interesting feature of this approach is illustrated by Equation (4). The data residual is not anymore dependent on the error of baseline reconstruction δd_{m_1}, making the inversion much more robust against the starting model, numerical modeling inaccuracies and non-linearity of the inversion.

RESULTS

The three different inversion approaches are applied to a synthetic case with a resistive and conductive anomaly (Figure 1). This shows how different can be these three different inversion schemes and how weak are the artifacts in the double difference strategy. Then we applied the three different inversion strategies to the Reykjanes geothermal field located at the south-west of Iceland at the landward extension of the Reykjanes Ridge (Darnet et al, 2020). Two surveys are acquired one year apart, a first one in September 2016, while drilling of RN-15/IDDP-2 well. The other is performed in August 2017,

after the thermal stimulation of the RN-15/IDDP-2 well. Darnet et al (2020) assess the influence of internal and external noise on survey repeatability between the two acquisitions. Over the whole frequency band, repeatability is within 2-3$\%$ and 2-3°for the amplitudes and phases respectively.

From the first data set, we build the baseline model noted m_1 by using a steepest-descent gradient optimization algorithm available in POLYEM3D. Once an acceptable baseline is found, we proceed to the inversion of the monitor data. Baseline reconstruction depicts the resistivity variations from the data set acquired in September 2016. Once an acceptable baseline is found, we proceed to the inversion of the monitor data by carrying out the three different time-lape inversion approaches. For parallel and sequential inversions: unfitted baseline structures, static shift structures and noise (correlated and not) are inverted in the same time as temporal resistivity changes. The parallel inversion is unable to discriminate between these different contributions, unlike the differential inversion which is focusing exclusively on time-lapse changes which limits drastically the number of artifacts.

CONCLUSIONS

In this study we investigate several time-lapse inversion strategies to infer the temporal changes of resistivity. We compare the commonly used parallel inversion framework with the sequential and double difference schemes. Unlike the parallel difference, the double difference inversion focuses on the time-lapse signal only. We show this approach is much more robust to noise since static noise and modelling errors are completely removed. Double difference is also less dependant on the starting model. Quantitative estimation of the time-lapse resistivity variations however is still dependant on the quality of the baseline model. It is also possible to image and localize resistivity variations even without a proper baseline reconstruction, or with a baseline model built with independent information. For instance, a large scale baseline model could be built with well logs, geological knowledge or a dense EM geophysical survey, and the monitoring performed with a reduced subset of the EM survey kept permanent between time steps.

ACKNOWLEDGEMENTS

The research and developments of the POLYEM3D code leading to these results has received fundings from the French ANR project EXCITING. Acquisition and processing of the Reykjanes dataset has been funded by the European research program H2020 in the framework of the project DeepEGS N$^{\circ}$690771. Large scale 3D EM modeling and inversion was performed with BRGM's POLYEM3D code on the Occigen supercomputer thanks to GENCI (Grand Equipement de Calcul Intensif) and CINES (Centre Informatique National de l$'$enseignement Supérieur) super computing facilities.

REFERENCES

Asnaashari A, Brossier R, Garambois S, Audebert F, Thore P, Virieux J (2014) Time-lapse seismic imaging using regularized full-waveform inversion with a prior model: which strategy? Geophysical prospecting 63(1):78–98

Darnet M, Wawrzyniak P, Coppo N, Nielsson S, Schill E, Fridleifsson G (2020) Monitoring geothermal reservoir developments with the controlled-source electro-magnetic methodâa calibration study on the reykjanes geothermal field. Journal of Volcanology and Geothermal Research 391:106437

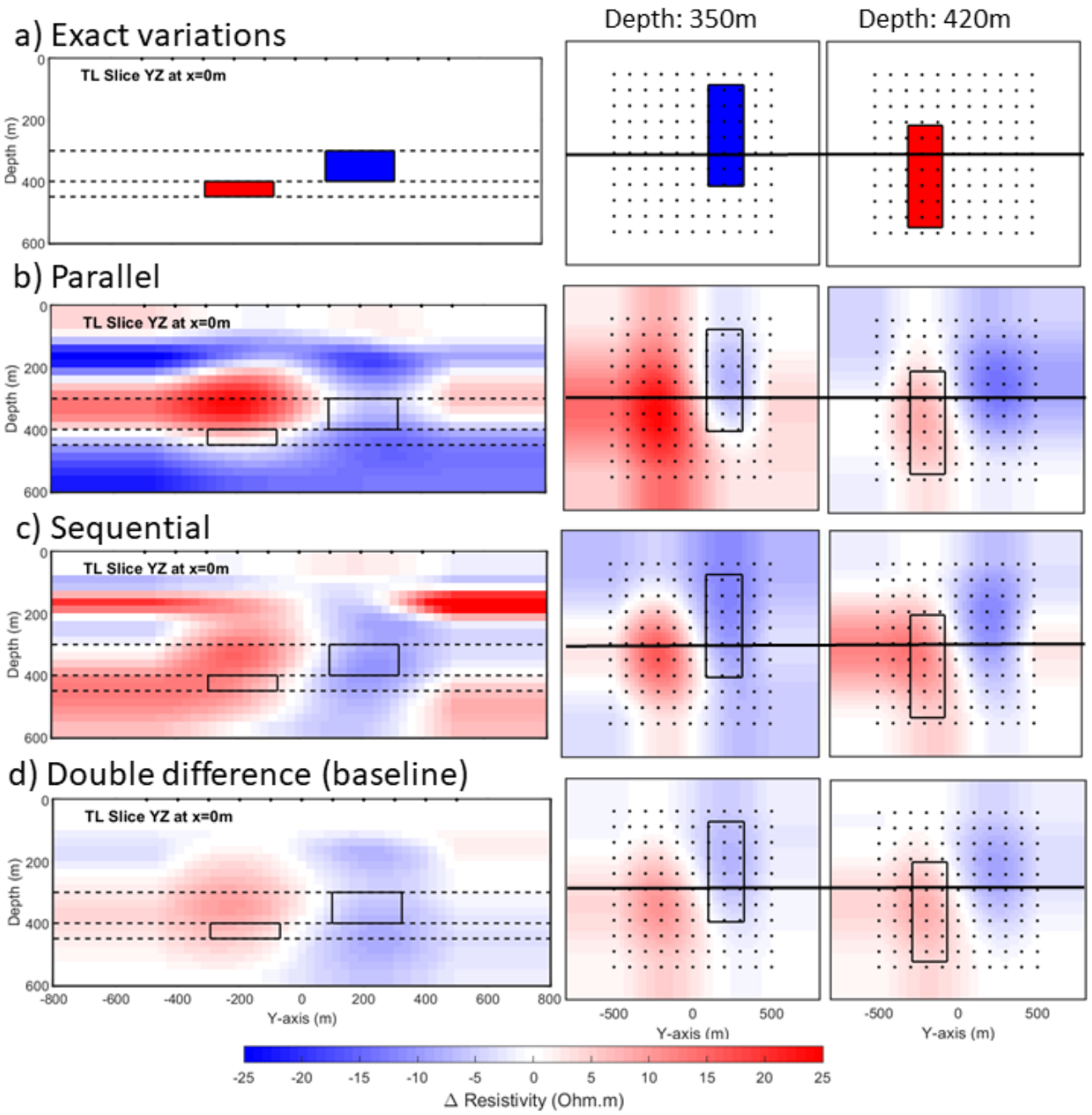

Figure 1: Slices of 3-D time-lapse resistivity models: (a) targets, (b) parallel, (c) sequential, (d) double difference, using a baseline reconstructed from the smooth 1D model, (e) double difference model using the exact baseline as a starting model and (f) double difference model using an homogeneous background as a starting model.

Abstract, 25th EM Induction Workshop,Çeşmeı, Turkey, September 11-17, 2022

Global Optimization Inversion of Horizontal Electric Dipole Time-Domain Electromagnetic Data Using Particle Swarm Optimization

C. A. Hapsoro[1], W. Srigutomo[2] and E. Agustine[3]
[1]Astronomy and Geophysics Research Group, Physics Department, Faculty of Mathematics and Natural Sciences, Universitas Negeri Malang, Jl. Semarang 5 Malang 65145, Indonesia, cahyo.ajihapsoro.fmipa@um.ac.id
[2]Physics of Earth and Complex System, Physics Department, Faculty of Mathematics and Natural Sciences, Institut Teknologi Bandung, Jl. Ganesa 10 Bandung 40132, Indonesia, wahyu@itb.ac.id
[3]Faculty of Mathematics and Natural Sciences, Padjadjaran University, Sumedang 45363, Indonesia, leo@geophys.unpad.ac.id contact

SUMMARY

We implement the global optimization of horizontal electric dipole-time domain electromagnetic (HED-TDEM) data through the application of particle swarm optimization (PSO) algorithm. This probabilistic approach is alternative to the widely used deterministic-local optimization approaches. In PSO algorithm, each particle that constitutes the swarm epitomizes a probable geophysical model comprised by subsurface resistivity values at several layers and thickness of each layer. The forward formulation of the TDEM problem for calculating the vertical component of the induced magnetic field is expressed first in Laplace domain. Transformation of the magnetic field from Laplace domain into time domain is performed by applying the Gaver-Stehfest numerical method. The implementation of PSO inversion to the TDEM problem is straightforward. It only requires adjustment of few inversion parameters such as inertia, acceleration coefficients and numbers of iteration and particles. The PSO inversion scheme was tested to synthetic noise-free data and noisy data, as well as to field data recorded in a volcanic-geothermal area. The results suggest that the PSO inversion scheme can efficaciously solved the HED-TDEM 1D stratified earth problem.

Keywords: time-domain electromagnetic, horizontal electric dipole, particle swarm optimization, resistivity

Singular Value Decomposition of the Phase Tensor

M.Karaş[1] and S.B.Tank[1]
[1]Boğaziçi University, Kandilli Observatory and E.R.I., İstanbul, Türkiye, karasm@itu.edu.tr
[1]Boğaziçi University, Kandilli Observatory and E.R.I., İstanbul, Türkiye, bulent.tank@boun.edu.tr

SUMMARY

To understand the detailed characteristics of magnetotelluric data (MT), the current study proposes a decomposition based on the singular values of the phase tensor. This mathematical methodology is inspired by the conventional ellipse illustration of the distortion free phase tensor however, it uses the full singular value decomposition (SVD) in a traditional manner. The outcomes of the SVD are utilized to illustrate the dimensionality information of the MT data by comparing the configurations of two associated ellipses. As another illustration method, Mohr circle diagrams are utilized in this study. To control the orientation of the singular value-based ellipses and to check the dimensionality of the data, Mohr circles were plotted for comparative purposes. Furthermore, extension to earlier works is provided by implementing the error-based weighted-least-square (WLS) analyses of multi-site and multi-frequency combinations. Our extension may be used to clarify the discrepancy between the two-dimensional and the three-dimensional modeling approach necessities. Synthetic tests were performed to observe validity of the developed methodology for both single-site-single-frequency and multi-site-multi-frequency handling of the data.

Keywords: Singular value decomposition, Phase tensor, Dimensionality

Abstract, 25^{th} EM Induction Workshop,Çeşmeı, Turkey, September 11-17, 2022

Modelling tippers in a spherical geometry

M. Kruglyakov[1] and A. Kuvshinov[2]
[1]University of Otago, New Zealand, mikhail.kruglyakov@otago.ac.nz
[2]ETH Zurich, Switzerland, kuvshinov@erdw.ethz.ch

SUMMARY

Several continental-scale magnetotelluric (MT) surveys have been initiated in the past decades. This motivates exploiting spherical geometry to model MT responses. However, while the MT impedances in spherical coordinates can be modelled by using different polarizations of a uniform external magnetic field as the source, for tippers, one needs another type of excitation. This is because the uniform external magnetic field of any polarization contains a non-zero radial component.

To overcome this issue, we elaborate a new source model, which leads to valid MT tippers in spherical geometry. This, in particular, allows researchers to exploit an immense amount of magnetic field data around the globe and probe the three-dimensional distribution of electrical conductivity at lithosphere and upper mantle depths on a global or semi-global scale.

The proposed source model has been validated by a novel, accurate, computationally efficient solver called GEMMIE. This solver is based on the nested domain integral equation approach and allows us to calculate high-resolution EM fields and responses, including tippers, globally and regionally, taking into account realistic oceans, sediments and mantle structures.

Keywords: Magnetotellurics; Electromagnetic theory; Geomagnetic induction; Numerical modelling

Abstract, 25th EM Induction Workshop, Çeşme, Turkey, September 11-17, 2022

Anomalous Phase in Elongated Prism Body: A Synthetic 3D MT Forward Modelling

Dharmendra Kumar[1], Arun Singh[2], M. Israil[1]

[1]Indian Institute of Technology, Roorkee, 247667, India,

[2]Indian Institute of Technology (ISM), Dhanbad, Jharkhand 826004.

Summary:

The magnetotelluric (MT) method is one of the successful geophysical techniques to investigate subsurface structures from shallow to great depths. In this method, two horizontal components of the electric field and three components of magnetic fields are measured and are transformed into transfer functions such as impedance tensor. Normally, the impedance phases for the off-diagonal components of the impedance tensor lie in the first ($0°<\Phi<90°$) and third quadrant ($-90°<\Phi<-180°$) for the XY and YX components, respectively. Sometimes, some phases may lie out of these quadrants. Such phases are termed Anomalous phases (AP). The AP acts as a barrier to the proper interpretation of the MT data. Simple 1D or 2D structures do not cause AP. Previously, complex 3D models are used to demonstrate and discuss the AP. In this study, we present a simple 3D model that can also generate AP. A conductive prism orientated N60°W is embedded in half space at a shallow depth. The impedance tensor was computed at a regular grid. From the simulated data, we observed AP near the two edges of the prism. The electric field vector rotates more than 90° at these places for a period greater than 10 s. The simple structure is able to produce the AP due to the current channeling toward the conductor and reversal of the electric field. The AP depends on the length/width ratio and orientation of the prism and the conductivity contrast between the prism and the background. Further, a discontinuity was introduced at the center of the prism. Using the computed forward responses, AP was observed around the discontinuity region.

Keywords: Magnetotelluric, Anomalous phase.

Electrical resistivity tomography image enhancement using neural network

K. Phueakim[1], C. Vachiratienchai[2] and P. Amatyakul[3]
[1]Department of Physics, Faculty of Science, Mahidol University, kittipong.phueakim@gmail.com
[2]Curl-E Geophysics Co., Ltd., chaichai.vac@gmail.com
[3] Department of Physics, Faculty of Science, Mahidol University, puwis.ama@mahidol.ac.th

SUMMARY

The development of neural networks is gradually improving in recent years. It shows excellent performance in data pattern learning for several applications. Several types of neural networks are successful in image processing. This work applies the neural network to enhance subsurface resistivity tomography images given by a geophysical prospecting method called the direct-current resistivity (DCR) method.

The resistivity tomography images or resistivity models from the inversion process of the direct-current resistivity (DCR) method are mostly vague, requiring professional analysis to deduce the appropriated models of the subsurface. A framework of image enhancement using a neural network, ResEN, is constructed to reduce professional biases and increase the resolution in the interpretation process of DCR.

The data used in the neural network are synthetic resistivity models and their corresponding inverted models. Resistivity models from the inversion process are computed by reliable software. Several validation cases are tested to show the enhancement ability of the developed framework using a neural network architecture. The results show that the framework can improve over 90 percent of inverted models in validating data. The framework is also tested with our developed straightforward data-driven inversion and commercial software with edge enhancement feature. Results show that the developed algorithm gives a reasonable accuracy in recovering true resistivity models compared to those approaches. The developed algorithm shows the ability to resolve the ambiguity problem of the resistivity distribution from the DCR method for various structures depending on the training set of the data.

Keywords: Neural network, Direct-current resistivity survey, Image processing

Hydrothermal system beneath Mt.Erciyes inferred from Three-dimensional Magnetotellurics, Central Anatolia, Türkiye

R.Yazıcı[1], M.Karaş[1] S. Üner[2] and S.B. Tank[1]

[1]Boğaziçi University, Kandilli Observatory and E.R.I., İstanbul, Türkiye, ruken.yazici@boun.edu.tr
[1]Boğaziçi University, Kandilli Observatory and E.R.I., İstanbul, Türkiye, karasm@itu.edu.tr
[2]İstanbul Technical University, Faculty of Mines, Dept. of Geophysics,
[1]Boğaziçi University, Kandilli Observatory and E.R.I., İstanbul, Türkiye, bulent.tank@boun.edu.tr

SUMMARY

Thirty-five wide-band magnetotellurics (MT) data were collected in three survey campaigns in 2013, 2014 and 2018 to decipher the electrical structure beneath the Erciyes Volcanic Complex and the surrounding Erciyes pull-apart basin in Central Anatolia, Türkiye, within the context of an NSF funded project, Continental Dynamics / Central Anatolian Tectonics (CD/CAT). Bounding the Erciyes volcanic complex in the west and in the east, the Erciyes basin is made up three major faults, the Yeşilhisar, Gesi and Develi faults. While the Yeşilhisar and DEveli faults define the west and east of the basin, the Gesi fault runs in the middle of the pull-apart basin making up the main branch of the Central Anatolian Fault (CAF) Zone, and crosses Mt. Erciyes. The Erciyes volcanic complex is proven to form in two stages: (i) Koçdağ (>2.8 Ma) and (i) New Erciyes (<2.8 Ma) stages, with various magmatism types. For determining the dimensionality of the MT data, phase tensor analyses were performed and three-dimensional models were developed using ModEM including topography to image the electrical conductivity variations beneath the volcanic complex, major faults and the basin. As a result significant and widespread conductive layer was observed beneath the volcanic complex that extends to around 5 km. The conductive layer, which appear to have deeper roots in the west when compared to east of the basin, was clearly marked by conductive-resistive interfaces near the three major faults.

Keywords: Mt.Erciyes, Hydrothermal system, Fluids

Static shift correction in sedimentary basins

D. Yakovlev[1] and A. Yakovlev[2]
[1]STC Nord-West, stcnordwest@gmail.com, Moscow, Russia
[2]Lomonosov Moscow State University, Moscow Russia

SUMMARY

The work considers the problem of static shift of magnetotelluric (MT) curves obtained in sedimentary basins. The MT data of recent years obtained in Argentina, Bolivia, Brazil, Iran, Kazakhstan and Russia were used. The problem of static shift is considered in detail on the data obtained in the Yenisei-Khatanga regional Megatrough (Northern Russia). This trough is composed of Jurassic-Cretaceous terrigenous rocks with almost horizontal bedding. To study the effect of near-surface inhomogeneities on MT curves, such conditions are ideal, since they make it possible to simplify the accounting for the effects of the background section, considering it to be one-dimensional. In the Yenisei-Khatanga regional Megatrough, about 25 thousand MT soundings were performed, accompanied by 2-D seismic and time-domain (TDEM) measurements. Such a large amount of data made it possible to test various methods for detecting static shift and correcting it.

As a reference result, a static shift correction was used based on geoelectric models obtained from the TDEM data. All other correction methods were compared with this reference result. The work shows that for regional studies, a statistical static shift correction based on the spatial filtering of the MT impedance at a certain frequency gives satisfactory results. For oil and gas and more detailed survey, it is necessary to use third-party data to correct the static shift. In more cases the best fit are the TDEM data. In their absence, seismic survey results can be used.

The work also shows examples when TDEM data cannot be used to correct static shift: due to complex topography (Bolivia), due to strongly inhomogeneous upper part of the section (Siberia), due to intensive high-frequency induced polarization effects in permafrost (Taimyr). Based on the TDEM data, examples of systematic underestimation of the level of amplitude MT curves (Bolivia, Taimyr) are shown.

Keywords: sedimentary basins, static shift correction, TDEM

Near surface resistivity structure estimated from time domain electromagnetic data recorded along a profile in HFT Zone in Mohand area, Uttarakhand, India

M. Israil[1], Rehan Raza Ansari[1], M. Zubair[1], P. Yogeshwar[2], B. Tezkan[2]

[1] Indian Institute of Technology Roorkee, Roorkee, Uttarakhand, India, mohammad.israil@es.iitr.ac.in
[2]Institute of Geophysics and Meteorology, University of Cologne, Cologne, Germany, pyogeshw@uni-koeln.de, tezkan@geo.uni-koeln.de

SUMMARY

Time-domain electromagnetic (TDEM) data were recorded using Fast TEM device deployed in a coincidence loop geometry at 24 stations along a profile in the Himalayan Frontal Thrust (HFT) zone in Mohand area, Uttarakhand, India. The profile is approximately 1.6 km long and extends from the Indo-Gangetic plain in the south to the north of HFT in the Khajnawar Rao, a seasonal river bed. The processed data at each station was inverted using Occam and Marquardt inversion techniques to obtain 1D resistivity depth models at each station. A stacked geoelectrical section is generated along the profile from the inverted models. North and south-dipping beds are reflected on either side of the Mohand anticline thrust, passing nearly through the middle of the profile. Resistivity variations are interpreted in terms of the tectonics geometry of the fault zone, geological and geo-hydrological scenario of the area. A near-surface resistive layer (> 200 Ω-m) consisting of dry fluvial deposits, gravels, pebbles, and boulders of varying sizes can be seen throughout the profile. A very low resistivity (~ 10 Ω-m) is observed in the fault core zone. This zone is exposed along the river terrace zone on the west bank of Khajnawar Rao. The derived resistivity variations explain the geological and geo-hydrological scenario of the area and are consistent with the information available in the literature.

Keywords: Near-surface resistivity structure, Himalayan Frontal Thrust (HFT), Time Domain Electromagnetic (TDEM), Sub-Himalaya

INTRODUCTION

Loop source time-domain electromagnetic is a controlled source electromagnetic (EM) method in which the transient decay of the magnetic field is measured after switching off the current injected through a transmitter (Tx) loop. The switching-off of the Tx current induces eddy currents in the finitely conducting subsurface. This induced current diffuses downward and outward in the subsurface. The diffusion process generates a time decaying secondary magnetic field in the absence of primary field. The measured decay characteristics of the secondary magnetic field are a function of the resistivity distribution of the subsurface formation. The decay rate of the transient is slower in a conductive formation, whereas it is faster in a resistive formation. The theoretical concepts of TDEM are given in various literature (Kaufman, A. A. et al., 1983, Nabighian et al., 1991). The recorded transient response is inverted in terms of resistivity distribution of subsurface formation (Danielsen, 2003). The TDEM method is fast and accurate for mapping the depth and thickness of resistivity structure. It is less sensitive to the lateral variation of resistivity than the DC resistivity method, thus used as an efficient and accurate alternative to the conventional DC resistivity methods. In the present study, we have used the TDEM method to delineate resistivity structure along a profile passing through the HFT zone in the Sub-Himalayan region in and around Mohand, Uttarakhand, India. The resistivity structure is further interpreted in terms of geological, tectonics and geo-hydrological formation of the area. Additional Radiomagnetotelluric data were recorded along the complete profile and perpendicular shorter transects to retrieve shallow high resolution data. However, here we only focus on the TDEM data.

The main aim of our study is to improve the near-surface geological information for an improved understanding of the tectonic process and its surface manifestations.

DATA RECORDING AND INVERSION

We recorded TDEM data using TEM-FAST 48 portable device. Twenty-four stations spread along a 1.6 km long profile in the HFT zone in the Mohand area were recorded. A coincident loop setup geometry with a single square of 50m x 50m wire loop was used in the field measurement. The transmitting current was 3.8A, and the recording time range was set from 4 to 2024 μs. The southern end of the profile is located in the Piedmont zone, which is the northern limit of the Indo-Gangetic plain in the study area. As defined in the geological literature (e.g. Srivastava et al. 2016), the Himalayan Frontal Thrust (HFT) passes nearly perpendicular to the profile line at the 10th station from the south with visible outcrops at the surface. The remaining 14 stations are located in the HFT hanging wall zone on the north of the HFT. The location of stations are shown in Figure 1.

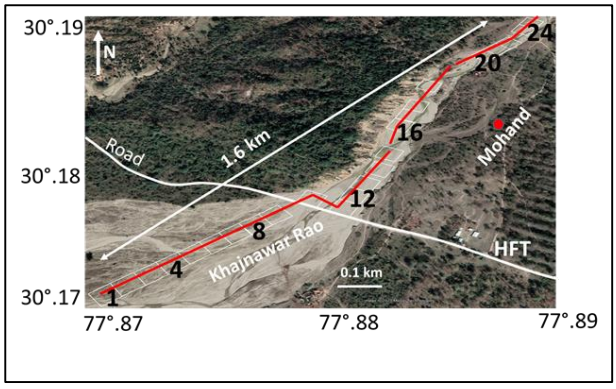

Figure 1 Location map of the study area showing TDEM stations.

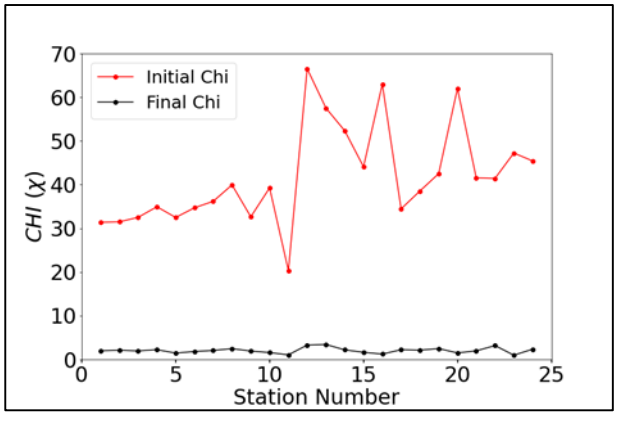

Figure 2 Initial and final error (chi) for all stations data using Marquardt inversion.

1D inversion of transient response at each station is done using the EMUPLUS code (cf. Haroon, A., Yogeshwar P., et al., 2015; Yogeshwar et al., 2020) for smooth model (Occam's) and minimum layered model (Marquardt) inversion. Initial and final errors (Chi) are shown in Figure 2. Convergence is achieved in all station data; however, some stations show larger misfit errors. The used field data error is set a minimum percentage error of 3%.

Comparison of smooth and layered inverted models at selected station along with the data and the fitted responses are shown in Figure 3. All three models

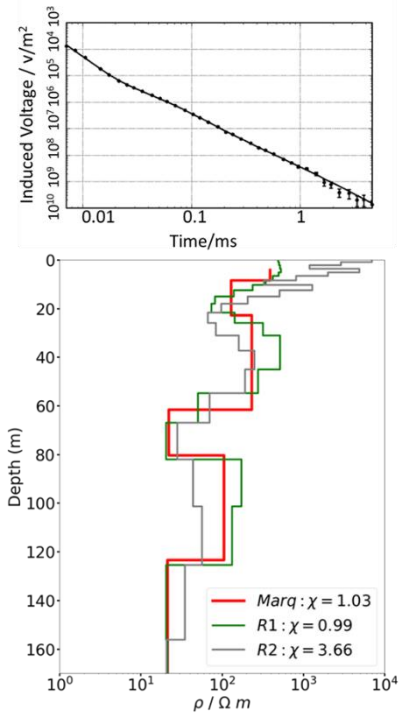

Figure 3 Top panel shows data and fitted response and bottom panel shows comparison of 1D layered and smooth inversion of TDEM response recorded at station 11.

are in general consistent within small variations. Subsequently, 1D inverted models were stitched together and interpolated between the stations to generate a smooth 2D image along the profile, as shown in Figure 4.

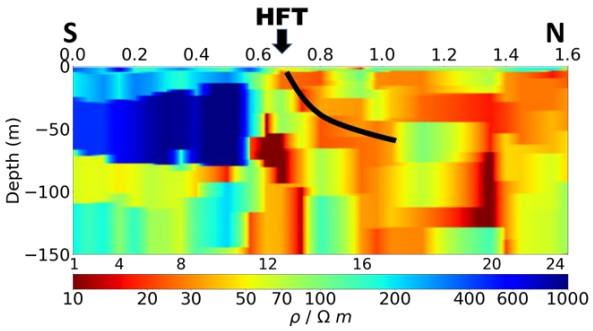

Figure 4 2D resistivity-depth section obtained by stacking and smoothing of 1D models along the profile.

The profile distance from station one in km, and TDEM station numbers are shown on top and bottom of the Figure 4, respectively.

RESULTS AND DISCUSSION

The study area is located in the Sub-Himalayan region, where the Upper and Middle Siwaliks Group of rock are exposed in the immediate vicinity of the Indo-Gangetic plain (IGP). TDEM stations are passing through the HFT, which is the northern limit of the IGP. Upper Siwaliks conglomerate in the area has been classified as a sandy matrix showing both coarsening and fining upward in stratigraphic sequence (Rohtash et al., 1991). The conglomerate is mainly composed of cobble to pebble clasts of quartzite, limestone, sandstone, and shale. Exposure of Middle and Upper Siwaliks subgroups can be seen in the area. The middle Siwalik subgroup comprises sandstone dominated intervals which pass upward transitionally into the Upper Siwaliks boulder conglomerate sequence. The general stratigraphy of the hanging wall zone can be described from top to downward: Top thin soil cover are fluvial sediments, 1-3 m thick loamy sand soil, and 2-3 m thick pebble-cobble (Wesnousky et al., 1999). A trench in the study area shows that the HFT reaches the surface and is covered by a thin (~ 10 m) fluvial material on top of the bedrock (Senthil et al., 2006). The boundary between Siwalik bedrock and alluvial deposits of the floodplain is abrupt and steep.

A 2D resistivity-depth section was obtained by stitching and smoothing 1D models along the profile, as shown in Figure 4. The derived resistivity-depth image shows a resistivity discontinuity at the HFT location. High resistivities are observed in the south of the HFT, whereas relatively low resistivity and low angle dipping resistivity features are observed in the north of the HFT. Based on the low resistivity trend in the north of the HFT, low angle north dipping beds are shown by a black line. This low resistivity zone is consistent with the fault core zone exposed on the west bank of the Khajnawar Rao (Srivastava et al., 2016). TDEM stations 12, 13 and 14 correspond to the low resistivity fault core zone, a highly pulverised fault gouge with a resistivity value (~10 Ω-m). On the north of the HFT, a gouge dominated damage zone is observed; these zones are dipping and represented by a resistivity between 20-50 Ω-m. The low resistivity indicates highly fractured and water-saturated thrusting beds. Similar alternative low resistivity zones are continued in the north along the profile.

In the southern zone of the HFT, the near-surface top layer is fluvial deposits represented by resistivity in the range of 200-400 Ω-m. The thickness of this layer is minimum (~ 3m) near HFT, which increases in the south and reaches up to 20 m. These are older alluvial flood plain deposits (Wesnousky et al. 1999). Beneath this resistive (> 300 Ω-m) thick Middle Siwaliks sandstone layer is present. Further, low resistivity (~ 50 Ω-m) thick, saturated aquifer zone is present beneath this layer.

CONCLUSIONS

TDEM data at 24 stations along a profile passing through the HFT zone in Mohand, Uttarakhand area were recorded and inverted in terms of resistivity distribution of the near-surface formation. The dry top surface layer is resistive (> 200 Ω-m), representing thin fluvial sediments deposited of Khajnawar Rao, seasonal river. The thickness of this layer varies along the profile from 3 -20 m. Followed the fluvial sediments cover, in the northern zone of profile highly jointed and fractured, partially and fully saturated with water, Upper and Middle Siwaliks formations are present. The average resistivity of this zone is 40 Ω-m. The dominant rocks in Upper Siwaliks and Middle Siwaliks are conglomerate and sandstone respectively. In the southern end of the profile, the rocks are more compacted and represented by high resistivity (> 500 Ω-m) formations. The fault core zone is a fine material partially and fully saturated with water, represented by low resistivity (~ 10 Ω-m). Further analysis of 2D and possible 3D effects in TDEM data and the integration of existing RMT data will further improve the interpretation.

Acknowledgements

This work is carried out in the frame of INDO-GERMAN joint research collaboration, DST-DAAD, Project no. DST/INT/DAAD/P-19/2019. Financial support from funding agencies (DST and DAAD) are thankfully acknowledged.

REFERENCES

Haroon, A., Yogeshwar P., ockmann J. B, Ossen D. November 30, 2015, EMUPLUS Manual

Jens, E. D., Esben Auken, Flemming Jørgensen, Verner Søndergaard, Kurt I. Sørensen (2003) The application of the transient electromagnetic method in hydrogeophysical surveys, Journal of Applied Geophysics, Volume 53, Issue 4, ISSN 0926-9851, Pages 181-198,

Kaufman, A. A. and Keller G. V. (1983) Frequency and Transient Sounding Methods in Geochemistry and Geophysics, Vol. 16, Elsevier, Amsterdam, pp. 686

Kumar, R. and Ghosh, S.K. 1991. Sedimentological

studies of the Upper Siwalik Boulder Conglomerate Formation, Mohand area, district Saharanpur, U.P., Jour. Him. Geol., 2,159-167

Nabighian, M. N. & Macnae, J. C., 1991. Time Domain Electromagnetic Prospecting Methods, in Electromagnetic Methods in Applied Geophysics, vol. 2, chap. 6, ed. Nabighian, M. N., Society of Exploration Geophysicists

Senthil Kumar, Steven G. Wesnousky, Thomas K. Rockwell, Richard W. Briggs, Vikram C. Thakur, and R. Jayangondaperumal (2006), Paleoseismic evidence of great surface rupture earthquakes along the Indian Himalaya, Journal of Geophysical Research, Vol. 111, B03304, doi:10.1029/2004JB003309, 2006.

Srivastava, V., Malay Mukul, Jason B. Barnes, 2016 Main Frontal thrust deformation and topographic growth of the Mohand Range, northwest Himalaya", Journal of Structural Geology, Journal of Structural Geology 93, 131-148

Wesnousky, Steven G., Senthil Kumar, R. Mohindra, and V. C. Thakur, (1999), Uplift and convergence along the Himalayan Frontal Thrust of India, TECTONICS, VOL. 18, NO. 6, PAGES 967-976

Yogeshwar, P., Küpper, M., Tezkan, B., Rath, V., Kiyan, D., Byrdina, S., Cruz, J., Andrade, C.& Viveiros, F. (2020). Innovative boat-towed transient electromagnetics—investigation of the Furnas volcanic lake hydrothermal system, Azores. *Geophysics*, *85*(2), E41-E56

Some fragments of my 70 years activity in EM geophysics

I.I.Rokityansky
Subbotin Institute of Geophysics of the National Academy of Sciences of Ukraine, Kiev, Ukraine
E-mail: rokityansky@gmail.com

SUMMARY

It is my farewell to EM community. I recall some earlier published half-forgotten results which can be useful today and express my opinion how can be improved some methodological details of EM studies.

Keywords: geoelectromagnetics, electrical conductivity anomalies, Carpathian anomaly

INTRODUCTION

In 1953, I was graduated from the Faculty of Physics of St. Petersburg University (SPbU) with a degree in geophysics and was allocated to Moscow for postgraduate studies at the Institute of Physics of the Earth (IPE). An outstanding mathematician (regularization theory) and geophysicist (magnetotelluric sounding (MTS)) academician Andrei Nikolaevich Tikhonov were appointed as my supervisor. I chose the topic "Induced polarization of ion-conducting rocks" and defended my PhD thesis in 1957 (Rokityansky 1957, 1959). At that time a great event began - the International Geophysical Year (IGY), and I was sent to Alushta, Crimea to equip the observatory and carry out registration and processing of natural variable electric **E** and magnetic **B** fields with a period from 1 s to 1 day. I had unique materials in my hands. I was interested in the relationship between **E** and **B** and its variability along the Earth's surface, that is, in essence, the MTS-MVP (Rokityansky 1961, Rokityansky et al. 1964). In the first decade of the MTS method, the Tikhonov-Cagniard (T-C) model was used in its purest form - a plane wave over a horizontally layered Earth. As a result, depth to the conductive base of the upper mantle was obtained at depths from 100 to 2000 km, even at close observation points. Such a spread did not correspond to the theory of EM induction and the results of other geophysical methods. I analyzed many practical MTS curves, made model calculations and was the first who discovered the existence of static distortions, and formulated simple methods for minimizing them – binding (tying in) to trusted data, static shift to global GDS data, grouping, which made it possible to carry out deep MTS on the real geological structures with local distortions (Rokityansky 1971, 1982, p. 201-209).

In 1957-1965 I worked in IPE department EM fields headed by

Valery Troitskaya.

Valery was outstanding personality, scientist and organizer of international cooperation in the «cold war» times. She was born in 1917. In the years of repressions of 1936-1939, her father was arrested and awaited an execution. To save him Valery, a student of SPbU, decided to ask for an audience with the formidable head of KGB, Lavrenty Beria, and managed to convince him of her father's innocence. Father was released (the rarest case). During IGY and after, Valery decisively for the benefit of cooperation violated the ridiculous KGB restrictions on the behavior of Soviet citizens abroad.

She established a network of electromagnetic observatories across USSR, in Arctic and Antarctica and studied ULF micropulsations with period 1-600 s. She organized the first experiment between magneto-conjugate points Sogra-Kerguelen and measured geomagnetic fluctuations at the depth 2.6 km in the French bathyscaphe «Archimed». She made 2 internationally recognized discovery: micropulsations «Pearls» and «DPO» - decreasing period oscillations indicating contraction of the magnetosphere. Troitskaya was member of the IUGG Bureau (1963-1967), the first woman president of IAGA (1971-1975), since 1985 - Honorary IAGA Member, member of the first Steering Committee of the International Geosphere-Biosphere Program (1986-1990). I participated in some of these studies, as well as in the registration of USA nuclear tests on a Pacific island and Soviet underground tests in Central Asia. I also organized an EM observatory in Cuba.

In 1960 academician M.A.Sadovsky became the Director of IPE. He obliged all departments to

participate in the Earthquakes (EQ) Forecast. This topic also was proposed to me. I refused and in 1965 moved to Institute of Geophysics in Kiev for

Geoelectromagnetic investigation of the Earth's crust and mantle

I organized the EM Research Laboratory and led it 25 years. In the first 5 years I have tested, studied and understood the possibilities of various methods of the deep electrical conductivity study and formulated a methodology for the interconnected use of the three main methods MVP-MTS-GDS (Rokityansky 1970 and in all my consequent monographs). Search and study of the anomalies of geomagnetic variations and associated conductive anomalies was a hobby for me. Every year we carried out field works for 3-4 months. I went out into the field and manually processed and interpreted the photorecords in order to determine where the next observation sites should be placed in order to optimally map the anomaly.

Many anomalies have been found and studied using induction vectors and anomalous field in horizontal magnetic components, that is by MVP method. Large anomalies in Eastern Europe: Kirovograd (1969), Carpathian (1972), Moscow-Tambov (1977), Ladoga (1981, moreover, MTS were carried out there before the MVP, but the anomaly was not discovered), Donbas (1988, but in the data of more than twenty MTS and records of pulses from the Volgograd-Donbas long (487 km) line the anomaly cannot be clearly distinguished).

Physics of the anomalous field formation

Anomalous currents in a high conducting body arise due to local electromagnetic induction inside this body, as well as due to conductive redistribution (and concentration) of currents induced in the host medium on the large territory comparable with the external source size. Quantitative estimates were made in the early 1970s based on analytical solutions for a cylinder and sphere presented as an infinite series which first term is proportional to the applied electric field (it forms the conductive anomaly), the second – to magnetic field – it forms the magnetic eddy type anomaly. Available results of 2D and 3D numerical calculations and physical modeling were also considered.

Analysis of natural situations showed that conductive type anomalies are predominate for elongated conductors, and a corresponding theory was developed for them (Rokityansky 1975-a and -b; 1982 p. 247-277, 290-307). The frequency characteristics of the conductive type anomalous field are equal to the product of the non-decreasing function of the period V ($0 \le V \le 1$, V=1 corresponds DC), which describes the degree of filling of the conductor by anomalous currents and the normal impedance of the given region, apriori studied by the GDS-MTS soundings. The impedance is a decreasing function of the period, so its product with function V has a maximum at some period T_O. The position T_O is closely related to the total longitudinal conductance G [S×m] - of the anomalous body, that is, the scale of the anomaly. On the period T_O, the anomalous fields and the induction vector become real C=Cu, the imaginary induction vector Cv passes through zero changing sign. On shorter periods Cu and Cv are parallel, on longer periods they are anti-parallel for 2D anomaly.

Short specification of the MVP method

Necessary and sufficient condition to make the conclusion on the existence of an electrical conductivity anomaly is the existence of a geomagnetic variations anomaly.

The existence of an anomaly of geomagnetic variations is evident from the stable presence of vertical component and from the difference in horizontal components at moderately spaced sites.

The shape of the profile curves of the anomalous field yields reliable estimation of the maximum possible depth of the anomalous currents **center** *d* and the width 2*L* of the anomaly.

Frequency response of the anomalous field yields estimate of the total longitudinal conductance *G* of the elongated anomalous body.

- It is a simple completely reliable MVP pre-computer results, which (anomaly location, *d*, *L* and *G* with their uncertainties) **should be used as apriori information** for consequent thorough MVP-MTS inverse problem computer modeling.

MTS

MTS can give false results even in relation to such a fundamental category as the existence or absence of an anomaly. For example, on the southern slope of the Ukrainian Shield (US), a dozen MTS curves above the axis of the Kirovograd anomaly, which is confidently identified according to the MVP data, show the absence of this anomaly (the reason is screening by sloping sedimentary layers).

However, MTS can more accurately than MVP determine the depth h of the upper edge of the anomaly although harmful distortions from near-surface inhomogeneities remain. So, a dozen MTS over the axis of Kirovograd anomaly in US made it possible to determine only the average

result of *h*=15±5 km (Rokityansky et al 2018)

Carpathian anomaly.

Let me remind of the Carpathian anomaly. Having data of more than 200 MVP points, the position of its axis was determined with good uncertainty of 5-10 km, and according to 8 profile graphs of the anomalous field in the Western Carpathians, the maximum possible depth of the center of anomalous currents was estimated: 24, 16, 19, 18, 18, 24, 26 and 21 km (Jankowski et al. 1985). The next step should be MTS to clarify the depth of the upper edge of the anomaly. In Ukraine, in the 1970s and 80s, we made about 50 MTS, identified 6 zones and, using 11 curves directly above the axis, determined the depth of the anomaly upper edge of 12±4 km.

At 22EMIW in Murnau I proposed «Project of the Carpathian anomaly depth study by means of detailed MTS over its axis». Project was not supported with a criticism: «for the MTS interpretation 2D profiles across the anomaly are necessary» - I strongly disagree with the latter. When the anomaly axis is known, only longitudinal curves are needed to determine its depth.

The anomaly in the center of Europe should be better studied. It can be, for example, a source of geothermal energy. I recommend to accept and realized «Project of the Carpathian anomaly depth study by means of detailed MTS over its axis» and would be happy to participate in it.

On 2D inversion and regularization

And in general, I think the mandatory 2D inversion is not justified. Exact 2D structures do not exist, the inevitable presence of deviations from 2D creates a systematic error in the 2D inversion results, which cannot be predicted and described using a statistical uncertainty obtained during data processing.

Unlike practical science (electrical prospecting), deep geoelectrics is regarded as a fundamental science, which sets the task of an honest, reliable study of the objective reality — the Earth. Since observation of electromagnetic fields is possible only on/above the Earth in a limited number of sites with limited accuracy, the conclusions of geoelectrics are always ambiguous. Providing only a single solution, in particular resulting from the use of regularization, can lead to false conclusions, and regarded as a manipulation of facts, that can discredits both the authors and the whole science of geoelectrics. So, many products of inversion (in particular 2D) should be regarded not as a well proven geological result but as one of possible transformation of response functions.

Esotericism and related issues

In 1989 I became interested in dowsing considering it as geophysical method but without support in physics which I planned to achieve. In next 5-years laboratory Plan-Project instead of the MT topic (which I led 25 years), I naively proposed a topic on dowsing, which was not accepted in institute. I was left without a Project and was sent to retire.
2 years I worked in a private company on esoterics, in 1994-1998 in «Ukranian Natational Research Center for Defense Technologies» was the only geophysicist and had the task of developing geophysical weapons. There, I tried to improve Kozyrev's theory (Rokityansky II 2008, 2012), studied the locality of thunderstorms and their confinement to geological structures, studied experiments on informational weather control and proposed its explanation (Pokityansky II 2014), studied the tectonic factor of the Chernobyl disaster and so on. After the collapse of the USSR, the economy constantly degraded in independent Ukraine and nobody's developments were used.

Return to geophysics

In 1999, at the EGU Assembly in Nice, I organized a Session on Quasi-spontaneous Variations (Rokityansky 1999). In 1999-2001, I collaborated with the discoverer of seismic electric signals (SES) prof. P.Varotsos (Greece). To explain high SES sensitivity in Ioannina place, Varotsos supposed existing under the place highly conducting channel. ≈40 MTS were made and interpreted, 2 PhD dissertations were defended but channel was not found. I made MVP and joint MVP-MTS data revealed conductor and its parameters.

I returned in Institute of geophysics, but no instruments for field works, no money for business trips to conferences and field works, for purchasing and printing articles. I and 3 PhD students processed worldwide Intermagnet data, Japanese geomagnetic data and obtained some results (Rokityansky en al 2019). Very low salary in academic institutes made my students move from the institute to private IT companies.

REFERENCES

Jankowski J et al. (1985) The results of GDS in west Carpathians. Geophys JRAstrSoc 80:561-574

Rokityansky II (1957) Laboratory study of induced polarization of sedimentary rocks. Izv AS USSR ser geophys 2: 217-227

Rokityansky II (1959) On the nature of induced

polarization of ion-conducting rocks. Izv AS USSR ser geophys 7: 1055-1060

Rokityansky II (1961) On the application of magnetotelluric method on anisotropic and inhomogeneous massifs. Izv AS USSR ser geophys 11: 1607-1613

Rokityansky II et al (1964) The coast effect in the variations of the Earth's electromagnetic field. J Geomagn Geoelectr 15: 271-274

Rokityansky II (1970) Study of deep electrical conductivity. Geophys comm AS UkrSSR 38: 102-108

Rokityansky II (1971) Deep magnetotelluric soundings at the presence of distortions from horizontal inhomogeneities. Geophys Comm AS UkrSSR 43: 71-77

Rokityansky II (1975-a) The interpretation of anomalous fields by using their frequency characteristics. PEPI 10: 271-281

Rokityansky II (1975-b) Investigation of electrical conductivity anomalies by the method of magneto-variational profiling. Naukova Dumka, Kiev, 279 p.

Rokityansky II (1982) Geoelectromagnetic invtstigation of the Earth's crust and mantle. Springer-Verlag, Berlin Heiderberg New York, 381 p.

Rokityansky II (1999) Phenomenon of quasi-spontaneous globally synchronized variations of physical parameters (QSV). Phys Chem Earth (A) 24: 705-710

Rokityansky II (2008) Absolute motion as the basis of Kozyrev's theory of time. Acta Geod Geoph Hung **43**(4): 461-469.

Rokityansky II (2012) North-South asymmetry of planets as effect of Kozyrev's causal asymmetrical mechanics. Acta Geod Geoph Hung **47**(1): 101-116.

Rokityansky II (2014) Physical basis of weather informational correction. Geoinformatics 2(50): 77-80.

Rokityansky II, Sokolova EYu, Tereshyn AV, Yakovlev AG (2018) Electrical conductivity anomalies in the junction zones of the Archean and Proterozoic geoblocks of the Ukrainian and Baltic shields. Geophys J 40(5): 208-244. Doi: 10.24028/gzh.0203-3100.v40i5.2018.147490

Rokityansky II, Babak VI, Tereshyn AV, Hayakawa M (2019) Variations of Geomagnetic Response Functions before the 2011 Tohoku Earthquake. Open J Earthquake Res 8: 70-84. https://doi.org/10.4236/ojer.2019.82005

Improving geophysical model resolution with magnetotelluric and gravity joint inversion: application to the Asal Rift geothermal region, Republic of Djibouti.

Rachid Robleh Rageh[1,3], Pascal Tarits[1,2], Sophie Hautot[2], Mohamed Jalludin[3]

[1]University Western Brittany, Brest, France

[2]IMAGIR Sarl, Saint Renan, France

[3]Center for Studies and Research of Djibouti (CERD),

SUMMARY

Magnetotellurics (MT) provides images of low resistivity alteration characteristic of hydrothermal alteration generally associated with active up flow. The accuracy of the resistivity images is therefore an important factor in defining the conceptual model. The sensitivity of the MT decreases with depth. To improve the geophysical image, we investigate how to combine MT, gravity and drilling data in the Asal Rift region of the Republic of Djibouti. In this study, we present a new gravity inversion approach constrained by a 3D MT resistivity model on the Asal Rift data. The results are conclusive and promising in the application to natural resources exploration.

Keywords: Magnetotellurics, gravity, constraint inversion, geothermal,

INTRODUCTION

Geothermal exploration in the Republic of Djibouti (Figure. 1) has led to several boreholes being drilled (BRGM, 1975a, b and AQUATER 1989, Caver, 2019). Field studies and deep drilling revealed high salinity, low permeability, dry boreholes despite positive indications from geophysical models.

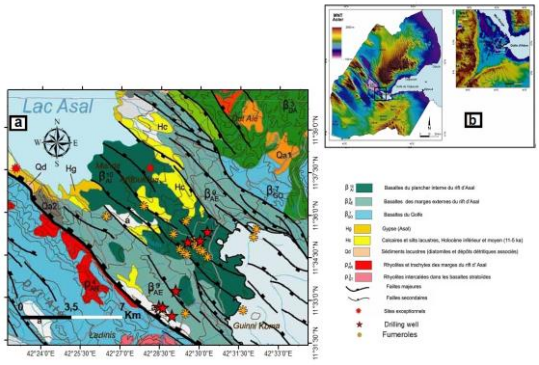

Figure 1. (a) Geological and structural characteristics with the main geothermal drillings of the Asal Rift (modified from Le Gall et al., 2015). (b) an ASTER digital elevation model, the black rectangle is the study area.

The major difficulty in obtaining a global vision of the resource is to have a methodology to characterize the geological and geothermal structures at depth (heat source, circulation of hydrothermal fluid, impermeable roof) and to understand how the areas of real interest for exploitation can be evaluated. Because of their complementarity, magnetotelluric (MT) and gravity measurements are generally used to characterize this geothermal resource. We present in this study a linear gravity inversion approach constrained by the MT resistivity model through cross-gradient coupling. This approach could help reduce the non-uniqueness of gravity inversion with a short computational time compared to the traditional joint inversion collected in the Asal Rift Zone, Djibouti (Figure 1).

MT AND GRAVITY INVERSION

We used data from 79 MT sites in this study (Figure. 2), obtained during an exploration undertaken in 2008 through a collaboration between ISOR in Iceland and the Centre d'Etudes et de Recherches de Djibouti (CERD). The data were recorded using a Phoenix MTU-5A system. Tthe gravity data come from a large survey carried out by the Bureau de Recherches Géologiques et Minières (BRGM, France) in the Asal rift in 1979 and 1980 (Demange and Puvilland, 1990,). In total, we used 641 data points (Figure. 2), acquired with a Worden gravity meter n°641 and a Lacoste-Romberg graviteters. The 3D MT inversion of the full impedance tensors was performed with the MINIM3D code (Hautot et al, 2007) for all stations (Figure. 2) and at all available times in the Asal Rift. The MT inversion was performed on a 29×28×15 grid oriented along the -40° N direction which corresponds to the rift propagation direction (Magnighetti et al., 1998). The initial root mean square (RMS) of 23.2 is reduced to 3.2. We developed a 3D gravity inversion scheme

and inverted the residual gravity data on a grid similar to the one used for the 3D MT inversion

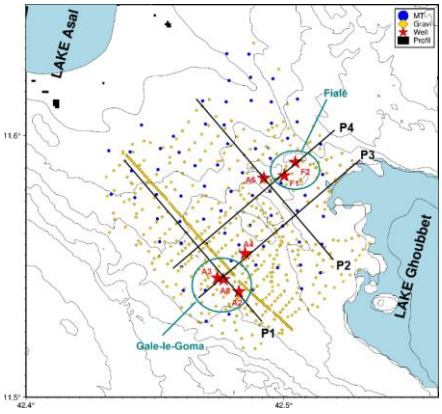

Figure 2. Asal Rift study area, gravity data in orange, MT data in blue, boreholes in red star and black lines are the profiles (P1 to P4).

CONSTRAINED INVERSION

In this section, we propose a constrained linear inversion to combine these two methods. The advantage of this approach is to couple gravity and MT data, to identify the same structures with extremely reduced computational time unlike the classical joint inversion. The most widely used method is the cross gradient developed by Gallardo and Meju (2003, 2007). The cross gradient coupling function is defined by (eq. 1): The cross-gradient coupling function in a joint inversion formulation is nonlinear as density and resistivity vary. Here, we are actually dealing with a resistivity-constrained inversion and, therefore, relation 1 becomes linear with respect to the density, as we have considered the resistivity to be constant. The new cost function is now defined as follows(eq.2):

$$CO^2 = \sum_{m=1}^{M} |\nabla d \times \nabla r|^2 \quad (1)$$

$$L^2 = \|\overrightarrow{g_{obs}} - G\vec{d}\|^2 + \lambda\|W_z\vec{d}\|^2 + \alpha CO^2 \quad (2)$$

The solution of equation 2 is written as follows:

$$\vec{d} = (tGG + \lambda W_z + \alpha Z)^{-1} tG\overrightarrow{g_{obs}} \quad (3)$$

Where G is the sensitivity kernel matrix, g_{obs} is the observed data. A weight Wz is introduced in the cost function, which depends on the mean depth for each cell (Li and Oldenburg 1998)

RESULTS

The results of the inversions are presented in the form of the following vertical sections 4 profiles that cross the boreholes (Figure. 2).
Figure 3 shows the results of the P1 to P2 profiles (Figure 2) of the resistivity model. We have also represented in Figure 4, the unconstrained density model of these 4 profiles.

Figure 3 shows the results of the P1 to P2 profiles (Figure 2) of the resistivity model. We have also represented in Figure 4, the unconstrained density model of these 4 profiles.

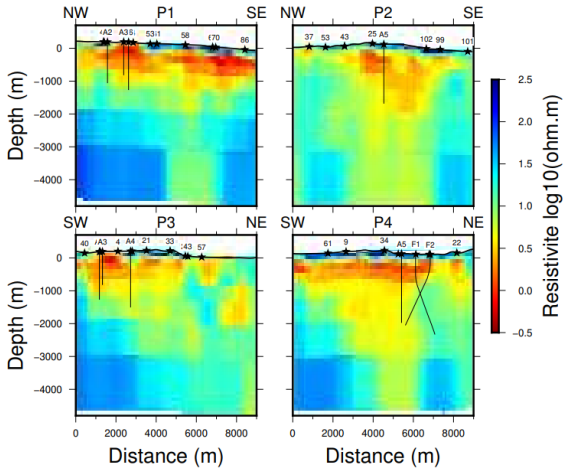

Figure 3. Vertical section of the 3D resistivity model, along the profiles of Fig. 2

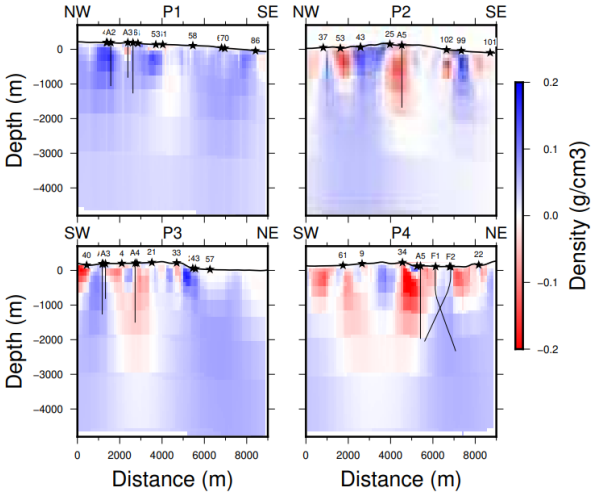

Figure 4. Vertical cross-section of the 3D unconstrained density model, along the profiles in Fig. 2.

In the 4 resistivity profiles (Figure. 3) at the level of the boreholes, we have a very resistive layer that appears from ground level to 400 m depth, due to the presence of basalts and hyaloclastites that occurred during the last basaltic eruption in 1978 (Demange et al, 1980). Then comes a very conductive layer from 400 to 1200 m, due to the presence of Pleistocene clays and trachyte. This is followed by a less conductive layer up to 2200 m which probably corresponds to basalt having

undergone alteration, rhyolites (AQUATER, 1989).

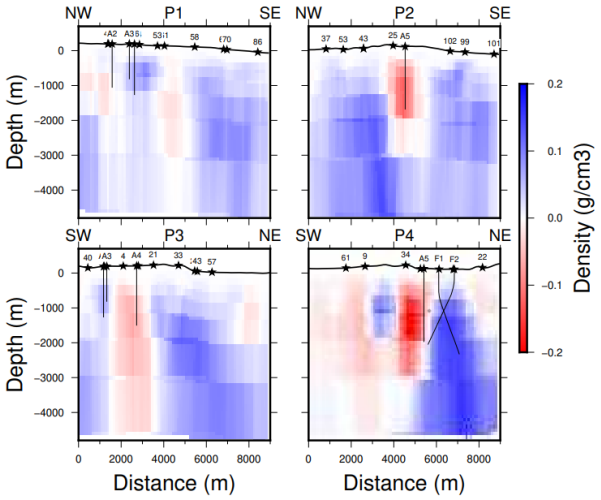

Figure 5. Vertical cross-section of the 3D unconstrained density model, along the profiles in Figure 2

The unconstrained density models (Fig. 4), show mainly two features: two positive anomalies in the NW-SE and SW-NE directions, separated by negative anomalies in the center of the 4 long profiles. However, these structures have low lateral resolution within the first kilometer in depth.
The result of the resistivity-constrained density model (Figure, 5), differs significantly from the unconstrained density model. Especially in the deep layers between 800 and 4806 m, where positive and negative anomalies due to resistivity constraints appear (Figure, 3). For the individual profiles (Figure, 5), the constrained model describes well with good vertical resolution the structural features that are present in both individual models (Figures, 3 and 4). Furthermore, due to the resistivity constraint, the boundaries separating the negative and positive anomaly domains are clearly visible in the constrained density model (Figure, 5)). The highly conductive layers in the resistivity model of the different profiles (Figure. 3), present between depths 143 and 1046 m, are placed almost at the same level in the constrained model, but with a small density contrast close to 0 g.cc. This may be due to the fact that the density and resistivity gradient tends to zero, or it may be due to the fact that there are no structural similarities between these two physical parameters in the near surface. With the exception of borehole F1 (Figure. 2) which shows a strong anomaly in the P4 profile, all other drill holes show negative densities in the correlation of conductors showing the resistivity pattern. These two indices are positive for geothermal exploration.

DISCUSSION

Gravity inversion constrained by the 3D resistivity model of the Asal Rift data led to a density model (Figure. 4), with clear visibility of fault zones at depth. Notably in the Fialé caldera area (Figure. 4, P4), where a negative density contrast zone associated with a hydrothermal metamorphic zone or possibly a mineralized water-saturated basaltic zone is observed to the southwest and a heavy unit zone possibly due to a volcanic (basalt) formation to the northeast (Figure. 4, P4). Numerous open faults are observed in the fialé caldera zone and numerous fumaroles are also present (Figure. 1). In profiles P2, P3 and P4, the constrained density model highlights a rising structure with very low densities -0.2 g.cc (Figure. 14 b). This structure corresponds to the upward flow directly connected to the magma chamber. This is in good agreement with the resistivity model and the seismic model (Doubre, 2004) which respectively interpret a zone of very low resistivity and a seismic zone between 1500-4000 m originating from the interaction of hot rock and overlying rocks (rhyolite, basalt) or perhaps molten magma in a strongly faulted zone. Gravity inversion constrained by the 3D resistivity model, adds information on structural geometries, fault zones, water intrusions and allows visualization of upward fluid flow.

CONCLUSIONS

We tested the linear inversion approach using the cross-gradient technique on real data on the Asal Rift without any a priori geological information. This method allows the recovery of individual models. These tests also showed that a joint inversion can be performed in a geological context that does not require a priori petrophysical knowledge. The results of these tests are conclusive and promising in the application of natural and other resources.
The drawback of this joint inversion of the different physical parameters is the determination of the coefficients of the cost function (eq. 2). Although the coupling coefficient plays a role in calibrating the constraint of the physical parameter targeted in this case for us the density, it is, therefore, necessary to perform several inversions by varying the weight of the cross gradient coupling. However, from this type of inversion, the speed of the computation time, with a good resolution of the lateral of the constrained model, follows.

ACKNOWLERGEMENTS

We thank the International Gravity Bureau, for helping us with the geographical coordinates of the Asal rift gravity data. IPG Paris provided the Ghoubbet bathymetry

REFERENCES

AQUATER. (1989). Djibouti geothermal exploration project: Republic of Djibouti. AQUATER.

BRGM : Territoire Français des Afars et des Issas: rapport de fin de sondage: résultats des premiers essais de production. BRGM75-SGN-442-GTH (1975a) 18p.

BRGM : Territoire Français des Afars et des Issas: rapport de fin de sondage, interprétation des données géologiques de Asal 1 et Asal 2. BRGM75-SGN-443-GTH. (1975b) 19p

Carver, C. T., Garg, S. K., Davis, L. C., & Jalludin, M. Reservoir Characterization from Exploration Well Completion Tests in the Fiale Caldera, Djibouti.(2019)

Demange, J., Stieltjes, L., & Varet, J. (1980). L'éruption d'Asal de novembre 1978. Bull. Soc. Geol. Fr, 7, 837-843.

Demange, J., & Puvilland, P. (1990). Champ géothermique d'Asal. Synthèse des Données. Bur. de Rech. Geol. et Min., Orléans, France.

Doubre, C. (2004). Structure and mechanisms of volcano-tectonic rift segments: studies of ancient rifts (Scotland, Iceland) and an active rift (Asal-Ghoubbet) (Doctoral dissertation, Le Mans

Gallardo, L. A. (2007). Multiple cross-gradient joint inversion for geospectral imaging. Geophysical Research Letters, 34(19). 178, 198

Gallardo, L. A. and Meju, M. A. (2003). Characterization of heterogeneous near-surface materials by joint 2d inversion of dc resistivity and seismic data. Geophysical Research Letters, 30(13). 178, 198

Hautot, S., Single, R., Watson, J., Harrop, N., Jerram, D., Tarits, P., Whaler, K., Dawes, D., 2007. 3-d magnetotelluric inversion and model validation with gravity data for the investigation of flood basalts and associated volcanic rifted margins. Geophysical Journal International 170 (3), 1418-1430.

Le Gall, B., Daoud, M. A., Maury, R., Gasse, F., Rolet, J., Jalludin, M., ... & Moussa, N. (2015). Carte Géologique de la République de Djibouti, Echelle 1/200 000. *Geological Map of the Republic of Djibouti. Scale1/200000*

Li, Y., Oldenburg, D. W., 1998. 3-d inversion of gravity data. Geophysics 63 (1), 109-119. Lucazeau, F., Vasseur, G., 1989. Heat flow density data from france and surrounding margins. Tectonophysics 164 (2-4), 251-258.

Manighetti, I.; Tapponnier, P.; Gillot, P.Y.; Jacques, E.; Courtillot, V.; Armijo, R.; Ruegg, J.C.; King, G. Propagation of rifting along the Arabia-Somalia Plate Boundary: Into Afar. J. Geophys. Res. Space Phys. 1998, 103, 4947-4974.

3D inversion of drone EM data -- the DroneSOM project

Longying Xiao[1], Cedric Patzer[2], Jochen Kamm[3]
Geological Survey of Finland (GTK), [1] longying.xiao@gtk.fi; [2] cedric.patzer@gtk.fi; [3] jochen.kamm@gtk.fi;

SUMMARY

The application of electromagnetic geophysical methods has been actively contributing to various engineering, environmental and economic fields. In Finland, forests and lakes cover more than 75% and 10% of the land area, respectively. This makes geophysical fieldwork such as mineral exploration and groundwater mapping more challenging and costly. Drone measurements are therefore a cost-effective and environmental-friendly approach, especially for large-scale mapping.

The DroneSOM (Drone Geophysics and Self-Organizing Maps) project, funded by EIT RawMaterials, intends to develop drone-based gravity and electromagnetic (EM) exploration instruments and associated data interpretation software. Together with the partners from both academia (i.e., Technical University of Denmark) and industry (i.e., RADAI Oy, Beak Consultants GmbH.), we aim to provide commercial geophysical solutions, as well as free educational tools at the end of the project. In particular, a set of efficient and robust 3D EM modeling and inversion code will be the kernel for EM data interpretation. We hereby present the framework of 3D frequency-domain EM inversion envisioned by project.

In this work, we present numerical examples, where we solve Maxwells equations using a total field electric field formulation. For the model meshing, the code supports rectilinear, curvilinear, and octree grids (Kamm et al., 2020; Xiao et al., 2022). The edge finite element method was used to discretize the diffusion equation derived from Maxwell's equations. To solve the resulting linear system of equations, we use for now the direct solver MUMPS. The object-oriented code is implemented in C++ to allow for easy adaptation for various source and data types.

For the inversion, we use the standard multi-component objective function, which includes data norm and model regularization norm. To solve the adjoint modeling and obtain the model update at each iteration, we use PETSc library. In general, we employ deal.II library (dealii.org/) to perform the heavy computation, such as the modeling equation discretization, linear system equation solving, and inversion model update, as it comes with interface wrappers to MUMPS and PETSc. Currently, the code is parallelised using the MPI framework for both forward and inverse modelling.

Keywords: DroneSOM, 3D, Inversion, frequency-domain, electromagnetic

REFERENCES

Kamm, J., M. Becken, and R. Abreu, 2020, Electromagnetic modelling with topography on regular grids with equivalent materials: Geophysical Journal International, 220, no. 3, P 2021–2038.

Xiao, L., G. Fiandaca, B. Zhang, E. Auken, and A.V. Christiansen, 2022, Fast 2.5D and 3D Inversion of transient electromagnetic surveys using the octree-based finite element method: Geophysics, 0: 1-53.

Drone based experimental TEM surveys over Lake Baikal and a uranium occurrence

V. Hallbauer-Zadorozhnaya[1], Yu. A. Davydenko[2,3], Parshin A.V[-2], and E. Stettler[1,4]
[1]AeroPhysX (pty) Ltd, South Africa, valeriya.hallbauer@gmail.com
[2]Irkutsk National Research Technical University, Russia, dya@geo.istu.edu
[3]Gelos Ltd, Russia, davidenkoya@gmail.com
[4]University of Witwatersrand, South Africa, stettlere@gmail,com

SUMMARY

The results of experimental TEM surveys using drones, carried out at the Bolshoe Goloustnoye site on Lake Baikal and at a uranium deposit are presented. L Baikal is a unique geoelectrical situation, where low-resistivity lacustrine sediments are located under a relatively isotropic water body. The upper part of the sedimentary sequence is represented by diatomaceous silt with high conductivity, the lower part has denser clayey sediments. The task was to investigate the possibility of using a drone based TEM survey for delineating the electrical stratigraphy of the subsurface at depths between 50-200 m separated into layers and blocks.

The geology of the uranium bearing area consists of a high-resistivity crystalline basement, overlain by low-resistivity sedimentary deposits (sands, clays) and effusive rocks and the TEM survey was undertaken to determine if the U mineralized strata have a distinctive resistivity signature.

The combined instrumentation unit consisted of an EGI-500 generator providing bipolar current pulses, a Mars 4.0 which is a multi-channel electrical prospecting potential difference recorder, a PDI-50 receiver loop and a SibGIS UAS - unmanned 6-rotor aircraft with a payload of up to 10 kg.

In both cases, a grounded electrical line AB was used as a source of the electromagnet field. Sixteen traverses of survey data were measured over the Baykal ice sheet and five traverses over the uranium deposit.

For the interpretation of the TEM data the $S\tau$ technique was used, which allows tracing the change in the apparent longitudinal conductivity with depth. On the sections, a high-resistivity layer is clearly distinguished, corresponding to the water of Lake Baikal as well as sedimentary deposits, composed by several blocks of low resistivity. The U-bearing layers are confidently identified in all profiles at depths of 120-170 m.

Keywords: Unmanned Aerial Vehicles (UAV), drone, TEM, S-plane, conductance

INTRODUCTION

In the first two decades of the 21st century airborne electromagnetic surveying has become widespread. In recent years, drones have been used in the transient EM soundings method. The UAS technology has several advantages over conventional airborne platforms to collect geophysical data such as resolution, accuracy, and cost but off-course presently have limited endurance and weight carrying capabilities. But in comparison to ground surveying a drone can collect in several days hundreds of thousands of sounding points. In the aircraft and helicopter version, as a rule, the field source (transmitter loop) is mounted directly on the wings of the aircraft or suspended on a cable under the helicopter. The weight restriction of a drone does not allow carrying a weight of more than 10 kilograms, where the transmitter source are located on the ground. As a rule, an ungrounded rectangular loop is used as a source of electrical current. In our cases, a long grounded AB line with a current of 5 A was used.

Experimental TEM surveys have been carried out on two sites: at the coastal part of Lake Baikal (delta of Bolshoe Goloustnoye river) and over a uranium occurrence in Easter Siberia. TEM surveying at both sites were made within one, two day period and one single day, with a high data density: the flight line spacing varied between 50 and 100m, the data sampling rate along flight lines is about 10 m.

INSTRUMENTATION AND OPERATIONS TECHNOLOGY

The UAV-MPP technology applied on Lake Baikal and on at the uranum deposits used a special versions of the components of the 'Mars' electrical survey system (*Patent No. 2574861*), and the SibGIS UAS unmanned platform (*Patent No. 2736956*).

The instrumentation assembly consist of the following units described below. On the ground we have:

a) EGI-500 generator that delivers bipolar 50% duty cycle current pulses. It consists of two separate units, one delivering the stabilized current and the second a pulse switcher. The duration of the block shaped current pulse is 5 ms on and 5ms off.
b) A long (2.2 km) grounded transmitter line AB is used as a source of the current pulses. The iron stakes (electrodes) of the transmitter cable are grounded into the water through holes drilled into the ice.
In the air we have:
a) A SibGIS UAS which is an unmanned 6-rotor hexacopter with a payload of up to 10 kg.
b) The "Mars 4.0" which is a multi-channel electrical prospecting potential difference recorder that collects the full TEM data series and functionally consists of an ADC, a GPS-enabled synchronization unit, a data storage module and a USB interface for connecting to a PC.
c) A PDI-50 receiver loop hanging below the hexacopter and has an equivalent surface area of 50 m^2 that records the secondary induced field.
d) Microcomputer with a GNSS-reference system mounted on to the drone. The onboard software stores the data.
The Figure 1 demonstrates the drone with suspended receiver box and vertical magnetic dipole (loop).

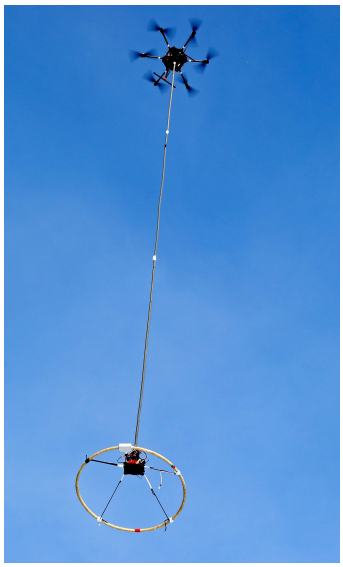

Figure 1. Unmanned Aerial Vehicles with receiver box and VMD. Diameter of VMD is 1 m, surface are 2500 m^2.

INTERPRETATON VIA MODIFICATION OF THE CALCULATION OF APPARENT LONGITUDINAL CONDUCTANCE ST

The so-called method of differential transformation of emf signals into the curves of apparent longitudinal conductance as function of time or depth (method Stau, $S\tau$) was proposed by Sidorov and Tikshaev (1970). The $S\tau$ method has certain advantages. Its use allows determining the conductance of the section and determining the depth (or time) where $S\tau$ increases noticeably. Usually increasing conductance is associated with the presence of a low resistive object (bodies and/or layers) in the resistivity section. We used this property when interpreting airborne data. The procedure of the modified method is described by Davydenko et al. (2022) as well as presented in another abstract presented on the 25th EM Induction Workshop (Hallbauer-Zadorozhnaya and Stettler, 2022).

RESULTS AND DSCUSSION
LAKE BAIKAL

An electrical line 2.16 km long was grounded (floated) into water of Lake Baikal along the shore at the Bolshoe Goloustnoye site (Figure 2). Six profiles were conducted parallel to the electrical line AB, nine – perpendicularly. The TEM points located directly above the current line were not interpreted due to the powerful noise generated by it.

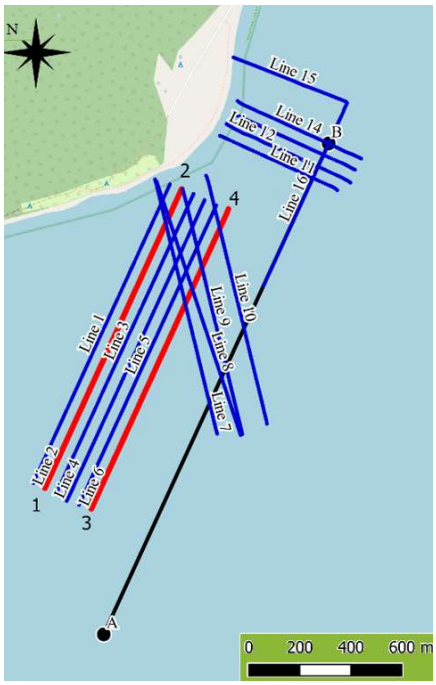

Figure 2. The layout of the profiles on the site Bolshoe Goloustnoye site on Lake Baikal. The black line indicates the location of the AB line. The profiles of electromagnetic induced polarization soundings (EMS-IP) are marked in red.

The emf curves were smoothed and after applying the procedure of the modified Stau method for each sounding, St(H) curves are calculated. An example of a cross-section of apparent longitudinal conductance for profile 6 is shown in Figure 3.

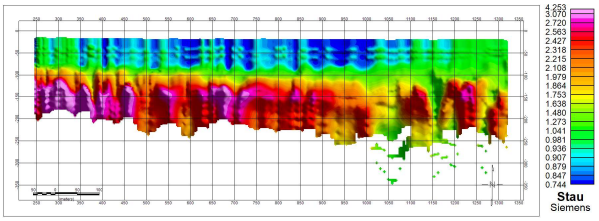

Figure 3. Apparent longitudinal conductance along profile 6 (close to current line AB). The section clearly shows a high-resistivity layer corresponding to Lake Baikal water and sedimentary deposits.

However, noise, instrumental interferences and geological distortions make it difficult to develop software for interpretation, especially when the TEM profile crosses the electrical transmitter line. The change in the shape and intensity with distance from the current source are now recorded and will aid in future surveys and interpretation.
A sufficiently dense network of profiles made it possible to present a three-dimensional visualization of the TEM data using the model of a "floating" plane. Figure 4 demonstrates the geo-electrical cuts at different elevations (200 m, 100 m, -30 m, -200 m).

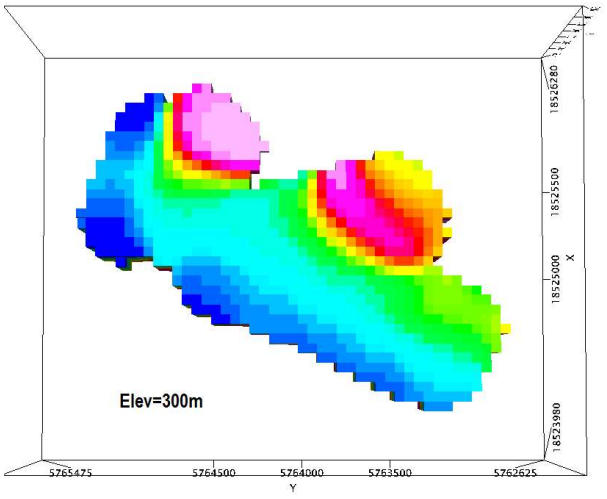

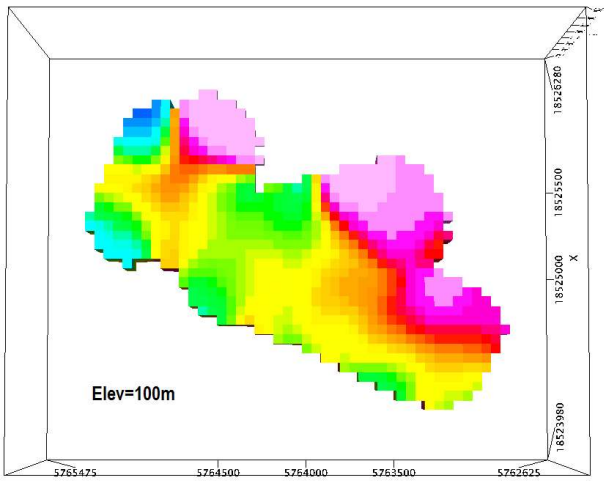

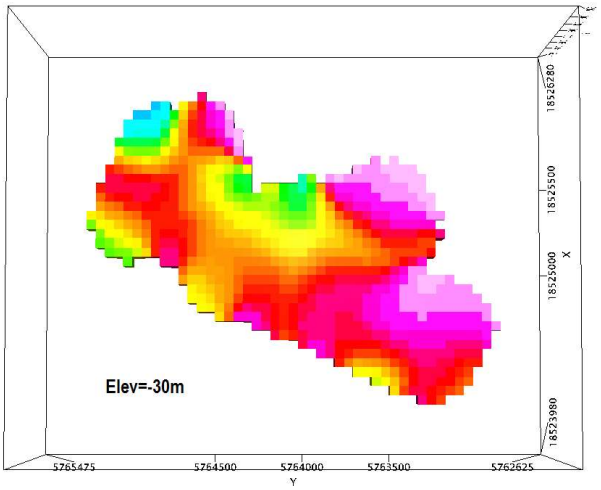

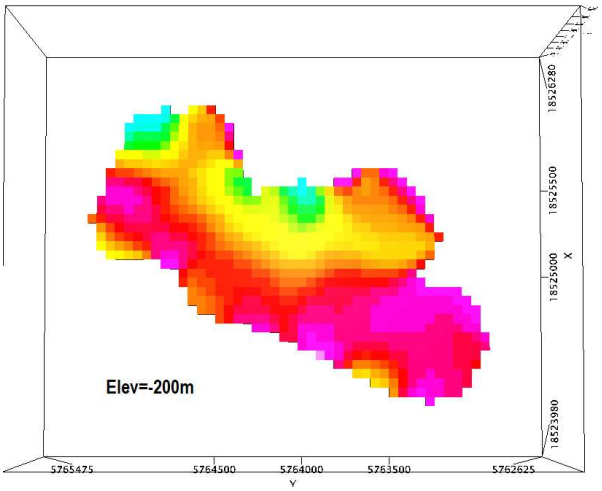

Figure 4. Geo-electrical cuts at different elevations (200 m, 100 m, -30 m, -200 m). colour bar is in Figure 3.

Conductivity of the lacustrine sediments increase with depth. A low resistive ring structure is located at some distance from the delta of the Goloustnaya River.

URANIUM OCCURRENCE

The area investigated is located on the Viktim Plateau, West Siberia. Five profiles have been carried out. Permafrost is ubiquitous in the area, its lower boundary is fixed at depths of 55-90 m from the surface. In the first approximation, the geoelectric section can be represented as follows:-
- crystalline rocks of the basement (granitoids, diorites, limestones, metamorphic shales and sandstones) have a resistivity (190 - 2000 Ohm.m) and occur at a depth of 120-160 m;
- Overlying U enriched sedimentary deposits (sands, clays with a thickness of 40-150 m) have la ow-density (2.0 g/cm^3), are weakly magnetic (0.024 SI units), low-resistivity (40 Ohm.m) and low-velocity (2150 m/s);

- the effusive stratum (several covers of basalts separated by tuff layers) is characterized by an average density (2.5 g/cm3), high magnetic susceptibility (2.0 - 230 SI units), high resistivity (1200 - 8000 Ohm.m) and acoustic velocity (3800 m/s).

The contrast of physical properties predetermines the effective use of the geoelectric methods to identify the enriched strata of rocks in the section.

Figure 5 demonstrates structures on the west side (5a) and on the east side (5b).

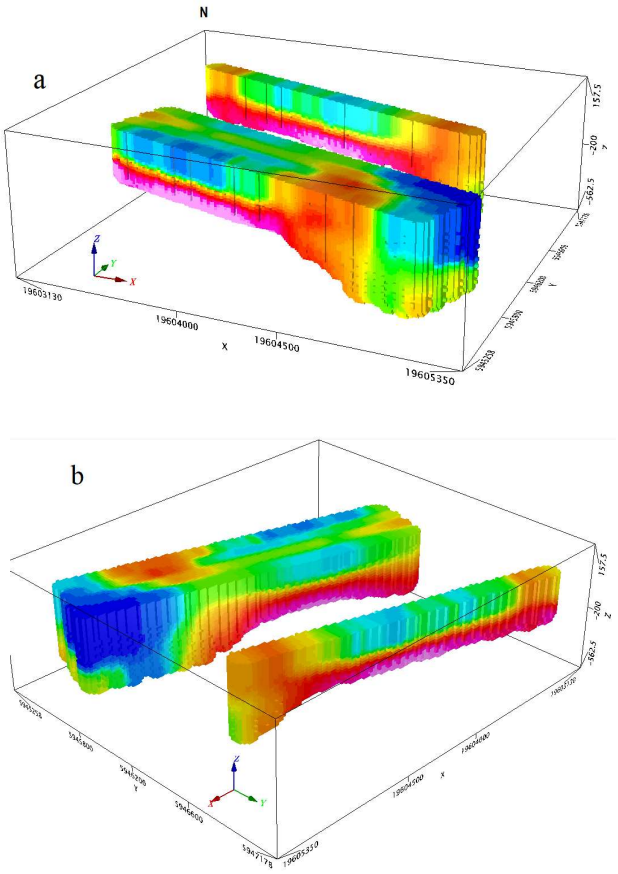

Figure 5. 3D visualization of apparent longitudinal conductance. a) View from the west, b) view from the east. Colour bar is on the Figure 3

These structural features of the section are characteristic of all five profiles. In the west part of the site at depths of 120-160 m, a remarkable conductor is observed, which we identify as a enriched complex. The east side of the site is highly restive. It is known that another thin layer of sedimentary rocks (also enriched) is located above the main deposit. In this case, it is quite possible that in the geoelectric section both layers appear as one with a slightly changed (convex) surface shape. We also note that a decrease in the longitudinal conductivity of the upper layer (basalts) is observed. This occurs because the secondary electromagnetic field rapidly propagates in the resistive rocks but concentrates in the conductor. Figures 5a and b show a three-dimensional image of the geoelectric sections. It is obvious that the correlation of the main elements of the block is correlated both horizontally and in plan, which indicates the stability of the transformation algorithm $S\tau$ and its applicability for interpreting the TEM data.

CONCLUSIONS

Experimental airborne TEM surveying using a drone demonstrates the effectiveness of TEM operations as shown in the Lake Baikal example that senses an conductor below a thick layer (100-250 m) of fresh highly resistive water.

Interpretation of the TEM data using the “floating” plane model indicates the stability of the transformation algorithm $S\tau$ and its applicability for interpretation the TEM namely for lateral differentiation in the upper part of the sedimentary material and the identification of large structures of various resistivity’s.

To optimize the interpretation process, it is essential to place the sounding profiles parallel too and removed from the current (transmitter) line.

The survey carried out at the site of the uranium occurrence showed the high efficiency of the airborne TEM in identifying and contouring the conductor at a depth of 150 m.

ACKNOWLEDGEMENTS

The research was supported by the Russian Science Foundation grant No. 20-67-47037 "Methodological and software for processing large amounts of data from electromagnetic soundings, gravity surveying and UAV magnetic exploration based on a comprehensive solution of three-dimensional inverse problems for ore delineation by geophysics".

REFERENCES

Sidorov V.A., Tikshaev V. V (1970) Interpretation of transient electromagnetic signals registered in near zone. Expolration Geophysics, M. Nedra. 42: pp.45-54 (in Russan).

Davydenko Yu.A., Hallbauer-Zadorozhnaya V., Bashkeev A.S., Parshn A.V (2022) UAV-TEM data inversion with S-Plane method to highlight coastal geological structure of Lake Baikal. The Near Surface Geoscience Conference & Exhibition 2022. Belgrad, Serbia.

Abstract, 25^{th} EM Induction Workshop,Çeşmeı, Turkey, September 11-17, 2022

Regional to Deposit scale exploration in Fennoscandia based on mineral systems approach

Maxim Yu. Smirnov[1], Graham Hill[2], Jochen Kamm[3], Jan Vozar[4], Jirigalatu[1], Pankaj Mishra[3], Kenneth Muhumuza[2] and DREX WG

[1] Luleå University of Technology, Sweden, maxim.smirnov@ltu.se
[2]Institute of Geophysics Czech Academy of Sciences, Prague, Czech Republic
[3] Geological Survey of Finland, Espoo, Finland
[4] Earth Science Institute Slovak Academy of Sciences, Bratislava, Slovakia

The D-REX (Deposit to Regional scale Exploration) project is based upon the application of the mineral systems concept a potential paradigm shifting approach to mineral deposit identification. Transport, precipitation and concentration of metals into economic mineral deposits involves a combination of processes occurring over different scales and depths. Regions with similar surficial geologies often have widely disparate metal endowment levels especially in cratonic environments. By applying the mineral systems approach we can elucidate lower crustal structures that may play a key role in the processes responsible for metal endowment in the upper-most crust.

Mineral deposit formation is often driven by deeply originating large scale fluid transfer (magmatic and/or metamorphic), which requires; a source region for metal bearing fluids, an energy source for driving fluid circulation, pathways for the migration of these enriched fluids, a depositional mechanism responsible for the formation of the deposit, and a fluid outflow. The overarching goal of the D-REX project is to identify previously unrealised metal endowed regions, via application of a new workflow inclusive of large-scale regional data sets with the ability to identify the deep fluid source regions and transport pathways/mechanisms to the upper crust, for targeted exploration and characterisation of the near surface zones of metal deposition and concentration. 3D magnetotellurics can provide information at all scales of the mineral system, as such it is the primary tool of investigation used in D-REX. MT data sets have been collected at three 100x100 km^2 regions of economic potential in the Fennoscandian shield (central Norway, northern Sweden, and central Finland).

D-Rex Working Group (D-REX WG):

Luleå University of Technology (LTU): *Maxim Yu. Smirnov, Jirigalatu, Thorkild M. Rasmussen, Tobias Bauer, Oskar Rydman*

Institute of Geophysics Czech Academy of Sciences (IG-CAS): *Graham Hill, Kenneth Muhumuza, Svetlana Kovachikova, Jorge Puente, Nazia Hassan, Nooshin Najafipour*

Geological Survey of Finland (GTK): *Jochen Kamm, Pankaj Mishra, Cedric Patzer, Uula Autio, Jarkko Jokinen, Jouni Luukas*

Earth Science Institute Slovak Academy of Sciences (ESI-SAS): *Jan Vozar , Jozef Madzin, Lenka Ondrasova, Peter Vajda*

Boliden Minerals AB: *Tobias Hermansson, Kirsi McGimpsey, Janne Kaukolinna*

Boliden Kevitsa Mining OY: *Katri Vaittinen*

LKAB: *Niklas Juhojuntti, Harald Van Den Berg*

Geological Survey of Norway (NGU): *Sofie Gradmann, Jomar Gellein*

Keywords: magnetotellurics, mineral systems, data inversion, Fennoscandia, metal endowment

Abstract, 25^{th} EM Induction Workshop,Çeşmeı, Turkey, September 11-17, 2022

Results from the DESMEX semi-airborne EM survey at the Gosetal/Rammelsberg (Harz Mountains, Germany)

A. Thiede, M. Becken, P.O. Kotowski and the DESMEX Working Group
Institute of Geophysics, University of Münster, Germany; athiede@uni-muenster.de

SUMMARY

The nowadays depleted world-class SEDEX Rammelsberg deposit and its adjacent areas are a prime location to test and demonstrate new geophysical exploration methods. Here, we present preliminary results of a semi-airborne EM survey centered at the Gosetal and the Rammelsberg, which was conducted in September 2020 as part of the DESMEX II project. Previous airborne EM exploration surveys, carried out about a decade ago in that area, revealed a high-conductivity anomaly in the Gosetal, but subsequent drillings could not verify its existence. Therefore, the results of the airborne EM survey remained enigmatic. Semi-airborne EM has the potential to image deeper than pure airborne EM and may detect conductivity anomalies from the near surface to about $1000\,m$, including a possibly deeper root of the enigmatic Gosetal anomaly.
We installed four electrical dipole transmitters of 2-$3\,km$ length and injected an alternating current with a fundamental frequency of 9.26 and $4.63\,Hz$ and covered an area of about $45\,km^2$ with the Helicopter induction coil DESMEX system. EM Transfer functions were derived in the frequency range up to $4\,kHz$. Analysis of the data is complicated due to the presence of steep topography and over $500\,m$ altitude differences in the surveyed area. Synthetic 3D modeling using the unstructured finite element code custEM shows that strong topographic effects are evident in the collected data and must thus be taken into account in any inversion. We discuss these effects as well as topography correction schemes for flat surface inversion models based on normal field corrections. Ongoing work is focused on comparison of 3D inversion applying the custEM code supporting complex survey geometry and the 3DINV code using corrected data on a flat surface model.

Keywords: semi-airborne electromagnetics; Rammelsberg mine; electrical resistivity; topography effects

INTRODUCTION

The Harz Mountains (Germany) are widely known for its long mining history. One of the outstanding sites in the Upper Harz Mountains is the Rammelsberg mine, a world-class SEDEX (sediment exhalative) deposit highly enriched in Zn- and Pb-sulfides (Large and Walcher, 1999). Nowadays, the mine is fully exploited but past airborne EM surveys revealed a shallow high-conductive anomaly in the adjacent Gosetal. However, subsequent drillings up to $500\,m$ depth could not verify the existence of an ore body and the Gosetal-anomaly remained enigmatic. Considering the mining background of this region, it is perfectly suited as location for a demonstration survey for novel geophysical exploration methods. The DESMEX project seeks to develop and establish such methods, including semi-airborne electromagnetics (EM), for exploration of deep-seated ore bodies. Previous DESMEX surveys (Smirnova et al, 2019, 2020) demonstrate the capability of semi-airborne EM in flat terrain. The Gosetal area features high altitude differences of more than $500\,m$ and very steep valleys making the location a challenging environment for EM data evaluation.
The Gosetal survey was conducted in September 2020. Four grounded dipole transmitters (Tx) of 2-$3\,km$ length were installed in the survey area (see Figure 1). We injected a rectangular current waveform with fundamental frequencies at $9.26\,Hz$ (Tx1, Tx2), $4.63\,Hz$ (Tx3) and $9.6\,Hz$ (Tx4) and a $100\,\%$ duty cycle. Flight areas were chosen for each Tx individually and with an overlapping area at the survey target. Tx were operated sequentially and flight lines are $250\,m$ apart and control lines have $1\,km$ spacing.

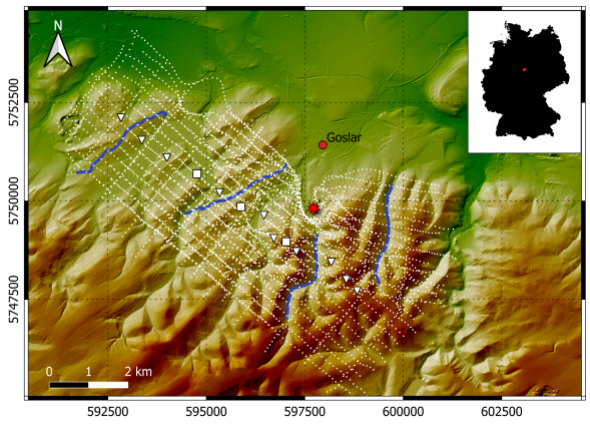

Figure 1: Survey Area: Blue lines show Tx locations (Tx1 to Tx4 from NW to SE), white dotted lines depict flight lines. Triangles and squares mark telluric and full-MT ground site positions. The red star shows the position of the Rammelsberg mine.

THE SEMI-AIRBORNE EM METHOD AND TRANSFER FUNCTIONS

The semi-airborne EM method combines advantages of purely airborne and purely ground-based controlled source EM methods. Using a powerful ground-based Tx, the method provides a great penetration depth of up to $1000\,m$ while maintaining the high efficiency and spatial resolution of an airborne system.
The injected current induces a magnetic field consisting of the normal field produced in a homogeneous halfspace and the anomalous field produced by anomalies therein. A linear relation can be stated between the observed magnetic flux density ($\vec{B}(\omega, \vec{r})$) and current amperage ($I(\omega)$) recordings

$$\vec{B}(\omega, \vec{r}) = \vec{\mathcal{B}}(\omega, \vec{r}) I(\omega) \tag{1}$$

where ω is the angular frequency and $\vec{r}$ denotes the point in space. The transfer function $\vec{\mathcal{B}}$ relates both quantities and holds information about the subsurface conductivity structure.
Transfer functions were estimated in the frequency range up to $4\,kHz$ following the procedure described by Becken et al (2020). Figure 3 shows amplitudes of transfer function estimates at three different frequencies along a coincident flight line for Tx1 to Tx3. The amplitudes produced by Tx2 and Tx3 decrease abruptly at all frequencies when crossing the Gosetal which indicates a conductive anomaly in the valley.

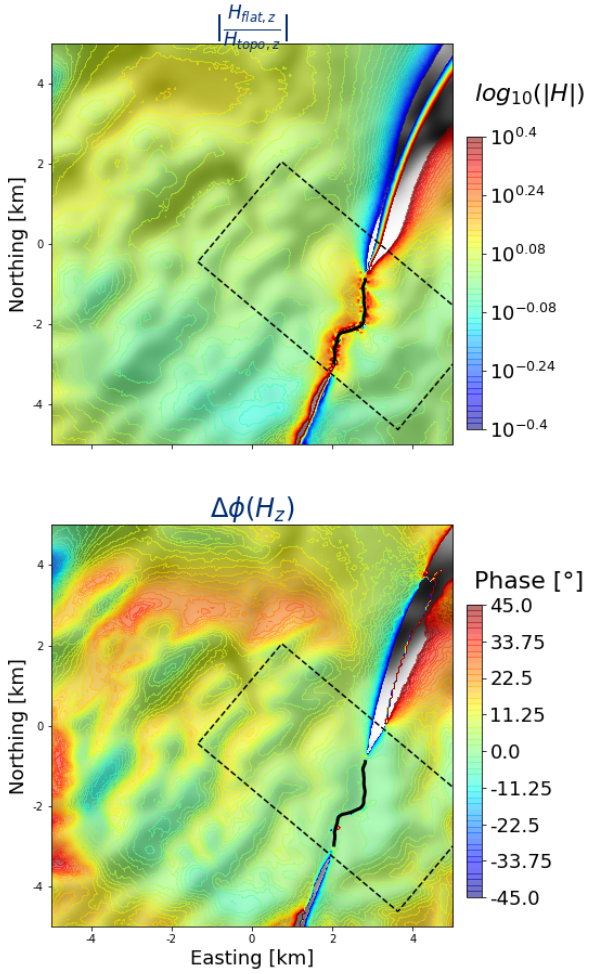

Figure 2: Amplitude ratio (top) and phase difference (bottom) of normal field responses ($\mathcal{B}_z$) for Tx3 (black line) received from models with and without topography using an electrical resistivity of $500\,\Omega m$. The dashed line gives the corresponding flight area.

TOPOGRAPHIC EFFECTS AND PRELIMINARY INVERSION RESULTS

The semi-airborne EM data are strongly distorted by topography (see Figure 2). A comparison of simulated transfer functions of models with and without topography imply distinct differences even aside from the vicinity of the Tx and zero crossings. Calculated phase differences of $> 10°$ are in the same order of magnitude as field variations produced by

anomalies and thus need to be taken into account for inversion.

Only few open source inversion codes can handle semi-airborne EM data and mostly do not allow for complex survey geometry such as in the Harz Mountains. Preliminary 3D inversion results are shown in Figure 4. We used the finite difference code 3DINV (Grayver et al, 2013) which only supports flat surface models. To reduce topography effects on the data, we applied a Normal Field Correction that substitutes the normal field $\vec{\mathcal{B}}_{topo}$ of a homogeneous half space with topography by the normal field $\vec{\mathcal{B}}_{flat}$ of a half space with a flat surface.

$$\vec{\mathcal{B}}_{inv} = \vec{\mathcal{B}}_{obs} - \vec{\mathcal{B}}_{topo} + \vec{\mathcal{B}}_{flat} \tag{2}$$

The residual $\vec{\mathcal{B}}_{inv}$ still includes topographic effects but these are expected to be less dominant. We estimated the normal field response of $\vec{\mathcal{B}}_{topo}$ and $\vec{\mathcal{B}}_{flat}$ using the unstructured finite element code custEM (Rochlitz et al, 2019) for $500\,\Omega m$ electrical resistivity. Corrected transfer functions $\mathcal{B}_{inv,z}$ were used as inversion input in a frequency range of 9 to $1000\,Hz$. The model box had a size of $9 \times 15 \times 4.02\,km$ plus padding cells with a $500\,\Omega m$ halfspace as starting model. The model was rotated to fit the general strike direction of $45°$. Data with a relative error $> 20\%$ and in the vicinity of the Tx were masked. A RMS of 1.48 was reached after 10 iterations.

Inversion results indicate a 500 to $1000\,m$ deep conductor in the Gosetal slightly dipping to SE direction (**A** in Figure 4). However, the conductor is not a unique feature as assumed from raw data. Strong anomalies in the vicinity of the transmitter (**B**) as well as conductors following the structure of valleys (**C**) indicate incomplete topography correction. Other anomalies (**D**) seem to be artefacts placed at the model edges with low data point coverage and low sensitivity.

CONCLUSIONS

We conducted a semi-airborne EM survey in the mining area Rammelsberg (Harz Mounatins, Germany). Estimated transfer functions indicate the presence of a conductive anomaly in the adjacent Gosetal. Analysis of the data is complicated, though, by the presence of steep topography that needs to be taken into account. Available 3D inversion codes only support flat surface models so we tested a Normal Field Correction to reduce topography effects. Preliminary results using corrected data show a good conductor in the Gosetal at 500 to $1000\,m$ depth but remaining topography effects can lead to artefacts. Ongoing work is focused on 3D inversion using the unstructured finite element code custEM that was recently extended to perform inversions.

ACKNOWLEDGMENTS

DESMEX Working Group members: Raphael Rochlitz, Thomas Günther, Mathias Ronczka, Annika Steuer, Olaf Cortes Arroyo, Hauke Petersen, Pritam Yogeshwar. We would like to thank all students and technical staff for helping with field work, flight operation and bird assembling. We are grateful to A. Grayver and R. Streich for providing the 3DINV code for 3D inversion. This project series (DESMEX I & II) is funded by the German Federal Ministry for Education and Research under grant no. 033R130.

REFERENCES

Becken M, Nittinger CG, Smirnova M, Steuer A, Martin T, Petersen H, Meyer U, Mörbe W, Yogeshwar P, Tezkan B, Matzander U, Friedrichs B, Rochlitz R, Günther T, Schiffler M, Stolz R, the DESMEX Working Group (2020) DESMEX: A novel system development for semi-airborne electromagnetic exploration. GEOPHYSICS 85(6):E253–E267

Grayver AV, Streich R, Ritter O (2013) Three-dimensional parallel distributed inversion of CSEM data using a direct forward solver. Geophys Journal International 193(3):1432–1446

Large D, Walcher E (1999) The Rammelsberg massive sulphide Cu-Zn-Pb-Ba-Deposit, Germany: an example of sediment-hosted, massive sulphide mineralisation. Mineralium Deposita 34(5):522–538

Rochlitz R, Skibbe N, Günther T (2019) custEM: Customizable finite-element simulation of complex controlled-source electromagnetic data. Geophysics 84(2):F17–F33

Smirnova M, Juhojuntti N, Becken M, Smirnov M (2020) Exploring Kiruna iron ore fields with large-scale, semi-airborne, controlled-source electromagnetics. First Break 38(10):35–40

Smirnova MV, Becken M, Nittinger C, Yogeshwar P, Mörbe W, Rochlitz R, Steuer A, Costabel

S, Smirnov MY, the DESMEX Working Group (2019) A novel semiairborne frequency-domain controlled-source electromagnetic system: Three-dimensional inversion of semiairborne data from the flight experiment over an ancient mining area near Schleiz, Germany. GEOPHYSICS 84(5):E281–E292

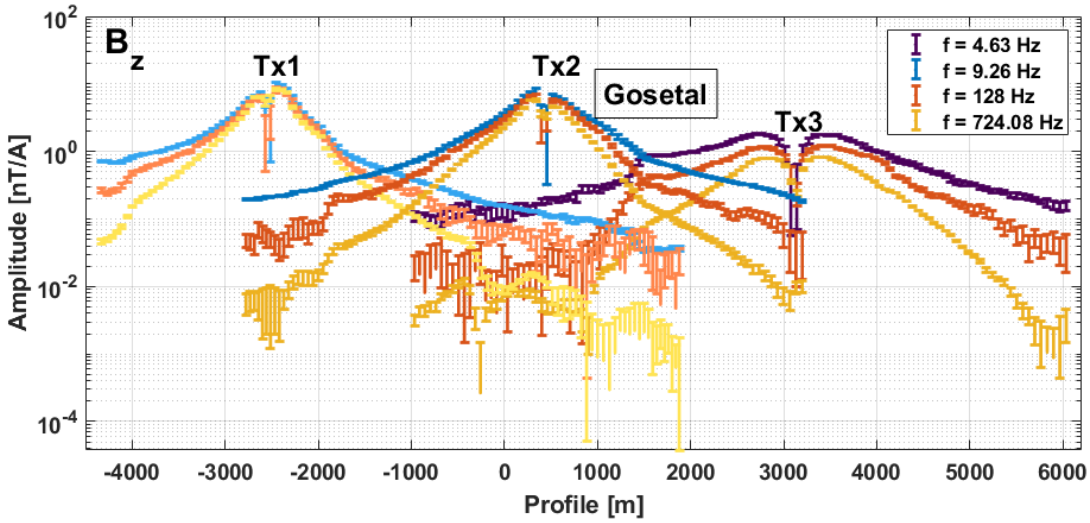

Figure 3: Amplitude of the $\mathcal{B}_z$ magnetic transfer function at Tx1 (light color), Tx2 and Tx3 (dark color). The lowermost frequency of Tx3 differs from the ones at Tx1 and Tx2 due to different base frequencies.

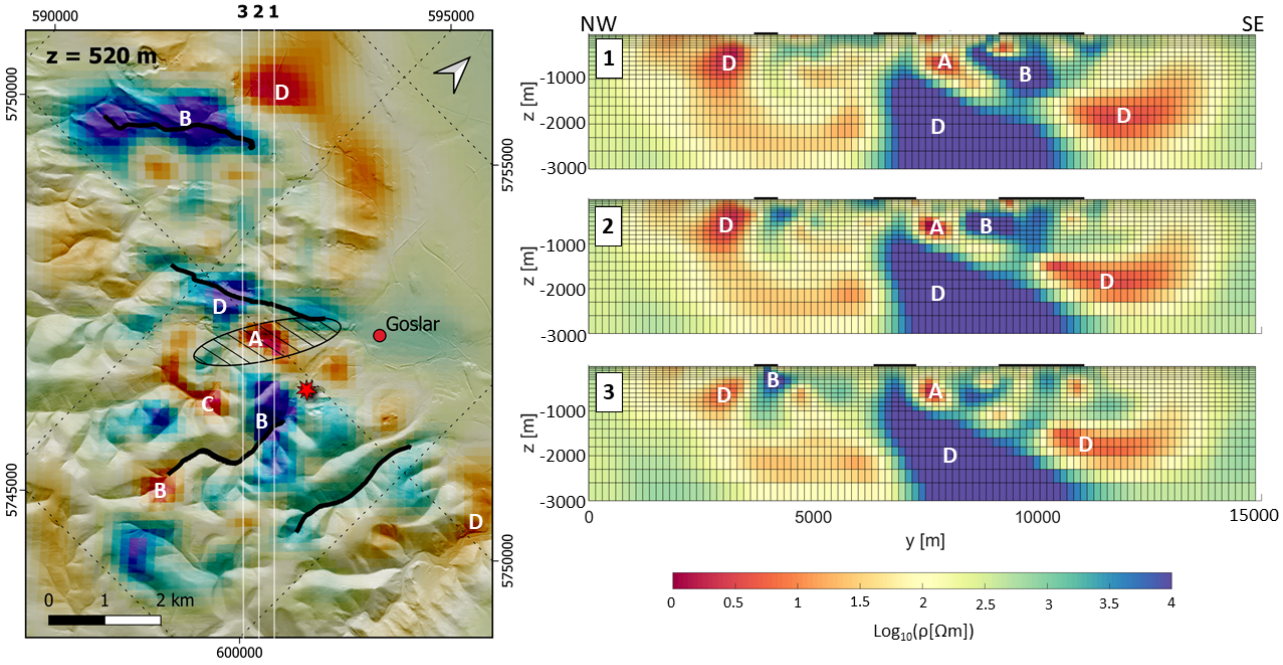

Figure 4: Horizontal slice (left panel) and cross sections (right panels) of the inversion results using normal field corrected data. The horizontal slice is shown on a topographic map to compare conductivity structures and mountain shapes. The hatched area and the red star mark the Gosetal and the Rammelsberg mine, respectively. Black lines show Tx positions.

Examination of geomagnetic data as precursors of the September 5, 2018 (MW = 6.6) and August 20, 2016 (MW = 6.0) earthquakes in Japan

Hamideh TAHERINIA[1], Shahrokh POURBEYRANVAND[2]
[1]M.S. student, International Institute of Earthquake Engineering and Seismology, Tehran, Iran, hesar.t.n266@gmail.com
[2]Assistant Prof., International Institute of Earthquake Engineering and Seismology, Tehran, Iran, beyranvand@iiees.ac.ir

SUMMARY

Magnetic anomalies have been discussed long ago as an earthquake precursor. In this study, the characteristic curves are obtained by frequent overplotting of magnetic data per 24-hour time frames on each other for three geomagnetic stations in Japan (MMB, KAK, KNY). All three components (Z, Y, X) or (Z, D, H) were processed in one year. In order to increase the intensity and distinction of the anomalies observed before the earthquake compared to the original data, we tried to eliminate the effect of daily variation of the magnetic field on the geomagnetic records by this method.

Keywords: anomaly, characteristic curve, Earthquake, Japan, magnetic field

INTRODUCTION

Earthquakes are one of the most devastating natural disasters, and their impact on human society, in terms of casualties and economic damage, has been significant throughout history. Earthquake prediction can aid in preparing for this major event, and its purpose is to identify earthquake-prone areas and reduce their financial and human losses. Any parameter that changes before the earthquake in a way that one can predict the earthquake with a careful study of its variations is called a precursor. Recently, more attention has been paid to geophysical, geomagnetic, geoelectrical, and electromagnetic precursors. The term Tectonomagnetism has been used in this context which involves changes in the magnetic field associated with an earthquake. The effect of magnetic seismicity was investigated by Ricky Taki (1976) (Meloni et al., 1998). The effect of magnetic seismicity is quite evident from comparing simultaneous data of a geomagnetic network (Liu et al., 2006). In the present study, the geomagnetic data of three stations, obtained through INTERMAGNET, with a distance of less than 500 km to the September 5. 2018 and August 20, 2016, Japan earthquakes are investigated.
Then the method of characteristic curves is used to remove the effect of diurnal variation of the geomagnetic field. After that, by examining the more distinct anomalies after implementing the method, the cases are matched with the seismic activities of the region. The pure anomaly can be observed by separating the noise from the desired signal. Among the various magnetic components, the horizontal components are more suitable than the others for the proposed process because of more variations in the geomagnetic field in the vertical direction due to f the geomagnetic gradient. Each component behaves differently as a function of the geological and geomagnetic conditions of the station site. In the present study, one year of magnetic data, including three stations and for X, Y, and Z components in addition to seismic data for Japan, are used to implement this method. The method is based on plotting different magnetic field components in specific time intervals in the same 24 hours frame. This will lead to a plot that shows the geomagnetic nature of each component of the geomagnetic field for each station. After averaging the values for every point at the horizontal axis of the plot, which is a unit of time depending on the sampling (hourly mean, minute mean, etc.), a curve will be obtained called the characteristic curve. Then we reduce the characteristic curve values from geomagnetic data to reveal the anomalies free of diurnal variation noise so that the possible anomalies related to earthquakes will be shown more distinctly. After drawing the components of the magnetic field and removing the daily changes from each of the components, we can observe the anomalies related to the earthquakes to justify the observed anomalies better and considering the standard deviation for each component, pre-seismic anomalies have a more significant distinction than the original data for being studied as a seismic precursor.

One of the problems with using this indicator is the ambiguity in separating seismic anomalies from the data (Hayakawa et al. 2007) because the number of factors affecting the earth's magnetic field is large and how some of them affect it is not completely clear. There is ample practical evidence

for specific magnetic and electrical oscillations before an earthquake occurs. Previous studies have used discrete wavelet transform to process geomagnetic data to automatically detect the sudden occurrence of magnetic storms (Gamri et al., 2013).

The study of changes in the earth's magnetic field before, at the same time, and after an earthquake has continued from the middle of the last century to the present day, and its related scientific formulations have evolved. Existing theories for interpreting magnetic anomalies related to seismic activity can be classified into three theories: magnetohydrodynamic, electro-synthetic and piezomagnetic. For more information on these theories, refer to the relevant references (Edwin and Roberts 1983).

Methods

According to the research in this field in the present study, this research has been done for Japan using geomagnetic data from three stations with a distance of less than 500 km. The geomagnetic stations used in this study are three stations, MMB, KAK and KNY and this information has been received from the INTERMAGNET site. Based on the Dobrowolski relationship $P = 10^{0.43M}$ (Dobrowolski et al. 1979), it is expected that the prediction phenomena will be observed in a radius of about 700 km. However, due to the lack of data and geomagnetic stations in the region, one of the stations in a radius of about 950 km was inevitably used for this purpose.

Figure (1) shows the location map of the studied stations, as well as the epicenter of the earthquake and seismicity of the region from 1900 to 2014.

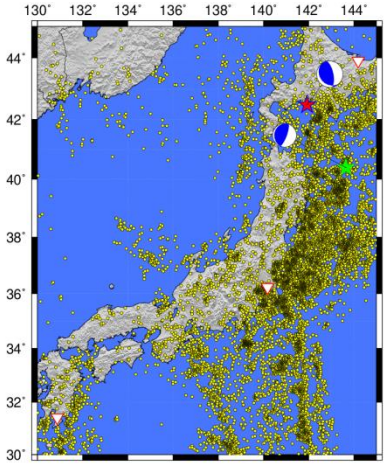

Figure 1. Location map of the studied stations (white triangle), as well as the epicenter of two earthquakes (red star position of the first earthquake and green star position of the second earthquake) and seismicity of the region from 1900 to 2014 (yellow circles).

In this research, the method of characteristic curves has been used to eliminate the effect of factors affecting the earth's magnetic field at the location of magnetometric stations. Relevant is removed from the data.

Then, by examining the abnormalities that have become clearer after the above steps and eliminating the noise due to daily changes, these cases are matched with the seismic activities of the region. Then, by isolating the noise from the desired signal and finally the observed abnormality, it is amplified as much as possible to make more use of the data in question as a precursor to the earthquake.

Among the various magnetic components, the X component is more suitable for the proposed process than the Y and Z components. Of course, other components can also be used depending on the geological and geomagnetic conditions of the station. In the present study, to show examples of the application of this method, the magnetic and seismic data available on the Japan Indicator Database website have been used. To display the data, you must first delete the values that have been registered as unsuitable data, which in the program written in PYTHON, these values have been replaced with their previous values. After selecting the appropriate time period using the available data from each station, the diagram of repeating the observed values over 2 hours on different days shows the desired station's geomagnetic nature; thus, the characteristic curve for a period of one year in the station in question. Comments were made on the magnetic components X, Y and Z in question. Figure (2) shows the characteristic curve at one of the stations for the Y component of the magnetic field of two earthquakes.

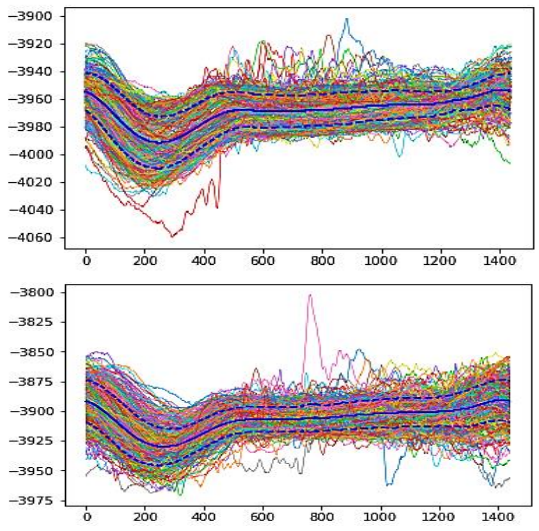

Figure 2. The characteristic curve (continuous line) is drawn at one of the stations for component Y of the magnetic field of two earthquakes (the first figure for the earthquake of 05/09/2018 and the second figure for the earthquake of 20/08/2016). The standard deviation dashes are based on 1s calculations. The horizontal axis represents time (minutes) and the vertical axis represents the amplitude of the magnetic field (nanotesla).

After drawing the magnetic field components and removing the daily changes from each component, one can observe the anomalies related to earthquakes better; to justify the observed anomalies and consider the standard deviation for each component, which is the definition of each component. It is shown in Figure (3) for the first earthquake and in Figure (4) for the second earthquake.

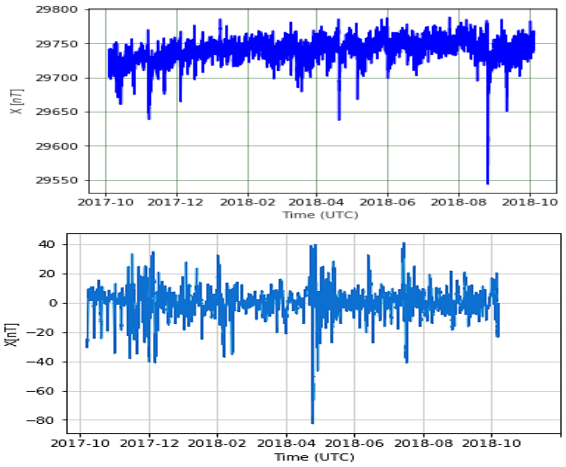

Figure 3. The Characteristic curve for one year of raw data at one station (Figure above) and data processing at the same station (Figure below) for the magnetic component (X).

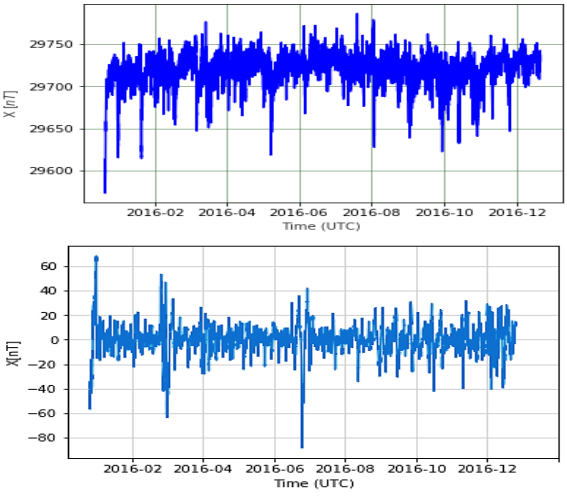

Figure 4. The Characteristic curve for one year of raw data at one station (Figure above) and data processing at the same station (Figure below) for the magnetic component (X).

Due to the fact that an earthquake occurs between 5-15 days after the geomagnetic anomaly, an anomaly is observed in the first earthquake on 26/08/2018, which can be used as an indicator of an earthquake with a magnitude of 6.6 on 05/09/2018. In the second earthquake, the anomaly of 05/08/2016 can be considered as a precursor to the earthquake with a magnitude of 0.6 on 20/08/2016 in Japan. Component X is more suitable for detecting this anomaly and shows a better anomaly. Component X of the magnetic field is compared for raw and processed data and related anomalies to observe the changes made by the characteristic curve method and its application in geomagnetic prediction studies. The first earthquake is shown in Figure (4) and the second earthquake in Figure (5).

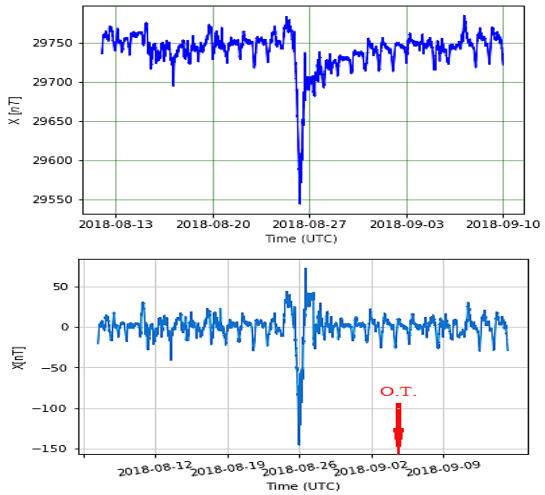

Figure 5. Curves of nature related to raw data (unprocessed, figure above) and data processing along with the time of the first earthquake for the magnetic component (X) (figure below).

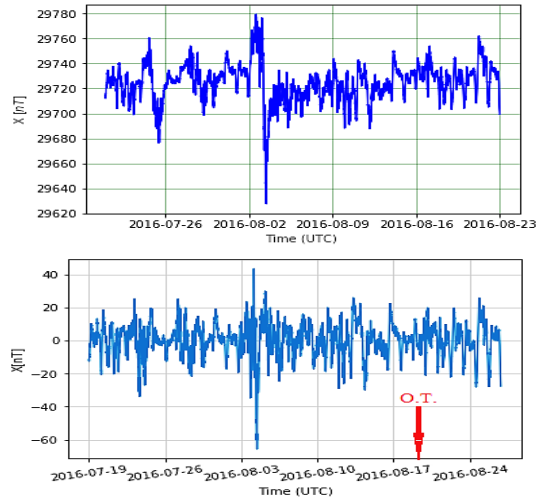

Figure 6. Curves of nature related to raw data (unprocessed, figure above) and data processing along with the time of the second earthquake for

the magnetic component (X) (figure below).

By comparing these two earthquakes, which are related to close geographical points and have approximately equal magnitudes (6.6 and 0.6), it was found that the earthquake of 05/09/2018 occurred at a depth of 35 km and the earthquake on 20/08/2016 Occurred at a depth of 10 km. As shown in Figure (7), the focal mechanism of earthquakes is inverse.

Figure 7. Focal mechanism of earthquake 05/09/2018 (left) and earthquake 20/08/2016 (right).

As shown in the diagrams, between these two earthquakes, the earthquake that occurred at a greater depth has a higher CLVD and has a more non-tectonic component and has a more specific anomaly.

CONCLUSIONS

Based on the obtained results and the processing performed on the magnetic records of three geomagnetic stations in Japan, abnormalities related to the change in the magnetic field have been identified. Finally, by comparing these two identified earthquakes, an earthquake that occurred at a greater depth has a higher CLVD and a more specific anomaly.

ACKNOWLEDGEMENTS

The Intermagnet is appreciated for providing access to the digital geomagnetic data used in this study.

REFERENCES

Dobrovolsky, I.P., Zubkov, S.I. & Miachkin, V.I., 1979. PAGEOPH (1979) 117: 1025. doi:10.1007/BF00876083

Edwin, P. and Roberts, B., 1983. Wave propagation in a magnetic cylinder, Sol. Phys., 88, 179.

Ghamry, E., Yumoto, K. and Yayama, H., 2013. Effect of SC on frequency content of geomagnetic data using DWT application: SC automatic detection. Earth Planets Space, 65, 1007-1015.

Hayakawa, M., Httori, K., and Ohta, K., 2007. Monitoring of ULF (Ultra-Low-Frequency) Geomagnetic variations associated with earthquakes. Sensors, 7, 1108-1122.

INTERMAGNET (hosted by Natural Resources Canada, G. O. (2018, June 18). INTERMAGNET. Retrieved from http://intermagnet.org/index-eng.php.

Meloni A., Mele G. and Palangio P., 1995, Tectonomagnetic field observations in central Italy 1989-1995, Physics of Earth and Planetary Interiors, vol 105, pp 145-152.

Liu J.Y, Chen C.H, Chen Y.I. and Yen H.Y., (2006, Seismo-magnetic anomalies and M $\geqslant$ 5.0 earthquakes observed in Taiwan during 1998-2001, Physics and Chemistry of the Earth, 2006, vol. 31, pp 215-222.

Rikitake, T., 1976. Earthquake Prediction, Elsevier Scientific Publishing Company.

Recognition of pre- and co-seismic electromagnetic signals in magnetotelluric measurements: a case study in the northern region of Algeria

Ahmed Seddik. Kasdi[1,2], Mohamed. Hamoudi[2], Abderrezak. Bouzid[1] and Naïla. Kerbadj[1,2]

[1] Center of Research in Astronomy, Astrophysics and Geophysics, Subsurface Geophysics Division, 16340, BP 63 route de l'Observatoire Bouzarèah, Algiers, Algeria.

[2] University of Science and Technology Houari Boumediene, Department of Geophysics - FSTGAT, BP 32 El Alia Bab-Ezzouar, 16111, Algiers, Algeria.

Summary

Seismo-electromagnetic signals are anomalous electromagnetic (EM) signals related to seismic activity. In recent years, the northern part of Algeria has experienced numerous moderate earthquakes. This seismic activity provided a rare opportunity to study earthquake-related temporal patterns of EM signals using magnetotelluric (MT) measurements. In this paper, we present an analysis of the MT time series using wavelet transform for several cases where co-seismic EM signals were observed. We present the precursor signatures of two main earthquakes using the spectral polarization technique. The results of the wavelet analysis revealed the time-frequency characteristics of the co-seismic EM signal with a high spectral amplitude at different frequency ranges. The spectral polarization technique revealed the existence of anomalies related to the earthquake several hours before its occurrence. This anomaly is correlated with the Dst index. We inferred that the unusual pre-earthquake behavior is related to the precursor signature but not to the solar-terrestrial effect.

Keywords: Northern Algeria, Magnetotelluric, Earthquakes, Seismo-electromagnetic, Time Series Analysis

Introduction

Seismo-electromagnetic signals (SES) have been reported over a wide frequency range (Hattori et al. 2006 and references therein). These EM signals may be precursory (prior to an earthquake) or co-seismic (coinciding with earthquakes). The observation and analysis of these EM phenomena is being used for seismic prediction and to understand the subsurface physical mechanisms related to the generation of these EM signals.

Various physical mechanisms have been proposed to explain the pre-and co-seismic EM signals, such as piezoelectric effect, piezomagnetic effect, microfracture electrification, seismic dynamo effect, and electrokinetic effect (Molchanov and Hayakawa 1998; Ogawa and Utada 2000; Matsushima et al. 2002; Honkura et al. 2002; Huang, 2002; Kasdi et al. 2022). The focal zones are mainly characterized by mechanical deformations, or fracturing generates EM signatures during and before the earthquake in the ULF band (Dudkin et al. 2010).

Previous studies suggest that EM earthquake precursors have emerged as a potential candidate for short-term earthquake prediction (Hayakawa et al. 2007; Dudkin et al. 2010). In this study, we use the spectral polarization technique to identify seismogenic emissions. This method is more flexible with respect to other methodologies that exist for obtaining the precursory signatures (Hayakawa and Hobara 2010).

Northern Algeria is in an active seismic zone in the Mediterranean region. The seismic activity is the result of the convergence between the two main Afro-Eurasian plates. Over the last two decades, northern Algeria has experienced numerous moderate-to-strong earthquakes (Khelif 2019). The recent seismic activity in Northern Algeria provides an opportunity to observe and study SES.

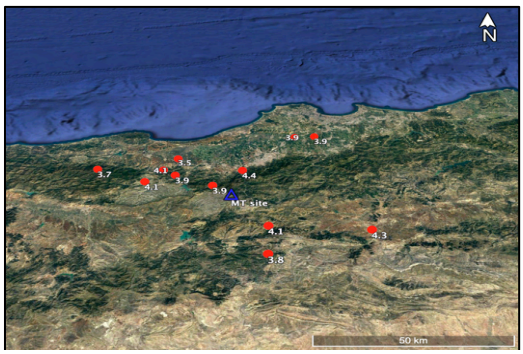

Figure 1. Map of the MT site and the distribution of earthquake epicenters cited in Tab 1.

Observational Database

The geomagnetic observatory of Medea, located about 60 km south of Algiers (Algeria), was chosen to conduct a MT experiment. The MT station was installed in December 2018 (labelled MT-site, Lat: 36.31° N, Log: 2.72° E). The station is equipped with an MTU-A System device from Phoenix-Geophysics. We measured the five components of the EM fields (Ex, Ey, Hx, Hy, and Hz). The sampling rate of the MTU-A is set to 15 Hz. Table 1 summarizes the origin time, position, magnitude, and epicentral distance (d) of earthquakes that

occurred near to the MT site where a co-seismic EM signal was observed in the MT time series. Figure 2 illustrates examples of the observed EM signals after the occurrence of the 4.4Mb earthquake cited in Table 1, where t=0 indicates the earthquake origin time. The distinct change in the components of the electric and magnetic fields a few seconds after the earthquake origin time marks a co-seismic EM signal related to the seismic events.

Date	Time	Lat °N	Lon °E	Mag (Mb)	d (Km)
26/09/2018	20:24:35	36.37	2.41	4.1	28.3
29/09/2018	08:00:09	36.35	2.65	3.9	08.6
29/09/2018	14:43:37	36.48	2.52	3.5	27.3
05/11/2018	16:51:56	36.43	2.24	3.7	45.4
12/12/2018	22:11:33	36.60	3.03	3.9	44.5
01/01/2019	04:26:12	36.42	2.47	4.1	26.2
13/05/2019	06:31:57	36.40	2.51	3.9	21.3
19/05/2020	21:06:03	36.06	2.82	3.8	27.7
13/08/2020	**08:04:48**	**36.42**	**2.75**	**4.4**	**14.9**
10/10/2020	15:52:48	36.60	2.95	3.9	40.3
23/12/2020	**18:36:52**	**36.15**	**3.16**	**4.3**	**43.2**
17/01/2021	02:59:56	36.17	2.83	4.1	17.2

Table 1. The location of earthquakes occurred near the MT site (from: https://www.emsc-csem.org).

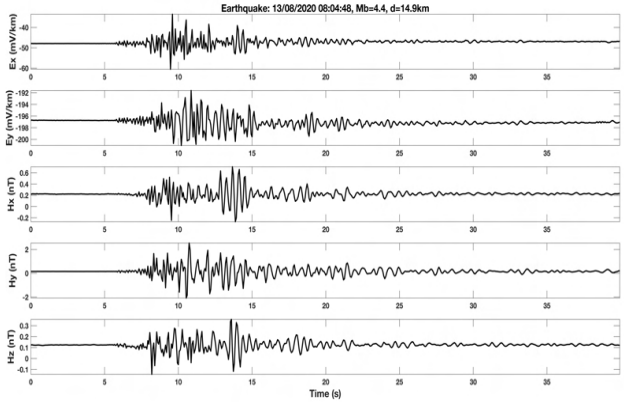

Figure 2. The observed time series data of the five magnetotelluric components measured at the MT site related to the 4.4Mb earthquake.

MT Time Series Analysis Methodology

Wavelet Analysis

Wavelet analysis (Morlet et al. 1982) is a powerful mathematical method in signal analysis that allows one to locate the temporal-frequency change in a time series. The wavelet transforms are further available in two forms, i.e., the continuous wavelet transform (CWT) deals with arbitrarily selected scales, A discrete wavelet transform (DWT) deals with only specific scales. CWT is more appropriate than DWT as it decomposes continuous-time functions into wavelets, whereas, in DWT, wavelets are discretely sampled (Lui and Najmi 1997).

Consequently, we used CWT to obtain the time-frequency representation for the MT time series. The wavelet spectral power values were derived in the 0.05–6 Hz frequency range. As an example, the five component wavelet spectra plots of the MT field signals components related to the 4.4Mb earthquake are presented in Figure 3.

Spectral Polarization Ratio Analysis

The polarization method is based on the measurement of the ratio of spectral power of the vertical magnetic field to the horizontal magnetic fields. This ratio is known to provide us with a lot of information, whether the observed variation is of ionospheric origin (or solar-terrestrial effect) or seismic-related. The polarization ratio analysis, has been demonstrated by prior studies to be effective, especially in the ULF range (Hayakawa et al. 2007; Yusof et al. 2019).

The procedures of the spectral polarization ratio analysis are briefly described. Hourly data is examined and a Fourier transform is applied to each hourly window. The method is repeated for the entire duration of the data set. We used a hamming function for windowing. The FFT transforms time-domain data into the frequency domain in terms of a power spectral density (PSD). The PSD spectrum was obtained in the frequency ranges between 0.05 and 1 Hz. The values of the amplitude spectra were averaged to attain an hourly mean (μ_{hourly_mean}). The normalization approach was implemented on the observation of the total duration of the data considered for this analysis to remove cyclic or daily variations. The standard deviation (σ_{std_td}) of the total duration of observation along with the mean of the data set (μ_{mean_td}) calculated for obtaining the normalized hourly value. The normalized hourly value $(N_{hour,k})$ calculated by using the above values is as follows;

$$N_{hour,k} = \mu_{hourlymean,k} - \mu_{mean\_td,k}/\sigma_{std_{td},k} \quad (1)$$

Here, k represents the three different geomagnetic field components (Hx, Hy, and Hz). 'td' refers to the total duration of data considered for this analysis. The spectral polarization ratio can be calculated using the following formula:

$$P_{Z/G} = N_{hour,H_z}/\sqrt{N^2_{hour,H_x} + N^2_{hour,H_y}} \quad (2)$$

Here, G indicates the total horizontal field components $(G = \sqrt{H_x^2 + H_y^2})$.

The spectral polarization ratio of different magnetic components shows an anomalous behavior before the earthquake (Yusof et al. 2019; Vijaya Kumar et al. 2021).

The spectral polarization technique has been implemented on the magnetic time series for two earthquakes, 4.4Mb and 4.3Mb mentioned in Table 1, respectively. The magnetic data is analyzed for earthquake precursors in the frequency band 0.05–1 Hz. The magnetic data was analyzed to determine the temporal variations of $P_{Z/G}$.

Geomagnetic index

In order to eliminate the effects of global geomagnetic activity and avoid false precursory signals, this study used a global geomagnetic index, namely the disturbance storm time (Dst) index, recorded during the same observation period. The Dst index is used to understand the difference between quiet and disturbed geomagnetic ambiance (Borovsky and Shprits 2017). The Dst index is derived on a one-hour basis from the H component measured by geomagnetic observatories at the middle to low latitudes. The Dst index was taken from the World Data Centre (Nose et al. 2015). A Dst index of less than -30 nT indicates solar activity known as a geomagnetic storm (Gonzalez et al. 1994).

Results and Discussion

The time-frequency representation obtained from the CWT supports the existence of co-seismic EM signals related to the seismic events. The analyzed MT components exhibit spectral enhancement in the frequency range of 2 Hz to high frequency (6 Hz in our case) for all of the earthquakes listed in table 1. The enhancement in the spectral content starts after a few seconds (8 to 15 seconds) of the onset of the mainshock of the earthquake. The increase in the spectral content after the mainshock depends on the epicenter distance as well as the magnitude of the earthquake.

Figure 4 demonstrates the hourly polarization ratio $P_{Z/G}$ (1st panel) and Dst index (2nd panel) from 10/08/2020 to 15/08/2020 (Fig. 4a) and 18/12/2020 to 24/12/2020 (Fig. 4b). The two earthquakes that occurred on 13/08/2020 (Mb = 4.4) and 23/12/2020 (Mb = 4.3) are represented by the vertical blue line. The threshold value defined $\mu p \pm 2\sigma p$ is consistent throughout the recorded duration. An anomalous peak appeared in the $P_{Z/G}$ panel before 10 and 32 h of the occurrence of the Mb = 4.4 and Mb = 4.3 earthquakes, respectively. We correlated these two peaks with the Dst index, suggesting that a value greater than -30 nT defines non-geomagnetic activity during this time. From these results, it is suggested that the anomalous peaks should be considered as precursors of the two earthquakes.

Conclusions

The installation of a MT station in the northern part of Algeria provided the opportunity to study SES. Co-seismic EM signals were observed during several earthquakes. Wavelet analysis has revealed the time-frequency content of the co-seismic EM signals observed simultaneously in the electric and magnetic field components. In the present work, we try to explain the precursor signatures using the spectral polarization technique. It is observed, for the frequency band 0.05–1Hz, a significant increase in the value of the polarization ratio several hours before the occurrence of earthquakes. After comparing the precursor results of each earthquake with the Dst index, we deduced that the unusual behavior before the earthquake is related to the precursor signatures.

These results will help in understanding the SES associated with earthquake activities in the North Algerian region. This kind of analysis should be carried out for many earthquakes to understand the seismo-electromagnetic phenomena.

Acknowledgements

This research was conducted with the support of the Research Center of Astronomy, Astrophysics and Geophysics (CRAAG, Algeria). Data collection was carried out using Phoenix Geophysics MTU-A system devices belonging to the Geophysics Laboratory (USTHB/Algiers). We thank the Geomagnetic Observatories (Kakioka [JMA], Honolulu and San Juan [USGS], Hermanus [RSA], INTERMAGNET, and many others for their cooperation to make the final Dst index available.

References

Borovsky J E, & Shprits YY (2017) Is the Dst index sufficient to define all geo-space storms? Journal of Geophysical Research: Space Physics, 122(11), 11-543

Dudkin F, Rawat G, Arora BR, Korepanov V, Leontyeva O, Sharma AK (2010) Application of polarization ellipse technique for analysis of ULF magnetic fields from two distant stations in Koyna–Warna seism-oactive region, West India. Nat Hazards Earth Syst Sci, 10:1513

Gonzalez WD, Joselyn JA, et al. (1994) What is a geomagnetic storm? Journal of Geophysical Research: Space Physics, 99(A4), 5771-5792

Hattori K, Serita A, Yoshino C, Hayakawa M and Isezaki N (2006) Singular spectral analysis and principal component analysis for signal discrimination of ULF geomagnetic data associated with 2000 Izu Island Earthquake Swarm. Physics and Chemistry of the Earth, Parts A/B/C, 31(4-9), pp.281-291

Hayakawa M, Hattori K, Ohta K (2007) Monitoring of ULF (ultra-low-frequency) geomagnetic variations associated with earthquakes. Sensors 7:1108–1122

Hayakawa M, Hobara Y (2010) Current status of seismo-electromagnetics for short-term earthquake prediction. Geomat Nat Hazards Risk 1(2):115–155

Honkura Y, Matsushima M, Oshiman N, Baris S, Ito A, Iio Y, Isikara AM (2002) Small electric and magnetic signals observed before the arrival of seismic wave. Earth Planets Space 54(12):e9–e12

Huang Q (2002) One possible generation mechanism of co-seismic electric signals. Proc Jpn Acad Ser B 78(7):173–178

Kasdi AS, Bouzid A and Hamoudi M (2022) Electromagnetic Signal Associated with Seismic Waves: Case Study in the North Central Algeria Area. Pure and Applied Geophysics, pp.1-15

Khelif MFA, (2019) La sismicité récente de la région algéroise. *Phd Thesis. Universite des Sciences et de la Technologie Houari Boumediene* (USTHB, Algeria), (in French)

Lui ATY, & Najmi AH (1997) Time-frequency decomposition of signals in a current disruption event. Geophysical research letters, 24(24), 3157-3160

Matsushima M, Honkura Y, Oshiman N, Baris S, et al. (2002) Seismo-electromagnetic effect associated with the Izmit earthquake and its aftershocks. Bull Seismol Soc Am 92:350–360

Molchanov OA, Hayakawa M (1998) On the generation mechanism of ULF seismogenic electromagnetic emissions. Phys Earth Planet Inter 105:201–210

Morlet J, Arens G, Fourgeau E, & Glard D (1982) Wave propagation and sampling theory—Part I & II: Complex signal and scattering in multilayered media. Geophysics, 47(2), 203-221

Nose M, Iyemori T, Sugiura M, & Kamei T (2015) World Data Center for Geomagnetism. Kyoto-Geomagnetic Dst index

Ogawa T, Utada H (2000) Coseismic piezoelectric effects due to a dislocation: 1. An analytic far and early-time field solution in a homogeneous whole space. Phys Earth Planet Inter 121(3–4):273–288

Vijaya Kumar, PV, Rawat, VS, Patro, PK, Gupta, AK and Babu, N (2021) Assessment and recognition of pre-and co-seismic electromagnetic signatures from magnetotelluric data: a case study from Koyna–Warna seismo-active region, India. Acta Geophysica, 69(1), pp.1-15

Yusof KA, Abdul Hamid NS, Abdullah M, Ahadi S and Yoshikawa A (2019) Assessment of signal processing methods for geomagnetic precursor of the 2012 M6. 9 Visayas, Philippines earthquake. Acta Geophysica, 67(5), pp.1297-1306

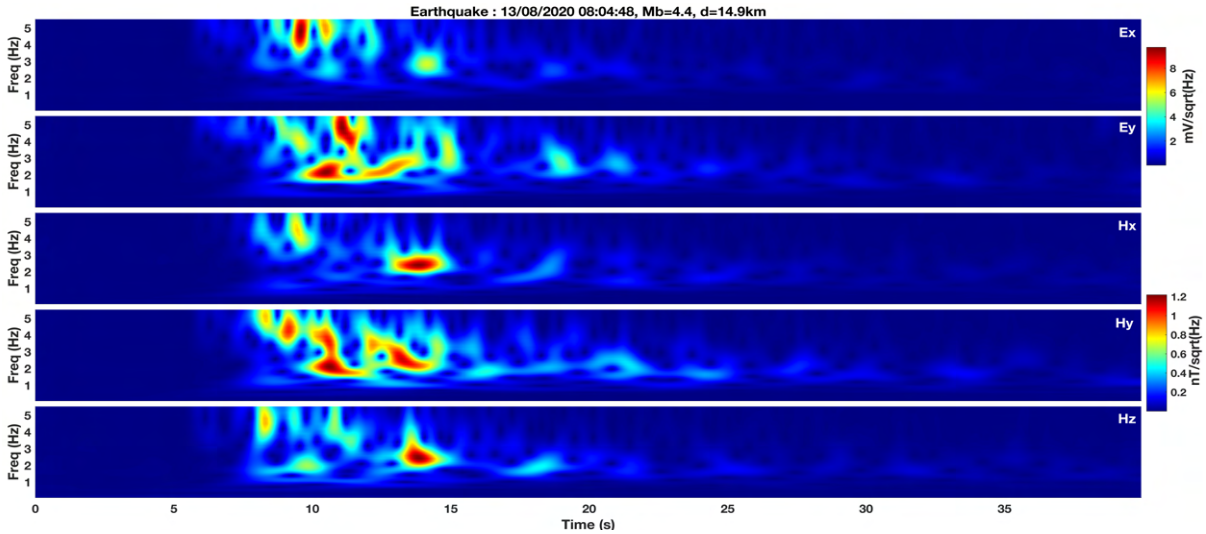

Figure 3. The wavelet power spectrum for the five magnetotelluric components time series data. The time t = 0 is the earthquake origin time. The used wavelet is the Morlet wavelet

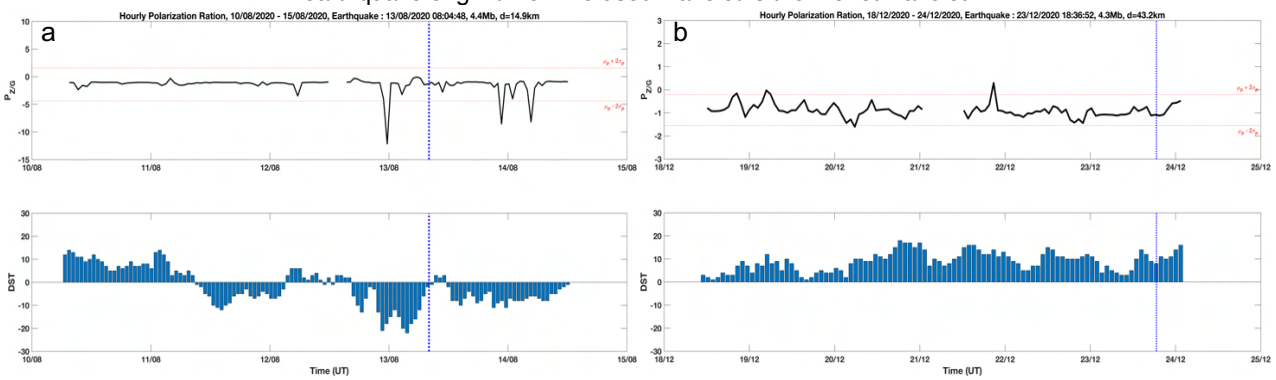

Figure 4. The temporal variation of the hourly spectral polarization of the component $P_{Z/G}$ (1st panel) and Dst index (2nd panel), (a) from August 10, 2020, to August 15, 2020, and (b) from December 18, 2020, to December 24, 2020. The vertical blue line indicates the earthquake origin time (August 13, 2020, Mb = 4.4 and December 23, 2020, Mb = 4.3 for a and b, respectively). The red dashed lines represent the threshold value ($\mu_p+2\sigma_p$) for Δf=0.05–1 Hz.

Investigation of Earthquake Swarm and Buried Geothermal Resources By Magnetotelluric, Gravity Modeling and Seismological Analyses of Upper Crust Structure of Yalova-Termal Region

E. Pekşen*[,1], D. Çaka[2], B. Tunç[3], B. Oruç[4], E. Budakoğlu[5], T. Türkmen[6], F. Sevim[7], D. Durdağ[8], K. Zengin[9], M. E. Erkan[10], G. Durdağ[11], Ş. Barış[12]

[1]Kocaeli University, ertanpeksen@kocaeli.edu.tr, [2]Kocaeli University, caka@kocaeli.edu.tr, [3]Kocaeli University, berna@kocaeli.edu.tr, [4]Kocaeli University, bulent.oruc@kocaeli.edu.tr, [5]Sakarya University, ebudakoglu@sakarya.edu.tr, [6]AFAD-Yalova, taylanturkmen@gmail.com, [7]TÜBİTAK-MAM Earth and Marine Sciences Research Group, fatih.sevim@tubitak.gov.tr, [8]Kocaeli University, dogukan.durdag@kocaeli.edu.tr, [9]Kocaeli University, zenginkaderrr@gmail.com, [10]Kocaeli University, eezgibabir@gmail.com, [11]Kocaeli University, gamzeayhandurdag@gmail.com, [12]Kocaeli University, sbaris@kocaeli.edu.tr

SUMMARY

In this study, velocity, resistivity, and density structure of Termal district and its surroundings were investigated. The seismic activity of the region was monitored for three years. During this period, 4792 earthquake data were read. 3D tomography of the region was obtained by performing the LOTOS program. Thus, the lateral and vertical distributions of seismic wave velocities were obtained from local earthquake tomography studies as well as Vp / Vs ratios. Resistivity distributions in three dimensions from 39 MT and TEM data were obtained in the vicinity of Termal district. As for the gravity method, the topography of basement in three dimensions was obtained up to 1.1 km using gravity data measured at 268 points. Density distributions of the corresponding area were estimated by an inversion method with the gravity data. Although the resolution of the three different geophysical methods performed in the study area varies, their results support each other.

Keywords: Local Earthquake Tomography, Magnetotelluric, Gravity, Geothermal, Earthquake

INTRODUCTION

The Armutlu Peninsula has very active seismicity. The study area and its territory has been monitored by an earthquake network station (Armutlu Earthquake Network Stations-ARNET) since 2005. The most important and highest of these activities as took place in August 2014. After this event, the earthquake activity of the Termal district and its vicinity for 3 years was monitored using the ARNET by adding 8 temporary stations to the existing network more detail. The places where the station to be established were determined specifically. To do this, the measurements were taken in these locations whether the selected places were suitable for the earthquake station by analyzing the measured data. After locations of the temporary station were determined, the installation of earthquake stations was completed.

Beside earthquake data and tomography study, three different geophysical methods applied in the study area. These were Transient electromagnetic (TEM), magnetotelluric (MT) and gravity methods. Standard MT (EDI) files were created by analyzing the data of MT measurements. The static shift effect in the MT measurements was eliminated by using TEM measurements (Pellerin and Hohmann, 1990). Consequently, 3D MT data (impedances) was performed using ModEM software (Egbert and Kelbert, 2012; Kelbert et al., 2014). Gravity data were measured in the corresponding area and Bouguer anomaly map was obtained as well. 3D gravity inversion (Oldenburg, 1974) and 2D gravity density inversion (Constable et al., 1987) were achieved using gravity data. Earthquake data were collected and read from stations periodically. Using earthquake data, tomography results were obtained (Koulakov, 2009). By using all these methods and results, comments were suggested about the region. Alteration zones, fault and dyke systems, and intrusive intrusions associated with possible heat sources were modeled depending on the density variations.

GEOLOGICAL SETTING

The geological map of the study area is shown in Figure 1. Neotectonic features of the district of Termal and its surroundings was studied by Yiğitbaş et al. (2006). Thermal hot water is on the border of Gemiciköy formation and Kızderbent Volcanite in Termal. The boundaries of our study area are generally located in these two units according to the geological map of the Armutlu Peninsula. Our study area consists of Eocene younger units and Eocene older units. Eocene aged rocks are andesitic and basaltic volcanics (Akbayram, 2011; Genç et al, 2004).

METHODS

In this study, seismic tomography, MT, and gravity methods were applied to examine the earthquake activities, to understand the location of faults and the boundaries of the hot water reservoir in the region.

Seismic Tomography

To obtain the tomography result of the study area, 5228 earthquakes with Ml magnitudes ranging from 0.1 to 4.9 were utilized. The data set contains a total of 92642 phase, 49232 P and 43410 S readings. The local earthquake tomography study was carried out using the LOTOS algorithm (Koulakov, 2009). Thus, the velocity structure of the study area was obtained. Figure 2(a) shows the variation of Vp perturbations at 1 km depth. The variation of Vs perturbations is illustrated in Figure 2(b). Figures 2(a) and 2(b) are superposed on a digital elevation map of the study area and faults with all together.

Magnetotellurics

MT measurements were acquired at 39 locations. MT locations are shown in Figure 1 with orange squares. Four set of Metronix equipment were utilized to measure MT data with one of the equipment fixed at a reference point. After collecting the data, the data processing was applied to get EDI files. The inverse solution was applied to the measured TEM data. TEM result was applied to static shift correction. Thus, the corrected MT data was obtained. 3D MT inversion was achieved using ModEM program with the corrected MT data set. The inversion of 3D MT data are illustrated at 1 km depth in Figure 2(c). One can distinguished the difference between the scanned area by tomography and MT methods from Figure 2(a), (b) and Figure(c). The reason for this is the distribution of the earthquake and the MT stations.

Gravity

The location of the gravity measurement points is shown in Figure 1 with white circles. The gravity data were measured at 268 points. The gravity data requires some basic data processing as latitude, free-air, Bouguer, terrain corrections to obtain Bouguer anomaly map of the study area. The low pass filter was also applied to the data to get rid of some noise from the measurement. The base undulation at 1.1 km depth was estimated by 3D inversion algorithm. 3D inversion was developed by Oldenburg (1974). Besides the 3D inversion of gravity data, 2D inversion of some of profiles were inverted by Occam inversion to estimate density variation.

CONCLUSIONS

Seismic Vp and Vs velocities were obtained by local earthquake tomography. MT resistivity volume of the study area was achieved by a 3D MT inversion program. 3D undulation depth of the base was estimated by a 3D gravity program. The seismic velocity structure of the region was revealed in detail with the local earthquake tomography study. Although the Vp/Vs distributions were expected at high values due to the geothermal fluid, low Vp/Vs ratios were obtained, especially at a depth of approximately 1 km. We also observed that the earthquake focal depths were concentrated in regions where the Vp/Vs ratios change sharply laterally. The electrical resistivity sections modeled from the MT data provided a solution up to a depth of 3.5 km, where the geothermal resources that cause changes in the local earthquake tomography velocity sections. Gravity anomalies provided solutions for revealing shallow lineaments of the project area and distribution of density differences. Using spectral analysis of Bouguer anomalies, the depth of the metamorphic basement rock to the medium was estimated as 1.15 km. Further, the geometric structure of the basement rock, modeled by the Parker-Oldenburg algorithm, varies between 0.75-1.5 km. This rapid changes in a local area reveals the importance of tectonic forces in the structural deformation of the basement rock and magma activity feeding deep geothermal processes. We also suggest that the aquifer of Termal city needs to be characterized more details. The drilling activities around the study should be controlled by the local authority.

ACKNOWLEDGEMENTS

This study was supported by the Scientific and Technical Research Council of Turkey (TÜBİTAK) under grant 117Y184. We would like to thank to PhD. Cemal Kaya for MT data processing. Unfortunately, PhD. Cemal Kaya passed away very sadly. He had a very helpful personality. We will never forget him with his very good memories.

REFERENCES

Akbayram K (2011). İstanbul ile Sakarya Zonları Arasındaki Potid-İçi Kenedinin Armutlu Yarımadası Doğusu'ndaki Evrimi. PhD thesis, İstanbul Technical University, İstanbul.

Constable SC, Parker RL, Constable CG (1987). Occam's inversion: A practical algorithm for generating smooth models from electromagnetic sounding data. Geophysics, 52, 289-300.

Genç C, İşseven T, Keskin M, Tüysüz O (2004). Armutlu Yarımadası (KB) Eosen manyetik kayalarının petrolojik evrimi ve paleomanyetizma özelliklerinin araştırılması: *TÜBİTAK Project No: 102Y032.*

Egbert GD, Kelbert A (2012). Computational recipes for electromagnetic inverse problems. Geophysical Journal International, *189*(1), 251-267.

Kelbert A, Meqbel N, Egbert, GD, Tandon K (2014). ModEM: A modular system for inversion of electromagnetic geophysical data. Computers & Geosciences, *66*, 40-53.

Koulakov I (2009). LOTOS code for local earthquake tomographic inversion. Benchmarks for testing tomographic algorithms. Bulletin of the Seismological Society of America, 99, 194-214.

Pellerin L, Hohmann, GW (1990). Transient electromagnetic inversion: A remedy for magnetotelluric static shifts. Geophysics, *55*(9), 1242-1250.

Oldenburg DW (1974). The inversion and interpretation of gravity anomalies. Geophysics, *39*, 526-536.

Yiğitbaş E, Bozcu M, Aylan E, Gürer ÖF, Yılmaz K, (2006). Armutlu Yarımadası'nın Yalova Batısında kalan kesiminin morfotektonik-jeolojik niteliklerinin incelenmesi: *TÜBİTAK Project No:101Y068.*

Web of General Directorate of Mineral Research and Exploration. http://yerbilimleri.mta.gov.tr/home.aspx Accessed 29 July 2022

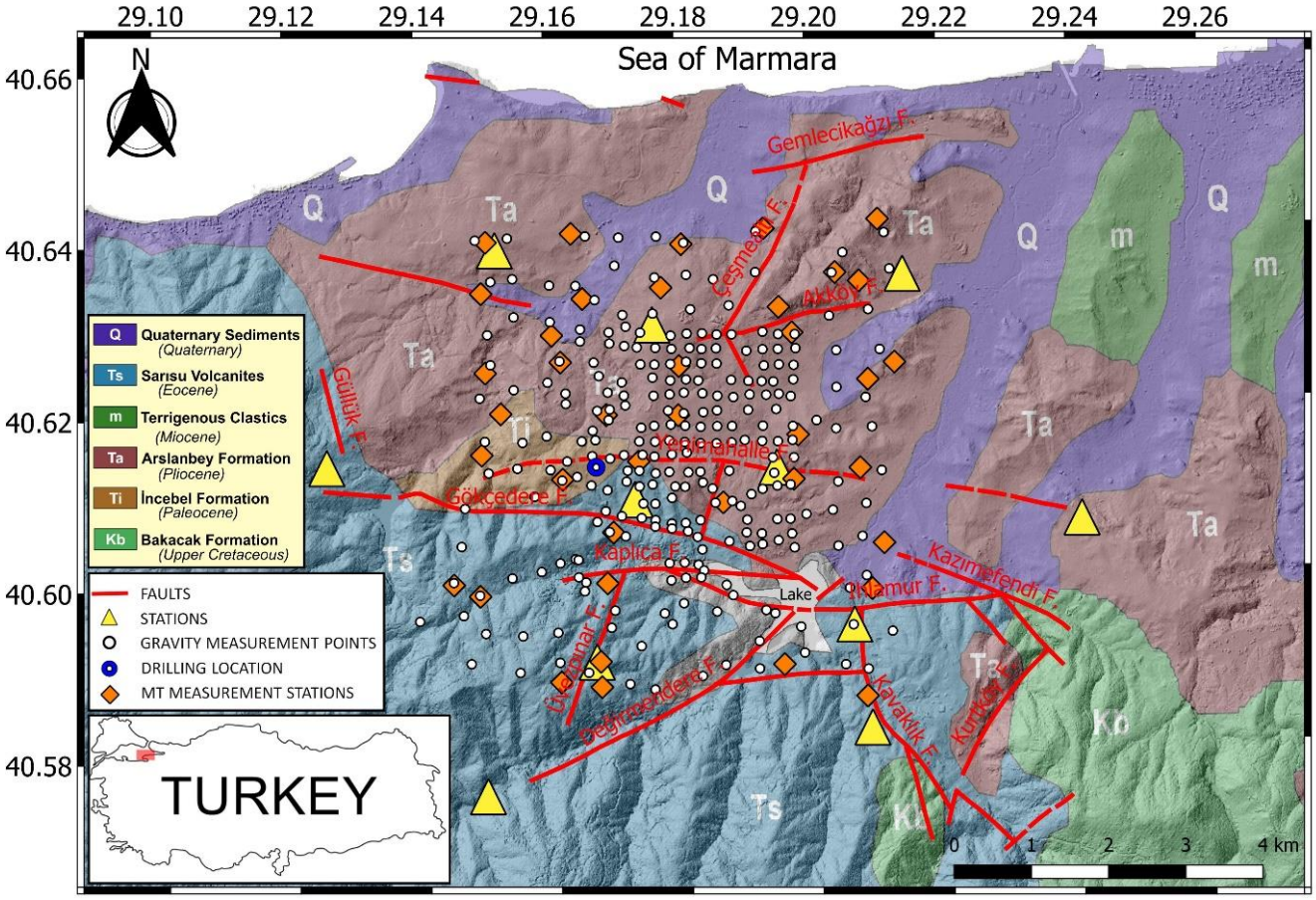

Figure 1. The geological map of the study area (Web of General Directorate of Mineral Research and Exploration). Faults are compiled by Yiğitbaş et al. (2006).

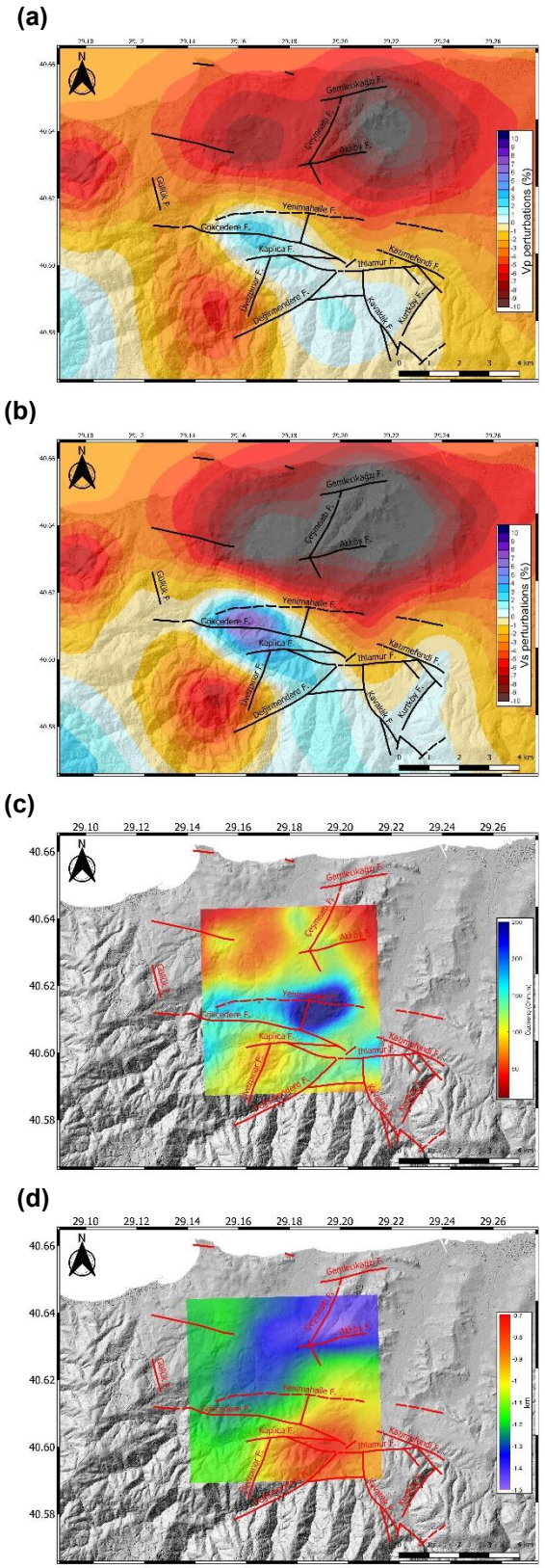

Figure 2 (a) Vp perturbations, **(b)** Vs perturbations, **(c)** MT resistivity variations, **(d)** Topography of basement at 1 km depth based on gravity data.

Assessment of geoelctric field variability in Yenisei-Khatanga oil and gas province and space weather hazards for infrastructure

E. Yu. Sokolova [1, 2], E. E. Marshalko [3], O. V. Kozyreva [2], I. S. Kupriyanov [1], D. V. Epishkin [4], G. E. Slinchuk [4, 5], D. V. Yakovlev [4]

[1] All-Russian Research Institute of Oil Geology, Moscow, Russia, sokol_l@mail.ru

[2] Schmidt Institute of Physics of the Earth, Russian Academy of Sciences, Moscow, Russia, kozyreva@ifz.ru

[3] Finnish Meteorological Institute, Helsinki, Finland, elena.e.marshalko@gmail.com

[4] Nord West Ltd, Moscow, Russia, dmitri_epishkin@mail.ru

[5] Moscow State University, Moscow, Russia, slin4ukgr@yandex.ru

SUMMARY

The geoelectric (telluric) field variability caused by the Earth's magnetic field disturbances during space weather anomalies is analyzed for the area of Yenisei-Khatanga regional through (YKRT) - a perspective oil and gas-bearing province located in Siberian Arctic within the auroral zone. For the analysis of telluric fields and estimation of their extreme values, we use a unique experimental magnetotelluric impedance tensor database collected by Nord West *Ltd* during the regional stage of the geophysical investigations of the trough and adjacent territories. The geoelectric field spatial-frequency distributions on the Earth's surface are calculated via the impedances and harmonic approximation of external geomagnetic excitation. The correlation of obtained distributions with geological map and MT array data helps to explain the position of the areas with maximal geoelectric field distortion accounting for their geological\geoelectrical heterogeneities.

Variations in time of telluric fields at a subset of YKRT MT sounding sites are synthesized via the impedance dependences on frequency and magnetic field time series recorded during intensive geomagnetic events at the nearest stationary monitoring sites. The snap-shoots of telluric field vectors' spatial distribution are presented for the characteristic time steps of the geomagnetic variations considered, specific features of these distributions are outlined. As geoelectric responses to rapid changes of external magnetic field are the drivers of geomagnetically induced currents (the most serious threat to the grounded industrial constructions in subpolar regions) the results of the study can be used to mitigate possible damaging space weather effects on operating and projected YKRT infrastructure facilities.

Keywords: geoelectric fields, geomagnetically induced currents, crustal heterogeneities, Yenisei-Khatanga regional trough and oil-gas-bearing province, auroral zone

INTRODUCTION

The theoretical and practical value of studying the Earth surface manifestations of space weather events significantly increased in the 21st century marked by the rapid economic development of high-latitude regions of Eurasia and North America. In the central sector of the Russian Arctic, of top priority are geomagnetically-induced currents' (GICs) problems in the oil and gas infrastructure.

This region offers experimental opportunities for such studies: a network of stationary magnetic observatories is being restored, large-scale arrays of magnetotelluric (MT) surveys are being collected in the frames of the hydrocarbon prospecting.

The geoelectric responses to the Earth's magnetic field rapid disturbances are drivers for most intensive GICs in earthen industrial constructions. So the analysis of geoelectric (telluric, **E**-) field variability for the territory of Yenisei-Khatanga oil and gas province, located within the highest level geomagnetic activity auroral zone (Fig. 1, 2), has clear relevance for studying possible negative space weather effects on the infrastructure facilities.

We present the results of such an analysis using the experimental data on 3D Earth conductivity and carried out this way for the first time in YKRT area.

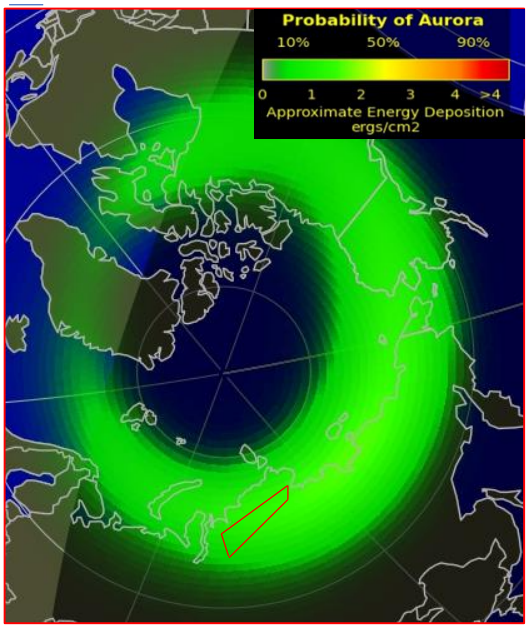

Figure 1. A case of NOAA Space Weather Prediction Center Aurora forecast (for 2022-07-01 19:41, UTC, NOAA Homepage). Red box marks the area of Yenisei-Khatanga regional trough (similar oil and gas province) on Taimyr peninsular.

Data And the Analysis Approaches

The study is based on unique collection of high quality broad-band MT impedance estimates for more than 650 (x_i,y_i) sounding sites assembled for YKRT by Nord West Ltd (Fig. 2, Slinchuk et al., 2022) during the regional phase of Taimyr peninsular geophysical investigations and applies two approaches to calculate geoelectric responses: in frequency and time domains, similar to (Lukas et al., 2018; Sokolova et al., 2019) .

The geoelectric field spatial-frequency distribution on the Earth's surface is calculated via all the ensemble of experimental **Z** tensors on the basis of classical dependence of telluric (**E**) and magnetic (**B**) fields with harmonic approximation of the plane-wave external magnetic excitation (Fig. 3).

Variation in time of telluric fields at a subset of YKRT MT sites are synthesized also in planar paradigm via the impedance frequency dependences and real time series of magnetic field on the base of stable forward and inverse Fourier transform routines. For calculations GIS INTEGRO (Cheremisina et al., 2022) are also used. Specially selected magnetic data were recorded during intensive space weather events at the nearest stations of the Russian Arctic geomagnetic monitoring network (Kozyreva et al., 2022) (Fig. 2).

The variation of the voltage in pipelines are estimated as simple line integral of vector $\mathbf{E}(x_i,y_i,t_j)$ estimates over pipe geometry for a set of fixed time steps t_j.

Discussion of the Results

The variability of the geoeletric fields on the area of Yenisei-Khatanga trough are represented in the study results by spatial distributions of the amplitudes of horizontal electric field $\mathbf{E}(x_i,y_i,T)$, induced by the homogeneous harmonic 1 nT geomagnetic field $\mathbf{B}_h(T)$ oriented geographically N-S and E-W for number of characteristic periods (Fig. 3). The temporal variability is described through $\mathbf{E}(x_i,y_i,t)$ variations with time, synthesized on magnetic storm or sub-storm records in NOK and DIK for some YKRT sites(x_i,y_i) representin different geoeletric structures. Also snap-shoots of telluric field $E(x_i,y_i,t)$ vector spatial distribution are presented for the characteristic time steps t_j of the geomagnetic variations considered.

YKRT stretches for over 1,000 km and has nearly 20 km-thick MZ sedimentary cover (electrical resistivity of 5-20 Ohm·m) with several basement uplifts geophysically established within the trough bed. It is surrounded by East Siberian Platform in the South and the Taimyr orogen in the North, which are composed of Paleozoic and older consolidated sedimentary\metamorphic complexes (100-400 Ohm·m) partially, penetrated by even more resistive intrusive bodies and broken by faults (Fig. 2). Spatial distributions over the YKRT area of effective apparent resistivity estimated on regional impedance collection reflect these geoelectrical contrasts at corresponding skin depths. The correlation of obtained **E**-field variability maps (amplitude for specific frequencies) and vector snap-shoots (for specific time steps of magnetic storms) with geological and resistivity data helps to explain the significant features of geoelectric distortions' field as products of 3D geological\geoelectrical heterogeneities.

Both maps of spatial geoelectric responses and time series of synthetic **E**-fields provide the ideas of possible extreme values/directions of geoelectric variations on the studied area, which are correspondent with but give much more details then similar small scale maps constructed recently in (Kozyreva et al. 2022) for central segment of Russian Arctic on the base of global 3D conductivity model (Alekseev et al., 2015).

The geo-induced voltage across operating and projecting pipelines in the region, calculated on synthetic geoelectric field time series, can exceed the regular levels of pipeline cathodic protection.

Conslusion

Our study describes the spatial and temporal variability of geoelectric field on the territory of perspective Yenisei-Khatanga oil and gas province. This component of the Earth's electromagnetic sphere is the main prerequisite for calculations of GICs in grounded technological systems, particularly – in pipelines. The following inferences seems to be useful for mitigation of possible

destructive impacts of space weather on operating and future YKRP infrastructure facilities.

- For an adequate assessment of these risks it is necessary to carefully analyze the geoelectric structure of the area where a facility to be constructed. Heterogeneities in the distribution of electrical conductivity of the Earth's crust are the major factor for the GIC patterns, by damping or, in opposite, significantly amplifying amplitudes of the currents and modulating the spectral composition. The most sever GICs are foreseen in the frames of YKRT, where perspective for hydrocarbons, resistive and highly heterogeneous in geoelecrtic properties Paleozoic formations are spread. The maps describing variability of regional geoelectric fields can serve as space weather hazard maps for subpolar oil and gas provinces.
- The estimates of vectors of the horizontal geoelectric field **E**(x,y,T), induced by the harmonic oscillations $\mathbf{B}_h(T)$, vary greatly in magnitude and direction. At frequencies that carry most of the disturbed field's energy, they have the maximum amplitudes in the range from <1 to ~50-100 mV/km at a unit amplitude of external magnetic field variations. Thus, even with moderate amplitudes of geomagnetic variations during substorms (300-500 nT), their geoelectric responses in the area of Pz formations can reach 15 V/km and more. As synthesized E-field time series reveal, during considered real mild magnetic storm (Dst ~-60 nT) telluric field variations for several geoelectrical structures of the YKRT might have exceeded 5-7 V/km.
- Voltage variations estimated using as input data synthetic time series of the geoelectric field in sites along projected or operating (Messoyaha-Norilsk) pipelines might be rearded as threshold values' objective porxi for cathodic protection scheme design/optimization for mitigation of severe spase wether impacts.

ACKNOWLEDGEMENTS

The studies were carried out as part of state assignments of All-Russian Research Institute of Oil Geology and Schmidt Institute of Physics of the Earth, Russian Academy of Sciences as well as by geophysical company Nord West Ltd and grant 314670 of the Academy of Finland.

REFERENCES

Alekseev D., Kuvshinov A., Palshin N. (2015) Compilation of 3D-global conductivity model of the Earth for space weather applications. Earth, Planets and Space.. 67:108. doi:10.1186/s40623-015-0272-5

Cheremisina E. N., Finkelstein M. Ya., Spiridonov V.A., Lubimova A.V. (2022) Chapter 6.5 - New computer technology to solve geological problems for prospecting and exploration of mineral resources. In: Moitra A.K., Kayal J.R. et al. (ed) Innovative Exploration Methods for Minerals, Oil,Gas, and Groundwater for Sustainable Development. Elsevier, Kolkata, p. 439-453. doi.org/10.1016/B978-0-12-823998-8.00056-9

Kozyreva O.V., Pilipenko V.A., Marshalko E.E., Sokolova E.Yu., Dobrovolsky M.N. (2022) Monitoring of Geomagnetic and Telluric Field Disturbances in the Russian Arctic. Appl. Sci. 2022. V. 12. P. 3755. doi.org/10.3390/app12083755

Lucas G.M., Love J.J., Kelbert A. (2018) Calculation of voltages in electric power transmission lines during historic geomagnetic storms: An investigation using realistic earth impedances // Space Weather.. V. 16. P. 185–195. doi.org/10.1002/2017SW001779

Slinchuk, G.Ye.E., Yakovlev, D.V., Yakovlev, A.G., Andreev, M.A. and Shirokova, Ye.P. (2022) A depth three-dimensional geoelectrical model of Taimyr. Physics of the Solid Earth, 2022, No. 5, Accepted.

Sokolova, E.Yu., Kozyreva, O.V., Pilipenko, V.A., Sakharov, Ya.A. and Epishkin, D.V. (2019) Space-Weather-Driven Geomagnetic- and Telluric-Field Variability in Northwestern Russia in Correlation with Geoelectrical Structure and Currents Induced in Electric-Power Grids. Geophysical Processes and Biosphere, No. 18, Iss. 4: pp. 66–85. DOI: 10.21455/GPB2019.4-7

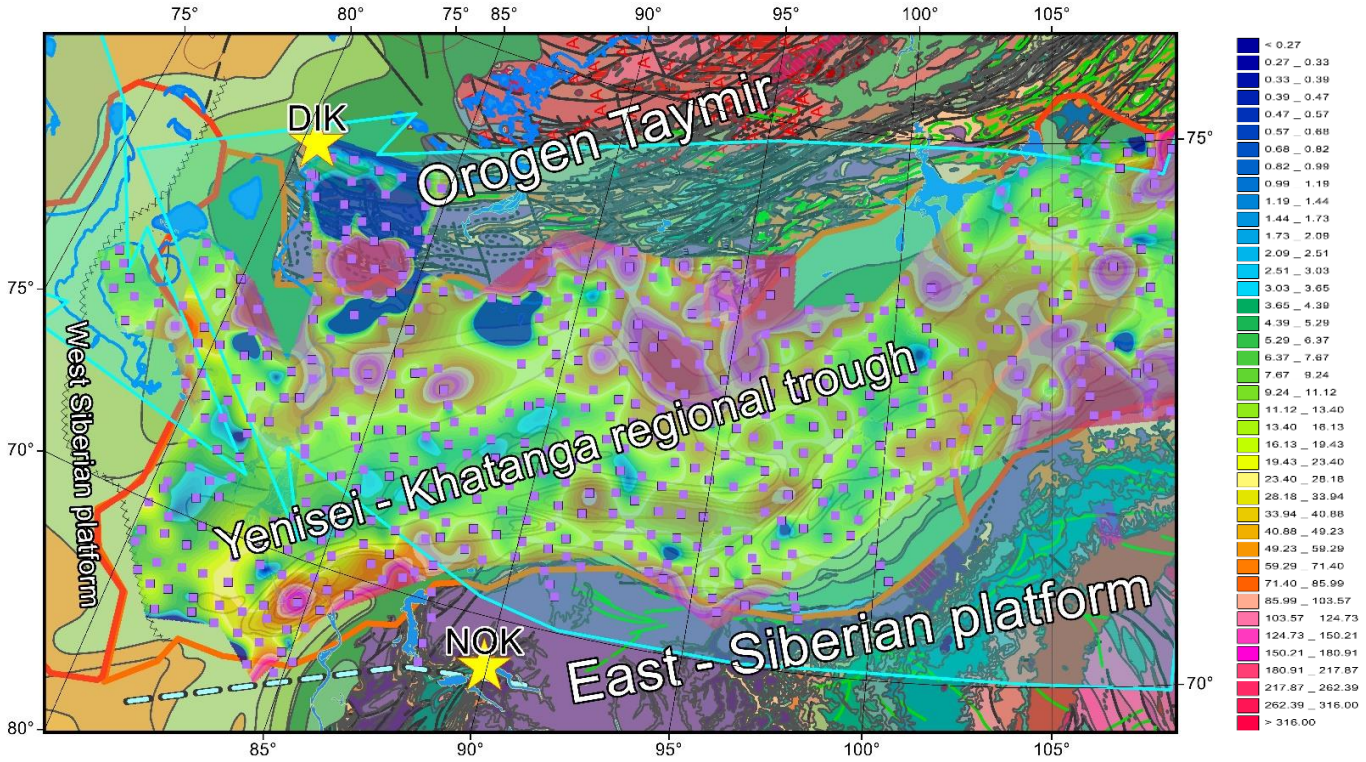

Figure 2. Yenisei-Khatanga oil and gas province MT sounding sites (Slinchuk et al., 2022) (purple squares inside orange contour line) and the nearest magnetic stations (DIK- Dikson, NOK- Norilsk, yellow stars) on the background of the regional geological map on Northern margins of East Siberian platform and distribution of corresponding effective apparent resistivity estimates (for T=100c), according to the color palette (in Om·m). Blue dotted line – operating Messoyakha-Norilsk gas pipe. Transparent blue arrows show a schematic position of western and eastern electrojets at local midnight on the meridian 100°E.

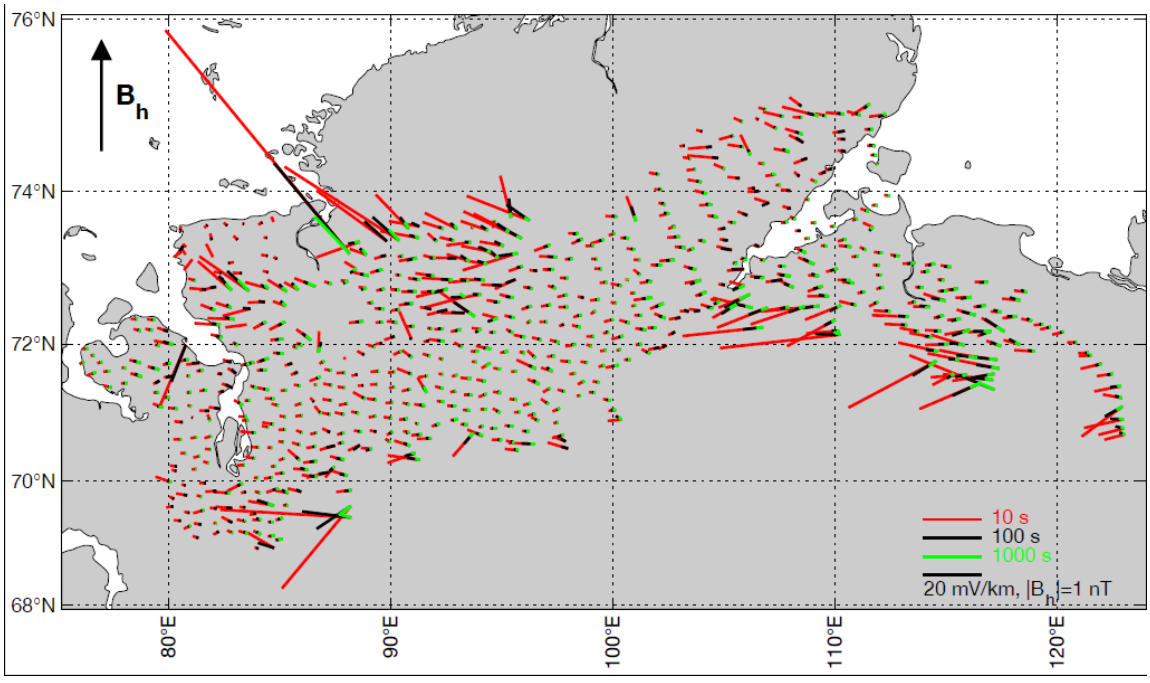

Figure 3. Spatial distribution on the Yenisei-Khatanga trough of the experimental impedance data-based vectors of the horizontal geoelectric field **E**(x,y,T), induced by the homogeneous harmonic geomagnetic field $\mathbf{B_h}$(T) with an amplitude of 1 nT and oriented geographically N-S, for the periods T=10 s (red), 100 s (black), and 1000 s (green). The scale bars show 20mV/km length of geoelectric field vectors.

Induction Responses from Magnetotelluric Transfer Functions in Southland, New Zealand

K. Pratscher[1], M. Ingham[2] , W. Heise[3], T. Bertrand[4], D. Mac Manus[5], C. Rodger[6], M. Dalzell[7], T. Petersen[8]
[1]Victoria University of Wellington, Wellington, New Zealand, Kristin.Pratscher@vuw.ac.nz
[2]Victoria University of Wellington, Wellington, New Zealand, Malcolm.Ingham@vuw.ac.nz
[3]GNS Science, Lower Hutt, New Zealand , W.Heise@gns.cri.nz
[4]GNS Science, Lower Hutt, New Zealand , T.Bertrand@gns.cri.nz
[5]University of Otago, Dunedin, New Zealand, craig.rodger@otago.ac.nz
[6]University of Otago, Dunedin, New Zealand, macda381@student.otago.ac.nz
[7] Transpower New Zealand, Wellington New Zealand, michael.dalzell@transpower.co.nz
[8]GNS Science, Lower Hutt, New Zealand , T.Petersen@gns.cri.nz

SUMMARY

The impact of geomagnetically induced currents (GIC) on the New Zealand power grid has previously been studied using a thin-sheet model of electrical conductance variations across the country. Due to its relative proximity to the auroral zone observed GIC are greatest in the south of the South Island in the Otago/Southland region. Recent acquisition of 62 long period magnetotelluric (MT) sites in this region provides the opportunity to better understand how GIC are related to the conductivity structure and tectonics. MT 1Hz impedance data in the period range between 10 and 10000 seconds have been combined with 1s resolution magnetic data to calculate the induced electric fields during the 2015 St. Patrick's Day Storm. Direct current measurements from sensors installed along the transmission network are compared with the induced electric fields to analyze the GIC and phases of the storm in detail.

Cumbre Vieja volcanic eruption (La Palma, Canary Islands): Magnetotelluric monitoring experiment

P.Piña-Varas[1], J. Ledo[2], D. Martínez Van Dorth[3,4], P. Queralt[1], I. Cabrera Pérez[3], L. D'Auria[3,4], N. Pérez[3,4]

[1] Department Dinàmica de la Terra i de l'Oceà, Universitat de Barcelona, Barcelona, Spain. p.pina@ub.edu.
[2] Physics of the Earth and Astrophysics, Faculty of Physics, Universidad Complutense de Madrid, Spain
[3] Instituto Tecnológico y de Energías Renovables (ITER), 38600 Granadilla de Abona, Tenerife, Canary Islands, Spain
[4] Instituto Volcanológico de Canarias (INVOLCAN), 38320 San Cristóbal de La Laguna, Tenerife, Canary Islands, Spain

SUMMARY

The last volcanic eruption in the Canary Islands took place in La Palma (September 19th - December 14th, 2021). For over 90 days the so-called Cumbre Vieja volcano was active, the longest volcanic eruption ever registered in this island, which represented a unique opportunity to assess the electrical resistivity changes related to this type of activity. On the one hand, the presence of magma generates strong resistivity contrasts with the hosting units, since magmas contain dissolved water in their composition that reduces its resistivity. On the other hand, the whole hydrothermal system which was characterised by the 3-D resistivity model of La Palma Island performed in 2019 will be most likely modified by the strong changes associated to this new geodynamic context. Under these circumstances, several experiments have been performed in the island since the beginning of the volcanic eruption, in order to understand the changes of the electrical resistivity associated to the magma intrusion, as well as the potential of the magnetotelluric method for the volcanic monitoring. Here, we present some preliminary results of this monitoring experiment, where important changes on the electrical properties of the subsoil have been detected and correlated to other information available, such as the seismicity. Additionally, the tests conducted against the 3-D resistivity model of the island (baseline model performed in 2019) help to understand the meaning and implications of such changes. These results remain preliminary, but they are definitely encouraging, as demonstrate the potential of the magnetotelluric method for the volcanic monitoring activities.

Keywords: Magnetotelluric 3D, volcanic monitoring, Canary Islands.

Geothermal exploration via magnetotelluric surveys in non-volcanic geothermal fields in northern Thailand

P. Amatyakul[1], T. Rung-arunwan[2], C. Vachiratienchai[3] and W. Siripunvaraporn

[1] Department of Physics, Faculty of Science, Mahidol University, Thailand, puwis.ama@mahidol.ac.th

[2]Curl-E Geophysics Co., Ltd., Thailand, t.rungarunwan@gmail.com

[3]Curl-E Geophysics Co., Ltd., Thailand, chatchai.vac@gmail.com

[4] Department of Physics, Faculty of Science, Mahidol University, Thailand, wsiripun@gmail.com

SUMMARY

Thailand's geothermal fields are non-volcanic and mostly located in northern part of the country where there are relatively high tectonic activities. Government agencies had conducted the geothermal potential assessment projects for electricity generation in 4 geothermal fields distributed around Chiang Mai, Chiang Rai, and Mae Hon Son provinces. Magnetotelluric (MT) surveys were then proposed and conducted in the mentioned provinces. More than 150 MT stations were deployed during 2013 – 2018, mainly to locate shallow geothermal reservoir and delineate the geothermal system in each area. The 3D resistivity models with the investigation depth of up to 2,000 meters were then obtained from the off-diagonal components of the impedance tenser within the frequency ranging from 3,000 – 0.003 Hz. The resistivity feature in all areas share the similar manner relating to the non-volcanic geothermal system: (1) the conductive geothermal reservoir (2) the conductive hydrothermal alteration zone (3) fluid pathway in term of fault and fracture, and (4) resistive granite heat source. To assess the potential in electricity generation, the testing boreholes were then proposed using the model derived from MT surveys. Several drillings were success in producing the hot water from the shallow reservoirs. In addition, the borehole results help confirming the reliability of the 3D resistivity models and reveal an important relation between resistivity structure and the geological targets.

The case study from the Mae Chan hot spring (MCH) in Chiang Rai province and the Fang hot spring (FGH) in Chiang Mai province also demonstrate the development made in the past ten years since the 3D MT survey was introduced to the local agencies in the early of 2010s. MT surveys of the first phase in those fields started with a very sparse clusters of MT stations to get the big picture of the geothermal system. The detailed MT surveys with denser MT stations (up to 50 meters) were then conducted in the focusing area pinpointed by the previous phase of the survey. The drilling results mostly agreed with resistivity model of both MCH and FGH which will be used as a guidance in future developing production and re-injection wells. The strategy and procedures used in these geothermal explorations can be shared with other non-volcanic geothermal exploration in Thailand and worldwide.

Keywords: geothermal exploration, magnetotelluric survey, northern Thailand

CSEM/MT imaging for deep EGS geothermal project derisking in the Upper Rhine Graben (France)

Mathieu Darnet[2], François Bretaudeau[2], Pierre Wawrzyniak[2,], Jean-François Girard[3], Guy Marquis[3], Vincent Maurer[1], Albert Genter[1],

[1]*ES-Géothermie, 5 Rue de Lisbonne 67300 Schiltigheim – France.*
[2]*BRGM, 3 Avenue Claude Guillemin 45000 Orléans – France*
[3]*EOST, 5, rue René Descartes 67000 Strasbourg – France*

SUMMARY

In the present paper, we present a combination of 3D Controlled-Source Electromagnetics (CSEM) and Magnetotellurics (MT) adapted to image electrical resistivity of deep granitic fractured reservoirs. This method is applied in the Upper Rhine Graben (URG) to locate and describe accurately the geothermal resource in order to reduce the risk of future Enhanced Geothermal System (EGS) projects planned in this area. Electrical resistivity logs data from Soultz-sous-Forêts geothermal wells (Alsace, France) have been used to design an optimal survey, since knowledge of resistivity variation in the sedimentary cover is required to properly image deep fluid circulation. As a validation step, a large-scale 3D CSEM/MT acquisition campaign was carried out to cover 150 km2 in Northern Alsace.

Keywords: geothermal reservoirs, EGS, electrical resistivity logs, CSEM, MT

INTRODUCTION

Electricity and heat production using Enhanced Geothermal System (EGS) technology rely on our knowledge and prediction capacity of hydrothermal fluid property, mainly temperature and flow rate. Most of hydrothermal fluid properties are obtained from post-drilling phases, whereas proxy information is hard to access in an economically viable way. The main challenge is then to develop methods to access these properties at the early stage of the exploration phase.

Deep fractured reservoirs are usually characterized by non-destructive geophysical methods (seismic, gravity, etc.). However, these techniques have a low sensitivity to geothermal fluids and so, do not predict accurately the geothermal resource, and more particularly the flowrate, before drilling operation.

Due to their sensitivity to fluids and particularly brine water in rocks (Archie, 1942), passive electromagnetic (EM) techniques (e.g. Magnetotellurics or MT) or active (Controlled-Source Electromagnetic or CSEM) have been traditionally used to investigate the subsurface conductivity. EM methods have shown to be effective to characterize geothermal reservoir geometry in volcanic area (Munoz, 2014), hydrocarbon reservoir geometry in offshore sedimentary area or onshore mineral exploration. Nevertheless, the ability of EM methods to image targets with high geothermal potential in deep fractured reservoir and in a high man-made noise environment still need to be demonstrated. Indeed, CSEM sources must compete with high noise levels and a conductive sedimentary cover resulting in low signal to noise ratio. In the framework of DEEP-EM project, we propose to adapt EM methods layout and imaging techniques to overcome these constraints and so reduce the risk of EGS projects exploration.

The benefit of the developed method will not be limited to deep fractured reservoirs but could be adapted to different settings like shallow geothermal reservoirs (e.g. Dogger layer in Paris Basin) and used to characterize other kinds of fluid content (e.g. CO2 storage).

Design of the CSEM exploration campaign using electrical resistivity logs

For about thirty years, the Upper Rhine Graben (UGR) has been a main target for research on geothermal exploration in deep fractured formations. Favorable targets are mainly deep and fractured hard rocks. In the last twenty years, geothermal activity in the Upper Rhine Graben has been on-going with several French (Soultz-sous-Forêts, Rittershoffen, Vendenheim, Illkirch), German

(Landau, Insheim, Bruchsal, Bruhl) and Swiss (Riehen, Basel) deep geothermal sites which are active from exploration to exploitation. All these projects deal with deep fractured geothermal reservoirs located within Triassic-sediments and/or crystalline basement (Aichholzer and al., 2016).

Predictive modelling suggests that CSEM anomalies in sedimentary basins are controlled at first order by the sedimentary cover resistivity (layer geometry and resistivity variation between and within the layers) and in a second order by hydrothermal fluid circulations. Hence, the knowledge of resistivity variations in the sedimentary cover is required to properly image deep fluid flow with high accuracy.

The Soltz-sous-Forêts and Rittershoffen (Alsace, France) geothermal wells data have provided electrical resistivity logs to study the electrical signature of deep fluid circulations. Preliminary results show a conductive trend for hydrothermally altered fractured zones and a highly resistive trend for unaltered facies (Figure 1) and hence a strong link between conductivity and permeable zones.

These results will help to design an appropriated acquisition campaign, since investigation and resolution depth in EM measurements mainly depend on formation resistivity and on the transmitted frequency (Zonge and Hughes,1991).

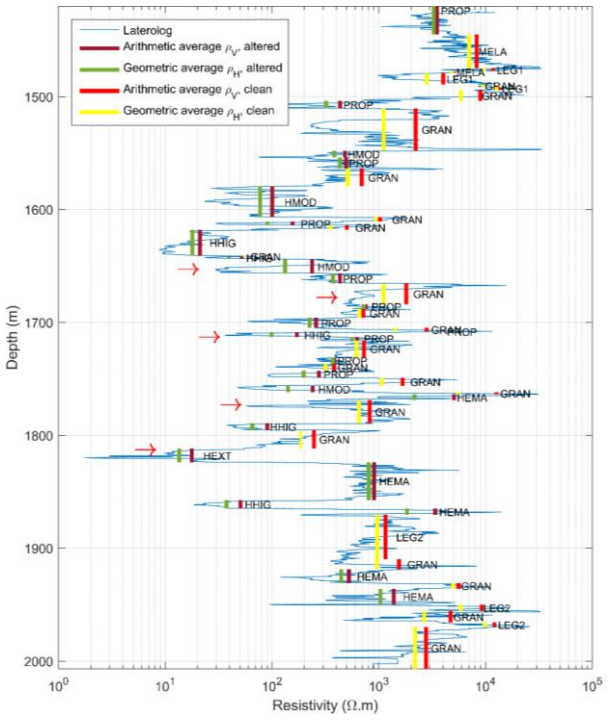

Figure 1. GPK1 resistivity laterolog in granite (geothermal well from Soultz-sous-Forêts) linked with cuttings observation. Red arrows correspond to the position of the main permeable fracture zones (Genter and al., 1997). Red and yellow line correspond to resistivity average for unaltered facies and green and purple to altered facies. GRAN: Biotite porphyritic standard granite. PROP: Propylitised biotite porphyritic granite. MELA: Biotite-rich granite. LEG1: Leucogranite 1. LEG2: Leucogranite 2. HEMA: Hematitised biotite porphyritic granite. HMOD: Moderately altered granite. HHIG: Highly altered granite. HEXT: Extremely altered granite (Traineau and al., 1991).

Field trial and exploration campaign

A CSEM/MT field trial (12 receivers (RX) installed every kilometre between Soultz-sous-Forêts and Rittershoffen plants) was performed to validate the design of a large-scale exploration campaign. The main goal of this test was to prove that despite the anthropogenic noise in the area, the CSEM setup was appropriate to image resistivity variations in the deep fractured granitic basement. In particular, the distance (~3km) between electrodes transmitter (TX) was increased that resulted in an amplification of the dipole moment (product of dipole length by an inject current intensity) and allowed to obtain a good signal to noise ratio more than 10km away from the TX.

CSEM data were inverted with MARE2DEM software (Key, 2016) and inversion results showed that the signal to noise ratio was sufficiently low to image resistivity variations within the basement. During the inversion process, the basement/sediments interface defined by seismic imaging was used to constrain the subsurface geometry to improve the vertical resolution of resistivity. Interestingly, inverted resistivity shows a good match with electrical resistivity logs within the sedimentary cover and granitic basement (Figure 2).

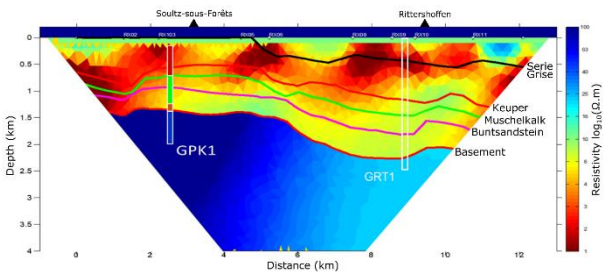

Figure 2. CSEM results from 2019 acquisition linked with the main formation isohypses. GPK-1 (Soultz-sous-Forêts) and GRT-1 (Rittershoffen) geothermal wells are located on the W-E profile (Figure 3). Electrical resistivity logs from GPK-1 show a good match with the inverted resistivity.

Three geothermal power plants projects consisting of quadruplets (2 injection wells and 2 production wells) are planned in Northern Alsace with the aim to reach temperatures over 150°C and flow rate over 250 m3/h per well. The results of this field trial have been used to define the acquisition parameters of a large-scale exploration campaign (6 transmitters and 100 receivers spread on 150km², Figure 3) carried out subsequently. It covered the whole exploration license and aimed at providing additional subsurface information to prioritize the geothermal areas of interest.

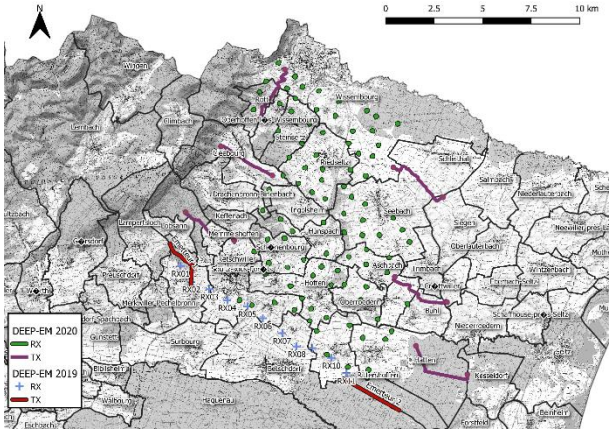

Figure 3. 3D CSEM/MT exploration campaign.

CONCLUSIONS

EM methods have been traditionally used to characterize shallow geothermal targets in volcanic context. The aim of DEEP-EM project is to develop these methods in order to use them for deep geothermal targets in sedimentary basins. Preliminary EM results showed the ability of resistivity measurements to provide information on deep fluid circulations at two different scales (borehole and reservoir). Electrical resistivity logs reveal a clear separation between altered/unaltered facies and furthermore a link between conductivity and permeable zones. At the reservoir scale, a CSEM field trial demonstrated the ability of the technique to image resistivity variations underneath a thick sedimentary cover (>1.4 km). These results have been used to design the acquisition of a large-scale EM exploration campaign and provide additional subsurface information to prioritize the geothermal areas of interest.

ACKNOWLEDGEMENTS

The authors wish to thank the ADEME (French Agency of Energy and Environment) in the framework of the DEEP-EM project. The authors acknowledge the GEIE EMC and ECOGI for their grateful help in this project.

REFERENCES

Aichholzer, C., Duringer, P., Orciani, S. and Genter, A.: New stratigraphic interpretation of the Soultz-sous-Forêts 30-year-old geothermal wells calibrated on the recent one from Rittershoffen (Upper Rhine Graben, France). Geotherm Energy 4, 13, (2016).

Archie, G. E.: The Electrical Resistivity Log as an Aid in Determining Some Reservoir Characteristics. Petroleum Transactions of the AIME, 146, (1942), 54–62.

Genter, A., Traineau, H. and Artignan, D.: Synthesis of geological and geophysical data at Soultz-sous-Forêts (France). Rapport BRGM R39440, (1997), 36.

Key, K.: MARE2DEM: a 2-D inversion code for controlled-source electromagnetic and magnetotelluric data. Geophysical Journal International, 207, (2016), 571–588.

Munoz, G.: Exploring for geothermal resources with electromagnetic methods. Surveys in geophysics, 35(1), (2014), 101-122.

Traineau, H., Genter, A., Cautru, J.P., Fabriol, H. and Chevremont, P.: Petrography of the granite massif from drill cutting analysis and well log interpretation in the HDR borehole GPK1 (Soultz, Alsace, France). Geothermal Science and Technology, 3, (1991), 1-29

Zonge, K.L., and Hughes, L.J.: Controlled Source Audio-Frequency Magnetotellurics. Investigations in Geophysics, (1991), 713-810.Baba K, Tarits P, Chave AD, Evans RL, Hirth G, Mackie RL (2006) Electrical structure beneath the northern MELT line on the East Pacific Rise at 15 degrees 45’S. Geophys Res Lett 33(22): L22,301

Cartwright J (2007) Big stars have weather too. IOP Publishing PhysicsWeb. http://physicsweb.org/articles/news/11/6/16/1. Accessed 26 June 2007

Integration of magnetotelluric data with ambient seismic noise and gravity models in order to characterize geothermal fault-controlled systems. The Vallès Basin case of study (NE Spain).

G. Mitjanas[1], J. Ledo[2], P. Queralt[3], P. Piña-Varas[4], A. Martí[5]
[1]Universitat de Barcelona, gmitjanas@ub.edu
[2]Universidad Complutense de Madrid, jledo@ucm.es
[3]Universitat de Barcelona, pilar.queralt@ub.edu
[4]Universitat de Barcelona, p.pina@ub.edu
[5]Universitat de Barcelona, annamarti@ub.edu

SUMMARY

In the framework of a project aimed at the development of low enthalpy geothermal energy in urban areas, the Vallès-Penedès Basin (Catalan Coastal Range, NE Spain) has been investigated by means of an integrated geophysical methodology. Among the different investigation methods deployed, two magnetotelluric profiles integrated with gravity and ambient seismic noise data have been performed. Although a definitive 3D magnetotelluric and gravity model covering the Vallés-Penedès Basin is still being worked on, preliminary results have already allowed us to image the geological structure of the area as well as to characterize the functioning of the main geothermal system.

Keywords: Geothermal exploration, Integration methods

INTRODUCTION

In the Vallès-Penedès (VP) Basin area, the thermal anomalies are located in the northeastern horst-graben limit, where a highly fractured Hercynian granodiorite is in contact with Miocene rocks by a major normal fault, the V-P Fault (Figure 1). This main structure seems to control the heat and the hot-water flow (Canals et al., 1989; Fernàndez & Banda, 1988; IGME, 1986; Mitjanas et al., 2021), nevertheless, the geological structure of this area, as well as the role of the different geological units, is poorly understood.

In this structural context, the electrical methods are those which offer a sufficient contrast to characterize the system, as they are usually used to the delineate geothermal reservoirs, locate aquifers, and sometimes, estimate porosity and physical conditions within a geothermal system (Georgsson, 2009; Hersir & Bjornsson, 1991; Piña-Varas et al., 2018). However, as seen in the conclusion of Mitjanas et al. (2021), the combination of different geophysical methods based on different physical properties, is an efficient option during the preliminary stages of geothermal exploration, even when they are used for low/mid-temperature systems, and also applicable in urban areas.

METHODS

This study is being carried out in the La Garriga-Samalús geothermal area which is located in the northeastern limit of the granodioritic thrust sheet (Figure 1). Affordable geophysical methods were chosen in order to try to define the main structure of the V-P crustal fault: two magnetotelluric (MT) profiles, gravity (GRV), and horizontal-to-vertical passive seismic (HVSR); which details of acquisition and processing follow the procedure presented in Mitjanas et al., (2021).

Two MT profiles were made in the eastern limit of the V-P Basin: MT-Samalús and MT-Vilamajor.
The MT-Samalús is located above a thermal anomaly previously reported in borehole exploration reports (IGME, 1982, 1984, 1986). This profile is made up of 16 sites in a NNW-SSE profile of approximately 6 km length from the granodioritic unit of the Prelitoral Range and across the V-P basin.
The MT-Vilamajor is strategically located outside the granodioritic sheet in order to identify the structural differences with a nearby area where no thermal anomalies have been detected. This profile is made up of 11 sites in a NNW-SSE profile of approximately 4 km long, which extends from the metamorphic Paleozoic rocks, towards the V-P Basin.

The HVSR survey includes 205 sites covering the basin area of the red outlined square (Figure 1), increasing the site density along with the MT profiles. The main objective of this method is to generate a basin-basement limit surface and supporting the MT inversion.

By the acquisition of new GRV measurements together with the previously available Bouguer anomaly data (IGC, 2012; Mitjanas et al., 2021), we have created a Residual Anomaly map made up of 1120 sites that cover the area between CM and MT-Vilamajor (Figure 1). The main objective of this

method is to interpret the basin and the fault geometry in the areas where no HVSR or MT data have been acquired (western part).

Moreover, 3D MT and GRV models are being developed.

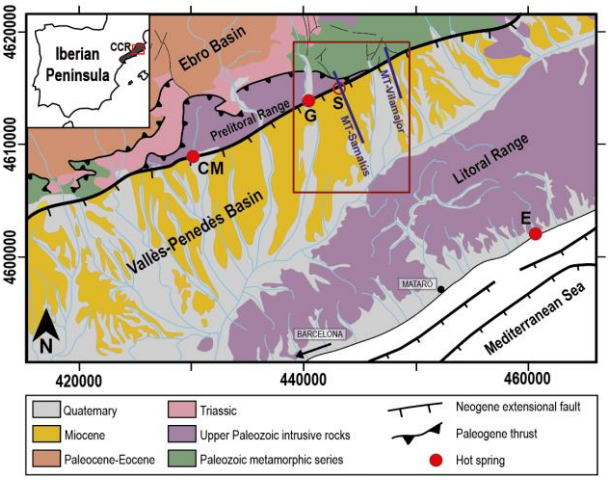

Figure 1. Geological map of the eastern part of the CCR. CM) Caldes de Montbuí (70ºC); G) La Garriga (60ºC); E) Caldes d'Estrac (38ºC); S) Samalús (90ºC at 1000 m depth) (Modified from ICGC, 2002; Martí et al., 1992).

RESULTS

MT-Samalús

The MT-Samalús final resistivity model (Figure 2) images the V-P Fault as a conductive vertical anomaly with a listric geometry. At the hangingwall, the conductive syn-kinematic deposits show a gradual deepening towards the SSE, towards the center of the Neogene basin.

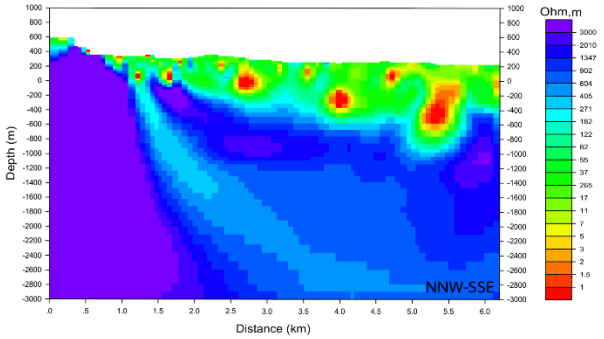

Figure 2. Resistivity model MT-Samalús (Mitjanas et al., 2021)

MT-Vilamajor

The MT-Vilamajor resistivity model (Figure 3) presents the same similar geoelectrical bodies as the ones presented in the previous MT-Samalús profile. The main difference relays on the V-P Fault geometry. Unlike the geometry defined in the MT-Samalús profile, in this case, the fault zone keeps its uprightness with depth.

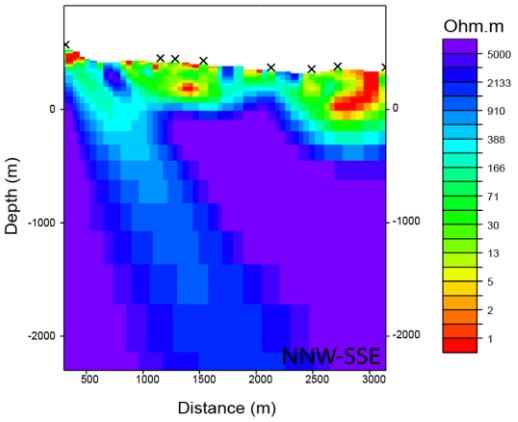

Figure 3. Resistivity model MT-Vilamajor.

HVSR

The basin-basement limit surface (Figure 4) shows that the deepest part of the basin is located at east of the Congost River. This river of La Garriga town, can be identified as the Quaternary sediments which have a N-S orientation (Figure 1).

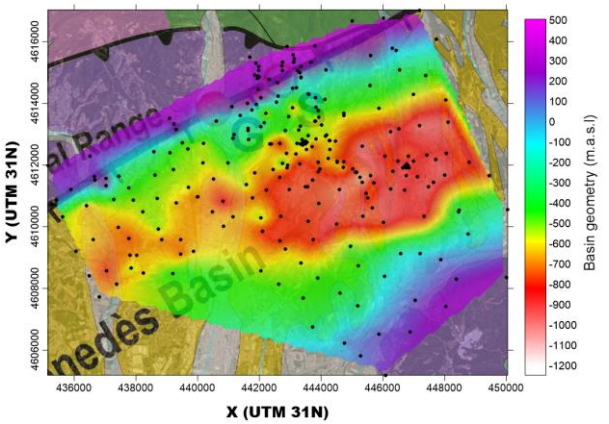

Figure 4. Sediment basin thickness along the region of study.

Gravity

The residual anomaly map (Figure 5) shows a large negative anomaly with an ENE-WSW direction. Towards the north, there is a high slope with higher values, and towards the east and south, the values increase slightly more gradually.

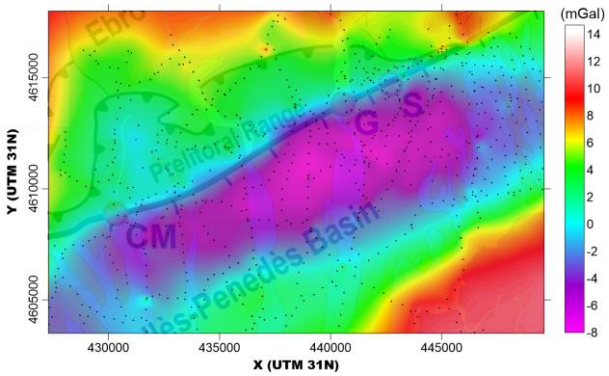

Figure 5. Residual anomaly map with the GRV sites and the base geological map.

DISCUSSION

The resistivity models, conditioned by the HVSR data, have allowed to constraining the basin geometry and the V-P Fault.

The V-P basin is characterized by a change in thickness (Figure 6), first, in the zone where the granodioritic thrust sheet intervenes (between CM and S, Figure 1); and within this zone, in the eastern part of the Congost River (G, Figure 1). The change of basin thickness in the Congost River could be related to a N-S Congost fault.

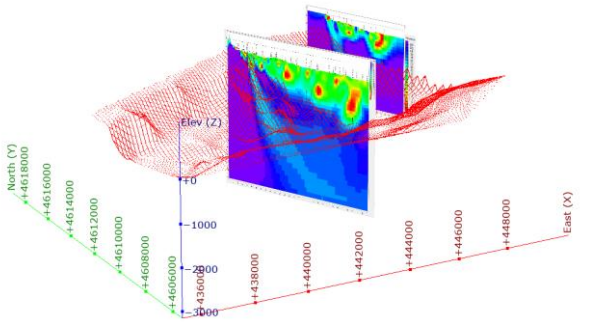

Figure 6. Basin base surface obtained using MT models and HVSR data. Leapfrog Software.

From CM and towards the eastern limit of the V-P Basin, the V-P Fault does not completely keep the same rectilinear orientation but forms non-aligned linear segments connected by fault trace bends (Figure 7). In La Garriga, this step is interpreted as a fractured relay ramp. The ramp rotations and the high degree of deformation in the relay zone could also favor the development of other major structures or could act as a potential area for the development of cross-fault river systems – as the identified in the Congost river –. In all such cases, it will, however, act as a site for both deformation and up-fault flow (Walsh et al., 2018).

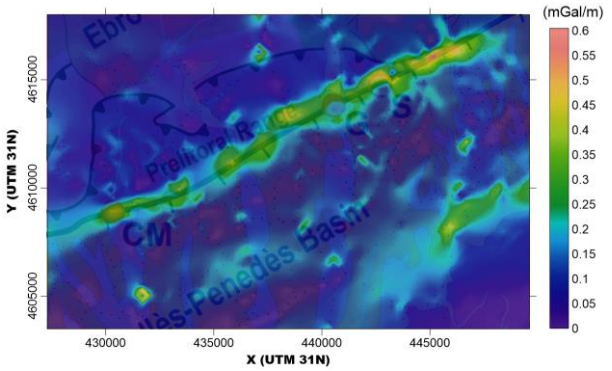

Figure 7. Slope gravity map. The maximum slopes would correspond with the V-P Fault trace.

CONCLUSIONS

The integration of the presented geophysical methods has allowed the identification and characterization of the V-P Fault and Basin.

The V-P Fault is imaged as a conductive body, fractured and water-saturated, which acts as a path for hot fluids which come from great depths. The presence of high-degree deformation zones along the V-P Fault trace and also the intersection with other potential faults, seem to control fast paths of up-fault flow.

The models presented, as well as preliminary interpretations, lead to the conclusion that the integration of the different methods is a very effective way to characterize geothermal systems, even if they are low-temperature systems or are located in urban areas.

ACKNOWLEDGMENTS

ICGC, the Catalan Geological Survey, for the HVSR data.

PIXIL project - (POCTEFA 2014-2020). https://pixil-project.eu/

Leapfrog Geothermal Software, ©Seequent, a Bentley Company.

REFERENCES

Canals, A., Albert, J., & Ayora, C. (1989). El sistema geotérmico de la Garriga-Samalús: : comparaciones con sistemas hidrotermales fósiles. In *Geogaceta* (Issue 7, pp. 88–90).

Fernàndez, M., & Banda, E. (1988). Aproximacion a la anomalia geotérmica de La Garriga - Samalus (Vallès - Penedès). *Acta Geológica Hispánica*, *23*(1), 1–20.

Georgsson, L. S. (2009). *Geophysical methods used in geothermal exploration. 50*(3–4), 227–249.

Hersir, G. P., & Bjornsson, A. (1991). *Geophysical exploration for geothermal resources: principles and application*. 94.

ICGC. (2002). *Mapa Geològic de Catalunya 1:250.000*. Institut Cartogràfic i Geològic de Catalunya.

IGME. (1982). *Informe sobre el seguimiento técnico del sondeo SAMALUS-1*.

IGME. (1984). *Proyecto de investigación geotérmica en el Vallés mediante sondeos de reconocimiento y síntesis hidrogeotérmica. Control geotermico de los sondeos SAMALUS 2, 3, 4 y 5*.

IGME. (1986). *Proyecto de seguimiento geológico del sonde de reconocimiento geotérmico SAMALUS-6 (1000 m) (Valles-Barcelona)*.

Martí, J., Mitjavila, J., Roca, E., & Aparicio, A. (1992).

Cenozoic magmatism of the valencia trough (western mediterranean): Relationship between structural evolution and volcanism. *Tectonophysics*, *203*(1–4), 145–165.

Mitjanas, G., Ledo, J., Macau, A., Alías, G., Queralt, P., Bellmunt, F., Rivero, L., Gabàs, A., Marcuello, A., Benjumea, B., Martí, A., & Figueras, S. (2021). Integrated seismic ambient noise, magnetotellurics and gravity data for the 2D interpretation of the Vallès basin structure in the geothermal system of La Garriga-Samalús (NE Spain). *Geothermics*, *93*(March).

Piña-Varas, P., Ledo, J., Queralt, P., Marcuello, A., & Perez, N. (2018). On the detectability of Teide volcano magma chambers (Tenerife, Canary Islands) with magnetotelluric data. *Earth, Planets and Space*, *70*(1).

Hydrothermal model of Aso volcano, Central Kyushu, Japan, inferred from AMT and ACTIVE datasets

T. Minami[1], M. Gresse[2] and M. Utsugi[3]
[1]Kobe University, Japan, tminami@port.kobe-u.ac.jp
[2]National Institute of Advanced Industrial Science and Technology, Japan, marceau.gresse@aist.go.jp
[3]Kyoto University, Japan, utsugi.mitsuru.5c@kyoto-u.ac.jp

SUMMARY

Aso volcano, Central Kyushu, Japan is one of the most active volcanos in Japan. It has an activity cycle with a period of about 15 to 20 years consisting of the active phase for about one year accompanied by mud, strombolian, and phreatic/phreatomagmatic eruptions and the other quiescent phase. Since the phreatomagmatic eruptions of Aso volcano are most devastating during the active period, our aim is to reveal the hydrothermal system of Aso volcano and understand the mechanism of the phreatic/phreatomagmatic eruptions. To reveal its shallow resistivity structure, two kinds of electromagnetic (EM) measurements have been conducted in Aso volcano: AMT and ACTIVE (Array of Controlled Transient-electromagnetics for Imaging Volcano Edifice, Utada et al. 2007). ACTIVE is a volcano monitoring system using transient EM method composed of a source electric dipole with earthing two electrodes and induction-coil receivers for measurement of the vertical component of the induced magnetic field. Our previous study (Minami et al., 2018) revealed the temporal change in the three-dimensional (3-D) resistivity structure through the magmatic eruptions of Aso volcano from August 2014 to August 2015 using the ACTIVE campaign datasets. With the aid of the hydrothermal simulation code TOUGH2 (Pruess, 1991), on the other hand, we recently found that a hydrothermal model assuming empirical porosity, permeability, and heat source at depth of the active crater explains well the 3-D resistivity structure inferred from AMT survey data (Kanda et al., 2019). We are currently integrating the hydrothermal model from the AMT dataset and the temporal variation in the resistivity structure revealed by the ACTIVE datasets. In the presentation, we present how our hydrothermal model explains the resistivity structure inferred from the AMT dataset and our project to integrate AMT and ACTIVE datasets into a hydrothermal model of Aso volcano.

Keywords: volcano, Aso, hydrothermal system, MT, CSEM

Abstract, 25^{th} EM Induction Workshop,Çeşmeı, Turkey, September 11-17, 2022

Using magnetotelluric and differential magnetometer data to quantify Space weather risk in the UK high voltage power transmission grid

Juliane Hübert[1] *, Ciaran Beggan[1], Gemma Richardson[1], Natalia Gomez Perez[1] and Alan Thomson[1]
[1]British Geological Survey, Edinburgh, UK
*juliane.huebert@bgs.ac.uk

SUMMARY

Geomagnetically induced currents (GICs) that occur during severe geomagnetic storms have been identified as a hazard to ground-based modern infrastructure like the power grid, gas pipelines and railways. During past extreme space weather events, disruption to the electricity supply in several mid- and higher latitude countries have been reported. In order to monitor, model and forecast GICs, sophisticated models of the ground electric field and the network topology are required in a multi-disciplinary approach. EM geophysics can provide realistic ground electric field estimates using magnetotelluric data and/or models of electrical conductivity of the earth.

We present a detailed analysis of newly collected differential magnetometer (DMM) and MT data in the UK that allow the verification and validation of our network model for the UK power transmission grid. Combining the observation of line GICs measured with DMM at several sites in the UK in the past four years and the electric fields derived from the MT data show an excellent fit of prediction and observation of GICs. This validation of the network model and electric field calculation allows us to use it with confidence for real time modelling and forecasting as well as extreme event analysis.

Keywords: Space Weather, Geomagnetically induced currents (GICs), Differential magnetometer method, geoelectric field model

Abstract, 25th EM Induction Workshop,Çeşmeı, Turkey, September 11-17, 2022

Time-lapse 3D CSEM for reservoir monitoring based on rock physics simulation

M. Ettayebi, S.Wang, M.Landrø [1]
[1]Norwegian University of Science and Technology (NTNU), mohammed.ettayebi@ntnu.no, shunguo.wang@ntnu.no, martin.landro@ntnu.no

SUMMARY

Marine controlled-source electromagnetic (CSEM) method measures EM fields transmitted by an active source either at seafloor or a few tens of meters above the seafloor, therefore it can image the electrical resistivity beneath the seafloor. Being able to resolve resistivity anomalies of high saturations of petroleum, marine CSEM sounding has gained increasing popularity after its introduction in 1981 by Cox. Nevertheless, the EM research community starts to extend its applications from petroleum exploration to an active production monitoring tool. Our study focuses on the latter.

By utilizing various dynamic reservoir properties made available through reservoir simulation of the Wisting field located in the Norwegian part of the Barents Sea, a realistic geoelectric model was created. To this end, we develop geologically consistent rock physics models, such that the available simulation results can be transformed into resistivity maps. We show that the resistivity map pertaining to each time-step can be used as an input model in a Finite Difference Time Domain (FDTD) forward modeling workflow to produce synthetic EM data. This synthetic EM data can be studied and analyzed in light of production induced changes in the reservoir for different production phases. This will allow us to acquire insights towards developing a technically feasible reservoir monitoring workflow suitable for time-lapse CSEM. Our result shows that at different production phases, the CSEM responses are different. Therefore, the method can be effectively used for production monitoring purpose. Moreover, this study will enable the testing of other time-lapse workflows with realistic complexities evaluating the potential of this technology for field application, through investigating the resolution limitations and the repeatability requirements.

Keywords: CSEM, time-lapse, reservoir monitoring, production monitoring, 4D

INTRODUCTION

The controlled-source electromagnetic (CSEM) experiment has for decades been established as a reliable method for hydrocarbon exploration. It is also widely acknowledged as a complementary tool to the seismic experiment, mainly due to the high sensitivity of the method to resistive and conductive anomalies, such as oil reservoirs and water. Recently, several studies have been devoted to extending the applications of the CSEM method from merely being a risk-reduction tool to time-lapse production monitoring tool. However, there is a lack of research that thoroughly studies the potential of the CSEM tool in capturing production induced changes in the fluid content for realistic and detailed reservoir models and production strategies.

Currently, an increasing attention is drawn towards understanding the time-lapse behaviour of the CSEM method in detail. Therefore, we conduct research on how to enable time-lapse 3D CSEM for reservoir monitoring. By developing a geologically consistent rock-physics model, the dynamic reservoir properties of the Wisting field located in the Norwegian part of the Barents sea can be converted into resistivity models for each time-step. These resistivity models can be utilized as inputs in a Finite Difference Time Domain (FDTD) workflow to generate synthetic EM data that can be studied and analyzed for time-lapse production effects.

The Wisting discovery was made back in 2013 by the wildcat well 7324/8-1. The well was drilled down-flanks on a structure in the Wisting Central prospect and hence got the name central well (Fig-

ure 1). The reservoir at this area shows good quality, and it belongs to the Realgrunnen Subgroup which consists of three formations: Fruholmen, Nordmela and Stø Formations. The well entered the top of the reservoir which is the Stø Formation at the depth of 662 m. The water depth here is 400 m and the structural crest is currently at 250 m burial depth. Wisting is known for its discernible electric properties where the background resistivity can reach up to 20 Ωm (Granli et al, 2017). The central well (7324/8-1) was drilled with the primary objective of investigating and evaluating the Jurassic Realgrunnen Subgroup for hydrocarbons (NPD, 2022), which indeed ended up as a discovery well.

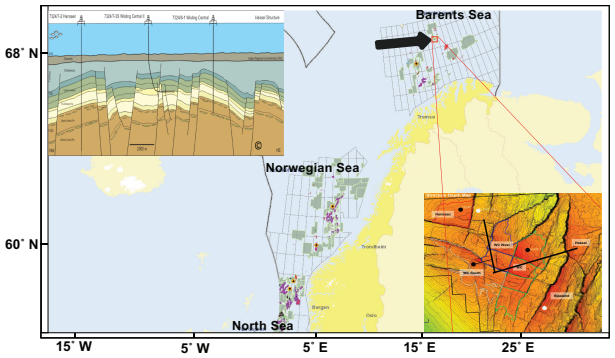

Figure 1: The Wisting field located in the Norwegian part of the Barents Sea as highlighted by the red rectangle. Lower right corner: the structure depth map of the Wisting field. The thick black lines are intersection lines going through specific wells. Upper left corner: schematic representation of the local structural and sedimentological geology along both of the thick black lines shown in the lower right corner.

A large database was made available for this time-lapse study, consisting of Eclipse production simulation models, well-logs, 3D CSEM inversion results and both conventional and P-cable 3D seismic data. The main objective of this work is to employ and combine the available data in various extents into a rock physics framework enabling us to create a serial of realistic resistivity models to represent oil production phases. These models can be utilized to investigate the survey parameters repeatability requirements and feasibility of time-lapse CSEM. With that in mind, this study consists of two main parts. The first one deals with the construction and calibration of the reservoir model while the second is devoted to studying the feasibility of time-lapse CSEM. As for the repeatability requirements, we will investigate that in future research.

RESISTIVITY MODELING FROM TIME-VARYING WATER SATURATION SIMULATIONS

CSEM data can be used to image resistivity structures. Subsequently, getting insight into the different rock properties that can alter subsurface resistivity is of critical importance for CSEM interpretation. Therefore, creating a reservoir model that will be used for time-lapse CSEM does depend on the resistivity distribution across the field considered. This brings into question the importance of a precise and realistic mapping of the resistivity. Time-varying water saturation can be transformed to time-varying resistivities and subsequently to time-varying Anomalous Transverse Resistance (ATR) maps. The Wisting field has demonstrated an excellent oppurtunity to show the ability of CSEM for reservoir monitoring.

The reservoir resistivity is dependent on a number of subsurface parameters. By Archie's law (Archie, 1942) it is clear that the saturation exponent n is one important parameter. Archie's law makes three implicit assumptions as pointed out by Mungan and Moore (1968); one is that the only conductive material is brine and that the rock matrix is non-conductive. However, if the reservoir contains clay, then rather more advanced models are required to model it.

Another physical property that has close interplay with reservoir resistivity is rock wettability and its distribution. Mungan and Moore (1968) state that the saturation exponent n appears to be saturation dependent increasing with the decrease of water saturation, and it can be as high as 9 when the water saturation is approaching connate water saturation in oil-wet formations. Bearing in mind that the reservoir at Wisting is possibly oil-wet as suggested by Alvarez et al (2018), this introduces the possibility of adjusting the saturation exponent n resulting in higher modeled resistivities.

As previously studied, there are many factors that can alter the saturation exponent and one of these factors is wettability (Adisoemarta et al, 2001). The model developed here and which is calibrated with the central well, elaborates further on this in conjunction with the conclusions made by Mungan and Moore (1968) on oil-wet formations. The model deals with the non-linearity of the saturation expo-

nent in oil-wet formations depending on water saturation. The saturation exponent should increase significantly in oil-wet formations to account for the isolated water globules in the larger pores, and which will not be able to conduct current (Anderson, 1986). Moreover, the wettability effects become more prominent as the brine saturation decreases. This stipulates establishing a connate water saturation $S_{w,connate}$ threshold or cut-off below which the rock changes its wettability from a state of mixed wettability to becoming oil-wet, resulting in a larger saturation exponent. The fact that Alvarez et al (2018) use a saturation exponent equal to 2.8 in their Wisting resistivity modeling supports the claim of Wisting being oil-wet. By incorporating information from both capillary pressure curves and Free Water Level (FWL) depth maps, the connate water saturation threshold was set to 10%.

Different gas caps scattered over the field have been recognized and these deserve special treatment in terms of the saturation exponent n. The latter should most likely be less than 2 in gas-bearing formations, introducing the necessity for choosing another threshold value for the gas saturation which for the reader's convenience will be given the name critical gas saturation. This may consequently demarcate the transition from oil-wet rocks with low water saturation combined with a large saturation exponent on one hand, and gas-bearing zones with relatively high gas saturation combined with a lower saturation exponent on the other hand. After multiple attempts, a gas saturation threshold value equal to 70% was deemed to produce the desired models. By desired models, the generated ATR maps are consistent with our understanding of the spatial distribution and magnitude of the most resistive targets and this conforms with the inverted 3D CSEM ATR maps.
With this background, a non-linear saturation exponent was modeled having its maximum value of 2.5 at the top of the reservoir and non-linearly decreasing with depth and the overall water saturation trend. Note that this only applies for intervals where the water saturation is lower than the connate water saturation 10%. On the other hand, if the gas saturation is higher than the critical gas saturation, then the saturation exponent n is assigned the value 1.8. To summarize, there are two main factors that decide what kind of value the saturation exponent is assigned, and these are the connate water saturation and critical gas saturation thresholds. The rock-physics model was used to transform detailed water saturation simulations to detailed resistivity maps that are used as inputs in a FDTD forward modeling workflow to generate synthetic CSEM data. Two resistivity maps are presented in Figure 2, in which the reservoir is marked by warm color.

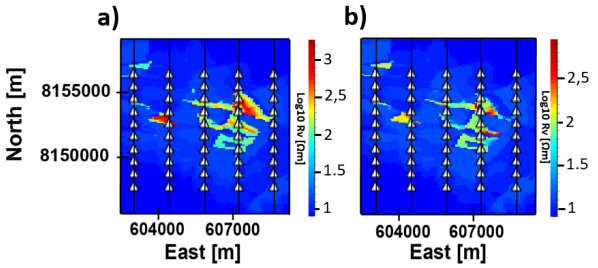

Figure 2: 2D resistivity maps for two different time steps. The year 2027 (plot a) when the field is expected to start producing and in the year 2057 (plot b) towards the predicted end of production. The white rectangles are receivers and the black vertical lines going through them are towlines. Note that the colorbar scales pertaining to the two different plots are different.

TIME-LAPSE PRODUCTION INDUCED RESPONSES

The time steps at the onset of production in the year 2027 and after 30 years of production in the year 2057 are used for simulation. Figure 3 shows the Ex-field normalized magnitude (NM) maps pertaining to the last time step. The source-receiver offset is set to 2667 m and the frequency is 5.0 Hz. Normalized value 1 represented by the lightish green implies that no change happens through the 30 years. If the NM is larger than 1, one can assume that there are changes to spot in the fluid content of the subsurface reservoir. It is clear that Figure 3 depicts discernible production-induced changes represented by the red positive anomalies. A clear and good spatial match exists between these anomalies and the resistivity maps in Figure 2, as we can clearly see that the epicentre of the anomaly is where most of the production is predicted to take place. A producing hydrocarbon field is expected to have decreasing petroleum volumes with time and hence lower resistivity values due to water-injection. Towards the end of the lifetime of a producing field, most of the target resistor will be gone and the end result is without the target resistor embedded in it. Figure 3 underpins this fact with the positive anomaly, which implies that the target response in the year 2027 is larger than the pseudo-background response in the year 2057. Another observation worth mentioning is the relatively

high frequency depicted here, and the higher resolution that offers. We think that a combination of relatively high background resistivity and shallow burial depth might contribute to a setting that is favorable for slightly higher frequencies.

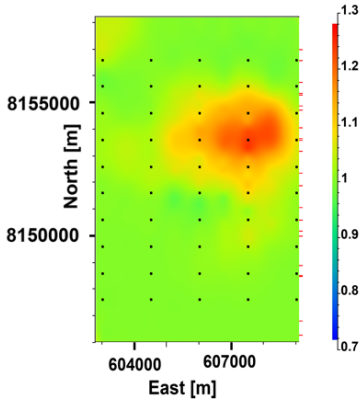

Figure 3: Normalized magnitude (NM) 2D map of the E_x field component for the year 2057 towards the predicted end of production. The source-receiver offset is 2667m while the frequency is 5.0 Hz. The black dots are receiver positions.

CONCLUSION

We showed how dynamic reservoir simulations related to different time steps can be converted to resistivity spatial distributions through a detailed, realistic and geologically consistent rock-physics model. These resistivity maps can be used as inputs in a FDTD forward modeling workflow to generate synthetic CSEM data. The CSEM data are studied and analyzed in different approaches towards understanding and developing a feasible workflow for time-lapse CSEM studies. What comes forth through this study is the ability of CSEM data to detect and capture production induced changes in the fluid content of a producing hydrocarbon reservoir. In addition, the presented workflow proves itself to be a feasible one, demonstrating how time-lapse CSEM can be used. The future work is to take a closer look at the repeatability requirements and limitations of time-lapse marine CSEM.

ACKNOWLEDGMENTS

We would like to thank the operator Equinor and the license partners for sharing with us valuable data that are essential for this research to be conducted, and also for permission to publish this work. We are grateful to Friedrich Roth for his software support and to Jan Petter Morten for his inputs. The study was funded by the Norwegian Research Council together with the GAMES consortium and the Center of Geophysical Forecasting (grant nos. 294404, 309960, and 324442). The modellings were performed on resources provided by Sigma2 - the National Infrastructure for High-Performance Computing and Data Storage in Norway (nn9872k).

REFERENCES

Adisoemarta PS, Anderson GA, Frailey SM, Asquith GB (2001) Saturation exponent n in well log interpretation: Another look at the permissible range. SPE Permian Basin Oil and Gas Recovery Conference DOI 10.2118/70043-ms

Alvarez P, Marcy F, Vrijlandt M, Skinnemoen Ø, MacGregor L, Nichols K, Keirstead R, Bolivar F, Bouchrara S, Smith M, Tseng HW, Rappke J (2018) Multiphysics characterization of reservoir prospects in the hoop area of the barents sea. Interpretation 6(3):SG1–SG17, DOI 10.1190/int-2017-0178.1

Anderson WG (1986) Wettability literature survey-part 3: The effects of wettability on the electrical properties of porous media. Journal of Petroleum Technology 38(12):1371–1378, DOI 10.2118/13934-pa

Archie G (1942) The electrical resistivity log as an aid in determining some reservoir characteristics. Transactions of the AIME 146(01):54–62

Granli JR, Veire HH, Gabrielsen P, Morten JP (2017) Maturing broadband 3D CSEM for improved reservoir property prediction in the Realgrunnen Group at Wisting, Barents Sea. SEG Technical Program Expanded Abstracts 2017 pp 2205–2209

Mungan N, Moore E (1968) Certain wettability effects on electrical resistivity in porous media. Journal of Canadian Petroleum Technology 7(01):20–25, DOI 10.2118/68-01-04

NPD F (2022) 7324/8-1 general information. https://factpages.npd.no/en/wellbore/pageview/exploration/all/7 accessed: 2022-06-11

3D modeling and inversion of ground-based TEM data, a case study of seawater intrusion on the eastern coast of the Gulf of Aqaba, Jordan

J. Abu Rajab[1], H. El-Kaliouby[2], E. Al Tarazi[1] and H. Al-Amoush[3]
[1]Department of Earth Sciences and Environment, Prince El-Hassan bin Talal Faculty for Natural Resources and Environment, The Hashemite University, Jordan, jafars@hu.edu.jo; eid@hu.edu.jo
[2]Department of Geophysical Sciences, National Research Center, Egypt, hkaliouby@gmail.com
[3]Department of Applied Earth and Environmental Sciences, Faculty of Earth and Environmental Sciences, Al al-Bayt University, Jordan, hani.alamoush1@gmail.com

SUMMARY

The research describes the ground-based transient electromagnetic (TEM) survey design and modeling/inversion scheme used to recover detailed geoelectrical structures at seawater intrusion in coastal areas. We analyzed the simulated and experimental TEM data along the profile using side-to-side 25 m × 25 m loop dimensions, conducted perpendicular to the coastal line. In addition, a coarse grid of experimental TEM loops of 100 m ×100 m dimensions was also evaluated for deeper investigation in view of the 3D inversion scheme conducted along the coastal area. In our 2D and 3D simulated models, we created multiple simplified geoelectrical structures that approximated seawater intrusion in sandy aquifers while allowing for topographical variations. The transient responses of the saline zone (seawater 1 Ω·m), the mixing zone (brackish water 3 Ω·m) and the fresh zone (freshwater 100 Ω·m) were calculated based on the modified Druskin-Knizhnerman finite-difference algorithm. Modeling of an inclined seawater interface of less than 45° shows subparallel horizontal layering; however, a wedge-like structure becomes more visible at a higher angle. In the presence of two zones (saline and brackish) and three zones (saline, brackish, and fresh), the geometry of inland intrusion is fairly determined using 1D inversion, but the resistivity values among intrusion phases are severely overestimated, and the transient transformation images provide minimum information about intrusion characteristics like depth to boundaries and lateral extension. However, 3D inversion along the TEM profile yields improved geometrical characteristics of intrusion, particularly for resistivity values. A 3D inversion of experimental TEM data distributed along profile and across the seawater interface reveals that resistivity values and interface structure agree much better with the inclined wedge-like structure. A 3D inversion of experimental grid TEM data spread along the seawater interface allows for high contrast at major contacts like brackish water-bearing sediments and saline water-bearing sediments, and the recovered model is comparable to reference sites like total dissolved solids measurements from well data.

Keywords: seawater intrusion, TEM, 2D/3D modeling and inversion, Gulf of Aqaba, Jordan

INTRODUCTION

Coastal aquifers, particularly in arid and semi-arid locations, are an essential source of drinking water for urban development. Because seawater contains more dissolved salts and minerals and is denser than terrestrial freshwater, it has a higher hydraulic head along the coastal margin than freshwater. Seawater moves into coastal aquifers in a wedge shape under freshwater due to its higher pressure and density (Bear et al.1999). A transition zone develops where seawater and freshwater meet and interact. Because fresh groundwater levels, or the height of the freshwater column, rise with land elevation, the inland extent of the seawater wedge is varied. The transient electromagnetic method (TEM) has been extensively used to study coastal aquifers since it is capable of defining groundwater resistivity with a resolution of a fraction of an Ω·m. The TEM method is used to study the geometry of seawater intrusion, utilizing information from geological research and boreholes exploration. Furthermore, two-dimensional (2D) and three-dimensional (3D) TEM surveys are a cost-effective solution to improve TEM data interpretations and gain a better understanding of seawater intrusion. Furthermore, substantial progress has been achieved in the development of TEM instruments, surveying methods, and 3D interpretation techniques (Newman and Commer 2005; Everett 2012; Barsukov and Fainberg 2013; Oldenburg et al. 2013; Barsukov et al. 2015). Nonetheless, there is debate about the efficiency and necessity of using 3D modeling and inversions for transient induction data. Even though a 1D assumption might work in a 1D environment, larger current flow patterns in transient induction electromagnetic systems are more likely to require 3D modeling and inversion to improve the physical contrasts in complex geological conditions like fractures, faults, cavities, and changes in the aquifer's hydraulic properties.

METHOD

In this study, we analyzed TEM data obtained using the TEMFAST 48 instrument in the area of seawater intrusion in Aqaba, Jordan. The first group of TEM data was optimized using a 25 m side-to-side single turn loop across the coast line. The second TEM group data was collected with coarsely spaced TEM of 100 m loop side length that was performed as a grid area along the coast line where the lithology and total dissolved solids ("TDS") of some boreholes are presented. We also simulated and analyzed TEM data-based 2D/3D structures in sandy aquifer with saline, brackish, and fresh water. TEM-RES Software (AEMR, Inc., Netherlands) was used for processing TEM measurements and for one-dimensional (1D) inversion purposes. The resistivities and thicknesses at each sounding site of the locally 1D earth's layered model was inverted based on a modified Levenberg–Marquardt approach (Barsukov et al., 2015).In case of 3D environment, the quasi-stationary approximation is used to model the 3D problem based Druskin and Knizhnerman (1988) method; this approximation is feasible when the displacement currents are infinitesimally smaller than the conduction current. The approach for 3D modeling/inversion of TEM data is conducted using the code TEM-3D WIZARD (AEMR, Inc., Netherlands).

simulated TEM data along profile (2D/3D subsurface structure)

TEM-3D WIZARD created simple geoelectrical structures to simulate seawater intrusion in sandy aquifers while taking topographical effects into consideration. Figure 1 depicts the 3D model of seawater intrusion data from a 2 × 2 km^2 area and 200 m depth. The x-axis is aligned with the profile of soundings with a 25 × 25 m^2 using single loop configuration, which passes through the center of the 2D seawater intrusion (x: -500 to 500, y=0). The transient responses of the saline zone (seawater 1 Ω·m), the mixing zone (brackish water 3 Ω·m) and the fresh zone (freshwater 100 Ω·m).

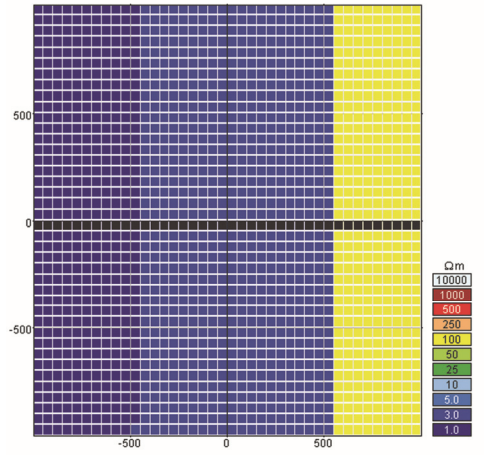

Figure 1. A 3D model of seawater intrusion was utilized to simulate TEM data from a 4 km^2 area. The aquifers' resistivities were constructed with a 45° inclination. A resistivity slice is shown below the topography.

RESULTS

Figure 2 shows the transient responses in terms of the apparent resistivity measured at several transient times for the 2D seawater intrusion model.

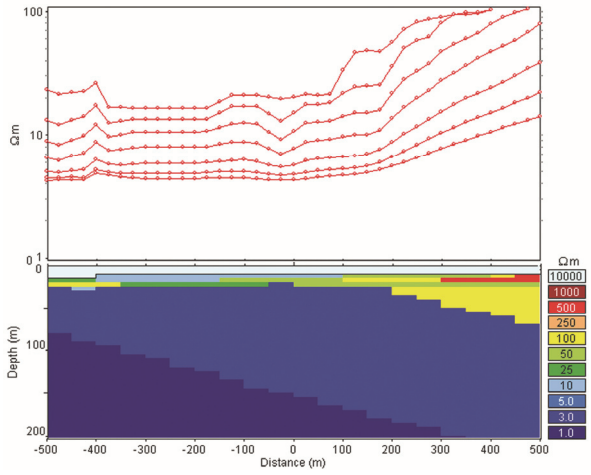

Figure 2. A 2D model of seawater intrusion and the transient responses of the saline zone (seawater 1 Ω·m), the mixing zone (brackish water 3 Ω·m) and the fresh zone (freshwater 100 Ω·m).

The response for the transient curves obtained at three positions: -450m for seawater, +0.0 for brackish water and the +450m for freshwater. The modeling were calculated for the same positions considering 2D/3D effect and presented in Figure 3.

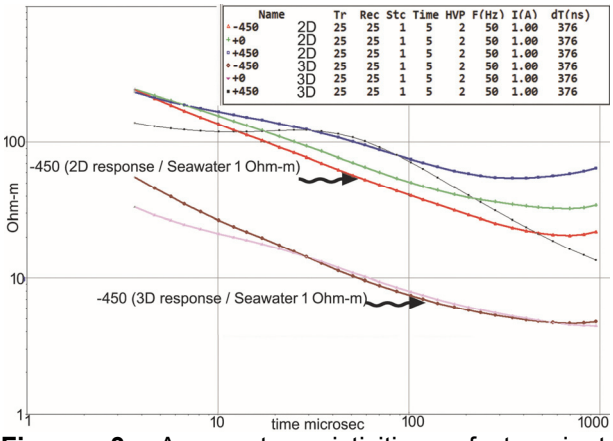

Figure 3. Apparent resistivities of transient responses for 2D and 3D intrusion structures, i.e., at -450 location, seawater response shows a significant resistivity difference for early and late-time response between 2D and 3D intrusion structures.

Figure 4 shows seawater intrusion using a 2D object effect and the results of a stitched 1D pointwise inversion. This made-up example was used to figure out the range of resistivity and the shape of the resulting layer structure.

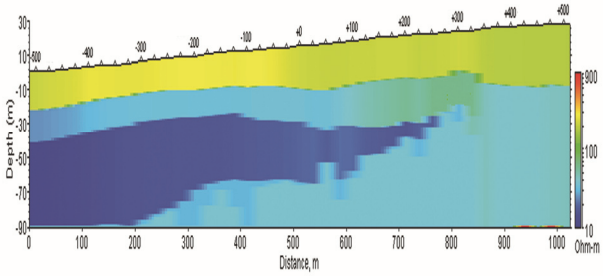

Figure 4.TEM resistivity simulated model based 2D structure of seawater intrusion, 1D RMS%=0.2.

The synthetic data in Figure 4 was, on the other hand, subjected to a 3D modeling and inversion procedure and modeled using the maximum 3D effect (Full space of X,Y,Z cells). This approach (Barsukov et al. 2015) includes 1D point inversion (each point in the profile is independent of the results of inversion on adjacent points), a global 1D inversion process to optimize the resistivity scale, and mutual 3D modeling computation and 3D inversion (Figure 5).

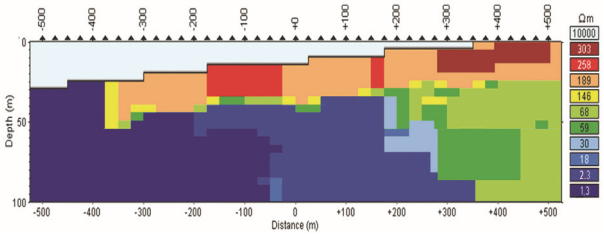

Figure 5. TEM resistivity simulated model based 3D structure of seawater intrusion,3D RMS%=6.5.

A case study from the east coast of Aqaba Gulf

71 TEM sites of 100 loop side length were selected to be included in the 3D inversion and modeling processes. We incorporated TEM data with station spacing averaging 350 m in most places. The geometrical skeleton of a region produced a discretized volume of approximately 130,000 cells in the domain of 1D TEM data using a grid of X = 4900 m, Y = 2200 m, and Z = 300 m. In this area, a 3D inversion resistivity map is shown for an elevation of -30 m below sea level (Figure 6). The slice map reveals a considerable contrast between saline water-bearing strata (<1Ω·m) and brackish water-bearing strata along the coast (>10Ω·m). Figure 6 presents the location of a TEM profile on the study area's southwestern side. The profile is composed of 20 loops with a loop side length of 25 m. Figure 7 shows the resistivity model based 3D inversion along profile and considering underlying 3D structure, the outcomes reveal three zones; saline water zone (<1Ω·m), brackish water zone (~3 Ω·m) and possible fresh water zone (>100 Ω·m). These resistivity ranges match the local aquifers' resistivities.

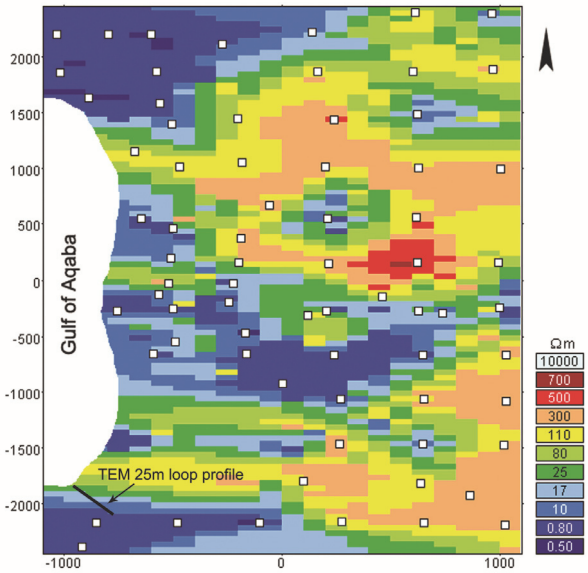

Figure 6. TEM resistivity model (Level=-30m) constructed from 3D inversion of 71 TEM loops, 3D RMS%=15.White square is 100×100 m^2 loop.

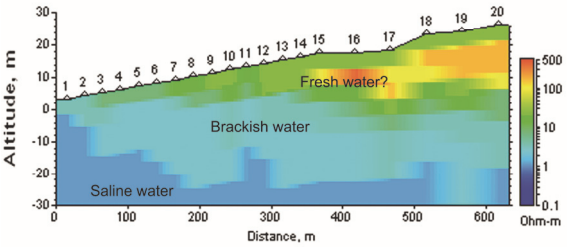

Figure 7. TEM resistivity model constructed from 3D inversion along profile and across seawater intrusion interface, 3D RMS%= 11.1, its location is presented in Figure 6. White square is 25×25 m^2 loop. Distances become inconsistent after TEM 15 due to site constraints.

Figure 8 shows the 3D inversion obtained from 71 TEM sites. The derived four resistivity cross-sections provided a high contrast at major contacts and along seawater intrusion interface, such as those between brackish water-bearing sediments and saline water-bearing sediments. In the direction of S1 profile near VES3 (i.e., 10 and 1 Ω·m, see Figure (8b)), and in the direction of S2 profile near Tour1 (i.e., 5 and 0.9 Ω·m. Another significant contrast has been defined at the boundary between alluvium deposits and the seawater intrusion zone (i.e., 200 and 0.6 Ω·m) Figure (8d).

CONCLUSIONS

The TEM method was used to establish resistivity modeling of seawater intrusion; however, modeling of seawater intrusion is challenging due to the complex geology, which includes numerous

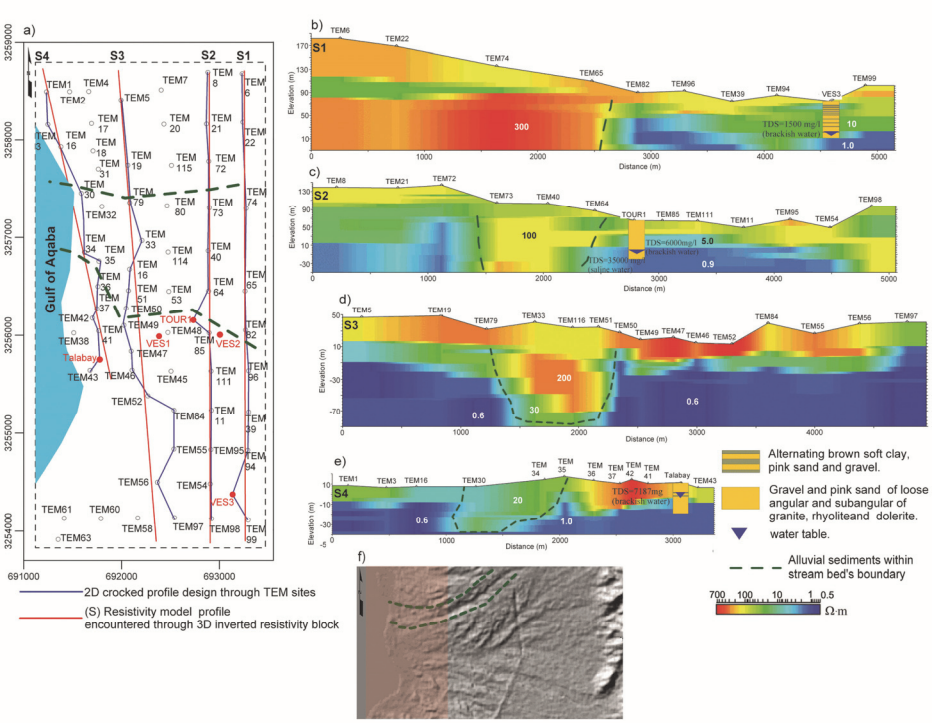

Figure 8. 3D inversion model of a 100 m × 100 m TEM loop: a) Map shows the distribution of near coast 71 TEM sites and the designed models' profiles (S), b) 2D geoelectrical model along (S1) profile, c) 2D geoelectrical model along (S2) profile, d) 2D geoelectrical model along (S3)profile, e) 2D geoelectrical model along (S4) profile, and f) Shaded relief topography of the study area shows the boundary of deep incised wadi (green dashed line) and the area of selected TEM sites (transparent pink rectangle).

layers types and the presence of possible fractures, faults, cavities and variations in the aquifer's hydraulic properties. So we model sandy aquifer to mitigate these parameters. TEM along profile employing single loop and side-to-side survey followed by 3D inversion and considering subsurface 3D structure is required for better resolving subsurface structure, especially in the area of seawater intrusion where resistivity variation is small. False resistivity interpretations may result from 1D point inversion or 2D stitching of 1D models. In the case of electromagnetically coupled station distances, 3D model-based 3D inversion is feasible and desirable. Reconstructing the geoelectrical structure of the medium is an ill-posed problem, and the final solution is a user-dependent issue that must be geologically accepted (details and stability). In the 71 TEM data set at the Aqaba coast, these requirements were not optimal; site restrictions have always limited the choice between densely spaced profiles without 3D information or too coarsely spaced 3D data. Cross sections can be used to interpret aquifer resistivity near reference boreholes.

ACKNOWLEDGEMENTS

The Ministry of Higher Education and Scientific Research/Jordan and The Hashemite University are thankful for funding this study (grant number WE/1/11/2019).

REFERENCES

Barsukov PO and Fainberg EB (2013) Three-dimensional interpretation of TEM soundings. Izvestiya, Physics of the Solid Earth 49: 517–525

Barsukov PO, Fainberg EB, Khabensky EO (2015) Shallow investigations by TEM-FAST technique: methodology and examples. In Spichak VV(ed) Methods of Geochemistry and Geophysics. Elsevier 40, pp 47–78

Bear J, Cheng A, Sorek S, Ouazar D, Herrera I (1999) Seawater intrusion in coastal aquifers: concepts, methods and practices. Springer Science, Business Media

Druskin V and Knizhnerman L (1988) A spectral semi-discrete method for the numerical solution of 3-D nonstationary problems in electrical prospecting. Izvestiya, Earth Physics 24: 641–648

Everett ME (2012)Theoretical developments in electromagnetic induction geophysics with selected applications in the near surface. Surveys in Geophysics 33: 29–63

Newman GA, Commer M (2005) New advances in transient Electromagnetic inversion. Geophysical Journal International 160: 5–32

Oldenburg DW, Haber E, Shekhtman R (2013) Three dimensional inversion of multisource time domain electromagnetic data. Geophysics 78: E47–E5

Using 3-D electrical conductivity model for understanding geological units of nonvolcanic geothermal reservoirs

B. Erdenechimeg[1], F. Samrock[1], A.V. Grayver[1], A. Kuvshinov[1], M.O. Saar[1], D. Sodnomsambuu[2], Ts. Shoovdor[2] and P. Dorj[3]

[1]ETH Zurich, erdenecb@ethz.ch

[2]Institute of astronomy and geophysics of Mongolian academy of science

[3]Renewable energy center of Mongolia

SUMMARY

Understanding the geological setting of nonvolcanic geothermal systems is vital to explaining the formation of geothermal reservoirs and their observable surface manifestations. The magnetotelluric method, used to determine the subsurface electrical conductivity distribution, is a common tool in geothermal exploration. In this study, we present an integrated interpretation of an electrical conductivity subsurface model, together with geological analyses and geochemical probes from a nonvolcanic, intermediate-temperature geothermal system in Mongolia. We conducted magnetotelluric (MT) and telluric-magnetotelluric (TMT) measurements at the Tsenkher geothermal area in the Mongolian Khangai dome during the summers of 2019 and 2020. The 20km*20km large area is characterized by three major hot springs with water temperatures up to 87°C. From a total of 196 MT and TMT stations, we obtained a 3-D electrical conductivity model of the subsurface. To interpret the data, we used a high-order finite-element electromagnetic modelling code (GOFEM) with locally refined hexahedral meshes that allows including accurate topography while ensuring high numerical accuracy with a sufficiently fine discretization of the inversion domain.

The best-fitting model provides essential insights into the subsurface structure of the Tsenkher geothermal area. The model is characterized by a strong vertical crustal conductor that appears south of the hot springs area and rises from depths of more than 10 km to the surface. We interpret this conductor as a remnant of past local volcanism and a zone of former magma ascent, indicating the potential source for the observed enhanced surface heat flow in the hot springs area around Tsenkher. Additionally, the model includes a prominent striking conductor beneath the hot springs at depths down to more than 3 km below the surface. The conductor is spatially aligned with a major fault that intersects the survey area, and is accompanied by several basaltic dyke intrusions. We interpret the fault-aligned conductor as the major area of deep fluid circulation and an accumulation zone for heated fluids. The interpretation agrees with theoretical concepts of topography-driven deep fluid circulation and local fault zones playing a major role in the transport of hot water from a reservoir to the surface. Inferred reservoir temperatures from geochemical fluid analyses are inagreement with interpretations of the maximum depth of fluid circulation inferred from the MT model.
Our MT subsurface model serves to better understand the formation of the Tsenkher hot springs in particular and intermediate-temperature geothermal systems in general.

Keywords: MT-TMT data acquisition, 3-D inversion, geothermal exploration, amagmatic geothermal systems, deep fluid circulation

Exploration of deep aquifer in North Jordan using TEM and MT

Gerhard Kapinos[1], Nedal Atteyat[2], Nidal Jahed[2], Florian Brückner[1], Falk Lindenmaier[1], Armin Margane[1], Mathias Toll[1], Pritam Yogeshwar[3]
[1] Federal Institute for Geosciences and Natural Resources (BGR), Germany, Gerhard.Kapinos@bgr.de
[2] Ministry of Energy and Natural Resources (MEMR), Jordan
[3] Institute of Geophysics and Meteorology, University of Cologne, Germany

SUMMARY

Deep aquifers at depths of 300 m to 1000 m have rarely been the focus of groundwater research. However, their importance for groundwater supply, especially in arid regions, is increasing, not least since the unmistakable climate change.
In order to quantify the location, extent and size of such deep aquifer systems, to understand them and thus to be able to use them sustainably, we used a combined transient electromagnetics (TEM) and magnetotellurics (MT) approach to investigate the distribution of electrical conductivity in relation to hydrogeological structures in a field study in northern Jordan.
42 TEM and 24 MT soundings were conducted in 2018 and 2019, mostly along profiles.
The TEM and MT data are complementary. MT resolves structures below 600 m, which is below the depth of investigation (DOI) of TEM. This allows deeper aquifer systems and their bases to be explored. In addition, lateral variations in conductivity can be detected with MT. Since the MT-data seem to indicate a one-dimensional (1D) background in the period range between 10^{-4} and 10^{1}s, the TEM-data could be used to correct the observed static shift in the MT data. Subsequently, both separate inversions of TEM and MT and joint inversions of TEM and MT were performed.
Another added value of the combined use of two methods is the strengthening of the robustness of the results by the joint inversion.
The joint 1D inversion confirms and complements the results of the separate inversion of the TEM- and for static-shifted corrected MT-data. The conductivity models, which provide a two-dimensional image of the conductivity in the subsurface, confirm hydrogeologic structures that are already known or suspected at a few points from well data, but also reveal new structures and new insights that are very valuable for understanding the aquifer system.

Keywords: Magnetotellurics, Transient electromagnetics, deep aquifers, joint inversion

Exploration of geothermal areas at the central part of Mexico through the application of Magnetotellurics and Transient Electromagnetics

Ruiz-Aguilar, D., García-Suárez, E., Cruz-Aquino, I.J., Pioquinto-Arcos, E., Roque-Pineda, L.S., Peiffer, L., Inguaggiato, C., Delgado-Argote, L., Contreras-López, M., Arango-Galván, C.

In the framework of a collaborative project funded by the Mexican government, we applied Magnetotellurics and Transient Electromagnetics in two geothermal areas located in Michoacán, a state placed in the central part of Mexico. These geothermal areas (Araró and San Agustín del Maíz) are located around Cuitzeo lake, where several geothermal surface manifestations have been reported. In Araró, a total of 31 MT stations and 30 TEM soundings were acquired. Whereas, in San Agustín del Maíz, we only acquired 21 MT soundings. At both areas, the soundings were spatially distributed around the locations of the thermal springs and water wells with high temperature. The acquired MT time series were robust processed to estimate the transfer functions. We perform the 3D inversion modeling of both MT data sets using ModEM. Regarding the TEM data, we interpreted them using 1D Occam and Marquardt techniques and the derived information was integrated in the corresponding 3D MT inversion scheme. Finally, the 3D resistivity models are appraised and correlated to geochemical and geological data, that were also obtained within the framework of this project.

Determination of the cap rock integrity in the Çanakkale-Tuzla hydrothermal system from inversion of magnetotelluric data by using particle swarm optimization

E. Büyük[1] and A.Karaman[2]

[1]Department of Geophysical Engineering, Faculty of Engineering and Natural Science, Gümüşhane University, Gümüşhane, Turkey,
[2]Department of Geophysical Engineering, Faculty of Mines, Istanbul Technical University, Istanbul, Turkey,

SUMMARY

Earthquakes of tectonic or magmatic intrusion origin around a geothermal field sometimes inflict irreversible damage to the caprock and cause temperature drop in reservoir temperature by altering the integrity of the cap rock structure. In a healthy reservoir, intact caprock seals the reservoir, maintains temperature and pressure build up for better well yield, and prevents cold water of overlain aquifers entering the system. The integrity of the caprock with these characteristics ensures the long-term preservation of a reservoir. However, loss of caprock integrity or weaken sealing capacity leads to leakage in and around the reservoir and reduces the sustainability and economic feasibility of a geothermal reservoir. Therefore, the geometry and integrity of the caprock are important, and any means of inspecting a caprock integrity is valuable for sustainable exploitation of a geothermal reservoir.

Caprock is usually identified with its striking conductive nature, which occurs because of mineral alteration and high clay content. Usually, the thickness of the caprock, which is usually several times less than its depth, is difficult to discern with the utility of conventional inversion techniques because of the structural complexity emanating from the non-sealing nature of the caprock. Starting model dependency as required for the conventional inversion methods usually forces the inversion procedure to produce a final model that is trapped about a local minimum due to the gradient of an objective function that is explicitly evaluated by a numerical method. On the other hand, evaluating partial derivatives with respect to the model parameters in some non-linear mathematical models may be impossible, or approximate schemes may not yield a sensible solution.

This study is n attempt for identifying the integrity of the caprock after the earthquake of Mw=5.3 on January 6, and subsequent swarms until March 26, using magnetotelluric data at Tuzla, Çanakkale geothermal field. One-dimensional magnetotelluric modeling approach with higher resolution for determining caprock structure compared to two- or three-dimensional modeling was carried out using particle swarm optimization (PSO) as an alternative to conventional inversion techniques. PSO is one of the modern global optimization methods based on a metaheuristic approach and has been recently preferred to overcome the subtle difficulties encountered in modeling geophysical data. Our modeling approach appeared to be successful in determining the caprock geometry, and the findings further strengthened our conviction that PSO is a powerful modeling technique for the MT data obtained on a geothermal field. It is critical that the modeling results provide important hypotheses for the loss of caprock integrity above a speculative magmatic intrusion, which extends to the hydrothermal reservoir above non-sealing caprock, and possibly triggers seismic events on the Tuzla fault.

Magnetotelluric investigations in the Ubaye valley, Western Alps: a connection between electrical conductivity, fluids, and earthquakes?

S. Byrdina[1], J-L. Got[1], L. Metral[1], P. Hering[2], M. Baques[3], L. De Barros[3], S. Garambois[1], P. Gueguen[1], V. Rath[4]

[1]Univ. Grenoble Alpes, Univ. Savoie Mont Blanc, CNRS, IRD, IFSTTAR, ISTerre, Grenoble, France, (svetlana.byrdina@univ-smb.fr)

[2]Goethe University Frankfurt, Institute of Geosciences, Frankfurt, Germany, (Hering@geophysik.uni-frankfurt.de)

[3]Université Côte d'Azur, CNRS, Observatoire de la Côte d'Azur, IRD, Géoazur, 250 rue Albert Einstein, Sophia Antipolis 06560 Valbonne, France, (debarros@geoazur.unice.fr)

[4]School of Cosmic Physics Dublin Institute for Advanced Studies 5 Merrion Square, Dublin 2, Ireland, (vrath@cp.dias.ie)

SUMMARY

The Ubaye valley is a seismically active region in the Western Alps (France), regularly struck by seismic swarms, e.g., in 2003–2004 or 2012–2015. While some earthquakes could be associated with known faults, the character of the observations (high seismicity – low deformation rate) requires complex driving processes beyond local or regional tectonics. Most conceptual models involve pressurized fluids present down to depths of several km, and/or long-range transport.

During 2020/21, a data set of 30 MT sites was acquired, covering a signal period ranging between 10^{-4} to 10^{4} s. Data quality was generally satisfactory up to 3 s and sometimes up to 100 s. For the 3-D inversion performed using the ModEM code, we have chosen a joint inversion of induction vectors, phase tensors and off-diagonal impedances (previously corrected for static shift with help of phase tensor inversion and few TDEM measurements).

The main findings include (a) a prominent conductor (down to 20 Ωm) located along the axis of the swarm zone, though generally above it; (b) a regional dominance of the Peninic Front in the East and the overridden Mesozoic (Dauphinoise) sediments in the West; (c) strike directions that agree well with most of the mapped faults and focal mechanisms of the strongest seismic events.

Our sensitivity reaches the border of the seismic swarm activity, but does not cover its depth extent. Conceptual models proposed for the origin of the seismic swarm activity will be discussed in the light of the MT imaging, and the associated uncertainties.

Keywords: magneto-tellurics, pressurized fluids, seismic swarms, Penninic Front, Western Alps

Two-dimensional electrical resistivity model of Sabalan geothermal field using Magnetotelluric data

Gholam Abbas Fanaee Kheirabad [1], Behrooz Oskooi [2]

[1] Mining Department, Birjand University of Technology, Birjand, Iran, afanaee@birjandut.ac.ir
[2] Institute of Geophysics, University of Tehran, Tehran, Iran, boskooi@ut.ac.ir

SUMMARY

The Sabalan Magnetotelluric (MT) survey discussed in this paper was carried out in November 2007. MT field components in the frequency band 0.002 – 320 Hz were collected at 28 sites at an average distance of 1.4 kilometer. The selected profile with seven MT stations in the region crosses over the hydrothermally altered zones and perpendicular to the main geological structures. The subsurface resistivity structure was modeled to assess the size of the geothermal resources and to prepare conceptual model for the hydrology of the geothermal fluid reservoirs. The MT sites were projected to a line for two dimensional (2-D) modeling. Electrical resistivity and impedance phase models were computed for TM and joint TE and TM mode data. These models resolved a good correlation between the features of the geothermal field and resistivity distribution at depth. The resulting models reveal the presence of a resistive cover layer underlain by an anomalous conductive layer at about 500 -1000 m below the ground surface. A very low resistivity (3 - 5 ohm-m) feature at the depths below 2000 m, bounded by two more resistive (100 - 500 ohm-m) features that interpreted as the main heat source of the geothermal system. At shallow depths, the resistivity model obtained from the MT data is consistent with the general conceptual resistivity model proposed for high-temperature geothermal systems at literatures.

Keywords: Geothermal exploration, Magnetotelluric, 2-D inversion, Electrical resistivity, Sabalan.

INTRODUCTION

Geothermal resources are ideal targets for electromagnetic (EM) methods since they produce strong variations in underground electrical resistivity. In thermal areas, the electrical resistivity is generally lower than in areas with colder subsurface temperature (Oskooi et al., 2005). Magnetotelluric (MT) studies have been conducted over geothermal systems (Spichak et al., 2009; Heise et al., 2008).
In 1998 a dense grid of 212 MT stations carried out on the Sabalan area that highlighted its resestivity structure and the relations between conductive anomalies and the geothermal reservoir condition (Talebi et al., 2005; Fanaee et al., 2010).
The most productive areas of Sabalan geothermal field were explored in November 2007. The primary objective of this survey was to delineate any resistivity anomalies that may be associated with high temperature geothermal resources. During recent years Mount Sabalan is considered as the subject of detailed volcanological, petrological and geophysical investigations (Oskooi et al., 2016; Fanaee et al., 2021; Oskooi et al., 2015; Ghaedrahmati et al., 2013).
Figure 1 show the geological setting in Sabalan area and the broader geological and geophysical settings of the area are described by Bromley et al. (2000).

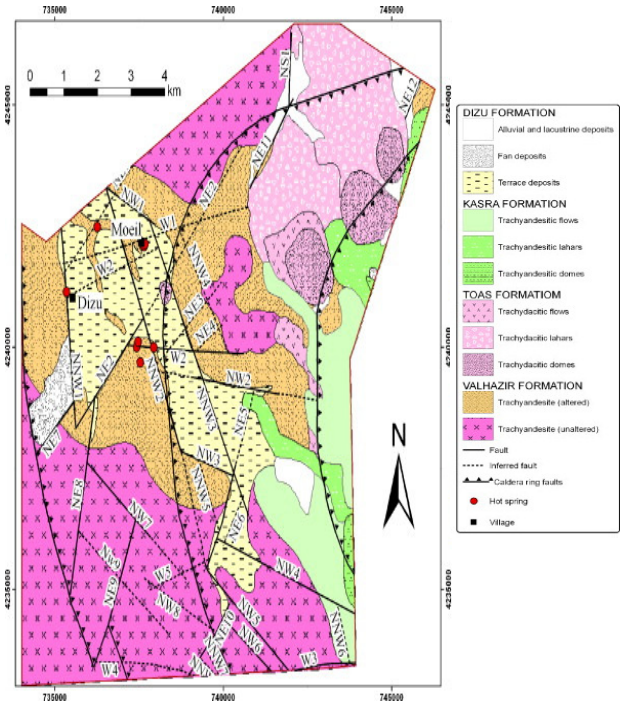

Figure 1. Simplified geological map of the study area (Emami, 1994).

METHODS

The basic principles of the MT method were introduced by Tikhonov (1950) and Cagniard (1953). The impedance tensor (Z) is defined as the relation in frequency domain between the components of the magnetic field B and those of the electric field E measured at the surface of the earth:

$$\begin{pmatrix} E_x \\ E_y \end{pmatrix} = \frac{1}{\mu_0} \begin{pmatrix} Z_{xx} & Z_{xy} \\ Z_{yx} & Z_{yy} \end{pmatrix} \begin{pmatrix} B_x \\ B_y \end{pmatrix} \quad (1)$$

indices x and y denoting magnetic North and East, μ_0 being the magnetic permeability of vacuum.

Z is usually displayed as apparent resistivity and phase which depend on the angular frequency:

$$\rho_a(\omega) = \frac{1}{\omega\mu_0}\left|Z(\omega)\right|^2 \quad (2)$$

$$\phi(\omega) = \arctan\frac{\mathrm{Im}\left(Z(\omega)\right)}{\mathrm{Re}\left(Z(\omega)\right)} \quad (3)$$

Simultaneously the variation of the vertical component (z-direction) of the magnetic field is also measured. Various skew parameters were estimated in order to analyze the dimensionality of the data. Swift's skew defined as the ratio of the on- and off diagonal impedance elements, approaches zero when the medium is 1-D or 2-D (Swift, 1967). Skew values below 0.2 in majority indicate that the study area could be approximated to a 2-D structure geoelectrically. MT sounding curves show a 2-D effect with a clear separation between the curve with the electric field parallel to the strike (TE mode) and the curve related to current circulation normal to the strike (TM mode). Skew values of the impedance strike shown in Figure 2 for the data from almost all sites and frequencies.

In cases where MT data display overall 2-D characteristics despite some 3-D effects, results obtained using 2-D inversion algorithms can be valid (Ledo, 2005).

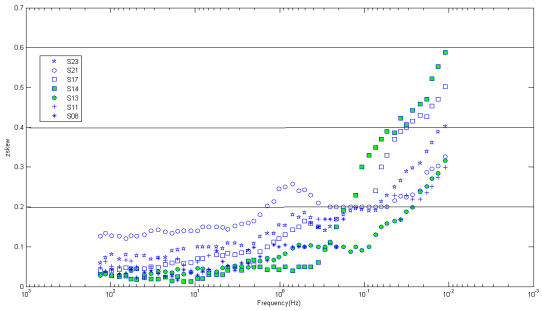

Figure 2. Variation of Swift's skew values (dimensionality factor) for all sites along the profile.

To obtain the subsurface structure along the profile, 2-D inversion code of REBOCC by Siripunvaraporn and Egbert (2000) was used. The code seeks a smooth model with the minimum amount of features required by the data. The data points were carefully selected between frequency ranges 0.002–320 Hz. The inversion started from a homogeneous half space with resistivity of 100 ohm-m.

In the inversion, apparent resistivity and phase data of both TE and TM modes were used. Reasonable RMS misfit was achieved usually after 10 iterations. The MT transfer functions along the strike (TE-mode) and orthogonal (TM-mode) directions were inverted simultaneously, to derive the 2-D subsurface resistivity distribution. Static shifts were not corrected at this stage of the work, as we were missing shallow subsurface information. However, apparent resistivity data on most sites show little difference between the two polarization curves at high frequencies and vary smoothly passing from one site to the next. Several inversions were performed of the TM and joint TM+TE modes. Since TM mode typically suffers less 3-D distortion than TE (Wannamaker et al., 1984), some inversions took into account only the TM mode data. The apparent resistivity was down-weighted during the inversion process to help to accommodate the possible static shift effects in the data. Error floor of 20% for the apparent resistivity and of 5% on the phase were assumed.

RESULTS

The inversion result of TM mode data is shown in Figure 3, respectively. By these levels of error on the data, the fit of the computed model response to the observed data was satisfactory (Figure 4). The resistivity and layer thickness of the obtained models depend on the mode used for the inversion. The normalized root mean square (rms) misfit was around 3 for obtained models.

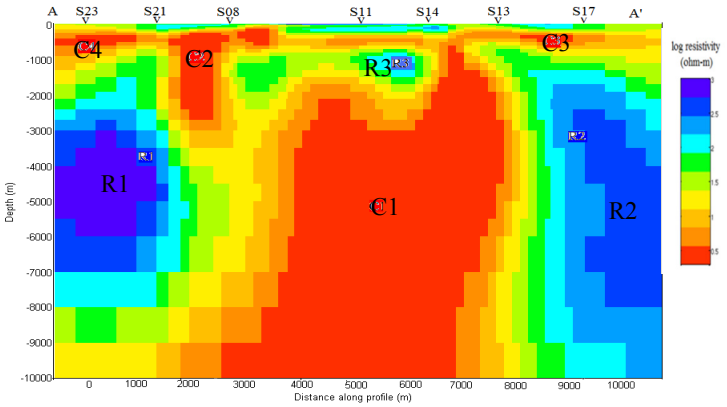

Figure 3. The resistivity model resulting from the inversion of TM mode data. C; conductive, R; resistive features.

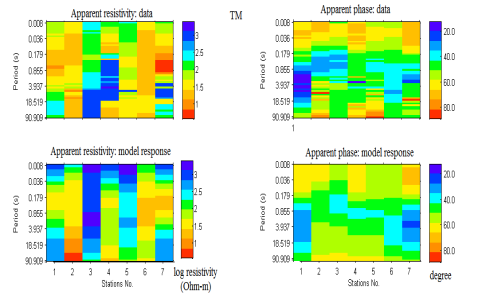

Figure 4. TM-mode data and model responses of the 2-D inversion.

The resulting model and data misfit for joint TE and TM-mode data is shown in Figure 5 and Figure 6.

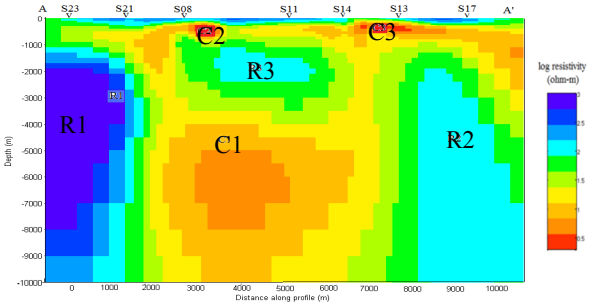

Figure 5. The resistivity model resulting from the joint inversion of TM and TE mode data.

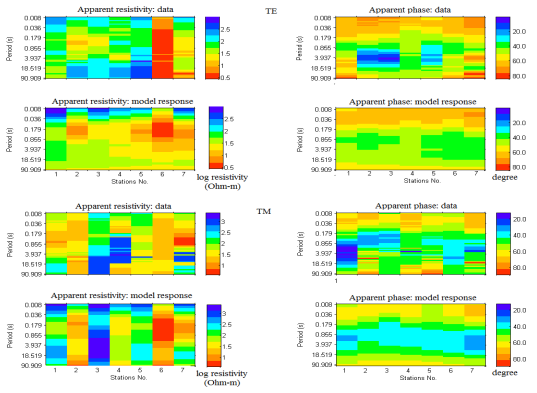

Figure 6. The TE and TM mode data and model responses from the joint inversion results.

DISCUSSION

In our case study, the inversion provides the valuable results. The prominent structures in the obtained resistivity models (Figure 3 and Figure 5) are discussed below:
A resistive layer (>400 ohm-m) is recognized at the top. At depth 300-1300 m there is a resistive feature (R3) among three separate conductive bodies (C1, C2, C3).

Conductive bodies show variable thicknesses along the 2D section, passing from a few hundred meters above R3 to about 3000m at C2. Below these conductors there is an increase of resistivity with depth along the whole profile, except under sites 8, 13 and 14, where the resistivity is always lower than a few tens of ohm-m in depth (<10 ohm-m). The opposite ends of the profile are characterized by a high resistivity (1000 ohm-m) structure, whereas in the middle of the profile the conductive feature, C4, (<10 ohm-m) is followed by a resistive layer R3 (>100 ohm-m), which in turn is overlying a very conductive structure C1 (<5 ohm-m).
The conductive structure is clearly constrained to the central part of the profile. The uppermost 0.5–4 km of the obtained 2-D resistivity structures is fairly like the previous results from 1998 MT data modeling (Fanaee et al., 2011). There is a highly conductive (<5 ohm-m) structure at depth of about 2.5 km in the middle of the profile. Most naturally magmatic intrusions acting as a heat source for the geothermal system, although there are no temperature data to confirm the presence of magma in Sabalan area. Another peculiar feature is the area beneath sites 8,21 and sites 13,14, where the 2-D model shows an abrupt transition to moderate resistivity values down to depths of 2-3 km where the deep conductive body begins. Most probably, an almost vertical fluidized or altered fault zone connecting the shallow and deep conductors together.

CONCLUSIONS

The magnetotelluric method and its ability to map deep conductive features, can make a valuable role in the reconnaissance of deep geothermal systems. A pilot MT survey was carried out in the Sabalan area, deploying seven broadband sites along a nearly 10 km profile. 2-D inversion results show conductivity models with stable features, identifying the main geological units. Analysis of the different skew parameters indicates that the impedances are well described in terms of 2-D models. Some deviations from 2-D behavior were noted for the data of some frequencies and sites where misfits were relatively large. The final 2-D model was stable and not depending on the a priori or starting models. Generally, the main result is that the two-dimensional electrical resistivity model is perfectly comparable to the structures found in literature as conceptual resistivity model of a high-temperature geothermal system (Berktold, 1983).

ACKNOWLEDGEMENTS

The authors would like to thank Siripunvaraporn and Egbert for academic use of their REBOCC code. Also, we are grateful to Renewable Energy Organization (SUNA) of Iran for preparing the data.

REFERENCES

Berktold, A., (1983) Electromagnetic studies in geothermal regions. Geophysics. Survey. 6, 173–200

Bromley, C.J., Khosrawi, K. and Talebi, B., (2000) Geophysical Exploration of the Sabalan Geothermal Prospects in Iran. Proceedings, World Geothermal Congress 2000: 1009-1014.

Cagniard, L., (1953) Basic theory of the magnetotelluric method. Geophysics 18, 605–635..

Emami H., (1994) Me□hkin□hahr 1; 100, 000 Scale Geological Map. Geological Survey of Iran.

Fanaee Kheirabad, G. A., Oskooi, B., (2021) Two-dimensional magnetotelluric modeling of the Sabalan geothermal field, North-West Iran, Journal of the earth and space physics,46(4), 27-37

Fanaee Kheirabad, G. A., Oskooi, B., (2010) Magnetotelluric modeling of Sabalan geothermal field, NW Iran, Presented in 20th international electromagnetic induction workshop, Giza, Egypt.

Fanaee Kheirabad, G. A., Oskooi, B., Porkhial, S., Rahmani, M. R., (2010) Investigation of Sabalan geothermal field structure using Magnetotelluric data, Presented in 14th Geophysics Conference of Iran, Tehran, Iran.

Fanaee kheirabad, G.A., Oskooi, B., (2011) Magnetotelluric interpretation of Sabalan geothermal field in northwest of Iran. Journal of the earth and space physics 37(3):1-11

Ghaedrahmati, R., Mradzadeh., A., Fathianpour., N., Kon Lee, S., (2013) Investigating 2-D MT inversion codes using real field data. Arabian Journal of Geoscience, 7, 1-16

Ghaedrahmati, R., Mradzadeh., A., Fathianpour., N., Lee, SK, Porkhial S., (2013) 3-D inversion of MT data from the Sabalan geothermal field, Ardabil, Iran. Journal of Applied Geophysics, 39: 12-24

Heise, W., Caldwell, T.G., Bibby, H.M., Bannister, S.C., (2008) Three-dimensional modelling of magnetotelluric data from the Rotokawa geothermal field, Taupo Volcanic Zone, New Zealand. Geophysical Journal International 173, 740–750.

Ledo, J., (2005) 2D versus 3D magnetotelluric data interpretation: Surveys in Geophysics, 26,671-806.

Oskooi, B., Pedersen, L.B., Smirnov, M., Árnason, K., Eysteinsson, H., Manzella, A., (2005) The deep geothermal structure of the Mid-Atlantic Ridge deduced from MT data in SW Iceland. Phys. Earth Planet. Inter. 150, 183–195.

Oskooi, B., Fanaee Kheirabad, G. A., Habibian Dehkordi, B., Nieuwenhuis, G., (2015) Three-dimensional conductivity model of the Sabalan geothermal field, NW Iran, interpreted from magnetotelluric data, Arabian Journal of Geosciences, (8) 3149-3157

Oskooi, B., Takalu, M., Montahaei, M., Rahmani, M.R., (2016) A recent magnetotelluric investigation of the Sabalan geothermal field in north-western Iran, Bollettino di Geofisica Teorica ed Applicata , Vol. 57 Issue 3, p261-274.

Siripunvaraporn, W. and Egbert, G., (2000) An effient data-subspace inversion for two dimensional magnetotelluric data, Geophysics, 65, 791-803.

Spichak V. Manzella A. (2009) Electromagnetic sounding of geothermal zones, Journal of Appl. Geophysics, 68 (4), 459-478.

Swift, C.M., (1967) A magnetotelluric investigation of electrical conductivity anomaly in the southwestern united states. PhD Thesis Massachusetts Institute of Technology.

Talebi, B., Khosrawi, K., Ussher, G., (2005) Review of resistivity surveys from the NW Sabalan geothermal field, Iran. Proc. World Geothermal Congress, Antalia, Turkey.

Tikhonov, A.N., (1950) On determining electrical characteristics of the deep layers of the Earth. Doklady Akademii Sel'skohozaÃjstvennyh Nauk 73, 295–297.

Wannamaker, P.E., Hohmann, G., Ward, S., (1984) Magnetotelluric responses of three-dimensional bodies in layered earths. Geophysics 49, 1517-1533.

Analysis of Geothermal Manifestation Distribution at Blawan-Ijen Geopark, East Java, Indonesia based on Magnetotelluric and Gravity Data for Determining the Recommendation of PLTP Location

Ibrahim, A[1*], Hapsoro, C., A.,[1] and Zulaikah S.[1]
[1] Astronomy and Geophysics Research Group, Department of Physics, Faculty of Mathematics and Natural Sciences, Universitas Negeri Malang, Jl. Semarang 5 Malang 65145 East Java, Indonesia,
alpanibrahim33@gmail.com
[1]cahyo.ajihapsoro.fmipa@um.ac.id
[1]siti.zulaikah.fmipa@um.ac.id

SUMMARY

Magnetotelluric (MT) and gravity investigations have been carried out at the Blawan-Ijen Geopark. Blawan-Ijen Geopark is located in Bondowoso-Banyuwangi, East Java, Indonesia. This investigation aims to find the subsurface resistivity structure of the area that may be correlated with geothermal in the area of unknown geothermal potential. MT surveys have been carried out in the area using a magnetometer located 3-5 km from the survey area. On the other hand, a gravity survey has been carried out at the same location as the MT survey site. The results of gravity data interpretation are used to support or check the results of MT data interpretation. The result of interpretation of MT and gravity data shows that the subsurface structure of the area correlates with the structure of the geothermal reservoir. The emergence of the Blawan fault is a way for geothermal fluid to flow to the earth's surface in the form of gas or steam. The distribution flow of Blawan's geothermal manifestations originates from the caldera of the older Ijen Mountains which spreads towards the Kendeng Mountains. It is also known that the geothermal manifestations of Blawan follow the flow of the Banyu Pahit river as evidenced by several hot springs along the river.

Keywords: Magnetotelluric, Gravity, Blawan-Ijen Geopark, Geothermal

Abstract, 25th EM Induction Workshop, Çeşme, Turkey, September 11-17, 2022

Interpretation and modeling of airborne and ground magnetometry data for a geothermal reservoir in the Abgarm region of Mahallat in Iran

Behrooz Oskooi[1,2*], Andreas Junge[1] ,Seyed Hossein Hosseini[2], Banafsheh Habibian Dehkordi[2] and Seyed Masoud Ghiasi[2]

[1]Institute of geosciences, Goethe University, Frankfurt, Germany

[2]Institute of Geophysics, University of Tehran

boskooi@ut.ac.ir, junge@geophysik.uni-frankfurt.de,
Hosseini.hossein@ut.ac.ir, bhabibian@gmail.com, masoud.ghiasi10@alumni.ut.ac.ir

SUMMARY

Abgarm of Mahallat is a well known geothermal region in central Iran on which many geophysical surveys are already conducted. To validate and compare the results with previous studies on this area, we take the opportunity to analyze the region by using magnetic and aeromagnetic methods simultaneously. Generally, this study tries to estimate the profound expansion of the leading geothermal anomaly and its sub-branches. The form of the anomaly was determined from aeromagnetic and ground magnetic grids, and in order to investigate the anomalies thoroughly, 3D inverse modeling has been utilized. Using several methods to estimate the depth of anomaly would approach us to the actual values. Hence, Euler's depth estimation and power spectrum depth estimation are applied to the aeromagnetic and magnetic data. As results, the interpretation of both methods afforded the consonant and comprehensive interpretation that perfectly accommodates previous studies on this region.

Keywords: Abgarm, Aeromagnetic, Geothermal, Mahallat, Magnetometry, 3D inversion.

INTRODUCTION

The earth is an extreme thermal energy resource that its heat is directed to the ground surface by volcano eruptions and underground water. The heat is continuously transferred to the upper levels by hydrothermal liquids. Hot water through the fractures and porosities emerges as hot water springs and geysers. A huge part of hot liquids are trapped in porous rocks and crustal fractures and provide the natural warm water resources, known as geothermal resources (Huenges et al. 2010). By studying geothermal anomalies, it turns out that superficial and groundwaters carry heat to the surface or shallower areas by penetrating to the deeper layers; this heat circulation is caused by the specific gravity of the cold and hot subsurface fluid (Dickson et al. 1995). Mahallat is one of the essential geothermal areas in central Iran. Some of the geological evidence to back up this claim are numerous hot springs, intrusive granite, granodiorite on sedimentary beds, and obvious alterations (Oskooi et al. 2016; Darijani et al 2014; Geological specifications of Mahallat 2008; Kahak and Golpayegan geological maps, 1995). Oskooi et al. (2016) have indicated that a structure with a 1.82 structure index shows a vertical cylinder; it is a geothermal spring formed by a significant mass of mafic or ultramafic intrusive igneous rocks. Oskooi and Darijani (2013) also confirm that the top of the cylinder anomaly is cone-shaped. In this study, Abgarm of Mahallat hot springs were explored using magnetic and aeromagnetic methods simultaneously. In general, magnetic studies can help us study the geothermal resources. Mafic intrusive bodies are closely associated with magnetic rocks, which are highly susceptible. This article locates the geothermal heat source by interpreting the magnetic and aeromagnetic data together.

Methodology

By using standard Euler deconvolution, we can estimate the position of the target body. This approach utilizes three orthogonal gradients of potential quantities. Three-dimensional Euler's equation is shown as below (Reid et al. 1990):

$$(x_i - x_0)\frac{\partial \Delta T_i}{\partial x} + (y_i - y_0)\frac{\partial \Delta T_i}{\partial y} + (z_i - z_0)\frac{\partial \Delta T_i}{\partial z} = -N\Delta T_i \quad (1)$$

where. $x_0, y_0, and\ z_0$ are the coordinates of magnetic source, T is the total magnetic anomaly and $\frac{\partial}{\partial x}, \frac{\partial}{\partial y}, and\ \frac{\partial}{\partial z}$ are derivatives in directions of x, y, and z, respectively. N belongs to the structural index (SI) that has been explained in the following. Using deconvolution can obtain the source anomaly specifications; because it is a procedure that uses the output to gain input.

Spectral analysis is a proper approach for

estimating the average depth of large-scale magnetic or gravity anomalies that concentrates on statistical specifications of sources. By taking the natural logarithm of both sides of azimuthally averaged power spectral equation, obtains:

$$\ln(\Phi|k|) = \ln(A) - 2|k|d + 2\ln(1 - e^{-|k|t}) \quad (2)$$

where, A is a constant value that depends on magnetization direction and regional magnetic fields, and k is wave number. Equation (3) in the high wave-number mediums, belongs to straight-line with -2d coefficient. approximately. Thus, we can obtain half of angle coefficient, which is estimation of (d) by fitting a straight line on the mediocre and high wavenumber section of logarithm power spectral curvature (Blakely 1995).

Li and Oldenburg (1996, 1998) provided algorithms for inverse modeling of the magnetic and gravity data. Because of the comprehensiveness of recommended method, it is one of the useful and classical methods for this purpose. The following Equation 3 (the general form of $Ax = B$), is principle of magnetic and gravity inversion modeling as has been used in this paper (Li and Oldenburg 1994, 1996, 1998):

$$(G^T W_d^T W_d G + \beta W_m^T W_m)m = G^T W_d^T W_d d^{obs} + \beta W_m^T W_m m_0 \quad (3)$$

G is $N \times M$ matrix known as data kernel, $d^{obs} = [d_1 d_2 d_3 \dots d_N]^T$ is observed data (magnetic or gravity), $m = [m_1 m_2 m_3 \dots m_M]^T$ is model parameter, W_d is weighted data matrix as diagonal matrix $W_d = diag[{}^1/_{\sigma_1} \dots {}^1/_{\sigma_N}]$ that σ_i is ith data standard deviation, m_0 is geological reference model, and W_m is a matrix for weight factor for calculating m length.

Geological Setting

Mahallat is located in the central volcanic zone of Iran. This zone has been active through the centuries and looks like a triangle in central Iran. The western boundary of Mahallat is limited to The Sanandaj-Sirjan metamorphic zone. The central zone of Iran is restricted to Alborz and Makran zone from Northern and southern boundaries, respectively, and in the eastern border of the mentioned zone can observe the Lut block. Minor superficial-shearing erosion of the zone is noticeable. Due to the extension of dolomite and limestone units and their fractures, the zone illustrates a good permeability. As mentioned above, The Eocene sediments consist of conglomerates that emerge in the southern section of the zone as hills. The most critical fault in the area is the Mahallat fault with an east-west extension. This fault near Delijan finds northeast-southwest, then north-south direction. The outcropped formations of the area are as follows: Shemshak formation (with Jurassic shale and limestone lithology), cretaceous Orbitolina limestone, Qom formation (with Marly - Limestone lithology), and igneous granodiorite has formed in the vicinity of sedimentary rocks (Hosseini et al. 2020).

Results

In order to investigate the Mahallat geothermal zone generally, which is a large-scale area, aeromagnetic data of the mentioned area have been utilized. The altitude of the flight is 400 to 500 meters with a flight spacing of 7.5 kilometers. The dimension of the region is $18800 \times 15500\ m^2$ and the residual magnetic map's minimum and maximum magnetic intensity are 18.8 and 525.8 nT, respectively. The lack of a negative value for the magnetic intensity states that the bottom part of the anomaly could be profound, therefore, the surveying cannot detect the negative pole of the anomaly. The RTP filter (Figure 1) was exerted to simplify the interpretation and increase the resemblance of the map and the actual shape of the anomaly. The shape of the anomaly in the RTP filter is very similar to the shape of the mass in inverse modeling, shown in the following. In order to investigate the sub-branches of the main anomaly discussed in the aeromagnetic section, a ground magnetic survey has been acquired. The dimension of the surveyed zone is 4660*2600 square meters, and 10000 stations have been used. Figure 1 indicates the residual aeromagnetic map of Iran (with 7.5 KM flight spacing) and the studying area. The red and blue rectangular in the zoom box picture illustrates the geographical locations of the aeromagnetic and ground magnetometry. In order to illuminate the main anomaly and sub-branches anomalies positions, the aeromagnetic and ground magnetometry RTP grids have been overlayed on the geographical projection of the surveying zone. The minimum magnetic field intensity is 47391.3, and the maximum is 48988.1 nT. The inclination and declination angles are 52.4 and 4.4 degrees, respectively. It is worth noting that the main intrusive anomaly of the Mahallat, which has been

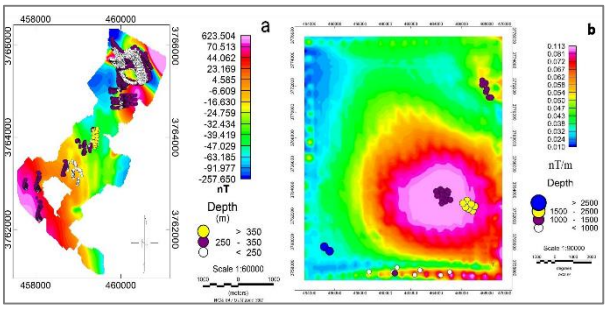

Figure 1. The residual aeromagnetic grid of Iran (the aeromagnetic and ground magnetometry surveying zones and their RTP grids have been superimposed)

investigated in the aeromagnetic section, is in the

northeast of the Abgarm area (ground magnetic grid).
Spectral analysis depth estimation is applicable for large-scale anomalies (Blakely 1995). Figure 2 shows the power spectrum function of Mahallat aeromagnetic data.

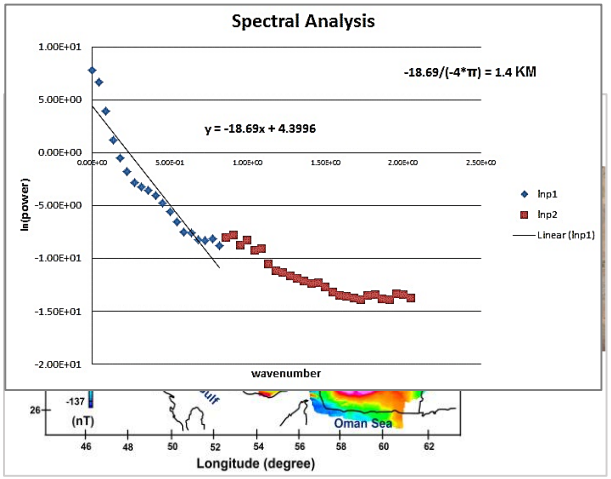

Figure 2. Depth estimation by power spectrum function.

As shown in Figure 2, the depth of the top of the anomaly is 1.4 km. This value fits well with previous studies that have suggested a depth of 1280 meters. (Oskooi et al., 2014). Figure 3a illustrates the located Euler depth estimation for structure index of 2 (cylinder). Conquerors of the solutions demonstrate the depth of 1000 to 1500 meters and 1500 to 2500 meters. In order to estimate the basement depth, the standard Euler was acquired. Euler's method depends on the shape of the anomaly that interferes with the differential equation as the structural index. Due to the area dimension and the anomaly expansion, $400 \times 400\ m^2$ window was considered for depth estimation in its center. According to the obtained inverse modeling from ground magnetometry data in the following, a structural index of 1 was presumed. Due to the Figure 3b, three depth ranges have been considered. White circles indicate 250 meters depths and lesser, purple circles are related to 250 to 350 meters, and yellow points are more than 350 meters depths representative.
Figure 3. (a) Standard Euler's depth estimation for structural index 1 (ground magnetic data), (b) located Euler depth estimation for structure index 2 (aeromagnetic data).

Figure 4a indicates 3D inverse modeling, which has been obtained from the Li-Oldenburg algorithm for Mahallat aeromagnetic data. The minimum and maximum of the susceptibility value are 0 and 0.03, respectively. The upper section of the anomaly has cone-shape geometry, and prior studies in this region have provided the same shape in their modeling, which confirms the inverse modeling accuracy (Oskooi et al. 2016). Li-Oldenburg inversion modeling algorithm also has been utilized for ground magnetometry survey of Abgarm region. Figure 4b views the ultimate inverse modeling obtained from the Li-Oldenburg algorithm. The Minimum and Maximum values of the susceptibility are 0 and 0.1, respectively. In order to present the model nicely, a depth of 2000 meters has been considered.

Discussion and conclusions

This study continues the previous studies in the Mahallat geothermal region that simultaneously benefits from a multi-method interpretation. The proliferation of the studies in this zone facilitates validation by matching the outcomes with prior ones. As mentioned before, first, the aeromagnetic data was investigated. Due to the Mahallat geothermal expansion, exploitation of the long flight spacing aeromagnetic data would be passable. Afterward, the power spectrum depth estimation and Euler's depth estimation have been utilized to obtain the aeromagnetic data anomaly upper depth. The upper depth of the anomaly in 3D inversion modeling is 1500 meters approximately in the power spectrum, depth estimation is 1.4 kilometers, and Euler's depth estimation is 1000 to 1500 meters. In the following, the Abgarm zone of the Mahallat ground magnetometry has been used. The ground magnetometry surveying was supplementary data through the main Mahallat geothermal zone. First, we applied Euler depth estimation on the data, and the upper sector depth of the anomaly is about 250 meters. In order to study the Abgarm-Mahallat area perfectly, 3D inverse modeling has been employed. The upper depth of the modeling shows 250 meters, which matches Euler's depth estimation.
The obtained depths in this study is in accordance with prior studies. For instance, Hosseini (2020), according to the 2D inverse modeling sections of MT, the depths of 250 to 1500 meters as granodiorite lava proposed. In addition, the cooling volcanic mass (heat source) has been set in the depth of 3 to 4 kilometers (Hosseini et al. 2020). As mentioned before, this study is a supplementary investigation in the Mahallat region. It utilizes aeromagnetic and ground magnetic data and their inverse modeling as verification implement, and the results indicate perfect analogy.

Acknowledgements

Authors would like to express their sincere thanks to the Institute of the Geophysics, University of Tehran and Goethe university, for all supports and utilities that were provided freely for fulfilment of this research.

References

Blakely R., Potential Theory in Gravity and Magnetic Applications. Cambridge University Press, 1995.

Dickson, M. H., & Fanelli, M. (2013). *Geothermal energy: utilization and technology*. Routledge.

Hosseini, S. H., Habibian Dehkordi, B., Abedi, M., & Oskooi, B. (2021). Implications for a Geothermal Reservoir at Abgarm, Mahallat, Iran: Magnetic and Magnetotelluric Signatures. *Natural Resources Research*, *30*(1), 259-272.

Huenges, E., & Ledru, P. (Eds.). (2011). *Geothermal energy systems: exploration, development, and utilization*. John Wiley & Sons.

Oskooi, B., Mirzaei, M., Mohammadi, B., Mohammadzadeh-Moghaddam, M., & Ghadimi, F. (2016). Integrated interpretation of the magnetotelluric and magnetic data from Mahallat geothermal field, Iran. Studia Geophysica et Geodaetica, 60(1), 141-161.

Oskooi, B. and Darijani, M. (2014). 2D inversion of the magnetotelluric data from Mahallat geothermal field in Iran using finite element approach. *Arabian Journal of Geosciences*, *7*(7), 2749-2759.

Oskooi, B., Darijani, M. and Mirzaie, M., 2013. Investigation of electrical resistivity and geological structure on the hot springs in Markazi province of Iran using magnetotelluric method. Bollettino di Geofisica ed Applicata 54, 245-256.

Reid A.B., Allsop J.M., Granser H., Millet A.J. and Somerton I.W., 1990. Magnetic interpretation in three dimensions using Euler deconvolution. Geophysics, 55, 80-91.

Li Y. and Oldenburg D. W., 3-D inversion of gravity data, Geophysics, vol. 63, no. 1, pp. 109-119, 1998.

Li Y. and Oldenburg D. W., 3-D inversion of magnetic data, Geophysics, vol. 61, no. 2, pp. 394-408, 1996.

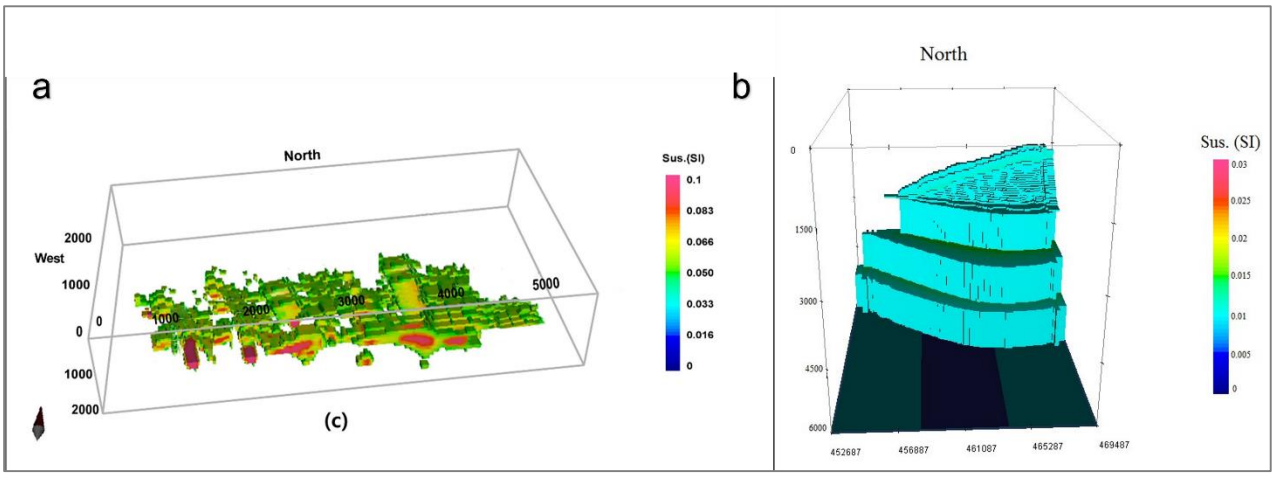

Figure 4. Inversion model of (a) Abgarm magnetometry data, (b) and Mahallat aeromagnetic data .

New insight of the hydrothermal system beneath Tolhuaca volcano (South Chile) revealed by magnetotelluric observations.

M. Pavez[1], D. Diaz[2], V. Goldberg[3], H. Brasse[4], I. Budach[5], G. Kapinos[6] and E. Schill[1,7]
[1]Karlsruhe Institute of Technology - Institute for Nuclear Waste Disposal, maximiliano.pavez@partner.kit.edu
[2]University of Chile - Department of Geophysics
[3]Karlsruhe Institute of Technology - Institute of Applied Geosciences
[4]Freie Universität Berlin - Fachrichtung Geophysik
[5]Geothermie Neubrandenburg GmbH
[6] Bundesanstalt für Geowissenschaften und Rohstoffe
[7]Technical University Darmstadt - Institute of Applied Geosciences

SUMMARY

On the NW flank of the Tolhuaca volcano an active geothermal system has developed with reservoir temperatures estimated of 220° - 300°C, characterized by several surface thermal manifestations with fumaroles, solfataras and hot springs. The interplay between heat-fluid-rock interaction processes is fundamental in the development of geothermal systems. However, the heat source of the geothermal system are poorly constrained. The work presented here address this issue by studying the electrical properties of the active Tolhuaca geothermal system in the Andes of southern Chile. Using newly recorded magnetotelluric data in the surrounding of Tolhuaca, we present a 3-D model of electrical resistivity of the crust. We used temperature measurements in deep wells and geochemical analyses of borehole fluid samples and new water samples to constrain present-day fluid conditions. The magnetotelluric model reveals different electrical structures below the western flank of Tolhuaca. The derived model endorses a previous study that drew the conclusion that there was highly conductive region associated with a low permeability clay-cap directly under the NW flank of the Tolhuaca volcano. Additionally, the electrical resistivity model shows a shallow conductive anomaly, ~3km below the Tolhuaca volcano, connected with a sub-vertical anomaly of intermediate resistivity. As we found no indications of a deep conductor, such as those observed in other high enthalpy geothermal systems, we conclude that the shallow magmatic deposit that is cooling but still hot enough to provide the heat source of the geothermal system. This magmatic compartment would have been fed from deep crustal zones by a sub-vertical dipping basaltic-andesitic mush column, which would act as a preferential pathway for the ascent of hydrothermal fluids.

Keywords: magnetotellurics, electrical structures, hydrothermal system, geothermal reservoir

Magnetotelluric imaging of a shallow groundwater system in central Zagros, Iran

M. Montahaei[1],
[1]Institute of geophysics, University of Tehran, Tehran, Iran, mmontaha@ut.ac.ir

SUMMARY

The results of an AMT exploration carried out in the Mond river basin, Bushehr province, southwest Iran are presented in this study. We aim to find the overall conductivity structure of the geological features controlling the aquifer in a basin where subsurface structure is little known. Dimensionality analysis of the data was performed by the phase tensor and the WAL invariants and distortion effects were removed employing the Groom-Baily decomposition method. Distortion corrected data were then modeled by a 2D smooth inversion approach and the results were further explored by applying sensitivity analysis to find the range of relevant models representing shallow aquifer system in the study area.
2D smooth inversion resolves a shallow conductive layer, extending throughout the model and a resistive basement detached by a moderately conductive zone. Another conductive anomaly exists at deep part beneath the NW of the profile.
A different class of resistivity model was derived using a distinct regularization approach which seeks the smoothest variation away from a starting model. The result shows the possible brine circulation between water-filled fractures constituting the conductor in the deep part of the model and the shallow alluvial aquifer layer.

Keywords: magnetotellurics, electrical conductivity, aquifer, Zagros

INTRODUCTION

Tectono-sedimentary basin evolution controls groundwater resources in alluvial aquifer systems. The Sena- Shonbe aquifer system, one of the 64 alluvial aquifers comprising the Mond river basin in southwest Iran, where only scarce information about subsurface is available. The Mond river is among the most important rivers originating in the high elevation areas of the Zagros region, generally flowing NE-SW for ~600 km to the Persian Gulf. The geology of the Mond river basin is complex and strongly affected by tectonic events in the Zagros Fold and Thrust Belt, a subdivision of the Zagros collision zone.

Here, we investigate an AMT data set obtained along a profile in Sena- Shonbe aquifer system. We applied different methods to unravel the dimensionality of the subsurface resistivity structure and a 2D inversion approach for further interpretation of the measured AMT data.

Dimensionality and Directionality Analysis

We applied the phase tensor (Caldwel et al., 2004) and Groom- Baily (McNise and Jones, 2001) decomposition approaches for dimensionality and directionality analysis of the measured data. At short periods, phase tensor ellipses are circles representing an electrically layered earth. At longer periods they represent a quasi 2-D geo-electric structure.

the orientation of phase tensor ellipses at periods, where principal phase splits are garter than 3˚ are presented in figure 2. The results reveal a trend of about 30˚ for the regional strike direction.

2-D inverse modeling of MT data

Two-dimensional isotropic inversions of distortion corrected MT data were run using the WingLink software (Rodi and Mackie, 2001). Figure 3 shows the result of an inversion constrained to fit within 3.5% of apparent resistivity and 1˚ of phase data for both TM and TE modes. Model misfits are acceptable (RMS=1.48) with the general trends of the apparent resistivity and phase curves reproduced at all sites.

In the next step, we applied a-priori inversions to validate main features recovered in figure 3. all the conductive or resistive structures have been removed from the inversion. The outcomes were then used as starting models and allowed to evolve through the inversion procedure, where the closest model to the starting model was looked for. This strategy confines the starting district of the inversion and spotlights undetected or poorly constrained features (Schwalenberg et al., 2002). The experiment results (Figure 4) suggest that the main features in Figure 3 are data supported and their shapes do not change significantly through the sensitivity studies.

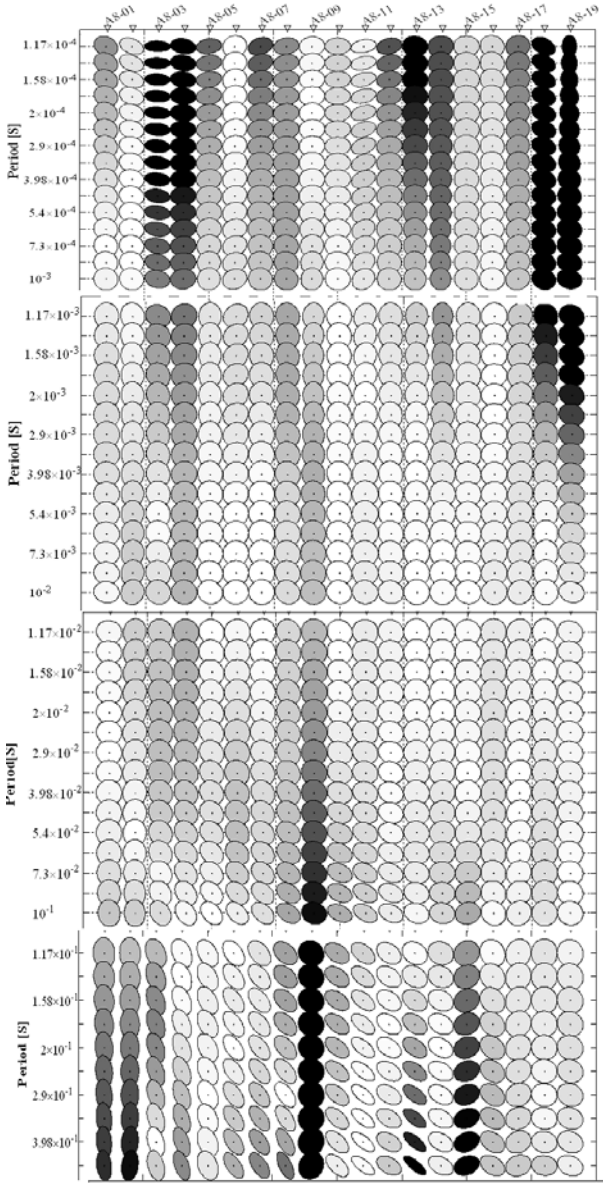

Figure 1. Pseudosection of phase tensors from the AMT survey, filled with the β skew angle.

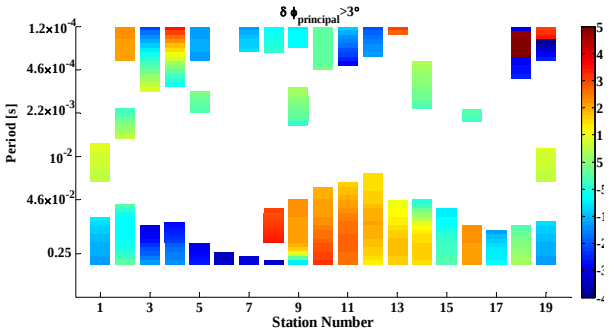

Figure 2. Pseudosection of phase tensor azimuths for the AMT survey. Azimuths are only shown for tensors with a split in the principal phases greater than 3˚.

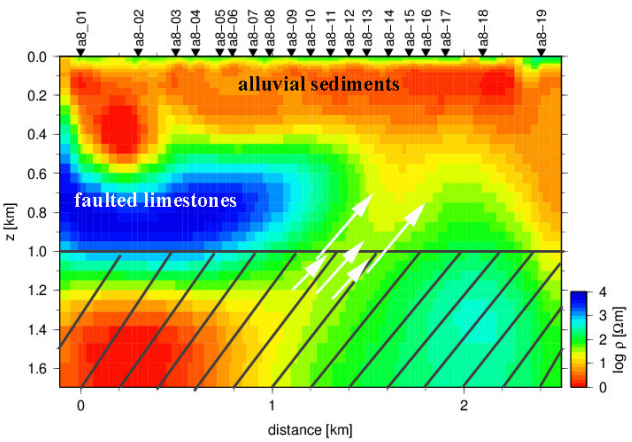

Figure 3. Final two-dimensional model produced from AMT data along profile A8 in central Zagros. The model used the TM and TE mode impedances as well as tipper data and reached an RMS value of 1.48.

CONCLUSIONS

In the course of this work, we outlined the results of dimensionality analysis and inversion results of an MT data set from central Zagros, Iran. The inversion model contains a thick conductive layer extending throughout the model, a deep conductor beneath the NW of the profile. Sensitivity tests support the existence of the narrow dipping conductive zone that connects the upper conductive layer and deeper conductor.

ACKNOWLEDGEMENTS

The author wishes to acknowledge Iran Office of Vice-presidency for Science and Technology, Office of drought, erosion and environmental affairs for kindly providing the field data used in this work.

REFERENCES

Caldwell, T.G., Bibby, H.M. & Brown, C., 2004. The magnetotelluric phase tensor, Geophys. J. Int., 158, 457–469.

McNeice, G. W., & Jones, A.G. (2001). Multisite, multifrequency tensor decomposition of magnetotelluric data. *Geophysics*, 66, 158–173.

Rodi, W., and R. L. Mackie (2001), Nonlinear conjugate gradients algorithm for 2-D magnetotelluric inversions, Geophysics, 66, 174–187.

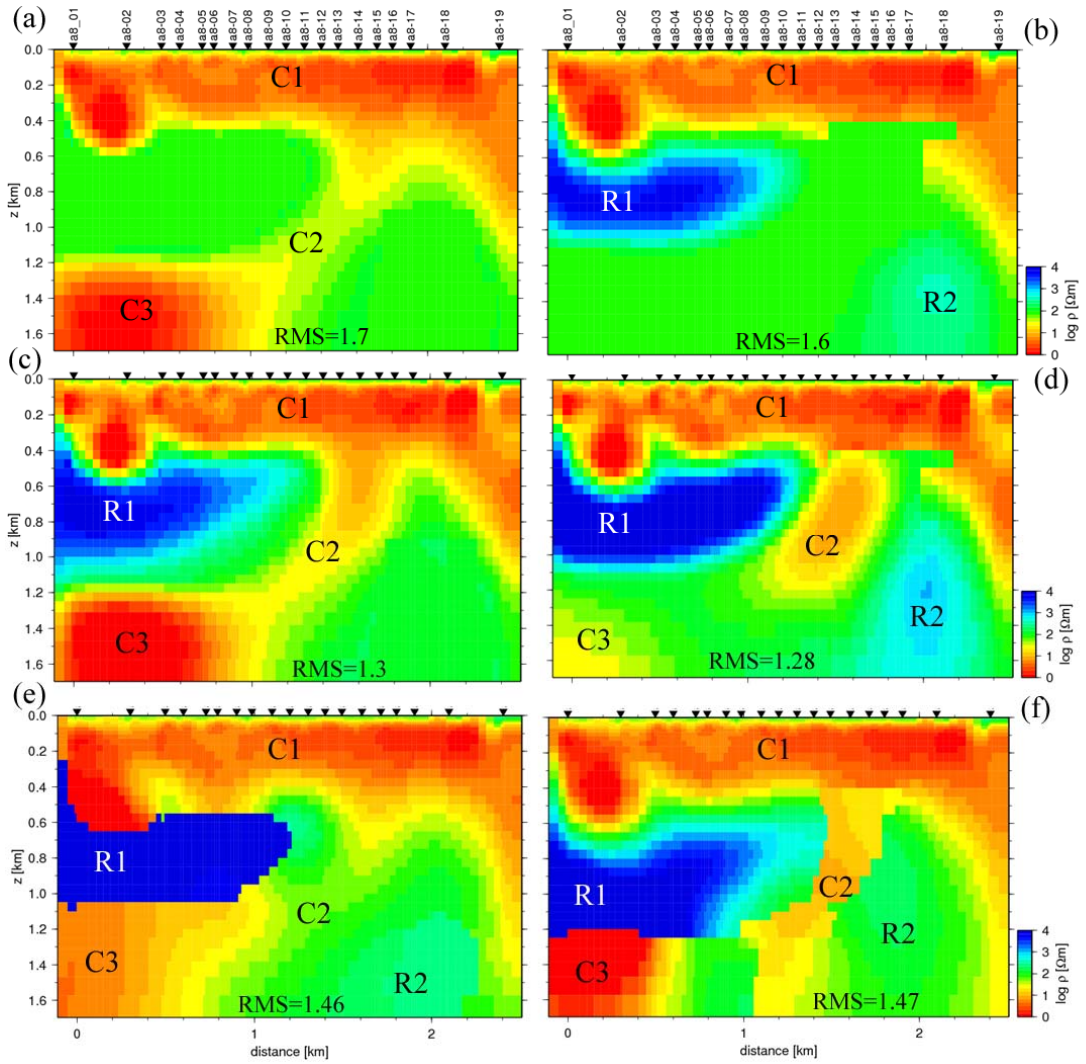

Figure 4. Inversion results where the closest to starting model was sought. (a, b) show the starting models, where the resistors (R1, R2) or the conductors (C2, C3) have been removed, respectively. (c, d) inversion results of (a, b). (e, f) inversion results where tear zones are introduced throughout the regions containing the resistors (R1, R2) and the conductors (C2, C3).

Abstract, 25^{th} EM Induction Workshop,Çeşmeı, Turkey, September 11-17, 2022

Large-scale mineral system study in Finland using 3D magnetotellurics

P. K. Mishra[1], J. Kamm[1], C. Patzer[1], U. Autio[1], K. Vaittinen[2], K. Muhumuza[3], M. Yu. Smirnov[4], G. Hill[3] and D-REX WG[5]
[1]Geological Survey of Finland, pankaj.mishra@gtk.fi
[2]Boliden Kevitsa Mining OY
[3]Institute of Geophysics Czech Academy of Sciences, Prague, Czech Republic
[4]Luleå University of Technology, Sweden

SUMMARY

The study of mineral systems has been demonstrated to be a paradigm shift in mineral potential assessment of mineral belts in cratonic environments by revealing lower crustal structures associated with metal concentration and emplacement in the upper-most crust. Magnetotellurics is a powerful tool for imaging these lower crustal structures and their connections to surficial interest zones. However, it has largely been applied in a two-dimensional fashion. In complicated Precambrian environments, 3D magnetotellurics is effective for production of more stable and less ambiguous conductivity models. Within the framework of the D-REX project we have examined three regions across the Fennoscandian shield and here we present results from the Pyhäsalmi mineral system, a part of the Rahe-Ladoka zone, Finland, on a regional scale and in 3D.

[5]**D-Rex Working Group (D-REX WG):**

Luleå University of Technology (LTU): Maxim Yu. Smirnov, Jirigalatu, Thorkild M. Rasmussen, Tobias Bauer, Oskar Rydman

Institute of Geophysics Czech Academy of Sciences (IG-CAS): Graham Hill, Kenneth Muhumuza, Svetlana Kovachikova, Jorge Puente, Nazia Hassan, Nooshin Najafipour

Geological Survey of Finland (GTK): Jochen Kamm, Pankaj Mishra, Cedric Patzer, Uula Autio, Jarkko Jokinen, Jouni Luukas

Earth Science Institute Slovak Academy of Sciences (ESI-SAS): Jan Vozar , Jozef Madzin, Lenka Ondrasova, Peter Vajda

Boliden Minerals AB: Tobias Hermansson, Kirsi McGimpsey, Janne Kaukolinna

Boliden Kevitsa Mining OY: Katri Vaittinen

LKAB: Niklas Juhojuntti, Harald Van Den Berg

Geological Survey of Norway (NGU): Sofie Gradmann, Jomar Gellein

Keywords: magnetotellurics, mineral systems, data inversion, Fennoscandia, metal endowments

Deep mineral exploration using semi-airborne electromagnetics: Investigation of a graphite deposit

W. Mörbe[1], P. Yogeshwar[1], B. Tezkan[1], P. Kotowski[2], A. Thiede[2], M. Becken[2], A. Steuer[3], H. Petersen[3] , M. Schiffler[4], R. Stolz[4], R. Rochlitz[5], T. Günther[5]
[1]University of Cologne, Institute of Geophysics and Meteorology, Germany, moerbe@geo.uni-koeln.de
[2]University of Münster, Institute of Geophysics, Germany
[3]Federal Institute for Geosciences and Resources (BGR), Hannover, Germany
[4]Leibniz-Institute for Photonic Technology (Leibniz-IPHT), Jena, Germany
[5]Leibniz-Institute of Applied Geophysics (LIAG), Hannover, Germany

The overarching goal of the collaborative project DESMEX-II is the development of methods for efficient exploration of deposits at great depths (~1000 m). Within the framework of the project, a large scale semi-airborne controlled source electromagnetic (CSEM) survey was conducted over a graphite deposit in eastern Bavaria, Germany. Due to the presence of graphite, an additional focus of this survey is the investigation of induced polarization effects on electromagnetic data and subsequently the development of suitable interpretation schemes.

At the ground, several horizontal electrical dipole transmitters with lengths between 1-3 km were deployed, utilizing a rectangular current function with a base frequency of 11.9 Hz. Sensors installed in a helicopter-towed bird measure the EM field on flight lines with a dense spacing and within several overlapping flight areas, covering offsets of several km to the ground-based transmitter. In addition, multi component magnetic as well as electric field measurements utilizing a low transmitter base frequency were conducted at the ground. Additional measurements of electric field data inline with the transmitter deliver complimentary information. After data processing, high quality transfer functions for frequencies between several Hz up to 8 kHz could be obtained.

Here, we will present the concept and first results from the conducted survey, including 2D and 3D inversion results of the semi-airborne EM dataset using multiple transmitters. The resulting inversion models exhibit strong conductivity contrasts. Shallow regions of high conductivity can be correlated with the occurrence of graphite and agree with high frequency helicopter borne EM measurements. The applicability of performing 2D inversion of single flight line data for interpretation is investigated. Effects of topography are analyzed with synthetic modelling studies and show a considerable large influence for high frequency data. Obtained ground based electric field data is evaluated in time and frequency domain and is utilized to identify effects of induced polarization on the EM dataset and to improve the overall modelling resolution of the semi-airborne CSEM data.

Keywords: DESMEX, semi-airborne CSEM, 3D Inversion, Induced Polarization

Abstract, 25th EM Induction Workshop, Kuşadası, Turkey, September 13-19, 2020

The value of full tensor magnetotellurics, gravity and electrical resistivity tomography for Lithium prospecting. A case study in Argentina.

A. Curcio[1], E. Chanampa[2], L. M. Cabanillas[3] and R. D. Piethe[2]
[1]Proingeo SA, acurcio@proingeo.com.ar
[2]Litica Resources (a Pluspetrol Mining Company), echanampa@litica.com; rpiethe@litica.com
[3]Independent Consultant, lmcabanillas@gmail.com

SUMMARY

The energy transition drives the energy sector to renewable energy and electrification, being the critical minerals key players in the industrial development map. They comprise rare earth elements and 35 other elements including lithium that holds the 60% of its world reserves in the so-called lithium triangle located in Argentina-Bolivia-Chile.
The low electrical resistivity, variations in salt concentrations, low acoustic impedances, and dynamics of the hydrogeological system, makes brine monitoring a complex geophysical exploratory problem. So, the objective is to find a suitable combination of geophysical techniques that fit the lithium exploration objectives, which are the characterization of the salt flat in depth, fluid detection, basement delineation, definition of the main structures and main faults and detection of semi-freshwater aquifers that contribute to its recharge and that are key to the water balance of the endorheic basin, which has the resource in solution. For this purpose, the evaluation of several prospecting methods in different salt flats was executed, concluding that full tensor magnetotellurics, electrical resistivity tomography and gravity comprises a toolkit that fit the objectives set. The results are validated with production and exploration wells and a methodology through pseudo wells will be discussed. Finally, similarities between lithium and hydrocarbon industry as well the exploration frontiers will be discussed.

Keywords: Lithium, multiphysis, magnetotellurics, electrical resistivity tomography, gravity.

Whole-lithosphere architecture of a mineral system and signatures of the sources and pathways of ore-forming fluids

Matthew Joseph Comeau[1], Michael Becken[2] and Alexey V. Kuvshinov[3]
[1]Institut für Geophysik, Universität Münster (WWU), Münster, Germany, matthew.comeau@uni-muenster.de
[2]Institut für Geophysik, Universität Münster (WWU), Münster, Germany, michael.becken@uni-muenster.de
[3]Institute of Geophysics, ETH, Zürich, Switzerland, kuvshinov@erdw.ethz.ch

SUMMARY

Mineral systems can be thought of as a combination of several critical elements, including the whole-lithosphere architecture, favorable geodynamic/tectonic events, and fertility. There are open questions regarding the source of ore-forming fluids, the depth of genesis, and their transportation through the upper crust to discrete emplacement locations. In this study, we investigate an Au–Cu metal belt located at the margin of an Archean-Paleoproterozoic microcontinent in central Mongolia. We explore three-dimensional models of the electrical resistivity and shear-wave velocity throughout the lithosphere. Directly beneath the metal belt, narrow, vertical, finger-like low-resistivity features are imaged within the resistive upper-middle crust and are connected to a large low-resistivity zone in the lower crust. A broad low-resistivity zone is imaged in the lithospheric mantle, which is well aligned with a zone of low shear-wave velocity. In the upper-middle crust, the resistivity signatures give evidence for ancient pathways of fluids, below the metal belt, constrained by structure along a tectonic boundary. In the lower lithosphere, the resistivity and velocity signatures are interpreted to represent a fossil fluid source region. We propose that these signatures were caused by a combination of factors, particularly those related to refertilization and metasomatism of the lithospheric mantle by long-lived subduction at the craton margin, and discuss several possibilities.

Keywords: mineral exploration; fertilization; fluid pathways; electrical resistivity; shear-wave velocity

3-D Magnetotelluric Forward and Inversion of the Chicontepec oil basin.

O. Avila[1], F. Corbo[2], and C. Castro[3]
[1]Posgraduate, Center of Geosciences-UNAM, oavila@geociencias.unam.mx
[2]Center of Geosciences-UNAM, fercorbo@geociencias.unam.mx
[3]Institute of Geosciences, Goethe University Frankfurt, castro@geophysik.uni-frankfurt.de

SUMMARY

According to the National Hydrocarbons Commission (CNH), in the Chicontepec Paleocayon, belonging to the oil province of Tampico – Misantla, that is one of the largest proven and possible oil reserves in Mexico. For this reason, it is important to improve the geological/structural knowledge in the area to have greater precision to determine the best areas to be exploited. This Paleocanyon has complex geology comprised of significant volumes of clay-stone sediments produced by multiple turbidite flow events, forming the reservoir-producing rock.

In this investigation, a 3-D resistivity model was generated from the inversion of 83 broad-spectrum Magnetotelluric sites (BMT), measured during an average acquisition time of 1 day, distributed along 5 profiles. The MT stations were acquired in different campaigns since 2019 using Phoenix MTU5-A dataloggers. The time series were processed following a robust single-site approach using the FFMT software package (Castro et al., 2020), Furthermore, we included the analysis of the electromagnetic response in surveys close to drilled wells, to constrain the conductivity distributions.

The 3-D inversion started from a homogeneous half-space, including main topographic features within the inner and outer mesh, and cells with fixed resistivity representing the high conductivity of the Gulf of Mexico. model was developed in a semi-homogeneous space with the local topography and the proximity to the Gulf of Mexico. The algorithm applied was ModEM (Egbert and Kelbert, 2012; Kelbert et al. 2014), which follows an inversion scheme based on nonlinear conjugate gradients (NLCG).

We present a resistivity model which reveals the geometry of the Paleocanyon both in extension and in-depth, geological structures, and geoelectrical anomalies embedded in the sedimentary deposits that can be associated with the presence of fluids, oil, and/or gas.

Keywords: Magnetotellurics, Oil, Gas, Chicontepec, Inversion,

Acknowledgements

This investigation was possible with the support of the 1787 CONACYT FC project, and the students that collaborated with the fieldwork in the different campaigns.

References

Egbert, G. D., Kelbert, A, 2012. Computational recipes for electromagnetic inverse problems. Geophysical Journal International, 189(1), 251-267.

Kelbert, A., Meqbel, N., Egbert, G. D., Tandon, K., 2014. ModEM: A modular system for inversion of electromagnetic geophysical data. Computers & Geosciences, 66, 40-53.

Castro, C.D., Hering, P. Junge. A., 2020. FFMT: A Matlab-based toolbox for Magnetotellurics (MT). RAUGM 2020 Reunión Mexicana de la Unión Geofísica Mexicana, Guadalajara, México.

Sedimentary copper mineral systems: Large scale resistivity footprints in the Adelaide Rift Complex, South Australia

B. Kay[1], G. Heinson[2], K. Brand[3], S. Thiel[4] and G. Boren[5]
[1]University of Adelaide, ben.kay@adelaide.edu.au
[2]University of Adelaide, graham.heinson@adelaide.edu.au
[3]Beurea of Meteorology, kate.e.brand01@gmail.com
[4]Geological Survey of South Australia, stephan.thiel@sa.gov.au
[5]University of Adelaide, goran.boren@adelaide.edu.au

SUMMARY

A significant challenge for the global mineral exploration industry is to identify the deep signature of world-class mineral deposits and the conceptual understanding of terrane scale fertility under cover at which mineral systems operate (Griffin, Begg, & O'Reilly, 2013; Groves & Santosh, 2015; Tassara et al., 2017). The fundamental caveat of the mineral systems approach is that ore deposits are part of a much larger system, evident at a variety of temporal and spatial scales (Hronsky & Groves, 2008; McCuaig & Hronsky, 2014). It is this scale dependency that is fundamentally important in exploration targeting, as the direct detection of ore deposits at the project scale is very difficult due to upper crustal heterogeneity, but potentially easier to predict at lithospheric scales (Hronsky & Groves, 2008).

In the sedimentary copper mineral system, it's generally agreed that the first order control is their location adjacent to failed rift basins and passive margin settings (Hitzman et al., 2010), that typically form during the breakup of the super-continents. The basinal architecture allows the deposition of oxidised syn-rifted red beds, sometimes with mafic or bimodal volcanics, which act as the source for the leaching of metals (Hitzman et al., 2010). Post rift marine and lacustrine sediments deposited later can produce areas of contained organic rich reductants necessary to form a chemical trap for the precipitation of sulphides, sometimes with large lateral extent (Hitzman et al., 2010). Evaporite sequences above the permeable post-rift sediments act as a hydrological seal, and occasionally as a source for downward moving brines through evaporite dissolution, which allows the possibility of long lasting intra-basinal fluid flow systems within which convective cells can develop with additional heat (Hitzman et al., 2010).

The Adelaide Rift Complex, itself part of the larger Adelaide Superbasin, is a large Neoproterozoic to middle Cambrian sedimentary system composing the Adelaide Rift Complex (ARC), the Torrens Hinge Zone, the Stuart Shelf, and the Coombalarnie Platform (Lloyd et al., 2020; Preiss, 2000). The stratigraphy of the ARC comprises five major successive rift cycles, evident by associated faulting, minor volcanism and distinct depositional sequences (Preiss, 2000; Lloyd et al., 2020), with the development of the ARC commencing as Laurentia began to rift from Australia-East Antarctica with Rodina.

In this study, we collect broadband MT data from 82 sites across the Northern Mount Lofty Ranges in the Adelaide Rift Complex. Sites are arranged at 10 km intervals in a rectangular grid covering 100 km N-S and 80 E-W. We supplement our newly collected MT sites with a further 80 long-period MT and broadband MT sites from previous surveys in the region and invert the entire dataset using a 3D inversion algorithm. The resulting 3D resistivity model reveals a localised elongated upper crustal conductor (~ 5 Ohm.m) spanning from the Burra to Kapunda Copper deposits which is constrained by structural dynamics from basin inversion during the Delamerian Orogeny. We argue that that this crustal conductor, is essentially the large-scale footprint of a sedimentary copper mineral system where highly saline fluids were sourced from evaporitic dissolution from the Callana Group strata.

Keywords: Sedimentary copper mineral systems, camp-scale, mineral exploration

Crustal geoelectrical distribution of Kalgoorlie gold camp mineral system (Western Australia)

P. Piña-Varas[1,2], M.C. Dentith[2]

[1] Department Dinàmica de la Terra i de l'Oceà, Universitat de Barcelona, Barcelona, Spain

[2] Centre for Exploration Targeting, School of Earth Sciences, The University of Western Australia, 35 Stirling Highway, Crawley, Western Australia 6009.

SUMMARY

The East Yilgarn craton (Western Australia) is a highly mineralized area that contains several large gold deposits, including the giant Kalgoorlie gold camp. Structural controls on gold deposition have resulted in the general acceptance in the Yilgarn craton covered by the concept of the “Mineral Systems”, according to which major faults between the fundamental crustal blocks are expected to control the movement of metal-bearing fluids within the system. For mapping such deep structures under cover, deep penetrating geophysical methods are required. Here we present the preliminary results of the broadband magnetotelluric experiment performed across the world class Kalgoorlie gold camp. The survey, with more than 100 MT sites with 5 km spacing, encompasses important orogenic gold deposits including the Golden Mile/Mt Charlotte, Kanowna Belle and Paddington. Data analysis shows a complicated 3D geoelectrical structure and therefore, impedance and tipper data were inverted accordingly using the modEM code. The resulting crustal conductivity distribution shows a series of conductive zones associated with known orogenic gold deposits. These zones appear to merge at depth and link to the conductive zone in the lower crust that trends oblique to the surface geology. The data suggest that orogenic gold mineral systems can be mapped into the deep crust using MT methods; and such surveys represent a valuable tool for exploring at the district scale for such deposits.

Keywords: 3D Magnetotelluric, Mineral system, Mineral exploration, Western Australia

Geophysical signature of the sedimentary/basement transition zone from seismic and CSEM. Analysis from a shallow analogue of the Rhine Graben

F. Bretaudeau [1,*], M. Darnet [1], J. Porté [3] C. Lerouge [1], S. Neeb [1], J.F. Girard [2], J.M. Baltassat [1], N. Coppo [1], C. Dezayes [1]

[1]BRGM (French Geological Survey) f.bretaudeau@brgm.fr
[2] Strasbourg University, ITES-CNRS, UMR7063, France
[3] Formerly 1 & 2, now at SINTEF Industry

SUMMARY

Exploiting high temperatures geothermal resources in sedimentary and basement rocks, rifts or flexural basins to produce electricity is now possible because of the development of binary geothermal power plant technology. However it remains challenging because the presence of fluid and permeability at 4–5 km depth is necessary. A multi-scale and multi-disciplinary approach to increase our knowledge of the transition zone between the sedimentary cover and the basement have been undertaken to provide fundamental knowledge for the assessment of its geothermal potential. We report out the results of a study performed on an exhumed transition zone in the Ringelbach area in the Vosges Mountain, on the flank of the Rhine graben. In this analogue of a deeply buried transition zone of the Rhine Graben, Triassic sandstones are still present on the top of the fractured and altered granitic basement providing the unique opportunity to study in-situ the physical properties of this transition zone. We focused here on both electrical (from CSEM) and seismic properties of the transition zone as they are the main physical parameters usually assessed with the help of geophysical methods during the exploration phase of a geothermal project. We show that altered porous and potentially permeable granite targeted in deep geothermal exploration has a clear signature on both electrical conductivity and seismic measurements that can be measured at core scale, borehole scale, and are still visible with surface geophysical methods such as refraction and reflection seismic and Controlled Source EM at a few hundred meter depth. The results suggest that best discrimination between permeable and non permeable rocks may be provided by the joint interpretation of both resistivity and seismic velocities.

Keywords: Geothermal exploration in sedimentary basins, CSEM, transition zone, multi-physics / multi-scale

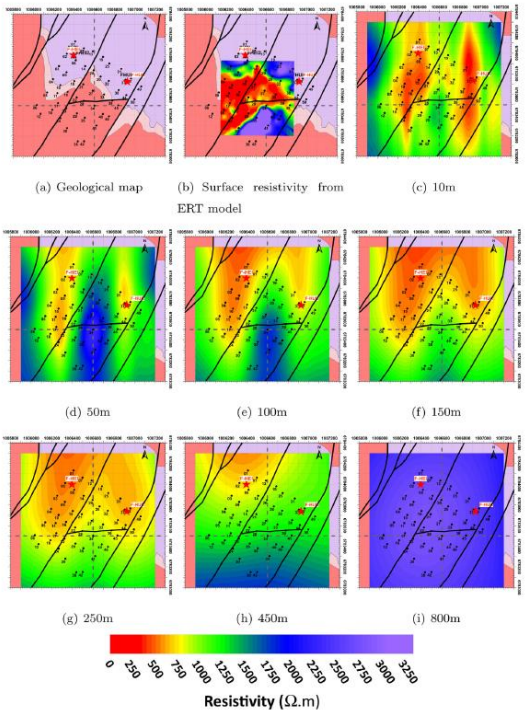

Figure 1: 3D CSEM resistivity model showing 1) a 200m thick conductive layer above the fresh granite associated with granite alteration, 2) very large variations of alteration marked by blocks with very high variation of resistivity.

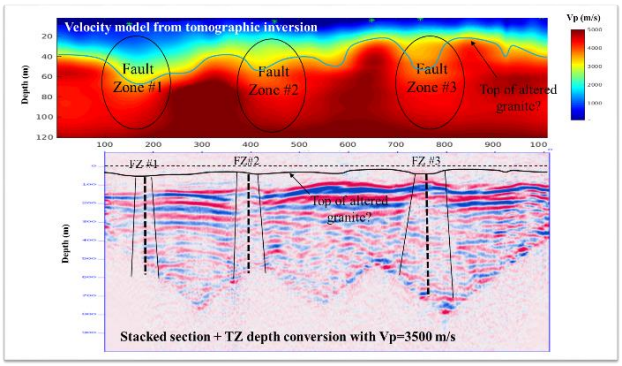

Figure 2: Seismic refraction velocity model and shallow seismic reflection showing 1) reflection on the top of the unaltered granite, 2) very large velocity variations associated to level of alteration and correlated with the known faults.

Combined 3D inversion of MT and CSEM-data from Malmberget northern Sweden.

O. Rydman[1], M.Yu. Smirnov[2], and H.V.D. Berg[3] N. Juhojuntti[4]
[1]Luleå university of technology, Sweden, oskar.rydman@ltu.se
[2]Luleå university of technology, Sweden, maxim.smirnov@ltu.se
[3]LKAB, Sweden, harald.van.den.berg@lkab.com
[4]LKAB, Sweden, niklas.juhojuntti@lkab.com

SUMMARY

During 2020-2022 both MT and CSEM surveys have been conducted around Malmberget in northern Sweden. Malmberget is the location of one of Europe's largest underground iron mines with iron oxide-apatite ore and mafic-intermediate metavolcanic host rock. In the area two different CSEM surveys were conducted, one in the summer of 2021 with a 4km long grounded dipole source and 150 measurements with 250m spacing in a 3x4km^2 rectangle, and another one done in the winter-spring of 2022 with a 1x1km^2 loop source with 100 measurements with 250m spacing in a 2x2 km^2 area. In the 2021 summer survey all five field components where measured (Ex,Ey,Hx,Hy,Hz) but in the 2022 winter-spring survey only the magnetic fields (Hx,Hy,Hz) were acquired due to weather limitations. The Magnetotelluric survey spans the whole area and consists of roughly 130 1km spaced measurements in a 10x15km^2 rectangle. These measurements were done in the summers of 2020,2021 and some during the winter-spring of 2022. CSEM surveys were processed to estimate univariate transfer functions between field components and current recording in frequency range 8 – 3000Hz. This approximates to a depth of investigation of about one to two km. The data are jointly inverted using the MR3Dmod code and the results compared to single inversions and a 3D geological model. The surveys were conducted in cooperation between Loussavaara-Kiirunavaara Aktiebolag (LKAB) and Luleå university of technology (LTU) and are part of two different projects. One focusing on Common Earth modelling (CEM) on deposit scale and the other being (D-Rex) which focuses on connections between regional and deposit scale exploration.

Keywords: Magnetotellurics, Controlled source electromagnetics, Combined inversion, 3D inversion, multiresolution grid

Experience of the solution of engineering and environmental tasks using the CSRMT method

A. Saraev[1], A. Shlykov[2] and B. Tezkan[3]
[1] St. Petersburg State University, a.saraev@spbu.ru
[2] St. Petersburg State University, a.shlykov@spbu.ru
[3] Cologne University, tezkan@geo.uni-koeln.de

SUMMARY

We have an experience of application of the controlled source radiomagnetotelluric (CSRMT) sounding method in the solution of engineering and environmental tasks in remote regions. Here the radiomagnetotelluric (RMT) cannot be successfully applied because of limited possibilities of measurements of radio transmitter's signals. As a source in the CSRMT method we use a horizontal electrical dipole, which ensures measurements of field components in a frequency range of 1-1000 kHz at a significant distance (up to 3–4 km) from the source. The extended frequency range of the CSRMT method compare to the RMT one (10-1000 kHz, depth of investigations up to 30-50 m) permit us to study deeper horizons of sections up to 100-150 m. An example of the study of a landfill of industrial wastes in the Vyborg area (Leningrad region) using the CSRMT method is considered. The high conductivity and a relative large thickness of the wastes did not allow us to map the bottom of the landfill by the RMT method. Also, a small amount of signals from radio transmitters reduced the informative value of the RMT method when studying the top part of the section (first meters). Results of the CSRMT method show its high efficiency in the study of the top and deep parts of the landfill. An example of application of the CSRMT method is obtained in the area of a railway bridge construction in the Northern part of Siberia (Yamalo-Nenets region). The aim of this survey was the estimation of the depth of solid sands serving as a basement for bridge piles. The resistivity model derived from the CSRMT data shown a good correlation with the existing boreholes information. The presented results were obtained with the support of the Russian Science Foundation, project No 21-47-04401.

Keywords: Controlled source radiomagnetotellurics, Waste site, Bridge construction

Joint 3D inversion of nearshore and land MT and CSEM data in coastal areas of volcanic islands: application to the Bouillante geothermal field

S. Védrine[1,2], P. Tarits[2], F. Bretaudeau[1], S. Hautot[3], M. Darnet[1]
[1]BRGM, 3 Av. Claude Guillemin, Orléans 45060, France, s.vedrine@brgm.fr
[2]Laboratoire GEO-OCEAN UMR6538, UBO, IUEM, Rue Dumont d'Urville, 29280, Plouzané, France, pascal.tarits@univ-brest.fr
[1]BRGM, 3 Av. Claude Guillemin, Orléans 45060, France, f.bretaudeau@brgm.fr
[3]IMAGIR Sarl, 1 rue des Ateliers F, 29290 Saint Renan, France, sophie.hautot@imagir.eu
[1]BRGM, 3 Av. Claude Guillemin, Orléans 45060, France, m.darnet@brgm.fr

SUMMARY

A large-scale magnetotelluric (MT) and controlled-source electromagnetic (CSEM) acquisition campaign was conducted around the exploited Bouillante geothermal field in Guadeloupe in the Lesser Antilles, supplemented by a regional airborne transient electromagnetic survey (AEM). The target is the characterization of the geothermal reservoir and the associated clay cap, generally identified by its highly conductive electrical signature, typical of a conventional volcanic geothermal system in an andesite-type geological environment. MT allows targeting the deepest parts of the subsurface, but the natural signal on which it relies is on average weak at low latitudes and can be much weaker than anthropogenic noise, making its use with dense acquisition challenging close to inhabited areas. CSEM allows completing and densifying the data coverage in the most urbanized areas thanks to the use of high power active current sources and less demanding measurement systems. Moreover, MT and CSEM 3D modeling, as well as inversion, in the coastal areas of volcanic islands can be challenging due to numerical errors induced by the presence of the sea/land interface and large variations in nearshore bathymetry and topography. These errors must be estimated and corrected to best invert the field data. Here we present the workflow and results of the 3D CSEM and MT modeling and inversion independently. The resistivity model obtained with CSEM is consistent with the known geology and the 3D MT model, but provides improved resolution as well as new information on the extension of the reservoir nearshore. We also discuss the complementarity between MT and CSEM in this context, and how to perform their joint inversion in order to benefit from the high resolution and sensitivity of CSEM on the first 2 km and the ability of MT to provide deeper information.

Keywords: Joint 3D inversion, Volcanic islands, Geothermal exploration, MT, CSEM

INTRODUCTION

3D exploration with electromagnetic methods in coastal areas of volcanic islands can be challenging due to the high level of anthropogenic noise, proximity to the sea/land interface, strong variations in near-shore bathymetry and topography, and near-surface heterogeneity. To overcome these limitations, our goal is the multi-scale integration of AEM, nearshore and land MT and CSEM to improve the reconstruction of deep geologic structures in 3D by inversion. The contribution of the CSEM method is a key to overcome anthropogenic noise and increase data coverage over urbanized areas while the AEM method aims to constrain the first 200 meters of our model. Finally, MT can reach the deepest part of the subsurface. In order to study how to integrate the different EM data, we apply our methodology to data from a geothermal exploration campaign carried out around the Bouillante geothermal field operated in Guadeloupe, in the French West Indies.

METHODS

The nearshore and land MT and CSEM acquisition campaign was conducted in the coastal area of Bouillante, near the geothermal power plant. The acquisition setup is shown in Figure 1 with: land CSEM transmitters, nearshore and land CSEM receivers, nearshore and land MT sites and AEM flight lines. In total, during the 2 weeks of acquisition, 5 CSEM transmitters, 70 CSEM receivers and 21 MT sites were deployed in the field. In addition, we obtained persmission to use MT data acquired by ORMAT (Owens et al. 2018) for inversion increasing the number of MT sites by 54. This dataset is very dense and diverse and also provides a unique opportunity to develop our multi-method integration of MT, CSEM and AEM.

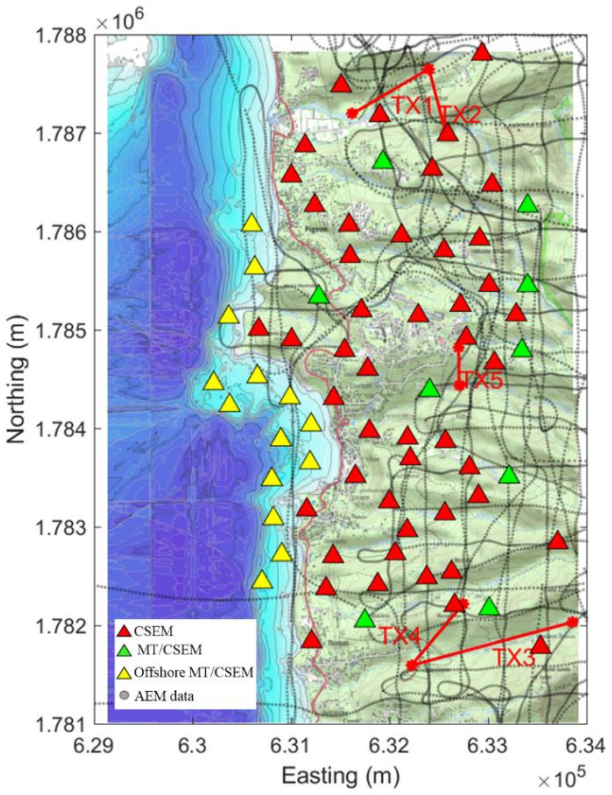

Figure 1. Bouillante survey area. land CSEM transmitters in red lines, land CSEM receivers in red triangles, land MT sites in green and nearshore CSEM receivers and MT sites in yellow. Projected UTM 20 N, WGS 84.

The 3D modeling of CSEM is done with a mixed finite element and finite difference approach using the open-source code custEM (Rochlitz et al. 2019), and POLYEM3D (Bretaudeau et al. 2021) respectively. The 3D inversion of CSEM data is done with the inversion code POLYEM3D, whereas the 3D inversion of MT is done by the code MINIM3D (Hautot et al. 2007).

RESULTS

We present a first CSEM 3D inversion result. We used a finite difference modeling grid of about 1.4 million cells. We inverted the real and imaginary part of the electric field in the north and east direction for 5 land transmitters, 70 nearshore and land receivers and for 6 frequencies (between 32 s and 32 Hz). A total of 81,000 parameters were inverted using the Guauss Newton minimization algorithm and using a jacobi-like preconditoner to avoid sensitivity buildup around transmitters and receivers and ensure convergence to a smooth solution. The starting model was an isotropic homogeneous medium of 20 Ω.m incorporating nearshore bathymetry variations with seawater fixed at 0.25 Ω.m and topography variations. Figure 2 shows the inverted model after 12 GN iterations among with bathymetry and the topographic relief map, the ”Plateau” fault (Calcagno et al. 2012), and two geothermal wells.

This first result is in good agreement with both the previous MT 3D inversion from ORMAT and our new 3D MT model. A clay cap is inferred on the shallow part of the model. A low resistive zone is inferred along the ”Plateau” fault crossed by a production well. A resistive structure is inferred not far north of the production well, and remains to be interpreted. Finally, from -2000 m below sea level, a low resistive zone is inferred that could be related to the temperature increase, but a sensitivity study remains to be done to confirm its existence. Although this result is interesting, it should be improved by combining it with the new MT 3D inversion which includes new nearshore marine sites and with the AEM logs.

DISCUSSION

The methodology for joint inversion of MT and CSEM data can be based on several strategies, such as cooperative, successive or joint inversion. Choosing one or the other inverted model as a prior or starting model to constrain the inversion of th other method is key to improving the physical and geological consistency of our final inverted resistivity model. A pitfall could be to perform a joint inversion from a blank starting model without further thought, and face minimization problems because MT and CSEM, although based on the same physics and inverting the same parameter, have different resolutions and sensitivities to subsurface anomalies. In the coastal areas of volcanic islands, one may choose to first constrain the deep geological structures by performing a MT inversion, and then add another layer of refinement by inverting the CSEM data. On the other hand, the MT inversion may benefit from the AEM and CSEM data to constrain the near surface and intermediate depth. Ultimately we plan to perform a joint inversion of the MT and CSEM data with the prior constraint of the AEM data, and adapt the relative weight of either method during the inversion process.

CONCLUSIONS

We have shown that CSEM can lead to results in good agreement with previous investigations of the area, and furthermore highlight new features that still need to be rigorously interpreted geologically. This dataset is a unique opportunity to develop a multi-method integration and define the best joint inversion methodology between MT, CSEM and AEM. We will likely begin by performing successive inversion tests to evaluate the best case scenario of

whether MT or CSEM should be inverted first. Then, we will try to adapt our inversion code to perform joint inversion with adaptive weights between both methods.

ACKNOWLEDGEMENTS

This work was conducted under the TEC project funded by the European program Interreg Caribbean. We thank our partners ADEME, OECS, Region Guadeloupe, MAPPEM Geophysics and the computing center occigen of CINES. We particularly thank ORMAT for allowing us to use their MT data.

REFERENCES

Bretaudeau F., Dubois F., Bissavetsy Kassa S. G., Coppo N., Wawrzyniak P., & Darnet M. (2021). Time-lapse resistivity imaging: CSEM-data 3-D double-difference inversion and application to the Reykjanes geothermal field. *Geophysical Journal International*, *226*(3), 1764-1782.

Calcagno P., Bouchot V., Thinon I., & Bourgine B. (2012). A new 3D fault model of the Bouillante geothermal province combining land and offshore structural knowledge (French West Indies). *Tectonophysics*, *526*, 185-195.

Hautot S., Single R.T., Watson J., Harrop N., Jerram D.A., Tarits P., Whaler K., & Dawe D. (2007). 3-D magnetotelluric inversion and model validation with gravity data for the investigation of flood basalts and associated volcanic rifted margins. *Geophysical Journal International*, *170*(3), 1418-1430.

Owens L., Perkin D., & Garanzini S. (2018). 3D MT Characterization of the Bouillante Geothermal Resource.

Rochlitz R., Skibbe N., & Günther T. (2019). custEM: Customizable finite-element simulation of complex controlled-source electromagnetic datacustEM: customizable 3D CSEM modeling. *Geophysics*, *84*(2), F17-F33

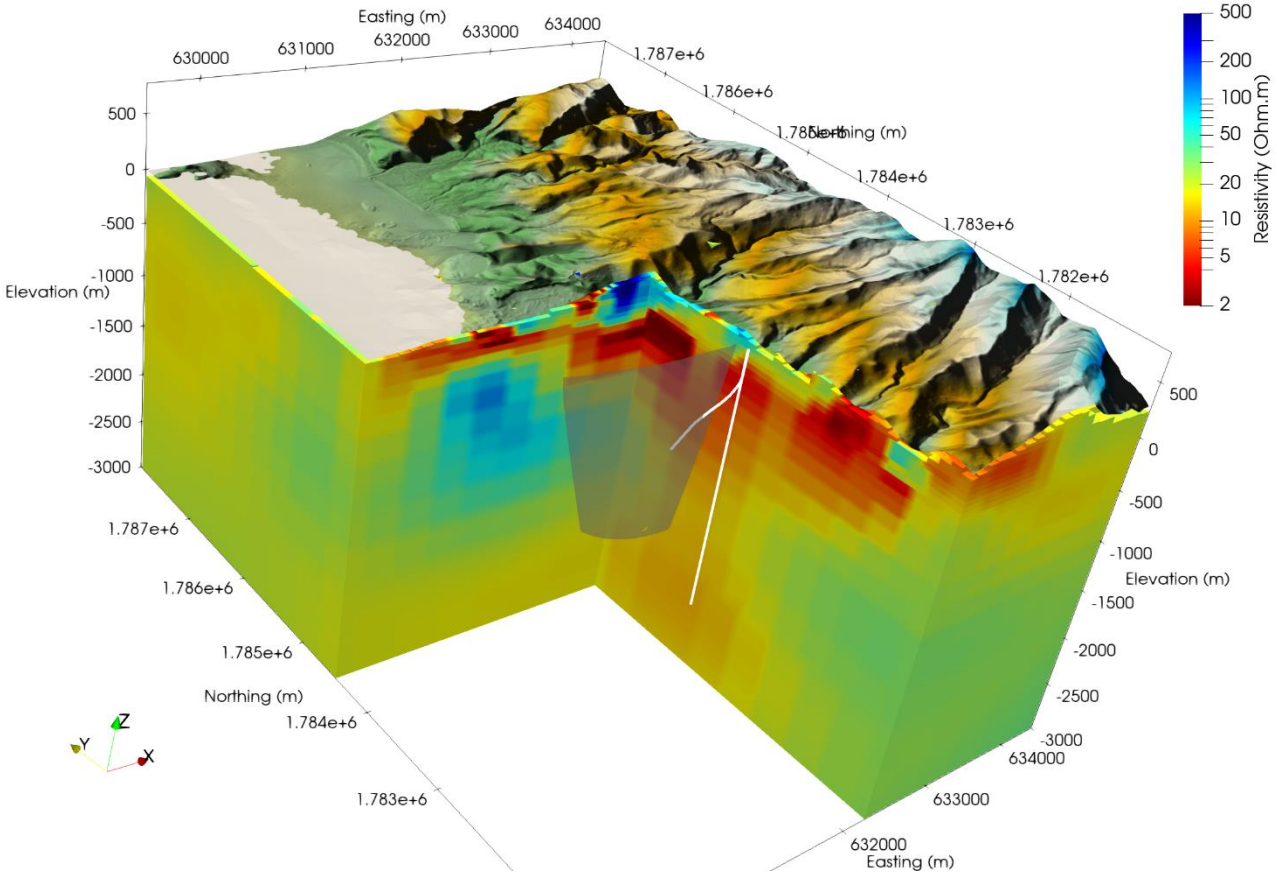

Figure 2. 3D CSEM inversion result after 12 GN iterations, warm colors correspond to low resistivity areas and cold colors to more resistive areas. Variations in bathymetry and topography are shown on top of the model. Two wells of the Bouillante geothermal plant are shown in white. The "Plateau" fault is shown in gray transparency (Calcagno et al. 2012). Projected UTM 20 N, WGS 84.

CSEM monitoring in Izu-Oshima volcano, Japan

Takao Koyama[1] and Makoto Uyeshima[2]

[1]Earthquake Research Institute, The University of Tokyo, tkoyama@eri.u-tokyo.ac.jp
[2]Earthquake Research Institute, The University of Tokyo, uyeshima@eri.u-tokyo.ac.jp

SUMMARY

Izu-Oshima volcano is one of the most active volcanos in Japan. The most recent eruption occurred in 1986, and the next event is expected in the near future. A monitoring of the volcanic activity is important to catch a precursory signal for mitigation of the volcanic disaster. A CSEM monitoring is carried on in Izu-Oshima caldera in order to detect the electrical conductivity change beneath the central cone. Two cables were deployed at south and east in the caldera floor to inject the electrical current into the ground. The length of south and west cables is 650 m and 1,700m, respectively. Five receivers, vertical induction coils, were installed on the rim of the central cone. The measurements are done by injecting a 50% duty cycle alternating current of one-second period for one hour every night. Data analysis and some three-dimensional modeling reveals that the electrical conductivity model beneath Izu-Oshima caldera, which is the two-layer structure with a 1 Wm conductive column beneath the central cone. The top unsaturated layer is as resistive as 200 Wm and the bottom saturated layer is 50 Wm. Running spectrum at five stations shows that every in-phase of the response function between an injection current and observed vertical magnetic field is almost stable, and out-of-phase has a remarkable annual change with the same polarity in all of sites. This change cannot be explained by the volcanic activity, but by a change of elevation of the boundary of the top and bottom layer beneath the caldera. It indicates it may be due to the annual variation of precipitation. If the conductive column rises up, that is, the volcanic fluid approaches to the surface before the next event, the changes of the response must show the opposite polarity of the in-phase data at some stations.

Keywords: Izu-Oshima volcano, CSEM monitoring, annual variation

Magnetotelluric Images of Volcanic Zones in NE Japan Arc and Co-seismic Deformations during the 2011 Tohoku M9 Earthquake

Masuda, S.[1], Ogawa, Y.[1,2] and Ichiki M.[3]
[1]Department of Earth and Planetary Sciences, Tokyo Institute of Technology, Japan
[2]Volcanic Fluid Research Center, Tokyo Institute of Technology, Japan
[3]Research Center for Prediction of Earthquakes and Volcanic Eruptions, Tohoku University, Japan

We have compiled wide-band magnetotelluric data collected at 590 sites over the last 30 years in NE-Japan. The period ranges are from 3ms to 2000s. Previous studies have focused on specific volcanic or seismic zones and had restrictions such as two-dimensional modeling methodology or three-dimensional modeling with 20kmx20km scale limitations. After compilating all the datasets, we have found strong current-channeling due to the elongated distributions of thick sedimentary layers, which introduce high three-dimensionality data around them. We identified such strong channeling by the induced electric field distribution and induction vectors for hypothetical event analyses using Hx and Hy inducting fields. This nature of the dataset requires complete three-dimensional modeling incorporating a large survey area with a 100 km x 100km scale.

We have used 410 sites in the central part of the survey area and inverted the resistivity structure from the full impedances and induction vectors in 8 periods using WSINV3DMT code. The most significant feature is the distribution of electrical conductors below 20 km along the volcanic arc, which runs in the SSW-NNE directions with a 10 km width. Its extension to the uppermost upper mantle depth shows resistivity of less than ten ohmm. These conductors get shallower toward Quaternary volcanoes as plume-like conduits, implying magmatic melt with potentially saline fluids in their upper part.

The distribution of those anomalous conductors at the volcanic zones has good spatial correlations to the co-seismic crustal depressions of the M9 Tohoku earthquake in 2011 inferred by InSAR (Takada and Fukushima, 2013).

Keywords: magnetotellurics, 3D modeling, volcano, deformation

First experience with high power EM towards the energy transition

K. Strack [1], S. Davydycheva [1], T. Hanstein [1], Y. Martinez [1], A.Y. Paembonam [1,2], V. Pronenko [3], M. Smirnov [1,4], P. Soupios [5], X. Xu [1]

[1] KMS Technologies, Houston, Texas, USA
[2] Sumatera Institute of Technology, Indonesia
[3] Lemi LLC, Lviv, Ukraine
[4] Lulea Technical University, Sweden
[5] King Fahd University of Petroleum and Minerals, Dhahran, Saudi Arabia

SUMMARY

During the energy transition, key applications for electromagnetics (EM) (including magnetotellurics - MT and controlled source electromagnetics - CSEM) are CO2 monitoring, geothermal exploration and monitoring, enhanced oil recovery (EOR & EOR+) monitoring, and lithium exploration. The most important of these is monitoring, which is required to measure time-lapse anomalies in the subsurface to be better than 0.5%. This requires a completely different approach to hardware, survey design, workflow, and interpretation.

To maintain the accuracy and controllability of the hardware, special care must be taken about sensors, the continuous recording of transmitter performance, and the monitoring of changes with time and temperature. We used the system in -200 C as well as +500 C with the entire range included in the system specification. The survey design usually requires a 3D anisotropic model-based exercise, including on-site noise measurements, well logs to define the resistivity variation before and after fluid injection, and petrophysical analysis. The results from this are optimized receiver spacing and the recording times for the magnetotelluric and CSEM measurements. Even though it is not immediately included, it also impacts the processing and interpretation design.

For monitoring CO2, geothermal or hydrocarbon reservoirs, we must always consider that for repeat measurements, everything could be changed (equipment, environmental noise conditions, and geophysical processing algorithms). Thus, we must minimize the impact of these on any baseline data to the point where we almost exclusively rely on average statistics.

For effectiveness and efficiency, we usually acquire MT during the night and CSEM during the day unless weather conditions demand differently. Thus, both methods and their results will be compared to the 3D anisotropic well log for calibration and they must be consistent within their resolution capabilities. The case histories from the US and Saudi Arabia used the Cloud to support near real-time quality assurance during the acquisition. We compare the inversion results with the 3D anisotropic log-based model response and include the seismic horizons. If everything is done correctly, the match allows us to certify even the baseline measurements based on the 3D model response. This significantly reduces the risk and provides us confidence in further time-lapse measurements.

Keywords: Controlled source electromagnetics, energy transition, reservoir monitoring, CO2 monitoring

Multidimensional inversion of transient electromagnetic data for the exploration of clay pans in the Atacama Desert, Chile

B. Blanco-Arrué [a], P. Yogeshwar [a], B. Tezkan [a], Y. Liu [c], R. Peng [c], V. Wennrich [b]

[a] *University of Cologne, Institute of Geophysics and Meteorology, Pohligstrasse 3, 50969 Cologne, Germany,*
[b] *University of Cologne, Institute of Geology and Mineralogy, Zülpicher Str.49a, 50674 Cologne, Germany,*
[c] *University of Geosciences, Institute of Geophysics and Geomatics, 430074 Wuhan, China.*

Summary

The Atacama Desert along the Chilean Coastal Cordillera is a unique landscape to understand the evolution of the Earth in hyper-arid and arid environments. Clay pans are crucial to understand the surface and subsurface processes in areas limited by water availability. This work aims to provide the sedimentary architecture and bedrock topography of selected clay pans through multidimensional inversion and interpretation of loop source transient EM data. The investigated sites are study areas of the *CRC 1211- Earth evolution at the dry limit*, established at the University of Cologne, Bonn and Aachen. In this context, our work contributes to a better comprehension of the investigated sites.

A total of 116 soundings were carried out on a 3D grid in the Paranal clay pan during December 2019. The TEM data were processed, analyzed, and inverted to investigate the resistivity distribution of the site. The resulting models show a maximum thickness of about 160 ± 10 m, interpreted as layers of colluvial and fluvial sediments. The major stratigraphy and the basement depth were confirmed with a drill core carried out in February this year. The shape of the conductive sediments suggests the presence of a former channel that might be part of the main drainage network in the surrounding study zone. However, multidimensional effects can lead to misinterpretations of TEM data if the subsurface is not 1D. In those cases, the quasi-2D resistivity distribution might be influenced. Therefore, a 2D inversion of the TEM data using the recently developed TEM3DInv code is performed to derive a more accurate geometry of the clay pan.

The TEM3DInv code is suitable for the time domain and is based on 3D Finite-Volume. The algorithm uses a Gauss-Newton inversion scheme coupled with a preconditioned conjugate gradient method to avoid explicit Jacobian calculation in each iteration. The performance and accuracy were tested using synthetic models that are representative of the PAR clay pan. Since the code is implemented for 3D, a very large smoothing in the y-direction is used to force a 2D subsurface reconstruction. Typically, the inversion converges in around six iterations, and the data is fitted well with a RMS of about 2. The derived 2D models are consistent and resolve the basement of around ~160 m depth. Thus, the 2D inversion provides an independent and improved solution compared to the 1D models. Finally, a 3D inversion of the whole 3D grid TEM shall be derived, although the computational resources are significant.

Keywords: Transient electromagnetic method, clay pans, sedimentary deposits, electrical conductivity.

Characterization of a landfill using magnetotellurics: the Garraf case

A. Martí[1], P. Queralt[1], A. Marcuello[1], J. Ledo[2], G. Mitjanas[1], P. Piña-Varas[1], A. Freixes[3], J. Solà[3], P. Pons[3]

[1]Institut Geomodels. Universitat de Barcelona, Spain annamarti@ub.edu
[2]Physics of the Earth and Astrophysics, Faculty of Physics, Universidad Complutense de Madrid, Spain
[3]Geoservei Projectes I Gestio Ambiental Sl, Spain

SUMMARY

Landfills are a highly environmental impact solution to waste disposal. In the Garraf Massif (Catalan Coastal ranges, SE Spain), a urban waste disposal landfill had been in operation between 1974 and 2006, where more than 26 milions of metric tonnes were deposited. This landfill was projected over a karstic terrain, which had important consequences over the underwater circulation system, among others. ERT profiles were acquired and imaged part of the infill and relevant pipes and man-made impermeabilization layers but were not able to penetrate below the landfill original vase. In 2019 and 2020 we performed a MT study over the landfill and its surrounding, with the goals of characterizing the electrical resistivity of the infill and imaging the electrical structures below the original topography previous to the landfill operations. The 2D and 3D resistivity models confirmed the highly conductive nature of the leachates and allowed us to quantify the depth below which it had penetrated below the original vase, proving the filtrations produced through the original permeabilizations, enhanced by the karstic rocks.

Keywords: landfill, leachates, electrical resistivity, magnetotellurics

Corrections for near surface effects contaminating MT data over a salt diaper, North West Kashan, Iran

E. Zare[1],
M. Montahaei[2],
H. Esmaili Oghaz[3]

[1]Institute of geophysics, University of Tehran, Tehran, Iran, elham.zare.99@ut.ac.ir
[2]Institute of geophysics, University of Tehran, Tehran, Iran, mmontaha@ut.ac.ir
[3]Natural Iranian Gas Storage Company for Nasr-Abad Area, Tehran, Iran

SUMMARY

In this study, we investigate an MT data set recorded over buried Nasr Abad salt diaper, in Qom Basin, west Central Iran. Central Iran (CI), Zagros folded belt (ZFB), Sanandaj-Sirjan zone (SSZ), Alborz Mountain Range, Kope- Dagh mountains, Makran and Sistan-Baluchestan are seven tectonic blocks, originated from Arabian-Eurasian collision which constitute the Iran plateau. Many majestic salt extrusions (diapers, glaciers (Nmakiers)) in ZFB, Saveh-Qom area and Grate Kavir desert in Central Iran provide a natural laboratory to test different dynamic models of salt flow.

Due to its large dimension, Nasr Abad salt diapir has been selected as an ideal site for gas storage and industrial waste disposal.

A challenging task arises from small scale conductive bodies distributed at surficial depths which generate distortion effects contaminating measured MT transfer function. We present here a systematic study of dimensionality analysis and decomposition of an MT data set, recorded at 25 stations along a profile in North West Kashan, Qom basin, Iran.

The Bahr and WAL invariants confirm regional 1D and 2D structures with local galvanic distortion, at most periods. Based on the phase tensor ellipses, we argue that most of the MT data represent regional 1-D and 2-D structures with local galvanic distortions. The Groom Baily decomposition of MT impedance tensors data reveals approximately period-independent distortion parameters and a set of smoothly varying regional strike directions. 2-D inductive effects were also retrieved by removing distortion effects from the measured data.

Keywords: magnetotellurics, electrical conductivity, salt dipir, Central Iran

Current use of Frequency-domain Electromagnetic Induction in precision agriculture: Knowledge gained from six years of experiments in Portugal

Mohammad Farzamian[1,2*], Fernando A. Monteiro Santos[2], Nadia Castanheira[1], Ana Marta Paz[1], Francisco José Martinez Moreno[2], Tiago B. Ramos[3], Maria Catarina Paz[4], and Maria C. Gonçalves[1]

[1]INIAV, Instituto Nacional de Investigação Agrária e Veterinária, Oeiras, Portugal
[2]Instituto Dom Luiz (IDL), Faculdade de Ciências da Universidade de Lisboa, Lisboa, Portugal
[3]Instituto Superior Técnico, Universidade de Lisboa, Lisboa, Portugal
[4]CIQuiBio, Barreiro School of Technology, Polytechnic Institute of Setúbal, Lavradio, Portugal

SUMMARY

Sustainable Agricultural Intensification aims at reducing the environmental footprint of agricultural production by promoting a sustainable use of limited resources to limit the use of agrochemicals, salt accumulation, land degradation and greenhouse gas emissions while increasing productivity and profitability. Such an emphasis requires efficient field-assessments to evaluate continuously the performance of the implemented management strategies. Traditional soil sampling methods, which require boreholes for soil sampling and laboratory analysis, cannot provide a comprehensive answer to this problem as they provide only limited spatial coverage and may therefore lack representativeness at the management scales. Furthermore, they are highly time and work consuming, resulting in costly surveys.

Frequency-domain Electromagnetic Induction (FDEM) provide a non-invasive and cost-effective technology for soil survey and monitoring based on innovative sensors, advanced algorithms for 2D and 3D tomographic imaging, and new technologies for field surveying allowing to assess soil properties in the management scale. Measurements obtained using FDEM can be related to several soil attributes, such as soil mineral composition, clay content, moisture, salinity, organic carbon, and cation exchange capacity (CEC), which are all relevant for agriculture. This technique provides also an opportunity to monitor the processes relevant for agricultural production from the analysis of time-dependent change of water content and soil salinization to the study of soil–root plant interactions.

During the last six years, we conducted several experiments in different regions of Portugal within two national and European projects, SOIL4EVER and SALTFREE, evaluating the application of the FDEM method in plot and field assessments of soil properties. The proposed methodology in these series of experiments consists of 4 main steps: 1) use of time-lapse FDEM surveys to measure the soil apparent electrical conductivity (ECa) and its changes during the experiment period; 2) inversion of time-lapse ECa data to assess the spatiotemporal distribution of the soil electrical conductivity (σ); 3) calibration process consisting of a regression between σ and different soil properties including moisture content, electrical conductivity of the saturated soil paste extract (ECe), sodium adsorption ratio (SAR), exchangeable sodium percentage (ESP), clay content, CEC, and pH; 4) conversion of spatial-temporal distributions of σ into soil properties using calibration equations and properties that are strongly correlated with σ.

Our results indicate that FDEM can be used as strong tool in precision agriculture to monitor soil salinity, sodicity, and moisture content variability, groundwater fluctuation, and to map soil texture and CEC. A high-precision determination of soil properties using FDEM is not always straightforward and feasible. This is because σ is a complex function of several soil properties, which can vary significantly over time and space. The soil salinity dominates the FDEM signal in wet saline soils, and we were able to assess soil salinity dynamics with high precision in our experiments. Clay content, CEC, and water content influence the FDEM signal in non-saline soils, allowing these properties to be predicted.

Acknowledgements

This work was developed in the scope of SOIL4EVER “Sustainable use of soil and water for improving crops productivity in irrigated areas” project supported by FCT, grant no. PTDC/ASPSOL/28796/2017.

Keywords: Precision agriculture, Soil electrical conductivity, inversion, efficient field assessment

An electrical resistivity model of the San Pedro – Ceboruco graben: 3-D inversion studies and comparisons between standard and advanced Magnetotelluric transfer functions

C. Castro[1], A. Junge[1], H. Eysteinsson[2], P. Hering[1], L. González-Castillo[3] and L. Ferrari[4]
[1] Goethe-Universität Frankfurt am Main, castro@geophysik.uni-frankfurt.de
[1] Goethe-Universität Frankfurt am Main, junge@geophysik.uni-frankfurt.de
[1] Goethe-Universität Frankfurt am Main, phhering@geophysik.uni-frankfurt.de
[2] Reykjavik Geothermal, hjalmar@rg.is
[3] Universidad de Granada, lgcastillo@ugr.es
[4] Universidad Nacional Autónoma de México, luca@geociencias.unam.mx

SUMMARY

A large set of Magnetotelluric (MT) surveys has been carried out along the Tepic-Zacoalco Rift (TZR) for geothermal exploration and to determine the deeper electrical conductivity distribution of the subsurface.

The available data set was carefully analyzed and the time series of those low-quality stations were reprocessed using a multivariate robust remote reference approach (Hering, 2019), improving the estimation of the frequency-dependent MT response functions, especially for Tippers.

Here, we perform a dimensionality analysis of the data using the MT Phase Tensor (PT, Caldwell et al., 2004) and the Complex Apparent Resistivity Tensor (CART, Brown, 2016, Hering et al., 2019). Both parameters have distinct features and sensitivities, which can be directly related to the conductivity distribution of different geological units. The comparison highlights the benefits of the interpretation of MT data sets using the novel CART. A spatially-constant phase split within the PT and coincident small induction vectors were observed between 10^1 – 10^2 period range, followed by a decrease in the phases for the longer periods, associated with an increase of the electrical resistivity.

Subsequently, 110 MT broadband stations were used to derive a high-resolution resistivity model of the San Pedro-Ceboruco (SPC) graben. 3-D inversion models derived from Impedance tensor and Tipper (Z and T) are compared to those resulting from PT and CART inversions. The model results reveal improvements for the advanced MT transfer functions, which result in a better resolution of vertical and horizontal resistivity gradients.

The resistivity model reveals a high conductivity ascent path, which connects the Ceboruco volcanic edifice to a mid-to-lower crust mush zone within the Tepic-Zacoalco Rift. Furthermore, the observed constant phase split and the small induction arrows coincide with the electrical anisotropy zone previously identified in the Ceboruco volcano by Hering et al. (2021).

Keywords: Magnetotellurics, Complex Apparent Resistivity Tensor, Electrical Anisotropy

REFERENCES

Caldwell TG, Bibby HM, Brown C (2004). The magnetotelluric phase tensor. Geophys. J. Int. 158, 457–469. doi: doi.org/10.1111/j.1365-246X.2004.02281.x.

Hering P (2019). Advances in Magnetotelluric Data Processing, Interpretation and Inversion, Illustrated by a Three-dimensional Resistivity Model of the Ceboruco Volcano. PhD Thesis. Goethe-Universität Frankfurt am Main, Germany.

Hering P, Brown C, Junge A (2019). Magnetotelluric apparent resistivity tensors for improved interpretations and 3-D inversions. J. Geophys. Res. Solid Earth 124, 7652–7679. doi: 10.1029/2018JB017221.

Hering P, González-Castillo L, Castro C, Junge A, Brown C, Márquez-Ramírez, VH, Pinzón JI, Gutiérrez QJ (2021, in press). Tectonic controls on magmatic systems: Evidence from a three-dimensional anisotropic electrical resistivity model of Ceboruco Volcano. Journal of Volcanology and Geothermal Research, 107382. doi: doi.org/10.1016/j.jvolgeores.2021.107382.

The use of the ''floating'' S-plane for effective interpretation of airborne TEM data

V. Hallbauer-Zadorozhnaya[1] and E. Stettler[1,2]
[1]AeroPhysX (Pty) Ltd, South Africa, valeriya.hallbauer@gmail.com
[2]University of Witwatersrand, South Africa, stettlere@gmail.com

SUMMARY

B-field TEM data due to a pulsing ground loop and collected with a DJI 600Pro hexacopter with MagArrow magnetometer as well as helicopter borne VTEM d**B**/dt data was modelled with the 'floating' S-Plane interpretation technique. The former stems from the Flat Mine North copper deposit and the later was recorded at the Hondekloof nickel occurrence, both in South Africa. Since interpretation routines for B-Field recordings are not well known the main objective of our research was to develop a single procedure for the interpretation of B- and dB/dt airborne TEM data. For the drone survey a transmitter (Tx) loop 1000x800 m^2 in size, on the ground and a MagArrow magnetometer below the drone was used as receiver to record both the magnetic and TEM variations. Soundings were recorded both inside and outside the Tx loop (up to ~500 m from all sides) and are 15m apart resulting in a total of about 1000 TEM soundings. After digital separation of the magnetic and electromagnetic field components a modified method for calculating the apparent longitudinal conductivity $S\tau$ (Stau) was applied. Firstly, the parameters of an equivalent conducting S-plane with longitudinal conductivity at a fixed depth, are determined. Then the theoretical emf curve was calculated for known parameters of the "floating" plane. To comply with the conditions of the near zone, the calculation of theoretical curves was carried out for the in-loop configuration but simulated by using Tx loops with smaller dimensions. Then $S\tau$ as a function of depth H was calculated according to the well-known usual technique and converted into a resistivity voxel showing possible deeper ore bodies.
For the VTEM data at Hondekloof the classical method of calculation $S\tau(H)$ was used, taking into account the excess of the transmitter-receiver configuration above the ground. At the site, exposed ore bodies are reflected in zones of increased longitudinal conductivity. Numerous anomalies have been identified, possibly associated with unexplored reserves of nickel ores.

Keywords: drone, airborne TEM, S-plane copper and nickel deposits

INTRODUCTION

During the first two decades of the 21st century transient airborne electromagnetic surveying became widespread. Presently we are witnessing the development of a new branch of electromagnetic exploration with the use of airborne TEM surveying by drone. Drones, also referred to as Unmanned Aircraft Systems (UAS), Unmanned Aerial Vehicles (UAV) or Remotely Piloted Aircraft (RPA), signify pilotless aircraft. The UAS technology has several advantages over a conventional airborne platform to collect geophysical data such as resolution, accuracy and cost but off-course presently have limited endurance and weight carrying capabilities. In comparison to ground surveys a drone can collect hundreds of thousands of sounding points in 2-3 days, weather permitting.
Airborne TEM have brought with them new problems in processing and interpretation of the data. Although the primary processing is today quite well established the modelling algorithms for a 1D inversion for every sounding can still take a long time and only visualize along the flight lines. This is too time consuming an approach to be used for a quick interpretation. Then heterogeneities in the upper part of the subsurface section can mask conductive bodies because changes in flight altitude can drastically change the amplitude of signals. In contrast to drone surveying neither a helicopter nor a fixed wing can fly at the same constant altitude above surface and changes in flight altitude can result falsely or in not identifying a conductive object. All this must be taken into account when creating a general interpretation/modelling algorithm.
We have carried out experimental work using a 50% duty cycle pulsing ground loop and a DJI 600Pro copter with a Geometrics MagArrow magnetometer suspended below sampling at 1 KHz to collect B-field decay TEM values. This data as well as dB/dt measurements from a VTEM (GETECH) survey were interpreted with the 'floating' S-plane method based on a modification of the Stau ($S\tau$) technique. The 'floating' technique also subdivides a subsurface section into a certain number of layers, but only identifies the conductive ones together with their depths.
The specifications of the drone and

magnetometers are given by Smit et al. (2022) and are outside the scope of this abstract.

INTERPRETATION VIA MODIFICATION OF THE CALCULATION OF APPARENT LONGITUDINAL CONDUCTANCE $S\tau$

The so-called method of differential transformation of emf signals into curves of apparent longitudinal conductance as function of time and depth was proposed by Sidorov and Tikshaev (1970) The $S\tau$ method has certain advantages. Its use allows determining the conductance of the section and determining the depth where $S\tau$ increases noticeably. Usually increasing conductance is associated with the presence of a low resistive object (bodies and/or layers) in the section.

According to Smythe's (1950) regardless of the position of the observation point at each moment in time, the amplitude of the potential vector Ax (and, accordingly, Bz and emf e(t), will be equal to the amplitude of a certain "floating" conductive plane lying at a depth h with conductivity S equivalent to the total longitudinal conductivity of the entire section up to depth h. Dividing up the transmitter loop in small segments AB we have for a dipole (or a short electric line AB):

$$Bz=(I\mu/4\pi r^2)\ (1/[r^2+4m^2]^{3/2)}), \quad (1)$$

$$e(t)=(IABQ/4\pi Sr^3)(1/[r^2+4m^2]^{3/2)})=KF(m)/S, \quad (2)$$

where I is an electrical current (in A), Q is the effective surface area of the receiver loop (in m^2), *r* is the distance between of center of AB and the observation point M, $\mu=4\pi10^{-7}\,H/\mu\varepsilon\tau\varepsilon\rho$ is the magnetic permeability, z_0 is distance between the S-plane and M, $m=z_0/2r+h/r+t/\mu$ Sr, $K=IABQ/4\pi r^3$.

Note that the St method can only be used for the 'near' zone condition, while with our setup we use either a big loop around which we integrate along small segments AB or if use is made of a long grounded line AB we integrate along the line and as the airborne receiver position Q can be a significant distance removed from AB it is then more likely to correspond to the transition zone between the 'near' and 'far' zone.

The parameters of the "floating" plane at each sounding are determined as follows:

1. After separating the ambient magnetic field and the TEM signal, the smoothing of the TEM signals to suppress noise;
2. From eq.2 the emf contains two unknowns S and m, while Bz contains only m. The transformation of the emf into Bz is performed by numerical integration, taking into account the additional time sequence;
3. Comparing the calculated values Bz with theoretical ones for the same setup (with fixed h, we get the parameters of the "floating" plane m(t) at each time;
4. Now for a given function m(t) we calculate the theoretical curve Bz for a new setup, i.e. for a small loop-in-loop configuration (AB=25 m) located on the ground (z_0=h).
5. Differentiating the theoretical Bz with respect to time t we obtain e(t)for "floating" plane as a function of m(t)
6. Subsequent smoothing of the emf signals.
7. Transformation of the signals into the $S\tau$(H), according to (Sidorov V.A. Tikshaev V.V., 1970). The depth of the "floating" plane can be calibrated using available drilling data. However many years of experience in using the St method shows that in most cases the empirical formula H(t)=0.5mr can be applicable.

RESULTS AND DISCUSSION
O'KIEP. RESULTS OF DRONE TEM.

The Flat Mine North (FMN) Cu ore body is one of many that constitutes the O'Kiep Cu district in extreme northwest South Africa. The FMN mine closed in 1995 due to low Cu prizes. Cu bearing sulphides occur in lumpy noritic intrusives in highly resistive granitic-gneissic basement material and are characterized by low or reduced resistivity values for larger Cu orebodies and TEM IP effects when disseminated. Figure 1 shows a 3D geo-electric model constructed from a TEM survey measuring the B-field decay and data collected with a 1kmx1km single loop transmitter with 75A, 50% duty cycle, 250ms on 250ms off waveform. The dipole moment was 750 000 Am^2. The receiver was a Geometrics MagArrow magnetometer hanging 4m below a DJI 600Pro hexacopter recording at a 1 KHz rate. The B-field data was not conducive to being modelled directly with a plate-like algorithm (Barnett,1984, Smit et al.,2022) and converted from B-field to dB/dt for 'floating' S-Plane modelling. On the northern side of the model, the conductive body is dipping as clearly seen and confirmed by numerous historic boreholes that discovered the copper body in the distant past. However the results indicate better conductors below the previously mined ore and show that previous drill holes without the foresight of geophysics stopped too short. These better conductors' start at a depth of 350m plus and show that if they are not due to geology containing graphite could signify much better ore at depth going down another 350m. It also shows the deep penetration advantage of recording the B-field.

HONDEKLOOF. RESULTS VTEM USING HELICOPTER.

Historic VTEM data conducted by GETECH at the Hondekloof Ni occurrence site in extreme central western SA was made available to us for re-valuation of the data. The total number of

soundings were about 330,000. The sounding density was 5m along flight lines, 25m between flight lines. The highly conductive nickel sulphides occurrences are confined to a ring-sharped structure surrounding a highly resistive granite–gneiss dome. Figure 2 shows a 3D resistivity model (ρ=H/S) where the colour bar displays the log of the resistivity and. areas of low resistivity are shown in blue. The massive bodies of Ni sulphides have a resistivity of 1Ohm.m and less.

Because of clear TEM IP evidence it is believed that some resistive zones are associated with the presence of disseminated NiS particles, which are also of exploration interest. In these sections, the TEM curves are distorted by the effects of induced polarization.

CONCLUSIONS

The data from both the drone B-field survey carried out at FMN (O'Kiep) and at the Hondekloof site that was surveyed according to the classic helicopter VTEM technique measuring db/dt, the modified Stau method was applied for interpretation of the TEM data. New potential reserves of copper at FMN and nickel deposits at Hondekloof were discovered at two sites in South Africa. The total number of TEM points in both sites are 1000 and 330,000, respectively. Full preparation and calculation of files for visualization of flight line subsurface sections for 143 profiles took 8 hours on an off the shelve i5 laptop (for the Hondekloof site).

As a result, three-dimensional images of geo-electric sections of the study area were constructed by gridding across flight lines. All available boreholes agree with the 3D geo-electric construct which show the potential of extra ore beyond that encountered in the boreholes.

REFERENCES

Barnett CT (1984) Simple inversion of time domain electromagnetic data. Geophysics 49(7):925–933. https:// doi. org/ 10. 1190/1. 14417 38

Sidorov VA, Tikshaev VV (1970) Interpretation of transient electromagnetic signals registered in near zone. Exploration Geophysics, M. Nedra. 42: pp.45-54 (in Russian).

Smit JP., Stettler EH, Price ABW, Schaefer MO, Schodlok MC, Zhang R (2022) Use of drones in acquiring B-field total-field electromagnetic data for mineral exploration. Mineral Economics doi:10.1007/s13563-021-00292-1.

Smythe VR 1950 Static and Dynamic Electricity. McGraw Hill Book Company Inc.

e 1: 3D geo-electrical model, Hondekloof Ni occurrence.

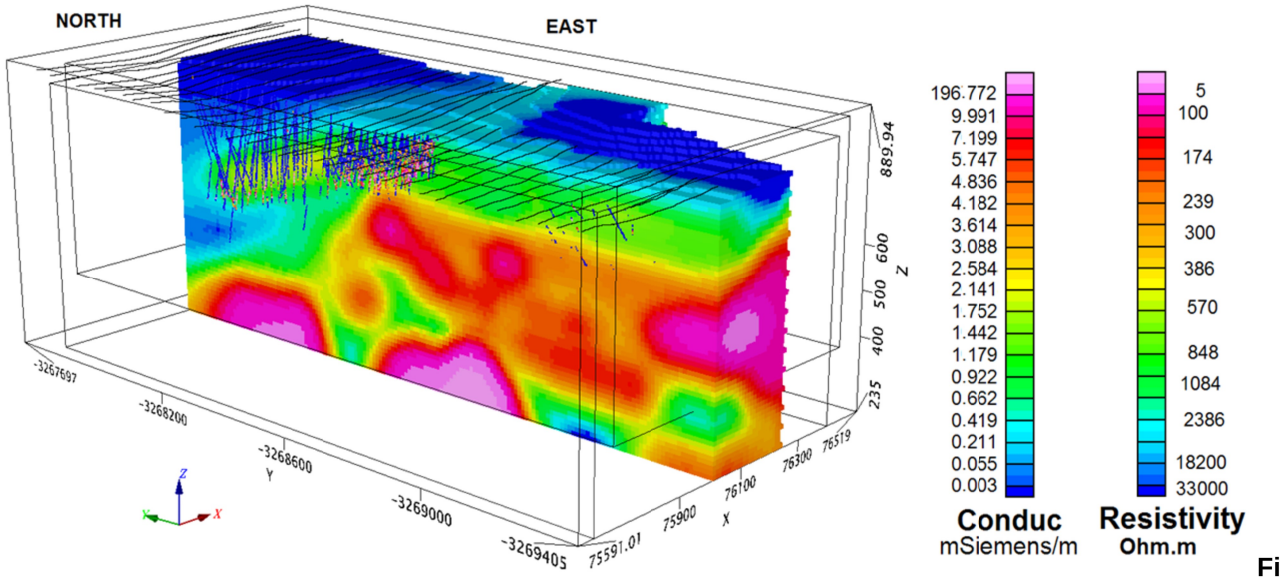

Figure 1: 3D geo-electrical model, Flat Mine North O'Kiep

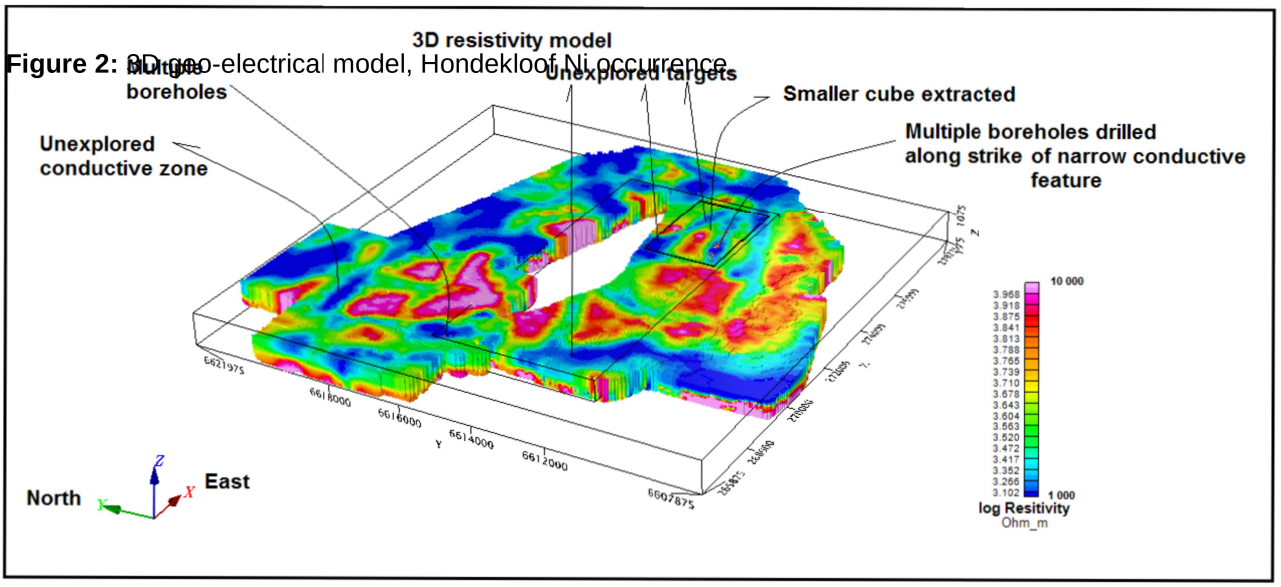

Figure 2: 3D geo-electrical model, Hondekloof Ni occurrence

Abstract, 25th EM Induction Workshop,Çeşmeı, Turkey, September 11-17, 2022

Local to Regional Scale 3D Study around Gällivare, Sweden based on Integration of 3D Magnetotellurics with other Geophysical Data

Jirigalatu[1], Maxim Yu. Smirnov[2], Thorkild M. Rassmussen[3], Oskar Rydman[4], Jan Vozar[5], Tobias Bauer[6], Jingyu Gao[7], Svetlana Kovachikova[8], Niklas Juhojuntti[9], Tobias Hermansson[10], Kirsi McGimpsey[11], Harald Van Den Berg[12], Graham Hill[13], Jochen Kamm[14] and DREX WG

[1]Luleå tekniska universitet,jirigalatu.jirigalatu@ltu.se

[2]Luleå tekniska universitet,

[3]Luleå tekniska universitet,

[4]Luleå tekniska universitet,

[5]Earth Science Institute of Slovak Academy of Sciences,

[6]Luleå tekniska universitet,

[7]Chinese Academy of Sciences,

[8]Institute of Geophysics of Czech Academy of Sciences,

[9]LKAB,

[10]BOLIDEN,

[11]BOLIDEN,

[12]LKAB,

[13]Institute of Geophysics of Czech Academy Of Sciences

[14]Geological Survey of Finland

SUMMARY

Geologically, Norrbotten has historically been one of the most active mining areas in Europe. Norrbotten hosts a world-class iron ore mine (in Kiruna), the largest copper mine (in Aitik) in Europe, which is also the largest gold producer in Sweden, together with other mines scatted in the county. Specially, Gällivare and Kiruna are probably the most productive mining areas of Fennoscandia. As a result, the areas have been extensively surveyed with mainly passive and non-invasive geophysical techniques such as ground and airborne gravimetry, aeromagnetics, and magnetotellurics. Therefore, it can be beneficial to understand the mechanism behind for its extreme enrichment in Norrbotten by using multi-scale multi-physics observations and the knowledge of the existing mineralization and polymetallic deposits. During summer 2021 regional and local scale magnetotelluric data were collected in Sweden around Gällivare. Area of about 100x100 km2 was covered with average site spacing of 5 km. Additional deposit scale measurement around Gällivare and Pyhasalmi were measured to compliment the regional data set as well as all previously available geophysical data. Extra CSEM data were also acquired.

Original data are processed and analysed to derive impedance and tipper transfer functions using conventional robust remote reference processing. We will continue to work with data and apply multivariate techniques which we expect will improve estimates of transfer functions at problematic sites and provide additional information to be used in inverse modelling. Overall the data quality is from excellent to good with some few exceptions related to instrumental and measurements problems.

Keywords: mineral systems, geophysics, magnetotellurics, data processing inversion

MTHEK Project: MagnetoTelluric Assessment of the HEKla Volcano

Duygu Kiyan[1], Ásdís Benediktsdóttir[2], Gylfi Páll Hersir[2], Magnús T. Guðmundsson[3], Christopher J. Bean[1], Colin Hogg[1], Þorsteinn Jónsson[3] and Jón Einar Jónsson[2]
[1]Dublin Institute for Advanced Studies, duygu@cp.dias.ie
[2]Iceland GeoSurvey, asdis.benediktsdottir@isor.is
[3]University of Iceland, mtg@hi.is

SUMMARY

Hekla is one of Iceland's most active and dangerous volcanoes having had 18 summit eruptions in the last 1,100 years, with the most recent eruption in 2000. Hekla volcano has been studied extensively using various geodetic methods. The most recent deformation studies (InSAR) in relation to the 2000 eruption of Hekla have addressed the proposed location of a deep-seated magma reservoir at approximately 10 km (Sturkell et al., 2013), where other studies indicate a greater depth (Ofeigsson et al., 2011). A regional-scale magnetotelluric (MT) survey (Eysteinsson and Hermance 1985) conducted in 1982 suggested the estimated depths for the magma chamber beneath the volcano to be between 5 and 24 km. The objectives of the MTHEK project are to (1) study the present electrical resistivity structure of the volcano through exploiting deep-probing broad-band MT data and (2) identify low-resistivity zones at depth, which may be a proxy for melt accumulation and migration pathways and thus, may constrain the location of the proposed magma reservoir. The geoelectrical models obtained will enable us to highlight potential real-time electromagnetic monitoring locations which may complement the current real-time seismic/deformation monitoring. In September 2020, broadband MT data were acquired at 20 stations around and to the south of Hekla volcano. The horizontal electric field components were recorded using 50-60 m dipoles, and the three components of the magnetic field were measured using induction coils. MT data were collected for a minimum of 13 hours up to a maximum of 53 hours. A distant remote reference site (approximately 100 km away) was recording during the whole survey. The period range of good quality data obtained is about 300 Hz to 1,000 - 2,000 s. In addition, at 17 MT stations central loop transient electromagnetic (TEM) data were collected using a transmitter loop of 200 m × 200 m and a 1 m^2 receiver loop with 100 windings (effective area 100 m^2). The TEM data are used to correct the MT data for static shift effects caused by near surface inhomogeneities or steep topography. State of the art data processing and analysis methods were applied to the data. Preliminary inversion models will be presented and provide a first idea of the resistivity structure of the volcano.

Keywords: Magnetotellurics, Electrical conductivity, Hekla Volcano, Iceland

Abstract, 25th EM Induction Workshop, Çeşme, Turkey, September 11-17, 2022

Calculating geoelectric fields using a lithospheric resistivity model of the Iberian Peninsula

R. Hafizi[1], A. Martí[1], P. Piña-Varas [1], G. Mitjanas[1], J. Campanyà[2], A. Marcuello[1], J. Ledo[3], P. Queralt[1]

[1] Institut Geomodels, Dept. Dinàmica de la Terra i de l'Oceà, Universitat de Barcelona, Barcelona, Spain, raha.hafizi@ub.edu

[2] Department of Build Environment, South East Technological University, Ireland

[3] Physics of the Earth and Astrophysics, Faculty of Physics, Universidad Complutense de Madrid, Spain

SUMMARY

As part of the IBERGIC-CAST (Modelling and forecasting of Geomagnetically Induced Currents in Spain) multidisciplinary project, funded by the Spanish Research Agency, we aim at improving the geoelectrical resistivity models of the lithosphere below the Iberian Peninsula, and use them to create the geoelectric field hazard maps for different geomagnetic storm scenarios.

In this work we present the modelling of the geoelectric fields using Magnetotelluric transfer functions computed from measured time series, and calculated from the most recent resistivity model of the Iberian lithosphere. Three-dimensional inversion of Magnetotelluric data and forward modeling give us the required impedances for geoelectric calculations for the Iberian Peninsula. The interstation function analysis also provides information about the difference of the electrical underground structure between the sites. For the geomagnetic field, we used data from geomagnetic observatories and hypothetical scenarios. Nearest-site and Spherical Elementary Currents Systems (SECS) were considered to interpolate geomagnetic fields from magnetic observatories to the sites of interest. The results are analyzed in views of the underlying geology and the coast.

The outcome of this study can be used for developing hazard maps of the geoelectrical field of Iberia for specific events or averaged years.

An assessment of galvanic distortion effects contaminating MT data from Central Iran

M. Sajedi[1],
M. Montahaei[2],
H. Esmaili Oghaz[3]

[1]Institute of geophysics, University of Tehran, Tehran, Iran, mehrdadsajedy13@gmail.com
[2]Institute of geophysics, University of Tehran, Tehran, Iran, mmontaha@ut.ac.ir
[3]Natural Iranian Gas Storage Company for Nasr-Abad Area, Tehran, Iran

SUMMARY

Salt extrusions (Diapir, dome and glaciers) have a high electrical resistivity contrast with their surrounding sediments and consequently are good exploration targets for electromagnetic (EM) methods. However, diffusive EM fields, employed in MT exploration technique, have restrictions in resolution and sensitivity and cannot model the earth at the full scale. Furthermore, galvanic distortion effects caused by shallow and small scale lateral inhomogenities contaminate measured EM fields and cause unreliable imaging of subsurface electrical resistivity.

In this study, we investigate dimensionality, directionality and distortion analysis of an MT dataset from 35 stations recorded along a profile in Nasr Abad region, west central Iran. The region is composed of five salt diapirs, developing close to the Abshirin Shurab fault zone which is a dextral strike slip fault with a NNW-SSE strike direction in the west Central Iran.

Considering the limitations of different dimensionality analysis method, we applied a combined approach, comprising a subsequent use of the WAL invariants, phase tensors and the Groom-Baily (BG) decomposition methods. At the first step we classified dimensionality and distortion effects at different period bands. Then, for the bands where MT data appear to arise from a superimposed model of 3D/2D structures, we switched to the GB decomposition method for distortion effect removal and retrieving regional impedances. At the first step, the application of rotational invariants showed that there is no sign of electrical anisotropy in dimensionality pattern and the regional conductivity structure can be considered predominantly as 2D with some superimposed distortions from local 3D conductivities. 2-D inductive impedance responses were also retrieved by removing distortion effects from the measured data.

Keywords: magnetotellurics, electrical conductivity, salt diaper, Central Iran

Towards a new 3D conductivity model of the British Isles: Revisiting MT data from Isle of Skye, Scotland

Aideliz Montiel-Álvarez[1], Juliane Hübert[2] and Kathy Whaler[3]
[1]School of GeoSciences, The University of Edinburgh, UK, a.montiel@ed.ac.uk
[2]Geomagnetism, British Geological Survey, UK, jubert@bgs.ac.uk
[3]School of GeoSciences, The University of Edinburgh, UK, kathy.whaler@ed.ac.uk

SUMMARY

Potential ground-level impacts of space weather on infrastructure include so-called Geomagnetically Induced Currents (GICs). These currents result from electromagnetic induction during geomagnetic storms and can damage power networks, pipelines, and railways. Estimating geoelectric fields at the Earth's surface is a critical element to evaluate the hazard and model GICs. Although the increase in computational capabilities has led to a wide range of GIC estimation techniques, the accurate incorporation of the Earth's electrical conductivity is probably the least explored aspect. However, large-scale magnetotelluric (MT) surveys are emerging as a suitable way to fill this gap and improve GIC modelling.

The SAGE (SWIMMR Activities in Ground Effects) project, led by the British Geological Survey, is one of eleven projects within the UK Strategic Priorities Fund (SPF) Space Weather Instrumentation, Measurement, Modelling, and Risk (SWIMMR) program. As part of the SAGE project, we are acquiring long-period magnetotelluric (LMT) data across Great Britain. These new sites, in addition to legacy datasets, will be used to build a 3D conductivity model of the British Isles. The legacy data include a broadband MT survey in the Isle of Skye that we used as a mini-scale pilot experiment to analyze effects and modelling parameters expected to be crucial in the model of Great Britain (GB). Although the ocean depth is shallow around the Isle of Skye (up to 250m), and in contrast to the argument of negligibility in the previous study, we show that the coast effect is significant. Another aspect related to the coast effect that has been recently investigated is the impact of conductive sediments. We show that adding sediment conductivity variation improves Skye's model, and we discuss the potential impact on the GB model. Finally, we investigated the effects of varying parameters including resistivity, extension, and cell dimension of the starting model as well as damping and covariance for the 3D inversion. The results from this study not only allowed us to build a new, robust 3D model of the Isle of Skye but set the bases to optimize the future modelling of the British Isles.

Keywords: 3D conductivity model, parameter test, British Isles

Abstract, 25th EM Induction Workshop,Çeşmeı, Turkey, September 11-17, 2022

Geophysical Imaging of the Roter Kamm Crater in the Sperrgebiet National Park, Namibia, using TEM and AMT

H. Nienhaus[1], P. Yogeshwar[2], W. Mörbe[3], B. Tezkan[4], B. Lushetile[5] and M. Melles[6]
[1]Institute of Geophysics and Meteorology, University of Cologne, h.nienhaus@uni-koeln.de
[2]Institute of Geophysics and Meteorology, University of Cologne, yogeshwar@geo.uni-koeln.de
[3]Institute of Geophysics and Meteorology, University of Cologne, moerbe@geo.uni-koeln.de
[4]Institute of Geophysics and Meteorology, University of Cologne, tezkan@geo.uni-koeln.de
[5]Geological Survey of Namibia, Bufelo.Lushetile@mme.gov.na
[6]Institute of Geology and Mineralogy, University of Cologne, mmelles@uni-koeln.de

SUMMARY

The Roter Kamm Crater is a 3.7-million-year-old meteoritic impact crater in the Sperrgebiet National Park in southern Namibia. The Sperrgebiet National Park, officially Tsau ǁKhaeb (Sperrgebiet) National Park, is a national park and former diamond mining area in southern Namibia. Since 1908 the public has had no access to the area and even when it was proclaimed a national park in 2008 most of the restrictions remained, leaving the environment mainly undisturbed and unexplored.

The geophysical exploration of the Roter Kamm Crater can lead to valuable information about its internal structure, as only a very limited number of geophysical studies had been carried out at this site. Prior gravimetry and (airborne-)magnetic measurements indicate a bowl-shaped anomaly underneath the crater, which was expected for an impact crater with a diameter of 2.5 km. However, the estimated depths of the basement vary between 100 m and 400 m.
To be able to image the basement in the crater in this wide range of possible target depths, two electromagnetic methods were selected: the Transient Electromagnetic (TEM) and the Audiomagnetotelluric (AMT) method. TEM is an active time domain method and has already proven its capability imaging sedimentary deposits. It is suited for investigations in shallow (up to 200 m) subsurface. AMT, on the contrary, is a passive, frequency domain method that can reach penetration depths up to a few kilometres. Both methods are sensitive to good conductive structures.

Within two weeks of fieldwork at the Roter Kamm Crater 153 TEM and 15 AMT soundings were carried out along three profiles. We used the TEM-FAST 48 (AEMR) for all TEM measurements with a coincidence-loop setup for quadratic transmitter/receiver loops with an edge length of 50 m (58 soundings) and 100 m (11 soundings). Additionally, TEM measurements were carried out in a fixed-loop-setup using 4 large transmitter loops (edge length: 200 m). At each transmitter loop 11 soundings were conducted in profile and perpendicular to profile direction with a maximum offset of 400 m. We used the ZT-30 Transmitter (Zonge) with the SMARTem24 (EMIT) + 3D LF induction coil triple (Geonics Limited)/KMS 820 (KMS Technologies) + 2 TEM-3 induction coils (Zonge). For the AMT measurements the SPAM MK IV system from the Geophysical Instrument Pool Potsdam (GIPP) was used to measure the horizontal electric and magnetic fields.
The 1D inversion models of the TEM data showed a good conducing anomaly in a depth of 100 m, but was not capable of imaging its lower boundary. The 2D inversion model of the AMT data, on the other hand, has a good resolution in higher depths and could resolve the basement at a maximum depth of over 300 m in the centre of the Roter Kamm Crater. Overall, AMT and TEM are in very good agreement with each other and show the expected bowl-shaped anomaly in the impact. These results proved, that both methods complement each other well and it was necessary to use AMT for resolving the basement within the crater and to use TEM for resolving structures within the upper 100 m of sediments.

Keywords: Transient Electromagnetics, Audiomagnetotelluric, Sedimentary Deposit, Impact Crater

The site selection procedure for a high-level radioactive waste repository in Germany: Future application of electromagnetic methods for exploration activities

Dennis Rippe[1], Katharina Bairlein[1], and Frank Meier[1]
[1]Bundesgesellschaft für Endlagerung mbH (BGE) Peine, Germany, dennis.rippe@bge.de

SUMMARY

According to the 'Repository Site Selection Act' (a German federal law called Standortauswahlgesetz – StandAG), the BGE, Germany's federal company for radioactive waste disposal, has been assigned to implement the site selection procedure for a German high-level radioactive waste repository in a deep geological formation with best possible safety conditions for a period of at least one million years. The site selection procedure is an iterative process consisting of three phases with increasing level of investigation while the considered area becomes smaller in the process. Starting with an empty, so-called white map of Germany, the BGE completed Step 1 of Phase I in September 2020 with the submission of the sub-areas interim report, which identified 90 individual sub-areas with favorable geological conditions for safe disposal of radioactive waste. According to the site selection act, the host rocks claystone, rock salt and crystalline rock are considered. In the current Step 2 of Phase I, regions for upcoming surface exploration will be identified. Surface exploration will take place in Phase II, including geophysical surveys, geological mapping, hydrogeological investigations, borehole drilling and tests. Surface exploration programs will be developed based on comparison of existing data and the demand for additional information to assess the disposal system.

Electromagnetic (EM) surveys can provide information of the subsurface rock properties relevant to the safety of a high-level radioactive waste repository. Due to the large variety of possible geological settings (different host rocks, depths, cap rock geology, etc.) it is necessary to consider various methods and their combinations for the surface exploration. In addition, surface conditions might influence the selection of methods, e.g. airborne EM in areas that are difficult to access. The BGE is involved in research regarding application of novel sensors, analysis and inversion tools for EM methods and combination of EM and other geophysical methods.

Keywords: Radioactive waste disposal; Site selection; Surface exploration

Donbas geoelectrical structure

I.I.Rokityansky, A.V.Tereshyn
Subbotin Institute of Geophysics of the National Academy of Sciences of Ukraine, Kiev, Ukraine
E-mail: rokityansky@gmail.com

SUMMARY

Donbas was formed by Late Devonian rifting of the East European Craton. Then subsidence and sedimentation formed 15-km thick Carboniferous deposits. The next long event was folding. Then inversion lifted the folded Donbas and subsequent erosion exposed the Carboniferous coal-bearing strata. Dominated strike of the Donbas structures is WNW-ESE. Deep electrical conductivity was studied by the methods of magnetic variation profiling (MVP) and magnetotelluric sounding (MTS). The MVP data at long (5-180 min) periods reveal the intense Donbas electrical conductivity anomaly (DECA) which runs along the main anticline of the folded Donbas and continues in DDB and Karpinsky swell (Figure 1). Interpretation conducted according to ideas described in (Rokityansky 1982). DECA parameters obtained by **MVP**: Profile graphs of the anomalous field give an estimate of the maximum possible depth of the anomalous currents center h=18±2 km. Frequency response maximum T_0≈3600 s yields the total longitudinal conductance G = (8±2)×10^8 S×m. Mapping the anomaly axis (Figure 1) and effective width L=36 km estimation also reliably made by MVP. 70 **MTS** at periods 0.1-3000 s yield: the upper ≈0.5 km thick layer have, as a rule, resistivity in the range of 5—50 Ohm·m. Deeper low resistivity objects are located in two conductive stripes, which upper edge varies from 0.3 to 5 km. The stripes are parallel to the DECA axis and considered as part of DECA. A very large value of G leads to assumption that the anomalous body extends to considerable depth (Figure 2). DECA axis spatially coincides with intense (up to 90 mW/m^2) deep heat flow anomaly. This fact suggests that the nature of the DECA lower part can be a partial melting. Geoelectric results support the idea of the modern tectonic activation in Donbas developed by V.V. Gordienko.

Keywords: magnetotelluric sounding, magnetic variation profiling, folded Donbas

Methods

Anomalous currents in a conducting body arise due to local electromagnetic induction in this body and due to conductive redistribution of currents induced in the enclosing media on territories with the size of an external source. Conductive type usually dominates. Its anomalous field is the product of decreasing function of period (it is the impedance of the normal cross-section) by a non-decreasing function V (0<V<1) that describes the degree of the conducting body filling with anomalous currents. Frequency response of such product has a maximum T_O which is directly related to integral longitudinal conductance G and open possibility to estimate it (Rokityansky 1982, p.247-256, 294-297)

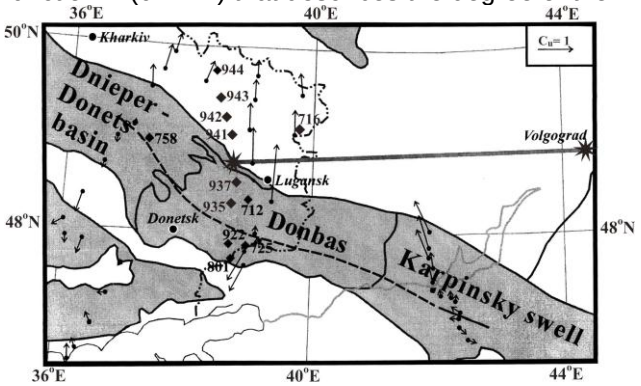

Figure 1. Donbas anomaly axis – dashed line. Arrows – induction vectors for periods 30-90 min. Rhombus – sites where impulses (±700 A, 800 kV, duration 100 s) from 473 km long line Volgograd – Donbas (grey line between stars) were recorded.

REFERENCE

Rokityansky II (1982) Geoelectromagnetic investigation of the Earth's crust and mantle. Berlin-Heidelberg-New York: Springer Verlag 381p.

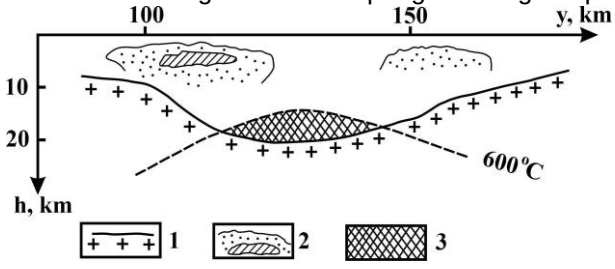

Figure 2. Model of the DECA cross-section assuming the well-conducting zone of partially molten rocks existence: 1 - surface of crystalline basement; 2 - two conductive stripes, oblique shading highlights resistivity less than 1 Om·m; 3 - zone of (partial) melting; dashed line - isotherm 600°C according to V.V. Gordienko.

Abstract, 25th EM Induction Workshop, Çeşme, Turkey, September 11-17, 2022

Imagery down to one kilometer depth by airborne electromagnetics: New constraints for geological and hydrogeological modeling in volcanic contexts

Anne Raingeard[1], Pierre-Alexandre Reninger[1], Aurélie Peyrefitte[1], Guillaume Martelet[1], Bertrand Aunay[2], Arnauld Malard[3], Frédéric Dubois[1]

[1]1BRGM, 3 Av. Claude Guillemin, Orléans 45060, France
[2]BRGM, 5 Rue Sainte Anne, Saint-Denis 97400, La Réunion, France
[3]ISSKA, Rue de la Serre 68/4eme étage, 2300 La Chaux-de-Fonds, Suisse

SUMMARY

We present an original approach to combine airborne magnetic data and five different airborne electromagnetics data sets going from 3 000 NIA up to 1 000 000 NIA magnetic moments (three different TDEM systems were used) in La Réunion island. A 3D geological model of the first kilometer bellow the Plaine des Fougères was built and then used for 3D hydrogeological interpretation.

Keywords: Airborne electromagnetics, Time Domain ElectroMagnetics, volcanic island, geological modeling

INTRODUCTION

To bring water to the northern part of La Réunion island (Indian ocean volcanic island), a new gallery will be drilled bellow the Plaine des Fougères and connected to the existing deep underground gallery called 'Salazie amont', covered by up to 1000 meters of volcanic materials. County council of la Réunion (CD974) has asked BRGM to produce a 3D geological model that will be used to create a 3D hydrogeological model, in order to prevent hydrogeological risks related to the drilling of highly permeable surrounding aquifers under high pressure. This work is presented in technical report by Peyrefitte et al (2022).

METHOD

A first airborne electromagnetics (AEM) survey was carried out in La Réunion island in 2014 using the SkyTEM 304 system. It resulted in the imagery of the first 300 m in depth over the whole Réunion island. A second survey was flown in 2021 over the Plaine des Fougères area, using the SkyTEM 306HP and the SkyTEM 312HP systems in order to extend the imagery, down to 1 000 m depth. During both AEM surveys, airborne magnetic data were also acquired. New deep bodies can now be imaged and mapped for geological or hydrogeological purposes. Figure 2 is an example of two South-North resistivity profiles in the same area, illustrating the gain in depth of investigation between SkyTEM 304 and SkyTEM 306HP systems. Combining both data sets, a high-resolution resistivity image of the Plaine des Fougères from the surface to 1000 meters depth was obtained. The processing methodology of AEM data is presented in Reninger et al (2020) and includes the use of the singular value decomposition and a manual editing of the residual noise. A joint smooth SCI inversion (Viezzoli et al, 2007) was run considering all the AEM data. Finally, a 3D resistivity model was created by the interpolation of the 304 and 306HP resistivity models for the near surface (the first 200 m) and the interpolation of 306HP and 312HP resistivity models for greater depths.

2D profile magnetic modeling was performed, using the resistivity model as background preliminary geometry and rock sample magnetic measurements to constrain the geological magnetic responses. Taking into account the volcanic history, 2D profiles constrained by both AEM and magnetic modelling lead to geologically realistic cross-sections (An example is presented in Figure 3). The resistivity model provides the overall geometry of volcanic layers and their alteration degree. Magnetic data allows refining the geological model in depth, highlighting distinct geological units within relatively homogeneous resistivity layers.

RESULTS

Combining all the previous 2D information, 3D geological modeling was carried out from -1000 m to 1500 meters above sea level. Figure 1 displays a result of the modelling, where we can see PN0 to PN4 formations, classified by increasing age, and information about their alteration or saturation in water.

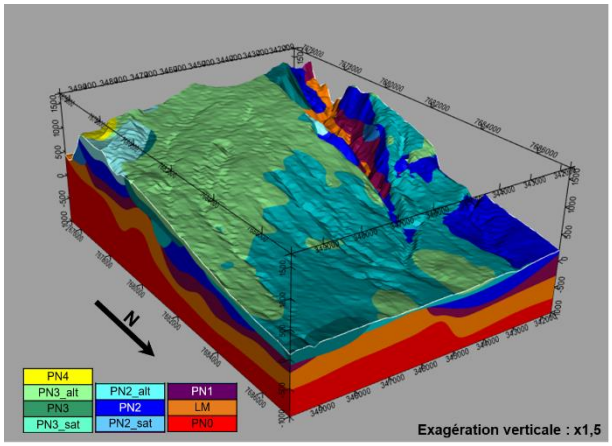

Figure 1: 3D geological model of the Plaine des Fougères.

This 3D model was then used for hydrogeological modelling in Visual KARSYS (Malard et al, 2018), in order to predict hydrogeological risk along several possible gallery routes.

CONCLUSION

Following an original approach consisting in the combination of high-resolution near surface and deep AEM surveys with aeromagnetic data and rock sample measurements, a realistic 3D geology was modeled down to 1000 meters depth. This made it possible to map the geometry of hydrogeological bodies within the first kilometer below the Plaine des Fougères in order to reduce the risk during the drilling of a deep gallery.

ACKNOWLEDGEMENTS

This project is funded by the county council of Réunion (CD974) and the water office of la Réunion.

REFERENCES

Peyreffite A, Reninger PA, Malard A, Raingeard A, Aunay B (2022) BRGM-RP-71628-28: Aide à l'implantation d'une gallerie souterraine (GANOR): acquisition et valorisation de données géophysiques héliportées pour la caractérisation profonde géologique et hydrogéologique de la Plaine des Fougères. Tech. rep., BRGM, URL http://infoterre.brgm.fr/

Reninger PA, Martelet G, Perrin J, Dumont M (2020) processing methodology for regional AEM surveys and local implications. Exploration Geophysics 51(1):143–154

Viezzoli A, Christiansen AV, Auken E, Sørensen K (2007) Spatially constrained inversion for quasi 3D modelling of aem data. ASEG Extended Abstracts 2007(1):1–4

Malard, A., Randles, S., Hausmann, P., Bucev, M., Lopez, S., Courrioux, G., Jeannin, P.Y., Vogel, M., 2018. Visual KARSYS, a web-platform for the documentation of karst aquifers including online geological modelling, in: Delivering Subsurface Models for Societal Challenges - 4th Meeting of the European 3D Geomodelling Community, 21st to 23rd February 2018, Orléans, France. p. 39.

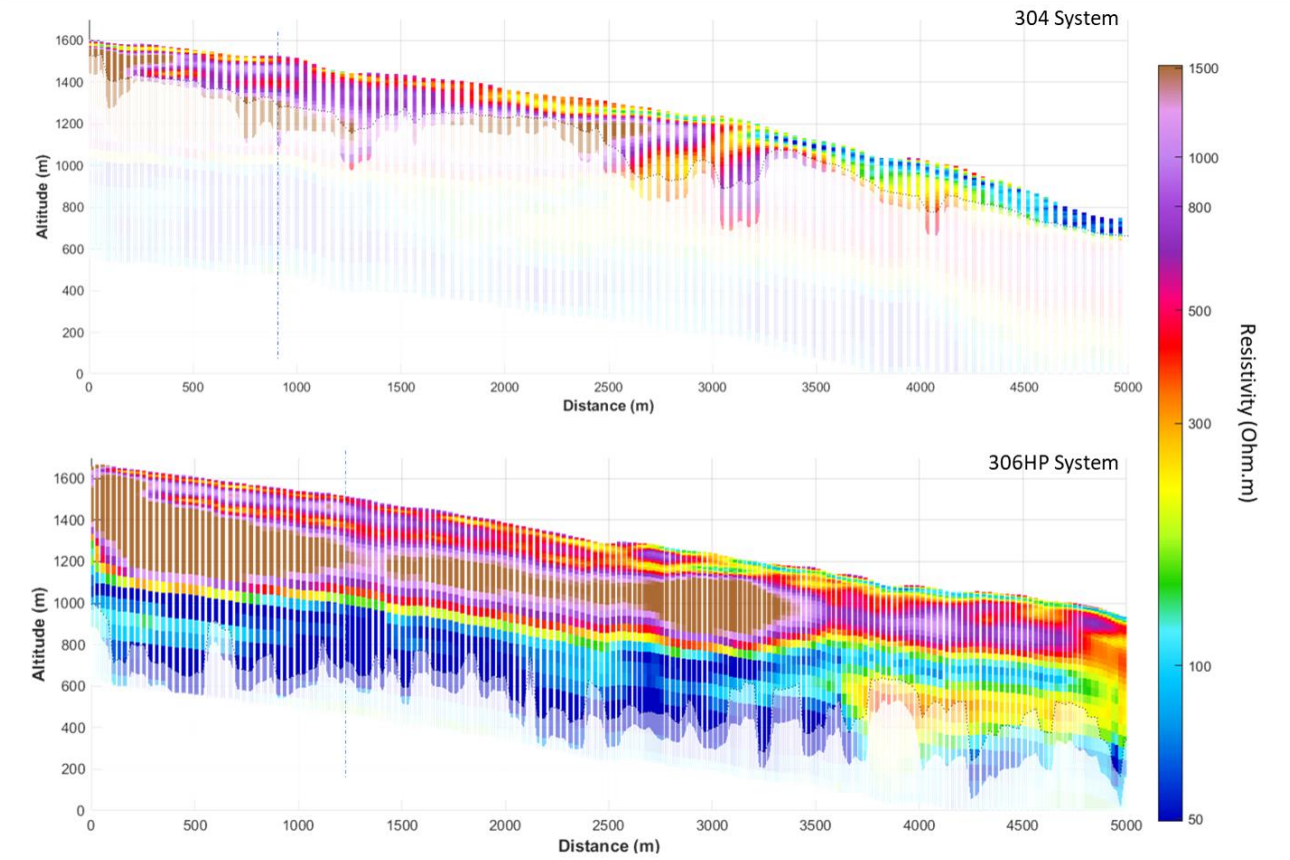

Figure 2: South-North resistivity profiles acquired with 304 (a) or 306HP (b) systems in the Plaine des Fougères area.

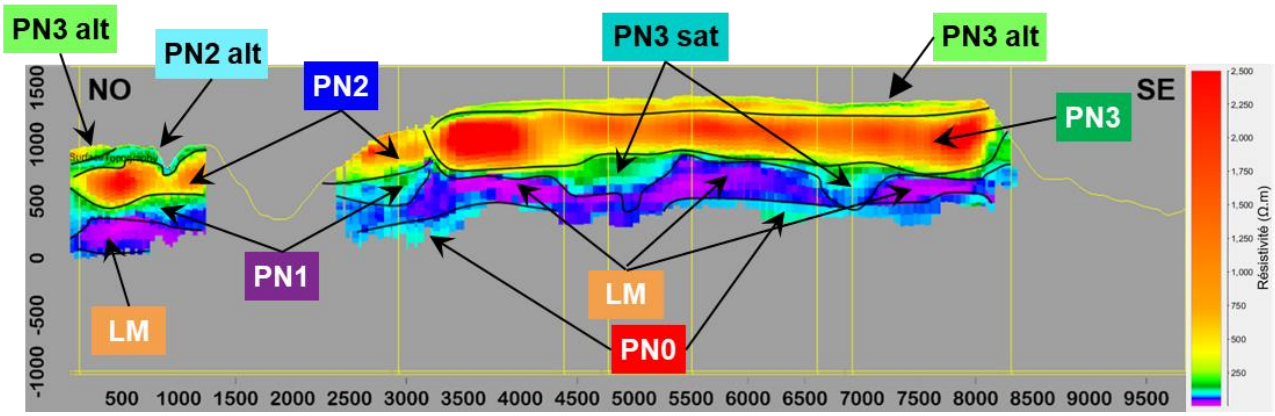

Figure 3: Example of an interpolated resistivity profile along the existing underground Salazie amont gallery, with geological interpretation. PN0 to PN4 represent old to recent volcanic formations.

Electromagnetic Studies on The Qarun Protected Area, Fayoum-Province, Egypt

M. Mekkawi[1], A. Ibrahim[1] , A. Awad, A. Khalil and M. Ibrahim[1]
[1]National Research Institute of Astronomy and Geophysics (NRIAG)
11421 Helwan, Cairo-Egypt.

SUMMARY

SUMMARY

The main object of our study are using suitable and fast tools of the Geoscience to evaluate the environmental impacts on the surrounding **Qarun Protected Area** (**QPA**) and natural resources. To achievement this target, Nuclear Magnetic Ressonnance (**NMR**) and Audio Magnetotelluric (**AMT**) were carried out on the **suggested area** for the first time in Egypt. In addition, land magnetic profile was conducted using GEM magnetometer (**Overhauser-19, Canada**). The daily variation of magnetic field is corrected using Misallat Magnetic observatory that is located at Kom Oshem village beside the Qarun Lake (about **25 km**). The results of NMR and AMT are conformed the depths of water table between 10 meters near Qarun Lake and 120 near Qatrani mountain.

Keywords: Nuclear Magnetic Ressonnance (**NMR**), Audio Magnetotelluric (**AMT**), Qarun Protected Area (**QPA**)

INTRODUCTION

Qaroun Protected Area (**QPA**) is established by the Egyptian national network of Protected Areas, which as on March 2007, as the Nature Conservation Sector of the Egyptian Environmental Affairs Agency (**EEAA**). It contains several features and areas of high value. The landscape is varied, attractive and includes some geological formations hosting fossil deposits of major importance site in the whole African continent in terms of fossil richness. The cultural heritage is also remarkable, with several archaeological sites of primary importance. A prominent feature of the area are the Eocene sediments of **Qasr el Sagha** and **Gebel Qattrani**, which represent the most complete record of Palaeogene mammals for all Africa, the fossil deposits of Qatrani, fossilized forest, ancient basalt quarries and other outstanding features. (Egyptian Environmental Affairs Agency, 2007).

Methods

We apply the NUMIS magnetic resonance which is the first time in Egypt, for exploration of ground water depth, its contents, porosity and permeability. Beside that, the high frequency magnetotelluric method to investigate the shallow subsurface structure of the area surrounded the Qarun Lake. Finally, the magnetic profile survey is conducted beside the magnetic resonance and magnetotelluric profiles figure (1).

The principle of Numis insturement is a pulse of current at a given frequency is transmitted into a loop. The signal produced in return by the H protons (water molecules) is measured within the same loop

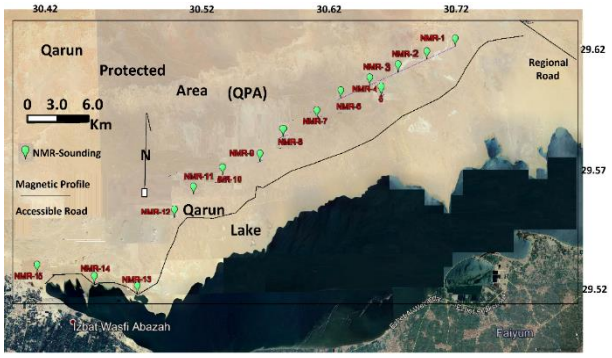

Figure 1:Location map showing NMR and AMT stations and magnetic profile (**Google Earth**).

Results

The magnetic profile was conducted every 25 m on the selected area and crossing the MT and MRS stations using GEM magnetometer(**Overhauser-19, Canada**), in order to see the shallow structures. The daily variation of magnetic field is corrected using Misallat Magnetic observatory that is located at Kom Oshem village beside the Qarun Lake (about 25 km).

The result of NUMIS magnetic resonance of stations 8, 9, 10 and 11 are showing in **Figure (2).**

Also, the 1D-MT inversion of high frequency magnetotelluric are shown **Figure (3)**.

.

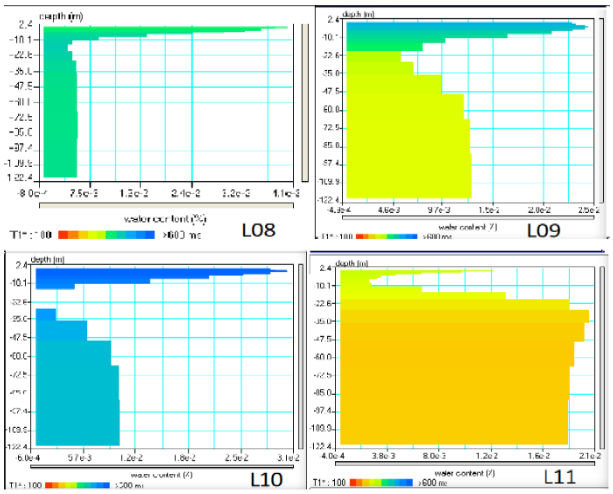

Figure 2: showing the results of Magnetic resonance (MRS)

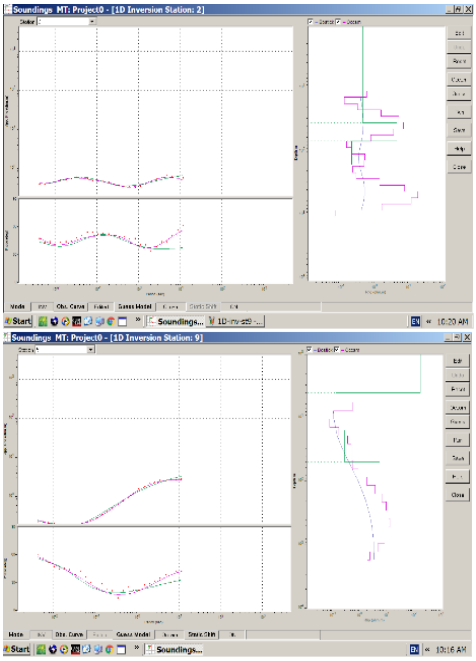

Figure (3): The results of 1D inversion of AMT.

Conclusion

The magnetic resonance method (MRS) able to investigate the ground water aquifer with easy way and measurements.-Also, evaluate the depth to water table, porosity (water contents) and permeability of the layers

- Correlated with the MT results which are good agrement.

*Aquifer water-model interpretation is required to integrate with the geological and remote sensing data.

Inferring the roots of volcano-geothermal systems in the Rotorua and Okataina calderas with Magnetotelluric models

E.A. Bertrand[1], P. Kannberg[2], T.G. Caldwell[1], W. Heise[1], S. Constable[2], B. Scott[3], S. Bannister[1], G. Kilgour[3], S.L. Bennie[1], R. Hart[1] and N. Palmer[1]
[1]GNS Science, 1 Fairway Drive, Avalon, Lower Hutt, 5010, t.bertrand@gns.cri.nz
[2]Scripps Institution of Oceanography, 8800 Biological Grade, La Jolla, California, USA
[3]GNS Science, 114 Karetoto Road RD4, Taupo, 3384

SUMMARY

A combination of 365 land and 34 lake-bottom magnetotelluric (MT) measurements at ~2 km spacing are used to investigate the structure of magmatic systems that drive high-temperature geothermal fields and volcanism in the northern part of the Taupo Volcanic Zone (TVZ), New Zealand. These data encompass the Rotorua Caldera and Okataina Volcanic Centre, covering an area of 2,800 km^2, and were inverted to create an image of the 3-D electrical resistivity structure of the crust to a depth of 20 km. Below shallow layers of quaternary volcanic deposits, the model is everywhere resistive, with the exception of a singular conductive zone (~500 km^2) below ~8 km depth that we interpret to be relatively mafic magma, consistent with petrologic and other geophysical data. Discrete fingers of low-resistivity (conductive) material rise from the margins of this inferred magmatic zone and connect directly with the locations of high-temperature geothermal fields at the surface.

Notably, one of the conductive fingers rises beneath the Haroharo Dome complex within the Okataina Volcanic Centre where 39 km^3 of silicic magma has been extruded in the last 9,000 years. These recent domes, which are electrically resistive, appear to cap and arrest the conductive finger (high-temperature fluids) at ~2 km depth, with surface geothermal activity displaced to the northeast, and along lake shorelines at the margin of the dome complex.

Keywords: Lake-Bottom Magnetotellurics, Taupo Volcanic Zone, Magma, Caldera, Geothermal

The formation of geothermal systems in the context of magma-assisted continental rifting: Magnetotelluric models from the Main Ethiopian Rift (MER)

L. Dambly[1a], F. Samrock[1], A.V. Grayver[2], H. Eysteinsson[3], M.O. Saar[1]

[1]ETH Zurich, Institute of Geophysics, Geothermal Energy and Geofluids Group, [a]luise.dambly@erdw.ethz.ch
[2]ETH Zurich, Institute of Geophysics, Earth and Planetary Magnetism Group
[3]Reykjavik Geothermal, Ltd., Reykjavik, Iceland

SUMMARY

The rise of geothermal development in Ethiopia has been strongly supported by magnetotelluric (MT) measurements. For placement of geothermal wells, the majority of MT studies focused on imaging the clay cap structure of volcano-hosted high-temperature geothermal systems. Most recent studies have succeeded to image the deeper magmatic feeding systems including the shallow magma reservoirs that drive geothermal systems in the MER, by applying modern 3-D inversion codes and by inverting MT phase tensors that are free of galvanic distortions.

To gain further insight into the geological setting of geothermal systems in the MER we constructed two new models obtained from 3-D inversion of MT data at Aluto and Corbetti volcanoes. Both geothermal systems play an important role in the Ethiopian energy development strategy. Although they have been thoroughly studied, open questions remain concerning their formation in the geological context of magma-assisted rifting. At Aluto the transcrustal distribution of magma was imaged by a local-scale MT survey, while at Corbetti evidence for the presence of a shallow intrusion was found, yet the intrusion was not yet imaged in 3-D.

To obtain a multi-scale model of the regional transcrustal distribution of melt beneath Aluto volcano we analyze two combined local- and regional-scale MT datasets. The datasets comprise regionally distributed stations across the rift valley (33 stations, 2000 km^2) and locally distributed stations measured at Aluto's volcanic edifice (165 stations, 145 km^2). In order to analyze the MT data we applied a modern 3-D inversion approach, based on a combination of impedance and phase tensor inversion. Doing so, we succeeded to obtain a 3-D multiscale subsurface model that images the lower crustal magma ponding zone in about 30 km depth beneath the rift. Furthermore, the model shows that this zone is connected to the shallow upper crustal magmatic heat source of Aluto's geothermal system via a structurally controlled transcrustal magma channel.

To shed light on the current state of the magma reservoir beneath Corbetti, we performed a 3-D phase tensor inversion utilizing a local dataset (127 stations, 340 km^2) covering the Corbetti caldera. In doing so, we could image for the first time a shallow intrusion, approximately 10 km deep, that acts as a heat source for the geothermal system of Corbetti. The location of this intrusion is in overall great agreement with previous predictions by InSAR surface deformation observations and geodetic and gravimetric modelling studies.

Our studies demonstrate the capability of MT to provide holistic images of volcano-hosted high-temperature geothermal systems from small scales relevant for geothermal drilling to large scales showing their formation in the context of an actively evolving rift.

Keywords: volcano imaging, geothermal exploration, 3-D multiscale inversion, Main Ethiopian Rift

Electromagnetic Study on The tenth of Ramadan City, Eastern Desert, Egypt

M. Mekkawi[1], A. Ibrahim[1] , A. Awad, A. Khalil and M. Ibrahim[1]
[1]National Research Institute of Astronomy and Geophysics (NRIAG)
11421 Helwan, Cairo-Egypt.

SUMMARY

SUMMARY

The main object of our study is evaluate the layers that contain fresh water at the tenth Ramadan City, Eastern Desert. Audio Magnetotelluric (AMT) were carried out on profile using G- EM3D instrument of Geometrics, USA.

The results of AMT show three layers that contain watre during Quaternary (shallow aquifer), Eocene (intermediate Aquifer) and Olgocene ((deep Aquifer). The results of 1D and 2D AMT are comparing with hydrogeological model near the stufy area.

Keywords: Audio Magnetotelluric (**AMT**), 1D and 2D AMT, tenth Ramadan City . Eastern Desert.

INTRODUCTION

The study area is located at an altitude of about 180 to 200 meters above sea level and is characterized by its flat where the factors of weathering in particular air play important role over thousands of years other than the water weathering, rain ages and wind weathering in the dry ages. However, some medium-height hills have been observed on the eastern border of the site as well as low-lying areas west and south of the site and are factors of topographical change due to human activity. The geological map and the location of the study area is showing in the (**Figure 1**).

Method

We apply the AMT magnetotellric profile using G-EM3D instrument of Geometrics, USA. The location map showing the elevation and AMT stations on the study area is showing in (**Figure 2**). The station separation is approximately 100 m. Every station has duration about 2 hours of the frequencies 10K, 4k, 1k until 0.1 Hz. The results are processed to remove cultural noise using appropriate filter to enhance the AMT data see (**Figure 3**). The AMT data seem good and have some large error bars especially at low frequency.

Results

The 1DMT results using (Bostick & Occam) codes and best fitting of Resistivities and phases are shown **Figure (3)**. It shows the three layers of low resistivity wet surface layers, shallow aquifer and deep aquifer, belonging to Quaternary, Eocene and Oligocene ages.

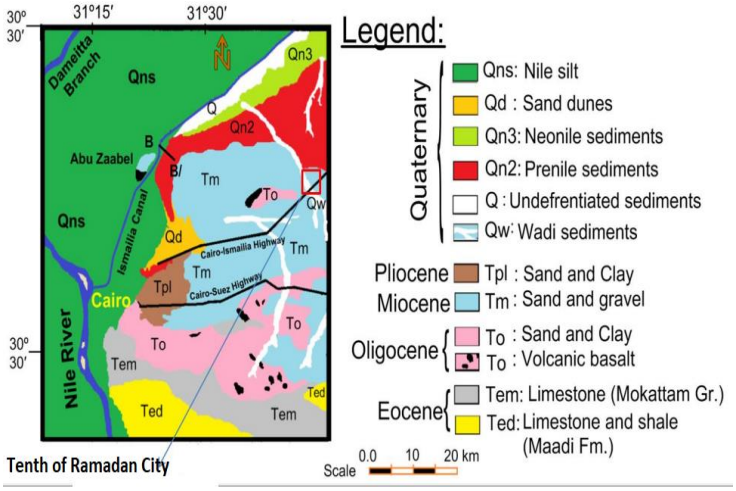

Figure 1: Geology map of the study area

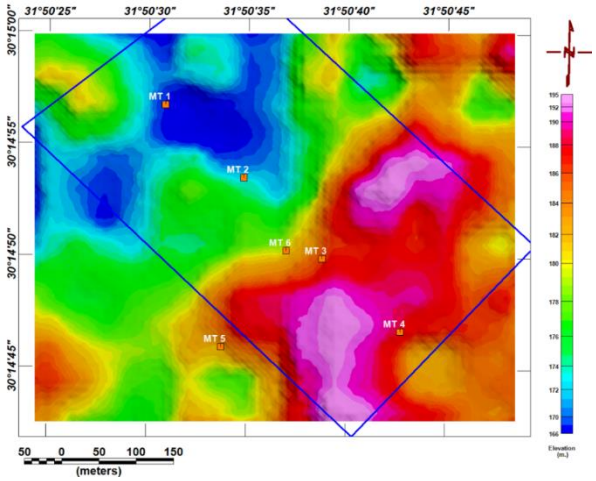

Figure 2. Location map showing the elevation and AMT stations on the study area.

.

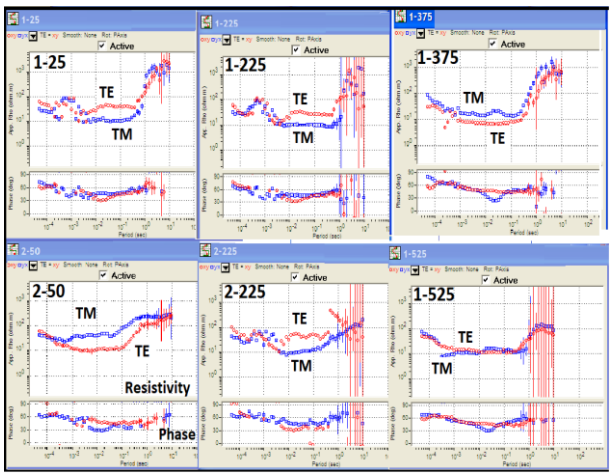

Figure 2: showing the results of G-EM3D

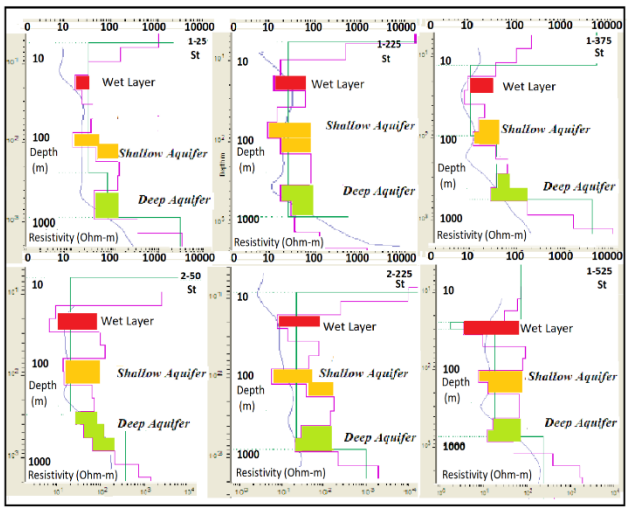

Figure (3): The results of 1D inversion of AMT.

Summary and Conclusion

In order to choose best place to drill well in the study area, 2DMT smoothing method (Rebocc code) is applied to see the horizontal and vertical change of resistivity in the study area (**Figure 4**). The result is correlated with the hydrological result near the study area which are good agreement with AMT result.. Aquifer water-model interpretation is required to compare with drilling data..

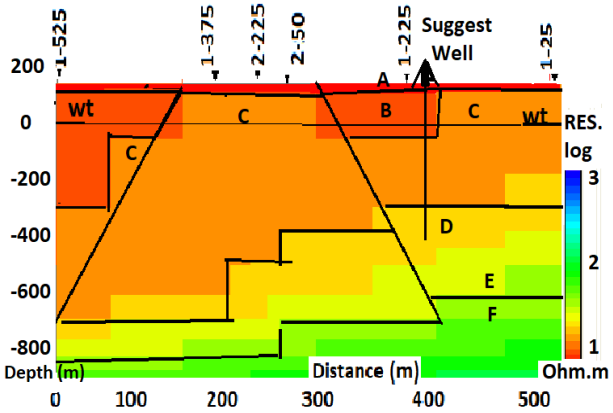

Figure 4. 2DMT results and suitable place for drill well.

Plate coupling at the northern Hikurangi margin: new results from magnetotellurics

W. Heise[1], G. Caldwell[1], T. Bertrand[1], Y. Ogawa[2], S. Bannister[1], G. Archibald[1], S. Bennie[1], R. Hart[1], N. Palmer[1], K. Seki[2], M. Fukai[2], K. H. Tseng [2], T. Nishizawa[2], J. McGrath[3]

[1] GNS Science, Lower Hutt, New Zealand, w.heise@gns.cri.nz

[2] Volcanic Fluid Research Center, Tokyo Institute of Technology, Tokyo, Japan

[3] School of Earth and Environment, University of Leeds, UK

SUMMARY

At the Hikurangi subduction margin along the east coast of New Zealand's North Island, plate coupling changes from weakly coupled in the northern part of the margin to locked in the south. Shallow slow slip events occur quasi-regularly in the northern weakly coupled part of the margin. While the conditions that lead to slow slip and changes in plate coupling are not fully understood, the presence of fluids within the subduction-interface-shear-zone is believed to play an important role. This is supported by the correlation between the resistivity at the depth of the plate interface inferred from MT data and the areal strain rate derived from GPS measurements. 52 new MT measurements have been done in the northernmost part of the Raukumara Peninsula in an area without previous MT data coverage. 3-D inverse modelling of impedance tensor data and geomagnetic transfer functions has been carried out at 322 at the northern half of the margin. The results data show that the dipping conductor above the subduction interface imaged previously to the south is present beneath the entire Raukumara Peninsula and correlates with the area of extensional strain rate consistent with weak plate coupling. Relocated seismicity within 3km of the interface shows a paucity of seismicity in the conductive areas of the plate interface. This confirms that fluid and/or clay-rich sediments are consistent with an area with a decreased density of asperities and stored strain.

Keywords: subduction, magnetotellurics, plate coupling

Investigation of Lithosphere Structure of Northwestern Anatolia with long-period magnetotelluric: Part 1. acquisition data by using remotely controlled system and comparison to previously collected broadband magnetotelluric data

İsmail Demirci[1], N. Yıldırım Gündoğdu[1], M. Doğukan Oskay[1] and M. Emin Candansayar[1]
[1]Ankara University, Faculty of Engineering, Geophysical Engineering Department, Geophysical Modelling Group, Ankara, TURKEY. E-mail: idemirci@eng.ankara.edu.tr

SUMMARY

In our previous study, we collected magnetotelluric (MT) data in broadband period ranges (T=0.0031s to 2000s) on 2006-2011 to reveal the crustal structure of North-Western Anatolia. Due to the low resistivity structure of the study area, the relationship between the crustal structure and the lithosphere could not be clearly defined in our previous project. Therefore, long period (T=0.00001s to 10000s) MT measurements are planned in order to reveal the relationship of deep earthquakes in the area with the lithospheric mantle and to complete the deficiencies in 3-D interpretation due to profile intervals. For this purpose, Long Period MT measurements were collected with a station spacing of approximately 15 km along four South-North profile. The data collected by new generation MT measurement system developed by Phoenix (MTU-5C) that enable us to remotely control the data during measurements. This part of the study describes and discusses the effectiveness of remotely controlled measurement system by using MT data collected in North-Western Anatolia. During the MT data collection phase, real-time data transfer was made with the help of a modem using a cellular network, which has recently been used in our country and in the world. Due to the very low signal amplitudes of long-term MT measurements, it is difficult to collect, especially in noisy area where settlements are located at frequent intervals. Thanks to remotely controlled measurement innovation, data quality is controlled during data collection. If the data quality is not good because of the unpredictable noise sources, the station location can be changed or precautions can be taken. In this study, real-time analysis of data and initial data processing results of measured data during long-period MT data collection will be presented. We also compare the broadband data collected from the same stations between the years 2008 to 2011.

Keywords: Long Period, Magnetotelluric, Remotely controlled, Lithosphere, North-Western Anatolia

INTRODUCTION

Magnetotelluric method is one of the most preferred geophysical electromagnetic methods in examining the deep resistivity structure of the earth (between 0.1 km and 40 km depth). There are many studies conducted in the last 15 years in the investigation of the upper crust-lower crust boundary and the tectonic structures, suture belts and fault zones in the crust using the magnetotelluric method (eg Becken et al. 2011; Zeng et al. 2015). Similarly, tectonic studies have been carried out in our country to examine the features of the North Anatolian Fault Zone, which is in the crust (first 20-30 km), especially in Western Anatolia (Tank et al. 2005; Ulugergerli et al. 2007; Kaya et al. 2009, 2013; Tank, 2012). Again, the studies on the upper-lower crust relationship, the suture belts and the fault zones in North-West Anatolia were carried out within the scope of our previous TÜBİTAK projects (Candansayar et al. 2008, 2010, 2012; Kaya 2010).

In recent years, many international projects have been carried out to investigate the relationship between the lithosphere and the crust. Studies carried out in the Tibet-Himalayan belt within the scope of the INDEPTH project have investigated continent-continent collision and crustal melting in the lithosphere (Unsworth 2010; Xie 2016). Similarly, the study on lithosphere research in northern Europe was carried out within the scope of the BEAR (Baltic Electromagnetic Array Research) project (Korja 2007).

In our country, there is only one study conducted in the Arab-European collision zone to investigate the lithosphere (Türkoğlu et al. 2015). In Western Anatolia, there is no study on the examination of the lithosphere. Within the scope of this study, long period Magnetotelluric measurements were taken for the first time in order to examine the lithosphere structure up to the first 100 km depth of the area surrounded by the provinces of Zonguldak, Kocaeli, Uşak and Konya in Northwest Anatolia. During the measurement, the data was transferred to a server computer via the cellular network in real time. In this context, in long-term MT data collection, a work flow chart for remote data management and real-time data analysis of these data and measured data in the workspace will be presented.

METHOD

In the MT method, two components of the electric field (Ex and Ey) and three components of the magnetic field (Hx, Hy, Hz) are measured as a function of time. By taking the Fourier transforms of these measured E and H fields, the impedance tensor and tipper tensor are estimated in the frequency domain. In classical magnetotelluric measurement systems, the measured electric and magnetic field components are recorded on an SD card (internal memory) located in the receiver unit (Figure 1a). In this study, during the MT data collection, the MT measurement system is connected to a modem with a cellular network (GSM operator) and the measurements are transferred to the computer used as server in the office via the cellular network with a 10 minute packages. Data quality is controlled by performing basic data processing of these transferred data in real time. Thus, during data collection phase, the data quality can be examined continuously, the negative effects on each component of the electric or magnetic field measurements can be intervened, shutdown of the instrument due to overheating can be overseen and instant information can be obtained.

In Long-Period magnetotelluric measurements, the measurement time at a station in the field takes 10-20 days to reach the desired period (T>10000 sec). For this reason, a box arrangement has been designed to ensure the safety of the Long-period MT measurement system in the field and to be affected by adverse weather conditions as little as possible. The assembly in question includes the Phoenix MTU-5C MT receiver system, the power supply (battery) and a modem for continuous transmission of measurements via the cellular network connection (Figure 2).

MAGNETOTELLURIC DATA ACQUISITION PHASE

Long-period magnetotelluric measurements were collected along four parallel directions from which broadband MT measurements were taken within the scope of our previous TÜBİTAK project number 105G145. Thanks to the simultaneous monitoring of the data, the measurement times at each Long Period MT station varied between 10-20 days to reach the targeted data quality. Based on the analysis of the broadband MT data measured in the previous project, station positions with low cultural noise were selected for the long-period MT data acquisition phase. Thus, measurements that have to be repeated and data losses were minimized. During the 15 years after the project, the changes in the residential area and energy transmission lines were taken into consideration and the site selections were made interactively in the light of all this information. A comparison of previously measured broadband MT and long-period MT measured in 2020 is presented in Figure 3. In this comparison, it is seen that the apparent resistivity and phases obtained from the non-diagonal elements of the impedance are almost same in the same period intervals. However, the apparent resistivity and phase obtained from the diagonal elements of the impedance are not very similar due to the fact that these components amplitude are very small amplitude and affected by noise and some unforeseen deficiencies in the data processing algorithm used before. Similarly, when comparing Tipper amplitudes and phases, it is seen that broadband data is scattered and long-period data has a less scattered character. The most important reason for this effect is that the coil used in the measurement of the vertical magnetic field cannot be fully buried due to the fact that it was too long in the previous equipment and so project.

CONCLUSIONS

In this study, for the first time, MT data covering broad and long period bands (0.0001 sec < T < 20.000 sec) were collected by real-time data transfer and data control. The main advantage of this type of measurement is that the time series data transferred to the host computer in packages within 10 minutes from the station installation can be analyzed. Thus, installation errors can be seen in the station setup and the error can be corrected. On the other hand, while collecting data, especially if the electric field is measured, rodents break the cables or for any reason, the problem in the cable connections can be observed and this problem can be resolved. The waiting time for long-period MT data acquisitionf15 takes an average of 10-20 days. In classical measurement systems, interruptions in cables, battery depletion, etc. situations occur frequently from the first day to the end. These sources of problems could have been noticed when going to the study area after 20 days. However, with this new system, it can be intervened as soon as a problem occurs.

On the other hand, the other experience gained in this study is that the changes in the signal amplitude according to the solar storms can affect the measurements and cause an increase or decrease in the noise content among the MT data measured at the same station after about 15 years. In this study, it was concluded that the data measured at the same station with an interval of 15 years were generally in harmony in accordance with the resistivity structure of the environment. Again, in this study, it was observed that the low amplitude components of the impedance (Zxx and Zyy) were greatly affected by the noise, and therefore these components were not in good agreement when the data measured at 15-year intervals were compared.

The same problem was observed in tipper amplitude and phase components. Therefore, in 3D inversion, care should be taken to include the main diagonal components of the impedance and the tipper components in the inversion according to the noise content.

ACKNOWLEDGEMENTS

This study was supported by the Scientific and Technological Research Council of Turkey (TÜBİTAK) under the project Grant No:119Y197. We thank TÜBİTAK for their valuable support.

REFERENCES

Becken M, Ritter O, Bedrosian PA, Weckmann U (2011) Correlation between deep fluids, tremor and creep along the central San Andreas fault. *Nature*, *480*(7375), 87-90.

Candansayar ME, Kaya C, Gürer A, et al. (2008) NW_Anatolia_CSGM Project: an investigation of N-W Anatolian Crust Structure by using Geophysical Methods. IAGA WG 1.2 on Electromagnetic Induction in the Earth, Beijing, China, October 23- October 29, 2008

Candansayar ME, Kaya C, Dikmen Ü, et al. (2010) Crustal structure of Northwestern Turkey, revealed by magnetotelluric surveys with the help of Seismology, Gravity and Magnetic Data. IAGA WG 1.2 on Electromagnetic Induction in the Earth 20th Workshop Abstract, Giza, Egypt , September 18-24, 2010

Candansayar ME, Kaya C, Dikmen Ü, et al. (2012) Deep Crustal Structure of Thrace Region Revealed by 2D Inversion of Magnetotelluric Data. Extended Abstract, 21st EM Induction Workshop, Darwin, Australia, July 25-31, 2012

Chen L, Booker JR, Jones AG, Wu N (1996) Electrically conductive crust in Southern Tibet form INDEPTH magnetotelluric surveying. *Science*, *274*(5293), 1694.

Kaya C (2010) Deep crustal structure of northwestern part of Turkey. Tectonophysics, 489(1), 227-239.

Kaya T, Kasaya T, Tank SB, Ogawa Y, Tunçer MK, Oshiman N, Matsushima M (2013) Electrical characterization of the North Anatolian Fault Zone underneath the Marmara Sea, Turkey by ocean bottom magnetotellurics. geophysical journal international, ggt025.

Kaya T, Tank SB, Tunçer MK, Rokoityansky II, Tolak E, Savchenko T (2009) Asperity along the North Anatolian Fault imaged by magnetotellurics at Düzce, Turkey. *Earth, planets and space*, *61*(7), 871-884.

Korja T (2007) How is the European lithosphere imaged by magnetotellurics?. Surveys in Geophysics, 28(2-3), 239-272.

Tank SB, Honkura Y, Ogawa Y, Matsushima M, Oshiman N, Tunçer MK, Işıkara AM (2005) Magnetotelluric imaging of the fault rupture area of the 1999 Izmit (Turkey) earthquake. *Physics of the Earth and Planetary Interiors*, *150*(1), 213-225.

Tank SB (2012) Fault zone conductors in Northwest Turkey inferred from audio frequency magnetotellurics. *Earth, planets and space*, *64*(9), 729-742.

Türkoğlu E, Unsworth M, Bulut F, Çağlar İ (2015) Crustal structure of the North Anatolian and East Anatolian Fault Systems from magnetotelluric data. *Physics of the Earth and Planetary Interiors*, *241*, 1-14.

Ulugergerli EU, Seyitoğlu G, Başokur AT, Kaya C, Dikmen U, Candansayar ME (2007) The geoelectrical structure of northwestern Anatolia, Turkey. *Pure and Applied Geophysics*, *164*(5), 999-1026.

Unsworth M (2010) Magnetotelluric studies of active continent–continent collisions. *Surveys in Geophysics*, *31*(2), 137-161.

Xie C, Jin S, Wei W, Ye G, Jing J, Zhang L, Xia R (2016) Crustal electrical structures and deep processes of the eastern Lhasa terrane in the south Tibetan plateau as revealed by magnetotelluric data. *Tectonophysics*, *675*, 168-180.

Zeng S, Hu X, Li J, Xu S, Fang H, Cai J (2015) Detection of the deep crustal structure of the Qiangtang terrane using magnetotelluric imaging. *Tectonophysics*, *661*, 180-189.

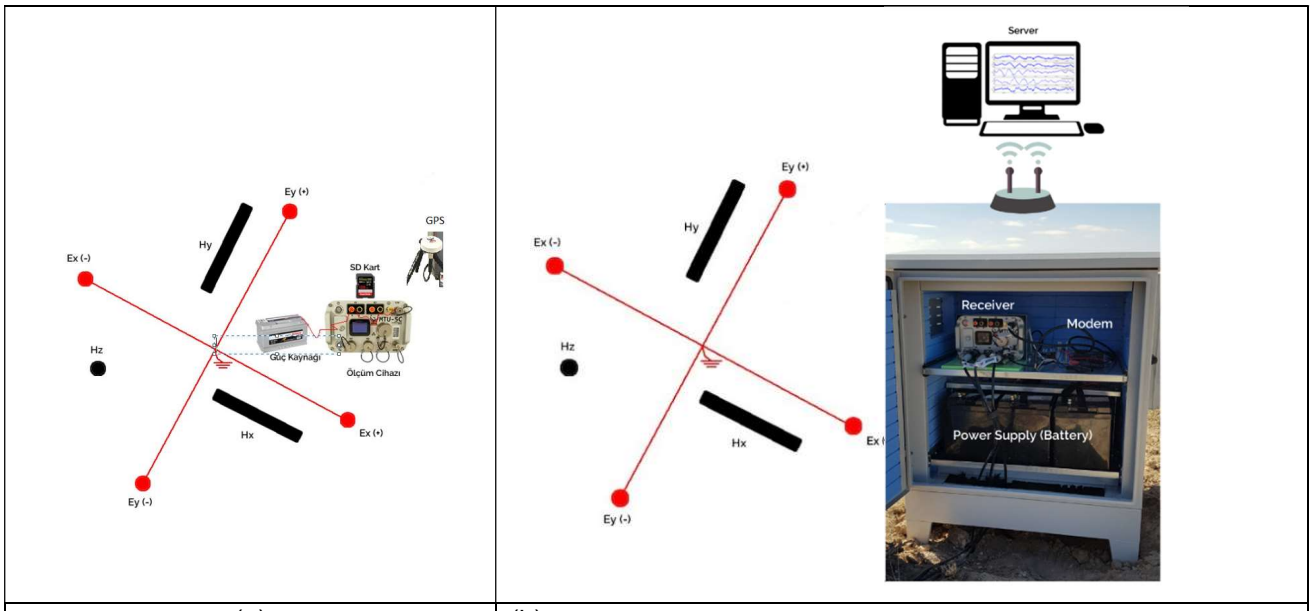

(a) (b)

Figure 1. a) Classical measurement system, (b) Remotely controlled measurement system

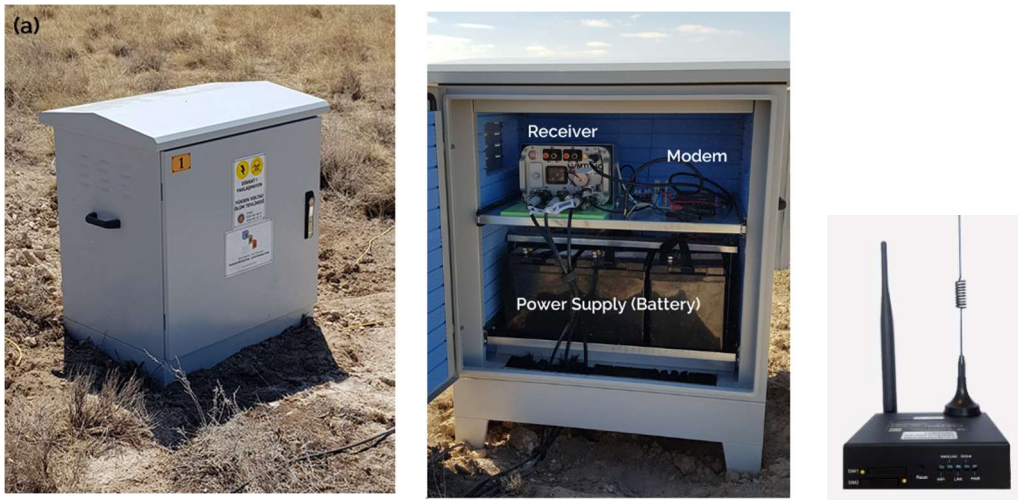

Figure 2. **a**) MT measurement system box designed in accordance with the field conditions, **b**) the layout of the system inside and **c**) the modem used.

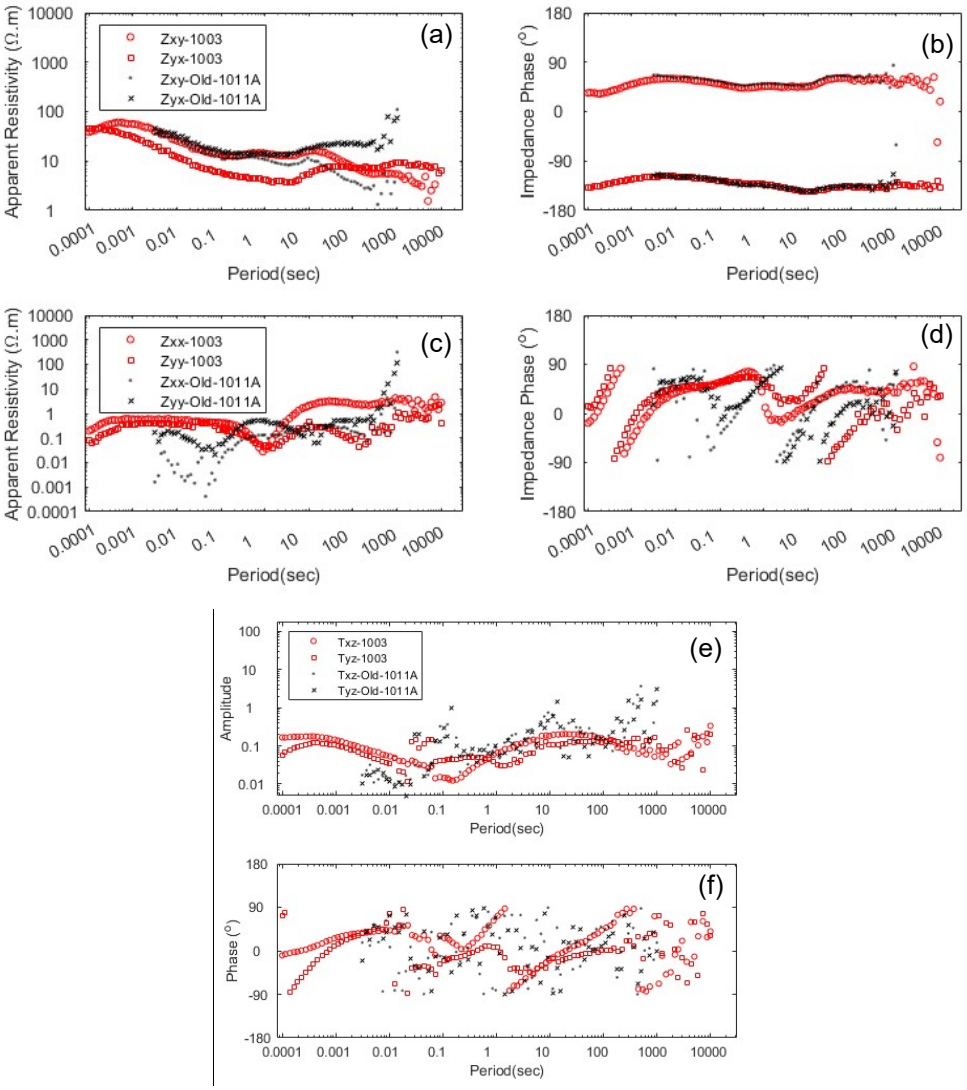

Figure 3. Presentation of Long Period MT (station 1003) measured in 2020 and broadband MT (old 1011A) measured in 2007 at the same point: (a) xy and yx component Apparent Resistivity curves, (b) xy and yx component Impedance Phase curves, (c) xx and yy component Apparent Resistivity curves, (d) xx and yy component Impedance Phase curves, (e) Txz and Tyz tipper amplitudes, (e) Txz and Tyz tipper phases. Red "circle and square" symbols indicate long period MT data, black "+ and x" symbols indicate broadband MT measurements.

3D lithospheric structure beneath the Marmara Sea by Magnetotellurics

T. Kaya-Eken[1,2,3], Y. Ogawa[2], Y. Usui[1,4], T. Kasaya[5], M. K. Tunçer[6], Y. Honkura[1,2], N. Oshiman[7], M. Matsushima[1], W. Siripunvaraporn[8].

[1] Earth and Planetary Sciences, Tokyo Institute of Technology, Tokyo, Japan
[2] Volcanic Fluid Research Center, Tokyo Institute of Technology, Tokyo, Japan
[3] Department of Geodesy, Boğaziçi University, Istanbul, Turkey, tulay.kaya@boun.edu.tr
[4] Earthquake Research Institute, The University of Tokyo, Tokyo, Japan
[5] Japan Agency for Marine–Earth Science and Technology, Yokosuka, Japan
[6] Department of Geophysics Engineering, Istanbul University-Cerrahpaşa, Istanbul, Turkey
[7] Disaster Prevention Research Institute, Kyoto University, Kyoto, Japan
[8] Department of Physics, Mahidol University, Bangkok, Thailand

SUMMARY

The North Anatolian Fault (NAF), a 1500 km long transform boundary between the Eurasian and Anatolian plates, is a seismically active zone in Turkey. During the 20th century, destructive earthquakes with magnitude Mw>7 took place on this fault zone increasing the seismic hazard in the Marmara Sea. Several studies have implied that segments in the Marmara Sea, not ruptured since 1766, are highly prone to generate a destructive earthquake (>Mw7.2) in the near future. Therefore, a proper understanding of lithospheric structure of the NAF Zone beneath the Marmara Sea is of utmost importance to the seismic hazard assessment studies. The energy released after an earthquake depends on the accumulated stress along fault zones and shear fracture strength that is controlled by the amount of pore fluid. The distribution of deep crustal fluids and connectivity of fluid-filled pores affect the electrical resistivity variation in the subsurface. Thus, electromagnetic methods, sensitive to the electrical resistivity, are powerful tools for imaging subsurface fluids in the deep crust. We present a study revealing the resistivity variation that reflects the rheological configuration of the lithosphere in relation to the fluid dynamics in the crust and mantle structure of the study region. We have collected magnetotelluric data at 25 sites in and around the Marmara Sea to elucidate 3D electrical resistivity distribution across the NAF zone and to determine the brittle-ductile zones. To achieve this we performed a 3D inverse modeling on magnetotelluric data using an unstructured tetrahedral mesh with the finite element method. The main findings from this study include resistive–conductive boundaries marking the trace of the NAF; prominent shallow (down to 5 km) and deep conductors located between Çınarcık and Central Basins and beneath them, respectively; a profound resistive structure below ~15 km consistent with the known seismic gap in this region.

Keywords: North Anatolian Fault Zone, Magnetotellurics, 3D modeling, Marmara Sea, Lithosphere.

3D imaging of the subsurface electrical resistivity structure in West Bohemia/Upper Palatinate covering mofettes and Quaternary volcanic structures by using Magnetotellurics

A. Platz[1], U. Weckmann[1,2], J. Pek[3], S. Kováčiková[3], R. Klanica[3], J. Mair[1], B. Aleid[1,2]
[1]Helmholtz-Zentrum Potsdam, Deutsches GeoForschungsZentrum, Potsdam, Germany, aplatz@gfz-potsdam.de
[2]University of Potsdam, Institute of Geoscienes, Potsdam, Germany
[3]Institute of Geophysics of the Czech Academy of Sciences, Prague, Czech Republic

SUMMARY

The region of West Bohemia and Upper Palatinate belongs to the West Bohemian Massif. The study area is situated at the junction of three different Variscan tectonic units and hosts the ENE-WSW trending Ohře Rift as well as many different fault systems. The entire region is characterized by ongoing magmatic processes in the intracontinental lithospheric mantle expressed by a series of phenomena, including e.g. the occurrence of repeated earthquake swarms and massive degassing of mantle derived CO_2 in form of mineral springs and mofettes. Ongoing active tectonics is mainly manifested by Cenozoic volcanism represented by different Quaternary volcanic structures. All these phenomena make the Ohře Rift a unique target area for European intra-continental geoscientific research. With magnetotelluric (MT) measurements we image the subsurface distribution of the electrical resistivity and map possible fluid pathways. 2D inversion results by Muñoz et al. (2018) reveal a conductive channel in the vicinity of the earthquake swarm region that extends from the lower crust to the surface forming a pathway for fluids into the region of the mofettes. A second conductive channel is present in the south of their model; however, their 2D inversions allow ambiguous interpretations of this feature. Therefore, we conducted a large 3D MT field experiment extending the study area towards the south. The 3D inversion result matches well with the known geology imaging different fluid/magma reservoirs at crust-mantle depth and mapping possible fluid pathways from the reservoirs to the surface feeding known mofettes and spas. A comparison of 3D and 2D inversion results suggests that the 2D inversion results are considerably characterized by 3D and off-profile structures.

Keywords: Magnetotellurics, Ohře Rift, Conductive channel, Fluid/magma reservoir, Earthquake swarm

Investigation of Deep Structure of Sultandağı Fault by Magnetotelluric, Gravity, GNSS, and Tectonic studies; First Results

Özcan ÖZYILDIRIM[1], İsmail DEMİRCİ[2], Çağlar ÖZKAYMAK[3,4], Özcan BEKTAŞ[5], Can BAŞARAN[1,3], Ibrahim TİRYAKİOĞLU[4,6], Doğukan Mert ÖZCAN[7] and Ahmet YILDIZ[1,3]

[1]Afyon Kocatepe University, Geothermal and Mineral Resources Application and Research Center, ozyildirim@aku.edu.tr

[2]Ankara University, Faculty of Engineering, Department of Geophysical Engineering

[3]Afyon Kocatepe University, Faculty of Engineering, Department of Geological Engineering

[4]Afyon Kocatepe University, Earthquake Application and Research Center

[5]Cumhuriyet University, Faculty of Engineering, Department of Geophysical Engineering

[6]Afyon Kocatepe University, Faculty of Engineering, Department of Map Engineering

[7]Afyon Kocatepe University, Graduate School of Natural and Applied Sciences

SUMMARY

Afyon-Akşehir Graben is one of the most seismically active neotectonic structures in Anatolia. There are previous scientific studies on the surface geometries, geomorphology, kinematics, and active tectonic features of the fault segments of the Sultandağı Fault, which is the most seismically active main edge fault of the graben. However, studies on the geometries and depths of these faults are very few at the crustal scale. The devastating earthquakes on the Sultandağı Fault in recent years show that segments of this fault are active, the seismogenic zone has reached 15 kilometers, and the geometry of these faults should be investigated in detail at the crustal scale by geophysical, geological, and geodetic methods. The first results of the main project, which includes developing a three-dimensional joint inversion algorithm for Magnetotelluric and Gravity data, are described in this study. In the study, the magnetotelluric data measured along the lines selected perpendicular to the main faults in the part covering the Sultandağı fault, which is the most important seismogenic belt of the region, were solved with the two-dimensional inversion algorithm and two-dimensional resistivity models were obtained. In addition, surface geology was used to analyze the active tectonic features of the fault segments on the Sultandağı Fault, and GNSS-based geodetic measurements were made to monitor the current tectonic activities of the segments. Preliminary findings have shown that the NW-SE trending and NE dipping Sultandağı Fault, which is a dip-slip normal fault, was formed between Sultandağı and Ilgın districts under NE-SW extensional forces. It also indicates that there are synthetic and antithetic fault branches extending approximately parallel to the Sultandağı Fault in the graben and that the fault has a depth of at least 10 km with an average angle of 70°.

Keywords: Magnetotelluric, Inversion, Gravity, Tectonics, Sultandağı Fault

INTRODUCTION

Sultandağı Fault is a 90 km long dip-slip normal fault. It can be traced along morphologically distinct steepnesses that show a linear course between Çay in the west and Doğanhisar in the east, well-developed alluvial fans are typical along the mountain front (Koçyiğit et al. 2000; Emre et al. 2011; Tiryakioğlu et al. 2015; Özkaymak et al. 2017). The northern margin faults located in the northeast of the graben are represented by NE-SW trending dip-slip normal faults from west to the east such as Bolvadin Fault, Büyük-Karabağ Fault, Çukurcak Fault, and Yunak Fault Zone (Emre et al. 2011; Özkaymak et al. 2017). On the seismically active Sultandağı Fault, during the instrumental period, many earthquakes occurred. While the right lateral GPS sliding speed determined on the Simav Fault is 3.9 mm/, the GPS-based opening speed value measured on the Sultandağı Fault is 3.4 mm/year (Aktuğ et al. 2013).

When tectonic studies supported by geophysical methods are classified, strike-slip faults that produce more earthquakes in the world are generally examined (Stanley et al. 1990; Ogawa et al. 2001; Tank et al. 2005; Türkoğlu et al. 2008; Kaya et al. 2013). Normal faults, which are generally located in the west of Turkey and cause Horst graben structures, are mostly studied from a geothermal point of view (Erdoğan and Candansayar 2017). It is observed that Normal faults are less frequently investigated in terms of tectonic and seismicity than strike-slip faults such as the North Anatolian and East Anatolian Fault Systems with the studies conducted with electromagnetic methods such as magnetotelluric. However, the earthquakes that have occurred in recent years show that the deep structures of normal faults in the Western Anatolia region should be investigated in detail with geophysical methods.

This study was carried out to fill this gap in the literature.

In the study, 2D resistivity models were obtained by inverting the MT data obtained on the Sultandağı Fault with the 2D MT algorithm using the unstructured mesh developed by Özyıldırım et al. (2017). The models were interpreted comparatively with the tectonic studies and gravity data in the field. In addition, within the scope of this study, the current slip rates, strain amounts, and directions of the fault segments in the region are measured using the GNSS technique; The geodynamic structure of the region is evaluated by comparing the findings obtained from the Geological and Geophysical studies carried out within the scope of the project.

METHODS

Along the Sultandağı Fault, it was planned to measure Magnetotelluric (MT) data as well as tectonic and GNSS studies in the determined area to view the deep structure of the part that intersects with Afyon K25, K26, and L26 sheets of 1/100,000. The distance between the MT lines is 3-3.5 km and consists of 24 lines. In each line, 10 MT points were determined with a distance of approximately 2.5 km from each other (Figure 1).

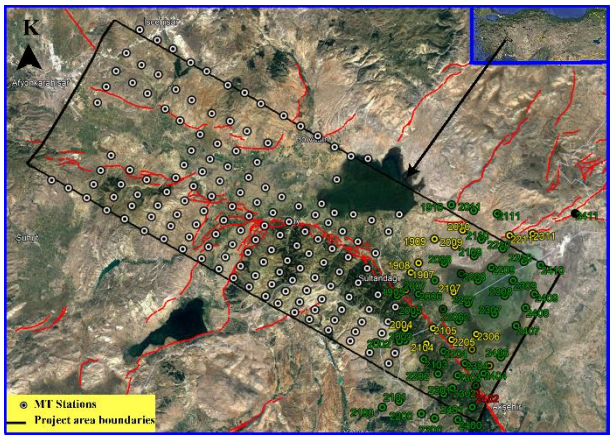

Figure 1. The location of the study area with locations of the MT stations on the Google Earth satellite image, the active faults (red lines) defined in the region (Emre et al. 2011).

In Figure 1, the MT stations that were measured at the study area and that will be measured in the future are shown together. The yellow and green stations show the measured data to be presented in this study on the Sultandağı fault, which is a segment of the AAG during the period.

MT data acquisition and analysis

In this study, MT data were measured on lines 19-24 from west to east(Figure 2).

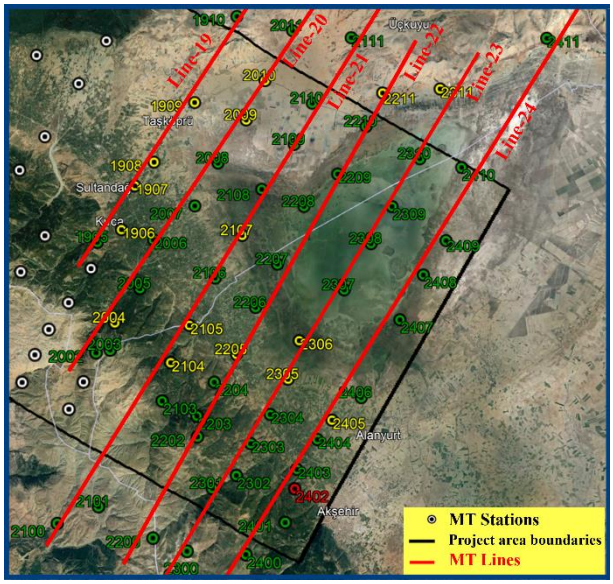

Figure 2. Locations of The MT stations measured data and designated MT lines for 2D inversion of these data

MT studies were carried out using “Metronix” brand “ADU07e” model receiver, “MFS06e and MFS07e” coils, and “Pb-$PbCl_2$” nonpolarized electrodes. The measurement period of the data collected as a time series at each station varies between 24-48 hours. Time series (raw) in four frequency bands (Sample frequencies: "128Hz-more than 24h", "512Hz-2h", "2048Hz-1h", "65536Hz-15min.") at each station were measured. Electric (E_x, E_y) and magnetic fields (H_x, H_y) were obtained in the frequency domain by taking the Fast Fourier transform (FFT) of the time series with the "ProcMT" software. Impedance values ($Z(\omega)$), including the ratios of Electric and Magnetic fields, were obtained for a total of 63 frequencies, 9 frequencies in each logarithmic period, in the range of 10kHz-10^{-3}Hz.

Files with the extension "edi" containing impedance values, apparent resistivity, and impedance phase values were recorded for each station and decomposition analysis was performed for global strike direction selection for 2D inversion. G&B decomposition was used as decomposition analysis (Groom and Bailey 1989). Analysis results are shown on the Rose diagram using three different frequency bands (10000-1Hz, 1-0.1Hz, 0.1-0.001Hz) and all frequencies (10000-0.001) on the same figure to see the dominant strike direction in different frequency bands. (Figure 3). In addition, the dominant strike direction was found by decomposing the data with the 'Strike' code of McNeice and Jones (2001) and the 'FNIDEC' algorithm developed in the master's thesis of the first author for the selected 3 frequency bands and all frequencies (Black arrows: Strike results, Red arrows: FNIDEC results in Figure 3). At the end of the analysis, the Strike was chosen as 5° for 2D

inversion. By rotating the Impedance Tensor to 5° Strike, the Zxy component of the diagonal elements was accepted as the TE-mode and the Zyx component as the TM-mode impedance.

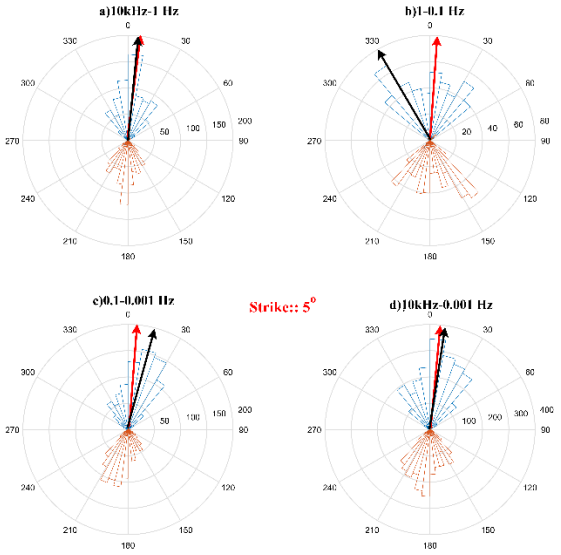

Figure 4. Presentation of G&B decomposition results in the rose diagram, with global strike angle values found from Strike (Black arrows) and FNIDEC (Red Arrows) codes

Gravity data

Measuring, correcting, mapping, filtering, modeling, and inversion Gravity data are the processing steps of the gravity method. This method is effective, especially in determining the density differences like as mines, sedimentary basins, fault zones, and buried geological structures. Due to the ill-definition of the Gravity method, modeling is performed rather than inversion in the literature, and deep and superficial tectonic edges are determined by filtering studies. Within the scope of this study, gravity data formed a basis for MT studies. Gravity data given in Figure 5, were obtained from the General Directorate of Mineral Research and Exploration of Turkey (MTA).

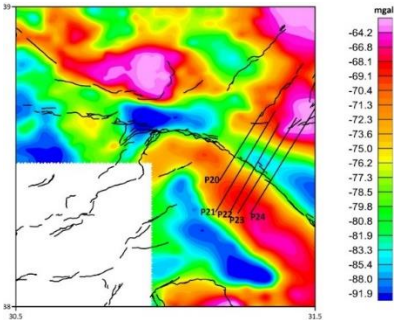

Figure 5. The gravity anomaly map of the study area and the locations of Lines determined for 2D gravity modeling.

Tectonic and GNSS studies

Tectonic studies were generally carried out in the form of field studies. In the study, data on the surface geometries, segmentation features, kinematic analyzes, and top/bottom block geology of the Sultandağı fault were collected. In this way, kinematic analysis studies were carried out in order to determine the kinematic properties of the region and the stress regime history. It was planned to make a GNSS measurement to determine the current tectonic movements of the faults in the region. GNSS measurement is one of the common geodetic measurement methods used to determine fault movements today. Source-fault parameters were tried to be obtained from the velocity fields to be obtained within the scope of the study.

RESULTS

The rotated MT data to the Global Strike were inverted by the inversion algorithm that use the unstructured mesh developed by Özyıldırım et al. (2017), and the resistivity models were obtained along the determined 6 lines. The resistivity model obtained from the data measured along Line-24 is presented in Figure 5c. Measured gravity data on the MT Line-24 were modeled two-dimensionally with the "Wingling" software. The gravity model on Line-24 is presented in Figure 5b. In Figure 5a, the MT station locations measured on Line 24 and the locations of active faults determined by tectonic studies in the region are shown. Detailed tectonic studies carried out within the scope of the study were interpreted with 2D density and resistivity models and the faults were drawn on the models (Figure 5b-5c). In GNSS studies, unlike other studies, the amount of slip on the main faults was calculated by using the fault depths and slopes obtained from the MT studies as inputs.

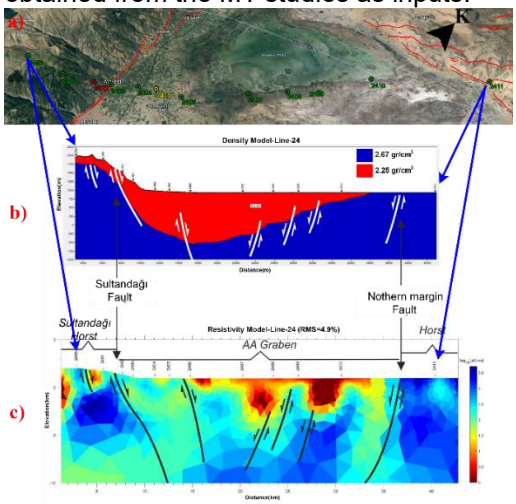

Figure 6. a. Line 24' de bulunan MT istasyonlarının konumları (red lines are active faults), **b.** 2D density model and **c.** 2D resistivity model on Line-24.

Conclusions

In the geological field studies carried out within the scope of the study, surface data such as the geometry, kinematic analysis, and active tectonic features of the Sultandağı fault were collected. Preliminary findings obtained from the studies carried out between Sultandağı and Ilgın districts indicate that segments of the Sultandağı Fault operate in dip-slip normal fault character, are shaped under NE-SW directional extensional forces, and are typical with linear trending mountain front, especially between Sultandağı and Akşehir. The dip angles measured from the NW-SE trending and northeastward dipping fault planes vary between 65° and 75°.In addition, MT data collected within the scope of geophysical studies were evaluated with the 2D inversion algorithm developed by Özyıldırım et al. (2017), and resistivity models were obtained. Preliminary evaluations were made for the gravity data measured along the relevant Lines, and density sections were obtained for fault zones and buried geological units and structures. Obtained resistivity and density models were interpreted in the light of tectonic studies. The preliminary findings indicate the existence of synthetic and antithetic fault branches extending approximately parallel to the main fault buried within the ceiling block of the Sultandağı Fault and the fault has a depth of at least 10 km with an average angle of 70°.

Acknowledgments

This study is supported by the Scientific and Technical Research Council of Turkey, TÜBİTAK, under grant no: 121Y01. We thank TÜBİTAK for its support.

References

Aktuğ B, Parmaksız E, Kurt M, Lenk O, Kılıçoğlu A, Gürdal MA and Özdemir S (2013) Deformation of central anatolia: GPS implications. Journal of Geodynamics **67**: 78-96

Emre Ö, Duman TY, Özalp S, Olgun Ş and Elmacı H (2011) 1:250.000 scale active fault map series of Turkey, Afyon (NJ 36-5) Quadrangle. Serial number: 16. General Directorate of Mineral Research and Exploration, Ankara, Turkey.

Erdoğan E and Candansayar ME (2017) The conductivity structure of the Gediz Graben geothermal area extracted from 2D and 3D magnetotelluric inversion: Synthetic and field data applications. Geothermics **65**: 170-179

Groom RW and Bailey RC (1989) Decomposition of magnetotelluric impedance tensors in the presence of local three-dimensional galvanic distortion. Journal of Geophysical Research-Solid Earth 94(B2): 1913-1925.

Kaya T, Kasaya T, Tank SB, Ogawa Y, Tunçer MK, Oshiman N and Matsushima M (2013) Electrical characterization of the North Anatolian Fault Zone underneath the Marmara Sea, Turkey by ocean bottom magnetotellurics. Geophysical Journal International **193**(2): 664-677.

Koçyiğit A, Ünay E and Saraç G (2000) Episodic graben formation and extensional neotectonic regime in west Central Anatolia and the Isparta Angle: a case study in the Akşehir-Afyon Graben, Turkey. Geological Society of London Special Publication 173: 405-421.

McNeice, GW and Jones AG (2001) Multisite, multifrequency tensor decomposition of magnetotelluric data. Geophysics, 66(1): 158-173

Ogawa Y, Mishina M, Goto T, Satoh H, Oshiman N, Kasaya T and Matsushima M (2001) Magnetotelluric imaging of fluids in intraplate earthquake zones, NE Japan back arc. Geophysical research letters **28**(19): 3741-3744

Özyıldırım Ö, Candansayar ME, Demirci İ and Tezkan B (2017) Two-dimensional inversion of magnetotelluric/radiomagnetotelluric data by using unstructured mesh. Geophysics **82**(4): E197-E210

Özkaymak Ç, Sözbilir H, Tiryakioğlu İ and Baybura T (2017) Bolvadin'de (Afyon-Akşehir Grabeni, Afyon) Gözlenen Yüzey Deformasyonlarının Jeolojik, Jeomorfolojik ve Jeodezik Analizi. Türkiye Jeoloji Bülteni **60**(2): 169-189

Stanley WD, Labson VF, Nokleberg WJ, Csejtey JB and Fisher MA (1990) The Denali fault system and Alaska Range of Alaska: Evidence for underplated Mesozoic flysch from magnetotelluric surveys. Geological Society of America Bulletin **102**(2): 160-173

Tank SB, Honkura Y, Ogawa Y, Matsushima M, Oshiman N, Tunçer MK and Işıkara AM (2005) Magnetotelluric imaging of the fault rupture area of the 1999 Izmit (Turkey) earthquake. Physics of the Earth and Planetary Interiors: **150**(1-3): 213-225

Tiryakioğlu İ, Baybura T, Özkaymak Ç, Sözbilir H, Sandıkçıoğlu A, Erdoğan S, Yılmaz İ, Uysal M, Yılmaz M, Yıldız A, Dereli MA, Yalçın M, Dumlupınar İM, Yalım H and Ertuğrul O (2015) Sultandağı Fayı Batı Kısmı Fay Aktivitelerinin Multidisipliner Çalışmalarla Belirlenmesi. Harita Teknolojileri Elektronik Dergisi 7(1): 7-16

Türkoğlu E, Unsworth M, Çağlar İ, Tuncer V and Avşar Ü (2008) Lithospheric structure of the Arabia-Eurasia collision zone in eastern Anatolia: Magnetotelluric evidence for widespread weakening by fluids?. Geology 36(8): 619-62

Integrated geophysical modeling of 2D/3D data in the Western Carpathians

J. Vozár[1], V. Bezák[1], M. Bielik[1], L. Ondrášová[1]
[1] Earth Science Institute of the Slovak Academy of Sciences, Bratislava, Slovakia, geofjavo@savba.sk

SUMMARY

We present crustal and lithosphere studies within Slovakia with magnetotelluric (MT) method, which were combined with other geophysical data.
The first part of research was focused on interpretation of MT measurements along the 2T seismic profile, which from north to south crosses all the basic tectonic units of the Outer and Inner Western Carpathians. The 3D MT model from data distributed along the 2T profile gives a qualitatively new information about physical properties of the crust along the profile and in its immediate vicinity. The new phenomena are highlighted in the 3D MT model, such as whole crustal conductivity zones at the boundary of physically contrasting blocks, namely the Carpathian conductivity zone (CCZ), the Pohorelá shear zone and the Zdychava fault zone. These identify major crustal blocks and structures typical for the Western Capathians. In comparison to older 2D model we see a significant difference, particularly in the case of the interpreted CCZ, which was not visible in the older 2D model. We assume that it reflects significant fault zones at the European Platform and Inner Western Carpathian junction. The model´s resolution and precision were supported by the integrated geophysical modelling, based on the crustal joint inversion with gravity data and geophysical-petrological thermally-self consistent mantle modelling.
Three MT profiles were modelled, which are distributed across the CCZ, farther to the East from the area of 2T profile. The dominant features are mostly middle-crust wide conductive zones, which are revealed on all profiles, although not always in the same position. Such structures have no equivalent in other profiles in central (2T) or western Slovakia, The only exception is the southern part of 2T profile, which was interpreted as a young crust alternated by volcanic activity or hydrothermal fluids. The conductive zones on our three profiles are also genetically young and we associate them with Neoalpine tectonic processes in the Neogene.
Further we continue with studies of dynamic processes at the contact of the Outer and Inner Carpathians. In a series of works, we focused on MT models across the Klippen Belt (KB) and the goal of these studies was to compare the deeper structures of the KB in its western and eastern sections. In the western section the tectonics is dominated by the Flysch Belt (FB), which overthrusts the KB. On the other hand, in the eastern section the situation is opposite - the KB is thrusted on the FB. By later processes the southern part of KB was cut off by steep faults. The contrasting tectonic style of the western and eastern sections of KB reflects the different kinematics of the Inner Western Carpathians (IWC) and the European Platform (EP) collision in the western and eastern part. While in the western part the transpression tectonics dominated, in the eastern part there were frontal thrusts on the EP. Only then the transpression movements along the BP began.

Keywords: magnetotelluric, tectonics, the Western Carpathians

Magnetotelluric investigation of the Denizli graben in the Western Anatolian Extensional Province

Ümit Avşar[1], Erşan Türkoğlu[2]

[1] İstanbul Technical University, Mining Faculty, Geophysical Engineering Department, 34469, İstanbul, Turkey, avsaru@itu.edu.tr

[2] Saudi Aramco, EXPEC Advanced Research Center, 31311, Dhahran, Saudi Arabia

SUMMARY

The Eastern Medditerranean region is known as a natural laboratory for earthsciences due to having tracks of opening and closing oceans (northern and southern tethys), subduction, obduction phenomenes in palaeotectonic era, and having active subduction, colision, and related tectonic structures in Neotectonic period. The most important structure of the region is Africa and Eurasia convergence which was a single subduction zone in east-west trending but it has been evolving into different tectonic parts through the geological time. One of the most significant of these tectonic fragments in the neotectonic period is called as Eastern Aegean arc which has a 40 mm/year subduction rate with high dip angle beneath Aegean sea – Western Anatolia, and also migration in the south-southwestward direction give rise to retreating of the slab. Furthermore, recent tomographic studies indicate that intersection area of the Aegean and Cyprus arc (just east of Aegean arc) which located beneath the Western Anatolia is defined as a slab tear that causes asthenospheric upwelling in SW Anatolia. Therefore, an extensional regime, accompied with volcanism, has been well established in Western Anatolia. And currently the region is dominated by horst graben systems and associated boundary faults. The aforementioned tectonic conditions which make the Western Anatolian graben systems candidates as geothermal potential regions. Since it provides the environment where three necessary components (heat Source, a reservoir with high porosity and permeability, liquid cycle system) of a geothermal system can be found. Thus it becomes important to reveal the structure of the graben systems. Magnetotelluric data were collected over a frequency range of 10,000 Hz to 0.001 Hz in Denizli graben-horst systems located in Western Anatolian Extensional Province. 3D MT inversions were performed to image the resistivity structure of the region.

Keywords: Denizli-Graben, Magnetotelluric, 3D-Inversion

Investigation of Lithosphere Structure of Northwestern Anatolia with long-period magnetotelluric data: Part 2. comparison to the 2D inversion of broadband and long period magnetotelluric data

M. Emin Candansayar[1], İsmail Demirci[1], N. Yıldırım Gündoğdu and M. Doğukan Oskay[1]
[1]Ankara University, Faculty of Engineering, Geophysical Engineering Department, Geophysical Modelling Group, Ankara, TURKEY. E-mail: candansayar@ankara.edu.tr

SUMMARY

In our previous study, we collected Magnetotelluric (MT) data along seven South-North and two East-West directional profiles in North-Western Anatoli between 2007 and 2010. The data were measured broadband frequency (T=0.0031s to 2000s) with the Phoenix MTU-5A system on 997 stations. The station interval was approximately 3 to 5 km. In this study, the data including AMT, broadband, and long-period MT data (T=0.0001s to 10.000s) were measured in four parallel lines from which broadband MT data were previously measured. The new MT data sets were measured with 15 km station intervals under the TUBITAK project (grant no. 119Y197). We used the new generation Phoenix MTU-5C system for a long period of MT measurement that allows us remote network data transfer via cell modem. This system enables us to make quality assessments of the measurements while the receivers are still active in the field. In order to obtain long-period MT data up to 10.000 seconds period, measurements were taken at each station for 10-18 days. The measurement was terminated after making sure that the data was obtained in a period of 10.000 seconds. Broadband MT data measured in 2010 and long-period MT data measured in 2020 and 2021 at the same station were compared. It was seen that the two data groups in the same period range were broadly similar. We individually interpreted long-period MT data collected along with four profiles. 2D resistivity models were obtained up to a depth of 150 km. The new models and the previous models obtained from 2D inversion of broadband MT data inversion are compared for the first 40 km according to the tectonic structure of the region. The main tectonic zones can be distinguished in both models. For the first time, in this presentation, preliminary results will be given about the lithosphere structure of northwest Anatolia up to a depth of 150 km.

Keywords: Lithosphere, Nort-Western Anatolia, Long Period, Magnetotelluric, Remotely controlled, 2D inversion

ACKNOWLEDGEMENTS

This study was supported by the Scientific and Technological Research Council of Turkey (TÜBİTAK) project under Grant No:119Y197. We thank TÜBİTAK for their valuable support.

Magnetotellurics reveals a hidden caldera and its relation to regional tectonics in the Cappadocia region, central Anatolia, Turkey

Ö. Hacıoğlu[1], A. T. Basokur[2], N. Meqbel[3], H. I. Arslan[2], T. Efeçınar[5]
[1]Karadeniz Technical University, ozlem.hacioglu@ktu.edu.tr
[2]Lemnis Geosciences, basokur@ankara.edu.tr
[3]National Observatory Rua General Jose Cristino, meqbeln@gmail.com
[2]Lemnis Geosciences, halilibrahimarslan@gmail.com
[5]Era Enerji Ltd., tevfik.efecinar@eraenergy.com.tr

SUMMARY

The Neogene-Quaternary volcanism in central Anatolia is characterized by ignimbrite sequences, and associated calderas have been partly dismantled and buried as a result of tectonic, volcanic, erosional and depositional processes, which cannot enable to identify of these structures from the surface expressions. To search the location of a concealed caldera, one of the probable ignimbrite source vents, magnetotelluric data acquired at 60 stations in the period range from 0.001s to 1000 s were used to derive an upper crustal three-dimensional electrical resistivity model in the Cappadocia region, central Anatolia, Turkey. The resistivity model provides constraints on the geometry and location of a buried caldera situated in the Çiftlik basin, which is characterized by a low resistivity (<10 Ωm) region coinciding with a caldera-like feature that is interpreted as a buried caldera complex (i.e., Çiftlik caldera) and attributed to the probable source area for the ignimbrites. The collapse and the burying process of the caldera complex have been linked with the transtensional tectonics of the Cappadocia region. The caldera margins are also compatible with the Quaternary fills of the Çiftlik basin and are bounded by faults related to the Cappadocian Volcanic Province fault system. Locating a buried eruption center beneath the Quaternary deposits may contribute to identify the source of Miocene-Pliocene ignimbrite emplacements.

Keywords: magnetotellurics, volcanism, caldera, Cappadocia

Estimating the melt fraction of magma reservoirs using MELTS and magnetotellurics

D. Cordell[1], S. Naif[2], J. Troch[3], and C. Huber[4]
[1]Georgia Institute of Technology, dcordell6@gatech.edu
[2]Georgia Institute of Technology, snaif@gatech.edu
[3]Smithsonian Institution National Museum of Natural History, trochj@si.edu
[4]Brown University, christian_huber@brown.edu

SUMMARY

Magnetotelluric data image the bulk resistivity of the subsurface which can be used to infer magma reservoir conditions beneath volcanoes. The bulk resistivity of magma depends primarily on the melt volume fraction, temperature, and dissolved water content. These variables are coupled via thermodynamic phase equilibria and saturation relationships yet mixing relations for bulk resistivity implicitly treat them as independent. Here, we use a parameterization of the rhyolite-MELTS thermodynamic modelling software to constrain relationships between melt fraction, temperature, dissolved water content and bulk resistivity for rhyolitic magmas. This method results in magnetotelluric interpretations which are (1) thermodynamically consistent, (2) independent of assumptions of temperature and water content derived from past eruptive episodes, and (3) able to investigate saturated melts containing crystal, melt, and volatile (i.e. aqueous fluid) phases. The utility of the method is demonstrated with three case studies of silicic systems at Mono Basin, Newberry Volcano, and the Laguna del Maule Volcanic Field (LdMVF). The moderately-conductive feature at Mono Basin can be explained by under-saturated partial melt (6-15 vol%) at <775°C, indicating relatively stable magma storage conditions since the last eruption. However, the relatively resistive feature at Newberry Volcano requires lower temperatures (<750°C) than previous estimates, suggesting that the system is saturated and has cooled since the last eruption (or that previous interpretations at 850°C are significantly out of equilibrium). The highly conductive feature at the LdMVF cannot be explained by saturated or under-saturated melt and requires additional non-magmatic conductive phases. These results demonstrate the potential of this new method to reduce uncertainty in magma storage parameters derived from magnetotelluric data and highlight the need for additional coupling strategies between petrology, geophysics, and thermo-mechanical models to better understand magmatic systems.

Keywords: magnetotellurics, MELTS, petrology, magma reservoir, volcano geophysics

Resistivity Models of Southwestern Canada: New insights into lithospheric structure, magma bodies, and geothermal systems

C. Hanneson and M.J. Unsworth
University of Alberta, Department of Physics, cedar@ualberta.ca

Summary

Three new 3-D resistivity models allow a fresh look at the lithospheric structure of southwestern Canada. The largest of these models is centred on the southeastern Canadian Cordillera and spans hundreds of kilometres. Another model is focused on the central Garibaldi volcanic belt, from Mount Garibaldi to the Bridge River Cones. The final model surrounds the Mount Meager volcanic complex, an area that is currently in the early stages of geothermal development.

The Cordillera model has a horizontal resolution of 5 km and extends to a depth of 400 km. It is the first regional-scale 3-D resistivity model of the southern Canadian Cordillera. This study focuses on crustal-scale resistivity anomalies including the southern Alberta-British Columbia conductor and the Canadian Cordilleran Regional conductor. It also investigates the transition from thin Cordilleran lithosphere to thick cratonic lithosphere, providing new insight into the deep structure of western North America.

The Garibaldi model has a horizontal resolution of 1.5 km and extends to a depth of 40 km. This 3-D resistivity model is preliminary, but it includes conductors below Mount Meager and Mount Cayley. Additional fieldwork at Mount Cayley is scheduled for August 2022 and an update will be provided at the 25th EM Induction Workshop.

The Mount Meager model has a horizontal resolution of 0.25 km and extends to a depth of 20 km. Following two field campaigns in 2019 and 2020, this study builds on magnetotelluric results from the 1980s and early 2000s. This 3-D resistivity model provides a regional view around the geothermal target, including a potential magma body and associated deep hydrothermal systems.

This abstract gives an overview of these three studies, along with key results. Together, they present an exciting new view of the geologic structure and geologic evolution of southwestern Canada.

Keywords: Canadian Cordillera, Garibaldi Volcanic Belt, Mount Meager, Magnetotellurics, Geothermal

Introduction

The Juan de Fuca plate, offshore southwestern British Columbia (BC) and northwestern Washington, subducts beneath the North American plate at the Cascadia subduction zone, as illustrated in Figure 1 at the end of the abstract. The tectonic convergence rate between these two plates is approximately 40 mm/year (Kreemer et al. 2014). In contrast to the Juan de Fuca plate, the Explorer plate to the north is subducting at a rate of only 5-20 mm/year (Hutchinson et al. 2020).

Dehydration of the subducting slab releases volatiles into the overlying mantle of the North American plate, lowering its melting point and creating a region of partial melt, which leads to volcanism at the surface (Stern 2002). The chain of volcanoes resulting from this subduction is called the Cascade volcanic arc. The northern segment of the arc, from Glacier Peak in Washington to Silverthrone Caldera in BC, is the Garibaldi volcanic belt (GVB; Figure 2).

Mount Baker is the most voluminous volcanic complex in the GVB, Glacier Peak is the most-recently active with an eruption in the mid-1700s and Mount Meager is the most-recently active in Canada with a major eruption ~2400 years ago (Hickson 1994). The most recent volcanism in the GVB has been rhyolitic-to-dacitic at Mount Meager, dacitic at Mount Cayley and Mount Garibaldi, and andesitic at Mount Baker and Glacier Peak (Hickson 1994). This illustrates a change from felsic composition in the north to intermediate silica content in the south.

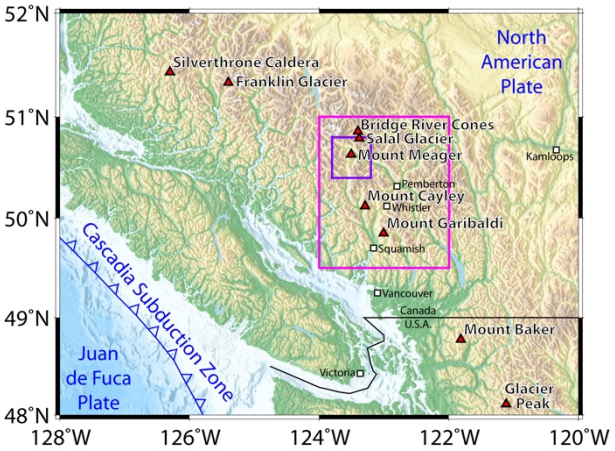

Figure 2. Map of southwestern BC and northwestern Washington with the Canada-U.S.A. border (black line), population centres (squares), volcanic centres (triangles) and two study areas: central GVB (pink) and Mount Meager (purple).

BC has a range of significant geothermal resources in settings that include volcanic systems, fault-hosted systems, and hot dry rock. Volcanic systems are found in the GVB, including at Mount Meager and Mount Cayley, and fault-hosted systems are found near the southern Rocky Mountain Trench (SRMT). Both fault-hosted geothermal systems and hot dry rock resources are found in the Columbia Mountains.

Data and Methods

The study centred on the southeastern Canadian Cordillera used magnetotelluric (MT) data from 331 locations (Figure 3). These data included 110 Lithoprobe sites, 22 EarthScope USArray sites, and 19 sites from other studies. The additional 180 MT soundings were collected by the University of Alberta between 2002 and 2018. The 3-D inversion used impedance and tipper data at 18 periods, logarithmically spaced between 1 and 18,000 s. The resistivity model has a horizontal resolution of 5 km and extends to a depth of 400 km.

The study focused on the central GVB used MT data from 77 locations (Figure 4). The 3-D inversion used impedance and tipper data at 24 periods, logarithmically spaced between 0.017 and 800 s. The resistivity model has a horizontal resolution of 1.5 km and extends to a depth of 40 km.

The study focused on Mount Meager used MT data from 66 locations (Figure 5). These data included 2, 30, 22 and 12 soundings from 1982, 2001, 2019 and 2020, respectively. The 3-D inversion used impedance and tipper data at 29 periods, logarithmically spaced between 0.0025 and 1,000 s. The resistivity model has a horizontal resolution of 0.25 km and extends to a depth of 20 km. ModEM (Kelbert et al. 2014) was used in all three studies.

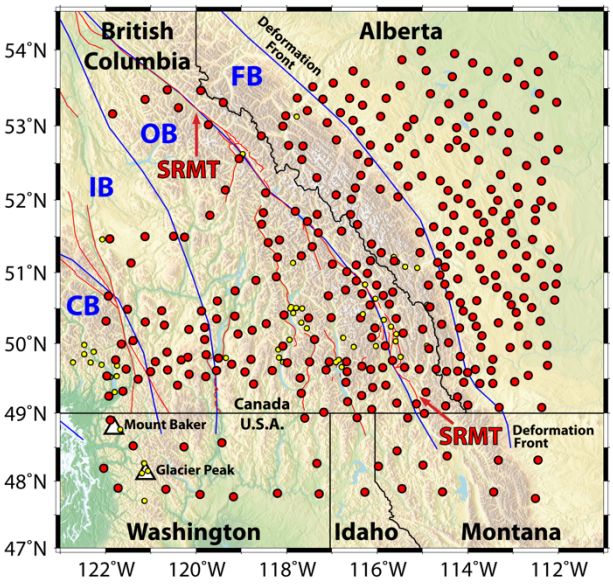

Figure 3. MT stations (red dots) used in the 3-D inversion to create the resistivity model centred on the southeastern Canadian Cordillera. Political boundaries (black lines), morphogeological boundaries (blue lines), major faults (red lines), thermal springs (yellow dots), and major volcanic centres (white triangles) are also shown. CB = Coast belt; IB = Intermontane belt; OB = Omineca belt; FB = Foreland belt; SRMT = southern Rocky Mountain Trench.

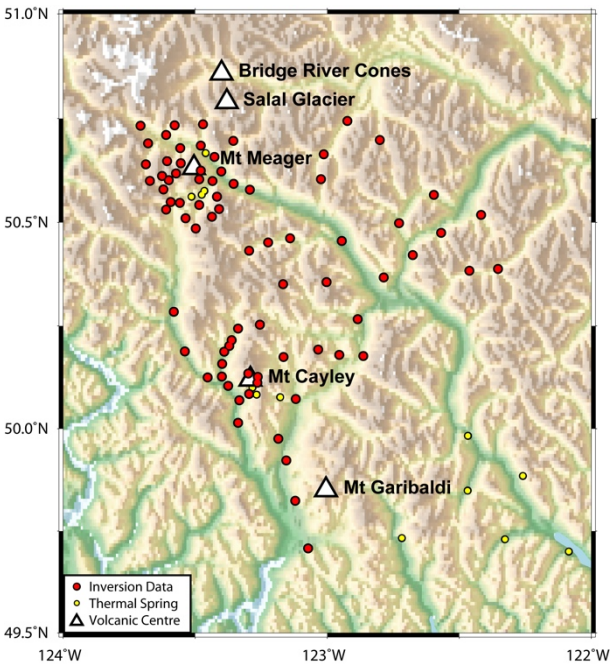

Figure 4. MT stations (red dots) used in the 3-D inversion to create the resistivity model focused on the central Garibaldi volcanic belt.

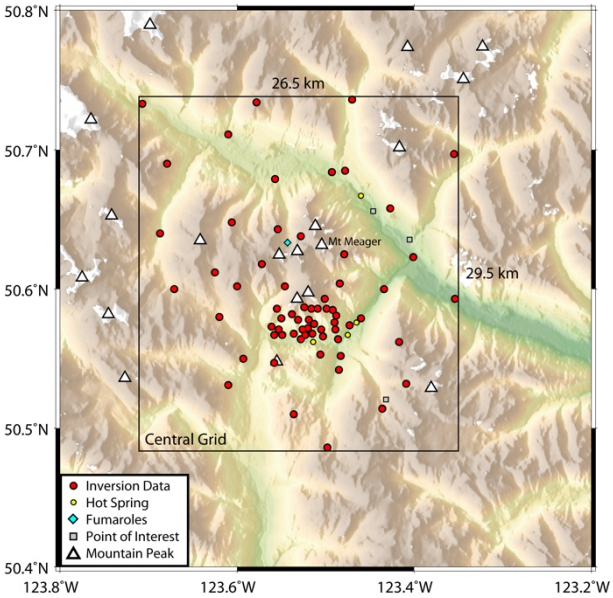

Figure 5. MT stations (red dots) used in the 3-D inversion to create the resistivity model surrounding the Mount Meager volcanic complex.

Resistivity Models

One horizontal slice from each of the three 3-D resistivity models is shown in this abstract (Figures 6, 7 and 8). The resistivity models will be shown in more detail at the 25th EM Induction Workshop.

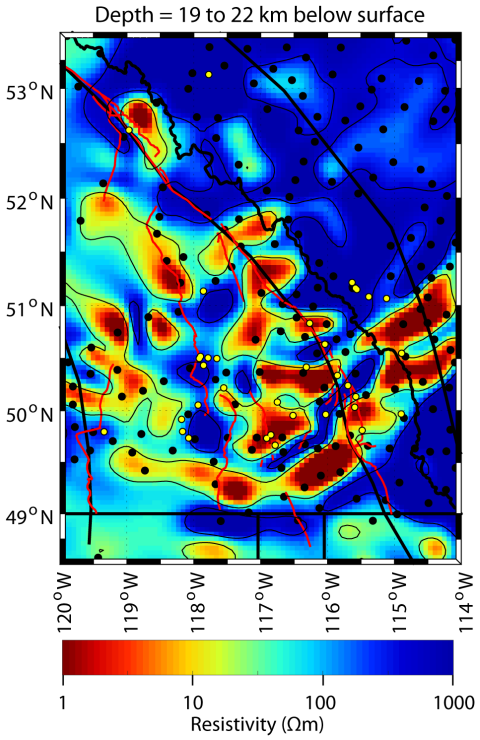

Figure 6. Horizontal slice of the 3-D resistivity model centred on the southeastern Canadian Cordillera. MT sites (black dots), thermal springs (yellow dots) and surface traces of major faults (red lines) are also shown.

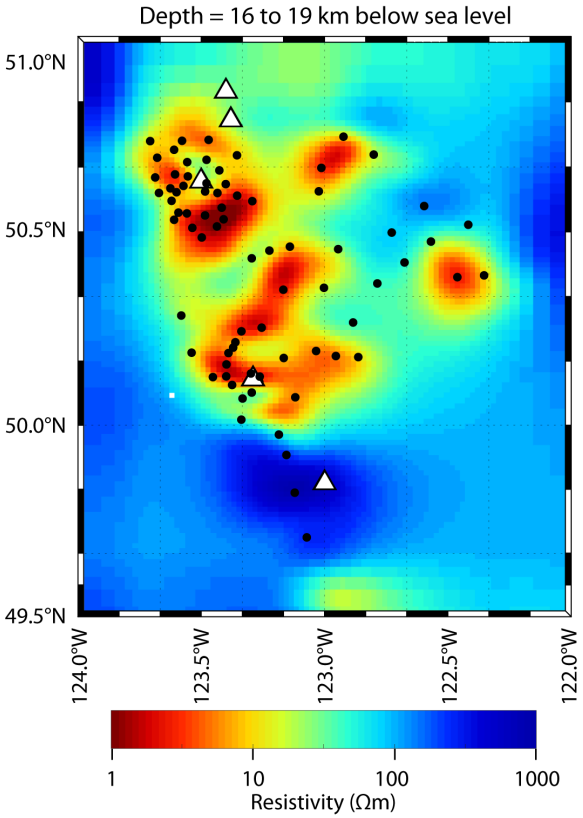

Figure 7. Horizontal slice of the 3-D resistivity model focused on the central Garibaldi volcanic belt. MT sites (black dots) and volcanic centres (triangles) are also shown.

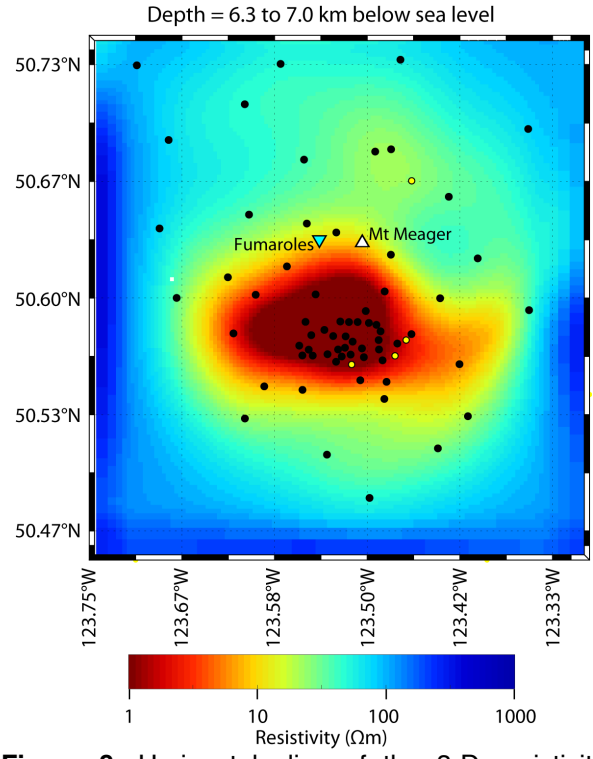

Figure 8. Horizontal slice of the 3-D resistivity model surrounding the Mount Meager volcanic complex. MT sites (black dots) and thermal springs (yellow dots) are also shown.

Conclusions

The resistivity model centred on the southeastern Canadian Cordillera exhibits low resistivity in the middle and lower crust of the Omineca belt. This is likely caused by interconnected saline fluids and possibly partial melt in the lowermost crust and uppermost mantle. Additional results, including detailed interpretations and deep lithospheric structure, will be presented at EMIW 2022.

The resistivity model focused on the central Garibaldi volcanic belt is preliminary, but it exhibits low resistivity below Mt Meager and Mt Cayley. Additional data will be collected at Mt Cayley this summer. An update will be provided at EMIW 2022.

The resistivity model focused on Mt Meager exhibits low resistivity beneath the volcanic complex in the depth range 5-10 km, possibly caused by a magma body. Additional results, including detailed interpretations, will be presented at EMIW 2022.

Acknowledgements

Funding was provided by an NSERC Discovery Grant to M.J. Unsworth and an award from the Future Energy Systems program at the University of Alberta. A Geoscience BC scholarship was awarded to C. Hanneson in 2021.

References

Hickson CJ (1994) Character of volcanism, volcanic hazards, and risk, northern end of the Cascade magmatic arc, British Columbia and Washington Stake. Geol Surv Can Bull 481:231. doi:10.4095/203253

Hutchinson J, Kao H, Riedel M, Obana K, Wang K, Kodaira S, Takahashi T, Yamamoto Y (2020) Significant geometric variation of the subducted plate beneath the northernmost Cascadia subduction zone and its tectonic implications as revealed by the 2014 MW 6.4 earthquake sequence. Earth & Planet Sci Lett 551:116569. doi:10.1016/j.epsl.2020.116569

Kelbert A, Meqbel N, Egbert GD, Tandon K (2014) ModEM: a modular system for inversion of electromagnetic geophysical data. Comput & Geosci 66:40. doi:10.1016/j.cageo.2014.01.010

Kreemer C, Blewitt G, Klein EC (2003) A geodetic plate motion and global strain rate model. Geochem Geophys 15:3849. doi:10.1002/2014GC005407

Stern RJ (2002) Subduction zones. Rev Geophys 40:3. doi:10.1029/2001RG000108

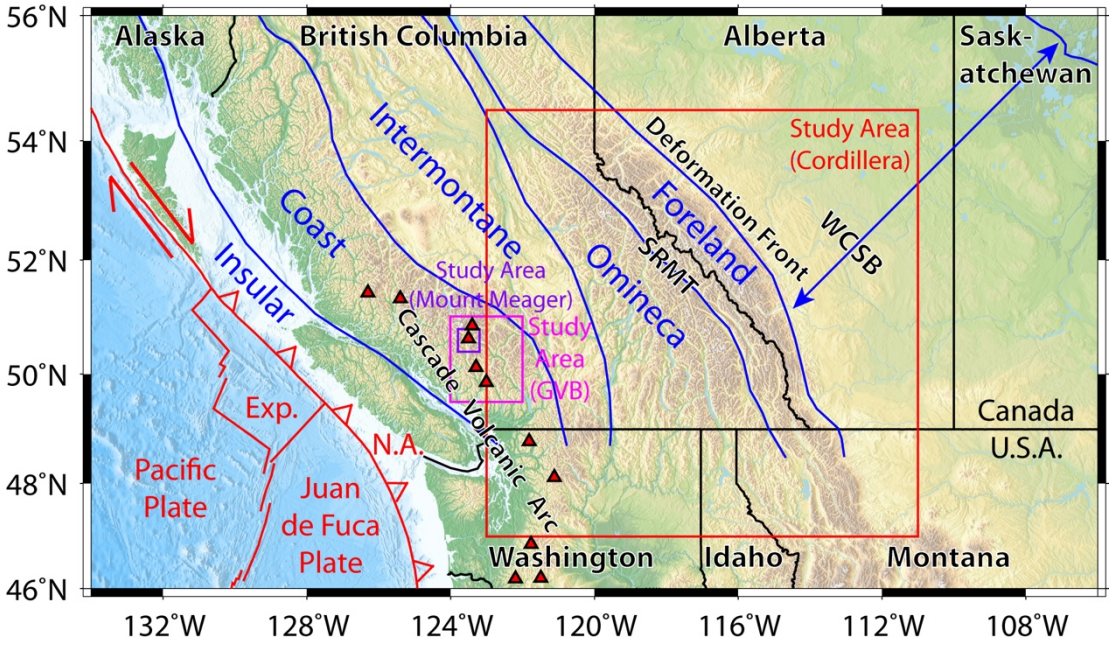

Figure 1. Map of southwestern Canada and northwestern U.S.A. with political boundaries (black lines), morphogeological boundaries (blue lines), tectonic plate boundaries (red lines), volcanoes (triangles), and three study areas: (1) centred on the southeastern Canadian Cordillera (red), (2) focused on the central Garibaldi volcanic belt (pink), and (3) surrounding the Mount Meager volcanic complex (purple). Exp. = Explorer plate, N.A. = North American plate, SRMT = southern Rocky Mountain Trench, and WCSB = Western Canada Sedimentary Basin.

Constraining the size and state of magma reservoirs through a quantitative approach combining MT, lab measurements and petrological modelling

F. Samrock[1], A.V. Grayver[2], O. Bachmann[3], Ö. Karakas[3], L. Dambly[1], M.O. Saar[1]

[1]ETH Zurich, Institute of Geophysics, Geothermal Energy and Geofluids Group, fsamrock@ethz.ch
[2]ETH Zurich, Institute of Geophysics, Earth and Planetary Magnetism Group
[3]ETH Zurich, Institute of Geochemistry and Petrology, Magmatic Petrology and Volcanology Group

SUMMARY

Magnetotelluric measurements are a powerful tool to image the subsurface under active volcanic regions. 3-D models, computed from magnetotelluric data, nowadays provide detailed multi-scale images of the electrical conductivity distribution. Since electrical conductivity is predominantly controlled by the presence of melt and fluid phases, conductivity models proved to be highly suitable for mapping the distribution of melt and for constraining melt fractions. Melt fractions can be estimated by combining laboratory models for melt electrical conductivity and mixing laws to derive the bulk electrical conductivity of multiphase systems. Melt electrical conductivity depends on the composition of the melt, the amount of dissolved water as well as temperature and pressure conditions. However, estimates of melt fractions are often based on arbitrary combinations of these parameters, and they do not consider the dependance of melt interconnectedness on melt fraction.
Here we present an interdisciplinary approach to interpret electric conductivity models from three volcanoes in the Main Ethiopian Rift. We use rhyolite-MELTS to model magma crystallization and storage conditions constrained by petrological analyses of on-site erupted products. To derive the electrical conductivity of melt during fractional crystallization we derive an expanded melt electrical conductivity model by interpolating between existing models for rhyolite, dacite and andesite melt. Thereby we obtain a generalized model that describes the electrical conductivity of melt in dependence on the SiO_2 and H_2O content, pressure and temperature. These parameters are given by rhyolite-MELTS. Decreasing melt connectedness with diminishing melt fraction is considered by varying the cementation exponent, *m,* in the generalized Archie's law whilst taking into account conservation of connectedness. Furthermore, we describe the magma reservoirs as three-phase systems consisting of crystals, melt and magmatic volatiles.
The results show that this approach enables us to constrain the current state of magma reservoirs in terms of melt fraction, temperature, and free volatile abundance. The latter is of eminent importance when discriminating between the two major mechanisms that drive volcanic unrest: magma on the move or increased degassing of a crystallizing magmatic system, so-called second boiling.
With this study we demonstrate the great capability of the presented interdisciplinary solution approach that combines geophysical observations, petrological probes, and laboratory models to capture the current state of volcanoes.
The outcome is of major importance when it comes to realistic volcanic hazard assessment and geothermal energy applications that require a detailed understanding of magmatic heat sources that sustain geothermal reservoirs.

Keywords: 3D inversion, volcano imaging, volcano deformation, interdisciplinary geophysical and petrological modelling

3-D model of the deep structure of the Yenisei-Khatanga regional trough

D. Yakovlev[1], G. Slinchuk[2] and A. Yakovlev[2]
[1]STC Nord-West, stcnordwest@gmail.com, Moscow, Russia
[2]Lomonosov Moscow State University, Moscow Russia

SUMMARY

This work is devoted to the study of the deep structure of the Yenisei-Khatanga regional trough (YKRT) in Northern Russia, where more than 25,000 MT soundings have been performed over the past 20 years over an area of 1200x400 km along a network of profiles. At present, two theories of the deep structure of this region and the origin of the trough are most popular: the “over-rift” and “eclogitic” hypotheses.

3-D inversion of MT data was performed using the ModEM code. From the entire data array, about 800 MT sites were selected over a 20x20 km network. Based on the results of 3-D inversion, a three-dimensional resistivity model of the deep structure of the Yenisei-Khatanga regional trough was obtained. Within the western half of the YKRT, there are no high-resistivity basement rocks; a sublatitudinal conductive zone is observed, which in general can indicate rifting processes. This testifies in favor of the “over-rift” theory of the origin of the western part of the YKRT. The eastern half of the YKRT at depths of more than 10 km has a geoelectric structure similar to the Siberian platform and similar structures in the northwestern and sublatitudinal directions. This suggests that rift processes did not occur here. The origin of the eastern part of the trough is rather explained by the “eclogitization” of the lower crust.

Keywords: 3-D inversion, deep structure, Yenisei-Khatanga regional trough

Compaction-driven fluid localization and stagnation can explain lower crustal low-resistivity zones

Matthew Joseph Comeau[1], Michael Becken[2] and Alexey V. Kuvshinov[3]
[1]Institut für Geophysik, Universität Münster (WWU), Münster, Germany, matthew.comeau@uni-muenster.de
[2]Institut für Geophysik, Universität Münster (WWU), Münster, Germany, michael.becken@uni-muenster.de
[3]Institute of Geophysics, ETH, Zürich, Switzerland, kuvshinov@erdw.ethz.ch

SUMMARY

We present electrical resistivity models that show discrete zones (width of ~25 km, vertical extent of <10 km) of low resistivity (<30 Ωm) in the lower crust (>20 km depth), from magnetotelluric data collected across the intracontinental Bulnay region, Mongolia. The top of these features is located approximately 5 km below the brittle-ductile transition zone and they are imaged as laterally extended (tube-like) features over 300 km long, parallel to the Bulnay fault zone, and perpendicular to the far-field compressive tectonic stress. Such features may be caused by unaccounted-for electrical anisotropy. However, when anisotropy is considered in the modeling, the features remain. We investigate an alternative explanation: we show evidence for a conceptual hydrodynamic model of fluid localization and stagnation by thermally activated compaction. We demonstrate that this is compatible with the observed low-resistivity zones, which are consistent with the presence of saline metamorphic fluids. Based on the thermal structure of the crust, the conceptual model predicts the size and shape of the zones: the fluid domains should have a vertical extent of ~9 km and their centres should be <9 km below the brittle-ductile transition zone. The conceptual model gives plausible values for the activation energy for viscous creep (270-360 kJ/mol), suggesting that the mechanism is dislocation creep. The electrical resistivity models constrain the lower crustal viscous compaction-length to be ~25 km, in this region. This length scale is consistent with independent estimates of hydraulic and rheological properties. The model can be used to independently constrain the lower crustal effective viscosity, the fluid salinity, and the porosity. Overall, the results imply tectonic deformation and compaction processes, rather than lithological-structural heterogeneity, control the regional lower crustal fluid flow.

Keywords: fluid; compaction; anisotropy; brittle-ductile transition; resistivity

The Curnamona Cube, new data and insights

B. Kay[1], G. Heinson[2], K. Brand[3], S. Thiel[4] and G. Boren[5]
[1]University of Adelaide, ben.kay@adelaide.edu.au
[2]University of Adelaide, graham.heinson@adelaide.edu.au
[3]Beurea of Meteorology, kate.e.brand01@gmail.com
[4]Geological Survey of South Australia, stephan.thiel@sa.gov.au
[5]University of Adelaide, goran.boren@adelaide.edu.au

SUMMARY

The Curnamona Province is a Paleoproterozoic to Mesoproterozoic domain that hosts the Broken Hill Pb-Zn ore body and a number of IOCG type Cu-Au deposits, but is mostly covered in Neoproterozoic to Quaternary cover from a few tens of meters to thousands of meters with much of the province remaining unknown. Three-dimensional resistivity modelling of 55-km gridded long-period magnetotelluric data collected as part of the Australian Lithospheric Architecture Magnetotelluric Project (AusLAMP) previously revealed the presence of the Curnamona Conductor that exhibits extremely low resistivities <1 Ω.m at upper-crustal depths (<15 km) which has a lateral extent of >200 km in a north–south orientation. The conductor appears to dip to the west, centred under the large igneous province Benagerie Suite Volcanics with resistivity ~10–100 Ω.m in a broader lower crustal region.

Here, we present 3D resistivity models of the Curnamona Cube, with approximately 200 magnetotelluric stations over the Curnamona Province. The AuScope funded program, the Curnamona Cube, was designed to collect approximately 150 broadband magnetotelluric and ambient noise tomography stations to characterise the crust and upper mantle from the surface down to several hundred kilometres in such a way as defining a cube of the physical properties of the Curnamona Province. This cube is designed to provide a physical model of the Curnamona Province in terms of its electrical resistivity and seismic velocity covering an area of around 400 x 400 x 400 km's.

Keywords: Curnamona Province, Undercover, Curnamona Cube, Magnetotelluric, Ambient Noise Tomography

First Magnetotelluric imaging of the northern Zagros orogenic belt (Preliminary report on measured data and processing techniques)

Sh. Zhian[1], A. Junge[1] and B. Oskooi[1]
[1]Goethe-Universität Frankfurt am Main, zhian@geophysik.uni-frankfurt.de
[1]Goethe-Universität Frankfurt am Main, junge@geophysik.uni-frankfurt.de
[1]Goethe-Universität Frankfurt am Main, email contact

SUMMARY

The Zagros orogenic belt, is a young and active orogen extending from the northwest to southeast in the western half of Iran, which, together with the Iranian plateau hold a record of the long-standing convergence history between Eurasia and Arabia across the Neo-Tethys, from subduction/obduction processes to present-day collision (Agard et al. 2011). On how this collision is accommodated in the northern part, currently there are two seismic models (Rahmani et al. 2019, Motaghi et al. 2017), proposing different geodynamic processes (lithospheric thickening or delamination) within the lithosphere and asthenosphere. An initial 2-D MT study based on these two seismic results indicates MT is a promising method to distinguish between different conductivity models within the lithosphere and upper asthenosphere beneath the Zagros.

To study the lithospheric structure and discriminate between the proposed seismic models in the northern Zagros, an MT survey was carried out at 22 sites (22 long-period and 22 broad-band measurements) along two parallel 450-km profiles in winter and spring 2022, with an approximately northeast and southwest direction from Tehran to Ilan provinces, crossing the Zagros.

Here, we present first results from the acquired data, an electrical conductivity model based on data processing using the robust processing technique implemented in Frankfurt software package, FFMT. The Matlab based programs follow the multi-station approach by Egbert [3] (1997) and has been extended to diminish the effects of anthropogenic noise (which so far, has caused challenges to process the data from some of the sites) by using an Eigenwert-criterium for the selection of the time segments (Hering, 2019). It allows for the minimization of coherent and incoherent noise between the field components of the local sites and improves results compared to standard processing approaches.

Keywords: Magnetotelluric, Zagros orogenic belt, Conductivity structure, Magnetotelluric transfer functions

REFRENCES

Agard, P. et al., 2011. Zagros orogeny: a subduction-dominated process, Geol. Mag., 148(5/6), 692–725.
Egbert, G., 1997. Robust multiple-station magnetotelluric data processing, Geophys. J. Int. 130, 475-496.
Hering, P., 2019. Advances in Magnetotelluric Data Processing, Interpretation and Inversion, illustrated by a three-dimensional Resistivity Model of the Ceboruco Volcano. PhD Thesis, Goethe-Universität Frankfurt am Main, Frankfurt, Germany.
Motaghi, K., Shabanian, E. & Kalvandi, F., 2017. Underplating along the northern portion of the Zagros suture zone, Iran, Geophys. J. Int., 210, 375–389.
Rahmani, M., Motaghi, K., Ghods, A., Sobouti, F., Talebian. M., Ai Y. and Chen, L., 2019. Deep velocity image of the north Zagros collision zone (Iran) from regional and teleseismic tomography, Geophys. J. Int. 219, 1729–1740.

Abstract, 25^{th} EM Induction Workshop,Çeşmeı, Turkey, September 11-17, 2022

What are the compositional causes behind electrical conductivity variations in continental lithospheric mantle? Methodology and practice for quantified interpretations.

S. Özaydın[1], K. Selway[2], M. Moorkamp[3], W. L. Griffin[1] and C. Manassero[1]
[1]School of Natural Sciences, Macquarie University, Sydney, Australia, sinan.ozaydin@mq.edu.au
[2]MinEx CRC, Future Industries Institute, University of South Australia, Adelaide, Australia, kate.selway@unisa.edu.au
[3]Department of Earth and Environmental Sciences, Ludwig-Maximilians-Universität, Munich, Germany, moorkamp@geophysik.uni-muenchen.de

SUMMARY

Since the electrical conductivity can be used as a proxy for many properties of the earth media, the magnetotelluric method remains one of the most powerful tools for unveiling the lithospheric architecture. However, the compositional nature behind variations in electrical conductivities is often under-interpreted. This practice primarily stems from the non-uniqueness in solutions acquired via deterministic inversion techniques and hardship in tying them to the vast literature of experimental petrology and electrical conductivity studies.

We demonstrate a review of methodologies used in making such quantified interpretations of magnetotelluric models centering the use of the MATE software (Özaydın and Selway, 2020, https://github.com/sinanozaydin/MATE) and portray the findings of such analysis from case studies in Southern Africa (Özaydın et al, 2021, 2022), Eastern Australia, Tanzania and Continental US.

Detailed comparison of xenoliths and xenocrysts from Southern Africa and recently-developed 3D magnetotelluric models demonstrate that such relationships between composition and electrical conductivity indeed exist. However, they constitute a complex phenomenon that requires careful analysis, which should include the emphasis on style, recurrence and intensity of metasomatism alongside the initial formation and age of the lithosphere in the first place.

Relationships between mantle-derived magma (e.g., kimberlites) and electrical conductivity; also exist according to analyses made from MT models around the Earth and spatial distribution of kimberlites. This finding supports magma transport mechanisms for kimberlites are controlled by lithospheric composition.

Keywords: lithospheric mantle, electrical conductivity, cratons, kimberlites, metasomatism

REFERENCES

Özaydın S, Selway K (2020) Mate: An analysis tool for the interpretation of magnetotelluric models of the mantle. Geochemistry, Geophysics, Geosystems 21(9):e2020GC009126

Özaydın S, Selway K, Griffin WL (2021) Are xenoliths from southwestern kaapvaal craton representative of the broader mantle? constraints from magnetotelluric modeling. Geophysical Research Letters 48(11):e2021GL092570

Özaydın S, Selway K, Griffin WL, Moorkamp M (2022) Probing the southern african lithosphere with magnetotellurics: 2. linking electrical conductivity, composition, and tectonomagmatic evolution. Journal of Geophysical Research: Solid Earth 127(3):e2021JB023105

Imaging of an intraplate volcanic system from source to surface

Matthew Joseph Comeau[1], Michael Becken[2] and Alexey V. Kuvshinov[3]
[1]Institut für Geophysik, Universität Münster (WWU), Münster, Germany, matthew.comeau@uni-muenster.de
[2]Institut für Geophysik, Universität Münster (WWU), Münster, Germany, michael.becken@uni-muenster.de
[3]Institute of Geophysics, ETH, Zürich, Switzerland, kuvshinov@erdw.ethz.ch

SUMMARY

The structure of continental intraplate volcanic systems — which occur far from active tectonic margins, unlike the majority of Earth's volcanism — is enigmatic and not fully understood, as are the underlying mechanisms responsible. Quaternary–Neogene aged, alkaline basalt flows and clusters of volcanic cones are found in Central Mongolia, which is in the continental interior. Using a high-resolution, multi-scale, magnetotelluric dataset, we generate both 3-D and 2-D electrical resistivity models of the lithosphere and uppermost mantle beneath this region. We focus on two volcanic fields that are separated by approximately 100 km. By examining the models and considering all available evidence we propose the following: 1) narrow, vertical, low-resistivity anomalies located in the upper–middle crust beneath the surface expressions of volcanism represent the remnant signatures of ancient, ephemeral magma pathways (or collection of pathways) and record the location of magma ascent; 2) widely distributed low-resistivity zones in the lower crust can be explained by very small amounts of saline fluids in a thermally perturbed region, and are hard to reconcile with magma storage; and 3i) a local low-resistivity zone in the lithospheric mantle and a broad, doming low-resistivity feature in the uppermost mantle are interpreted to represent a metasomatized lithospheric mantle and a mantle upwelling and thermal anomaly explained by low-percent partial melt, which is inferred to be the source for intraplate volcanism. Thus the geophysical images reveal magma generation and transport from a mantle source to the surface beneath a continental intraplate basaltic volcanic system. Furthermore, they are consistent with geochemical and petrological evidence from erupted lavas that point to a single common mantle source region for both volcanic zones and a volatile-enriched, metasomatized sub-continental lithospheric mantle, as well as limited crustal contamination and rapid magma ascent.

Keywords: magma plumbing; intraplate volcanism; mantle upwelling; partial melt; electrical resistivity

Crustal structure across Indus Tsangpo Suture zone NW Himalaya, India as revealed from Magnetotelluric study

C.K. Rao
ckraochinta@gmail.com
Adhiraj Gardens, Kharghar, Navi Mumbai

SUMMARY

Broad band magnetotelluric (MT) data were acquired at 18 stations along NE-SW profile crossing Tso Morari and Indus Tsangpo (ITS) suture in NW Himalayan region. Regional strike analysis indicates the MT data is consistent with an assumption of 2D geoelectric strike direction. The regional strike indicates $N40^0W$ and correlates well with the observed predominant geological strike of the region. The galvanic distortion corrected data were inverted with 2D inversion code for obtaining geoelectric model of the study region. The geoelectric section broadly reflects the resistivity pattern typically observed over Indus Tsangpo suture in other parts of Himalaya. A low resistivity zone of 20 km thick and 15 km wide with resistivity less than 2 Ohm-m is delineated corresponds to ITS is flanked on either side by the high resistivity bodies. The high resistivity bodies correspond to Rupshi granite on SW of ITS and Ladakh batholith and Chusul granite on the NE. Studies in different parts of ITS indicate that the low resistivity is a regional feature extending over the entire 2500 km length of Himalaya. The low resistivity observed in the present study is attributed to either saline fluids or partial melts of the rocks due to high temperature regime in deeper crust, and also the frictional heat generated in the process of Indian Plate sliding across the Tibetan block. The high surface heat flow of 180 mW/sq.m in the region suggest that most of contribution to the observed low resistivity is of thermal origin.

Keywords: Magnetotellurics, Higher Himalayas, Indus Tsangpo suture

Long period magnetotelluric at the Antarctica: The role of asthenospheric mantle anisotropy in Glacial Isostatic Adjustment.

González-Castillo L.[1], Madarieta-Txurruca A.[1], Hill G.[2], Castro C. [3], Galindo-Zaldívar J. [1,4] and Junge A. [3]

1 Dpto. de Geodinámica, Universidad de Granada, Granada, Spain. lgcastillo@ugr.es

1 Dpto. de Geodinámica, Universidad de Granada, Granada, Spain. amadatxu@ugr.es

2 Institute of Geophysics, Czech Academy of Science, Prague, Czech Republic. gjhill@ig.cas.cz

3 Institut für Geowissenschaften, Goethe Universität Frankfurt, Frankfurt am Main, Germany. castro@geophysik.uni-frankfurt.de

4 Instituto Andaluz de Ciencias de la Tierra CSIC-Universidad de Granada, Granada, Spain. jgalindo@ugr.es

3 Institut für Geowissenschaften, Goethe Universität Frankfurt, Frankfurt am Main, Germany. junge@geophysik.uni-frankfurt.de

SUMMARY

Understanding the behavior and geodynamic evolution of Antarctica is essential to determine the processes controlling future climatic warming and sea level rise. The Antarctic continent was isolated since 30-40 Ma ago by the tectonic opening of the Drake-Scotia and Tasman gateways creating the Antarctic Circumpolar Current. This change in oceanic circulation doubtlessly affected the global climate and Antarctic ice sheet evolution with consequent sea level change. Mantle rheology influences the motion of lithospheric plates and the Glacial Isostatic Adjustments (GIA) processes which imprint the mantle structure including anisotropic features. Mantle electrical anisotropy may be identified by means of long period magnetotelluric (LMT) measurements. In the first stage of our research, LMT data were collected at seven sites distributed on the Antarctic Peninsula and South Shetland Islands, from January to March 2022. Here we present preliminary data analysis that suggests possible presence of electrical anisotropy in the asthenospheric mantle of this portion of the Antarctic Peninsula and South Shetland Islands. Accounting for the tectonic evolution of Antarctica, is essential to identify the source of potential mantle anisotropy i.e. is it a result of geodynamic and /or GIA processes. These results will contribute to the improvement of GIA models currently developed in view of an isotropic mantle. GIA models allow for reconstructions of ice mass changes which help the understanding and prediction of sea-level changes.

Keywords: Antarctica, mantle anisotropy, Long Period Magnetotelluric, GIA.

Abstract, 25^{th} EM Induction Workshop,Çeşmeı, Turkey, September 11-17, 2022

Investigation into lithospheric mantle of Northern Tanzania utilising 3D magnetotellurics.

S. Özaydın[1], K. Selway[2], S. Foley[1], P. Tarits[3] and S. Hautot[4]
[1]School of Natural Sciences, Macquarie University, Sydney, Australia
[2]MinEx CRC, Future Industries Institute, University of South Australia, Adelaide, Australia
[3]Laboratoire Géosciences Océan, Institut Universitaire Européen de la Mer, 29280 Plouzané, France
[4]IMAGIR sarl, 29290 Saint Renan, France

SUMMARY

The relationship between mantle melting and its residual effects on the composition of the lithosphere has not been well documented. Neogene rifting system in Northern Tanzanian Divergence provides an excellent laboratory to investigate such a relationship since a variety of volcanic rocks in the vicinity are associated with different categories of recent incipient mantle melting (Foley et al, 2012). Electrical conductivity is sensitive to the products of metasomatism exerted on the mantle (e.g., water, hydrous minerals); therefore, the magnetotelluric (MT) method can be utilised to explore such relationships.

The electrical structure of North Tanzanian Divergence was investigated using 3D magnetotelluric modelling (Kelbert et al, 2014) of a dataset combining long-period and broadband MT stations (Selway, 2015; Plasman et al, 2019). Then the magnetotelluric model was interpreted using the MATE software (Özaydın and Selway, 2020) to understand the relationship between mantle composition and electrical conductivity. The preliminary results indicate that the Tanzanian craton and the rift region consist of a more heterogeneous mantle with patches of hydrated/conductive regions. On the other hand, a more dry/resistive mantle is present beneath the Mozambique Belt, possibly reflecting the destruction of metasomes via larger volumes of mantle melting.

Keywords: magnetotellurics, electrical conductivity, cratons, rifting, incipient melts

REFERENCES

Foley S, Link K, Tiberindwa J, Barifaijo E (2012) Patterns and origin of igneous activity around the Tanzanian craton. Journal of African Earth Sciences 62(1):1–18, DOI 10.1016/j.jafrearsci.2011.10.001

Kelbert A, Meqbel N, Egbert GD, Tandon K (2014) Modem: A modular system for inversion of electromagnetic geophysical data. Computers & Geosciences 66:40–53

Özaydın S, Selway K (2020) Mate: An analysis tool for the interpretation of magnetotelluric models of the mantle. Geochemistry, Geophysics, Geosystems 21(9):e2020GC009126

Plasman M, Hautot S, Tarits P, Gautier S, Tiberi C, Le Gall B, Mtelela K, Gama R (2019) Lithospheric Structure of a Transitional Magmatic to Amagmatic Continental Rift SystemâInsights from Magnetotelluric and Local Tomography Studies in the North Tanzanian Divergence, East African Rift. Geosciences 9(11):462, DOI 10.3390/geosciences9110462

Selway K (2015) Negligible effect of hydrogen content on plate strength in East Africa. Nature Geoscience 8(7):543–546, DOI 10.1038/ngeo2453

The Electrical Signature of the Manzaz and Atakor Intraplate Cenozoic Volcanism (Central Hoggar, South of Algeria)

Zakaria Boukhalfa[1], Abderrezak Bouzid[1] and Amel Benhallou[1]

[1]Centre de Recherche en Astronomie, Astrophysique et Géophysique (CRAAG), BP63, Route de l'Observatoire, Bouzereah, Algiers, 16340, Algeria, boukhalfa.zakaria@yahoo.com

SUMMARY

Volcanism occurs in several distinct geological settings. Most of these are associated with tectonic plate boundaries. In contrast, a relatively small number of volcanoes occur within plates far from their margins. The crustal and lithospheric mantle structure of such continental intraplate volcanic systems are enigmatic and the origins of volcanic activity remain controversial, which is due in part to a lack of high-resolution geophysical data. In Algeria, the intraplate volcanism is well presented in the Hoggar massif which belongs to the Tuareg shield. This region is associated with a lithospheric swell of about 1000 km in diameter in relation with the Cenozoic volcanism occurring in several regions. The origin of this activity is nowadays debated. The Atakor/Manzaz region is located in the center of the swell. In order to define its deep structure, broadband magnetotelluric (BBMT) data from 40 stations along three intersected profiles were collected. The BBMT soundings are scattered across an area approximately 170km from east to west, and 80 km from north to south. We performed 3-D inversion of full impedance tensor and vertical magnetic field transfer function. The obtained model exhibits very complex electrical features. It highlights three electrical levels reflecting the crust and the uppermost lithospheric mantle. The upper crust is mainly dominated by a sharp resistant structure interrupted by several conductors related to the known shear zones of the area, while the middle-to-lower crust shows a very conductive character, the whole set is underlined by more or less conductive part which materializes the uppermost lithospheric mantle. The architecture formed by the conductive bodies at different depths in this model, is reminiscent of the plumbing system, and known as the Flower Structure in geology.

Keywords: Intraplate volcanism, Broadband magnetotelluric (BBMT), Flower structure.

Abstract, 25th EM Induction Workshop, Çeşme, Turkey, September 11-17, 2022

Electrical resistivity structure beneath the southern Tohoku, Northeast Japan, inferred from a joint inversion of magnetotelluric and geomagnetic transfer functions

D. Diba[1], M. Uyeshima[2], M. Ichiki[3], S. Sakanaka[4], M. Tamura[5], and Y. Usui[6]
[1]Earthquake Research Institute, the University of Tokyo, dieno@eri.u-tokyo.ac.jp
[2]Earthquake Research Institute, the University of Tokyo, uyeshima@eri.u-tokyo.ac.jp
[3]Graduate School of Science, Tohoku University, masahiro.ichiki.b5@tohoku.ac.jp
[4]Graduate School of International Research Sciences, Akita University, sakanaka@gipc.akita-u.ac.jp
[5]Research Institute of Energy, Environment, and Geology, Hokkaido Research Organization, tamura-makoto@hro.or.jp
[6]Earthquake Research Institute, the University of Tokyo, yusui@eri.u-tokyo.ac.jp

SUMMARY

Significant in-land activities in southern Tohoku are implications of the ongoing subduction system in Northeast Japan. Knowing that fluids play an essential role in arc magmatism and the associated seismicity, this study is intended to understand the deep subsurface fluids distribution beneath the southern Tohoku to clarify the origin of the in-land activities. A magnetotelluric survey delineating the subsurface electrical resistivity structure is suitable for this purpose because bulk resistivity is sensitive to the composition and connectivity of fluids. Time-varying electric and magnetic field data were recorded at 15 stations along a profile line. The frequency-domain response functions of the measured fields were interpreted to yield a two-dimensional electrical resistivity structure using a newly developed joint inversion code. In addition to the commonly used response functions, the inter-station horizontal magnetic field transfer function was also considered to determine the regional trend and estimate the electrical resistivity structure. The result shows that in the southern Tohoku, especially beneath the survey line, a fluid-rich area is located under the back-arc side instead of the volcanic front. This understanding comes after inversion reveals an upper mantle – middle crustal conductor between a back-arc volcano and the volcanic front, well-correlated with a swarm of deep low-frequency events. The bulk conductivity of the conductor could be explained by some degree of partially molten rock and saline water originating from the upwelling flow above the subducting slab. In addition, a surficial, inclined conductive body is found on the back arc, the boundary of which is very consistent with the eastward dipping reverse fault of the Tsukioka fault zone.

Keywords: electrical resistivity structure, magnetotelluric method, geomagnetic transfer function, inversion, subduction zone

Crustal Structure beneath East Himalayan Syntaxis and the Relation to its Rapid Uplift and Exhumation

Hao Dong[1,2*], Jialin Qi[1], Sheng Jin[1,2], Gaofeng Ye[1,2] and Wenbo Wei[1,2]
[1]China University of Geosciences, Beijing,
[2]State Key Laboratory of Geological Process and Mineral Resources, Beijing
*donghao@cugb.edu.cn

SUMMARY

The unique East Himalayan Syntaxis (EHS) is featured with a sharp U-turn of all geological boundaries, geomorphic features and river systems at the east end of the Himalayan orogenic belt. The EHS is believed to be one of the regions with the strongest Cenozoic uplift and exhumation in Tibetan Plateau. Among the EHS, the most significant geomorphology feature is the Namcha Barwa (NB) peak, which rises abruptly to over 7700m from the surrounding Yarlung-Tsangpo canyon. The core Namcha Barwa area remains a high uplift rate since late Pliocene and forms a series of high-angle fault systems centered on EHS. To understand the mechanisms behind the rapid uplift of the study region, magnetotelluric array dataset were used to image the 3D electrical structure beneath the EHS. The inversion model reveals crustal high conductivity anomalies around the NB region, at the depth of 20-40 kilometers. The rapid uplift of the region may lead to decompression melts of the mid-to-lower crust, which is correlated with local leucogranites. The melts may provide the heat sources for the hydrothermal systems around Namcha Barwa. On the other hand, the crustal structure directly beneath NB is imaged as highly resistive NNE directed anomaly. This feature is consistent with previous regional magnetotelluric model and the high-velocity structure discovered by Rayleigh wave velocity results, but do not support the popular “tectonic aneurysms” model which involves crustal advective flows towards the topographic gap. The resistive “wedge” may reflect the northward intrusion of deep materials into the crust of the Lhasa block, which further induces the uplift of regional structure and the upwelling of hot materials at the front end. With the gradual intrusion of the wedge, the uplift may gradually expands to the northeast, forming the long and narrow compound anticline responses.

Keywords: East Himalayan Syntaxis, Namcha Barwa, Magnetotellurics, uplift and exhumation

Magnetotelluric investigations in south of Mexico to better understand the seismic hazard of the area.

Ruiz-Aguilar, D., Husker, A., Arango-Galván, C., Romo-Jones, J.M., García-Suárez, E., Constable, S.

As part of a collaborative project, we applied Magnetotellurics in the south area of Mexico to better understand its seismic hazard. In the framework of this NSF funded project, we propose an amphibous magnetotelluric sounding survey coupled with seismotectonic analysis to: (1) Determine differences in coupling/slip regimes in and around the Mexican Tehuantepec seismic gap; (2) Image the Tehuantepec Ridge within the subducted plate to determine its role in the coupling and if it contributes to the break between the Trans-Mexican Volcanic Belt (TMVB) arc system and the Chiapas arc; (3) Image any evidence of fluid infiltration in the Tehuantepec fault. The proposed study analyzes the unusually large Mw8.2 normal fault Tehuantepec earthquake which is downdip of a slab interface that has no recorded earthquakes. The proposed reasons for why the earthquake occurred are that it was due to slab pull below a strongly coupled interface or that it was due to slab bending along a reactivated, possibly fluid-filled and poorly coupled subducted outer rise fault. This study would represent the only physical measurement to directly determine which is correct and determine the link to possible future earthquakes. In this work, we present results of the MT land measurements that were recorded from January to March 2022. We used the long-period LEMI-424 systems that are provided by PASSCAL instrument center, and the MT Time Series were robust processed to estimate the MT transfer functions. A 3D inversion scheme was applied using ModEM and we present the obtained results.

Abstract, 25th EM Induction Workshop, Çeşme, Turkey, September 11-17, 2022

The Geometry of the Main Himalayan Thrust along the Satluj river valley, Northwest Himalaya, India retrieved from Magnetotelluric studies.

Authors: Dhamodharan S and Gautam Rawat

Abstract

The magnetotelluric (MT) data collected along the Nahan- Kourick-Chango transact in the Satluj river valley in the northwest Himalaya have been analysed to obtain subsurface resistivity structure. The objective is to study tectonics and the geometry of the major fault systems in the region. Dimensionality analysis of robustly estimated transfer functions indicates the distribution of electrical conductivity in the study area is complex specifically at low frequencies, whereas at middle and higher frequencies majority of MT responses are two-dimensional (2-D). Dimensionality and decomposition analysis recovers geoelectrical strike NE-SW striking with an angle of ~45° for the majority of responses. The geoelectrical strike coincides with the general trend of the major geological ruptures in the study area. The Non-Linear Conjugate Gradient (NLCG) algorithm was utilized to obtain the 2-D resistivity model of the study area. Near-surface resistivity distribution favours known geological findings of the medium to highly metamorphosed crystalline rocks of the Lesser Himalaya and Higher Himalaya. Shallow surface high conducting layer mapped throughout the profile, is characterized by the presence of trapped water/fluids expelled from the underthrusting sedimentary rocks. The Intra-Crustal Low Resistive Layer (IC-LRL) of the Himalayan wedge with a thickness of ~9 km marked with very low resistivity throughout the profile. The resistivity transition between the Indian basement and the base of the IC-LRL of the Himalayan wedge making the detachment or Main Himalayan Thrust (MHT) with a dipping angle of 3.5° in the Sub Himalaya, 6° in the Lesser Himalaya, and ramping with 21° to the south of the Munsiari Thrust and further dipping north-easterly with 5° at the north of the South Tibetan Detachment. Despite of some undulation in the scale, the observed geometry of the MHT with ramp structure in the present study is well reliable with the geometry of the MHT discovered by previous balanced geologic cross-sections in the study area and the adjacent Garhwal and Kumaun region.

Integrated geophysical study of the deep structure of Yenisei-Khatanga regional trough: new results and MTS contribution

E. Yu. Sokolova [1, 2], Bolshakov E.M.[2], Biserkin I.A.[1], Finkelshtein M.Ya.[1], I. S. Kupriyanov [1], Pimanova N.N.[1], Shirokova T.P.[1,3]

[1] All-Russian Research Institute of Oil Geology, Moscow, Russia, sokol_l@mail.ru

[2] Schmidt Institute of Physics of the Earth, Russian Academy of Sciences, Moscow, Russia,

[3] Moscow State University, Moscow, Russia, tpshirokova@yandex.ru

SUMMARY

The paper presents modern results of integrated interpretation of the data obtained by different geophysical methods in the region of Yenisei-Khatanga regional trough (YKRT) - oil and gas-bearing province located at Taimyr peninsular, the Northern frame of East Siberian platform. The regional stage of the geological-geophysical investigation of this hard to reach, remote but perspective province is going to the end. The goal of our study is to develop an integrated volume model of the deep structure of the trough as a basement for scientific forecasting in hydrocarbon prospecting. Solid ground for this model formation in its turn became the interpretation of the CCP seismic and MT soundings' data of the regional profile network (with attraction of several DSS geotraverses). This profile analysis was based on the results of gravity and magnetic fields' zoning, 2D and 3D geophysical (potential fields and MT) inversions and the classification of the main sedimentary and igneous rock formations by physical properties. This stage was finished by design of the spatial structural framework of the Mz sedimentary cover of the trough as well as underlain consolidated older crustal and upper-mantle layers. Then, this layered construction was endowed with material properties in the course of 3D inversions of gravity and magnetic field, constrained by profile seismic and MT data as well as 3D MT inversion (Slinchuk et al, 2022) results and geological information. Finally, layered distributions of density and magnetization with lateral inhomogeneities, which satisfy the observed potential fields, were restored for all the YKRT. The main instruments for potential fields' quality and quantity analyses were presented by geoinformation system INTEGRO developed in All-Russian Research Institute of Oil Geology RRIOG (Cheremisina et al., 2022), while MT data were inverted with a help of modern efficient open access codes.

The presentation of the course of geophysical YKRT model construction is focused on the contribution of magnetotelluric data to restoring the deep architecture of the through: identification of fault zones, fluidized areas and sedimentary grabens in profile sections, construction of the structural surfaces of the Pz formations and crystalline basement, as well as localization and determination of the morphology of magmatic formations of the period of geodynamic activation of the Pz-Mz boundary - buried intrusives and trap strata.

The information obtained is important for updating the structural-tectonic and geodynamic models of the YKRT – the main products of the regional stage of any oil and gas province investigations. Finally, we discuss the possibilities of using the results of the study as markers of the main stages of the YKRT formation associated with the evolution of the Khatanga local center of the Siberian superplume, as well as in the applied aspect – for searching potential hydrocarbon traps.

The authors are grateful to colleagues from Nord-West Ltd for providing unique magnetotelluric data for the integrated geophysical studies as well as for fruitful bilateral discussions of the results obtained. The research was carried out as part of state assignments of All-Russian Research Institute of Oil Geology and Schmidt Institute of Physics of the Earth, Russian Academy of Sciences.

Keywords: integrated interpretation of geophysical data, 2D and 3D inversions, deep architecture of oil and gas-bearing provinces, Yenisei-Khatanga regional trough, products of Siberian superplume activity

Mapping the geometry of volcanic systems with magnetotelluric soundings: results from a land and marine magnetotelluric survey performed during the 2018-2019 Mayotte seismovolcanic crisis

Mathieu Darnet[1], Pierre Wawrzyniak[1], Pascal Tarits[2], Sophie Hautot[3] and Jean-François D'eu[4]

[1]*BRGM – French Geological Survey, Orléans, France – m.darnet@brgm.fr or p.wawrzyniak@brgm.fr*
[2]*IUEM, Institut Universitaire Européen de la Mer, LGO, UMR 6538 - IUEM/UBO - pascal.tarits@univ-brest.fr*
[3] *IMAGIR Sarl, Saint Renan, France - sophie.hautot@imagir.eu*
[4] *MAPPEM Geophysics SAS, Saint Renan, France - jf.deu@mappem-geophysics.com*

SUMMARY

A major seismovolcanic crisis has afflicted the islands of Mayotte, Comoros Archipelago, since May 2018, although the origin is debated. Magnetotellurics (MT), which is sensitive to hydrothermal and/or magmatic fluids and can map the subsurface electrical resistivity structure, can provide insight by revealing the internal structure of the volcanic system. In this paper, we report the results of a preliminary land and shallow marine MT survey performed on and offshore the island nearest the crisis. The 3D inversion-derived electrical resistivity model suggests that the island is underlain by a shallow ~500-m-thick conductive layer atop a deeper, more resistive layer, possibly associated with a high-temperature geothermal system. At depths of ~15 km, the resistivity drops by almost two orders of magnitude, possibly due to partial melting. Further petrophysical and geophysical studies are underway for confirmation and to map the geometry and evolution of the volcanic system.

Keywords: magnetotelluric, electrical resistivity, seismovolcanic, geothermal

INTRODUCTION

Mayotte, located along a WNW-ESE oceanic ridge at the boundary of the Lwandle and Somalian plates, represents a region of islands within the volcanic Comoros Archipelago north of the Mozambique Channel between the northern tip of Madagascar and the eastern coast of Mozambique. The region of Mayotte is composed predominantly of two main islands, namely, Grande Terre (363 km2) to the west and Petite Terre (11 km2) to the east (figure 1).

In May 2018, an offshore seismovolcanic crisis initiated approximately 50 km to the east of Mayotte; the crisis included the largest seismic event ever recorded in the Comoros with a Mw=5.9 and an estimated 5 km3 of lava was released from an eruptive site in the same area (REVOSIMA bulletin, http://www.ipgp.fr/fr/actualites-reseau).
The seismicity subsequently migrated to the west and is now located between 5 and 15 km from the Petite Terre. The possible causes of the Comoros volcanism continue to constitute a topic of controversy (Lemoine et al., 2019), as its origin could be related to i) the presence of a hot spot, ii) lithospheric fractures, or iii) a combination of the two, i.e., regional extension in conjunction with asthenospheric processes. Forecasts regarding the evolution of this crisis remain very uncertain and require the gathering of additional geoscientific data, particularly geophysical data, to help understand the internal structure of the corresponding volcanic system.

In this paper, we present the results of an land and shallow marine Magneto-Telluric (MT) survey carried out during the seismovolcanic crisis of Mayotte.

MT DATA ACQUISITION AND PROCESSING

Due to its high degree of urbanization, Petite Terre island presents a challenging environment in which to perform passive electromagnetic (EM) measurements. To mitigate the impacts of ambient EM noise on the MT soundings, we deployed two MT stations on the most isolated parts of the island (sites L1 and L2) and one remote reference MT station on Grande Terre island (site L0), approximately 15 km away from Petite Terre (figure 1). We used ADU07 systems (Metronix, Germany) with unpolarizable Pb-PbCl2 electrodes (Wolf Ltd, Hungary) and MSF07 magnetic coils (Metronix, Germany). The sensors were oriented toward the north and east (x=north, y=east). MT recordings were performed synchronously for 4 days at both sites.

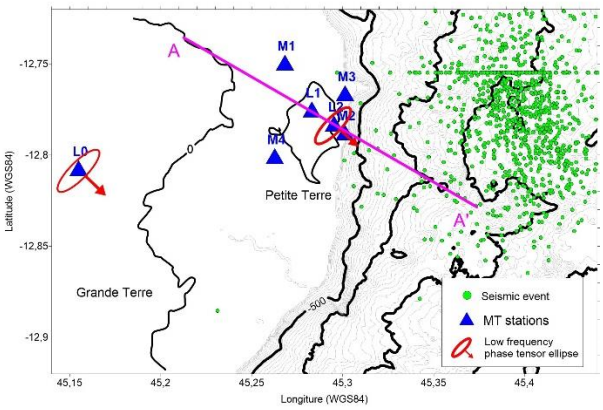

Figure 1. Location of the MT stations deployed onshore and offshore Petite Terre island. The blue triangles represent the MT sites. The green circles represent the epicenters of the seismic events recorded from May 2018 to May 2019. The red ellipses with an arrow represent the phase tensor ellipses at 1000 s at sites L0 and L2. Profile AA' is the location of the cross-section through the 3D resistivity model in Figure 3.

We processed the time series following the robust approach of Chave and Thomson. (2004) with a remote reference MT station. We computed the full impedance tensor at each site at periods ranging from 0.001 to 1000 s. An MT sounding example is shown in figure 2. Overall, the data were of good quality over the period range; however, at 1-10 s, noise could not be excluded due to the weakness of the primary field. The phase tensor ellipses shown in figure 1 were extracted from the phase tensors calculated using the formula of Booker (2014).

Because of the limited number of sites favorable for MT measurements on Petite Terre island, we deployed four new-generation low-power shallow marine MT systems (STATEM) around the island at water depths ranging from 15 to 25 m (figure 1). These STATEM systems were recently developed by MAPPEM Geophysics and the Ocean Geosciences Laboratory (LGO), European Institute for Marine Studies (IUEM). Each STATEM system records the two horizontal components of the electric field with 5m-long electric dipoles and marine Ag-AgCl electrodes. The three components of the magnetic field were obtained from a 3-component fluxgate sensor. With an optimized datalogger, the measurements were performed synchronously with the land stations for 2 days at a sampling rate of 512 Hz. The design of the system is such that motion of the system induced by oceanic current is minimized. During the survey, bidirectional tiltmeter measurements performed every second showed that motion and drift of the sensor were minimum (less than +/- 0.2 deg).

Similarly to the land case, the time series were robustly processed with the bounded influence, remote reference processing (BIRRP). The processing of shallow marine MT data is a challenging task due to the high level of ocean-induced EM noise that can mask the MT signal. For the electric field, noise can be generated not only by the movement of the water layer (e.g., waves, swells, tides) within the Earth's magnetic field but also by the current-induced motion of the electrodes. Similarly, magnetic field measurements can become contaminated by noise associated with not only ocean-induced electric currents but also the motion of the sensor. As a consequence, both electric and magnetic measurements may exhibit high levels of ocean-induced EM noise that is well correlated and difficult to distinguish from the MT signal. Therefore, the use of a land remote reference is of paramount importance to reduce the impacts of ocean-induced noise. Remote referencing between marine sites was sufficient at long periods (>100 s); hence, the challenge was to obtain the MT impedance at the shortest possible period (<0.1 s). Depending on the type of noise, magnetic and/or electric field measurements from the remote reference were used to filter out oceanic noise. An example of the MT transfer function is shown in figure 2. Despite the lack of high-frequency measurements (<0.01 s) due to the weakness of the MT signals recorded beneath ~20 m of seawater, the MT transfer function was reliably recovered over the 0.02 - 1000 s period band and was consistent with the nearby land site (site L2). Nevertheless, similar to the land data, the MT impedance results at 1-10 s were not reliable, as this period range is further impacted by a high level of swell-induced noise.

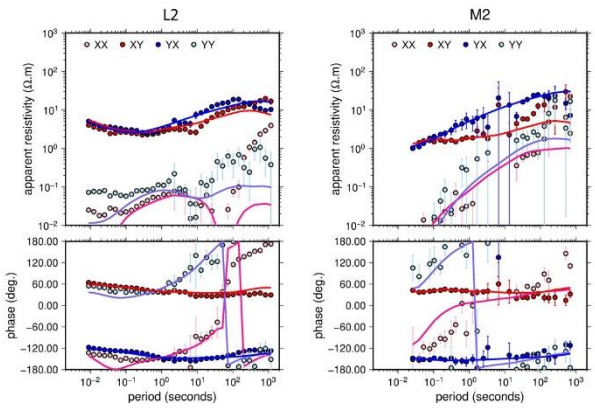

Figure 2. MT soundings for sites L2 (left panel) and M2 (right panel). The upper and lower panels display the apparent resistivity in Ohm.m and phase in degrees, respectively. The full lines signify the responses of the best-fitting model.

MT INVERSION RESULTS

The data recorded at the two land and the four marine MT sites were jointly inverted to image the electrical resistivity structure beneath Petite Terre island. We inverted the four components of the MT impedance tensors at all available periods; the period range for the land MT data was 0.009-1000 s, and that for the marine MT data was 0.02-1000 s. We excluded data with large errors, especially within the dead band. For the 3D inversion, we used the MININ3D code from Hautot et al. (2007). Given the small number of sites, we used a grid of 21x18x18 cells, which included the bathymetry of the study area. The total volume of the 3D model was 21x20x13 km3. The horizontal dimensions of the cells in the central part of the model is 500 x 500 m. The thickness of the layers increased from 5 to 5000 m. The 3D model topped a 1D model with three layers with thicknesses of 13, 38 and 88 km, whose resistivities were also included in the inversion. Except for the marine part (0.3 Ohm.m), the starting model was homogeneous (18 Ohm.m). The 3D inversion was applied to minimize a misfit function between the observed data and the 3D model response at all sites and frequencies weighted by the data variance. Data were the four complex components of the MT tensor. The starting RMS was 9.3, and the RMS decreased down to 2.2.

A cross-section through the shallow (until 5km depth) and deep (until 50km depth) section of the 3D resistivity model is shown in figure S2 and figure 3, respectively. The most prominent feature is the presence of a deep conductive layer (with a resistivity of less than 2 Ohm.m) beneath a depth of 13 km (labelled C1 on figure 3). A shallow conductive layer (resistivity of less than 5 Ohm.m) is also present within the first 500 m of the model (labelled C3 on figure S2). Between these two conductive structures, the resistivity increases up to ~100 Ohm.m. Toward the southeast, the resistivity in the 5-13 km depth range decreases to less than 10 Ohm.m (labelled C2 on figure 3); this conductor is located close to the hypocenters of the seismic events recorded during the seismovolcanic crisis.

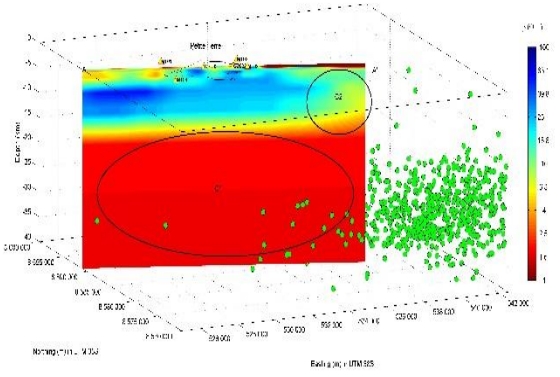

Figure 3. N120° cross-section through the 3D resistivity volume obtained from the inversion of the land and marine MT data. Green circles represent the hypocenters of the seismic events recorded from May 1, 2018, to May 28, 2019 \citep{lemoine2019volcano}. Yellow triangles represent the MT sites used in the MT inversion.

To assess the uncertainties in the deep resistivity structures identified in the 3D resistivity model, we performed a sensitivity analysis on both the resistivity of the conductive layer (below a depth of 13 km) and the depth to the top of this conductor (figure 4). The misfit rapidly increases with increasing resistivity below a depth of 13 km, confirming that a conductor of less than 4 Ohm.m is required to fit the data (figure 4a). The optimum depth of this conductor was found at approximately 16 km (figure 4b). However, the misfit increases slowly between this interval indicating that this depth is not very well resolved. We also tested the sensitivity of the model to the presence of the C2 conductor between depths of 5 and 13 km to the southeast of Petite Terre and on the edge of the MT network (figure 3). The absence of this conductor significantly increased the misfit (figure 4c), suggesting that this feature was not an artifact of the inversion process and was constrained by the MT data.

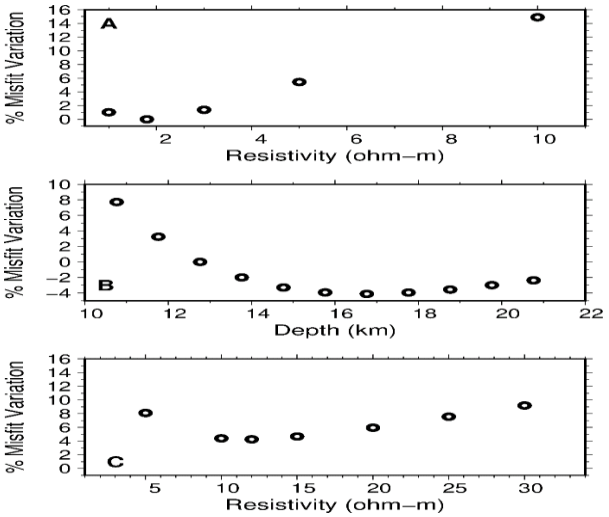

Figure 4. Variation of the misfit between the tested and preferred model as a function of a) the resistivity of the deep conductive layer, b) the depth of the top of this conductor and c) the presence of a conductor between 5 and 13km depth to the South-East of Petite Terre. The value 0 corresponds to the preferred model.

DISCUSSION

The presence of a shallow conductive layer overlying a more resistive body beneath the surface

of Petite Terre (labelled C3 in figure 3) is consistent with the electrical resistivity structure typically observed under volcanoes exhibiting well-developed hydrothermal systems (Flovenz et al., 2005). According to these models, this shallow conductive layer (resistivity of 1-10 Ohm.m) corresponds to a smectite-rich, low-temperature (<220°C), hydrothermally altered layer, often called a clay cap. For Petite Terre, this layer would be approximately 500 m thick. At greater depth and with increasing temperature (>220° C), the material is less rich in smectite, whereas the illite content increases. Furthermore, porosity tends to decrease with depth, which reinforces the modeled resistivity increase due to the change in alteration products with resistivity values ranging from 20 to 100 Ohm.m. On Petite Terre, such values are observed below depths of 500 m and deeper and could correspond to a high-temperature geothermal reservoir.

At depths of 13-16 km, the resistivity drops by almost two orders of magnitude, reaching values of a few Ohm-meters (labelled C1 on figure 3). These low resistivities could be caused either by the presence of altered rocks saturated with fluid below the supercritical point (<400°C) or by the presence of a small fraction of connected melt. At these depths, the temperature exceeds the supercritical point; hence, the most likely explanation for the observed conductive layer is the presence of melt. Similar observations have been reported beneath oceanic ridges on the basis of MT soundings (Baba, 2006) and interpreted as being indicative of the presence of melt (Laumonier et al., 2017). Nevertheless, additional laboratory data (e.g., electrical resistivity measurements on Mayotte volcanic rock samples) and geophysical observations (e.g., seismic tomography) are necessary to confirm this interpretation.

Finally, we noticed the presence of a conductive structure in the 5-15 km depth range to the southeast of Petite Terre (labelled C2 on figure 3) close to the seismic events recorded between May 2018 and May 2019. In this area, recent volcanic material and gas emissions have been observed on the seafloor. Accordingly, this conductive anomaly could be related to recent seismovolcanic activity. Additional deep marine MT sites are currently being deployed in this area to obtain more insight into the presence and geometry of this conductive anomaly and its relationship with the regional seismovolcanic activity. Furthermore, the land stations at sites L0 and L2 are currently being monitored continuously to perform robust-processing of the deep marine MT sites but also long-term monitoring of any resistivity changes at depth related to the evolution of the seismovolcanic crisis.

Conclusions

Since May 2018, a major seismovolcanic crisis has affected the islands of Mayotte in the Comoros Archipelago, providing a unique opportunity to monitor the development of an active volcanic system. Preliminary MT data acquired on and near this island were implemented to image the electrical resistivity structure of the volcanic system. The resulting model suggests the presence of hydrothermal fluids in the shallow part of the system (< 2 km) and magmatic fluids at greater depth (> 15 km). Further petrophysical and geophysical studies (e.g. additional land and offshore MT surveys, seismic surveys) are ongoing to confirm the origin and geometry of these deep conductors and to help better understand the associated magmatic and volcanic activity.

Acknowledgements

We would like to thank the General Directorate for Risk Prevention (DGPR) for financially supporting the geophysical work.

References

Baba, K., Chave, A.D., Evans, R.L., Hirth, G., Mackie, R.L., 2006. Mantle dynamics beneath the east pacific rise at 17 s: Insights from the mantle electromagnetic and tomography (melt) experiment. Journal of Geophysical Research: Solid Earth 111.

Booker, J.R., 2014. The magnetotelluric phase tensor: a critical review. Surv. Geophys. 35, 7–40.

Chave, A.D., Thomson, D.J., 2004. Bounded influence magnetotelluric response function estimation. Geophys. J. Int. 157, 988–1006.

Flóvenz, Ó., Spangenberg, E., Kulenkampff, J., Árnason, K., Karlsdóttir, R., Huenges E., 2005. The role of electrical interface conduction in geothermal exploration. In: Proceedings of the 2005 World Geothermal Congress. pp. 24–29.

Hautot, S., Single, R., Watson, J., Harrop, N., Jerram, D., Tarits, P., Whaler, K., Dawes, D., 2007. 3-d magnetotelluric inversion and model validation with gravity data for the investigation of flood basalts and associated volcanic rifted margins. Geophys. J. Int. 170, 1418–1430.

Lemoine, A., Bertil, D., Roullé, A., Briole, P., 2019. The Volcano-Tectonic Crisis of 2018 East of Mayotte, Comoros Islands

Laumonier, M., Farla, R., Frost, D.J., Katsura, T., Marquardt, K., Bouvier, A.S., Baumgartner, L.P., 2017. Experimental determination of melt interconnectivity and electrical conductivity in the upper mantle. Earth Planet. Sci. Lett. 463, 286–297.

Abstract, 25th EM Induction Workshop, Çeşme, Turkey, September 11-17, 2022

3D CSEM inversion data at Campos basin Brazil constrained by seismic and well log

A. Benevides[1], N. Meqbel[1], W. Lima[1], S. Fontes[1], G. Egbert[2], P. Werdt[1] and E. La Terra[1]

[1] Dept. Geophysics, Observatório Nacional Brazil, benevidesartur@gmail.com
[2] Oregon State University, Corvallis, egbert@coas.oregonstate.edu

SUMMARY

A set of 3D CSEM inversion runs of a real data in the Campos basin, SE Brazil is presented in this study. The Campos basin was formed during Neocomian (Cretaceous period 145–130 my) and its clastic reservoirs have been the largest oil producer in Brazil for the past three decades. This basin presents challenges in the exploration of clastic reservoirs due to the deeper waters and the complex geological configuration imposed by the tectonics associated with giant salt domes. Electromagnetic (EM) methods are sensitive to subsurface resistive variations and have been frequently used in exploration programs for hydrocarbon (HC). Reservoirs filled with HC are generally more resistive than the host rocks which is an advantage for EM method. Combining resistive models with seismic minimizes ambiguity in the interpretations and considerably improves the resolution of the subsurface structures and the geometry of the reservoir targets. In this study, a set of 40 EM receivers were deployed at the seafloor (water thickness around 1.7 km) in a grid-shape array varying spacing between 5 km to 10 km. The electric field components recorded from an active electromagnetic source towed 50 m above the seafloor was processed and generated signal in four frequencies: 0.125, 0.25, 0.5 and 1.25 Hz. Maximum polarization ellipses parameters obtained by rotating the horizontal electric components for the same transmitter azimuth is used as measured data during the inversion. For the 3D CSEM inversion we have used a modified version of the Modular System for EM inversion (ModEM code) which is under development within a research project at Observatório Nacional – Brazil. Preliminary resistivity model results yielded a good agreement with resistivity well logs. Strategies including seismic features as a-priori information has been analyzed and is showing improvements in resolution of the resistivity models.

Keywords: 3D CSEM inversion, Electromagnetic, Salt Structures, Campos basin

Abstract, 25th EM Induction Workshop, Kuşadası, Turkey, September 13-19, 2020

Comparing results from a new bottom-towed CSEM system against seismic and core data

Roslynn B. King[1,2], Amy Gusick[3], Steven Constable[1], Amy Gusick[3], and Jillian M. Maloney[2]

[1] Scripps Institution of Oceanography, University of California San Diego, California, USA, rbking@ucsd.edu, sconstable@ucsd.edu
[2] Department of Geological Sciences, San Diego State University, California, USA, jmaloney@sdsu.edu
[3] Department of Anthropology, Natural History Museum of Los Angeles County, California, USA, agusick@nhm.org

SUMMARY

Bottom-dragged marine EM systems minimize the attenuating effect of the seawater as well as achieve maximum coupling to the seafloor. Such systems have been developed to characterize and map the top tens of meters of the seafloor to study a range of targets from groundwater discharge to gas hydrates. However, the use of systems dragged across the seafloor is limited to settings that are heavily sedimented and without protective status. This limitation can significantly restrict potential survey areas as nearly 41 percent of U.S. marine waters have protected status and many offshore infrastructure projects require baseline studies during which the seafloor should not be significantly altered. To survey these regions, we are developing a controlled-source electromagnetic (CSEM) system that minimizes impact on the seafloor and is sensitive to the upper 50 meters of the subseafloor. The new CSEM system can be deployed in culturally and biologically sensitive regions and is designed to resolve small (~3 meter wide and 20 cm thick) subtle targets. The system is neutrally buoyant, flying between 1 to 2 meters above the seafloor, with a small counterweight to minimize impact on the seafloor. The system is made up of a transmitter that doubles as a depressor weight and three receivers for a final array length of 40 meters. The transmitter emits a waveform between 1 to 5 amps on a 2-meter horizontal electric dipole which is received by triaxial receivers. From preliminary results, the system can resolve the porosity of the shallow subseafloor with good agreement with seismic and core data. Initial inversions generated from a survey offshore California, USA indicate significant improvement in resolution from the new CSEM system when compared to surface-towed CSEM systems. Here, we will present results from 3 case studies testing the sensitivity and resolution of the new CSEM system.

Keywords: Marine CSEM; Near seabed resistivity; Resolution

Multi- EM surveying and data analysis for deep-sea seafloor massive sulfide exploration

K. Schwalenberg[1], H. Mueller[1], U. Barckhausen[1], and the INDEX Exploration Team
[1] BGR - Federal Institute for Geosciences and Natural Resources, Hannover, Germany,
katrin.schwalenberg@bgr.de

SUMMARY

Deep-sea hydrothermal vent fields associated with the formation of seafloor massive sulfides (SMS) may become a future source of high-tech minerals such as Cu, Ni, Pb, Co, and REE, which are all demanded for the energy transition away from hydrocarbon resources. The identification and evaluation of the-deposits in the deep ocean is a needle in a haystack problem. They are relatively small (size of a soccer field) and form in complex terrain at mid-ocean ridges, island arcs and back-arc spreading centres. The plume of active hydrothermal systems can be traced in the water column; however, active hydrothermal vents have an abundant, environmental sensitive fauna and low mineral potential. Inactive and extinct vent sites are generally missing characteristic seafloor expressions such as black smokers and distinct vent fauna, and may be hidden under a thin layer of sediments. An important aspect in mineral resource assessment is the inner structure and spatial extent of the SMS deposits, in particular their dimensions in depth, which can be addressed by geophysical methods.

In addition to magnetic and bathymetric surveying, we have collected a variety of marine frequency domain CSEM loop data and electric dipole-dipole data (DC conductivity, induced polarisation and self potential) over active and inactive hydrothermal vent fields associated with seafloor massive sulfides in the German licence areas located in the Indian Ocean. The data have been collected using BGR's unique deep-sea GOLDEN EYE CSEM profiler and newly acquired tandem Vulcan E-field receivers for self potential measurements. First results from the most recent cruise in 2021 indicate several anomalous features in the data that agree well with previously known, visually identified sulfide occurrences. The interpretation of the data is challenged by the complexity of the terrain and navigation issues. In our presentation we will give an overview of the current status of the data analyses and discuss our next steps to derive the 3D structure of the subseafloor mineral deposits.

Keywords: marine electromagnetics, seafloor massive sulfide exploration

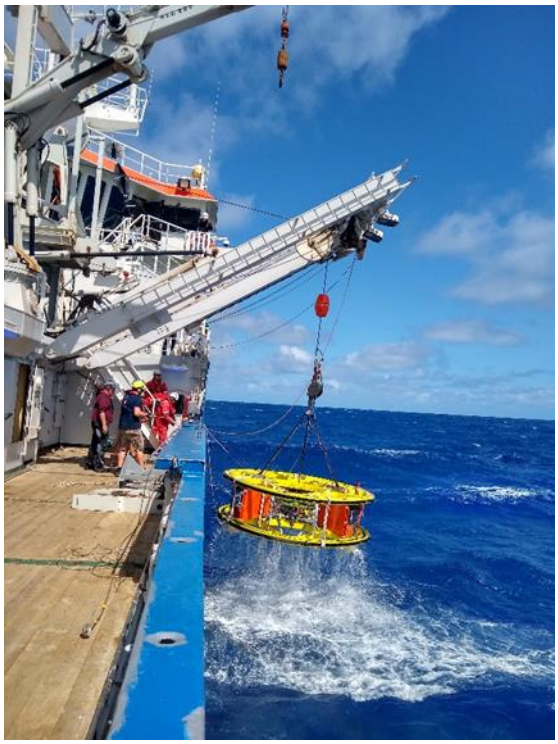

Figure 1. Left: Golden Eye recovery on RV Pelagia. Top: Vulcan E-field receiver being deployed at the aft deck.

Abstract, 25th EM Induction Workshop, Çeşme, Turkey, September 11-17, 2022

Characterizing Offshore Freshened Groundwater in a Carbonate Shelf Using Integrated Geophysical and Geochemical Analysis: A Case Study from the Maltese Islands

Zahra Faghih[1], Amir Haroon[1], Marion Jegen[1], Christian Berndt[1], Bradley A. Weymer[2], Konstantin Reeck[1], Thomas Müller[1], Mark Schmidt[1]
& OMAX Scientific Party

[1]GEOMAR Helmholtz Centre for Ocean Research Kiel, Germany
[2]Shanghai Jiao Tong University, China

SUMMARY

Coastal carbonate lithologies host considerable quantities of potable freshwater worldwide. However, the continuation of the terrestrial aquifers across the coastline into the marine realm, or the existence of carbonate-hosted offshore freshened groundwater (OFG) in general, are poorly constrained. Distribution, geometry, volume as well as the controlling factors of freshened groundwater beneath the present-day seafloor remain uncertain in many places across the world. To investigate whether freshened groundwater can exist offshore a semi-arid carbonate coastline like Malta and assess if such resource has the potential to serve as an alternative unconventional source of drinking water is addressed within a joint project between University of Malta and GEOMAR Helmholtz Centre for Ocean Research Kiel. Presently, OFG has been documented in coastal embayments and continental shelves worldwide. Geophysical studies carried out in Israel, New Zealand, Malta and the United States of America provide good examples of how integrating geophysical approaches and borehole data constrain the spatial extent of OFG systems, as well as provide estimates on the salinity of the pore-water. Here, we present an integration of marine controlled source electromagnetic (CSEM) data with 2-D seismic reflection profiles, core samples, geochemical data and borehole measurements targeting OFG along a carbonate shelf offshore the Maltese Islands. Electrical resistivity models derived from 2-D inversion of CSEM data identify a resistive anomaly (> 10 Ωm) offshore the northeastern coast of Gozo. If this resistivity anomaly is associated with a groundwater body at a depth of ~ 300 m below sea level or, alternatively, caused by lithological variability is discussed through an integrated geophysical model using 2-D resistivity models, multi-channel seismic reflection data and in-situ geochemical measurements. Preliminary results show that the resistivity anomalies indicate an OFG body located within the seafloor east of Gozo which extends northeastward. Furthermore, hydrogeological modeling is planned to quantitatively characterize the potential OFG system offshore Maltese Islands.

Keywords: Offshore Groundwater, Controlled Source Electromagnetics, Carbonate Margin, Integrated Geophysics

Abstract, 25th EM Induction Workshop, Çeşme, Turkey, September 11-17, 2022

The dependence of the tsunami electromagnetic signals observed at islands on the subsurface resistivity

R. Shibahara[1], T. Minami[2]
[1]Kobe University, Japan, 225s414s@stu.kobe-u.ac.jp
[2]Kobe University, Japan, tminami@port.kobe-u.ac.jp

SUMMARY

The electromagnetic (EM) field variations due to large tsunamis have been observed at seafloor stations and land ones close to coastlines. If the subsurface resistivity affects the tsunami EM signals, the phenomena could be applied to investigation of the resistivity structure as well as prediction of tsunami arrivals and heights. As for tsunami EM signals at the flat seafloor, Shimizu and Utada (2015) revealed that the EM field variations due to long waves are less affected by the subsurface resistivity. However, the dependence of the EM field observed at land and island stations has not been clarified and needs further investigation.

In this study, we investigated the subsurface resistivity dependence of the tsunami EM singles on island by numerical calculations for the following two cases. In Case 1, plane waves propagate in a flat seafloor with a constant depth and passes through a simple conical island; in Case 2, the 2011 Tohoku tsunami reached Chichijima Island. In both cases, we assumed a simple semi-infinite homogeneous resistivity structure below the island and the adjacent seafloor, and calculated the tsunami EM signals using the TMTGEM tsunami EM simulation code (Minami et al. 2017). In the EM field calculations for Case 1, we tested several radii of the island and three homogeneous subsurface resistivities of 1000,100, and 10 Ωm. We found in the result of Case 1 that the amplitude of the magnetic vertical component (Bz) varies by a maximum of 10% and the electric horizontal component (Eh) does by a maximum of 40%, in terms of those for 1000 Ωm. The variations in the amplitude were not so affected by the radius of the island. In Case 2, the case of Chichijima, we used the fault model of the 2011 Tohoku earthquake estimated by Tatehata et al. (2015) as the tsunami source for tsunami simulation and tested three subsurface resistivities in the same manner as Case 1. The results of Case 2 show that the amplitude of Eh varies by a maximum of 60%, and that of Bz varies by a maximum of 30%, in terms of those for 1000 Ωm. The results both in Case 1 and 2 indicate that the tsunami-generated Eh on the island is affected by the subsurface resistivity and may be possible to utilize in exploring the resistivity structure of islands. We succeeded in explaining the dependence of the amplitude of Eh on the subsurface resistivity by a simple stationary parallel circuit model. The stationarity of the circuit model accounting for the simulation results implies that the tsunami-generated electric field variation observed at islands are explained by the stationary process, and that the resistivity structure below the island could be explored by the tsunami electric sounding.

Keywords: tsunami, island, resistivity, simulation, FEM

Revisit of the mantle electrical structure beneath the Tristan da Cuna hotspot by using a 3-D inversion based on non-conforming deformed hexahedral mesh

Singh, R.K.[1], Baba, K.[2], Usui, Y.[3], Grayver, A.[4], Jegen, M. [5], Morschhauser, A.[6], Geissler, W.[7], Matzka, J.[8] , Haroon, A.[9] and Kuvshinov, A[10]

[1]ERI, The University of Tokyo, roshan@eri.u-tokyo.ac.jp

[2]ERI, The University of Tokyo, kbaba@eri.u-tokyo.ac.jp

[3]ERI, The University of Tokyo, yusui@eri.u-tokyo.ac.jp

[4]ETH, Zürich, agrayver@ethz.ch

[5]GEOMAR, Helmholtz Centre of Ocean Research Kiel, mjegen@geomar.de

[6]GFZ, Potsdam, mors@gfz-potsdam.de

[7]AWI, Helmholtz Centre for Polar and Marine Research, Wolfram.Geissler@awi.de

[8]GFZ, Potsdam, jmat@gfz-potsdam.de

[9]GEOMAR, Helmholtz Centre of Ocean Research Kiel, aharoon@geomar.de

[10]ETH, Zürich, kuvshinov@erdw.ethz.ch

SUMMARY

The Tristan da Cunha islands are located 450 km east of the Mid-Atlantic Ridge and 60 km north of the Tristan da Cunha transform fault, and fracture zone system in the Atlantic Ocean. The islands are products of intraplate hotspot volcanism. However, several controversies are associated with theories for the origin of the Tristan da Cunha hotspot. Previous magnetotelluric data 3-D inversion results based on finite-difference algorithm couldn't image plume-like vertical structure, unlike many geological and geochemical studies (Baba et al., 2017). In this study, we revisit the electrical structure of the region by inverting combined vertical magnetic transfer functions and the MT responses from seafloor stations around the islands and those newly obtained on the Tristan da Cunha and Nightingale islands. The topographic effect is one of the keys to obtaining a more reliable subsurface structure, and therefore, we use two finite-element-based inversion methods of Usui (2021) and Grayver (2015). For inversion analysis, we compared the topographic responses from these methods and a finite-difference-based forward modeling method (Baba & Seama, 2002; Baba & Chave, 2005) used in the previous study (Baba et al., 2017). The responses for sites with minimum topography effects are almost identical from all the three methods except for some sites where difference is observed in shorter periods. This could be due to the difference in the mesh resolution around the sites. The responses for sites with significant topography effects show a reasonable match for the finite-element methods in longer periods. In contrast a significant difference is observed in responses from all three methods for short periods. The comparison of modeled responses proves the applicability of Usui's inversion scheme to MT data from this region. In the workshop, the inversion results from Usui's inversion method will be presented.

Keywords: Non-conforming deformed hexahedral mesh, Finite-element, Marine magnetotelluric

Imaging deep resistivity in 3D in coastal areas and volcanic islands: Toward a multi-method and multi-scale approach combining land and shallow water passive and active EM

F. Bretaudeau[1], S. Védrine[1,2], P. Tarits[2], J-F d'Eu[3], Q. Daverdisse[3], N. Coppo[1], P. Wawrzyniak[1], S. Hautot[4], F. Dubois[1], E. Civallero[1], F. Beaubois[1], Y. Legendre[1], M. Darnet[1]

[1]BRGM (French Geological Survey), f.bretaudeau@brgm.fr
[2]GEO-OCEAN UMR6538, University of Western Britany, France, pascal.tarits@univ-brest.fr
[3]Mappem Geophysics, France, jf.deu@mappem-geophysics.com
[4]IMAGIR Sarl, France, sophie.hautot@imagir.eu

SUMMARY

3D resistivity imaging with Electromagnetic (EM) methods is commonly used in volcanic context. It is particularly useful to characterize geothermal reservoirs, thanks to the sensitivity of resistivity of the variation of types and levels of alteration (mapping clay cap to delineate reservoir). However, application of EM exploration techniques on coastal areas of volcanic islands can be challenging due to the high level of anthropogenic noise, proximity to the sea/land interface, strong variations in topography and near-shore bathymetry, and near-surface heterogeneities.

Magnetotellurics (MT) is the historical method and the only one capable of sounding at very large depths (>3km). But anthropogenic noise related to urbanization often limits its performances and therefore often restricts its use to quiet areas and coarse mesh surveys. Controlled Source EM in land, with the use of powerful active current source and lighter recording systems is an interesting alternative to overcome anthropogenic noise and increase data coverage and resolution close to populated or industrialized zones, but is more limited in depth (0-2km). Finally, Airborne EM shows limited investigated depth (0-300m) but can provide very dense coverage in the near surface poorly sampled by CSEM and MT.

Furthermore, all those methods are now quite common in land, but their use along the coast and in particular in shallow water is not obvious and almost never considered, whereas there is no reason for coastal geothermal reservoirs to be limited by the coastline. The two main reasons are: (1) costs and availability of deployment of adapted coastal /shallow water equipment (2) difficulty of modeling and inversion processing of the EM data considering accurately the topography, bathymetry and land/sea high resistivity contrast.

We try to summarize here the progress made in recent years to try to overcome those limitations and provide deep resistivity models of geothermal reservoirs bellow coastal areas on volcanic islands, based on the feedback from various coastal MT and CSEM surveys. We discuss the improvement provided by:

1) adapted instrumentation for shallow water MT
2) adapted instrumentation and protocols for land/shallow water CSEM
3) optimized processing of marine MT
4) 3D accurate modeling including topography/bathymetry and coastline
5) Marine shallow electrical resistivity mapping
6) 3D inversion of multi-method multi-scale workflow of MT/CSEM and including shallow resistivity

We illustrate the potential of this multi-scale multi-method approach with a large campaign conducted over the operated Bouillante geothermal field in Guadeloupe in the French Lesser Antilles, where a joint land/marine CSEM/MT + AEM + marine streamer was conducted in 2021-2022.

Keywords: Coastal EM, Volcanic islands, geothermal exploration, MT, CSEM, AEM, multi-method, multi-scale, joint 3D inversion

Links between slab mantle dehydration and forearc seismogenic zone structure in the Shumagin Gap, Alaska using magnetotelluric imaging

D. Cordell[1], S. Naif[2], R. Evans[3], K. Key[4], S. Constable[5], D. Shillington[6], and A. Bécel[7]
[1]Georgia Institute of Technology, dcordell6@gatech.edu
[2]Georgia Institute of Technology, snaif3@gatech.edu
[3]Woods Hole Oceanographic Institution, revans@whoi.edu
[4]Lamont-Doherty Earth Observatory, Columbia University, kkey@ldeo.columbia.edu
[5]Scripps Institution of Oceanography, sconstable@ucsd.edu
[6]Northern Arizona University, donna.shillington@nau.edu
[7]Lamont- Doherty Earth Observatory, Columbia University, annebcl@ldeo.columbia.edu

SUMMARY

Fluids in subduction zones influence many important geological processes as the hydrated incoming plate lithosphere (i.e. slab) releases pore-bound and chemically-bound water into the over-riding crust and mantle wedge. In particular, fluids released from the slab beneath the forearc seismogenic zone are thought to create conditionally-stable regions which have strain-dependent slip behavior and may control megathrust rupture. The Shumagin Gap is unique along the Aleutian arc for its paucity of historical megathrust (>8 Mw) rupture nucleating in the gap. Geodetic data suggest that gap is weakly-coupled relative to adjacent segments. The reasons for the weak coupling and lack of megathrust rupture are unclear. Furthermore, the adjacent Semidi segment ruptured in July 2020 with Mw 7.6 and propagated into the Shumagin Gap. To examine the role of fluids, marine magnetotelluric (MT) data were collected along a 250 km trench-perpendicular profile in 2019 as part of the Electromagnetic Alaskan GeoPRISMS Experiment. The resulting 2-D resistivity model contains a conductor near the plate interface and is correlated with a wide-band of reflectors from seismic studies, seismicity, and the July 2020 rupture patch. This suggests that fluids play an important role in controlling the slip behavior in the Shumagin Gap. The source of the fluids at the plate interface is commonly thought to come from the downgoing slab crust. However, the MT results indicate a significant slab mantle conductor >15 km below the slab Moho, directly beneath (and connected to) the conductor at the plate interface. This suggests that deeper slab mantle serpentinization may reach pressure-temperature conditions conducive to dehydration beneath the forearc seismogenic zone. This provides an additional source of forearc fluids not previously considered in subduction zone water budgets which can modulate slip behaviour.

Keywords: magnetotellurics, subduction zone, seismogenic zone, dehydration, Alaska

Abstract, 25^{th} EM Induction Workshop,Çeşmeı, Turkey, September 11-17, 2022

Modelling 3D coast effects in marine magnetotelluric data using edge-based finite element method

Jianbo Long, Shunguo Wang

jianbo.long@ntnu.no; shunguo.wang@ntnu.no
Norwegian University of Science and Technology (NTNU), Trondheim, Norway

SUMMARY

Magnetotelluric method has been an important method in investigating offshore geologic structures in a variety of applications. Previous studies have shown that coast distortion can affect measurements over a great distance. Often, 2D models are used in marine magnetotelluric studies, partly because the 2D assumption is acceptable in test regions and partly because 3D tools are unavailable. Here, we have developed a vector finite element based modelling code to study the 3D coast effect. Initial test results have confirmed the modelling accuracy and we are now able to analyze 3D coast effects over more complex scenarios.

Keywords: marine magnetotellurics, coast effect, finite element, modelling

INTRODUCTION

Coast and bathymetry effects are the primary terrain-related distortions when interpreting marine magnetotelluric (MT) data. In some experiment environments such as mid-ocean ridges, the underlying earth model may be approximated as a two-dimensional (2D) conductivity model where the conductivity does not change along the strike direction (i.e., ocean ridges). In this case, MT data analysis is commonly separated into that of transverse electric (TE) mode and transverse magnetic (TM) mode.

Coast effect does not just affect the close region of continental margin, but can propagate to a long distance (Worzewski et al, 2012). In the TE mode of the 2D scenario, the effect is due to the induction coupling between the coast and the rest of the earth model (i.e., sea water and sea floor) since the electrical current flows in parallel to the strike direction and no electric charges are built on conductivity interfaces. In the TM mode, in addition to the induction, galvanic diffusion of the electromagnetic (EM) field will also play a part in distorting the MT measurements. In both modes, these distortions can be indicated by the existence of abnormal apparent resistivity values and phase changes, which have been well observed in field (e.g., Key and Constable, 2011) and in numerical modellings (e.g., Santos et al, 2001; Worzewski et al, 2012; Wang et al, 2019).

In the three-dimensional (3D) scenario, it is reasonable to expect that both induction and galvanic diffusions will be present. In addition, unlike the relatively flat seafloor surface around mid-ocean ridges that can often be approximated as 2D models, 3D coastal lines are much more ubiquitous. These factors present a very challenging but important question: how can the coast distortions be recognized (and then removed if possible), or be taken into consideration in interpreting 3D MT data ?

Here, we have developed a 3D finite element modelling code in the hope that it will allow us to accurately model the coast effects on marine MT data, thus allowing us to better recognize 3D coast effects in real data. The code utilizes unstructured tetrahedral meshes which allow for efficient and accurate representation of coastal lines and bathymetry.

MODELLING CODE

Our finite-element based forward modelling code is developed using modern FORTRAN features and

can compute both 2D and 3D MT responses using unstructured meshes. 2D triangular and 3D tetrahedral meshes are used in this study and are generated using software Triangle (Shewchuk, 1996) and Tetgen (Si, 2015), respectively.

EQUATIONS AND BOUNDARY CONDITIONS

Common equations solved in the modelling include electromagnetic potential equations and the Helmholtz equation for electric field, $\mathbf{E}$ or magnetic field, $\mathbf{H}$. To best model the coast distortion in the MT data, we have chosen the $\mathbf{E}$-field equation. This is because the coastal lines can extend to a great distance making the vertical surfaces of a 3D model as essentially 2D models, as shown in Figs 1 and 2.

On 2D boundary surfaces, electric charges will accumulate when the external electric field is parallel to the surfaces (similar to the TM mode of a pure 2D model), giving rise to possible discontinuities in EM potential functions. In this case, specifying boundary EM field values will be much easier than specifying potential function values. Boundary $\mathbf{E}$ field values are from solving 2D modelling problems over the 2D boundary surfaces.

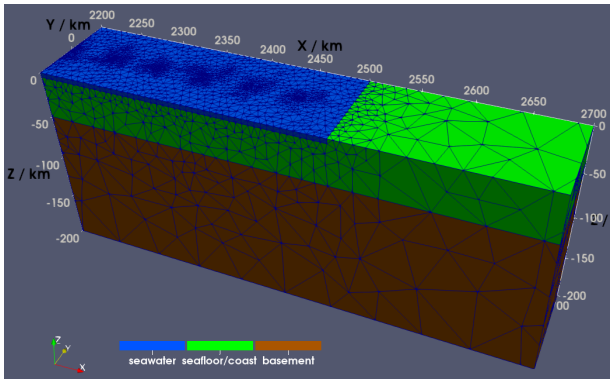

Figure 1: Example 3D tetrahedral mesh of part of the test 3D marine conductivity model with a vertical coast at x = 2500 km. Vertical boundary surfaces in the $x-z$ plane are 2D surfaces.

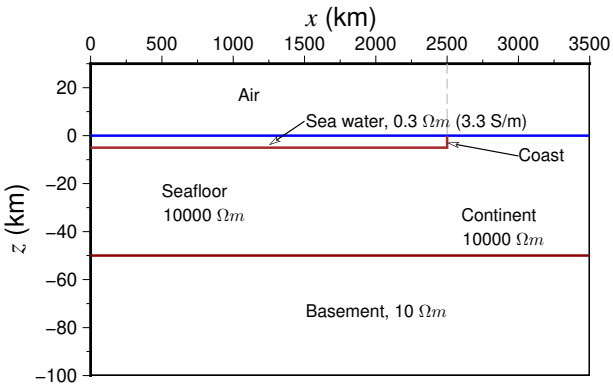

Figure 2: Corresponding 2D conductivity model of the 3D model shown in Fig1. Sea water layer has a thickness of 5 km and conductivity of 3.3 S/m.

EXAMPLE MODELLING RESULT

Our initial test model, which is shown in Figs 1 and 2, is a relatively simple 3D marine model with only 3 conductivity regions: sea water (3.3 S/m), seafloor (1.e-4 S/m) and an asthenosphere basement (0.1 S/m). The coast boundary is located at x = 2500 km. The sea water has a depth of 5 km. The top of the conductive basement is at z = -50 km. These parameters are taken from the example model from Wang et al (2019). A series of frequency value ranging from 1.e-5 Hz to 0.5 Hz was used to test the modelling. The actual computational domain of this test extends from x = -500 km to x = 4000 km in the horizontal direction and from z = -200 km to z = 80 km in the vertical direction. Due to the use of unstructured meshes, we were able to locally refine the mesh around regions of interest.

Since the conductivity contrast between sea water and the coastal region is high, large coast effect can be expected at measurements along sea floor. The calculated 3D impedance tensor, expressed in apparent resistivity and phase values, is shown in Fig 3 at site x = 2050 km, y = 0 along the seafloor (1 meter above seafloor), which is 450 km away from the coastal line.

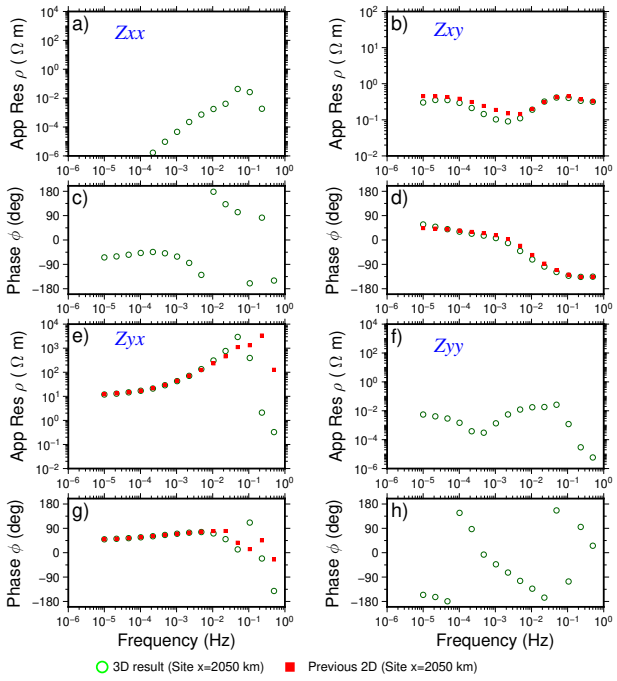

Figure 3: Apparent resistivity and phase values of 4 components of impedance tensor calculated at the site x = 2050 km (see Fig 2). Previous 2D result is from Wang et al (2019)

The 3D result is seen to be in good agreement with the 2D results previously presented in Wang et al (2019), with the latter only having TE (corresponding to Zyx here) and TM mode (corresponding to Zxy here) impedance components. Since this model is essentially the "3D version" of that 2D marine model from Wang et al (2019), the diagonals of the impedance tensor are expected to be trivial, as shown by the very small values of Zxx and Zyy here. The larger errors at high frequencies of the results, particularly in Zyx, are due to limited size of mesh used in the test.

Further vector $\mathbf{E}$ field flows are plotted in Fig 4 for the polarization mode of having the MT source $\mathbf{E}$ field parallel to the $x - z$ plane (i.e., TM mode in a 2D case). The vertical section of the plot is at $y = 0$. Results similar to previous 2D modellings are observed here. For example, there are only dominantly downward flows of current density in the resistive seafloor at low frequency, but at high frequency, downward flows of current density near the coast are seen upward flowing back to the sea water, causing coast effect at great distances away from the coast line.

Conclusions

3D coast effects are expected to be more complex than the 2D case. Our finite-element based modelling code for 3D coast effects has been initially tested and shown to be capable of accurately modelling the effect. More complex 3D marine conductivity models, possibly with bathymetry information, will be tested in the next stage.

Acknowledgments

The study was funded by the Norwegian Research Council (294404, 309960, and 324442) and the National Infrastructure for High-Performance Computing and Data Storage in Norway (nn9872k).

References

Key K, Constable S (2011) Coast effect distortion of marine magnetotelluric data: Insights from a pilot study offshore northeastern Japan. Physics of the Earth and Planetary Interiors 184(3-4):194–207

Santos FAM, Nolasco M, Almeida EP, Pous J, Mendes-Victor LA (2001) Coast effects on magnetic and magnetotelluric transfer functions and their correction: application to MT soundings carried out in SW Iberia. Earth and Planetary Science Letters 186(2):283–295

Shewchuk JR (1996) Triangle: Engineering a 2D quality mesh generator and Delaunay triangulator. In: Workshop on Applied Computational Geometry, Springer, pp 203–222

Si H (2015) TetGen, a Delaunay-based quality tetrahedral mesh generator. ACM Transactions on Mathematical Software (TOMS) 41(2):11

Wang S, Constable S, Reyes-Ortega V, Rychert CA (2019) A newly distinguished marine magnetotelluric coast effect sensitive to the lithosphere–asthenosphere boundary. Geophysical Journal International 218(2):978–987

Worzewski T, Jegen M, Swidinsky A (2012) Approximations for the 2-d coast effect on marine magnetotelluric data. Geophysical journal international 189(1):357–368

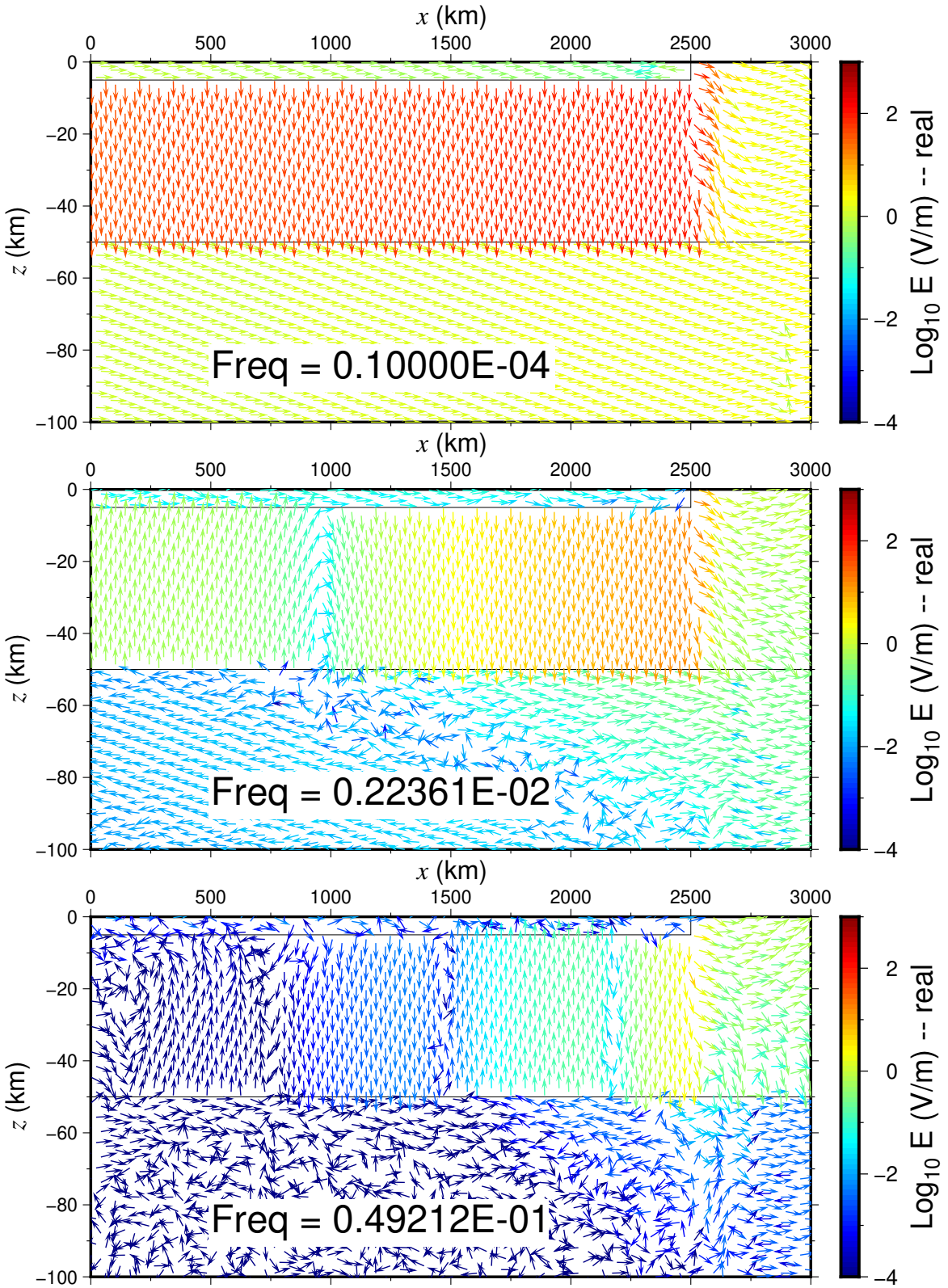

Figure 4: Calculated vector $\mathbf{E}$ field distribution in the $x-z$ plane with $y = 0$ from the 3D model at three different frequencies. Only real part of $\mathbf{E}$ field is shown. At frequencies f = 2.23e-3 Hz and f = 0.049 Hz, some vector arrows of the field become more random than others; this is due to insufficient modelling accuracy caused by limited element sizes of the mesh in those regions. Current density flows follow the same of $\mathbf{E}$ field.

Abstract, 25^{th} EM Induction Workshop,Çeşmeı, Turkey, September 11-17, 2022

Multi-Data Inversion Approach for Retrieving Rock Properties from Measurements on Drill Cuttings

J. H. Börner[1], V. Herdegen[2], J.-U. Repke[3] and K. Spitzer[1]
[1]Institute of Geophysics and Geoinformatics, Technical University Bergakademie Freiberg, Germany; jana.boerner@geophysik.tu-freiberg.de
[2]Institute of Thermal, Environmental and Natural Products' Process Engineering, Technical University Bergakademie Freiberg, Germany
[3]Process Dynamics and Operations Group, DBTA, Technical University Berlin, Germany

SUMMARY

Electromagnetic methods can be of great value in monitoring applications (e.g. for geothermal energy, carbon dioxide sequestration, enhanced oil recovery, natural gas discharge zones) due to their sensitivity to reservoir fluids and their properties. Quantitative evaluation of monitoring data requires knowledge of reservoir-specific petrophysical relationships. As sample material for establishing these petrophysical relationships, drill cuttings are often the only rock material available from deep formations due to related high costs and time-consumption of coring. Therefore, estimating various formation properties from cuttings is a common task. However, for physical rock properties like complex electrical conductivity this formation property retrieval is challenging.

We therefore systematically investigated the electrical and structural properties of four different carbonate rocks and one sandstone in both crushed (8 different particle sizes, between 0.03 mm and 10 mm particle size) and plug form with a vast set of methods at normal conditions: complex-valued electrical conductivity, NMR, mercury intrusion porosimetry, nitrogen adsorption, XRD, μCT, scanning electron microscopy. By means of the huge data set we are able to quantify the pore-space, surface and electrical properties as functions of particle size, understand their relations, differentiate between intra- and inter-particle responses. The samples show significant variation in their electrical conductivity depending on salinity, porosity, pore-space heterogeneity and – due to the peculiarities of the crushed samples – the organization of particles in the packing.

We present a three-level model for the crushed rock material, which accounts for particle size and inner structure. Based on this model, it is possible to computationally recover the corresponding properties of the original, undisturbed formation. We realize this by means of a multi-data inversion of complex electrical conductivity, specific surface and porosity data for each rock. The presented inversion approach allows for utilizing the available drill cuttings, while maintaining the direct connection to the original rock.

Keywords: Electrical rock conductivity; Petrophysical joint inversion; Microstructures

Abstract, 25th EM Induction Workshop, Çeşme, Turkey, September 11-17, 2022

Comparative 3D inversion of magnetotelluric phase tensors and impedances reveals electrically anisotropic base of Gawler Craton, South Australia

K. Tietze[1,2,3], S. Thiel[1,2], K. Brand[1,2,4] and G. Heinson[2]
[1] Geological Survey of South Australia, Department for Energy and Mining, Adelaide
[2] School of Physical Sciences, University of Adelaide
[3] Now at: Helmholtz Centre Potsdam - GFZ German Research Centre for Geosciences, Telegrafenberg, Potsdam,
[4] Now at: Australian Space Weather Forecasting Centre, Bureau of Meteorology, Adelaide
kristina.tietze@gfz-potsdam.de

SUMMARY

Isotropic three-dimensional (3-D) inversion has become a standard tool in the interpretation of magnetotelluric (MT) data. 3-D anisotropic inversion codes are under development, yet the number of unknowns increases by a factor of 6 rendering the problem extremely ill-posed. Presence of anisotropy is usually inferred from (i) spurious sequences of conductive and resistive bodies or (ii) comparison with two-dimensional anisotropic modelling approaches.

Here, we investigate the 3-D structure of the Gawler Craton down to ~250 km depth using 282 sites of the AusLAMP array located in the southern half of South Australia. Inversions of the MT impedance as phase tensors and real and imaginary parts result in diverging structures at depths > 70 km. We demonstrate that a unifying model which explains all data types similarly well is suggestive of an anisotropic resistivity structure at the base of the Gawler Craton lithosphere at depths of 120-210 km. Depth location and orientation of the anisotropy agrees well with results from analysis of seismic receiver functions. We suggest that electric anisotropy in the Gawler Craton is a result of lattice-preferred orientation of olivine crystals and metasomatic processes with macroscopic preferential orientation.

Our results illustrate that inversion of phase tensor data is superior for the direct imaging of anisotropic resistivity contrasts in otherwise isotropic resistivity models; inversion models obtained with impedances may miss such structures. 'Comparable' overall RMS misfits are often meaningless when comparing inversion results for various data types since sensitivities differ between data types. Reliable inversion results consistent with the entire data set can only be recovered if data fits are assessed systematically for all data representations. We also discuss the influence of error settings for phase tensors on the inversion.

Our study also revealed that, if persistent across large areas, (i) parallel orientation of phase tensor major axes, (ii) constantly high phase tensor maximum phases or (iii) diverging directions of phase tensor major axes and induction arrows are suggestive of anisotropic structures and corresponding hypotheses should be evaluated.

Keywords: Give 1 to 5 keywords

Electrical monitoring of dynamic drainage and imbibition processes in rock-fluid-gas systems

Martin Sonntag [1], **Jana Börner**[2], **Volker Herdegen** [3], **Franz Grahl** [3], **Klaus Spitzer** [2]
[1] **TU BAF, Institute of Geophysics and Geoinformatics, msonntag@geophysik.tu-freiberg.de**
[2] **TU BAF, Institute of Geophysics and Geoinformatics**
[3] **TU BAF, Institute of Thermal-, Environmental- and Resources Process Engineering**

SUMMARY

Understanding physico-chemical interactions and quantification of reaction kinetics during dynamic processes in multi-phase systems and their impact on the electric conductivity can help to interpretation EM-monitoring data. Therefor a multistage experimental setup was developed and performed on different reactive and non-reactive rock-fluid-gas systems.
The results shows that the real part of the el. conductivity decreases by about -90% in the dewatered states and after imbibition the el. conductivity increases differently depending on material and measuring height. A combination of reactive materials show the strongest conductivity changes after cycles of dynamic processes.

Keywords: Spectral Induced Polarization, carbonate rocks, non-equilibrium condition

ABSTRACT

Carbonate rocks host large fossil oil and natural gas deposits and are targets for Enhanced Oil Recovery and Carbon Capture and Storage applications. Although electromagnetic methods can be used for monitoring. The understanding of the electrical properties of carbonates is still incomplete due to their heterogeneous pore space and reactivity towards aqueous phases, especially in the presence of CO_2 (dissolution and precipitation processes).
Therefore, a systematic multistage experimental procedure was developed as well as the successful realization of test series on different multiphase systems for electrical monitoring and characterization of dynamic processes.
In each case, a combination of sand or carbonate as rock matrix, and nitrogen or CO_2 as gas component was used for the individual experiments. Thus, the combinations of rock matrix and gas can be divided into subsystems with different degrees of reactivity.
It can be seen that the carbonate systems show a strong response to the pressure increase, depending on their chemical reactivity potential. The sand systems, on the other hand, show no reaction to the pressure increase (inert matrix). The subsequent dynamic processes can cause significant changes in the characteristics of the complex conductivity spectra, where the chemical reactivity of the individual components plays an important role.

The results help to understand the physicochemical understanding and quantification of the reaction kinetics during long-term surface aging of carbonate rocks exposed to CO_2. A model-based relationship between complex electrical properties and long-term reaction kinetics for named conditions supports geoelectrical monitoring and enables prediction of parameter contrasts.

REFERENCES

Journal article

Börner J.H. et. al. (2017) Spectral induced polarization of the three-phase system CO_2 - brine - sand under reservoir conditions. Geophysics 208, Issue 1: p289–p305

Börner J.H. et. al. (2015) The electrical conductivity of CO_2-bearing pore waters at elevated pressure and temperature: a laboratory study and its implications in CO_2 storage monitoring and leakage detection, Geophysics 203, Issue 2: p1072–p1084

WaxmanM, Smits L, (1968) Electrical conductivities in oil bearing shaly sands, Society of Petroleum Engineers Journal, Vol.8

Abstract, 25th EM Induction Workshop, Çeşme, Turkey, September 11-17, 2022

Imaging and inversion of potential field data, a case study for exploring Iron-bearing zones in Golgohar, Iran

Behrooz Oskooi[1], Pardis Mansourshoar[1], Maysam Abedi[2]

[1]Institute of Geophysics, University of Tehran, Iran

[2]School of Mining Engineering, College of Engineering, University of Tehran, Iran

Abstract

Imaging and inversion of potential field data give us an estimation of the source property distribution and it is a powerful tool which yields a fast 3D representation of the source distribution. The execution time of these approaches is substantially different. Imaging methods are characterized by fast computation, simplicity and the results are quantities proportional, but not the real physical properties, on the other hand, the inverse modeling can always determine the real physical parameters distribution but it is computationally expensive.

In this work we want utilize both approaches of the inversion and the Depth from Extreme Points (DEXP) of magnetic data for the Golgohar Iron mine located in the Sanandaj-Sirjan zone in the province of Kerman of Iran. First both approaches are compared for three synthetic scenarios corrupted by 3% of Gaussian noise; which are a single source, a single sloping source and a multi source of magnetic anomaly. This is needed for the investigation on its reliability for the practical application on the real data. Reconstructed models from synthetic data are in close association with the sought geometry. Ultimately, the approaches are applied for the interpretation of the real data and the results shows a high correlation between imaging and inversion in terms of the magnetic anomaly positions, horizontally and vertically.

Keywords: DEXP, Potential field data, Imaging, Inversion, Golgohar Iron mine.

Abstract, 25th EM Induction Workshop, Çeşme, Turkey, September 11-17, 2022

Imaging the weathering zone in Chile with active Radio-Magnetotellurics

Weckmann, U. [1], Cruces Zabala, J. [1], Patzer, C. [1, 2], Ritter, O. [1], Araya Vargas, J. [3]

[1] German Research Centre for Geosciences Potsdam - GFZ, Germany (uweck@gfz-potsdam.de)
[2] now at:Geological Survey of Finland (GTK), Finland;
[3] Universidad de Atacama (UdA) Copiapo, Chileffiliation, email contact

SUMMARY

The interdisciplinary DeepEarthShape project focusses on the weathering zone with drillings and a suite of geophysical, geochemical and geobiological approaches. The weathering zone is the uppermost part of the Earth's crust where rocks and soils experience breakdown either mechanically or chemically through the impact of air/gases, water and/or biological organisms. Weathered bedrock and soil belong to the life-sustaining, layer of the Earth's surface. Its thickness depends on the balance between erosion, removing weathered material from the surface, and weathering processes that deepen the interface between weathered and fresh bedrock. Although at shallow depths of 1 – 2 m appreciable amounts of microbial biomass and DNA counts were observed that might be related to weathering processes, our insight into the entire critical zone and its processes is still limited. We do not know for instance a) the depth of weathering; b) the process advancing it; c) whether this advance is driven by water, gases, and/or biological activity and concentrated along faults. Since some of the properties and characteristics of the weathering zone seem to be linked with climate, a set of four study sites is studies within the framework of the DFG Special Priority Program 1803 which belong to different climate zones and thus experience different vegetation, precipitation and erosion. However, the long-stretched coast of Chile represents a prime location to be exposed to these climatic differences but allows at the same time to stay in a similar geological/tectonic complex - the Coastal Cordillera. Therefore, we expect to compare the obtained results from the different study sites and finally test hypotheses concerning the weathering zone.
We utilised a combined geophysical approach using P- and S-wave seismics as well as Radio-Magnetotelluric (RMT) measurements along approximately 200 – 300 m long profiles at the study sites along the Chilean coast. Within the framework of the RMT experiment, we used our horizontal magnetic dipole transmitter in combination with a classical MT station nearby. Here, we will show and discuss 2D and 3D inversion results together with geophysical logging data from the drill holes and lab measurements of core samples. First results indicate that precipitation and shallow fluid enhanced zones e.g. in minor faults and folds can be traced and into the active weathering zone.

Keywords Weathering Zone, Radio-Magnetotellurics, Chile, magnetic dipole transmitter

Anisotropy estimation using 1D joint inversion of DC resistivity and CSRMT methods in the granite-gneiss terrains of Eastern Ghats, India

Akarsh Singh [1], Sudha Agrahari [2], Arseny Shlykov [3], Alexander Saraev [4] and Abhishek Yadav [5]

[1] Indian Institute of Technology, Kharagpur, India, singhakarsh100@gmail.com

[2] Indian Institute of Technology, Kharagpur, India, sudha@gg.iitkgp.ac.in

[3] St. Petersburg State University, Russia, shlykovarseny@gmail.com

[4] St. Petersburg State University, Russia, asaraev51@mail.ru

[5] Indian Institute of Technology, Kharagpur, India, abhishek47268@gmail.com

SUMMARY

The joint inversion of a galvanic and an inductive method is a standard procedure for the estimation of resistivity anisotropy of the subsurface. Other advantages of the joint inversion include the enhancement in the resolution and the *importances* of the model parameters obtained after the joint inversion. The joint inversion of the DC resistivity method and far-field CSRMT method is utilized to evaluate the resistivity anisotropy in the fractured granite-gneissic terrains of Eastern Ghats, Odisha, India. A table depicting the *importances* justifies the accuracy of the joint inversion. The interpreted results validate the inferences made from a borehole lithology in the area. The anisotropy in the subsurface is found to increase with depth and is more pronounced near the fractured horizons. Also, the magnitude of the anisotropy varies up to 15.

Keywords: Anisotropy, joint-inversion, DC resistivity, CSRMT

Introduction

Geophysical interpretation is always susceptible to ambiguity, which can be resolved to a degree by taking various measures like the inclusion of apriori information or resorting to a combination of several geophysical techniques. A good possibility for the joint usage of more than one technique is by concatenating the parameter, data, and the parameter sensitivity (Jacobian) matrices to utilize the advantages of all the individual methods involved.

In the standard DC resistivity surveys, the individual consecutive layers are assumed isotropic and homogeneous. However, in a scenario where multiple thin layers coexist inside a thicker stratum, the assumption of an isotropic layer no longer holds. The terminology macro- and micro-anisotropy are worth considering at this point. Maillet (1947) referred to the single electrical equivalent of a set of thin distinct resistive layers as a macro-anisotropic layer and termed the phenomenon macro-anisotropy. Nevertheless, the individual thin layers are quite discernible in the well-logging measurements (Shlykov et al. 2018). The other type of anisotropy, which originates from the preferential orientation of mineral grains (crystals) in the layer matrix, is called micro-anisotropy. This may also be due to the presence of certain flaky and platy minerals like biotite and amphiboles respectively.

Jupp and Vozoff (1977) first elucidated anisotropy estimation using the joint inversion of a resistive and an inductive method. They used a set of four coupled equations as shown below (Equations 1-4):

$$\rho_{DC} = \sqrt{\rho_V * \rho_H} \quad (1)$$

$$h_{DC} = h * \sqrt{\rho_V / \rho_H} \quad (2)$$

$$\rho_{MT} = \rho_H \quad (3)$$

$$h_{MT} = h \quad (4)$$

where, ρ_{DC}, ρ_{MT} and h_{DC}, h_{MT} are the resistivity and thickness detected by the DC and MT methods. ρ_V and ρ_H are the actual vertical and horizontal resistivity while h is the actual thickness.

These equations clearly show that the resistivity perceived by the DC resistivity method is the product of the vertical and the horizontal resistivities, while resistivity measured by the MT method (present case: CSRMT in a far-field zone) is purely horizontal. Also, the thickness is over-estimated in the resistivity method by a factor of the anisotropy coefficient $\left(=\sqrt{\rho_V/\rho_H}\right)$ of the layer while the thickness estimated by the CSRMT method corresponds to the true (geological) thickness.

The accuracy of the Marquardt inverted model parameters can be evaluated in terms of their *importances* (Jupp and Vozoff, 1975) which is presented at the end, for all the soundings. Sudha et al. (2014) defined *importances* for model parameter (m_i) as shown in equation (5)

$$Imp(m_i) = \sqrt{[(\boldsymbol{VT})(\boldsymbol{VT})^T]_{ii}} \quad (5)$$

where V is the parameter eigen vector matrix (or V-matrix) obtained from the singular value decomposition of the Jacobian matrix. T is the diagonal matrix having damping factors as its elements. *Importances* are a measure, of how well

the parameters are resolved. Their high values imply a major influence on the modeled data. (Vozoff and Jupp, 1975).

Geology of the study area

High-grade metamorphosed rocks of the Eastern Ghats Mobile belt (EGMB) are found in the study area. The area lies in the Archean-aged Charnockite-Migmatites-Khondalite province (figure 1). Due to the intense shearing and metamorphism, the rocks were highly fractured. The borehole (figure 2) displays fractured granite gneiss in the depth interval of 12-13 m. The successive layers were mostly coarse-grained granite-gneiss with the presence of feldspar veins for an interval of 1 m at 30.5 m depth and then the same rock without veins.

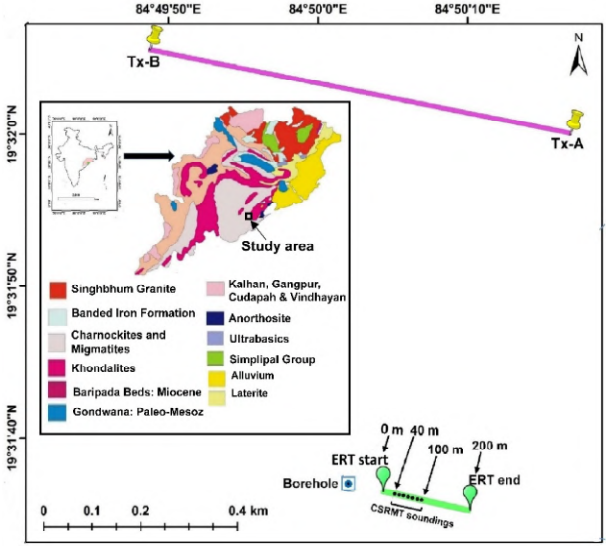

Figure 1. Study area map depicting the geology of Odisha (Mahalik, 1998) and the location of the DC resistivity and CSRMT soundings.

Instruments and Field experiment

The multi-electrode instrument ABEM Terrameter LS was used for 2D DC resistivity data acquisition in the Wenner-Schlumberger configuration using a 2x21-electrode protocol and 5 m inter-electrode spacing. The 1D data was extracted from the 2D acquired data at the profile distances (mid-points) from 40-100 m. Figure 1 depicts the location of the 2D resistivity profile and the CSRMT soundings.

SM-25 RMT-F receiver and a portable AC transmitter GTS-1 were used for CSRMT soundings (Saraev et al, 2017). The source was a grounded horizontal electrical dipole (HED) with 800 m length and a cluster electrode arrangement at each end. Two electric and three magnetic i.e. five channels were used in the receiver. A portable Gasoline generator powered the transmitter. The field experiment was carried out in the granite-gneissic terrains of the Eastern Ghats. Shallow clay layers provided good electrode connectivity. CSRMT data was acquired in the broadside configuration. The borehole was about 50 m WNW from the start of the ERT profile.

Frequency in the range of 1-1000 kHz was propagated from the transmitter. The data was recorded in the broadside direction of the HED. The far-field zone, which is least sensitive to vertical resistivity (Constable et al., 2010), lies in the broadside direction.

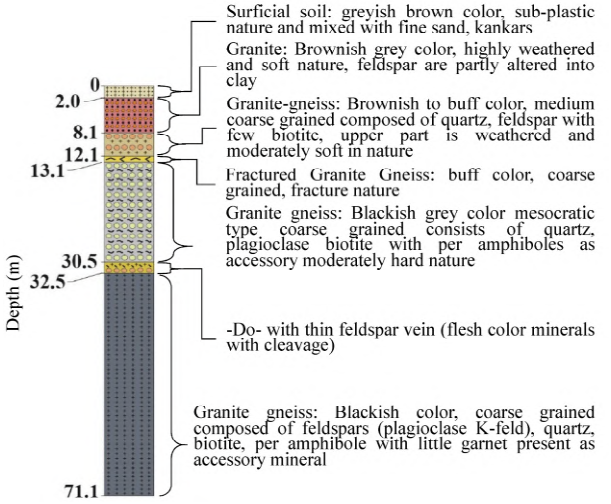

Figure 2. Borehole lithology from the study area.

Results

Single and joint inversion results of the sounding at a profile distance of 50 m have been displayed in table 1 and figure 4. The joint inversion results of seven CSRMT soundings coincident with 1-D DC resistivity soundings are shown in table 2 and figure 3. For the sounding at 50 m, the single DC resistivity inversion fitted most well for a three-layer model. For the DC method mean resistivity and the equivalent thickness are shown in table 1.

The parameter *importances* from the DC resistivity inversion are larger than 0.6. CSRMT method fitted better for the four-layer model and the horizontal resistivity and layer thickness parameters are found to be closer in magnitude to that obtained by the joint inversion. The *importances* obtained in the joint inversion are improved.

The variation of vertical and horizontal resistivity and anisotropy coefficient with depth for all soundings are shown in figure 3. The last layers in all the soundings are exhibiting a high anisotropy coefficient with the magnitude varying up to 10. However, the sounding at a profile distance of 90 m shows an anisotropy coefficient up to ~14 in the last two layers. The appearance of a high anisotropy coefficient (>4.0) below 10 m depth (figure 3c) conforms to the lithology (granite-gneiss) reported in the borehole.

Table 1. Inversion results along with the *importances* for the sounding at the profile distance of 50 m

method / param	DC Alone (ρ_{mean}, $h_{eq.}$)		CSRMT alone		Joint	
	model parameters	*importances*	model parameters	*importances*	model parameters	*importances*
ρ_{v1}	3.5	0.76			6.8	0.73
ρ_{v2}	10.0	0.63			4.8	0.17
ρ_{v3}	12.0	0.70			293.5	0.87
ρ_{v4}					1.4e4	0.11
ρ_{h1}			6.8	1.00	6.8	1.00
ρ_{h2}			1.7	0.89	1.7	0.92
ρ_{h3}			10.1	0.91	9.5	0.95
ρ_{h4}			142.7	0.96	140.2	0.96
h_1	1.8	0.63	1.2	0.97	1.2	0.98
h_2	11.4	0.72	1.3	0.66	1.2	0.80
h_3			8.2	0.95	7.8	0.96
RMS (%)	3.1		2.6 (ρ) 4.3 (ϕ)		2.5	

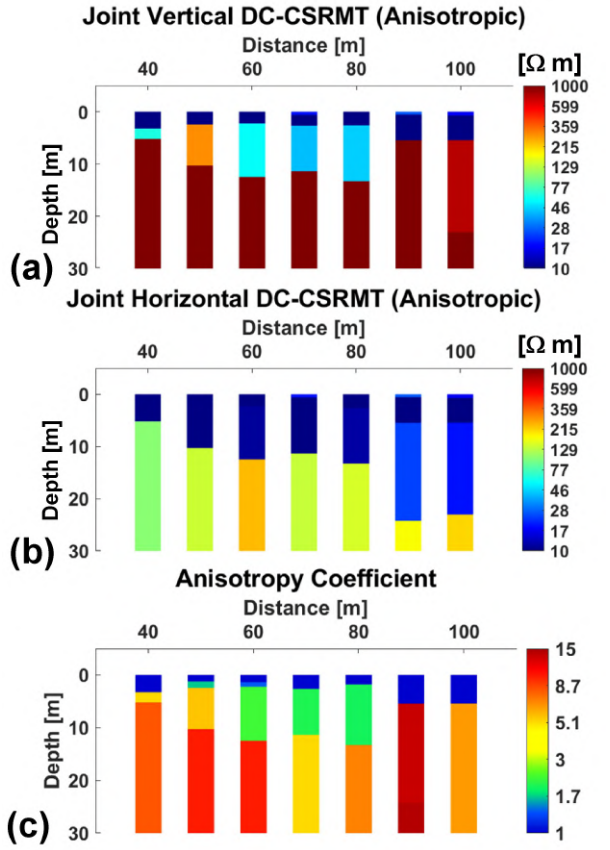

Figure 3. 1D joint inversion of DC and far-field CSRMT data: (a) vertical resistivity, (b) horizontal resistivity, and (c) Anisotropy coefficient.

Conclusions

Joint inversion of DC resistivity and far-field CSRMT data has successfully resolved the anisotropy present in the area. High anisotropy values (up to 15) have been observed in the deeper layers (>10 m). This might be due to the presence of fractured and foliated granite-gneiss rocks.

Acknowledgments

This work is done under the joint “DST-RFBR” project scheme with financial assistance from the “Department of Science and Technology, India, Project No: INT/RUS/RFBR/P-277” and the “Russian Science Foundation, project No 21-47-04401”.

References

Constable S (2010) Ten years of marine CSEM for hydrocarbon exploration. Geophysics, 75(5): 75A67-75A81.

Jupp DLB, Vozoff K (1975) Stable iterative methods for the inversion of geophysical data. Geophysical Journal International 42(3):957-976.

Jupp DLB, Vozoff, K (1977) Resolving anisotropy in layered media by joint inversion. Geophysical Prospecting 25(3):460-470.

Mahalik NK (1998) Precambrians. Geology and mineral resources of Orissa:43–81. SGAT Publ.

Raiche AP, Jupp DLB, Rutter H, Vozoff K (1985) The joint use of coincident loop transient electromagnetic and Schlumberger sounding to resolve layered structures. Geophysics 50(10):1618-1627.

Saraev A, Simakov A, Shlykov A, Tezkan B (2017) Controlled source radiomagnetotellurics: A tool for near surface investigations in remote regions. Journal of Applied Geophysics 146: 228-237.

Shlykov A, Agrahari S, Antaschuk K, Saraev A, Simakov, A (2018) Estimation of the anisotropy using CSRMT data in the transition zone of electric dipole. In 24th EM Induction Workshop, Helsingør, Denmark, August 12-19, 2018, At Helsingør, Denmark.

Sudha, Tezkan B, Siemon B (2014) Appraisal of a new 1D weighted joint inversion of ground based and helicopter-borne electromagnetic data. Journal of Applied Geophysics 62(3):597-614.

Vozoff K, Jupp DLB (1975) Joint inversion of geophysical data. Geophysical Journal International 42(3):977-991.

Table 2. Summary of the joint Inversion results along with the *importances* of all the soundings

sounding / param	40m		50m		60m		70m		80m		90m		100m	
	model parameters	*importances*	model parameters	*importances*	model parameters	*importances*	model parameters	*importances*	model parameters	*importances*	model parameters	*importances*	model parameters	*importances*
ρ_{v1}	3.9	0.37	6.8	0.73	8.2	0.81	19.0	0.71	8.5	0.93	26.3	0.87	17.0	0.41
ρ_{v2}	50.	0.14	4.8	0.17	3.4	0.09	3.1	0.24	6.3	0.13	3.6	0.43	3.9	0.25
ρ_{v3}	63.9	0.41	293.5	0.87	57.3	0.94	42.1	0.81	45.1	0.91	4356.9	0.36	786.7	0.83
ρ_{v4}	7326	0.13	14448	0.11	25147	0.09	3652	0.45	7310	0.27	37427	0.03	8771	0.11
ρ_{h1}	3.9	1.00	6.8	1.00	8.2	1.00	19.0	0.75	8.5	1.00	26.3	0.48	17.0	0.93
ρ_{h2}	5.0	0.75	1.7	0.92	1.8	0.83	3.0	0.98	1.6	0.80	3.6	1.00	3.9	1.00
ρ_{h3}	2.4	0.77	9.5	0.95	11.2	0.99	10.2	0.96	11.7	0.98	23.8	0.95	19.1	0.95
ρ_{h4}	106.3	0.99	140.2	0.96	241.6	0.96	137.3	0.94	149.4	0.97	173.8	0.71	212.4	0.71
h_1	1.9	0.76	1.2	0.98	1.4	0.98	0.6	0.93	1.8	0.99	0.5	0.97	0.7	0.98
h_2	1.4	0.60	1.2	0.80	0.8	0.65	2.1	0.91	0.8	0.64	4.9	1.00	4.8	0.99
h_3	2.0	0.78	7.8	0.96	10.2	0.99	8.7	0.97	10.7	0.98	18.7	0.90	17.6	0.94
RMS (%)	2.2		2.5		2.8		3.0		3.3		4.2		5.4	

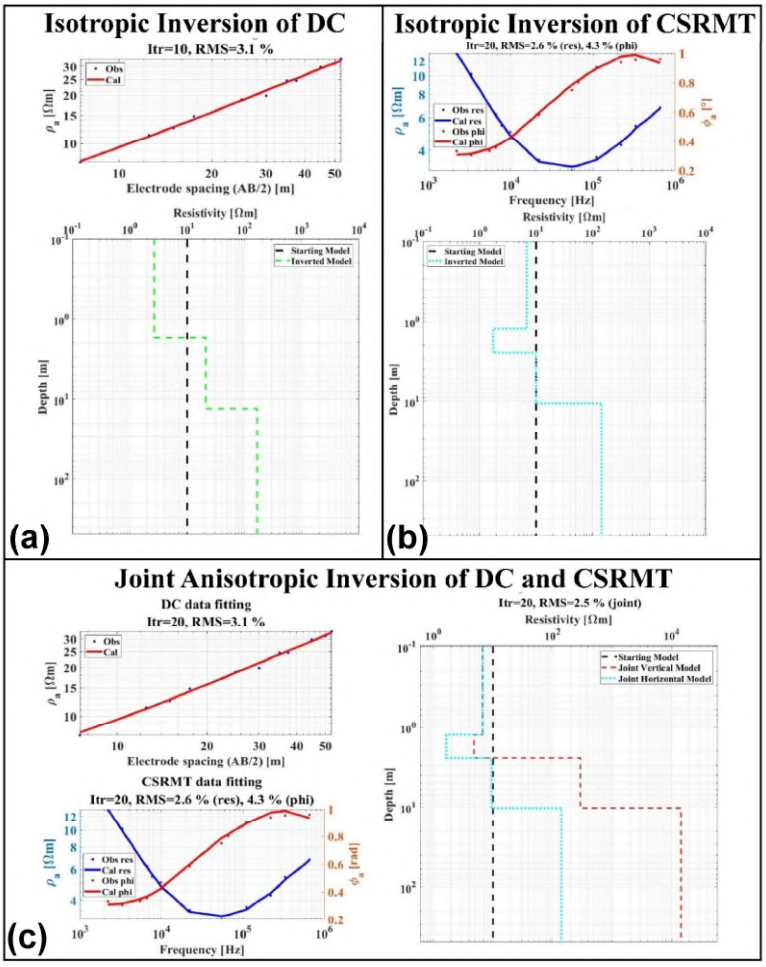

Figure 4. Single Isotropic inversion of (a) DC, (b) CSRMT. (c) Joint Anisotropic Inversion for sounding at 50 m.

Abstract, 25th EM Induction Workshop,Çeşmeı, Turkey, September 11-17, 2022

Global induction response to 11 year period and the conductivity of the lower mantle

S. Constable[1], C. Constable[1], M. Korte[2] and M. Morzfeld[1]
[1]Scripps Institution of Oceanography, USA, sconstable@ucsd.edu, cconstable@ucsd.edu, matti@ucsd.edu
[2]Deutsches GeoForschungsZentrum, Potsdam, Germany, monika@gfz-potsdam.de

SUMMARY

To date the electromagnetic response of Earth has been restricted to periods shorter than one year (with the exception of an estimate for the 11-year sunspot cycle by Harwood and Malin (1977)) because at longer periods the separation of the internal and external fields remains challenging. We adopt a simple approach to extracting the external P_1^0 variations and their inductive response from 117 years of hourly geomagnetic data from 192 observatories drawn from a recent compilation distributed by the British Geological Survey. Observatories were selected to be within 65° of the geomagnetic equator and data gaps of up to 48 hours were repaired using linear interpolation. Baseline corrections were made and the time varying International Geomagnetic Reference Field (IGRF) was removed from the data, which were rotated into geomagnetic coordinates year by year to allow for migration of the geomagnetic pole. Data were processed year by year by fitting hourly estimates of the internal and external coefficients of a P_1^0 field to the set of observatories that had no missing data for that year (a number that varies between 3 and 93), using one month overlaps between years to remove the small bias from year to year fits. Observatory years with excessive misfit were iteratively removed from the processing. Multi-taper spectral analysis and band averaging was used to estimate the power spectra and transfer functions between the two time series. A clear peak at the 11-year solar cycle appears in the external field spectrum, with a smaller but discernible peak at the first harmonic of 5.5 years, with associated peaks in the coherency spectrum. Error bars on complex admittance were estimated from the statistics of the cross-spectrum and a parametric bootstrap. The data can be fit to RMS 1.0 with a smooth Occam inversion model. A Bayesian inversion approach was also used, generating 10,000 models that fit acceptably well. A conductive core is seen in the models and is required by the data. The well-documented jump in conductivity between the upper and lower mantle is clearly seen, and a second jump in conductivity occurs at depth of 1,800 km.

Keywords: global induction, mantle conductivity, sunspot cycle

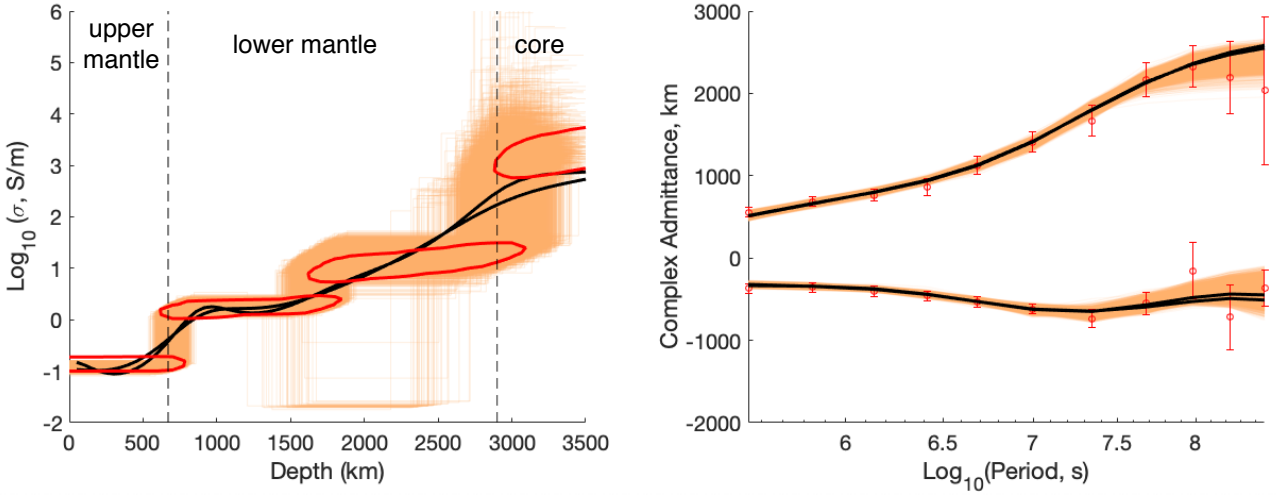

Figure 1: Inverted models, complex impedance data, and model responses. Orange lines are 10,000 4-layer models fitting between RMS 0.92 and 1.3. Black lines are Occam models and responses fitting to RMS 1.0 and 1.1. Red contours are the 95% bounds on acceptable model space.

Abstract, 25^{th} EM Induction Workshop,Çeşmeı, Turkey, September 11-17, 2022

Signatures of the global ocean circulation in geomagnetic secular variation and acceleration

C.C. Finlay[1], J. Velímský[2] and C. Kloss[1]
[1] DTU Space, National Space Institute, Copenhagen, Denmark, cfinlay@space.dtu.dk
[2]Dept. of Geophysics, Faculty of Mathematics and Physics, Charles University, Prague, Czech Republic, jakub.velimsky@mff.cuni.cz

SUMMARY

Changes in the global ocean circulation driven by winds and density gradients produce, via motional induction, time-varying geomagnetic signals. On long length and time scales these signals are hidden beneath larger core-generated signals but, due to their location at Earth's surface, on sufficiently short length scales and considering month to interannual timescales they could be detectable. Such signals would provide valuable information related to ocean circulation and conductivity variations. Here, we investigate this question using advanced forward simulations of the magnetic signals generated by (i) the oceans, using the ECCO v4r4 ocean circulation model and a realistic electrical conductivity model for the Earth's oceans, sediments, and upper mantle, (ii) the core dynamo, using an advanced numerical model that correctly simulates the relevant timescales of core processes (waves, advection etc.), and (iii) the ionospheric field, based on an empirical model derived from satellite measurements and scaled by the solar radio flux index. We use these to generate synthetic satellite observations on real Swarm orbits, and for simulated orbits of the proposed NanoMagSat mission. We find it is possible to recover ocean-generated secular variation (SV) and secular acceleration (SA) signals from 6 months of low-earth-orbit satellite data. It is expected that there will be significant benefits from using NanoMagSat data when considering shorter periods; further work is needed in this direction.

Keywords: global ocean circulation, motional induction, secular variations and acceleration

Abstract, 25^{th} EM Induction Workshop,Çeşmeı, Turkey, September 11-17, 2022

Limits of a-posteriori interpretation of electrical conductivity in terms of water content

O. Knopp[1]
[1]Dept. of Geophysics, Faculty of Mathematics and Physics, Charles University, Prague, Czech Republic, knopp@karel.troja.mff.cuni.cz

SUMMARY

Electrical conductivity profile of the mantle, derived from EM inversion, can be itself viewed as data for further interpretation. This interpretation in terms of the thermochemical state of the mantle rock can be obtained using Gibbs energy minimalization and experimental mantle rock electrical conductivity data. If we constrain the temperature and some dimensions of the chemical composition it is possible to obtain the water content from electrical conductivity. This inversion can have significant a-posteriori error margins. This is not only due to the a-priori error estimate of the electrical conductivity and the thermochemical data or the error of the forward problem derived from Hashin-Shtrikman bounds, but also due to the significant error of the experimentally derived mantle rock conductivity data. I would like to present a few examples of this local inversion and show how different errors are projected into the final a-posteriori distribution of the local water content.

Keywords: electrical conductivity, Gibbs energy minimization, mantle composition

Abstract, 25th EM Induction Workshop, Çeşme, Turkey, September 11-17, 2022

Regionality of mantle conductivity inferred from geomagnetic daily variation analysis

Takao Koyama[1], Shigeru Fujita[2], Ikuko Fujii[3], Kiyoshi Baba[4] and Hisayoshi Shimizu[5]
[1]Earthquake Research Institute, The University of Tokyo, tkoyama@eri.u-tokyo.ac.jp
[2]The Institute of Statistical Mathematics, sfujita@ism.ac.jp
[3]Meteorological College, Japan Meteorological Agency, ifujii@mc-jma.go.jp
[4]Earthquake Research Institute, The University of Tokyo, kbaba@eri.u-tokyo.ac.jp
[5]Earthquake Research Institute, The University of Tokyo, shimizu@eri.u-tokyo.ac.jp

SUMMARY

This paper report on regionality of the electrical conductivity of the global mantle, inferred from geomagnetic data analysis of daily variation. The mantle has a potential to reserve huge amount of water, and the electrical conductivity distribution can reveal water contents in the mantle. In this study, geomagnetic data of daily variation at 71 stations were analyzed, and a global distribution of the electrical conductivity in the mantle was detected. It is necessary to take into account the Sq field distribution, because the geomagnetic distribution of daily variation is complex, and it prevents a plane wave assumption. 71 stations, however, are still not enough to draw a Sq field with high resolution. Instead of it, the GAIA (Ground-to-topside model of Atmosphere and Ionosphere for Aeronomy) is used as the inducing field. The GAIA assimilates the meteorological reanalysis data (JRA-55) to the whole atmosphere-ionosphere coupled model and thus it is the well-modelled Sq field. First, we executed spherical harmonic expansion of the magnetic field of the GAIA for three-days time series, which correspond to sequent solar quiet days. Next, three-dimensional forward modeling in the spherical Earth was performed to compare with the observed geomagnetic data. Now, we suppose the one-dimensional structure in the Earth under the ocean-land lateral contrast. We tried several one-dimensional models and searched for the best-fitted model for each station. As the results, beneath Europe, the conductive model, in which the electrical conductivity exceeds 0.1 S/m in the upper mantle, is preferred. Conversely, the resistive model, in which the electrical conductivity is 0.01 S/m or less in the upper mantle, is likely beneath the northwestern Pacific. This difference may be derived from the water contents, which were carried by a subducting slab, because a maximum amount of water depends on the temperature of the slab.

Keywords: mantle conductivity, geomagnetic daily variation, Sq field, GAIA

Hunga-Tonga Hunga-Ha'apai Eruption lightning as seen by remote MT measurements in New Zealand and Japan

T. G. Caldwell[1], P. A. Jarvis[1], C. Noble[2], Y. Ogawa[3]

[1] GNS Science, New Zealand
[2] NZ Metrological Service, New Zealand
[3] Tokyo Institute of Technology, Japan

One of the astonishing aspects of the Jan-15 2022 Hunga-Tonga Hunga-Ha'apai (HTHH) eruption was the intensity of the volcanic lightning produced. Worldwide lightning detection networks recorded approximately $4x10^5$ lightning strokes centred on HHTH in 2 hours starting around 04:10 Jan-15th UTC. During the eruption, two continuously recording MT stations were operating on the east coast of New Zealand's North Island, approximately 2000 km from HTHH. These stations continuously record the magnetic field variations at a sample rate of 150 Hz using induction coils manufactured by Phoenix Geophysics. A similar recording site in Japan, about 8000 km from HHTH, was also operating during the eruption. The magnetic field signals in the 10^{-2} s to 1 s period range in both New Zealand (NZ) and Japan are tangentially polarized with respect to the direction of propagation from HHTH; consistent with the expected surface-guided electromagnetic-wave propagation in the resonant cavity formed by the earth and the ionosphere. The agreement between spectral-time plots of the MT data and lightning count-rate data recorded by the Vaisala Global Lightning Detection Network (GLD360) at HTHH is remarkably good.

The NZ and Japanese MT data indicate volcanic lightning associated with the main eruption commenced between 04:08 and 04:14 Jan 15th (UTC). This agrees with time estimates of the eruption initiation from visible satellite imagery and global seismic datasets. The intense electrical activity associated with the eruption lasted 2 hours, peaking about 50 minutes after onset. The NZ MT data also show that a less-intense burst of electrical activity first developed the day before the main eruption (Jan 13th), at about 17:00 UTC lasting about 0.5 hours. Later that morning, the Tongan Geological Service observed a towering eruption cloud with volcanic lightning at its margins. Additionally, a 0.7-hour-long episode of intense lightning occurred about 4.5 hours after the onset of the main eruption, indicative of a second significant eruption, also seen in satellite imagery and seismic data.

A remarkable feature of the eruption was the atmospheric pressure wave that propagated worldwide. Barometric pressure data recorded throughout NZ and on islands in the Pacific to the north and south of New Zealand shows that the origin time for the ‘detonation’ event that caused the pressure pulse occurred about the same time as the onset of lightning seen in the MT data. Such an energetic explosion suggests that large quantities of magma and seawater came into contact producing an eruption column that was water rich; conditions needed for ice formation and thus lightning production in the eruption column and in the high-altitude umbrella-cloud that spread outwards from the eruption centre.

Keywords: Hunga-Tonga Hunga-Ha'apai (HTHH), eruption, lightning, magnetotellurics

Abstract, 25^{th} EM Induction Workshop, Çeşme, Turkey, September 11-17, 2022

MagVector/MFX-2 – a Planetary Laboratory on the International Space Station (ISS): Electromagnetic Simulation and Inversion of Magnetic Field Data from Planetary and Asteroid Analogs

Jana Börner[1], Stefanie Garbade[2], Sarah Sophia Keßler[1], Detlef Konigorski[2], Volker Schmid[3], Lorenzo Schmitt[1], Carolin Schneider[1], Frank Sohl[4] and Klaus Spitzer[1]

[1] Institute of Geophysics and Geoinformatics, TU Bergakademie Freiberg, Germany, jana.boerner@geophysik.tu-freiberg.de, carolin.schneider@geophysik.tu-freiberg.de, sarah-sophia.kessler@student.tu-freiberg.de, lorenzo.schmitt@student.tu-freiberg.de, klaus.spitzer@geophysik.tu-freiberg.de

[2] Airbus Defense & Space GmbH, Bremen, Germany, stefanie.garbade@airbus.com, detlev.konigorski@airbus.com

[3] German Space Agency at DLR AR-AF BO - Forschung und Exploration, Bonn-Oberkassel, Germany, Volker.Schmid@dlr.de

[4] German Aerospace Centre (DLR), Institute of Planetary Research, Rutherfordstraße 2, 12489 Berlin, Germany, Frank.Sohl@dlr.de

SUMMARY

The MagVector/MFX-2 experiment was conducted in 2018 as part of Alexander Gerst's horizons mission on the International Space Station (ISS). It was planned and led by the German Space Agency at DLR and developed and built by Airbus Defense and Space GmbH with funds from the Federal Ministry for Economic Affairs and Energy. Its main objective was to enlarge the number of sensors for measuring effects of the Magvector/MFX core. Furthermore, the new sensor array gave an excellent opportunity to host 13 different material and planetary rock samples, for the first time measuring possible interactions with magnetic fields when travelling with orbital velocity in a laboratory experimental setup onboard the ISS. The magnetic environment around the samples was continuously monitored by 32 sensors measuring the magnetic flux density in three components. The meteorite samples and sample preparation were provided by the Museum für Naturkunde Berlin. The collected data material has been investigated using simulation and inversion software developed at the TU Freiberg. Here, we are going to report about the results of these virtual experiments that aim at reconstructing and understanding the observed magnetostatic and inductive responses generated by the samples. The magnetic susceptibility of the samples was successfully recovered by a newly developed magnetostatic inversion algorithm after preprocessing the data to remove unphysical signal components. Furthermore, we have carried out a series of induction experiments using our Nédélec finite element unstructured tetrahedral mesh time-domain forward modeling code. Both codes allow for a highly accurate incorporation of the experimental geometry and the shape of the samples. The induction experiments showed that a significant inductive effect of the samples at the nearest sensor location cannot be expected below 1 to 10 kHz. Based on these findings, the method can be scaled up for the investigation of larger objects.

Keywords: International Space Station (ISS), horizons mission, MFX-2 experiment, terrestrial planets, asteroids, magnetostatics, electromagnetic induction, numerical simulation

Abstract, 25^{th} EM Induction Workshop,Çeşmeı, Turkey, September 11-17, 2022

Deep geomagnetic sounding by Sq variations in Europe: A 3-D inversion based on the regional-to-local transfer functions

J. Velímský[1], L. Šachl[1] and O. Knopp[1]
[1]Dept. of Geophysics, Faculty of Mathematics and Physics, Charles University, Prague, Czech Republic,
jakub.velimsky@mff.cuni.cz

SUMMARY

The spatial configuration of the ionospheric currents precludes the use of simple local transfer functions in geomagnetic deep sounding by the solar quiet (Sq) variations. The global-to-local transfer functions relate the local vertical magnetic field at a particular observatory to the spherical harmonic coefficients describing the ionospheric source. The latter must be obtained by initial processing of the horizontal magnetic field measurements, and using an a-priori conductivity model.

The approach presented here introduces two novel points in this concept. First, the global spherical harmonic base is replaced on the regional scale with vector Slepian functions, concentrating the EM fields in the area of interest while still allowing to use the well developed spherical-harmonic formalism. Second, the Dirichlet boundary condition is applied in the forward problem, prescribing the total horizontal magnetic field in the Slepian base, and thus avoiding the use of an a-priori conductivity model. Such formulation allows a straightforward prediction of the regional-to-local transfer functions, which relate the vertical magnetic field at a particular point with the coefficients of the Slepian expansion of the horizontal component.

The methodology is tested on a synthetic quasi-realistic scenario for European observatories. A 3-D conductivity model WINTERC-e Wd-emax, based on a thermochemical state of the mantle and laboratory conductivity measurements, is used to generate the responses, and subsequently is successfully recovered from them by 3-D inversion.

In the next step, we obtain robust estimates of the regional-to-local transfer functions for the daily time harmonics from geomagnetic field measurements at European observatories, and invert them in terms of 3-D electrical conductivity distribution in the upper mantle below Europe. Finally, we look at the interpretation of the conductivity model in terms of the mantle thermochemical structure.

Keywords: Sq variations, geomagnetic deep sounding, transfer functions, upper mantle conductivity below Europe

Abstract, 25^{th} EM Induction Workshop, Çeşme, Turkey, September 11-17, 2022

3-D inversion of tippers estimated at a continental grid of Chinese geomagnetic observatories: Preliminary results

Shan Xu[1,2], Alexey Kuvshinov[2], Chaojian Chen[2], Mikhail Kruglyakov[3], Rafael Rigaud[2], Zhengyong Ren[4] and Xiangyun Hu[1]

[1]China University of Geosciences (Wuhan), Wuhan, China, shanxu0919@gmail.com

[2]ETH Zürich, Zürich, Switzerland, kuvshinov@erdw.ethz.ch

[3]University of Otago, Dunedin, New Zealand, m.kruglyakov@gmail.com

[4]Central South University, Changsha, China, renzhengyong@csu.edu.cn

SUMMARY

Deep 3-D electrical conductivity structures on a continental scale can be retrieved by the joint inversion of multi-source magnetic transfer functions (TFs) - tippers, and longer period global-to-local (G2L) TFs originated from the signals due to ionospheric and magnetospheric sources - which in their turn can be estimated from a regional network of continuous measurements of the geomagnetic field. In this study, we discuss a data set comprising measurements from a grid of continental Chinese geomagnetic observatories, present results of estimating tippers from these data and perform their forward and inverse modelling. Specifically, we sorted out and carefully calibrated twelve years (2008-2019) of data from 67 Chinese observatories. We estimated tippers at these observatories in a period range between 5 minutes and 3 hours; notably, tippers appeared to be extremely large at four stations in southwest China. We also present the first results of inverting tippers in terms of 3-D conductivity distribution in the crust and part of the upper mantle beneath China. Inversion is performed using a novel, accurate, and computationally efficient 3-D forward and inverse solver, GEMMIE, based on the integral equation approach. This work is considered as the first step toward joint inversion of tippers and longer period G2L TFs to obtain a 3-D conductivity model beneath China down to the lower mantle.

Keywords: Geomagnetic induction; Time-series analysis; Tippers; Three-dimensional conductivity structure.

Abstract, 25th EM Induction Workshop, Çeşme, Turkey, September 11-17, 2022

Investigation of the Impact of convectively coupled equatorial waves (CCEW) and total electron content (TEC) on the diurnal cycle in Indonesia as early warning system of equatorial climate change

M. K. Rifai, C. A. Hapsoro and E. Latifah
Physics Department, Univesitas Negeri Malang, Indonesia, mochamad.khoirul.2003228@students.um.ac.id
Physics Department, Univesitas Negeri Malang, Indonesia, cahyo.ajihapsoro.fmipa@um.ac.id
Physics Department, Univesitas Negeri Malang, Indonesia, eny.latifah.fmipa@um.ac.id

SUMMARY

Climate change has become a global issue that impacts the world community's perspective on preventing potential natural disasters in the future. One of the essential factors in the investigation of climate change dynamics is the Convectively Coupled Equatorial Wave (CCEW). Recent studies on the CCEW found very active climate dynamics in the Indo-Pacific warm sea region. This condition causes the Indo-Pacific region to have the potential for extreme conditions in the future. On the other hand, several previous studies have shown an unusual correlation between TEC (Total Electron Content) activity in the Ionosphere layer to climate dynamics in the lower atmosphere. TEC induces the propagation of gravity and Kelvin waves, which affects the formation speed of the weather phases. Although recent research has revealed a correlation between the two components with such a wide area coverage, the impact on Indonesia's territory is still not fully understood. This is important considering that the Indonesian archipelago has various large islands with different meteorological conditions. So, a more specific review regarding the impact of CCEW and TEC in the Indonesian archipelago needs to be carried out. The impact of these two components is focused on the diurnal cycle, considering that the Indonesian archipelago has high precipitation levels. CCEW data processing uses TMPA (TRMM Multisatellite Precipitation Analyses) and IR-WS (Infrared Weather State). Furthermore, the two types of data models are processed to identify the CCEW phase and finally perform a statistical analysis of the resulting diurnal cycle. TEC's behaviour was observed using Geostationary Satellite Radio Beacon Techniques for further statistical analysis of the intensity of its influence on the diurnal cycle. This research is intended as an early mitigation effort to the changing conditions of the equatorial tropical climate in Indonesia, which is expected to continue to increase in the next few decades.

Keywords: Climate change, Convectively Coupled Equatorial Waves (CCEW), Total Electron Content (TEC), diurnal cycle, Indonesia.

Variations of the induction vector, worldwide study

I.I.Rokityansky
Subbotin Institute of Geophysics of the National Academy of Sciences of Ukraine, Kiev, Ukraine
E-mail: rokityansky@gmail.com

SUMMARY

Real (in phase) and imaginary (out of phase) induction vectors (vertical response functions) were obtained for every day in the time interval from 1991 to 2014 years on 137 observatories of the global network «Intermagnet» for 5 intervals of periods: 150-300 c, 300-600 c, 600-1200 c, 1200-2400 c, 2400-3600 c. To reduce scatter and make it easier to work with great amount of data, the daily values were averaged to monthly mean values. Such global material from $+87^0$ to -88^0 geomagnetic latitudes was obtained for the first time and its analysis yields new scientific results. The annual variation with a period 1 year is visible at about 2/3 of the observatories (At the rest observatories it is below background of shorter period variations and/or noise). Its amplitude depends of geomagnetic latitude and sometimes attains such a high value as 0.4-0.5 (peak-to-peak) in high ($>65^0$) latitudes and varies within 0.01-0.15 in middle and low latitudes. Previous studies in middle latitudes led to conclusion that induction vector's northern component A_u is everywhere positive (maximum in June, minimum in December) and proposed a global source model for its description. This study states that in high latitudes A_u is negative. 11-years variation found in ≈30% of observatories distributed in all latitudes but more frequently in aurora zones. Non-periodic transient variations of the induction vector also occur, in particular before strong earthquakes. In common, the behavior of the induction vector variations is complex with many local exceptions and irregularities that leads to supposition that they are not a simple «source effect», but contain information from the Earth interior and its environment including interactions in the system Earth-Sun-Moon-planets.

Keywords: geomagnetic field, geomagnetic variations, annual variation, magnetic variation profiling.

Introduction

The Induction vectors were introduced by Parkinson (1959), Wiese (1965) and Schmucker (1970) for the study of strong conductivity contrasts like sea-land and looking for electrical conductivity anomalies in the Earth crust. To obtain an induction vector, three components of natural geomagnetic field **B**(t) are necessary.

Method

In the geoelectromagnetic studies of the Earth's interior natural source field $\mathbf{B}(t)=B_x\mathbf{e_x}+B_y\mathbf{e_y}+B_z\mathbf{e_z}$ (where $\mathbf{e_x}$, $\mathbf{e_y}$, $\mathbf{e_z}$ are unit vectors directed to North, East and downward) is used. **B**(t) contains rich information both from external source in ionosphere and magnetosphere and from the Earth interior. To clean out external influence and focus on the Earth interior study special processing transforms **B**(t) time series into Response Functions (RF) time series. Induction vector **C** is one of RF (response of the Earth to applied external field):

$$\mathbf{C}=A\mathbf{e_x}+B\mathbf{e_y} \quad (1)$$

where A and B determined from the linear equation

$$B_z = AB_x + BB_y \quad (2)$$

The quantities A and B are complex numbers, and a pair of induction vectors is determined: real $\mathbf{C_u}$ and imaginary $\mathbf{C_v}$ (Rokityansky 1982).
Real induction vector $\mathbf{C_u} = A_u\mathbf{e_x} + B_u\mathbf{e_y}$ possess an important property: in the Wiese notation used here, it is directed away from a good conductor.

Processing technique

The processing of the data recorded in the time interval Δ∓=t2-t1 (usually 1 day in this work) is a transformation from 3 synchronous time series Bx, By, Bz with a discreteness Δt (1 min – data Intermagnet) into the time series of the induction vector components for the set of obtained periods Tn (n=1-5) with discreteness Δ∓. Obviously, Δt«Tn«Δ∓.
Processing was carried out by programs of Varentsov (2007) and Klimkovich (2009) based on FFT, calculation of cross- and auto-correlation energy spectra between magnetic components, partial estimator procedure in a set of overlapping windows, and a multi-stage selection of acceptable estimators according to coherence criteria.

Data and results

Digital Intermagnet worldwide data **B**(t) (http://www.intermagnet.org/) with the discreteness of 1 min have been processed since 1991 to 2014

year and for every day the components A_u, B_u, A_v, and B_v of real and imaginary induction vectors were obtained for the intervals of periods 2,5-5 min, 5-10 min, 10-20 min, 20-40 min and 40-60 min. The daily components of the induction vector are characterized by a considerable scatter. For their smoothing and compact presentation of long-term data, the monthly mean values were calculated and used. This limited the resolution of the obtained time series to 2-3 months.

Observatories with induction vectors at period 1800 s are presented in Figure 1, the time series for 25 observatories at the same period are given in Figure 2, the time series at 4 periods are published in (Babak et al 2017) for 8 observatories. *When reading the following text, it is recommended to look at the mentioned figures.*

The annual variation (AV) with a period 1 year is visible at about 2/3 observatories of world (at the rest observatories it is below background of shorter period variations and/or noise). Its amplitude depends of geomagnetic latitude and sometimes attains such a high value as 0.4-0.5 (peak-to-peak) in high (>65^0) latitudes and varies within 0.01-0.15 in middle and low latitudes. AV amplitude as a rule increases with the period.

Previous works (Araya and Ritter 2016 and others referred in it) studied AV only in middle latitudes and found that northern component A_u is always positive, i.e. A_u has the maximum in June. Studies in high latitudes yield: polarity of A_u is usually negative (maximum in December) with few exceptions. All this clearly seen in Figure 2 at northern observatories THL and RES and in the southern one DRV, but in the most southern SBA A_u is positive (an «exception»). It means that annual variations are not only global source field effect but also effect of local factors.

Consider the results of 3 observatories:

THL (geomagnetic latitude 87.31^O, northwest of Greenland). AV is most intense at the longest period of 3000 s, sometimes reaching an amplitude of 0.5 on A_u and B_v components. With the period decrease, AV amplitude decreases to values of the order 0.2-0.05. AV is unstable, its amplitude at some components/periods changes by 1.5-2 times during 23 years. Also, there is an «overflow» of AV from one component to another. So, at periods 5-10 min at A_v in THL and at B_v in NAQ annual variation in 1991-2004 was rather intensive, then it was halved, and at A_u and B_u of both observatories AV amplitude was doubled. The same AV enhancement from 2005-2007 to 2011-2014 was observed in HLP (Poland), KOU (Guyana) … and Japan where it was supposed to be middle-term precursor of the Tohoku earthquake (Rokityansky et al. 2019).

RES (north of Canada), the induction vector is on average 0.2 directed to the north. The AV is slightly smaller in amplitude than in THL, but with a similar distribution over the components. Intense variations with a period little less than half of year are imposed on the AV. They deviate the shape of AV from a sinusoid and make the upper extremum of AV blunt and the lower extremum pointed (and similar form is observed also at observatories THL, DRV, SBA on A_u and B_v components); in other cases, vice versa, the upper one is pointed, the lower one is blunt (THL, SBA - on the B_u component).

NAQ (geom. latitude 69.46^0, south of Greenland). Marine currents of deep ocean create a significant real induction vector Cu≈0.9 at periods 20-60 min. The imaginary vector Cv at periods 450, 900, 1800 and 3000 s is equal to +0.3, +0.15, 0 and -0.15 respectively which is in full agreement with the theory and empirical formula (7.1) for the coast effect developed in [Rokityansky, 1982, p. 313]. In NAQ large annual (0.1-0.3) and 11-year variations (0.1-0.2 in all periods). And quite unusual thing - a large trend ≈0.2 over 23 years. Glaciers are melting in Greenland. May be the anomalous behavior of vectors in NAQ related with global warming?

11-years variation found in ≈30% of observatories distributed in all latitudes, more often in aurora zones.

REFERENCES

Araya JV, Ritter O (2016) Source effects in mid-latitude geomagnetic transfer functions. *Geophys J Int* 204, 606-630. doi: 10.1093/gji/ggv474.

Babak VI, Rokityansky II, Sokolova EYu, Tereshin AV (2017) Annual, 11-year and aperiodic variations of the induction vector at 8 observatories of the Intermagnet network. Geofiz j, 39, n. 1, 97-110, doi: org/10.24028/gzh.0203-3100.v39i1.2017.94013

Rokityansky II (1982) Geoelectromagnetic investigation of the Earth's crust and mantle. Berlin-Heidelberg-New York: Springer Verlag 381p.

Rokityansky II, Babak VI, Tereshyn AV, Hayakawa M (2019) Variations of Geomagnetic Response Functions before the 2011 Tohoku Earthquake. Open Journal of Earthquake Research, 8, 70-84. https://doi.org/10.4236/ojer.2019.82005

ACKNOWLEDGEMENTS

The author is grateful to I.M. Varentsov and T.A. Klimkovich for the processing programs, V.I. Babak and A.V. Tereshyn for processing a significant amount of data, and to the staff of geomagnetic observatories for the high quality records.

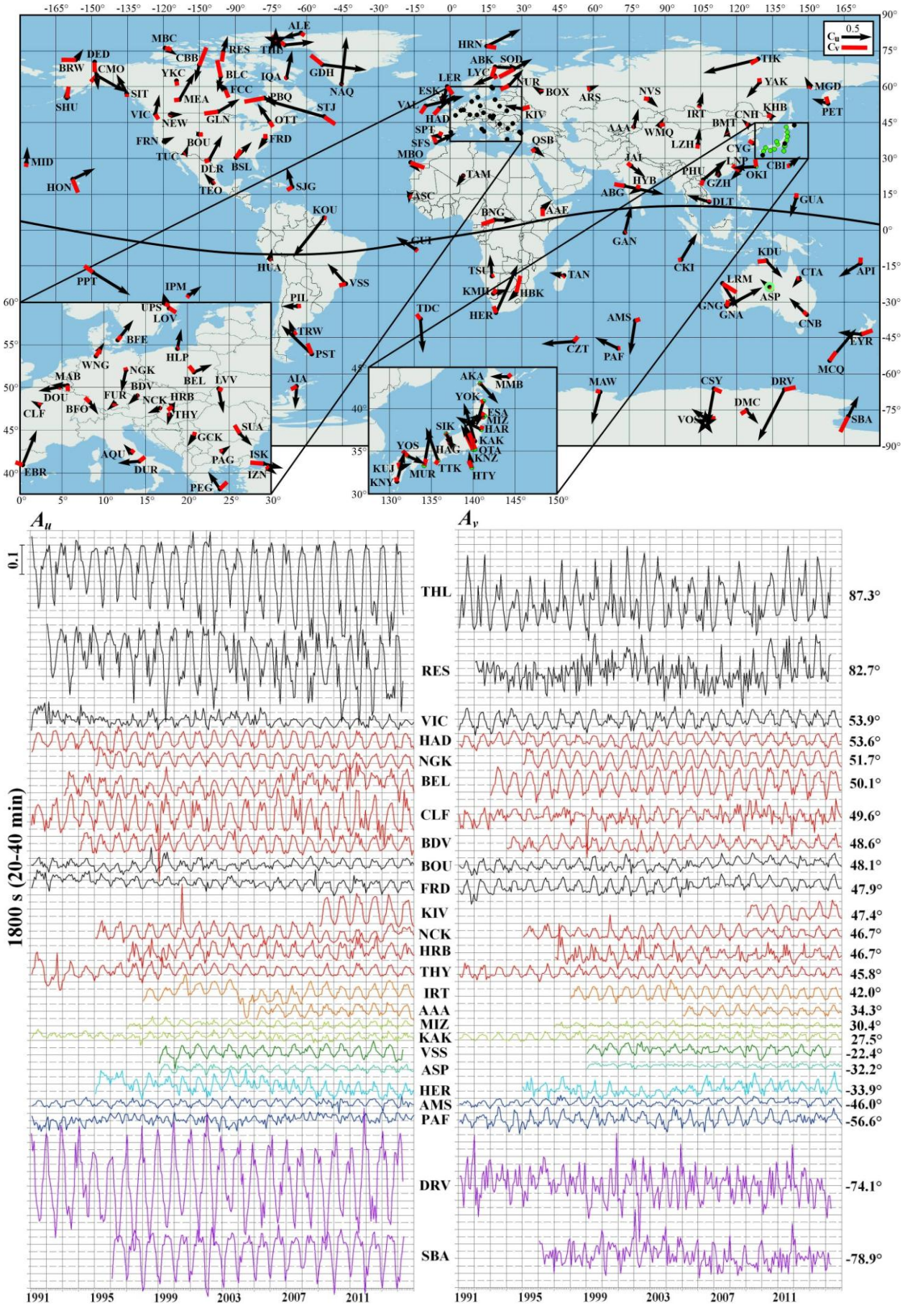
Cu
Cv
0.5
A_u
A_v
0.1
1800 s (20-40 min)
THL 87.3°
RES 82.7°
VIC 53.9°
HAD 53.6°
NGK 51.7°
BEL 50.1°
CLF 49.6°
BDV 48.6°
BOU 48.1°
FRD 47.9°
KIV 47.4°
NCK 46.7°
HRB 46.7°
THY 45.8°
IRT 42.0°
AAA 34.3°
MIZ 30.4°
KAK 27.5°
VSS -22.4°
ASP -32.2°
HER -33.9°
AMS -46.0°
PAF -56.6°
DRV -74.1°
SBA -78.9°
1991
1995
1999
2003
2007
2011

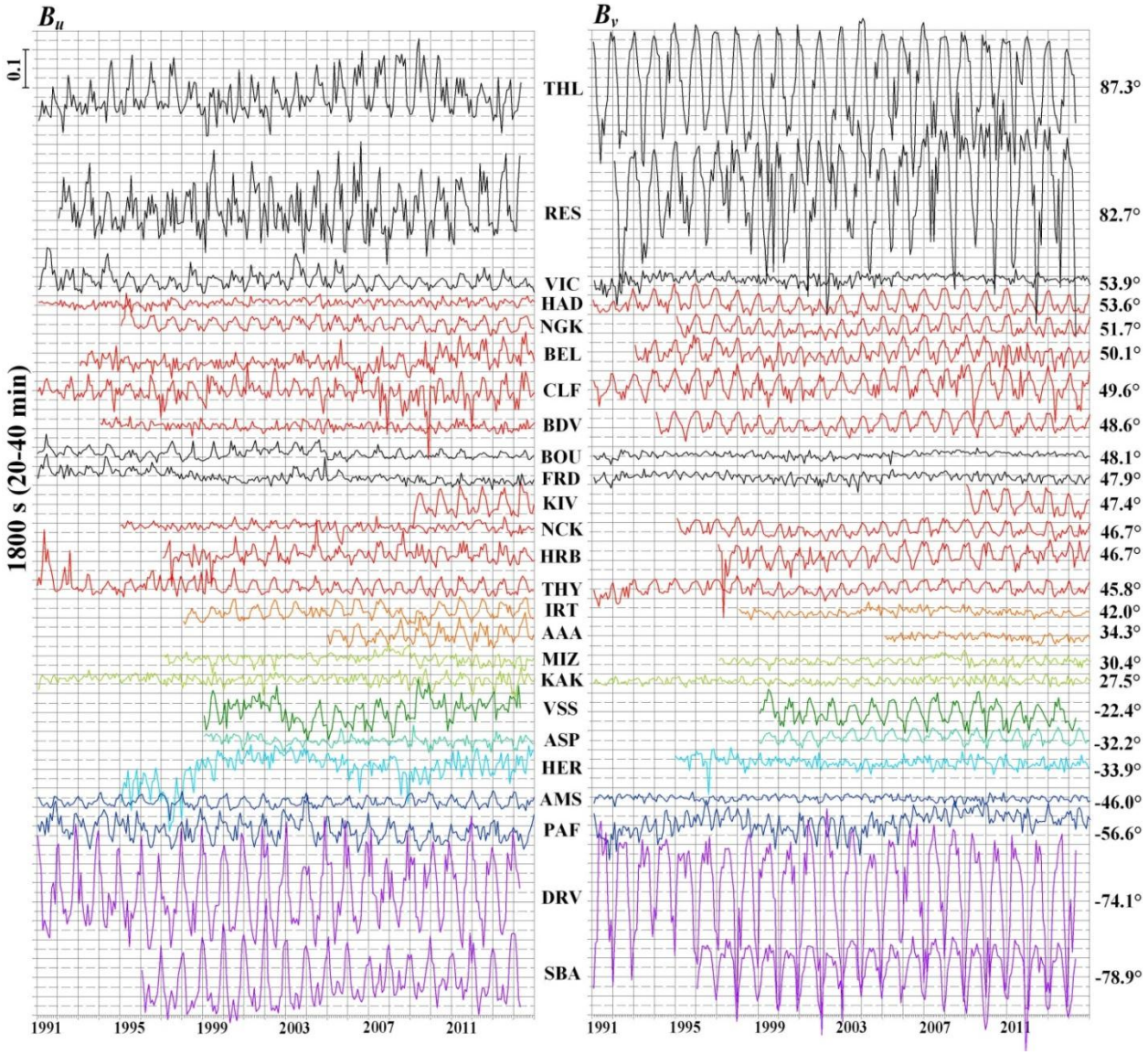

Figure 1. Map of 137 Intermagnet + 14 Japanese observatories with real $\mathbf{C_u}$ and imaginary $\mathbf{C_v}$ induction vectors for the period 1800 s (20-40 min), averaged for the entire observation period. Geomagnetic poles for epoch 2010 are marked by 5-ray stars, geomagnetic equator is also drawn.

Figure 2. Monthly average components A_u and A_v (upper graph), B_u and B_v (lower graph) in 1991-2014 for a period 1800 s (20-40 min) at 25 observatories selected with clearly visible annual variations. The geomagnetic latitudes of each observatory are inscribed on the right. The scale for all observatories is the same, the level is not saved. The color of the curves depends on the location: black - North America, red - Europe, faded red - Asia, light green - Japan, green - South America, green-blue - Australia, blue - South Africa, dark blue - Indian Ocean, orange - Antarctica.

CONCLUSIONS

Real and imaginary induction vectors were calculated for every day and month in the time interval from 1991 to 2014 on 137 observatories of the global network «Intermagnet» for 5 intervals of periods: 150-300 c, 300-600 c, 600-1200 c, 1200-2400 c, 2400-3600 c. Such global material was obtained for the first time and its analysis yields new results so far using only monthly mean values. The annual variation is visible at about 2/3 of the observatories. In high (>65^0) latitudes its amplitude attains such a high value as 0.4-0.5, in middle and low latitudes it varies within 0.01-0.15. Northern component of annual variations in low and middle latitudes is positive (maximum in June, minimum in December), in high latitudes - negative. 11-years variation found in 30% of observatories distributed in all latitudes but more frequently in aurora zones. Non-periodic transient variations of the induction vector also occur, in particular before strong earthquakes. Dependence of the induction vector variations on the magnitude and direction of the vector itself is not found in this study.

Constraining the crustal and mantle conductivity structures beneath islands by a joint inversion of multi-source magnetic transfer functions

C. Chen[1], A. Kuvshinov[1], M. Kruglyakov[2], F. Munch[3] and R. Rigaud[1]
[1]Institute of Geophysics, ETH Zurich, Switzerland, chaojian.chen@erdw.ethz.ch
[2]Department of Physics, University of Otago, New Zealand
[3]Berkeley Seismological Laboratory, University of California, Berkeley, United States

SUMMARY

In this study, we present a tool to simultaneously invert multi-source magnetic transfer functions (TFs), including tippers, solar global-to-local transfer functions (TFs) originating from the signals due to ionospheric source, and global Q-responses originating from the signals due to magnetospheric source. We jointly invert the aforementioned TFs to constrain the local conductivity structures beneath three islands in the Atlantic (Tristan da Cunha), Indian (Cocos), and Pacific (Oahu) Oceans. The recovered conductivity profiles appeared to be consistent with the presence of upper mantle plumes beneath the Tristan da Cunha and Oahu Islands. Our results indicate resistive lithosphere of different thicknesses beneath considered three islands. Besides, new conductivity profiles suggest warmer-than-average mantle temperatures and the presence of a small fraction of melt beneath Tristan da Cunha Island. At the same time, the conductivities beneath Cocos Island are in good agreement with estimates expected for ambient mantle conditions.
Keywords: Joint inversion; electromagnetic; transfer functions; mantle conductivity

Abstract, 25th EM Induction Workshop,Çeşmeı, Turkey, September 11-17, 2022

Making geo-electromagnetic (magnetotelluric) data accessible via EPOS portal

M.Yu. Smirnov[1], J. Hübert[2], O. Ritter[3], A. Neska [4], T.M. Rasmussen[1], P. Hejda [5], S. Flower [2], A. Chambodut [6], J.J. Curto [7], J. Matzka [3], A. Thomson [2], A. Viljanen [8]
[1] Luleå University of Technology, Sweden, maxim.smirnov@ltu.se
[2]British Geological Survey, Edinburgh, UK, juliane.huebert@bgs.ac.uk
[3] GFZ, Potsdam, Germany, Oliver.Ritter@gfz-potsdam.de
[4] Institute of Geophysics, Polish Academy of Sciences, Warsaw, Poland, anne@igf.edu.pl
[5]Institute of Geophysics, Prague, Czech Republic, ph@ig.cas.cz
[6]Ecole et Observatoire des Sciences de la Terre, Université de Strasbourg, France, aude.chambodut@unistra.fr
[7] Observatori de l'Ebre, Roquetes, Spain, jjcurto@obsebre.es
[8] Finnish Meteorological Institute, Helsinki, Finland, ari.viljanen@fmi.fi

Over the past decades a great wealth of magnetotelluric (MT) data have been collected by many researchers across the globe. Making the data accessible and available to other scientists within the same discipline and beyond poses a big challenge but also offers great opportunities for new and cross-disciplinary science. Since the last EM Induction workshop in Helsingor in 2018 we have continued to further develop the archiving of and access to European MT data within the European Plate Observing System (EPOS). EPOS is a multidisciplinary, distributed research infrastructure that facilitates the integrated use of data, data products, and facilities from the solid Earth science community in Europe and is funded by the European union. MT data is integrated in the Geo-Electromagnetic Thematic Core Service (TCS) in close collaboration with geomagnetic observations and data services. EPOS' main achievement is an openly accessible data portal that contains the metadata and download links to all data available through this service, thus making MT data searchable and accessible to a wide range of science, policy makers and other users.

Geo-electromagnetic data are currently held in a variety of formats, software and locations, which creates a barrier to access. Data provided through EPOS will have to conform to common standards. We have developed and implemented today's standard-de-facto for web metadata - the JSON container, a standard text-based format for representing structured data - as the data storage format for MT data and models. This data format is intentionally implemented to contain all the necessary information to fully describe EM metadata. Existing standards like .edi can be converted easily and software tools are openly available.

For EPOS, the data from all TCSs are searchable via the centralised Integrated Core Services (ICS) portal. The portal itself only provides a search function through metadata provided by various TCSs, but the data themselves are stored on individual TCS servers. We have established data storage of MT data at BGS and LTU facilities and discuss with other national research institutes to test and use their facilities for sustained MT data storage and access.

Keywords: EPOS, magnetotelluric data, database, data format

Multidimensional Interpretation of Controlled-Source Radio-Magnetotelluric (CSRMT) of a waste-site in Cologne, Germany

S. Fadavi Asghari[1], A. Shlykov[2], M. Smirnova[3], A. Saraev[4], P. Yogeshwar[5] and B. Tezkan[6]
[1]Institute of Geophysics and Meteorology, University of Cologne, sfadavia@smail.uni-koeln.de
[2]Institute of Earth Sciences, St. Petersburg State University, shlykovarseny@gmail.com
[3]Institute of Geophysics and Meteorology, University of Cologne, maria.smirnova@uni-koeln.de
[4]Institute of Earth Sciences, St. Petersburg State University, asaraev51@mail.ru
[5]Institute of Geophysics and Meteorology, University of Cologne, yogeshwar@geo.uni-koeln.de
[6]Institute of Geophysics and Meteorology, University of Cologne, tezkan@geo.uni-koeln.de

SUMMARY

Radio-Magnetotelluric (RMT) method is based on measurements of the electromagnetic (EM) field using military and civilian radio transmitters broadcasting in a frequency range between 10 to 1000 kHz as the source. In order to reach to higher signal to noise ratio and a deeper penetration depth, CSRMT measurements are performed using a controlled-source in a wider frequency range of 1 to 1000 kHz.

We accomplished a dense CSRMT survey over a waste-site in Cologne, Germany. The site was used as sand and gravel pit from 1940s to the 1950s. Afterwards, it was filled with different kinds of wastes including household refuse, construction and industrial waste, cinder, tires, wood, plastic, military fences, etc. The aim of the CSRMT survey is to detect the boundary and the basement of the waste body and possibly any signature of contamination leakage to the deeper subsurface.

Two perpendicular transmitters, each 265 and 580 meters long, were set-up to obtain the full impedance tensor and the tipper elements. In order to validate the far-field condition, RMT measurements were also carried out with the transmitters switched off. The far-field data have been acquired in a total of 177 stations from thirteen profiles. The separation between the stations and the profiles was 10 and 30 m respectively.

The RMT and CSRMT data acquired in this field experiment, were processed and the corresponding apparent resistivity, phase and tipper were calculated. Here, we present and discuss the 2D and 3D inversion of the computed transfer functions.

In general, we image a high conductive waste body extending to a maximum depth of 15 m. The exploration depth is around 50 m in average. The waste body indicates an internal structuring and is well confined to the former pit area. Below the waste, sandy gravel is deposited.

Outside the waste the subsurface is highly resistive.

The CSRMT results, are in a good agreement with former DCR results that are obtained from the same region indicating the reliability of the data acquisition, processing and inversion.

Keywords: electromagnetic, CSRMT, inversion, conductivity, waste-site

Delineating subsurface structures for deep aquifer study using MT, and airborne geophysics. Case study of the Voltaian sedimentary basin, Ghana West Africa.

R.A. Mejida[1,2], P. Tarits[1], T.E. Armah[2] , S. Hautot[3] and S.M. Yidana [2]
[1] IUEM, Geo-Ocean, rmejida@ug.edu.gh, tarits@univ-brest.fr
[2] University of Ghana, tekarmah@ug.edu.gh, smyidana@ug.edu.gh
[3] IMAGIR, sophie.hautot@imagir.eu

SUMMARY

Locating groundwater productive zones in the near surface in the Voltaian sedimentary basin in Ghana has been challenging over the past years causing water scarcity among residents in the basin. Resident relies sole on groundwater for their domestic supply as a result of extreme temperatures and high evapotranspiration following a prolong dry season, causes surface water bodies to dry up. To address this challenge, airborne geophysical data and magnetotellurics data has used to attempt to delineate aquifers deeper beyond the weathered zone in the basin. The results of the integrated geophysical approach suggest the presence of a low resistivity layer lies between 200m to 550 m within the sandstones and could have potential for holding groundwater.

Keywords: Magnetotellurics, Inversion, Airborne geophysics, water resources, Voltaian Sedimentary Basin

Groundwater is the main source of potable water for indigenes in the northern part of the several kilometers deep Voltaian Sedimentary Basin (VSB) in Ghana (Figure 1).

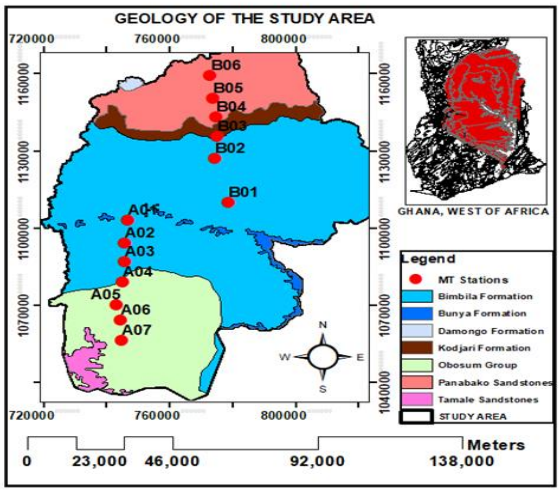

Figure 1 : Geology of Voltaian Sedimentary Basin

Groundwater exploration in the VSB over the years has yielded very little success with a failure rate of about 60 percent (Agyekum and Asare, 2016). Electrical resistivity tomography has been the main geophysical technique used for groundwater exploration in the VSB targeting the weathered zone of the near surface. The low yields of boreholes have pushed contractors to target deeper aquifers as against the shallow aquifers in the basin to supply sufficient water to cover the rapid economic development coupled with population growth in the basin. The complexity and paucity of the outcrops has hampered sufficient mapping of the basin structure down to the Proterozoic basement. To address this problem, and to offer a detailed description of the basin structure, a preliminary integrated geophysical investigation approach using existing airborne geophysical data (obtained from the Ghana geological survey authority) and magnetotelluric (MT) data obtained from field survey undertaken within the scope of this project in the north part of the VSB. The target areas for MT soundings were identified from airborne geophysical data (EM, magnetic and gravity, Fugro (2009)). Vertical gradient maps of the airborne magnetic data and Euler solutions of the airborne gravity data revealed the presence of several geological structures (faults and folds) within the thick platform sediment (Figure 3) revealing their potential as deep-seated aquifers. The depth to basement is observed to averaging about 4.5 km with the MT while with the

airborne gravity and magnetic data, the depth is 5.5 km and 4 km respectively. A total of 13 broad-band MT soundings along two profiles lines orienting north-south were conducted. A preliminary 3-D inversion of the whole data set showed the presence of conductive layers within the basin (Figure 2).

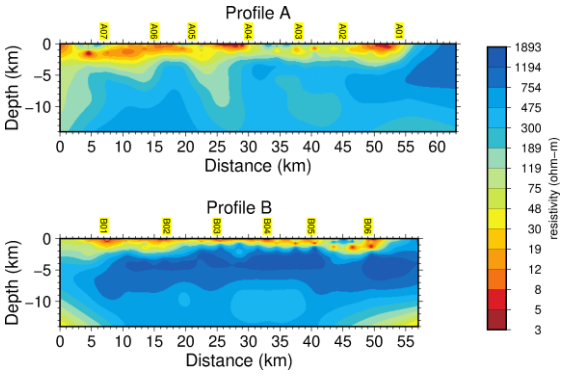

Figure 2. Southern and northern resistivity sections from the 3-D inversion results.

One dimensional MT inversion of the Berdichevsky invariant (e.g. Simpson and Bahr, 2005) was used to improve the vertical resolution at each site. The average thickness of the low resistive layer is about 300 m and with values which ranges between a few tens of ohm m corresponding to resistivity values of fresh groundwater. Further work will target proper delineation of the possible deep-seated aquifers possibly within the sandstones known to intercalate with the shales and siltstones in the area. Also, we will be carrying out composition analysis as well as porosity and permeability test of some outcrops in the region to further improve this work.

ACKNOWLEDGEMENTS

The authors thank the French embassy in Ghana and the Ghana government for their financial support toward this work.

REFERENCES

Agyekum W.A. and Asare E.B. (2016) Challenges associated with groundwater resource development in Northern Ghana. Ghana journal of science 56: 39-51

Fugro Airborne Survey (2009) Logistics and processing report, airborne magnetics and GEOTEM survey. Area 1 to 8, Ghana 92.

Simpson F. and Bahr K. (2005) Practical magnetotellurics. Cambridge University Press, Cambridge

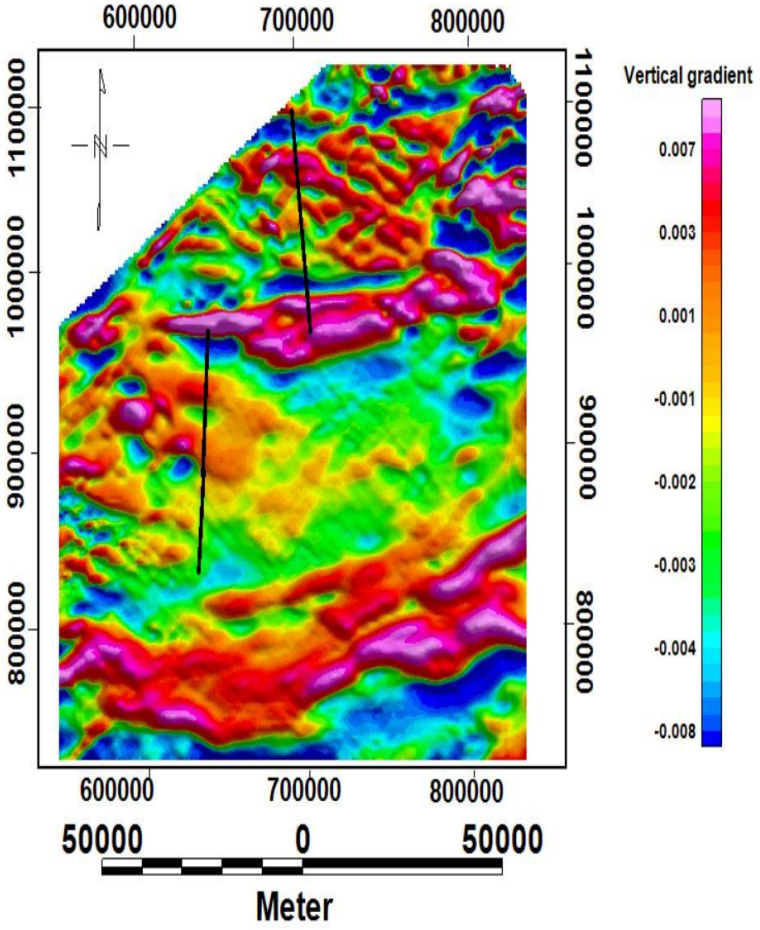

Figure 3. The vertical derivative of the magnetic data shows geological structures in the northern part of the Voltaian sedimentary basin in Ghana.

Investigation of the topographic effect in the San Pedro-Ceboruco graben: real data and synthetic studies

M. K. Díaz[1,2], C. Castro[1], A. Junge[1], F. Corbo[2]
[1]Goethe-Universität Frankfurt am Main, mdiazna@geociencias.unam.mx
[1]Goethe-Universität Frankfurt am Main, castro@geophysik.uni-frankfurt.de
[1]Goethe-Universität Frankfurt am Main, junge@geophysik.uni-frankfurt.de
[2]Universidad Nacional Autónoma de México, fercorbo@geociencias.unam.mx

Summary

The Magnetotelluric (MT) Transfer Functions (TF) establish the relationship between time variations of the electric and magnetic fields at the Earth's surface. Thus, they provide frequency-dependent information about the electrical resistivity structure of the subsurface. The TFs can be strongly influenced by topography and, cause misinterpretation in subsequent modelling. Therefore, modelling topographic effects could lead to a deeper understanding of the TF during the interpretation process.

A MT survey was carried out in the framework of the projects SPCG[a] and DEMITZ[b] along the NW Tepic-Zacoalco Rift (TZR), where important volcanic structures are present. The purpose of these projects is to investigate the magmatic systems and the conductivity distribution in the subsurface at the northern part of the TZR, known as the San Pedro-Ceboruco graben (SPCG). The processing results of measured time series, reveal induction arrows pointing away from the volcanic edifices (Wiese convention) for periods around 1s.

To determine the contribution of the topographic effect on the observed data, 3-D forward responses are calculated accounting for a simplified topography, including the actual dimensions and positions of the San Pedro Dome and Ceboruco Volcano, both located in the SPCG. The responses obtained in the synthetic study reveal a strong influence of topography at frequencies above 1Hz represented by large induction arrows and phase tensor split. Attempting to reproduce the observed data, the spatial and frequency distribution of TFs simulated for conductivity anomalies with different geometries and varying background resistivities.

The simulation study reveals that the observed TFs do not result from topography but give evidence for a conductive body centered in-between the existing volcanoes.

Keywords: Magnetotelluric Transfer Functions, Topography, Modelling, Magmatic Systems.

[a]PAPIIT funded project "Geothermal assessing and determination of the magmatic source in the San Pedro-Ceboruco graben (SPCG)".

[b]DFG funded project "Mid-to-Deep-crustal Electromagnetic Investigation of Tepic-Zacoalco Rift: Exploring Magmatic Systems and Electrical Anisotropy in Western Mexico (DEMITZ)".

emiw2022.emiw.org